**МІНІСТЕРСТВО ОСВІТИ І НАУКИ УКРАЇНИ**
**ДВНЗ «Прикарпатський національний університет імені Василя Стефаника»**
Фізико-хімічний інститут
Науково-дослідницький центр напівпровідникового матеріалонавства
**АКАДЕМІЯ НАУК ВИЩОЇ ШКОЛИ УКРАЇНИ**
**Державний фонд фундаментальних досліджень**
**НАЦІОНАЛЬНА АКАДЕМІЯ НАУК УКРАЇНИ**
Інститут фізики напівпровідників ім. В.Є. Лашкарьова
Інститут хімії поверхні ім. О.О. Чуйка
Інститут металофізики ім. Г.В. Курдюмова
Інститут загальної і неорганічної хімії ім. В.І. Вернадського
**Українське фізичне товариство**
**Університет Газі (Туреччина)**

# XV МІЖНАРОДНА КОНФЕРЕНЦІЯ З ФІЗИКИ І ТЕХНОЛОГІЇ ТОНКИХ ПЛІВОК ТА НАНОСИСТЕМ

## Програма

*Івано-Франківськ, 11-16 травня, 2015*

---

*Ivano-Frankivsk, May, 11-16, 2015*

## Program

# XV INTERNATIONAL CONFERENCE ON PHYSICS AND TECHNOLOGY OF THIN FILMS AND NANOSYSTEMS

**MINISTRY OF EDUCATION AND SCIENCE OF UKRAINE**
**Vasyl Stefanyk Precarpathian National University**
Physical-Chemical Institute
R&D Centre of Semiconductor Material Science
**ACADEMY OF SCIENCE OF HIGH SCHOOL OF UKRAINE**
**State Fund of Fundamental Research**
**NATIONAL ACADEMY OF SCIENCE OF UKRAINE**
V.E. Lashkarev Institute of Semiconductor Physics
Chuiko Institute of Surface Chemistry
G.V. Kurdyumov Institute of the Physics of Metals
V.I. Vernadsky Institute of General and Inorganic Chemistry
**Ukraine Physics Society**
**Gazy University (Turkey)**

**УДК 539.2**
**ББК 22.373.1**
**Ф 83**

**Фізика і технологія тонких плівок та наносистем.** ***Матеріали XV Міжнародної конференції*** / За заг. ред. заслуженого діяча науки і техніки України, д.х.н., проф. **Фреїка Д.М**. – Івано-Франківськ: п-ць Голіней О.М., 2015. – 400 с.

Представлено сучасні результати теоретичних і експериментальних досліджень з питань фізики і технології тонких плівок та наносистем (метали, напівпровідники, діелектрики, провідні полімери; методи отримання та дослідження; фізико-хімічні властивості; нанотехнології і наноматеріали, квантово-розмірні структури, наноелектроніка, тощо. Матеріали підготовлено до друку Організаційним комітетом та Редакційною колегією конференції і подано в авторській редакції.

Для наукових та інженерних працівників, що займаються проблемами тонкоплівкового матеріалознавства та мікроелектроніки.

Рекомендовано до друку науково-технічною радою Фізико-хімічного інституту ДВНЗ «Прикарпатський національний університет імені Василя Стефаника»

**Physics and Technology of Thin Films and Nanosystems.** ***Materials of XV International Conference*** / Ed. by Honored scientist of Ukraine, Dr. Chem.Sci., Prof. **Freik D.M**. – Ivano-Frankivsk: Publisher Goliney O.M., 2015. – 400 c.

The results of theoretical and experimental researches in directions of the physics and technology of thin films and nanosystems (metals, semiconductors, dielectrics, and polymers; and methods of their investigation; physic-chemical properties of thin films; nanotechnology and nanomaterials, quantum-size structures; thin-film devices of electronics, are presented. The materials preformed for printing by Conference's Organizational Committee and Editorial Board, are conveyed in authoring edition.

For scientists and reserchers on the field of thin-film material sciences and nanoelectronics.

Р е ц е н з е н т и:
**Литовченко В.Г.**
*чл.-кор. НАН України, завідувач відділенням Інституту фізики напівпровідників ім. В.Є. Лашкарьова НАН України*
**Матвеєва Л.О.**
*доктор фізико-математичних наук, заступник завідувача відділу напівпровідникових гетероструктур Інституту фізики напівпровідників ім. В.Є. Лашкарьова НАН України*
**Лепіх Я.І.**
*доктор фізико-математичних наук, професор, Одеський Національний Університет ім. І.І. Мечникова*

## ОРГАНІЗАЦІЙНИЙ КОМІТЕТ

**Бюро**

**Загороднюк А., Литовченко В., Фреїк Д.**

**Міжнародний**

**Анатичук Л**. (Україна), **Ахиска Р.** (Туреччина), **Бабанли М.** (Азербайджан), **Бєляєв О.** (Україна), **Блонський І.** (Україна), **Бродин М.** (Україна), **Булавін Л.** (Україна), **Власенко О.** (Україна), **Волков С.** (Україна), **Вуйцік В.** (Польща), **Галущак М.** (Україна), **Горбик П.** (Україна), **Готра З.** (Україна), **Грігоніс А.** (Литва), **Гриньов Б.** (Україна), **Гуревич Ю.** (Мексика), **Жуковскі П.** (Польща), **Зломанов В.** (Росія), **Івасишин О.** (Україна), **Калінкін І.** (Росія), **Картель М.** (Україна), **Кияк Б.** (Україна), **Кікінеші О.** (Угорщина), **Кучмій С.** (Україна), **Мазуренко Є.** (Україна), **Малашкевич Г.** (Білорусь), **Міттова І.** (Росія), **Младенов Г.** (Болгарія), **Мовчан Б.** (Україна), **Наумовець А.** (Україна), **Находкін М.** (Україна), **Нікіфоров К.** (Росія), **Новиков М.** (Україна), **Остафійчук Б.** (Україна), **Панасюк В.** (Україна), **Птушинський Ю.** (Україна), **Раренко І.** (Україна), **Свєчніков С.** (Україна), **Сидоренко С.** (Україна), **Сизов Ф.** (Україна), **Скатков Л.** (Ізраїль), **Солонін Ю.** (Україна), **Стасюк І.** (Україна), **Стріха М.** (Україна), **Харченко М.** (Україна), **Челідзе Т.** (Грузія), **Тигиняну І.** (Молдова), **Томчук П.** (Україна), **Уваров В.** (Україна), **Фірстов С.** (Україна), **Фістуль В.** (Росія), **Фодчук І.** (Україна), **Шпілевський Е.** (Білорусь), **Шпотюк О.** (Україна)

Національний

**Бойчук В.І.** (Дрогобич), **Бойчук В.М.** (Івано-Франківськ), **Буджак Я.** (Львів), **Гасюк І.** (Івано-Франківськ), **Гургула Г** (Івано-Франківськ)**, Горічок І.** (Івано-Франківськ), **Дзумедзей Р.** (Івано-Франківськ), **Дзундза Б.** (Івано-Франківськ), **Дмитрук М.** (Київ), **Дружинін А.** (Львів), **Запухляк Р.** (Івано-Франківськ), **Зауличний Я.** (Київ), **Зінченко В.** (Одеса), **Зиман З.** (Харків), **Ігнатенко П.** (Донецьк), **Кідалов В.** (Бердянськ), **Кланічка В.** (Івано-Франківськ), **Коваленко О.** (Дніпропетровськ), **Корбутяк Д.** (Київ), **Куницький Ю.** (Київ), **Лашкарьов Г.** (Київ), **Лєпіх Я.** (Одеса), **Ліщинський І.** (Івано-Франківськ), **Лоп'янко М.** (Івано-Франківськ), **Матвеєва Л.** (Київ), **Мельничук О.** (Ніжин), **Миколайчук О.** (Львів), **Миронюк І.** (Івано-Франківськ), **Никируй Л.** (Івано-Франківськ), **Похмурський В.** (Львів), **Прокопів В.** (Івано-Франківськ), **Проценко І.** (Суми), **Прокопенко І.** (Київ), **Пташенко О.** (Одеса), **Рогачова О.** (Харків), **Рубіш В.** (Ужгород), **Рувінський М.** (Івано-Франківськ), **Смертенко П.** (Київ), **Стасюк З.** (Львів), **Стронський О.** (Київ), **Студеняк І.** (Ужгород), **Ткач М.** (Чернівці), **Томашик В.** (Київ), **Чуйко Г.** (Херсон)

**Секретаріат**

**Межиловська Л.** – вчений секретар конференції;

**Биліна І., Борик В., Волочанська Б., Іванишин І., Костюк О., Матківський О., Паращук Т., Потяк В., Соколов О., Яворський Я.**

## ORGANIZING COMMITTEE

### Bureau

**D. Freik, V. Lytovchenko, A. Zagorodnyuk**

International

**R. Ahiska** (Turkey), **L. Anatychyk** (Ukraine), **M. Babanly** (Azerbaijan), **O. Belyaev** (Ukraine), **I. Blonskiy** (Ukraine), **M. Brodyn** (Ukraine), **L. Bulavin** (Ukraine), **S. Firstov** (Ukraine), **V. Fistulj** (Russia), **I. Fodchuk** (Ukraine), **M. Galushchak** (Ukraine), **P. Gorbyk** (Ukraine), **Z. Gotra** (Ukraine), **A. Grigonis** (Lithuania), **B. Grynyov** (Ukraine), **Yu. Gurevich** (Mexico), **O. Ivasyshyn** (Ukraine), **I. Kalinkin** (Russia), **M. Kartel** (Ukraine), **M. Kharchenko** (Ukraine), **O. Kikineshi** (Hungary), **S. Kuchmij** (Ukraine), **B. Kyyak** (Ukraine), **G. Malashkevich** (Belarus), **Ye. Mazurenko** (Ukraine), **I. Mittova** (Russia), **G. Mladenov** (Bulgaria), **B. Movchan** (Ukraine), **A. Naumovetsj** (Ukraine), **M. Nahodkin** (Ukraine), **K. Nikiforov** (Russia), **M. Novykov** (Ukraine), **B. Ostafiychuk** (Ukraine), **V. Panasjuk** (Ukraine), **Yu. Ptushynskiy** (Ukraine), **I. Rarenko** (Ukraine), **E. Shpilevsky** (Belarus), **O. Shpotyuk** (Ukraine), **F. Sizov** (Ukraine), **L. Skatkov** (Israel), **Yu. Solonin** (Ukraine), **I. Stasjuk** (Ukraine), **M. Striha** (Ukraine), **S. Svechnikov** (Ukraine), **S. Sydorenko** (Ukraine), **T. Tchelidze** (Georgia), **P. Tomchuk** (Ukraine), **I. Tiginyanu** (Moldova), **V. Uvarov** (Ukraine), **O. Vlasenko** (Ukraine), **S. Volkov** (Ukraine), **V. Wojcik** (Poland), **V. Zlomanov** (Russia), **P. Zukowski** (Poland)

National

**V. Boychuk** (Drogobych), **V. Boychuk** (Ivano-Frankivsk), **Ya. Budzhak** (Lviv), **G. Chuyko** (Kherson), **M. Dmytruk** (Kyiv), **A. Druzhynin** (Lviv), **R. Dzumedzey** (Ivano-Frankivsk), **B. Dzundza** (Ivano-Frankivsk), **I. Gasyuk** (Ivano-Frankivsk), **I. Horichok** (Ivano-Frankivsk)**, H. Hurgula** (Ivano-Frankivsk)**, P. Ignatenko** (Donetsk), **V. Kidalov** (Berdyansk), **V. Klanichka** (Ivano-Frankivsk), **D. Korbutyak** (Kyiv), **O. Kovalenko** (Dnipropetrovsk), **Yu. Kunitskiy** (Kyiv), **G. Lashkaryov** (Kyiv), **I. Lepikh** (Odesa), **I. Lishchynskyy** (Ivano-Frankivsk), **M. Lopyanko** (Ivano-Frankivsk), **L. Matveeva** (Kyiv), **Yu. Melnychuk** (Nizhyn), **O. Mykolaychuk** (Lviv), **I. Myronyuk** (Ukraine), **L. Nykyruy** (Ivano-Frankivsk), **V. Pohmursjkyy** (Lviv), **V. Prokopiv** (Ivano-Frankivsk), **I. Protsenko** (Sumy), **I. Prokopenko** (Kyiv), **O. Ptashchenko** (Odesa), **O. Rogachova** (Kharkiv), **V. Rubish** (Uzhgorod), **M. Ruvinskyy** (Ivano-Frankivsk), **P. Smertenko** (Kyiv), **Z. Stasyuk** (Lviv), **O. Stronsjkyy** (Kyiv), **I. Studenyak** (Uzhgorod), **M. Tkach** (Chernivtsi), **V. Tomashyk** (Kyiv), **R. Zapykhlyak** (Ivano-Frankivsk), **I. Zaulychnyy** (Kyiv), **V. Zinchenko** (Odesa), **Z. Zyman** (Kharkiv)

### Secretariate

**L. Mezhylovska** – Scientific Secretary;
**V. Boryk,I. Bylina, I. Ivanyshyn, J. Javorskij, O. Kostyk, O. Matkivskiy, T. Parashchuk, V. Potyak, O. Sokolov, B. Volochanska**

## Вельмишановні пані та панове! Колеги! Друзі! Учасники XV МКФТТПН – 2015!

У черговий раз раді зустрічі з Вами!

Коли свої результати мають змогу представити понад 250 науковців, серед яких майже 100 докторів наук, у тому числі академіки та членкори НАН України, зарубіжних академій наук, то такий солідний представницький форум додає певної ваги і нашому Прикарпаттю!

Конференція при цьому виступає вагомим об'єднувальним фактором для вчених різних наукових шкіл України та закордону, які займаються проблемами фізики і технології тонких плівок, нанотехнологіями, наноматеріалами і квантово-розмірними структурами та проблематикою їх прикладних аспектів.

Переконаний, що наша конференція буде належним внеском наукової спільноти у розв'язанні відзначних проблем.

**З великою повагою,**
**голова Оргкомітету**
**МКФТТПН-XV**

**Дмитро Фреїк**

*м.Івано-Франківська, Україна*
*11 травня 2015 р.*

## Ladies and Gentlemen! Dear Colleagues and Participants of ICPTTFN-XV – 2015!

Precarpathian region and precarpathians once again are pleased to meet you! The new time is flying relentlessly; new realities and new challenges are facing to science and to scientists. Besides the deep theoretical ideas, specific practical recommendations are necessary and even better developments that would embody the latest achievements in life, technology, determining the further progress of civilization.

I am convinced that our conference will properly contribute scientific community in solving of significant problems.

**With great respect,**

**Chairman of the Organizing Committee**
**ICPTTFN-XV**

**Dmytro Freik**

*Ivano-Frankivsk, Ukraine*
*May 11, 2015.*

**ПЛЕНАРНІ ДОПОВІДІ**
12-15 травня 2015 р.

**PLENARY REPORT**
May, 12-15, 2015

# Hybrid Nanostructures with Magnetic, Luminescent and Conductive Functions for Biomedical Application

Aksimentyeva O.I.[1,2], Horbenko Yu.Yu.[1], Soronovych I.I.[2], Dyakonov V.P.[3]

[1]*Ivan Franko National University of Lviv, Lviv, Ukraine,*
[2]*Lviv Medical Institute, Lviv, Ukraine*
[3]*Institute of Physics, Polish Academy of Science, Warsaw, Poland*

The polymer-magnetic materials attract a great attention due to their practical application in novel technologies and investigations. Of particular interest is the use of functionalized polymer capsules as drug carriers, microreactors and sensors. Multifunctionality of hybrid nanocomposites may be realized by providing various functions – magnetic, conductive or fluorescent, etc.

In the present work firstly we obtained the hybrid composites with all three functions – magnetic, luminescent and conductive, by modification of the polystyrene-magnetite nanocapsules by luminescent $BaZrO_3$ nanocrystals and by conducting shell of the polyaniline [1]. Obtaining hybrid composites were characterized by SEM, FTIR, XRD, EDAX analysis and cathodoluminescence (CL). It was found that adsorption of $BaZrO_3$ nanocrystals on polystyrene (PS) shell of nanoparticles leads to modification of CL spectra of $BaZrO_3$ with appearance of new bands at $E$ = 1.9, 2.15, 2.45, 3.0 and 3.96 eV; a conducting polymer did not affects the shape of CL spectrum. By XRD analysis it is found that modification of luminescence spectra in composites is caused by changing in substructure of nanocrystals under influence of PS matrix: decreasing of lattice parameter for nano-$BaZrO_3$ in composite; chemical interaction between PS and $BaZrO_3$ confirmed by FTIR spectra [2]. So, the described modifications of CL spectra can be connected with structural changes of $BaZrO_3$ nanograins under influence of the PS matrix.

Labelling of capsules by luminescent substances provides a possibility to trace their pathways within a tissue, whereas loading them with magnetic nanoparticles allows manipulation by an external magnetic field gradient. Conductive polymer shell provides a possibility to control the behavior of nanoparticles by an electric field, and track their movements in biological environments. Proposed method of surface modification may be used for developing biosensors and diagnostic methods in medicine.

1. Aksimentyeva O. , Savchyn V. , Dyakonov V. , Demchenko P. , Horbenko Yu. Modification of polymer-magnetic nanoparticles by luminescent and conducting substances // Molec.Cryst.Liq.Cryst. – 2014. – Vol. 590. – P. 35–42.
2. Aksimentyeva O. , Savchyn V. , Opaynych I. , Demchenko P. , Horbenko Yu. Effect of polymer matrix on the structure and luminescence properties of barium zirconate nanocrystals // Chem.Met&Alloys. – 2013. – Vol. 6. – P. 177–182.

# Nanostructural and Film Materials for Thermoelectricity

Anatychuk L.I., Gorsky P.V., Vikhor L.N.

*Institute of Thermoelectricity, Chernivtsi, Ukraine*

The possibilities for the increase in energy conversion efficiency within the latest decade are related to the use of nanostructural materials, such as nanowires, nanofilms and nanocomposites. The improvement of the figure of merit in the said structures is stipulated by two main reasons. The first one is the drastic decrease in thermal conductivity $\kappa$ due to the increase in phonon scattering at the boundaries of structures in nanofilms and nanowires, or at the grain boundaries in bulk nanocomposites. The second reason is the possibility of improving electronic properties, like Seebeck coefficient $\alpha$ and electroconductivity $\sigma$ by virtue of the increase in charge carriers' density of states at transition from monocrystals to 2D-superlattices with quantum wells, 1D quantum wires and nanocomposites with 0D quantum dots.

In the last few years certain successes in the development of technologies and creating of thermoelectric nanostructures have been reached. Fig.1 shows the results of the research on the figure of merit *ZT* of such materials obtained in various scientific laboratories.

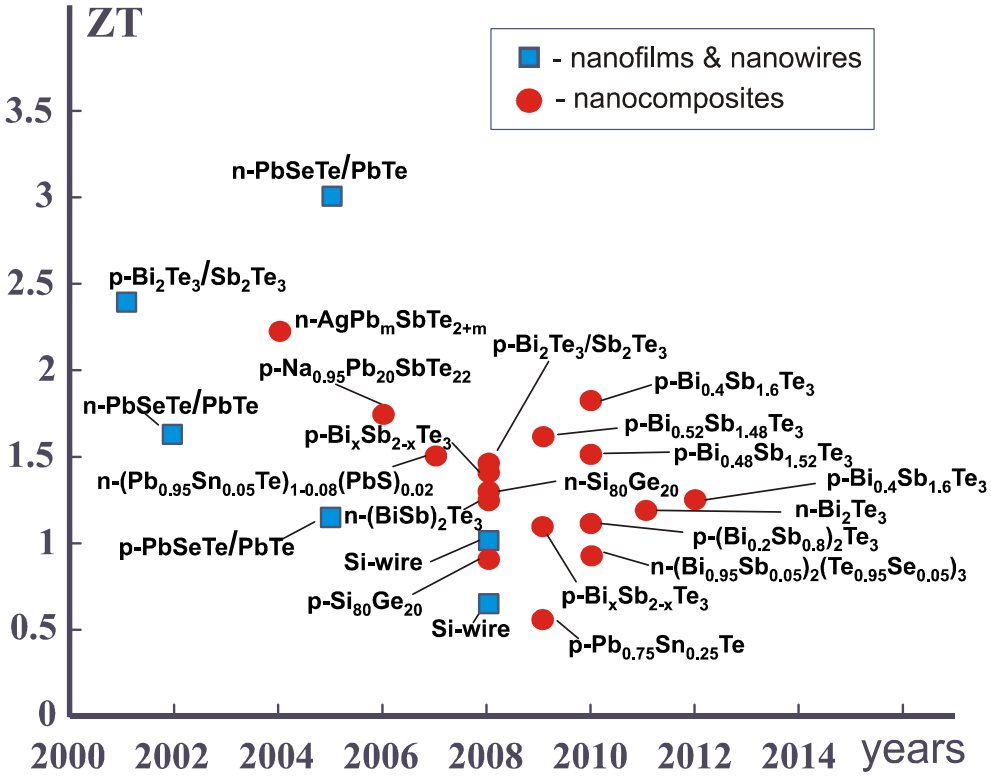


Fig. 1. Figure of merit of the experimental nanostructural samples.

The most meaningful results were obtained for the superlattice-based films and for the structures with quantum wells and quantum dots. The value of *ZT* ~

2 – 3 was obtained for them whereas the value of $ZT$ for monocrystals was equal to ~ 1.0. But these results have found no confirmation in any laboratory of the world as yet. Moreover, to fabricate nanofilms by depositing atomic layers, complicated and costly technologies are required. A more fruitful idea, therefore, was the development of nanocomposites in the form of bulk materials out of nanograins. They are fabricated by techniques that are cheap for mass production, such as, for instance, nanopowders pressing. The improved values of $ZT$ ~ 1.5 (Fig.1) were obtained for the majority of the developed nanocomposites, though not as high as expected.

It is obvious that characteristic dimensions of nanostructure have an influence on the $ZT$ value. For Bi-Te based materials the impact of nanolayers thicknesses in the films and sizes of particles in nanopowders on the figure of merit $Z$ was estimated. Only classic effects of charge carrier and phonon scattering at the boundaries of nanostructures that arise due to the comparability of the characteristic dimension of a structure with the lengths of phonons and charge carriers free paths were considered. The dependence of the phonons relaxation time on the frequency was also taken into account. The results of the research are given in Figs. 2 and 3.

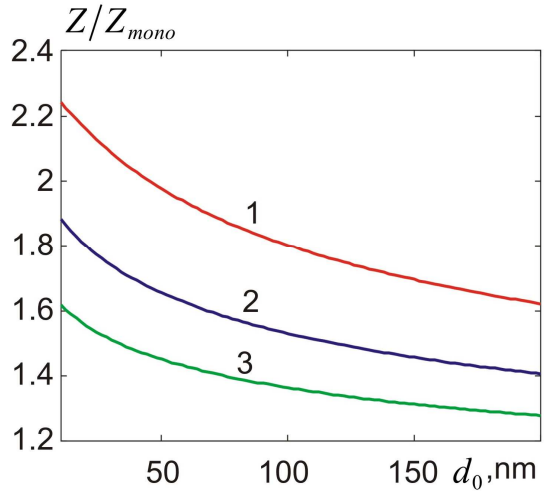


Fig.2. Dependences of ratio of the nanolayer figure of merit $Z$ to the monocrystal value $Z_{mono}$ on the layer thickness. 1 – $T$=200K, 2 – $T$=300K, 3 – $T$=400K.

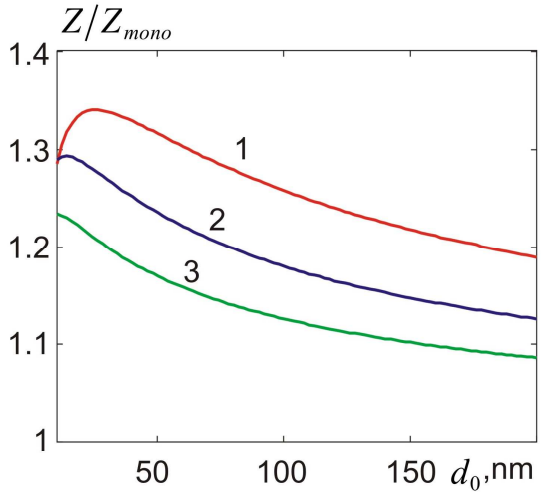


Fig.3. Dependences of ratio of the nanopowder figure of merit $Z$ to the monocrystal value $Z_{mono}$ on the nanoparticle radius. 1 – $T$=200K, 2 – $T$=300K, 3 – $T$=400K.

Downsizing the characteristic dimension of a nanostructure ensures the increase in $Z$ related to the value of $Z_{mono}$ in a monocrystalline material. A more significant increase in the figure of merit as compared to that in nanocomposites is obtained at films, which was clearly seen in experiments.

# Nanomaterials in Extreme Conditions: New Approaches and Non-Resolved Problems

Andrievski R.A.

*Institute of Problems of Chemical Physics, Russian Academy of Sciences, Chernogolovka, Moscow Region, 142432, Russia*

Practically all nanomaterials are very nonequilibrium. The specific features of nanomaterials, such as the numerous interfaces, segregations and residual stresses availability, define their high level of physical/mechanical properties. However, it is evident that some thermal, radiation, deformation, and corrosion actions can initiate the recrystallization, relaxation and homogenization that lead to the nanostructure annihilation and irreversible decrease of physical/mechanical properties. In this connection, the nanomaterials stability problem takes a great attention.

This report analyses the modern experimental and theoretical data on nanomaterials behavior at high temperatures, irradiation, deformation actions, and corrosion environments. The nanotwinned structures high stability in extreme conditions is marked. Non-resolved problems are underlined.

1. R.A. Andrievski. Review of thermal stability of nanomaterials. Journal of Materials
2. Science **49**, No 4, 1449-1460 (2014).
3. R.A. Andrievski. Nanostructures under extremes, Physics – Uspekhi **57**, No 10, 947-962 (2014).

# Bulk and surface micro- and nanostructures in chalcogenide glassy semiconductors induced by femtosecond laser pulses

Blonskyi I.V., Kadan V.M., Shpotyuk O.I., Korenyuk P.I.. Yarusevych O.I, Shynkarenko E.V.

*Institute of Physics NAS of Ukraine, Kyiv, Ukraine*
*[1]Scientific Research Company 'Carat', Lviv, Ukraine*

It is shown that femtosecond laser radiation induces the process of Kerr filamentation in chalcogenide semiconductor glass (ChSG) of $As_4Ge_{30}S_{66}$ composition, which is featured by the presence of structural mesh elements of nanometer scale. Formation of high-intensity filament core which hosts a variety of different nonlinear processes, including two-photon absorption, is closely related to this phenomenon. As a result, free charge carriers, photoinduced transformations and local change of refractive index occur in the plasma channel of the filament. Basing on this phenomenon, we proposed and tested a method filament-induced self-writing of micro-waveguides in bulk ChSG. Refractive index profile of the waveguide is calculated based on defocused microscopic images of the excitated area, using one-dimensional Transport of Intensity Equation and inverse Abel transform. We found that a zone of increased refractive index (up to $0.5 \times 10^{-3}$), appears along the waveguide axis, which is surrounded by a zone of negative refractive index changes of ~ 7 mm diameter.

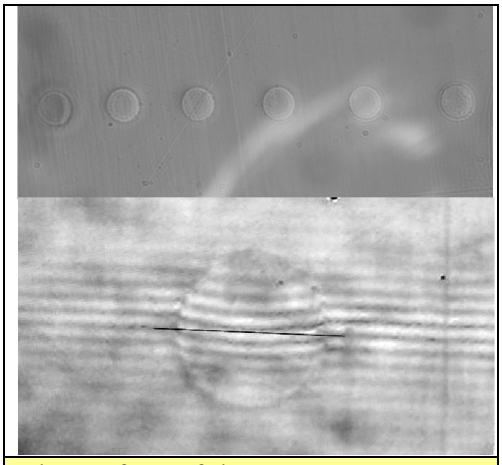

The surface of the 65GeS2-25Ga2S3-10CsCl ChSG the exposure by a number of single fs laser pulses, illustrating the produced microlenses, and micro-interferense pattern of a single microlens of 23 μm diameter.

We tested the possibility of production of microlenses using a single pulse of femtosecond laser radiation and proposed a method of microlens production, which can serve as a basis for the technology of rapid production of regular arrays of microlenses for telecom applications. The advantage of this method is its high performance that is limited only by the repetition rate of the laser pulses (1000 microlenses per second).

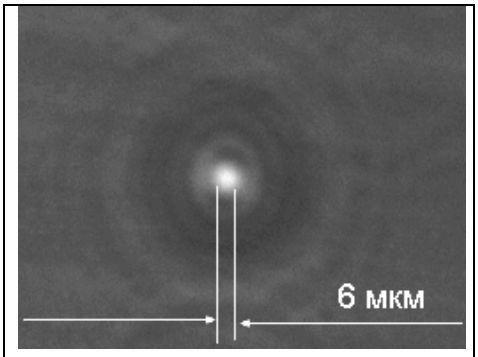


Imaginary focus of the microlens. The object plane is in the sample at a depth of 150 microns from the surface.

# Electrical and Optical Properties of 1d-, 2d- and 3d-Dimensional Spherical Semiconductor Quantum Dots Superlattices

Boichuk V.I., Bilynskyi I.V., Pazyuk R.I.

*Ivan Franko Drohobych State Pedagogical University, Drohobych, Ukraine*

Last decades physical properties of individual semiconductor quantum dots have been extensively studied both theoretically and experimentally. The effects of the size, shape, strain fields, and dielectric screening on electronic states and optical response of separated quantum dots (QD) are addressed in the literature in great detail. In a simplified picture, transport properties of arrays of weakly coupled quantum dots (its wave functions is well localized in a individual QD) are described in terms of hopping conduction, while optical response is defined by the energy spectrum of individual dots and inhomogeneous broadening due to the size distribution.

A more interesting and potentially practically important case is when strong coupling among dots leads to formation of 1D-, 2D- or 3D-dimensional extended minibands instead of localized quantum dot states. Regimented or partially regimented multiplearrays of quantum dots, also termed quantum dot superlattices, have already been fabricated by a variety of techniques. In these artificial crystals the role of atoms isplayed by quantum dots. Thus, we refer to these structures as quantum dot crystals or “supra crystals”. As a consequence, the energy spectrum of such supra crystals is characterized by emergence of minibands separated by complete stop bands. This situation observed at quantum dot superlattice.

Special optical and electric properties of this superlattices have already found their practical applications. For example, electrical conductivity perpendicular to the superlattice layers exhibits behaviour very similar to what is found in tunnel diode. Construction and properties of analogous device, based on quantum well structure fabricated from GaAs sandwiched between two $Ga_{1-x}Al_xAs$ barriers. The device could handle frequencies up to 2.5 THz, giving possibility to work at millimetre and submillimetre wavelengths.

In this paper we investigate the electron energy spectra in 1D-, 2D- and 3D-dimensional regimented GaAs/AlAs quantum dot superlattice by solving the Schrodinger equation in the envelope wave-function and strong coupling approximation. Electron densities of states, required for modeling of an electron transport and optical properties of quantum dot superlattices, were calculated. In addition, we obtained dependence of the electrical conductivity and Fermi energy on the temperature. Based on the results, it was found that the higher the temperature the more mini-bands are involved into the conduction process.

# Plasmonic Spectra and Cubic Optical Nonlinearity of Nanostructured Gold Films

Brodyn M., Liakhovetskyi V.

*Institute of Physics NAS of Ukraine, Kiev, Ukraine*

The aim of the report is to summarize spectral and nonlinear optical properties of the nanostructured Au films with random and regular positioning of the nanoparticles. Properties of the plasmon spectra and characteristics of the third-order nonlinearity are considered.

Plasmonic spectra of the structures under study were measured depending on their topography features. The third order optical susceptibility $\chi^{(3)}$ of the samples is measured in resonant and nonresonant conditions respectively to the plasmonic band. Maximum value of the $\chi^{(3)}$ was measured to be $8 \cdot 10^{-5}$ esu.

The nonlinear optical response dynamics was measured under femtosecond laser excitation at $\lambda$=400nm and 800 nm. It was shown that the nonlinear optical response is induced during less than 200 fs and is due to free electron generation and the following electron-electron scattering resulting in electron gas heating. The relaxation of the nonlinearity goes with two different times "fast" $\tau_1 \sim 2 \div 5$ ps and "slow" $\tau_2 \sim 200$ ps. It was shown that the "fast" relaxation corresponds to the time of hot electros thermalisation, meanwhile the "slow" one corresponds to Au nanoparticle lattice cooling down.

# Spin-Valve Film Structures with Nanoparticles Layers

Cheshko I.V., Protsenko S.I., Shumakova N.I.

*Sumy State University, Sumy, Ukraine*

Ordered arrays of nanoparticles (NP) can be used for creating film device structures of the spin-valve type with higher performance and stability. Moreover, in the classical scheme of forming a sequence of layers of spin-valve structures for magnetic/nonmagnetic/pinned magnetic layer, the magnetic array NP can be used to create tough magnetic lower working layer with high values of coercive power ($H_c$), and soft magnetic sparkling the upper working layer with low values $H_c$. Therefore, attention in the study of magneto-optical and magnetoresistive properties of arrays NP primarily aimed at establishing the dependence of $H_c$ on the size of the particles, since the maximum value of $H_c$ determines the physical limit their practical use. Experimental dates [1] which is confirmed in the framework of the cluster approach to the theoretical study of magnetization processes [2] showing that NP can have a larger atoms magnetic moment than the atoms of bulk material even at room temperature. In addition, according to [3], the magnetic moment of the NP at $T \rightarrow 0$ K more than the bulk metal, and at $T > 0$ K magnetization NPs shows a strong dependence on temperature.

In [4] ordered arrays of $Fe_3O_4$ NP on the $SiO_2$ substrate and embedded in a conductive matrix Cu or Au are considered as fragments of a film of spin-valve structures. It was shown that the ordered structure of one or more layers of NPs is lower $H_c$ than those that include arrays of NPs in a conductive matrix. And when termovar in vacuum this system up to T = 900 K, the value of $H_c$ is increased from 60 to 480 mT (for comparison: the authors [5] have reported the achievement of high values of $H_c$ = 100 mT for the Fe NP with a diameter of 25 nm). By the authors of [4] the growth of the $H_c$ explain the increase in the size of bass from 10 to 20 nm. It is also noted the formation under the influence of high temperature islet structure of the Au film with the inclusion of NP, which confirms the view that the size effects in the magnetic properties of NP to a large extent are determined by the properties of the environment in which they are placed. Uniaxial anisotropic character of $H_c$ $Fe_3O_4$ NP in the matrix Cu or Au noticeable at all stages of the heat treatment of the samples.

For some cases the sensory instrumentation the upper working magnetic layer of the spin-valve must have a minimum residual magnetization at high values of $H_c$. In this case, you can use arrays of magnetic NPs in a single domain state, which is achieved by reducing the volume of the NPs to a certain critical value. For $Fe_3O_4$ NP as 3d-metals the transition to a single-domain state at room temperature is observed when the size of 15 - 20 nm. Reducing the size of NP up to 5 - 8 nm and violations of the homogeneity of their crystal structure leads to a significant reduction of the effective magnetic moment and the disappearance of

the ferromagnetic properties of the entire array NP. However, it should be noted that, according to [2] in some cases, even with an average size smaller than 5 nm NPs can have high values of $H_c$. So the magnetic moment of Co atoms in the 20 atoms cluster bigger than the magnetic moment of atoms in the bulk layer. This can be explained by the high structural stability of such nanoclusters with a minimum number of defects on the surface.

Magnetic layers spin-valve structures based on nanoparticles of different degree of dispersion can be formed in the process of getting film samples with sequential layer-by-layer condensation of magnetic and non-magnetic component with subsequent annealing in vacuum. For example, in [6] studied the magnetic properties of Co NP arrays at different stages of the formation of granular alloys based on Cu and Co. It is shown that the concentration and size of the formed nanoparticles depend on the thickness of the Co layers in Co film system. Formed thereby Co NP in a range of sizes 10 - 40 nm had little coercive, indicating that the super paramagnetic state obtained NP. By increasing the size of 30 - 120 nm in film samples based on Co NP observed isotropy process magnetization values of $H_c$ = 30 mT.

This work was done in state project №52.20.01-01.15/17 ЗФ of the Applied Physic Department of Sumy State University.

1. Magnetic Nanoparticles: Surface Effects and Properties Related to Biomedicine Applications / B. Issa, I. Obaitad, B. Albis et al. // *Int. J. Mol. Sci*. – 2013. – № 14. – P. 21266-21305.
2. G. M. Paster. Teory of Clastur Magnetism. – 2012. – Berlin: Springer. – 400 p.
3. NMR and Spin Relaxation in Systems with Magnetic Nanoparticles: Effects of Size and Molecular Motion / N. Noginova, T. Weaver, A. Andreyev et al. // *J. Phys. Condens. Matter*. – 2009. - № 21. – P. 255301-255321.
4. Formation of the Granular (Cu,Co) Alloys with Uniform Distribution of Magnetic Granules Using Co Nanoparticle Arrays / V.A.Zlenko, M.G.Demydenko, S.I.Protsenko et al. // *J.Nano- Electron. Phys*. – 2012. – V.4, № 4. – P. 04023-1–04023-6.
5. Nanocrystalline Iron Particles Synthesized without Chilling by Chemical Vapor Condensation / D.W. Lee, T.S. Jang, , D. Kim et al. // *Glass Phys. Chem*. – 2005. – V. 31, № 4. – P. 545–548.
6. Magnetoresistive and Magneto-optical Properties of Fragment Spin-Valve Structures Based on the Ordered Arraysof Fe3O4Nanoparticles / M.G.Demydenko, D.M. Kostyuk, S.I.Protsenko et al. // *J.Nano- Electron. Phys*. – 2014. – V. 6, № 4. – P. 04046-1–04046-4.

# Surface-Enhanced Photophysical Phenomena in Surface Metal-Amorphous Semiconductor Composite

Dmitruk N.[1], RomanyukV.[1], Kondratenko O.[1], M. Taborska[1], S. Charnovych[2], S. Kokenyesi[2]

[1] *Institute for Physics of Semiconductors NAS of Ukraine, Kyiv, Ukraine*
[2] *University of Debrecen, Debrecen, Hungary*

It is known that the enhancement of the electric field in the vicinity of a metallic nanoparticle resulting from the excitation of eigen oscillations in the electron gas (surface plasmons) leads to the enhancement of many photophysical phenomena. Composites belong to a class of functional materials where variations of the effective dielectric function of heterosystem and the optical properties of the material are possible in the wide range [1]. Surface composites are created typically based on plasmon-carrying materials (metals, conducting oxides) with the structures with reduced dimensionality (nanoparticles, nanowires and thin films) deposited on the surface of the semiconductor or insulator. The main idea of surface composites is a realization of significant electromagnetic interaction in the near-field and in the far-field regions. Such interaction leads to various surface-enhanced photophysical phenomena, such as surface-enhanced infrared absorption (SEIRA), Raman scattering (SERS), tip-enhanced Raman scattering (TERS), photo- or electroluminescence (SEEL), generation of electron-hole pairs and, accordingly, photoelectric current of barrier structures etc.

We have fabricated single and multicomponent layered structures, which consist of granular (gold) nanoparticle film and chalcogenide ($As_2S_3$) layers on glass substrates. Morphology and structure of composites were investigated with AFM, TEM and SEM techniques. Optical properties were investigated with reflectance/transmittance spectroscopy of polarized light at several angles of incidence in the 400–1100 nm spectral range.

Spectroscopic investigations with transparent substrates allow us to obtain total absorption spectra $A(\lambda)=1-R(\lambda)-T(\lambda)$ of layered structures. In figure it is shown that beyond the fundamental absorption edge of the chalcogenide ($\lambda_g \approx 450$ nm) the absorption in the $Au/As_2S_3$ structure becomes much more complicated in comparison to the case of pure chalcogenide film on a glass. Apparently, the surface enhanced absorption of light in the region of transparency of the semiconductor is caused by the interaction of surface plasmons (near field) and interference modes in a Fabry-Perot like cavity (virtual modes) [2]. Since light passes many times across the near-field region of metal nanoparticles, the absorption coefficient attains a level comparable to that in the case of fundamental band to band absorption.

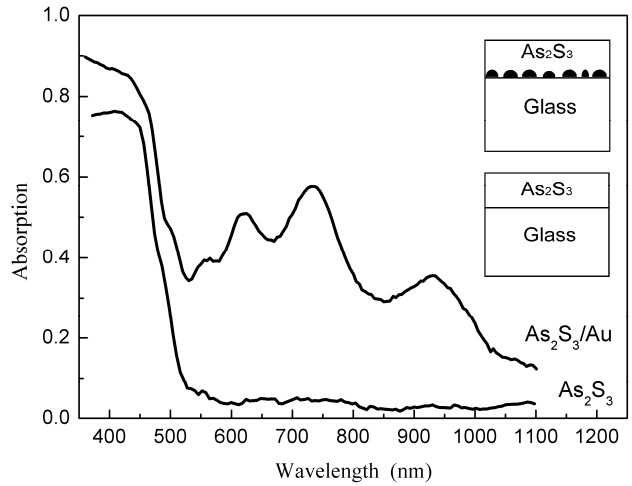


Chalcogenide glasses display the highest photoinduced effects among other materials and their photosensitivity does not involve chemical reactions. Photo-induced transformation processes, as some laser-stimulated changes of optical parameters in amorphous chalcogenide films ($As_2S_3$, $As_2Se_3$ etc.), are used for optical memory and recording, fabrication of photonics elements, direct laser writing of buried optical waveguides etc. Because of excitation of localized (surface) plasmons in metal nanoparticles accompanied by near-field enhancement is used for enhancement of various photophysical phenomena, it can be assumed that photo-induced transformation processes in chalcogenides also can be influenced by this way [3].

Thus, we have observed another surface enhanced photophysical phenomenon similar to such long familiar effects as the enhancement of the infrared absorption or Raman scattering by adsorbed molecules in the presence of a rough metallic surface or colloidal metal particles. This effect could be used for development of new active elements for opto- and nanoelectronic devices (sensors, photodetectors, solar cells etc.), where the excitation of surface plasmons or surface plasmon-polaritons is used. Also, results obtained enable further selection of optimized structures for optical recording.

1. N. L. Dmitruk, A. V. Goncharenko, E. F. Venger. Optics of Small Particles and Composite Media. Naukova Dumka. Kyiv. 2009. 386 p.
2. N. L. Dmitruk, V. R. Romanyuk, M. I. Taborskaya, S. Charnovych, S. Kokenyesi, N. V. Yurkovich. Interaction of Surface Plasmons with Interference Modes in Thin Film Nanostructures. *Pis'ma v Zhurnal Eksperimental'noi i Teoreticheskoi Fiziki.* – 2014, – V. 99, No.3. – P.146.
3. S. Charnovych, N. Dmitruk, I. Voynarovych, N. Yurkovich, S. Kokenyesi. Plasmon-Assisted Transformations in Metal-Amorphous Chalcogenide Light-Sensitive Nanostructures. *Plasmonics.* – 2012. – V.7, No.341. – P.345.

# Mechanical Properties of Composite Electrolytic Nickel Coatings Obtained by Pulsed Current

Dudkina V.V., Zabludovsky V.A., Shtapenko E.Ph.

*Dnepropetrovsk National University of Railway Transport named after academician V. Lazaryan, Dnepropetrovsk, Ukraine*

The electrolytic coatings based on nickel are widely used to protect metal surfaces from corrosion, mechanical damage, improve the strength characteristics and sliding strength of the products. In addressing the issue of improving the functional properties of electrolytic coatings the promising direction is to obtain nanocomposite materials with the use of ultrafine particles (UFP).

The deposition of composite coatings was carried out from aquosystem nickel plating with the adding up UFP particles of concentration 2 g/l by current rectangular impulse with the frequency of 50 Hz, the pulse relative duration from 2 to 50 and the average current density is 100 $A/m^2$. The microhardness of the coatings was measured on the microhardness tester PMT-3 at load indenter of 0.196 N.

The sample life service tests were conducted on friction machine with reciprocating samples in conditions of unlubricated friction. The electron microprobe analysis was made by using the electron-scan microscope JSM-64901LV (Japan).

The conducted researches showed that the structure and mechanical properties of the composite electrolytic nickel coating depend on the mode of electrodeposition, the contents and distribution of the co-deposition nanodiamond particles in matrix metal.

According to the spectral analysis results of composite coatings samples at increasing of current pulse relative duration from 2 to 50 and their invariable frequency is observed the increasing of particle content UFP in a covering from $17 \div 33$ to $35 \div 43$ of weight % and their more equal distribution in a covering that led to the formation of finely crystalline, more closely-packed coverings and defined the rising mechanical characteristics of the composite coatings. So the nickel coverings, deposited by means of direct current with density 100 $A/m^2$, in 5 hours of wearing process lose 10 % of the weight. At the pulse mode deposition with the frequency of 50 Hz and pulse relative duration equal 2, the coverings microhardness increases by 35-40 %, and wearing process makes 7 %. At increasing the current pulse relative duration from 2 to $50^{th}$ the microhardness increases by 20-25 %, and wearing process decreases to 3 %.

Thus, the increasing of co-deposition particles UFP contents in the nickel covering received by means of pulse current allows forming composite electrolytic nickel coatings with increased microhardness and wearing resistance.

# Teaching Material Science Subjects Using SES Program from Granta Design, UK

Duryagina Z., Tepla T., Pleshakov E., Bohun L., Semenuk O.

*National University "Lviv Polytechnic", Lviv, Ukraine*

The integration of Ukraine into the European educational and scientific space requires structural reform of the national education system, creating a single educational criteria and standards across the whole continent. The project TEMPUS MMATENG “MODERNIZATION OF TWO CYCLES (MA, BA) OF COMPETENCE-BASED CURRICULA IN MATERIAL ENGINEERING ACCORDING TO THE BEST EXPERIENCE OF BOLOGNA PROCESS”, which aims to facilitate the modernization of higher education in the partner countries, the Department of Materials Science and Applied Materials Processing Lviv Polytechnic received SES software on top of Granta Design, UK.

SES software was created jointly by leading programmers and material experts from Cambridge University (UK). It is based on an extensive database of engineering materials (steels and non-ferrous alloys, plastics, composites, biomaterials, etc.). With this program, the introduction of initial properties (mechanical, physical, economic, etc.) of products, you can define the desired group of materials, including by introducing a new additional options you want, isolate material that will fully meet the requirements. With this program the selected material can be completely described: serves its chemical composition, physical and mechanical properties and possible ways of making technological processing, economic and environmental feasibility of its use.

This program is used in almost every application in materials sciences in the department of Applied Materials and Materials Processing, National University "Lviv Polytechnic", for example "Material science", "Heat treatment" "Nonferrous metals", "Nonmetallic Materials", "Alloys with specific properties", "Powder and composite materials" and many others. Using this software, students can easily learn to choose materials for a particular product, assign technological modes of production and surface treatment, to provide the necessary material properties. This program, or equivalent, is widely used in European universities, so its introduction in Ukraine will allow our students need for easy integration into the educational process within the EU programs for exchange students.

# Polycrystalline bismuth films: fabrication, structure and electrophysical properties

[1]Fedotov A.S., [2]Poznyak S.K., [2]Tsybulskaya L.S., [1]Svito I.A., [1]Shepelevich V.G., [1]Mazanik A.V., [1]Fedotov A.K., [2]Gaevskaya T.V.

*[1]Belarusian State University, Minsk, Belarus*
*[2]Research Institute for Physical Chemical Problems, Belarusian State University, Minsk, Belarus*

Thin bismuth films provide a wide range of practical applications. Owing to a high magnetoresistive effect bismuth layers can be used as components of magnetic field sensors [1]. Many of today's conventional thermoelectric materials are bismuth-based compounds, for example $Bi_2Te_3$ [2].

The present work is focused on establishing correlation between electrophysical properties of polycrystalline bismuth films prepared by different methods and their microstructure. The films were fabricated by melt spinning and electrochemical deposition techniques.

Electrochemical bismuth deposition was performed from aqueous electrolyte containing 0.174 mol/l $Bi(ClO_4)_3$ and 3 mol/l $HClO_4$ onto plates made of a one-sided flexible foil-coated laminate. 70 μm thick Bi films were electrodeposited at room temperature and electrolyte stirring under galvanostatic regime with a current density of 2.5 A/dm$^2$. In the melt spinning technique, bismuth (99.9999 %) was melted and then spilled on the cold surface of rotating cylinder made of a polished copper.

Grain structure analysis (electron backscatter diffraction technique) showed that relatively fine-crystalline films (grain size $l_G$ is 0.5–1.5 μm) are formed by electrochemical deposition. Annealing of these films at 540 K for 5–6 h leads to a significant growth of the grain size (up to 10–50 μm). Melt spinning technique gives the coarse-grained Bi films ($l_G \sim$ 5–15 μm) at once.

Electrophysical characteristics such as resistivity, magnetoresistance, Seebeck coefficient and Hall coefficient of the prepared bismuth films were measured in 4–300 K temperature range under magnetic fields up to 8 T (Fig. 1). Relative magnetoresistance $\Delta\rho/\rho_o$ at 4 K under magnetic field 8 T reaches 4500 for annealed electrodeposited films, whereas $\Delta\rho/\rho_o$ does not exceed 12 for as-prepared electrodeposited films. Temperature dependence of the resistivity was found to be strongly influenced by Bi grain size. Semiconductor-like behavior is observed for the fine-grained samples and metal-like behavior – for the coarse-grained ones (Fig. 1a).

Mobilities and concentrations of electrons and holes were calculated using parabolic dispersion law for holes and Lax model, which takes into account a non-parabolicity of dispersion law for electrons [3]. Electron and hole concentrations were found to be practically independent of the film fabrication method and are around $10^{24}$ m$^{-3}$, increasing five to seven times as the temperature grows from 25 to 300 K. Mobilities for the electrochemically

deposited samples are close to 1 $m^2/(V \cdot s)$ and depend only slightly on temperature in the studied range. For the other types of Bi films, mobilities are approximately 10 $m^2/(V \cdot s)$ at helium temperatures and decline by an order of magnitude at room temperature.

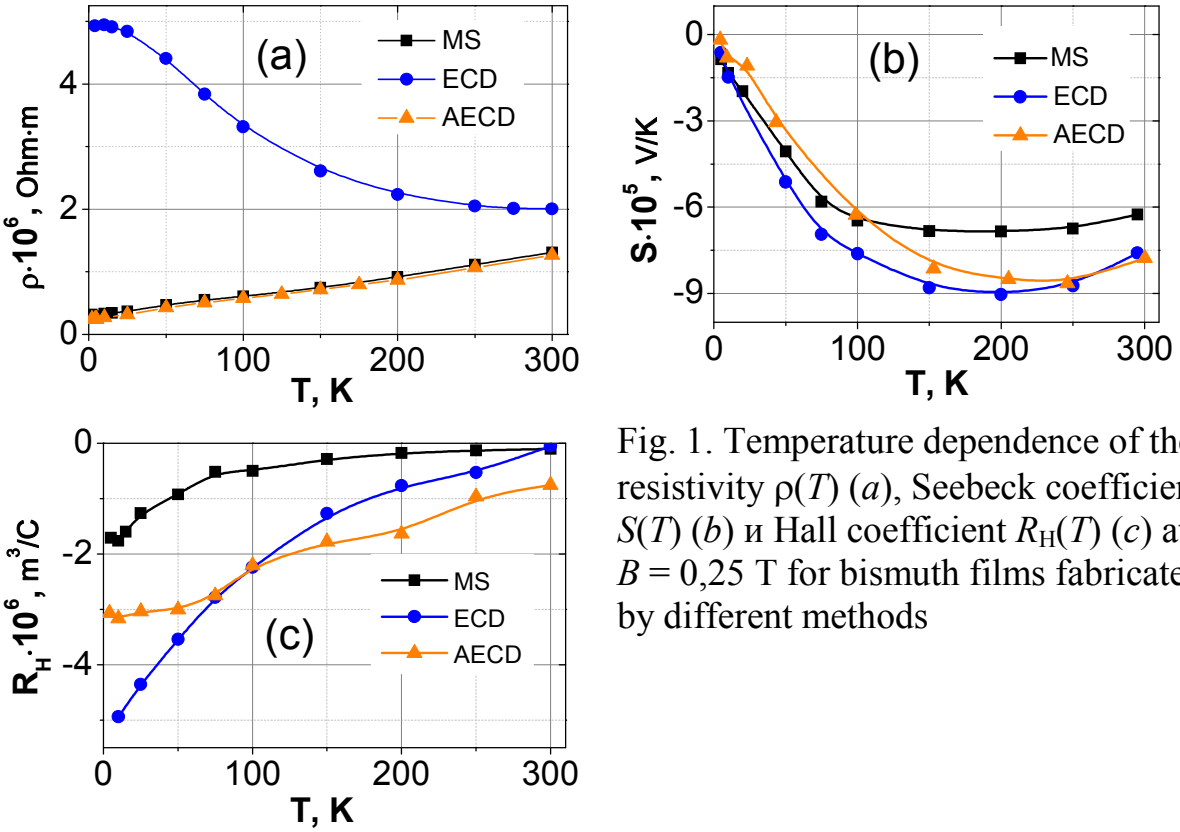


Fig. 1. Temperature dependence of the resistivity ρ(*T*) (*a*), Seebeck coefficient *S*(*T*) (*b*) и Hall coefficient $R_H(T)$ (*c*) at *B* = 0,25 T for bismuth films fabricated by different methods

The observed differences in electronic properties of the Bi films under study can be explained by a profound effect of grain boundaries on charge carriers scattering. For fine-crystalline films (as-prepared electrodeposited films, ECD) the grain-boundary scattering plays a significant role, which results in a weak temperature dependence of mobility and in a decrease of resistivity with increasing the temperature due to a rise of the charge carrier concentration. In the case of coarse-crystalline films (electrodeposited films after annealing, AECD, and films deposited by melt spinning, MS) a contribution of the temperature-dependent scattering by phonons enhances strongly. As a result, the charge carrier mobility decreases, and the resistivity monotonically rises with increasing the temperature.

1. Prinz G. A. Magnetoelectronics // *Science,* 282, (1998), 1660.
2. Xiao F., Hangarter C., Yoo B. [et al.] Recent progress in electrodeposition of thermoelectric thin films and nanostructures // *Electrochim. Acta*., 53, (2008), 8103.
3. Heremans J., Hansen O. P. Influence of non-parabolicity on intravalley electron-phonon scattering; the case of bismuth // *J. Phys. C*., 12, (1979), 3483.

# The Effect of $C_3H_5(OH)_3$ Intercalation on the Electrical Properties of InSe and $In_2Se_3$ Layered Crystals

Feshak T.M., Tsybulenko Y.M.

*Frantsevich Institute of Problems of Materials Science, NAS of Ukraine, Chernivtsi Department, Chernivtsi, Ukraine*

Intercalation [1] as nanotechnological approach to instrumentation in various fields of modern science and technology is difficult to overestimate.

The base materials for the experiments were InSe and $In_2Se_3$ layered crystals, which were grown by the Bridgman method. The samples which were studied had the appearance of rectangular parallelepiped. In the experiments was used a method of exposition intercalation. Samples were placed in a liquid environment $C_3H_5(OH)_3$, which had the same temperature of the material [2]. Therefore, the main parameter intercalation process was the time exposure.

Measurements of electrical parameters of the samples were carried out by Hall Effect. Samples were placed in a $C_3H_5(OH)_3$ cell. The experiment lasted 21 days.

The dependence of the electrical conductivity and majority carrier concentration from exposure time are shown in Fig. As can be seen from the figure, the intercalation $C_3H_5(OH)_3$ of samples leads to increase the electrical conductivity and majority carrier concentration for $In_2Se_3$ to a greater extent than for samples InSe. In addition, for samples InSe<$C_3H_5(OH)_3$> were performed measurements of electrical parameters at nitric temperature.

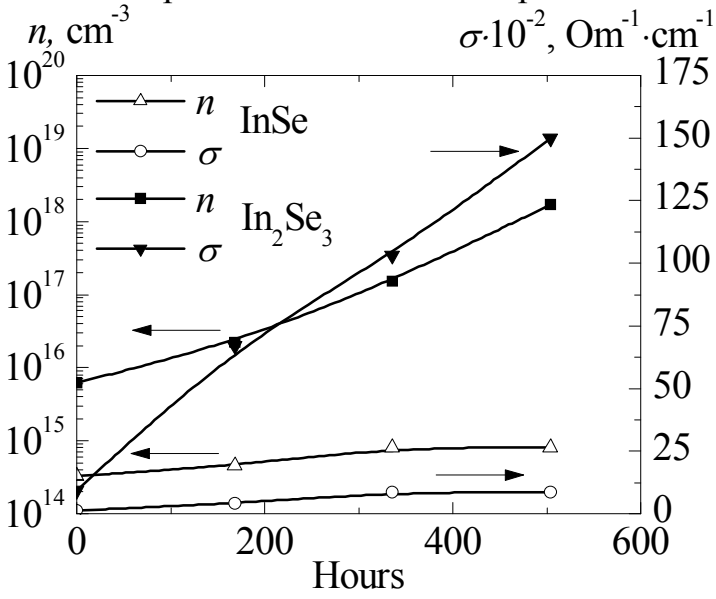


Fig. The dependence of the electrical conductivity and majority carrier concentration from exposure time for samples InSe та $In_2Se_3$.

1. McKinnon W.R., Haering R.R. Physical mechanisms of intercalation//Modern Aspects of Eiectrochemistry. New York. – 1983. – № 15. – P. 235-261.
2. Boledzyuk V.B., Kovalyuk Z.D., Pyrlya M.M., Barbutsa S.G. Optical and Electrical Properties of InSe and GaSe Layered Crystals Intercalated with Ethanol. Ukr. J. Phys. – 2013, – Vol. 58, N 9, – P. 857-862.

# Strain Tensor Measurement in Crystals Using the EBSD Technique

Fodchuk I.M.

*Yuriy Fedkovych Chernivtsi National University, Chernivtsi, Ukraine*

The advantages of Kikuchi method (EBSD technique) such as high locality (~ 40μm) and precision of lattice parameter determination (~$10^{-4}$ Å) have been used to develop the enhanced technique of residual strain tensor construction by means of new approaches.

In traditional procedures of determination of strain tensor components as a rule one of the components is being undetermined. Precise determination of position of zone axes on the Kikuchi pattern is complex and ambiguous task since the fragment of pattern around the area of Kikuchi bands intersection has no intensity maximum; moreover, intensity distribution has no symmetry. To solve this task the complex of methods for digital processing of EBSD patterns have been proposed and allow to determine not only the exact position of zone axis but also to analyze the profiles of intensity distribution across Kikuchi bands [1, 2]. To specify all components of strain tensor unambiguously it has been proposed to determine the diagonal components of strain tensor from the changes of integral intensity of Kikuchi bands.

Approbation of developed technique was carried out on diamonds samples, diamond films, metal sheets (Ni, Al), nanocrystalline metal films, weld joint of NiCrFe nickel alloy with crack. It should be noted that extended precision of strain tensor components can be achieved using the reference crystal.

Characteristic surfaces of strain tensor and strain ellipsoids were constructed for local areas, which demonstrably show the anisotropy in the distribution of residual strains. Particularly in the case of diamond crystal shear components of strain tensor $\varepsilon_{xz}$, $\varepsilon_{yz}$ for local areas, which correspond to different crystalline blocks, have almost equal values that indicate the absence of rotation in reference crystallographic directions. At the same time other components of strain tensor show significant variations.

1. Borcha M.D., Balovsyak S.V., Fodchuk I.M., Khomenko V.Yu., Tkach V.N. Local deformation in diamond crystals defined by the Fourier transformation of Kikuchi patterns // J. Superhard Materials Materials. – 2013. – **35**, № 4. – pp.34-42.
2. Borcha M.D. Balovsyak S.V., Fodchuk I.M., Khomenko V.Yu., Tkach V.N. Distribution of Local Deformations in Diamond Crystals according to the Analysis of Kikuchi Lines Profile Intensities // Journal of Superhard Materials. – 2013. – Vol. **35**, №. 4. – pp. 35–43.

# Strategy and Tactics in Thermoelectric Material Science

Freik D.M, Nykyruy L.I., Mezhylovska L.Y.

*Vasyl Stefanyk Precarpathian national University, Ivano-Frankivsk, Ukraine*

The thermoelectric effects of Seebeck, Peltier, and Thomson considered as core to the building of thermoelectric module which converts thermal energy into electrical energy or cooling systems creation [1]. The efficiency of thermoelectric materials characterized by dimensionless quantity – thermoelectric figure of merit

$$ZT = \frac{S^2 \sigma T}{\chi}.$$

In this expression S is the coefficient of Seebeck, $\sigma$ – specific electrical conductivity, T – temperature, and $\chi$ – coefficient of heat conductivity.

The better the efficiency of thermoelectric material determined of the higher value of ZT.

Glen Slack most clearly formulated the strategy in thermoelectric material: the best materials are agreement to the concept of "phonon glass – electronic crystal." Namely, phonons must be disordered, like glass, and electrons must have high mobility that is inherent in crystalline semiconductors.

As for tactics, they are different and should be attributed to the massive crystals, composites and quantum-dimensional structures.

*Massive crystals*. The substitution atoms of main matrix by impurities causes to reduction of $\chi$ and to growth of S (examples of these materials: Bismuth (Lead) Telluride, Skutterudite, Clathrates, LASTs, OCBs, JALTT).

*Composites*. There is a scattering of phonons (decrease $\chi$) and increase of S by throttling carriers on the grain boundaries.

*Quantum-size structures*: *walls, wires, dots*. These structures are characterized by power throttling carriers in the barriers, "carrier-pocket" engineering, and transition from semimetal to semiconductors.

*This research is sponsored by NATO's Public Diplomacy Division in the framework of "Science for Peace" (NATO SPS 984536)).*

1. J.-F. Li, W.-S. Liu, L.-D. Zhao, M. Zhou. *NPG Asia Mater,* 2 (2010), 152.
2. D.M. Freik, M.O. Galuschak, O.S Krunutcky, O.M. Matkivskiy, *Physics and Chemistry Solid State*, 13 (2014), 300.

# Charge Transport in Amorphous Metal-Oxide In-Ga–Zn–O Semiconductor Films and Their Use for Thin-Film Transistor Applications

Kadashchuk A.,[1,2] Fishchuk I.I.,[1,2] Heremans H.,[1] Genoe J.[1]

[1]*InterUniversity Microelectronic Center (IMEC), Leuven, Belgium*
[2]*Institute of Physics, NAS of Ukraine, Kyiv, Ukraine*
[3]*Institute for Nuclear Research, NAS of Ukraine, Kyiv, Ukraine*

In recent years transparent amorphous oxide semiconductor, In-Ga–Zn–O (a-IGZO) [1], attracted a lot of interest because it has a potential to overtake α-Si:H in applications in backplanes for large-area active matrix displays and holds much promise for emerging transparent flexible electronics due to its high mobility, reasonable bias stability and superior spatial uniformity over a wide area, and the films can be fabricated by a conventional sputtering method. a-IGZO belongs to new class of high-mobility thin-film semiconductors enabling the realization of the next generation of thin film transistor (TFT) technology and eventually opens new frontier for large-area electronics called 'flexible electronics,' which means electronic circuits fabricated on flexible plastic substrates. The high level of activity on these devices is because, even though the material is amorphous, it can offer a carrier mobility of 10-50 $cm^2/Vs$. This is 10–20 times greater than a-Si:H, and the higher mobility is advantageous for driving organic light emitting diode, OLED, displays. Also, due to the amorphous nature of the material, it may have better uniformity than poly-Si, which is the currently preferred TFT technology for commercial, hand-held AMOLED displays.

In this work [2] we describe electrical transport properties in a-IGZO TFTs. We suggest a model based on Effective Medium approximation (EMA) which is able to describe charge-carrier transport in a disordered semiconductor with a significant degree of degeneration realized at high carrier concentrations, especially relevant to a-IGZO TFT, when the Fermi level is very close to the mobility edge (transport band edge). The EMA model is based on a straightforward averaging of the Fermi-Dirac carrier distributions using suitably normalized cumulative density-of-state (DOS) distribution that includes both extended (delocalized) states and the localized states. The key assumption of the model is that the charge-carriers move through delocalized states and that, in addition to the tail of localized states, the disorder can give rise to spatial energy variation of the transport band edge being described by a Gaussian distribution. The principal advantage of the present EMA model is its ability to describe universally effective drift- and Hall mobility in heterogeneous materials as a function of disorder, temperature and carrier concentration within the same theoretical formalism. It can explain a puzzling observation of activated and a carrier-concentration dependent Hall mobility in a disordered system featuring

an ideal Hall effect. The present model has been successfully applied to describe experimental results on the charge transport in a-IGZO TFT. In particular, the model reproduces well both Meyer-Neldel (MN) compensation behavior for the charge-carrier mobility and inverse-MN effect for the conductivity observed in the same a-IGZO. The model was further supported by *ab initio* calculations revealing that the amorphization of IGZO gives rise to variation of the conduction band edge rather than to the creation of localized states. The obtained changes agrees with the one we used to describe the charge transport. We found that the band edge variation dominates the charge-carrier transport in high-quality a-IGZO TFTs in above-threshold voltage region, whereas the localized states need not to be invoked to account for the experimental results in this material. Moreover, charge scattering effects were shown to have a noticeable contribution to the temperature dependent transport in a-IGZO films.

[1] K. Nomura, H. Ohta, A. Takagi, T. Kamiya, M. Hirano, H. Hosono, Nature, 432, 488 (2004).
[2] A. Kadashchuk, I. I. Fishchuk, J. Genoe, P. Heremans, Phys. Rev. B. (submitted).

# Photoluminescence of $A_2B_6$ Nanocrystals

Korbutyak D.V.

*V.E. Lashkaryov Institute of Semiconductor Physics, NAS of Ukraine, Kyiv, Ukraine*

Advances in synthesis technologies of high-quality $A_2B_6$ nanocrystals (NCs) have stimulated their wide use in various fields of opto- and nanoelectronics. Among the most promising areas of $A_2B_6$ NC applications various light-emitting devices should be noted, such as LEDs, white light sources, low-threshold lasers etc. Due to the narrow emission spectrum of monodisperse NCs (half-width of the radiation band is about 20 nm) NC-based LEDs are characterized by rich colors with a much better spectral purity than liquid crystal or organic LEDs. Besides, NC-based LEDs are characterized by a number of advantages comparing to classic LEDs based on *p-n* junctions. They have high quantum yield of radiation, low power consumption, long useful lifetime, high-*speed operation*, resistance to vibrations and shocks. LED radiation of almost arbitrary color could be obtained by selecting the material of NCs and their sizes. Some of the light-emitting properties of $A_2B_6$ NCs have been described in our review [1]. In this paper we present new results of the studies of optical, luminescent and structural characteristics of $A_2B_6$ NCs incorporated in protective inorganic matrices or directly synthesized in polymer matrices [2]. Moreover, results are highlighted of research and development methods of stabilization of $A_2B_6$ NC optical characteristics, surface passivation and efficiency increasing by NCs incorporation in the matrix of alkali metal salts. A technology is described of synthesis in polymer matrices of CdS NCs doped with Cu and Zn impurities [3]. The results of X-ray analysis and comprehensive studies of optical absorption and photoluminescence spectra of CdS NCs are described (the results being dependent on concentration of copper and zinc impurities introduced). It has been found that copper atoms are concentrating on the surface of CdS NCs. This leads to passivation of vacancy type defects, which serve as surface radiative centers. *On the contrary*, zinc penetrates into the bulk of CdS NCs creating additional surface defects (the defects being the radiative recombination centers).

1. Д.В. Корбутяк, О.В. Коваленко, С.І. Будзуляк, С.М. Калитчук, І.М. Купчак. Світловипромінюючі властивості квантових точок напівпровідникових сполук $A_2B_6$//УФЖ. Огляди. – 2012.- Т. 7, № 1, С. 48-95.
2. Д.В. Корбутяк, С.М. Калитчук, С.І. Будзуляк, А.О. Курик, С.В. Токарев, О.М. Шевчук, Г.А. Ільчук, В.С. Токарев. Люмінесцентні властивості нанокристалів CdS, синтезованих у полімерних матрицях // ЖФД.- 2014. – Т. 18, № 1. – С. 1801-1805.
3. Д.В. Корбутяк, С.В. Токарев, С.І. Будзуляк, А.О. Курик, В.П. Кладько, Ю.О. Поліщук, О.М. Шевчук, Г.А. Ільчук, В.С. Токарев. Оптичні та структурно-дефектні характеристики нанокристалів CdS:Cu і CdS:Zn, синтезованих в полімерних матрицях//Фізики і хімія твердого тіла. – 2013. – Т. 14, № 1, С. 222-227.

# Calculation of optical waves propagation through gyrotropic anisotropic media: chalcogenide glass plates and thin films

Kozak M.I.

*Uzhhorod National University, Uzhhorod, Ukraine*

As is well known in the glass as in fluids have short-range order. In addition, numerous studies show that the glasses are typically somewhat middle order. Chalcogenide glasses in this respect demonstrate much higher rate than the canonical silicate glasses. Some elements, such as As, in combination with S or Se, the structure provide such polymers. It is also known assumption of the existence in glasses As - S (Se) even paracrystalline structure. This requires a large extent clarified electrodynamic model in optical studies of such media. At the microscopic level, it concerns the theory of the local field. In the macroscopic respect - this clarification of constitutive equations, which are used in the solution of Maxwell's equations. Necessary averaging microscopic theory when considering the spatial nonlocality of the medium response to the electromagnetic disturbance is extremely difficult. However, it is known that these difficulties cost, if we consider the spatial dispersion immediately phenomenologically. In this case, we write the dependence of the electric displacement vector of the electric vector $\mathbf{D} = \mathbf{D}(\mathbf{E})$ in some different from conventional ($\mathbf{D} = \varepsilon\mathbf{E}$, where $\varepsilon$ – dielectric tensor) form. If we consider only the spatial dispersion of the first order, you can use the representation $\mathbf{D} = \varepsilon\mathbf{E} + \gamma\mathrm{rot}\mathbf{E}$, where $\gamma$ is the second rank tensor. If $\gamma$ is scalar, then the last relation describes gyrotropic medium. It is for this constitutive equation in the present report shows the method for solving Maxwell's equations and application to thin films and plates.

According to the Berreman's 4×4-matrix formulation, the Maxwell's equations, along with the constitutive equations for a particular optical media shall be converted into a scalar system of four first order differential equations in four unknowns, which are the field components $E_x$, $E_y$, $H_x$, $H_y$ in the Cartesian coordinates system:

$$\begin{cases} E_x' = & \dfrac{\gamma k_x^2}{\varepsilon_{zz}} E_y & & -\dfrac{ik_z^2}{k_0\varepsilon_{zz}} H_y, \\ E_y' = & & ik_0 H_x, & \\ H_x' = & \dfrac{ik_y^2}{k_0} E_y & & +k_0^2\gamma H_y, \\ H_y' = & -ik_0\varepsilon_{xx} E_x & -k_0^2\gamma H_x, & \end{cases} \qquad (1)$$

where $k_y^2 = k_0^2\varepsilon_{yy} - k_x^2$, $k_z^2 = k_0^2\varepsilon_{zz} - k_x^2$, $k_x = k_0 \sin\phi_0$, $k_0 = \omega/c = 2\pi/\lambda$, $\phi_0$ – an angle of incidence, and $\lambda$ is the wavelength in vacuum. Here, the dependence of

the fields **E**, **H** and **D** from the time $t$ at a frequency ω is built according to the harmonic rule ~ exp($i\omega t$), where $c$ is the speed of light in vacuum. Hereafter, the prime (') denotes differentiation with respect to $z$.

In [1] was the first to show that the system (1) is reduced to the solution of the following fourth order equation

$$\left(E_y''\right)'' - \mathcal{A}E_y'' + \mathcal{B}E_y = 0,$$

where $\mathcal{A} = \frac{\varepsilon_{xx}}{\varepsilon_{zz}}k_z^2 + k_y^2 + k_0^4\gamma^2$, $\mathcal{B} = \frac{\varepsilon_{xx}}{\varepsilon_{zz}}\left(k_y^2k_z^2 - k_0^4k_x^2\gamma^2\right)$.

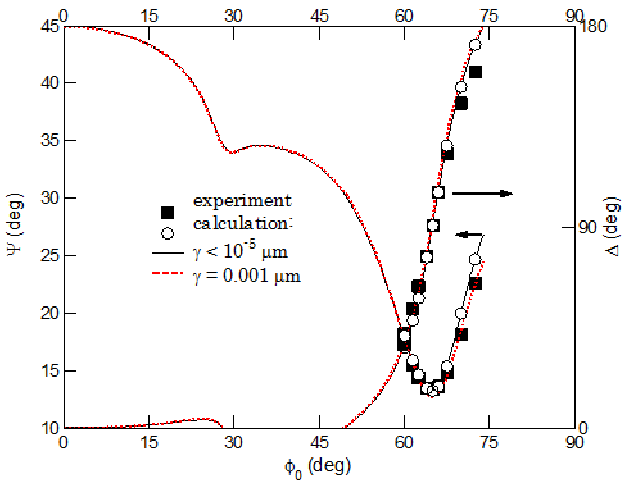


Fig. 1. Ellipsometric angles Ψ and Δ as a function of the incidence angle $\phi_0$ of $As_2S_3$ thin film, refractive index $n_f$ = 2.453, $d$ = 2.103 μm at different γ.

The remaining components of the field easily calculated from the system.

We see that there are four waves – apply two forward and two – in the opposite direction. The challenge for a plate or thin film is solved by using the usual boundary conditions. This leads to solving a system of linear algebraic equations of order eight. As an example, we show the effect of the degree of gyrotropy on ellipsometric spectra of thin films (Fig. 1). As you can see, to the extent gyrotropy $\gamma \sim 10^{-5}$ (corresponds to a rotation of the polarization plane of quartz 188 deg/cm) does influence unnoticed. When $\gamma \sim 10^{-3}$ observed contrast and improved agreement between the experimental and theoretical values for angles of incidence greater than the critical angle.

The calculation results of several common examples are listed in [1]. Detailed mathematical calculations will soon be published in expanded form.

1. Kozak M.I. , General approach in polarimetry-ellipsometric calculation, Proc. of the X Int. Conf. “Electronics and applied physics”, October, 22-25, 2014, Kyiv, pp. 197–198.

# The Effect of Nickel Intercalation on the Properties of $In_2Se_3$ Layered Crystals

Kushnir B.V., Boledzyuk V.B., Potsiluiko R.L.

*Frantsevich Institute for Problems of Materials Science, NAS of Ukraine, Chernivtsi Department, Chernivtsi, Ukraine*

$In_2Se_3$ is a layered semiconductor with defective structure of tetrahedral bonding, where one-third of the sites is vacant and forms a screw array along the c axis. $In_2Se_3$ layered crystals have been the subject of many investigations due to their peculiar electrical and optical properties, and their potential applications in various types of electronic and optoelectronic devices, phase-change random access memories, solid-state batteries, and solar cells, etc [1, 2].

$In_2Se_3$ single crystals were grown by the Bridgman modified method from a stoichiometric melt and characterized by a pronounced layered structure over the whole length of a sample. Intercalation of samples was performed by the electrochemical method in the course of the anodic reaction of intercalation in static gradient magnetic field of 50 A/m at the sample-electrolyte interface. $NiNO_3$ saturated aqueous solution was used as the electrolyte. The concentration of embedded Ni (x) was calculated according to Faraday's law.

The influence of $Ni^{2+}$ ions intercalation on properties of $In_2Se_3$ monocrystals was investi-gated. It was shown that at the increase the concentration of $Ni^{2+}$ ions the specific conductivity of $In_2Se_3$ crystals tends to decline (Fig.). The basic samples of $In_2Se_3$ single crystals are paramagnetic. It is found that $Ni_xIn_2Se_3$ samples have ferromagnetic properties at room temperature.

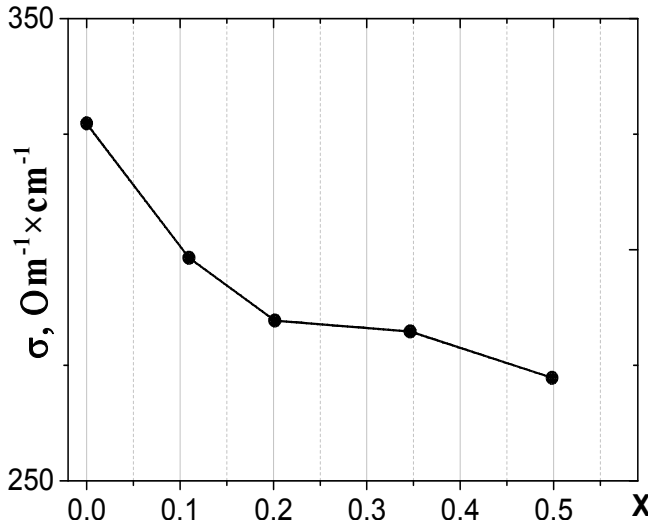


Fig. The dependence of σ⊥c layer-parallel electrical conduction for $Ni_xIn_2Se_3$

1. Julien C., Eddrief M., Kambas K., Balkanski M. // Mater. Sci. Eng. B. 1996.V. 38. N 1. P. 1–8.
2. Bakhtinov, A.P., Boledzyuk, V.B., Kovalyuk, Z.D., Kudrinskii, Z.R., Litvin, O.S., and Shevchenko, A.D., Phys. Solid State, 2013, vol. 55, no. 6, pp. 1148–1155.

# Degradation Processes on the Interface of Film Systems "Glass - Klaster Ag-Pd" - Sn-Pb

Lepikh Ya.I., Lavrenova T.I.

*Interdepartmental scientific - educational physicotechnical centre of MOS and NAS of Ukraine at the Odessa I.I. Mechnikov National University, Odessa, Ukraine*

Influence of structural - phase features of conductor films based on " glass - Ag-Pd " on processes of physical and chemical interaction of a film material with the solder STP-61 is investigated.

Researches have shown, that main reason of degradation (partial or full destruction of contact compounds "glass - Ag-Pd"-STP-61) is: bad adhesion of a film to ceramic substrate; dissolution of a film material in solder melt; solder melt penetration on pores and microcracks through the appreciable heterogeneity and nonthickened conductor macrostructure. System Ag-Pd-Sn-Pb element concentration distributions on diffusion zone depth are received. It is established, that interaction the Sn-Pb melt (at temperature $250^0$ C) with a thick film material results in a strong redistribution of the basic solder components (segregation) with Sn extracting in a contact zone and Pb crystallization on a distance of 60-70 microns from the interface. It is possible to explain such redistribution by the presence of dissolution process which passes on two mechanisms: a kinetic mode - diffusion through interphase border; diffuse (heterodiffusion of the dissolved metal in the liquid melt). The equations which describe solution kinetics are received. For a kinetic mode: $n = n_\infty \left\{1 - \exp\left[-\left(\varpi_\tau \rho / n_\infty\right)\left(S / V_{ж}\right)t\right]\right\}$; for diffuse mechanism: $n = n_\infty \left\{1 - exp\left[-\left(D / \delta\right)\left(S / V_{ж}\right)t\right]\right\}$, where n - metal solution concentration, $n_\infty$ - saturation concentration; ω – crystallization speed; $\omega_\tau$ - probability of the firm metal in liquid transition, $\rho$- firm metal surface density; S - contact area; $V_ж$ - liquid solder volume; δ - boundary layer thickness. In our case when both mechanisms operate: $n = n_\infty \left\{1 - \exp\left[-\alpha\left(S / V_{ж}\right)t\right]\right\}$, where $\alpha = \left(V_{ж} / S\right)\ln\left[n_\infty / \left(n_\infty - n\right)\right]$ - dissolution speed constant.

It is established, that formation in an initial glass matrix intermetallic compound $Ag_xPd_y$ and solvate systems complex spatial structure such as $Me(OH_2)$ blocks tin diffusion in a matrix and inhibits dissolution of its other components (Ag, Pd) in tin - lead melt. At presence in a glass matrix intermetallic compounds $Ag_xPd_y$ and solvate systems of complex spatial structure such as Me $(OH_2)$ film adhesion to a ceramic substrate is high and makes 5-10 MPa.

# Nano-phase Formation at Ion-Beam Synthesis

Litovchenko V.G., Melnik V.P., Romanyuk B.M., Popov V.G.

*V. Lashkarev Institute of Semiconductor Physics NAS of Ukraine, Kyiv, Ukraine.*

Intensive research of the nanocluster-conteining structures is caused by unique properties inherent to such structures that are not characteristic for a bulk material. One of such character of silicon nanoclusters (Si-nc) is the emission of light in the visible and near-infrared region of the spectrum.

At combined use of a number of technological procedures, such as ion-induced formation of nanoclusters, modifications of the Si-nc/$SiO_2$ interfaces, passivation of non-radiative recombination centers, it is possible significantly (by more than an order of magnitude) increase the photoluminescense efficiency compared with the traditional method of formation of luminescent structures (thermal decay of non-stoichiometric $SiO_x$ film, etc.).

We have investigated the effect of implantation a number of impurities (H, C, N, Al, Ti) on the formation and modification of luminescent structures containing silicon nanoclasters, embedded in the dielectric matrix. It was established that implantation of carbon, nitrogen and aluminum (stimulants of the $SiO_x$ phase decay) and the next high-temperature annealing (1100-1200 °C) during the formation of Si-nc in silica matrix significantly accelerates the nucleation and growth processes of silicon nanoclusters. The basic mechanisms of this effect is the binding of excess oxygen in the region of Si-nc growth, and reduction (offset) of local mechanical stress during silicon nano-inclusion growth. Controlled introduction of these impurities (at 0.1 - 2 atomic %) can influence the size and concentration of nano-clusters and thus change the spectral characteristics of the luminescent structures. In particular, the introduction of carbon and nitrogen increases the concentration of smaller clusters accompanied by increased (several times) photoluminescence intensity in the short-wave region of the spectrum that is consistent with the predicted quantum-dimensional mechanism. In addition, nitrogen effectively passivates non-radiative recombination centers, which leads to a general increase in the intensity of radiative recombination. Aluminum, intensely absorbing oxygen, creats conditions for rapid Si-nc nucleation in the early stages of their high-temperature formation.

Another way to influence the growth of nc-Si is proposed combined method of acoustic-stymulated ion beam doping (synthesis) of solid targets that can accelerate the redistribution of radiation defects generated by the interaction of accelerated particles with solid (Figure 1). This allows you to influence the rate of quasi-chemical reactions in nanoscale structures, stimulate (accelerate or reduce) processes of mass transport and thus change the conditions of the formation, growth and decay of the phases in solid matrices. The introduction of ultrasonic waves at ion-beam synthesis of metal clusters in $SiO_2$ matrix, as it is

shown by our experiments, leads to increased formation of metallic nanoclusters (Cu, Ag), Figure 2. The average size of clusters may be increased almost twice.

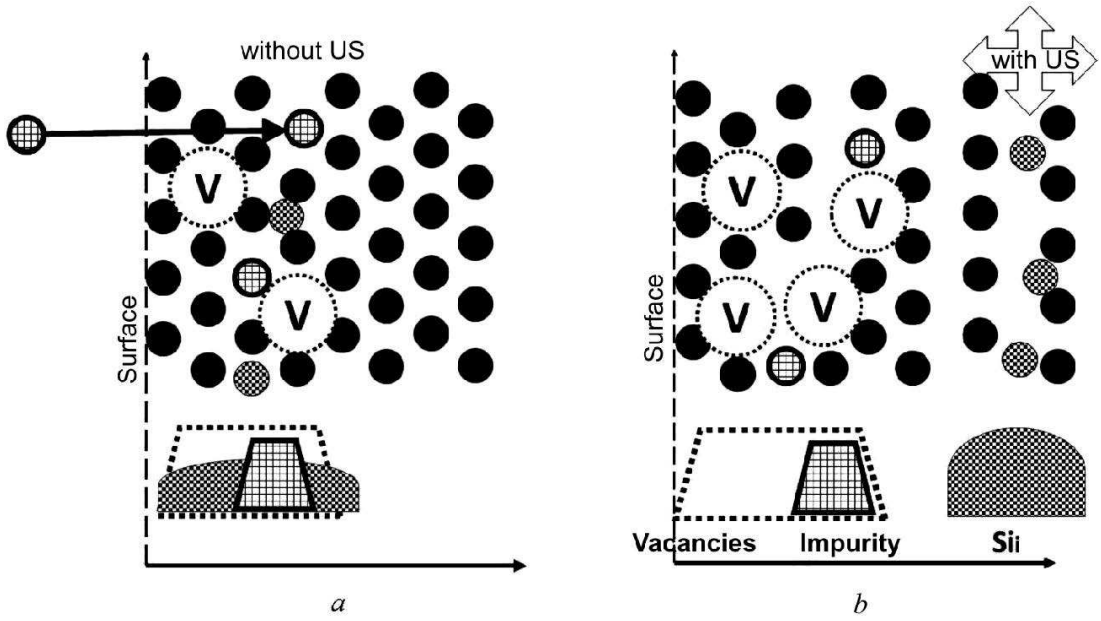


Fig. 1. Distributions of radiation-induced defects after the implantation (a) without and (b) with the in situ US treatment.

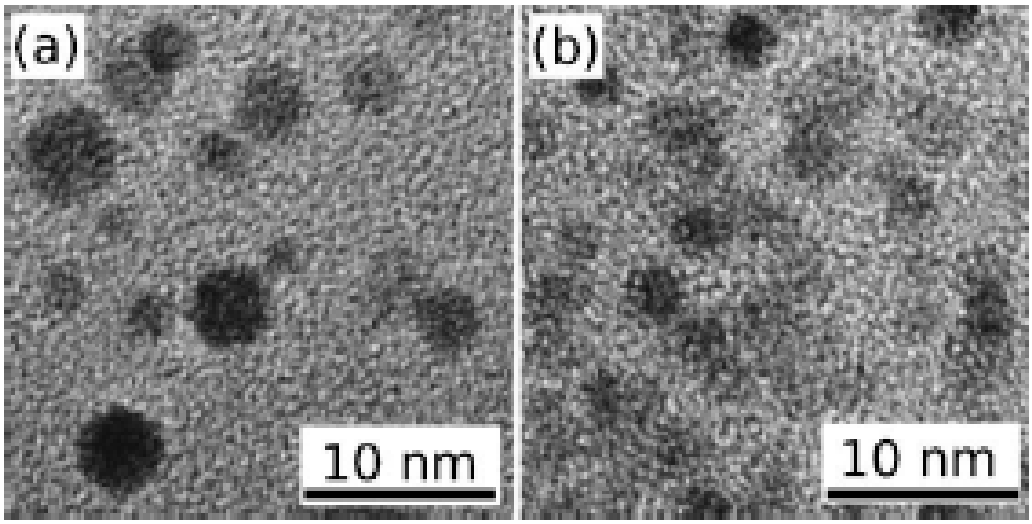


Fig. 2. TEM images of copper clusters in the $SiO_2$ film synthesized by implanting $^{63}Cu^+$ ions to the dose $D_{Cu} = 5\times10^{15}$ cm$^{-2}$: implantation (a) with and (b) without US treatment.

# The Influence Cylindrical Nano Defects Filling Volume on Heat-Resistant Metals Thin Films Effective Electronic Characteristics

Marenkov V.I.

*Odessa I.I.Mechnikov National University, Odessa, 65026 Ukraine*

Diagnostics and control of the parameters of the samples with NDFV are conducted with the help of different methods of metering of effective carrier density in the sample that represents the material under study. At the same time, the kinetic processes such as conductivity current in the sample with NDFV, lead to the change in the mictrostructure of the local electrostatic field and the redistribution of carriers in the region of local thermodynamic equilibrium. It is reflected in the behavior of the effective conductivity of microinhomogeneous sample (MIS), so the interpretation of the experimental data needs to take into account these effects. As it was shown in [1-5], the self-consistent exchange of electric charge between the base material (BM) and the NDFV subsystem happens in the way that the instantaneous electroneutral regions (electroneutral cells) emerge, transform and evaluate in the volume of MIS. They define the spatial scale of the coulomb microinhomogeneties of the sample. Their emergence is caused by the presence of non-zero effective density of the electronic component inside the ND volume. The statistical averaging on the system realizations ensemble within the framework of Thomas-Fermi approximation for the carrier dispersion equation gives the effective distribution of space charge and self-consistent electric field in the electroneutral cell $C_\xi^z$ of MIS. The $C_\xi^z$ cell is the result of the averaging of the instantaneous cell $C_\xi$ over the cell ensemble $C_\xi^z = \text{mean}\{C_{\xi n}\}_{n\to\infty}$. Further averaging of the of the local parameters for multiple statistical cells of the sample leads to the determination of the effective electrochemical potential F of the carriers in microinhomogeneous film and associate it with the initial thermodynamic, electronic and dielectric parameters of the MIS, external electric field $\vec{E}_0$, geometric characteristics of the NDFV and collective parameters of the defect microstructure dispersed in the sample.

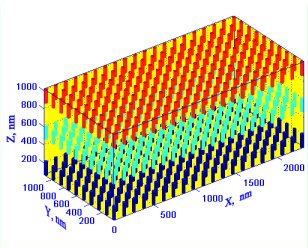


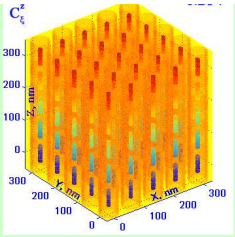


Fig.1. Electroneutrality cells in the nanoinhomogeneous film sample of the heat-resistant metal with cylindrical NDFV: A) three-layer film; B)the microinhomogeneous film element with cylindrical defects of filling volume in the electroneutrality cells .

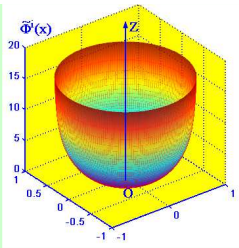


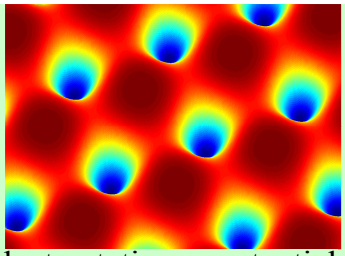

Fig.2.A). The electrostatic potential distribution in its own volume NDFV. The potential is normalized to the Fermi energy of the carriers of the base material film, the geometrical parameters are expressed in units of the Debye radius; B). The cross-section of a super lattice of cylindrical NDFV in a thin film in Wolfram. In conditi-onal colors presents a qualitative picture of the distri-bution self-consistent potential in the vicinity of defects. Red represents the BM-matrix, a blue region volumes nanodefects with a low concentration of carriers.

The most commonly used in applications types of film structures with defects of filling volume is shown in figure 1.

The spatial distribution of the self-consistent electrostatic potential in the individual volume of the defect, and in a thin film with a regular structure cylindrical NDFV demonstrate Fig. 2A) and Fig. 2B) .

3-D the dependence of the effective Fermi level of carriers in Fig. 3 reflects the effect of size and concentration of RDSO in a film of tungsten on the effective work function of electron transfer from the surface.

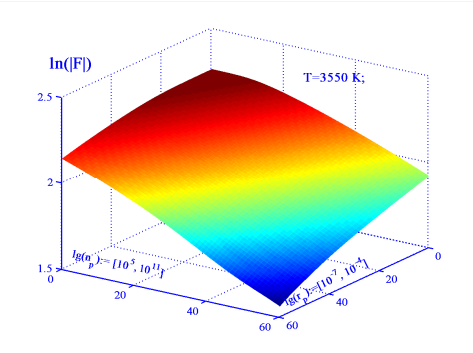


Fig.3. The effective Fermi level of carriers in micro-inhomogeneous film.

Conclusions:

1).The problem of the equilibrium ionization in the heterogeneous heat-resistant metal with the nano defects filling volume (NDFV) is solved in the framework of the statistical model of the quasi-neutral cells of heterogeneous plasma for the planar and cylindrical symmetry of the nano-inclusions in the matrix of base material of microinhomogeneous sample (MIS); 2).The functional dependencies of the effective NDFV charge and its Fermi level on the thermodynamic parameters of microinhomogeneous sample (temperature, size and concentration of defects, initial electronic and dielectric properties of the base material) are determined with the help of the averaged on the cell ensemble parameters of the microinhomogeneous sample with the defects filling volume; 3).The analytic equation, that determines the optimal relation between the NDFV geometry and the walls of base material matrix in case of maximum defect influence on the electronic properties of the sample, is obtained;.4).The structure of the local Maxwell field in the wall region of VFD and local volume charge distribution in the contact area between base material and defect are determined. The effect of the tension of the self-consistent electrostatic potential on the effective work function of electrons from the surface of the micro inhomogeneous films with nano defects of filling volume; 5). The computer simulation of the electrophysical properties of wolfram, rhenium, tantalum and microinhomogeneous aluminum oxide with VFND was performed in the temperature region T=[1000,3000]K, which is characteristic for the contemporary technologies of high-temperature plasma sensors.

1. V.I. Marenkov, Journal of Molecular Liquids.–2005.–Vol.120, Nu. 2.– P. 181.
2. Marenkov V.I..- 24-th Symposium on Plasma Physics and Technology, 14th-17th June, 2010, Prague, Czech Republic, P. 130-131.
3. V.I. Marenkov, Materials XIV International Conference Physics and Technology of Thin Films and Nanosystems.–May 20–25, 2013, Ivano-Frankivsk, Ukraine.– P. 317.
4. V.I. Marenkov, Ukr. J. Phys. 2014, Vol. 59, N 3.– P. 257.
5. 5. V.I. Marenkov Fermi Level of Carriers in the Volume Filling Defects Structure Based on Heat-Resistant Metals// Nanomaterials: Applications &Properties (NAP-2011). - 2011, P. 82-84.

# Electroreflectance and Electronic Processes in Nanostructures with Fullerenes

Matveeva L.A., Kolyadina E.Yu., Neluba P.L., Venger E.F.

*V. Lashkaryov Institute of Semiconductor Physics NAS of Ukraine, Kyiv, Ukraine*

Nanostructures with $C_{60}$ fullerenes are new promising materials for electronic, sensors and biomedical application. Their physical properties are determined by the film growth conditions and different external actions [1]. Inner mechanical stresses appears in the films during their manufacturing process. Their relaxation deteriorated the characteristics and reduced reliability of the corresponding devices. The $C_{60}$ energy gap value dispersion is of 1.43 to 2.35 eV [2]. Therefore, an investigation of internal mechanical stresses and electronic processes in nanostructures with fullerenes is important for the technology development and for $C_{60}$ films electronic properties prediction.

We present the results of studies on the films production and their structure perfection, mechanical stresses, the features electronic band structure and electronic processes in $C_{60}$ nanostructures depending on the substrate type, and the influence on them microwave treatment. To reduce internal mechanical stresses, the films were deposited onto various non-heated substrates (Si, glass). Sublimation of microcrystalline $C_{60}$ powder from effusion tantalum cell in vacuum at a pressure of $10^{-4}$ Pa and of 800 K temperature was used [3]. The films had a polycrystalline structures, their thickness was of 0.1 to 2 μm. The films mechanical stresses were determined on the heterosystems bending, using the Stoney's equation. The films were compressed on Si and too on glass substrate. The electroreflectance method was used to determination of mechanical stresses in $C_{60}$ films and in Si substrate on interface.

This method was applied for the control of electron parameters of the nanostructures. Study of electronic band structure modulation spectroscopy method should help in understanding the nature and mechanism of light absorption of $C_{60}$ solid. The high sensitivity of this method to details of the band structure is well known. The advantage of modulation spectra over classical spectra lies in the fact that they allow the find thin structure, usually hidden by the structureless background. This method is the most sensitive, since its signal is determined by the third energy derivative of the optical constants. He signal exist only at the critical points of the Brillouen zone in direct-transition region, vanishes as we move away from these point, and determined by both optical and electron properties of the semiconductor surface under investigation.

The electroreflectance spectra were measured by an electrolytic method in quartz electrolytic cells with 0.1 normal KCl water solution at the room temperature in of 1.5 to 3.6 eV range for $C_{60}$ films and Si substrate in interface. Calculation of the electron parameters was realized, using energy location of the dominant peaks in the spectrum and its intensity. There were determined the

transitions energy $E_g$, the value of the phenomenological broadening parameter Γ (they depend on the type electron transition), the relaxation energy time of charge carriers τ and their mobility μ. Important data were obtained too concerning the film and interface film - substrate band structures, their structure perfection, the conductivity type of the films and the substrate on the interface, change of elastic stresses and charge scattering processes, as well as the effect of microwave irradiation on the properties of the heterostructures.

It been established, that $C_{60}$ solid is direct - gap semiconductor with about 1.6 eV band gap ($E_0$) in the singular X point of the Brillouen zone. The next direct transition in this point ($E_1$) was observed in spectral range about 2.2 eV. The value of band gap depend on inner mechanical stresses. We calculated the value of this dependence on the basis of the data on electrorefletance spectra and the heterosystem bending. They were established: $-2.8 \cdot 10^{-10}$ eV/Pa and $-4.2 \cdot 10^{-10}$ eV/Pa for $E_0$ and $E_1$ transitions, respectively.

The electro-optical Franz-Keldysh effect in a built-in electric field was observed in $C_{60}$/glass on alternating-sign oscillations in electroreflectance spectra above fullerene optical absorption edge. There was determined the electro-optical energy and electric field value. In this heterosystem the doublet nature of the peaks of electroreflectance was observed. This was explained by the effect of surface size quantization of the electron energy in the electron enriched fullerene surface in interface and the presence of $E_g + e_1$ transitions.

To translate nanostructures in a state of equilibrium, we used the microwave irradiation. The relaxation mechanical stresses takes place, and after 10 s irradiation the mechanical stresses disappear, that is confirmed by substrate $E_0$ transition energy shift to a value 3.38 eV, which corresponds to the surface unstressed Si. In [1] it been show, that $C_{60}$ film can change composition with the formation of the other carbon structures both in processes of the films deposition and by γ - irradiation. By microwave irradiation, the possibility was found to reduce the mechanical stresses in heterosystems and technological defects, to improve electronic parameters of $C_{60}$ films and interface, and to fabrication of the nanostructures with $C_{60}$ fullerene without their decomposition and the bending deformation.

1. E.Yu. Kolyadina, L.A. Matveeva., P.L. Neluba, V.V. Shlapatskaya. Physical properties of $C_{60}$ fullerene nanostructures. – Material Science and Engineering Technology – 2013 – Vol. 44, № 2-3 – P. 144-149.
2. T.L. Makarova. Electrical and optical properties of pristine and polymerized fullerenes. – Semiconductors. – 2001 – Vol. 35, № 3 – P. 243-261.
3. P.L. Neluba. Peculiarities of fullerenes condensation from molecular beam in vacuum. – Technol. Konstr. Elektron. Appar. – 2011 – № 6 – P. 35-39.

# Oxidation and Photo-Eged Studies of Graphen-Like Two Dimentional Arsenic-, Germanium Sulfide Crystalls and Nanostructured Glasses

Mitsa V.[1], Holomb R.[1], Kondrat A.[1], Popovich N.[1], Veresh M[2], Csik A.[3],Vondráček M.[4], Tsud N.[5], Matolin V.[5], Kevin P.[6], Fekeshgazi I.[1]

[1]*Research Institute of Solid State Physics and Chemistry, Uzhhorod National University, Uzhhorod, Ukraine*

[2]*Wigner Research Centre for Physics of the Hungarian Academy of Sciences, Budapest, Hungary*

[3]*Institute for Nuclear Research of the Hungarian Academy of Sciences, Debrecen, Hungary*

[4]*Institute of Physics, Academy of Sciences of the Czech Republic, Cukrovarnická 10, 16253 Prague 6, Czech Republic*

[5]*Department of Surface and Plasma Science, Faculty of Mathematics and Physics, Charles University, Prague, Czech Republic*

[6]*Elettra-Sincrotrone Trieste S.C.p.A., Trieste, Italy*

Arsenic sulphide minerals are found naturally and have been used as artists' pigments since prehistoric times. Orpiment $As_2S_3$ gives a yellow pigment and realgar $As_4S_4$ usually gives an orange-red. Recently by macro FT-Raman and energy-dependent micro-Raman spectroscopy we found the light-induced structural changes in glassy As-S system with realgar inclusion [1,2]. New observed features in the Raman spectra of As-S glass are related to transformations of $As_4S_4$ molecules. Being initially in the structure of glassy closed and connected with glassy network only by weak Van der Vaals forces α (β)-$As_4S_4$ molecules are transformed into pararealgar p-$As_4S_4$ form during laser illumination. The effectiveness of transformations depends mainly from photon energies used for irradiation but transformation tendency observed for all used photon energies ranged from 1.65 to 2.54 eV. Our findings are multidisciplinary and may have a significant value to play in disciplines such as natural resources, prehistoric artistic expression, archaeology, art history and chalcogenide photonics. Based on our finding of light-induce realgar-paraleargar transformation the additional related investigations [3] also found realgar degradation by different halogen lamps and a LED lamp, used in museum exhibitions are helpful to describe the photo-degradation processes in pigment[4].The light remains unique because it can neither be eliminated nor completely controlled. The red colour of the pigment based on realgar α-$As_4S_4$ on exposure to light transformed to pararealgar p-As4S4 that exhibits yellow colour. Based on our investigations, the light necessary for viewing a work of art with realgar pigments, can damage the artwork starting from with photon energies equal 1.65 eV with relatively high intensities $10^2$ W/cm$^2$. Process of light induces polymorph transformation on air is accompanies with formation arsenolite $As_2O_3$ and finally lead to whitening of realgar. The process is not completely clarified so far. Based on SRPS, XPS and surface enhance Raman

and PL spectroscopy studies we found some photo-aged processes occurring on the surface of amorphous $As_2S_3$ film for chalcogenide photonics. In energy dependent luminescence in orpiment, realgar and glassy As-S with realgar inclusion we have found evidence of $As_2O_3$, $As_2O_5$ formation and PL band typical for substance known in general formula $As_2O_3xH_2O$. Last is show that is why the illuminated places with realgar in high humidity condition can by wet. May be this finding help to give answer why some places on paintings "dry". The positions of PL bands in excitation-dependent photoluminescence of aged and freshly fractured g-$GeS_2(T_iV_j)$ prepared with different rate of quenching ($V_j$) and melt temperature ($T_i$) are compare and analyse together with Raman PL , XPS spectra of GeS, β-$GeS_2$ . Excitation-dependent PL spectra of g-$GeS_2(T_iV_j)$ exhibit increasing intensity up to $E_{ex}$ = 2.75 eV . For this $E_{ex}$ the strong broad green band centred at 2.37 eV appear. Such behaviour of PL spectra of β-$GeS_2$ is typical for $GeO_2$ with quartz-like structure.

1. R. Holomb, V. Mitsa, P. Johansson, N. Mateleshko, A. Matic, M. Veresh. Chalcogenide Letters.- 2005.-Vol. 2, No. 7.- p. 63 - 69.
2. R. Holomb , N. Mateleshko , V. Mitsa , P. Johansson , A. Matic , M. Veres. Journal of Non-Crystalline Solids.- 2006.- Vol.352. -Pp. 1607–1611.
3. Andrea Macciha. Case of realgar photo-oxidation: looking for the best lighting system applied to cultural heritage. PhD thesis. Universita di Roma.-2012.

# Comparison of Light- and Particle-beam Surface Patterning in Amorphous Chalcogenide and Acrylic Polymer Layers

[1]Molnar S., [2]Nagy Gy., [3]Burunkova J., [1]Bohdan R., [2]Rajta I., [1]Kokenyesi S.

*[1]Institute of Physics, University of Debrecen, Debrecen, Hungary*
*[2]Institute of Nuclear Research Hungarian Academy of Scienecs, Debrecen, Hungary*
*[3]University ITMO, St.Petersburg, Russia*

Amorphous layers of chalcogenide glasses from As(Ge)-Se system with comparatively low softening temperatures (370-450 K) and acrylic polymers with different degree of cross-linking, synthesized from diurethane dimethacrylate, mixture of isomers, dodecanethiol functionalized gold nanoparticles, silica nanoparticles and 2,2-dimethoxy-2-phenylacetophenone, as well as nanocomposite structures from these materials, containing gold nanoparticles have been produced and used for *in situ* surface optical and geometrical relief fabrication by optical- or ion-beam recording. Recording was performed by different laser irradiation as well as by focused (r=3-4 μm) proton beams (2 MeV) in a Van-de-Graaff accelerator.

Investigations were focused on the formation of giant (height modulation from nanometers up to micrometers) geometrical reliefs and elements (dots, lines and diffractive elements) applicable in the 0.5 – 10 micrometer spectral range for optoelectronics. The efficiency of the recording, pattern formation was estimated from the data on surface relief profile heights, widths or depths vs. exposure (input energy), as well from the optical measurements. The mechanisms of the recording processes, which include important mass-transport components were considered, the efficiency of surface modulations were compared and the selection of the materials and processing with best recording parameters was done.

*This work was supported by the 4.2.2.A-11/1/KONV-2012-0036 project, which is co-financed by the European Union and European Social Fund.*

# Gas-Phase Synthesis and Structure of Needle-Shaped Silica Nanoparticles

Myronyuk I.F., Bezruka N.A., Dmytrutsa T.V.

*Vasyl Stefanyk Precarpathian National University, Ivano-Frankivsk, Ukraine*

Silica received by combustion of steam of silicon-containing substances ($SiCl_4$, $CH_3SiCl_4$) in hydrogen-air flame is an important product used as a thickener for liquid media, filler of polymers, abrasive material for chemical-mechanical polishing of monocrystals of electronic equipment, drug absorption of medical supplies etc.

Currently well-known methods of fumed silica synthesis allow receiving an aerogel-like product with a specific surface area of 50-400 $m^2 \cdot g^{-1}$, in which the fractal structure of the oxide material is formed from spherical nanoparticles.

Investigating the dependence of aerogel structure and the size of its primary particles on silica synthesis conditions (the components ratio in the reaction mixture, its homogeneity and outflow velocity from nozzle burner, flame temperature, and its turbulence), we concluded that turbulence and flame temperature are the main factors, which determine a morphological structure of the product and the degree of primary particles dispersion.

At the first stage of the fumed synthesis the origin and growth of proto-particles were carried out by the fleeting heterolytic reactions of siloxane bonds formation at condensation, for example, chlorine siloxane $SiCl_{3-n}(OH)_{n+1}$ (n = 1-3) and further condensation of hydroxide oxide oligomers $–[Si(OH)_2 – O – Si(OH)_2]_m–Si(OH)Cl$ (m = 5-10).

It should be noted, that protoparticles and primary silica particles formed at flame temperature of 1400-1650 K have too large surface energy, it causes a decrease of melting point of the oxide material on 250-400 K. Therefore they are in a molten state at those temperatures.

High turbulence of flame leads to rapid protoparticles coalescence and formation of $SiO_2$ primary particles. The primary particle of 6-14 nm in size has at those conditions a higher viscosity compared to protoparticles, therefore their adhesion occurs only at the collision.

The calculation of characteristic time of particles coalescence in the flame has shown that it is the same at the synthesis of silica with different specific surface area and is about $10^{-3}$ s, and turbulent diffusion coefficient is in the range of $10^{-3}$-$10^{-2}$ $m^2 \cdot s^{-1}$ that is in 2-3 times higher than the molecular diffusion coefficient.

In turbulent flame with Reynolds number (Re) less than 15000 small-scale pulsations provide a formation of aerogel-like structures formed mainly from linear clusters (fractals). The pulsations enhance diffusion processes in the flames at the large turbulence ($Re \geq 40000$), which leads to an increase in the

degree of volume concentration of primary particles and the formation of secondary gel-like structures.

Decisive influence of turbulence of reaction medium on the morphology of the secondary structures in a flame caused to seek ways of volume flame filling by ordered "tornado" type vortices, with the help of which the formation of $SiO_2$ two-dimensional nanoparticles would occur.

To ensure the necessary turbulent regime the flaming reactor diameter at the widest place was chosen such that the Reynolds number for this zone was 44000-50000, and the energy of the heat flux in the core of the flame was 1400-1700 $kW \cdot m^{-3}$. The temperature in the core of the flame reaches 2773 K at this energy, and the local flow velocity is accelerated almost to the sound speed. However, outside the core of the flame on the distance from the axis equal to two diameters of the burner nozzle, the flow reaction velocity decreases in 4-5 times, and the temperature of the flame reduces to 1400-1600 K due to leak of air. Significant gradient of speed change and temperature of the cross section of the flame results in the formation on the surface of its core a cascade of toroid-like vortices that break down into smaller cylindrical ones with virtually no energy loss. The process of such successive bifurcations stops when the forces of molecular viscosity in media are beginning to affect the structure of small-scale vortices and their energy is converted into heat.

Thus, smaller "tornado" vortices formed from toroid-like ones are oriented in the direction of flow, straightened, and involve in their volume $SiO_2$ primary particles and submitted to the zone of lower temperatures and speeds. "Tornado" vortices are enough stable and the time of their existence is sufficient for the concentration of primary particles along their axes and forming of monolithic needles as a result of sintering.

The needles formed in the flame have a diameter of 10-15 nm and their length is 1-3 microns. Small clusters of vortices are concentrated at the ends of the needles, namely in places where the entering of spherical particles into a vortices volume occurs. Synchronous process of vortices crushing and the formation in their bulk of the needle-shaped particles leads to the formation of the original product as a two-dimensional grid with rhombic windows.

The specific surface area of fumed product is 370-420 $m^2 \cdot g^{-1}$, and the contents of needle-shaped nanoparticles is 40-80 %.

The study of atomic structure of the needle-shaped $SiO_2$ particles using TEM and IR-spectroscopy allowed to find out that short openly branched chain clusters of 0.6-2.4 nm in length are the structural motifs of silica. Two $SiO_4$ tetrahedrons, with tops directed alternately down and up and connected to each other via a common oxygen atom, are in a one repetitive fragment of chain cluster. Intertetrahedral SiOSi angle along the chain is close to 180°. Due to the short length and spatial off-orientation of chain clusters needle-shaped particles are amorphous.

# The Film Materials of Sensor Technique: Solid Solutions, Eutectics, Pseudoalloys

Protsenko I.Yu., Odnodvorets L.V., Shumakova M.O., Tkach O.P.

*Sumy State University, Sumy, Ukraine, i.protsenko@aph.sumdu.edu.ua*

Classification film materials in terms of their relationship structural phase state and electrical and magnetoresistive properties was performed. The classification assigned degree of mutual solubility of atoms in the two-component film systems received simultaneous condensation or layers of multilayer films with subsequent heat treatment to 900 K. The comprehensive research of crystal structure, thermal and magnetoresistive properties can offer the following classification of film materials.

1. ***Solid solutions with unlimited solubility component:*** film materials based on Fe and Cr; Cu and Co; Fe and Pd or Pt; Co and Pd or Pt. In [1] presented some results of research of electro- and magnetoresistive properties of these films.

2. ***Eutectic based non-annealed film materials with limited solubility***, film materials based on Ag or Au and Co or Fe; Co and Cr. Since the films solubility component has a higher value compared with bulk samples, we implemented a stabilization granular alloys [2] in individual crystallites eutectic, as there may be excess concentration of atomic magnetic components. It must be emphasized that the granular state (correct to call it quasigranulare) can be realized not mentioned in "classic" version, and by condensation of magnetic metal island films between the lower and upper layers of nonmagnetic metal. An example of such a film structure can be Pd (Pt) / island film Fe (Co) / Pd (Pt), in which we observed the effect of GMR.

3. ***Annealing film systems with limited solubility components and granulated condition***: film materials based on Ag or Au and Co or Fe; Co and Cr; systems of this type should be classified as quasieutectic.

We analyze the possible use of considered film materials as sensitive elements of the spin-valve structures and temperature, pressure, strain and magnetic field sensors.

1. D.M. Kondrakhova, Yu. M. Shabel'nyk, O.V.Synashenko, I.Yu.Protsenko // *Uspehi Fiziki Metallov*, **13**, № 3, pp. 241 – 268 (2012).
2. I.Yu.Protsenko, I.V.Cheshko, L.V.Odnodvorets, D.M.Kondrakhova, O.V.Pylypenko, Yu.M.Shabel'nyk, O.V.Vlasenko // *Uspehi Fiziki Metallov*, 14, № 3, pp. 229 – 258 (2012).

# Si and GaAs Nanostructures as Chemical Sensors

Ptashchenko O.O.[1], Ptashchenko F.O.[2]

[1]*Odessa National I. I. Mechnikov University, Odessa, Ukraine*
[2]*Odessa National Maritime Academy, Odessa, Ukraine*

Si and GaAs nanostructures are perspective as chemical sensors. The porSi films with a broad size distribution ranging between 4 and 12 nm, are extensively studied during last decade as gas sensors [1]. The structures (□ 60 μ thick) were prepared by anodisation of boron-doped p-type substrates in HF containing solutions. The internal surface of pores was passivated due to nearly complete covering by hydrogen (Si–$H_x$ groups). This technology provides a porosity $P$□ 60% and specific surface area up to 600 $m^2$ $g^{-1}$. At low distance between pores, charged surface traps, particularly $P_b$ centers, block the conduction pathways by coulomb repulsion and cause a high resistivity of porSi. In an approximation of a regular cylindrical pores arrangement, the minimum density of ionized donor surface centers for coulomb blockade is defined by

$$N^{+}_{S\min} = d_P\left[(d_A / d_p)^2 - 1\right] / 2 \times N_A, \qquad (1)$$

where $d_P$ is the pore diameter; $d_A$ denotes the distance between the pores axes; $N_A$ is the bulk acceptor concentration. At $P$=60%, the pores diameter $d_P = 5$ nm and the bulk acceptor concentration $N_A = 1 \cdot 10^{18}$ $cm^{-3}$, the minimum surface centers density in pores, as required for coulomb blockade, amounts $N_S^{\min} = 0,78 \cdot 10^{11}$ $cm^{-2}$.

In real porSi films, there remain some paths for the *p*-current. In $NO_2$ (acceptor like) vapors, the record threshold concentration to be detected was 15 ppb [2]. However, in wet $NH_3$ (donor like) vapors the current non-monotonously depends on the ammonia partial pressure with a minimum at □ 5 Pa [1]. Therefore the minimum explicitly measured $NH_3$ molecules concentration is 300 ppm. The sensitivity to wet $NH_3$ vapors amounts up to 30 μA/kPa.

The Si nanowires (SiNWs) with diameters of 50–250 nm, formed with metal-assisted etching of intrinsic Si(111) wafers in HF containing solutions, were extensively studied as chemical sensors [3]. *P*-type conduction of SiNWs was consistently increased in acidic gases ($CO_2$, $SO_2$, $Cl_2$, $NO_2$, and HCl), acid vapors ($H_3PO_4$, HCl, $H_2SO_4$, and HF), or weakly acidic organic solutions (alcohol or acetone), whereas p-type conduction of SiNWs was consistently decreased after purging the acid vapor by dry neutral gas of $O_2$, Ar, or $N_2$. In $NH_3$ vapors (basic atmosprere), the conductivity non-monotonously dependends on the ammonia partial pressure, having a minimum at □ 70 Pa. Therefore the minimum explicitly measured $NH_3$ molecules concentration is □ 2000 ppm.

The minimum surface centers density on SiNW, as required for coulomb blocade, is given by

$$N^{+}_{S\min} = 0,25dN_A, \quad (2)$$

where $d$ is the SiNW diameter. At $d = 150$ nm; $N_A = 1 \cdot 10^{18}$ cm$^{-3}$, we obtain $N^{+}_{S\min} = 3,8 \cdot 10^{12}$ cm$^{-2}$, which is much higher than in porSi.

Thus, the porSi sensors have a very high gas sensitivity, however SiNWs are much lower in dimensions. And the processes, which cause the gas sensitivity of the porSi- and SiNWs structures, are similar to ones in *p-n* junctions [4]. The reverse current of the Si- and GaAs *p-n* junctions can be of $10^{-10}$–$10^{-11}$ A. This enables low threshold concentrations of vapors to be detected. The minimum surface centers density in the *p-n* junction, as required for the midgap Fermi level locking, is given by

$$N^{+}_{s\min} = \sqrt{\varepsilon_S E_g / q^2 N_A}, \quad (3)$$

where $\varepsilon_S$ is the dielectric constant of the semiconductor; $E_g$ denotes the band gap; $q$ is the elemental charge. At $\varepsilon_S = \varepsilon_0 \varepsilon = 1,04 \cdot 10^{-12}$ F/cm; *Eg*=1,12 eV; $N_A = 1 \cdot 10^{18}$cm$^{-3}$ we obtain $N^{+}_{S\min} = 1,9 \cdot 10^{12}$ cm$^{-2}$, which is between the corresponding values for porSi and SiNWs. The threshold $NH_3$ concentration for Si- and GaAs *p-n* sensors is of □ 10 ppm and 1 ppm, respectively, which is better than for porSi and SiNWs.

The main unsolved problem for all three chemical sensor types is the parameters instability, caused, particularly, by the surface oxidation. And the main direction for the enhancement of their sensitivity and stability is an appropriate surface doping.


1. Boarino L., Borini S., Amato G. Electrical properties of mesoporous silicon: from a surface effect to coulomb blockade and more // J. Electrochem. Soc. – 2009. – V. 156, No. 12. – P. K223–K226.
2. Pancheri L., Oton C. J., Gaburro Z. et al. Very sensitive porous silicon $NO_2$ sensor // Sensors and actuators B. – 2003. – V. 89. – P. 237–239.
3. Yuan G. D., Zhou Y. B., Guo C. S. et al. Tunable electrical properties of silicon nanowires via surface-ambient chemistry // ACSNANO. – 2010.– V. 4, No. 6. – P. 3045–3052.
4. Ptashchenko O. O., Ptashchenko F. O., Yemets O. V. Effect of ammonia vapors on the surface current in silicon p-n junctions. // Photoelectronics. – 2006. – No. 16. – P. 89 – 93.

# Schottky Photosesors on High Radiation Resistivity Semiconductors

Rarenko I.M.[1], Korbutyak D.V.[2], Klad'ko V.P.[2], Panchuk O.E.[1], Fochuk P.M.[1], Sklyarchuk O.F.[1], Zakharuk Z.I.[1], Dremlyuzhenko S.G.[1], Rarenko A.I.[1], Galochkin A.V.[1], Shafranyuk V.P.[1]

[1]*Chernivtsy National University*
[2]*V.E. Lashkaryov Institute of Semiconductor Physics NASU, Kiev, Ukraine*

Semiconductor $Hg_3In_2Te_6$ crystals and their analogous are solid solutions of $In_2Te_3$ and HgTe. $Hg_3In_2Te_6$ crystals are congruently melted as chemical compound. Like $In_2Te_3$ the $Hg_3In_2Te_6$ crystal has cubic crystal lattice with stoichiometric vacancies in their crystal structure. The electroconductivity, photoconductivity, mechanical, chemical properties of the crystals do not deteriorate after their irradiation by γ-photons with energies up to 1 MeV and doses up to $10^{18}$ $cm^{-2}$, by electrons with energies up to 300 MeV and doses up to $10^{19}$ $cm^{-2}$ and by mixed reactor irradiation (filtered slow neutrons) with doses up to $10^{19}$ $cm^{-2}$. This feature is determined by high concentration (~$5\cdot10^{21}$ $cm^{-3}$) of stoihiometric vacancies ($V_s$) in crystal structure, where every third In-cation node is empty. These $V_s$ are electroneutral, they capture all impurity atoms in these crystals and kept them in electroneutral state too. On the other hand, this feature does not allow forming direct p-n junctions in these crystals by introducing the impurities. However, we have developed p-n junction analogues in form of Schottky diodes and corresponding photodiodes with semitransparent metal layer on single crystal $Hg_3In_2Te_6$ substrate that allows irradiation to get into active region preserving this way all the advantages compared to p-n junction.

We have synthesized $Hg_3In_2Te_6$ single crystals and their more wide-gap analogues $Hg_2CdInGaTe_6$, $Hg_2MnInGaTe_6$ for Shottky diodes and photodiodes preparation.

Schottky diodes were fabricated using vacuum thermal or magnetron sputtering of semi-transparent nickel films of 200 Å thickness or $In_2O_3SnO$ films of 1000 Å thickness on the n-type substrates made of all the investigated crystals. The bottom ohmic contact was manufactured by indium fusing.

Comparison of I–V characteristics of Ni – $Hg_3In_2Te_6$ diode: measured (circles) and calculated according to the generation-recombination Sah–Noyce–Shockley theory (solid line). The dashed line shows the calculation results according to the thermionic theory (fig.1).

Schottky photodiodes based on these wide-gap semiconductors are designed for the detectors of near-infrared, visible (fig.2) and ionizing radiation emission, which do not require additional cooling. The latter is associated with a weak dependence of their photosensitivity on temperature.

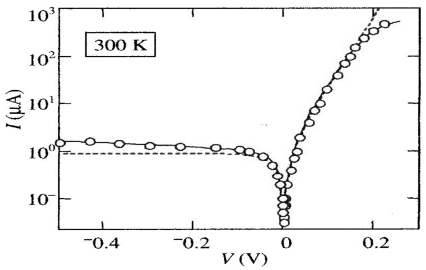


Fig.1

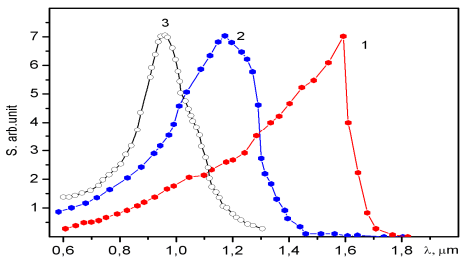


Fig.2

# Type-II Superlattice HOT Infrared Photodetectors

Rogalski A.

*Military University of Technology, Institute of Applied Physics, Warsaw, Poland*

Recently, a new strategy to achieve high-operating temperature (HOT) infrared photodetectors including barrier and cascade devices has been observed. Another method to reduce dark current is related to the limitation of the volume of detector material via a concept of a photon-trapping detector.

The paper presents approaches, materials, and device structures of the new types of infrared detectors. The intent is to concentrate on device approaches that are having the most impact today in the main stream of infrared detector technologies. A secondary aim is to outline the evolution of detector technologies showing why certain device designs and architecture have emerged as more useful today also as alternative technologies competitive to HgCdTe ternary alloy.

The performance of an innovative HOT detector designing so-called interband (IB) cascade type-II InAs/GaSb superlattice detectors is presented. Detailed analysis of the detector's performance (such as dark current, *RA* product, current responsivity, and response time) versus bias voltage and operating temperatures (220 to 400 K) is performed, pointing out the optimal working conditions.

The performance of nBn detector and cascade detector is compared with HgCdTe HOT detectors. At the present stage of technology, the experimentally measured $R_0A$ values of the IB cascade type-II superlattice detectors at room temperature are higher than those predicted for HgCdTe photodiodes. It is shown that these HOT detectors have emerged as the competitors of HgCdTe photodetectors.

# Optical and electrical properties of Al-doped ZnO films deposited by ALD process on Si and glass substrate

Romanyuk V.[1], Dmytruk N.[1], Kondratenko O., Taborska M.[1],
Lashkarev G.[2], Karpyna V.[2], Popovych V.[2], Dranchuk M.[2],
Dovbeshko G.[3], Dmytruk I.[3], PietruszkaR.[4], Godlewski M.[4]

[1]*Institute of Semiconductor Physics, NASU, prosp. Nauky 45, Kyiv, Ukraine;*
[2]*Institute for Problems of Material Science, NASU, ul. Krzhizhanovskogo 3, Kyiv, Ukraine;*
[3]*Institute of Physics, NASU, prosp. Nauky 46, Kyiv, Ukraine;*
[4]*Institute of Physics, PAN, al. Lotnikow 32/46, Warsaw, Poland*

Today transparent conductive oxides (TCO) are materials of a great importance for development "transparent electronics" and photovoltaics, irreplaceable for flat panel displays and thin film solar cells. Zinc oxide doped with III-group elements is one of extensively studied nonexpensive TCO materials for indium-tin-oxide (ITO) substitution. Though electrical and optical properties of weakly doped ZnO films are widely known, it is of interest to determine optical constants ***n*** and ***k*** as well as optical mobility, plasma frequency and effective mass for highly doped ZnO:Al films from measurements of reflectance in visible and near IR wavelength range accompanied with electrical measurements.

Al-doped ZnO films with Al content from 0.5 to 7 at.% and thicknesses in the range 260-420 nm were deposited by ALD process. Accordingly to Hall effect measurements the carrier concentration, mobility and resistivity were in the range $(0.9\text{-}4)10^{20}$ cm$^{-3}$, 16-6 cm$^2$/V·s, $(4.2\text{-}2.5)10^{-3}$ Ohm·cm, respectively. Measurements of reflectance in visible range were carried out at various incidence angles (10, 30, 50, 70°) by using p-polarized light what allow us to determine more carefully ***n***, ***k*** and thickness of films from fitting interference curves. The two models of Cauchy and Drude-Lorentz were used. At increasing aluminium content in ZnO film optical constant ***k*** also increases testifying to an absorption by free electrons at wavelength greater than 800 nm. IR reflectance spectra were measured in the range 1.6-25 μm with Fourier-transform spectrometer Bruker IFS-66. Fitting of these spectra allow us to estimate plasma frequency $\omega_p$ and damping constant $\gamma_p$ which describe relaxation processes related to optical mobility (or in-grain mobility). At increasing carrier concentration $\omega_p$ increases from 2380 cm$^{-1}$ for ZnO with 0.5 at.% of Al to 4985 cm$^{-1}$ for ZnO with 7 at.% of Al. At the same time $\gamma_p$ also increases from 995 to 1900 cm$^{-1}$. Using the Hall concentration we determined electron effective mass ***m****. In our films it grows from $0.29m_0$ to $0.5m_0$ with increasing of Al content. Optical mobility estimated from $\mu=e/\boldsymbol{\gamma_p m^*}$ was in the range 25-10 cm$^2$/V·s. It was found that optical mobility is larger than Hall mobility. The estimated contribution of grain boundaries scattering into electron mobility is about 60%.

For ZnO films with 5 and 7 at.% of Al we observed in IR spectra the band at 12-16 μm that can be related to Al-O phonon modes. PL measurements carried out at room temperature ($\lambda_{exc}$=266 nm) demonstrate one emission peak at 376-379 nm and two ones in visible range at 560 and 700 nm. At increasing Al content in ZnO films UV near band edge emission line drastically diminishes, red line diminishes as well. So we observe passivation of some extrinsic defects localized on film surface.

In accordance with optical investigations we can see the decrease of mobility and increase of electron effective mass at increasing Al content. The primary scattering mechanism is the scattering on grain boundaries. So, it is necessary to find out technological parameters and post-growing treatment for a reduction this process.

**Acknowledgements**

This work was partially supported by the National Science Centre (decision No. DEC-2012/06/A/ST7/00398).

# Nanocomposites in As-Sb-S-I System

Rubish V.M., Rigan M.Yu., Gasynets S.M., Kyrylenko V.K.,
Perevuznyk V.P., Shtets P.P.

*Uzhgorod Scientific-Technological Center of the Institute for Information Recording, NASU, Uzhgorod Ukraine*

In this report we present results of investigation of structure, physical parameters of $(As_2S_3)_{100-x}(SbSI)_x$ and $(Sb_2S_3)_{100-x}(AsSI)_x$ glasses and amorphous films and conditions of forming nanosized ferroelectric crystalline inclusions in their matrix.

Investigations of X-ray diffraction patterns of glassy, crystallized and crystalline materials were carried out on «ДРОН-3» X-ray apparatus (λ=1.5418 Å). Raman spectra were recorded using a ДФС-24 spectrometer on the λ=630 nm.

Nanoheterogeneous structure of $(As_2S_3)_{100-x}(SbSI)_x$ and $(Sb_2S_3)_{100-x}(AsSI)_x$ glasses and films established on the basis of Raman spectra investigations. It is shown that the glass matrix is formed by only binary structural groups with heteropolar bonds ($SbS_3$, $AsS_3$, $SbI_3$, $AsI_3$) and contains small amount molecular fragments with homopolar bonds (for example, As-As, S-S). Chain molecular associates $(SbI_3)_m$ and $(AsI_3)_n$ of different length can be formed in their matrix in case of considerable content of iodide in the composition of glasses or films.

The analysis of X-ray diffraction patterns and Raman spectra showed that crystalline SbSI inclusions are being formed in amorphous matrix at crystallization of $(As_2S_3)_{100-x}(SbSI)_x$ and $(Sb_2S_3)_{100-x}(AsSI)_x$ glasses. The forming of SbSI nanocrystals and their growth is taking place in the range of temperatures $T_g$-$T_c$ ($T_g$ and $T_c$ are temperatures of glassforming and crystallization) and are being accompanied by anomalies on temperature dependences of dielectric parameters (ε′ and ε′′). Glass crystallization is accompanied by a sharp increase of ε′ and ε′′.

Reflexes coinciding with diffraction lines for polycrystalline antimony sulphoiodide appear on X-ray diffraction patterns of crystallized glasses and their Raman spectra contain sharp bands at 107-110, 138-140 and 316-320 $cm^{-1}$.

The influence of annealing heat and time regimes on the structure of obtained composites has been studied. It is shown that with annealing temperature and time raising, the intensity of bands in Raman spectra and reflexes on X-ray diffraction patterns is growing while their half-width is decreasing. It testifies to growing of dimensions of crystalline inclusions in glassy matrix.

The mechanism of forming of nanosized crystalline SbSI inclusions in matrix of $(As_2S_3)_{100-x}(SbSI)_x$ and $(Sb_2S_3)_{100-x}(AsSI)_x$ glasses has been suggested. The effect of annealing regimes on dielectric properties of ferroelectric glassceramics is discussed.

# The Dependence of Material Atomization Degree, with Respect to Laser Source Parameters

Schukin S.O.[1], Nosov O.V., Zabello E.I., Batrak P.O.[2]

[1]*The National Technical University of Ukraine "Kyiv Polytechnic Institute", Kyiv, Ukraine*
[2]*International Center "Institute of Applied Optics", Nat. Acad. Sci. of Ukraine, Kyiv, Ukraine*

One of the techniques of deposition thin films is a pulsed laser deposition (PLD), which is characterized by simplicity, high efficiency and adaptability, purity and quality of the obtained films. The initial stage of laser deposition is a process of atomization, which is based on processes of thermalization laser pulse energy and heating material to temperatures close to the boiling point, that provided intense evaporation material. The formation of laser plasma is accompanied by processes which affect the quality of the film, it is the presence finely-dispersed phase of laser erosion and tough, deep character damage of material surface, this leads to inhomogeneity obtained films and spatial instability of the laser plasma plume. In order to reduce their impact was applied advanced techniques and equipments such as mechanical seperators, scheme of crossed beams, and etc.

According to our and other researches, the foregoing disadvantages can be eliminated in the implementation of certain requirements to parameters of laser source, which include pulse duration, pulse energy and pulse repetition rate, and the state of the surrounding atmosphere [1-3]. Depending from these parameters changes the concentration of vapor matter, atomic ratio and finely dispersed phase of ejected material. It was shown that using of multi-pulse mode of influence on material for laser emission analys leads to an increase of atomization of matter. As initial process of atomization is common for emission analysis and deposition, we should expect a similar effect for PLD.

In the report will be presented summarizes the results of this approach for the deposition of thin films.

1. Anokhov S., Berezhnoy E., Zabello E., Nosov. O. Spatial and spectral structure of a plasma plume induced by the multipulse laser evaporation of the material// Optics. Quantum electronics. Holography. ISSN 0503-1265. Ukr. J. Phys. V. 49? 2004, N 8, p. 763-765
2. Bukharov A. Y., Pershin S.M., Krivitskaya N.N., Orlov R. Yu. // Zh. Prikl. Spektr. - 1991. - 54, N 6. - P. 1011-1115
3. Zabello E., Syaber V., Khizhnyak A.. Influence of temporal parameters of laser irradiation on emission spectra of the evaporated material. // Semiconductor Physics, Quantum Electronics & Optoelectronics vol. 2, №1 (1999), p.142-146
4. Сухов Л. Т. Лазерный спектральный анализ (Физические принципы).// Новосибирск: Наука, 1990- 143 с.

# The Effect of Endless Activation on the Specific Characteristics of Nanoporous carbon Materials for Supercapasitors

Semenchuk I.I.

*Frantsevich Institute for Problems of Materials Science, NAS of Ukraine, Chernivtsi Department, Chernivtsi*

The important factors, that to determined use nanoporous carbon as component electrodes of supercapacitors (SC) is high specific capacity material and high electrical conductivity.

The effort to improve the specific capacity of nanoporous carbon by on-stage technology activation at high temperature was led.

The base material was feedstock of plant origin, which was subjected to carbonization at 650 $^{o}$C for 1 hour herein after. Then carbonated material was placed in an water solution of 30% KOH in 1:1 ratio. After that was on-stage process activation. Activation of the received carbon material was carried out in 3 stages.

In the first stage of activation carbonated material was mixed with 30% KOH water solution and was subjected to thermal treatment at 850 $^{o}$C with constant vacuum pumping (1-2·10$^{-1}$ mmHg) during 40 minutes.

As can be seen from the figure, on the current-voltage characteristics of the SC is not observed wale-like emission, that indicating a lack of electrode material impurities, and no peaks as in positive and in negative polarization indicates that in the SC during the charge-discharge does not occur Faraday's processes.

The three-time activation in an alkaline medium leads to increase of capacity by 35-40% was established.

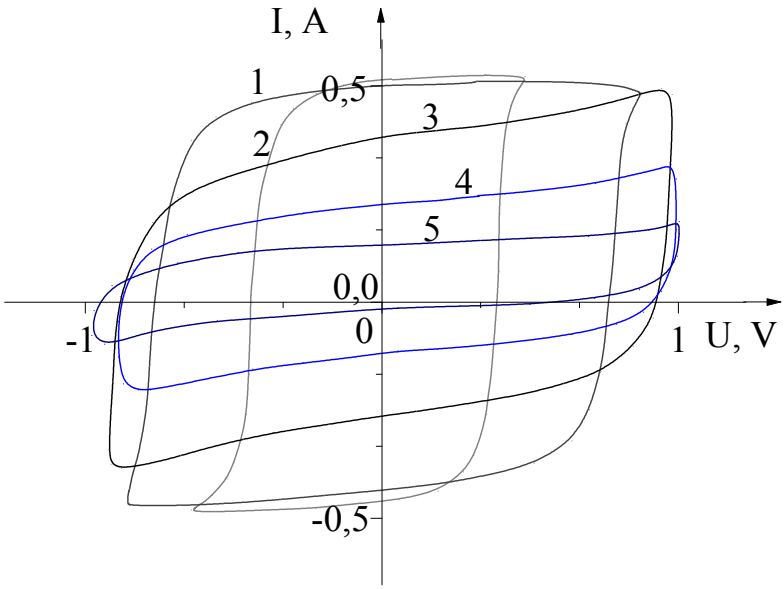


Fig. Cyclic I-V of activated carbon electrodes at:1 – 2 mV/s; 2 – 5 mV/s; 3 – 10 mV/s; 4 – 20 mV/s; 5 – 50 mV/s.

1. Kovalyuk Z.D., Yurtsenyuk S.P., Buharov V.A., Savchuk A.I. New electrode materials for supercapacitors//E-MRS IUMRS ICEM 2006 Spring Meeting (Nice, France). – 2006.

# The Melting and Solidification Loops of Cu-Ni Nanoparticle

Shirinyan A.S.[1], Wilde G.[2], Makara V.A.[1,3], Bilogorodskyy Y.S.[4], Komisarenko O.S.[3]

[1] *"Physical-chemical materials science" center of National Academy of Sciences of Ukraine and Kiev Taras Shevchenko National University, Kyiv, Ukraine*
[2] *Institut für Materialphysik, Westfälische Wilhelms-Universität Münster, Münster, Germany*
[3] *Kiev Taras Shevchenko National University, Kyiv, Ukraine*
[4] *Cherkasy regional ecological-naturalistic center, Minor Academy of Sciences, Cherkasy, Ukraine*

For the first time we calculate and present for individual Cu-Ni nanoparticle the nanomelting and nanosolidification loops at different nanometric sizes at temperature-composition phase diagram. Equilibrium states in two-phase region are investigated from 1000 K up to 1700 K. The limit amount of matter and surface-induced size effects can change the thermodynamics of first order phase transformation so that there are appearance of hysteresis in a form of nonsymmetry for forth and back transforming paths, the existence of compositional splitting and of the loops-like splitted path on the size dependent temperature-composition phase diagram, the difference between the size-dependent phase diagram and solubility diagram, between two-phase equilibrium curves and solubility curves, also intersection of nanoliquidus and nanosolidus. These findings lead to the necessity to reconsider such basic concepts in materials science as phase diagram and solubility diagram.

The work have been done in the framework of German-Ukraine collaboration Project (DAAD reference code A/14/02389).

# Intercalated stage-ordered layered structures in the framework of the periodic Anderson model

Stasyuk I.V., Velychko O.V.

*Institute for Condensed Matter Physics of the National Academy of Sciences of Ukraine, Lviv, Ukraine*

The periodic Anderson model is used for investigation of influence of intercalated particles on the electronic band structure of layered nanohybrid compound with stage ordering (three layers in the packet in the considered case) of the GaSe-type. Such compounds are considered as perspective materials for high-capacity secondary cells and supercapacitors.

Changes in the electron spectrum which is split compared to the standard Fivaz dispersion law due to intercalation (see Fig. 1) look like appearance of impurity branch (more strictly, a group of three branches for the case of three layers in the packet). This additional band can transform into the impurity level (being far away from the main band) or widen and hybridize with the main band.

More complete description of the spectrum transformation due to intercalation is given by the density of electronic states (see Fig. 1). A typical picture shows appearance of the narrow impurity bands near the bottom of the conduction band. The most pronounced transformation of the latter takes place in the vicinity of the impurity band while the rest remains practically intact. One can use the obtained results analysing the measured dynamical response and impedance spectra of stage-ordered compounds.

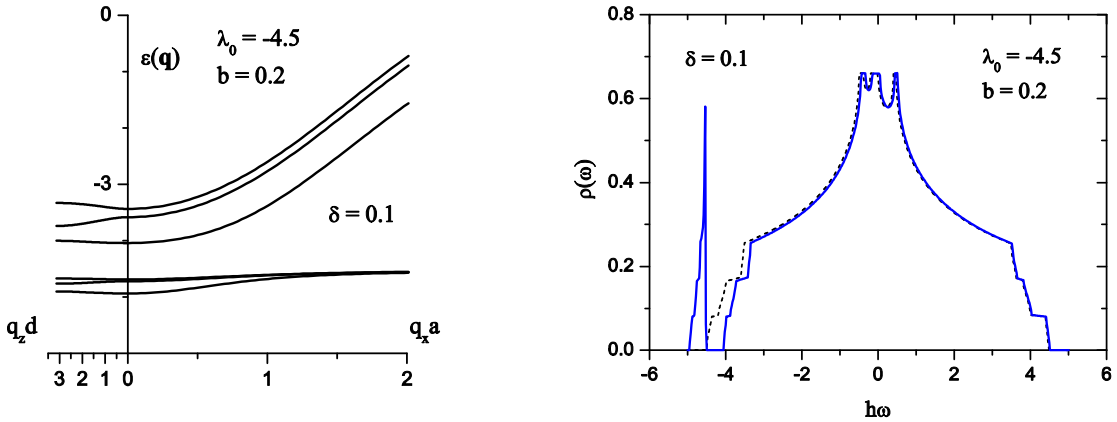


Fig. 1. Electron spectrum (left) and the respective density of states (right) transformed by intercalation. The dashed line (right) corresponds to the pure matrix. Energetic quantities (energy splitting δ in packet, hybridization parameter $V$ ($b = |V|^2$), intrapacket ($t$ = 0.3) and interpacket ($t'$ = 0.1) transfer parameters, etc) are given in the units of transverse intralayer transfer constant.

# Quantum and Classical Size Effect in "Quench Condensed" Ultrathin Metal Films

Stasyuk Z.V., Bihun R.I.

*Ivan Franco Lviv national university, Lviv, Ukraine.*

Thin layers of substance are basic elements of many devices of modern electronic techniques. The further development of electronics is impossible without microminiaturisation of electronic systems by nanotechnology, in particular, by techniques of electrically stable ultrathin-thickness covering formation. Properties of ultrathin slabs can essentially differ from properties concerning thick layers which are used in nowadays engineering. This difference first of all is caused by prevailing influence of the surface phenomena on ultrathin layer structure and electric parameters.

The current theoretical and experimental researches on electron charge transport in ultrathin (layer thickness are 2-10 nm) electrically continuous metal films (temperature coefficient of resistance $\beta > 0$) under the condition of inequality realization $d < l$ were analysed and reviewed. Here $d$ is the film thickness, $l$ is the charge mean free path. The peculiarities of film structure are meant as crystal lattice parametres and the crystalline average linear sizes.

The fabrication of ultrathin electrically continuous metal film on dielectric substrate surface is a problem of considerable difficulty due to the action of surface tension forces. These phenomena lead to coalescence of metal particles. As a result there is some critical thickness layer $d_c$ at which current starts to flows (*percolation threshold* is observed here). The technological features of film formation (the speed of material condensation, the substrate temperature at layer deposition, the modes of further heat treatment) defines the average of $d_c$ as well as the properties of condensate material, in particular fusion temperature. Essential decrease $d_c$ may be reached at epitaxial growth of metal film on the oriented substrate. The other effective way of $d_c$ decreasing is preliminary deposition of surfactant underlayers of superficially active substances of a subatom thickness on dielectric substrate or so called "quench condensed" method wich prevent coalescence in metal condensates. This technique allowed the formation of ultrathin conductive coverings. In particular, the Hall voltage investigation on 1-3 nm thicknees chrome films deposited on surfactant germanium underlayer was performed in [1]. The electron transport phenomena are essentially influenced by electron scattering on film surface when the mean free path of electron becomes commensurable to the thickness of a metal film $d$. Thus the contribution of surface scattering in the total electron relaxation time is close to the contribution of bulk scattering. The thickness dependence of kinetic parameters of electrically continuous metal films is described within the framework of the classical and internal size effect theories [2].

With further reduction of metal layer thickness when the electron mean free path satisfies the condition $d < l$, the quasiballistic electron transport in a film (without changes of the power spectrum of electron in metal film) is presented. Thus charge carriers surface scattering in metal film becomes dominating. The contribution of surface scattering has essentially influenced the macroscopic surface inhomogeneity because the mean linear grain sizes are commensurable to film thickness. The

quasiballistic electron transport in metal films can be described by size dependencies of kinetic coefficients proposed in Namba and Wissman theories [2]. The treatment of experimental data by the mentioned theories allows the reliable calculation of the average amplitude of one-dimentional surface asperity $h$. The calculated values $h$ well coordinate with experimental data of direct STM and AFM investigation.

When the film thickness does not exceed 5 - 8 nm the quantum effects which have influence on electron transport in film are possible. Quantum size effects are most brightly displayed in semimetal films. An electron de-Brogle wave length in these materials in 10 times exceeds interatomic distances and consequently the interference of electronic waves is influenced poorly by imperfections of film surface. In metal films the situation is essentially different as a de-Brogle electron wave length is commensurable to interatomic distances. Therefore, to observe oscillation of the kinetic coefficients in thin metals layers it is necessary to provide high perfection surface structure. In the quantum electron transport range of films thickness the laws of residual conductivity size dependensis $\sigma_{res}=1/[\rho(d)-\rho_{\infty}]$ takes place. The theoretical expressions are most convenient for direct experimental comparison with theoretical data has been received by Fishman and Calecki [3]. Modern theoretical approaches of quantum size effect in kinetic phenomena of metal films are based on assumption that the metal sample electronic structure is the same as in bulk materials. Quantum size effect in metal film is a consequence of electron system size limitation along Z axis in thin film thickness direction. That is why we developed one dimension model of metal films conductivity in Boltzmann approach for quantum electron transport. The fluctuation of film boundary has dramatic influents on electron spectra. It changes electron scattering under quantum size effect. In the frame work of developed model size dependences of metal films conductivity were calculated. The developed model was used for quantitative description of the experimental data of monocrystalline $CoSi_2$ films and fine-grained gold metal films. In the film thickness ranges of the quantum electron transport and transition to the semiclassical electron transport the comparison of calculations results of metal film size dependences conductivity were compared for our model with others theoretical approaches. The developed quantum model of charge transport in films with metallic conductivity can more successfully describe the transition from purely quantum to semiclassical charge transport in comparison to modern quantum theories [4]. This was possible because the proposed model considers the perturbation energy states in the whole volume of the film due to the existence of macroscopic inhomogeneities on the metal film surface. Perturbation calculated in the linear approximation with assumption that $\Delta h$ is $d$ independent.

1. Schroder K., Zhang L. Phys. Stat. Sol. B.- 1994.- Vol.183.- P.k5-k8.
2. Bihun R. I.., Buchkovska M. D., Koltun N. S., Stasyuk Z. V, Leonov D. S. Metallofizika i noveishie tekhnologii.– 2013.– V.35, № 12.– P. 1659-1674.
3. Calecki D., Fishman G., Phys.Rev.Lett.–1989.– Vol. 62.– P. 1302-1305.
4. Bihun R.I., Stasyuk Z.V. Metallofizika i noveishie tekhnologii.– 2014.– V.36, № 6.– P. 723 –734.

# Frequency limits for graphene conducting channel, imposed by quantum capacitance and kinetic inductance

Strikha M.V.

*V.Lashkaroiv Institute of Semiconductor Physics, Kyiv, Ukraine*

Dynamic conductance of quantum nano-scale conductors is an important problem of nanoelectronics theory [1]. Generally, electrostatic capacitance of the system "graphene strip – substrate – gate" plays a crucial role in grapheme physics, being responsible for the "gate doping" of graphene with electrons or holes [2]. However, later we examine the case of mono- and multilayer graphene dynamic conductivity in drain – source circuit, without gate doping, with gate not being included into such circuit. As it was demonstrated in [3], additional quantum capacitance and kinetic inductance arise for such a circuit a result of a correct solution of Boltzmann transport equation. Therefore equivalent circuit for the long strip of graphene can be presented as a combination of quantum capacitance $C$, and kinetic inductance $L$ (see Fig.1).

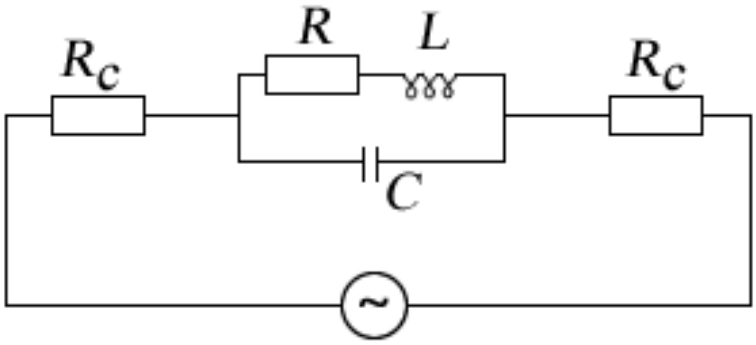


Fig.1. Equivalent circuit for a strip of graphene. $R$ – graphene strip resistivity, $R_C$ – contacts resistivity.

The quantum capacitance of the graphene strip can be presented [3] as:

$$C = e^2 \sum_{m,k} \left( -\frac{\partial f_o}{\partial E} \right) \tag{1}$$

Here $e$ is a charge of electron, $f_o$ is equilibrium distribution function, $E$ is energy. Summation in (1) is carried over all the sub-bands $m$, and wave-vectors $\boldsymbol{k}$ in $xy$ plane.

Kinetic inductance is introduced as:

$$\frac{1}{L} = \frac{e^2}{l^2} \sum_{m,k} v^2 \left( -\frac{\partial f_o}{\partial E} \right), \tag{2}$$

where $l$ is a strip length between the contacts, $v$ is electron speed in $x$ direction between source and drain. With allowance for the linear band spectrum of graphene

$$E = \pm \hbar v_F k, \tag{3}$$

where $v_F = 10^6$ m/s, (1) and (2) can be rewritten approximately as:

$$C \approx \frac{2e^2 Ml}{hv_F} \quad , \tag{4}$$

$$\frac{1}{L} \approx \frac{2e^2 M}{hv_F l}\left\langle v^2 \right\rangle . \tag{5}$$

Here $M$ is a total number of sub-bands, which is roughly equal to the number of electronic have-wavelengths which fit in the graphene strip cross-section in $yz$ plane (across the current), <…> means average for electron drift in $x$ direction (along the current).

The impedance of the circuit, presented in Fig.1, is given by:

$$Z = 2R_c + \frac{R(1-\varpi^2 LC) + \varpi^2 RLC}{(1-\varpi^2 LC)^2 + (\varpi RC)^2} + i\frac{\varpi L(1-\varpi^2 LC) - \omega R^2 C}{(1-\varpi^2 LC)^2 + (\varpi RC)^2} \tag{6}$$

For ω = 0 (6) obviously yields:

$$Z = 2R_c + R . \tag{7}$$

However, with the increase of the applied field frequency, the resonance occurs at $\omega_r$ frequency when the imaginary part in (6) is zero and the resistivity of the circuit reaches maximum:

$$\varpi_r = \varpi_o \sqrt{1 - \frac{R^2 C}{L}}; \varpi_o = \frac{1}{\sqrt{LC}} \tag{8}$$

With allowance for (4), (5) one can see, that $\varpi_r \approx \varpi_c$ in the case, when $\left\langle v^2 \right\rangle / v_F^2 << 1$.

Now let us estimate the frequencies, predicted by (8). For the high quality graphene Landauer resistor [1], where electron passes from source to drain without scattering and where with allowance for (3) $\left\langle v^2 \right\rangle \approx v_F^2$, (8) yields:

$$\omega_o \sim \sqrt{\left\langle v^2 \right\rangle} / l = v_F / l . \tag{9}$$

This leads to the frequencies of GHz range for the submicron length of graphene strip between the contacts. However, in a long graphene strip of mm length order with a diffusive movement of electron from source to drain, where $\sqrt{\left\langle v^2 \right\rangle} \sim \mu \overline{E}_{sd}$, $\mu$ is electron mobility, $\overline{E}_{sd}$ is average in time electric field in source-drain circuit, one can get for $\overline{E}_{sd} \sim 10^3$ V/m and $\mu \sim 1$ m$^2$/Vs (which is a typical value for CVD graphene) the frequency of MHz order. Therefore, by varying CVD graphene strip length (in hundreds μm – mm range) and mobility (in 0.1 – 1 m$^2$/Vs range), we can fabricate filters for tens KHz – MHz range.


1. Supriyo Datta. Lessons from Nanoelectronics: A New Perspective on Transport. – Hackensack, New Jersey: World Scientific Publishing Company. – 2012. – pp. 473.
2. S. Das Sarma, Sh. Adam, E.H. Hwang, and E. Rossi, Rev. Mod. Phys. 83, 407 (2011).
3. S.Salahuddin, M.Lundstrom, S.Datta. IEEE Transactions on Electron Devices, **52**, 1734 (2005).

# New Functional Materials Based on Chalcogenide Glasses, Polymers Obtained Via Modification and Nanocomposite Techniques and Their Applications

Stronski A.[1], Achimova E.[2]

[1] *V. Lashkaryov Institute of Semiconductor Physics NAS of Ukraine, Kyiv, Ukraine*
*E-mail: paiuk@ua.fm*
[2] *Institute of Applied Physics AS of Moldova, Chisinau, Moldova*

In this work design and synthesis of new nanocomposite materials based on chalcogenide glass semiconductors (ChGS), organic polymers, together with overview of their properties and some applications are reviewed.

Influence of doping of chalcogenide glasses by transitional metals and rare-earth elements on their properties is considered. X-ray diffraction measurements confirmed the amorphous structures of chalcogenide glasses doped by transition metals and rare-earth elements. Radial distribution functions have not shown significant changes in distance for nearest neighborhood with the change of dopant concentration. Differential scanning calorimetry (DSC) measurements have shown that $T_g$ values were smaller for doped glasses as compared to undoped ones. Activation energy of glass transition was estimated with the use of Kissinger's expression. The main feature of Raman spectra under the introduction of transitional and rare-earth impurities into chalcogenide glass matrix is change of relative concentration of the main and non-stoichiometric structural elements typical for initial glasses. Luminescence of chalcogenide glasses doped by transitional metals was studied in 800-1600nm region ($T=77K, \lambda_{ex} = 514nm$). Photoluminescence appears as a broad Gaussian-shaped spectrum with peak energy $E_{PL}$ approximately at $E_{PL} \approx E_g/2$. Chalcogenide glasses modified by Yb have two bands of luminescence in near IR region (near 980 and 1060nm) with excitation on 980nm wavelength at room temperature. In this case transitions observed are characteristic for $Yb^{3+}$ ion. Pure chalcogenide glasses are diamagnetics. Introduction of transitional and rare earth impurities changes the magnetic properties of investigated chalcogenide glasses. In the fields near 5T the specific magnetic moment M(T) dependence was observed which is characteristic for paramagnetic and ferromagnetic in the paramagnetic temperature range.

Two-component nanocomposites based on ChGS and metal phtalocyanine were obtained by simultaneous condensation of two components on the surface of substrates in a vacuum. Surface morphology of the samples was investigated using AFM. In the optical absorption spectra of composites the characteristic bands of phtalocyanine are present. Comparison of Raman spectra for nanocomposite films with ChGS and Me-ChGS allows identifying main structural bounds. Metal atom can form additional coordination bonds with chalcogen of nearby ChGS matrix.

Layers of polyepoxypropilcarbazole were studied as media for holographic recording. The polymer was synthesized as the host polymer matrix, and iodoform $CHI_3$ was introduced as the photosensitizing dye. As the pure polymer material is sensitive in the UV spectral range its sensitivity should be shifted to the type of recording laser region. To shift the spectral sensitivity to the blue spectral region the sensitizing dye such as iodoform $CHI_3$ has been doped into the polymer matrix. Thin polymer films with thickness ~ 1.3 μm were prepared from homogeneous polymer

solution in toluene by spin-coating procedure using programmable spin-coater "SGS Spincoat G3P-8". To determine the film thickness in this work the MII-4 interference microscope modified by developed interferometric software OPTIC METER and AFM measurements were applied. For holographic gratings recording 473 nm 100 mW DPSS laser was used. Diffraction gratings were recorded using these films as registering media by keeping the beams ratio 1:1 and spatial frequency 1000 lines/mm. After exposure of films by interference pattern the wet chemical treatment was applied for the surface relief formation. The etching was controlled by measuring the diffraction efficiency of the gratings in transmission mode at the 633 nm wavelength within the equal time intervals. Evolution of diffraction efficiency of the gratings in dependence on recording and etching times was studied. Diffraction efficiency values of obtained gratings were about 18%.

Nanomultilayer structures based on ChGS were studied as one-step recording media. Optical constants of nanomultilayers, thickness and optical band-gap energy were obtained from transmission spectra by Swanepoel method. Optical properties of nanomultilayer structures were analyzed within the frames of single-oscillator model. Diffraction gratings were recorded using DPSS green laser (λ=532nm and power 100mW) with synchronous diffraction efficiency measurement at λ=650 nm in the first diffraction order. AFM studies of surface relief of holographic gratings with a period Λ =1μm recorded in nanomultilayers $As_2S_3$ –Se and $Ge_5As_{37}S_{58}$–Se have shown high optical quality of the obtained relief. Diffraction efficiency η values of the gratings were ~ 20-30% in transmission mode at wavelength λ = 0.65 μm. Due to the changes in transmission, reflection, and in thickness under the influence of laser irradiation, $As_2S_3$–Se and $Ge_5As_{37}S_{58}$ –Se multilayers may be used for effective amplitude-phase optical information media and surface-relief optical elements.

Different surface relief patterns were recorded by e-beam irradiation of nanomultilayer structures on the base of ChGS. Diffraction gratings with 1, 2 and 4 μm period and other surface relief's structures were recorded by e-beam exposure using scanning-electron microscope Tesla BS 300 with programmable exposure control unit. The accelerating voltage was 25 kV and the size of the electron beam at this voltage was about 300 nm.

Obtained results show that optical, thermal, luminescent and magnetic properties of chalcogenide glasses can be changed by doping them with transitional and rare-earth metals. Chalcogenide glasses can be host for rare-earth metals which provide possibility to simultaneously change both luminescent and magnetic properties of glasses. Nanomultilayer composites based on chalcogenide glasses and inorganic (chalcogenide glass) - organic (polymers, dyes) composites are perspective as recording media. Direct surface recording or recording with consequent selective etching can be realized. New functional materials based on chalcogenide glasses, polymers and produced via modification and nanocomposite techniques are perspective for the applications in optics, optoelectronics and integrated optics.

*The research was supported by the project FP–7 SECURE–R21*

*Dedicated to the 50-th anniversary of the discovery of light-sensitivity effect of thin films of chalcogenide glasses:* M. T. Kostishin, E. V. Mikhailovskaya, P. F. Romanenko, G. A. Sandul, Journ. of Applied and Scientific Photography and Cinematography (in Russian), **10** (6), (1965) 450.

# Influence of Dopants on the Formation and Photoluminescent Properties of Colloidal CdTe Nanocrystals

Tomashyk V.M., Kapush O.A., Trishchuk L.I., Tomashyk Z.F.

*V.Ye. Lashkaryov Institute of Semiconductor Physics of NAS of Ukraine, Kyiv, Ukraine*

The unique properties of nanoscale systems led to their widespread use in several fields of science and technology. Recently, considerable interest to researchers cause II-VI semiconductor. The transition of the II-VI semiconductor particles size in the nanoscale leads to the spatial limitations carriers and quantum effects manifest that are uncharacteristic for bulk samples.

There is considerable interest in colloidal semiconductor nanocrystals (NCs) as active components for the next generation of solar cells and other optoelectronic devices. Potential advantages of colloidal NCs are that they can be deposited on any surface and that the band gap of a NC can be tuned by changing the size of the particle. However, along with the benefits in the synthesis of NCs is also a problem because the organic ligands using for the solution processing of the NCs, inhibit the separation of excitons and lead to a decrease in carrier mobility in densely packed layers NC.

Specific properties of some impurities [transition and rare earth elements (REE)] can use them for qualitatively new semiconductor materials with a wide range of opportunities to use in optoelectronics. Specific properties of some impurities [transition and rare earth elements (REE)] can use them for qualitatively new semiconductor materials with a wide range of opportunities to use in optoelectronics. Features of this application are due to unusual impurity states arising from the doping of II-VI semiconductors and related with the formation of heterovalent impurity centers. The behavior of REE impurities with unfilled 4f-shell in the semiconductors has been some peculiarities, for example, a combination of low solubility and an ability of REE to perform “cleaning” of the materials in which it is possible significantly reduce the concentration of background impurities and increase the electrons mobility.

Now especially actively researches concerned the doping characteristics and optical excitation local centers in terms of quantum limits in the semiconductor structures. The nature of radiating centers and radiating characteristics of optical transitions in the structures of II-VI semiconductor compounds, especially CdTe in polymer films and dielectric matrices is studying using luminescent methods.

Doping of CdTe NCs by the ions of transition elements and REE is of great interest due to the fact that allows substantially modifying their optical and electronic properties. Effective transfer of excitation energy from NCs to local center of REE and transition elements with quasiatom structure of energy levels opens the possibility of using these structures to create light emitting systems of

new generation. However, the introduction of heterovalent impurities into NCs is very difficult task and requires modification of synthesis methods.

Doping of CdTe NCs by ions of f-group is an interesting and promising task especially because their internal atomic transitions lie in the visible and near infrared spectral regions. For example, the maximum luminescence of Er is observed at a wavelength of 1550 nm, corresponding to the second window of transparency in optical fiber transmission system. However, these transitions are forbidden by the selection rules and the intensity of these lines is very small. Therefore the introduction of ion on NC, which characterized by strong absorptive ability and at the implementation of effective energy transfer, will significantly enhance the required luminescence.

The report will consider the problem of CdTe NCs doping during their colloidal synthesis and subsequent incorporation into the solid matrixes and their special and electronic properties.

At the synthesis, the introduction of a few impurity atoms into a NC that contains only a few hundred atoms may lead to their expulsion to the surface or degrade the crystalline structure. This will inherently create a heavily doped NC under strong quantum confinement. The electronic and optical properties in such circumstances are still unresolved.

Here, we describe a simple room-temperature method for doping CdTe NCs with f-elements impurities. Colloidal synthesis of CdTe NCs was carried out by the literature procedure [1], which was modified by a number of considerable alterations. Reaction chamber used was a 500 mL reactor equipped with partitions and valves, thermometer and electromagnetic stirrer. The process of CdTe synthesis was accomplished at 20°C in argon atmosphere with the use of the following reagents: 0.1 M solution of $CdI_2$ (reagent grade), thioglycolic acid (99 %), and electrochemically prepared hydrogen telluride. Nanocrystals of CdTe were modified with thioglycolic acid, while solution pH was maintained by addition of 1 M NaOH solution. f-Elements were used as an alloying agent in the synthesis. By changing the dopants and their concentration, it is possible to achieve a very high level of the electronic properties control, including the band gap and Fermi level energy.

1. Effect of thioglycolic acid on the stability and photoluminescence properties of colloidal solutions of CdTe nanocrystals / O.A. Kapush, L.I. Trishchuk, V.N. Tomashik, Z.F. Tomashik // Inorg. Mater., 2014, Vol. 50, No. 1, pp. 13–18.

# Luminescence and photoconductivity of zinc selenide crystals, doped with transition metal elements

Vaksman Yu.F., Nitsuk Yu.A.

*I.I. Mechnikov National University, Odesa, Ukraine*

The interest in research of zinc selenide crystals doped with transition metal elements has increased considerably during the past few years. High quantum yield of emission and small Stokes losses of transition metal ions in zinc selenide allow to use these crystals as active media and passive gates for IR-lasers. The practical application of such lasers includes spectroscopy, biology, medicine, optical communications and navigation systems.

Further practical application of these crystals is limited by lack of simple and reliable technology doping by transition elements with controlled optical and photoelectric parameters, as well as the lack of information about their optical properties in the visible and near-infrared spectral region.

In this study, ZnSe: Ti, V, Cr, Fe, Co, Ni crystals obtained by diffusion doping are investigated. In the photoluminescence spectra of these crystals revealed a new series of emission lines in the visible and near-infrared spectral range. It is established that the relative luminescence intensity of the investigated crystals heavily depends on the photon energy of excitation light. As the excitation photon energy is lowered, the contribution of low energy bands to the luminescence spectrum increases. At the same time, under changes in the excitation photon energy, the position of emission peaks remains unchanged. This effect is typical of intracenter luminescence. A comparison of the photoluminescence spectra with previously studied the absorption spectra allowed to establish one correspondence between the absorption and photoluminescence lines in these crystals and determine the value of the Stokes shift.

Temperature shift of the first two high-energy photoconductivity lines correlated with a shift of the fundamental absorption edge position of the crystals. Accordingly, the depth of the ground state level of transition metal ions in ZnSe crystals is determined.

In these crystals first discovered a series of high-temperature photoconductivity lines in the visible region. These lines were observed at temperatures above 300K. The spectral position of the photoconductivity lines remains unchanged with increasing temperature and matches with the position of the previously studied lines intracenter absorption. The mechanism of high-temperature photoconductivity is proposed. It is assumed that in this case a two-step process. At first, electrons execute intracenter optical transitions from the ground state to higher excited states. Then thermally activated transitions of electrons from the levels of excited states to the conduction band occur.

# Ostwald Ripening of Nanodispersed Phases in Metal Alloys

Vengrenovich R.D.

*Yuriy Fedkovych Chernivtsi National University, Chernivtsi, Ukraine*

Recently, due to the development of nanotechnology, there are significant deviations from the classical theory of Lifshitz-Slyozov-Wagner. An example of such deviations are many experimental works in which it is shown that the experimental particle size distribution obtained by chemical methods are not described the theoretical curve Lifshitz-Slezov and is not satisfied dependency $\langle r \rangle \sim t^{1/3}$. This means that in this example the experimental studies when the synthesis of nanoparticles (NPs) is performed by chemical methods, diffusion mechanism of NPs growth does not work.

In [1] was developed the modified theory of Lifshitz-Slyozov-Wagner for systems in which the growth of the particles is controlled by both diffusion and the rate of formation of chemical bonds or chemical reaction. At the same time, however, the question arises, how to be in the case of metallic systems in which growth can occur in clusters under the dislocation diffusion, ie, diffusion along of individual dislocations or dislocation tubes?

With this in mind, we have studied the growth (dissolution) mechanism of the nanoparticles is controlled simultaneously matrix diffusion, diffusion along dislocations and the rate of formation of chemical bonds in metal alloys systems $CuNiAl$ or $AlLi$, at the stage of Ostwald ripening (OR). Obtained the expression for distribution function of nanoparticle size, based on the calculation of which is dependent on the rate of growth of three fluxes - diffusion $j_v$, dislocation $j_d$ and kinetic $j_i$.

Theoretically calculated distribution quite adequate describes the experimental histograms in alloys $CuNi_{15}Al_5$ or $Al-Li$.

It means that the proposed mechanism of clusters growth in the process of OR, when taking into account all three fluxes $j_v$, $j_d$ or $j_i$, can be realized in practice, and the calculated distribution can be used to compare with experimental histograms to establish possible mechanisms of growth.

1. Vengrenovich R.D., Ivanskii B.V., Moskalyuk A.V. Generalized Lifshitz-Slyozov-Wagner distribution // JETP. – 2007, – Vol. 131, №6, – P. 1040-1047.

# Effect of Particles Sizes on Electronic Structure of Nanooxides and Character of Interatomic Bonds Formation in Composites at Mechanical Activation and Pyrogenic Synthesis

Zaulychnyy Ya.V.

*National Technical University of Ukraine "Kyiv Polytechnic Institute", 35 Politekhnichna Str., Kyiv, 03056, Ukraine*

Energy redistribution of valence electrons during dispersion of solids to nanosizes is a result of differences in splitting of energy levels of atoms in volume and atoms with broken bonds on the nanoparticles surface. Number of these bonds is commensurate. Such redistribution depends on atomic-crystal structure, chemical bonding and charge state of ions. The energy distribution of electrons gets narrow simultaneously with increasing density in a high-energy region at the top of valence band in crystals with significant bonds covalence while these bonds break and binding states dehybridize.

Relaxation processes in highly disordered crystals and amorphous phases leads to a shift of the energy distribution towards low energies due to absence of strictly directed dehybridized orbitals and their overlapping.

The energy distribution gets narrow in oxides with high-charged anions, where electrons transferred from cations occupy non-binding high-energy electronic states, occurs due to return of electrons to cations when bonds breaking during dispersion.

Mechanical activation of single-component nanoxides leads to narrowing of energy distribution of electrons due to particles dispersion. Mechanical activation of two-component mixtures of nanooxides results in significant widening of superposition of the O*p*-electrons energy distribution towards low energies, where O$p_\pi$-binding states concentrate.

Analysis of the O$K_\alpha$, Si$L_\alpha$ and Al$L_\alpha$ ultra-soft X-ray emission bands of alumina-silica nanocomposites, corresponding to the energy distribution of the O*p*-, Si*sd*- and Al*sd*-valence electrons showed that low-energy widening of the O*p*-electrons distribution is a consequence of splitting of O*p*-energy levels during π-overlapping of *p*-orbitals of oxygen surface atoms in $SiO_2$ and $Al_2O_3$ nanoparticles in the process of mechanical activation due to high local pressures and temperatures.

Decreasing occupation of the high-energy Si*sd*- and Al*sd*-levels indicates that split O$p_\pi$-levels were occupied by electrons transferred from silicon and aluminum cations. Therefore, oxygen charge in binding states significantly increased as a result of mechanical activation. This effect caused an increase of the charge capacity of lithium power supplies made of alumina-silica nanocomposites. Charge capacity increased during cycling. It is possible since increased oxygen ions charge increases number of $Li^+$ ions intercalated into structural channels of material and lithium ions can not tear electrons from

binding levels off in order to recombine to neutral atoms. Therefore, they go out from cathode and together with ions from anode increase number of charge carriers during the next cycle under deintercalation. $Li^+$ ions easily tear electrons from non-binding states in non-activated mixtures and recombine to free atoms, which are extremely active and oxidize creating LiO film that disable deintercalation and counteract the cycling.

Bonds between the surface atoms of nanoparticles during pyrogenic synthesis form with formation of $SiO_2$ layer on the $Al_2O_3$ particle. It was confirmed by half decreasing intensity of the Al$L_\alpha$ as compared to that of the Si$L_\alpha$ versus spectra obtained from mechanical and mechanically activated nanocomposites.

# Lead Telluride: Atypical Paramagnetism of Native Defects

Zayachuk D.M.

*Lviv Polytechnic National University, Lviv, Ukraine*

This report is devoted to atypical paramagnetic centers in solid recently the first experimentally revealed in lead telluride, which can be attributed to the native defects of *PbTe* crystal matrix. Atypical paramagnetism of the centers manifests itself in an unusual combination of temperature and magnetic field behavior of their magnetic susceptibility, which doesn't depend on temperature but drastically decreases when the applied magnetic field increases. Just this combination of temperature and magnetic-field behavior of the magnetic susceptibility allows asserting about a new type of paramagnetic centers in solid.

There are orientation and polarization paramagnetism in solid. Only one of them, namely van Vleck polarization paramagnetism is temperature-independent. It emerges when electronic shells of weakly interacting centers do not have spherical symmetry. Herewith magnetic susceptibility of the standard van Vleck paramagnetic non-spherical centers is independent of magnetic field too that is not the case for *PbTe*.

Magnetic investigations of *PbTe* samples show the existence of two different types of paramagnetic centers there. One of them is the typical paramagnetic centers, which create the temperature-dependent Curie-like component of the total magnetic susceptibility, $\chi \sim 1/T$. The concentration of such paramagnetic centers is rather low, about $(3\div4)\cdot10^{18}$ см$^{-3}$, namely the same order as a typical hole concentration for undoped *PbTe* crystals grown from melt by a Bridgman technique. Other one is the atypical paramagnetic centers, which create the temperature-independent component of the total magnetic susceptibility, which drastically depend on the applied magnetic field. The bulk and surface of crystal ingots strongly differ in concentration of the atypical paramagnetic centers. Towards the surface their concentration might increase so dramatically that it leads to the transition of *PbTe* from diamagnetic to paramagnetic state in quite broad range of low magnetic fields.

The nature of both types of paramagnetic centers in undoped *PbTe* is not entirely clear. Here we discuss the possibility to explain their by different native defects of crystal matrix. We believe that the typical paramagnetic centers can be formed by *Pb* vacancies, which are the source of free holes in *PbTe*. Creating a free hole, *Pb* vacancy binds an electron, which might lead to the emergence of orientation paramagnetism. A *Pb* atom shifted into interstitial site of *PbTe* lattice could be suggested as the atypical polarization paramagnetic center since polarization paramagnetism can arise from the breaking of spherical symmetry of outer electron shell when full magnetic moment of an atom is zero, $J = 0$, but spin and orbital moments are both non-zero, $L = S \neq 0$, what is consistent with configuration of the outer electron shell $6s^2 6p^2$ of *Pb*.

# CVD-Composites as Perspective Film-Forming Materials

Zinchenko V.F.

*A.V. Bogatsky Physico-Chemical Institute of NAS of Ukraine, Odessa, Ukraine*

Film-forming materials (FFM) are used as initial substances for obtaining coatings by so-called PVD (Physical Vapor Deposition) method more often. In a CVD (Chemical Vapor Deposition) method the coating is formed in a course of gaseous reactions between volatile components. Earlier [1] it is developed composite FFM on the basis of system ZnS-Ge, evaporating congruently at rather low temperatures. We [2] represent the evaporation mechanism in vacuum and condensation on a substrate of this material. It combines features both PVD, and CVD processes:

$$\underset{\text{FFM}}{ZnS_s + Ge_s} \xrightarrow{t,vac.} \underset{\text{vapor}}{Zn_v\uparrow + GeS_v\uparrow} \xrightarrow{t} \underset{\text{coating}}{ZnS_{s(n)} + Ge_{s(n)}}. \qquad (1)$$

The calculated value of conditional temperature ($T_a=T_{P\approx1.33Pa}$) is 590°C for a composite that is much lower, than for ZnS (820°C). Thus, according to XRDA (fig.), the nano-composite type coating occurs though the initial material being microcrystalline.

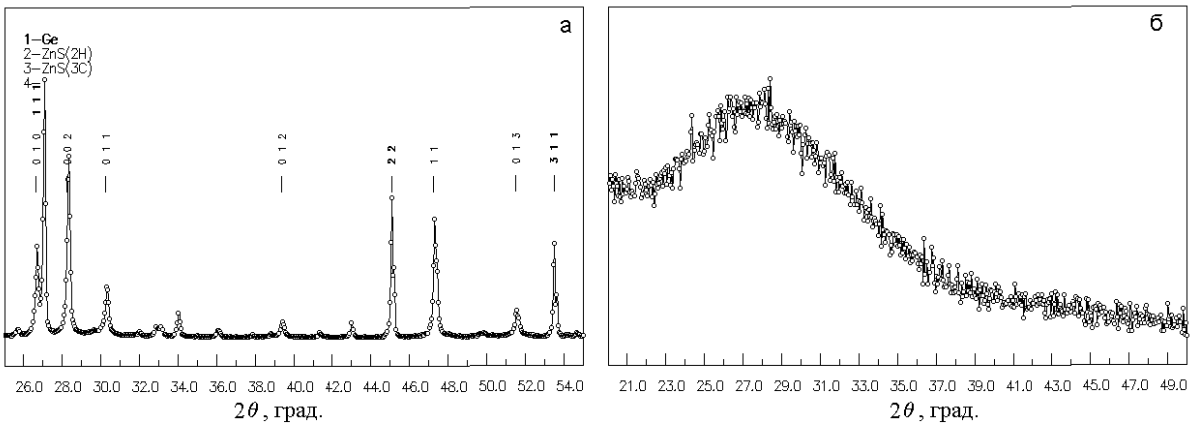


Fig. X-ray diffractograms of the initial CVD-composite ZnS-Ge (a) and the coating produced from it (b).

It makes possible to improve essentially optical and operational (especially, mechanical durability) parameters of coatings (tab.) and to expand domain of transparency of Ge up to border of a visible range of a spectrum.

The materials evaporating and condensed in a similar way are named CVD-composites. In addition to their application as FFM of new type, they are used, for example, in a finishing stage of a way of deep clearing of zinc sulfide from oxide admixture [2]. In it surplus of the sulfidizing agent, $Sb_2S_3$ is eliminated by processing by an additive disperse Ge under the scheme:

$$Sb_2S_{3,\,s} + Ge_s \xrightarrow{t,vac.} 2SbS_v\uparrow + GeS_v\uparrow. \qquad (2)$$

$Sb_2S_3$-Ge composite makes it possible obtaining coatings with much higher mechanical durability in comparison with a coating produced from pure $Sb_2S_3$.

*Table*

Some CVD-composites and parameters of thin-film optical coatings

| Composition | Patent of Ukraine, No | Development (year) | Parameters of coatings | | |
|---|---|---|---|---|---|
| | | | Refractive index, n | Scattering factor, % | Mechanical durability, rotations/group |
| ZnSe-Ge | 75529 | 2012 | 3.30 | 0.05 | 10000/0 |
| $Sb_2S_3$-Ge | 81076 | 2013 | 3.10 | 0.02 | 4500/0 |
| $Sb_2Se_3$-Ge | 87624 | 2014 | 3.66 | – | 7000/0 |
| $In_2Se_3$-Ge | 92947 | 2014 | 3.45 | – | 8000/0 |

Other CVD-composites as FFM on the basis of binary compounds are investigated also, namely: ZnSe-Ge, $Sb_2Se_3$-Ge, $In_2Se_3$-Ge, EuS-Ge, EuSe-Ge, ZnO-Ge, $GeO_2$-Ge, $SnO_2$-Ge, etc. [3]. Their considerable part has shown also high level of optical and operational parameters of coatings (tab.). Further as one of components of CVD-composites complex chalcogenides of chalcospinel $MM'_2X_4$ (M–Mn, Zn, Eu(II), Yb(II), M'–In, Yb(III), X–S, Se) type are applied. The fact of partial interaction of more volatile component of complex chalcogenide with Ge as a part of a CVD-composite is established. It affects both on process of evaporation of composites, and on parameters of obtained coatings.

It is supposed to expand circle of FFMs of CVD-composite type, using as one of components complex oxide that allows to hope that it will be possible to deposit in a soft technological mode nano-composite coatings with electro-conductive properties.

1. Zinchenko V.F., Kocherba G.I., Magunov I.R., Mozkova O.V., Sobol V.P., Belayavina N.M. Optical properties of the thin-film coatings obtained from the ZnS-Ge composites by CVD // Phys. Chem. Solid State.-2011.-V.12, No2.-P. 433-437.
2. Zinchenko V.F., Chygrynov V.E., Mozkova O.V., Magunov I.R., Kovalevska I.P. Effect of interaction in system ZnS(ZnO)-$Sb_2S_3$-Ge on parameters of the produced thin films // Phys. Chem. Solid State.-2014.-V.15, No3.-P.579-583.
3. Zinchenko V.F., Chygrynov V.E., Mozkova O.V., Magunov I.R., Sadkovska L.V. Influence of interaction on optical properties of composites of GeO-$GeO_2$ and Ge-$GeO_2$($SnO_2$) systems // Ukr. Khim. Jhurn.-2013.-V.79, No10.-P.91-95.

## СЕКЦІЯ 1 (усні доповіді)
## ТЕХНОЛОГІЯ ТОНКИХ ПЛІВОК (МЕТЕЛИ, НАПІВПРОВІДНИКИ, ДІЕЛЕКТРИКИ, ПРОВІДНІ ПОЛІМЕРИ) І МЕТОДИ ЇХ ДОСЛІДЖЕННЯ

12-15 травня 2015 р.

## SESSION 1 (oral)
## THIN FILMS TECHNOLOGY (METALS, SEMICONDUCTORS, DIELECTRICS, CONDUCTIVE POLYMERS) AND THEIR RESEARCH METHODS

May, 12-15, 2015

# Spectroscopic and Magnetic Characterization of ZnO:Co Diluted Magnetic Semiconductor Layers Prepared by Printed Electronics Method

Avramenko K.A.[1], Strelchuk V.V.[1], Rarata S.V.[1], Synhaivska O.I.[1], Pekar G.S.[1], Osipyonok M.M.[1], Syngaivsky O.F.[1], Koniakhina M.V.[2], Tronc P.[3]

[1] *V. Lashkaryov Institute of Semiconductor Physics, National Academy of Sciences of Ukraine, Kyiv, Ukraine*

[2] *Taras Shevchenko National University of Kyiv, Kyiv, Ukraine*

[3] *Ecole Superieure de Physique et de Chimie Industrielles de la Ville de Paris, Paris, France*

In recent years considerable efforts have been widely made in synthesis of dilute magnetic semiconductors (DMS) that could be used in future spintronic devices which utilize both spin and charge state of carriers. Co-doped ZnO is predicted to belong to such promising DMS, but no one has succeeded in producing ZnO:Co layers that satisfy simultaneously such criteria as desired physical characteristics, high reproducibility and availability of manufacturing techniques. Therefore, the search for new methods for preparation of ZnO:Co with required physical properties still remains an open question.

$Zn_{0,99}Co_{0,01}O$ layers have been synthesized for the first time by a rather simple printed-electronics method developed and patented by the authors. The layers of a high crystalline quality were grown at temperature about 1000°C on (0001)-sapphire substrates.

Magnetic force microscopy measurements of $Zn_{0,99}Co_{0,01}O$ layers showed the non-uniform surface distribution of magnetization revealing room-temperature ferromagnetic behavior of the samples investigated.

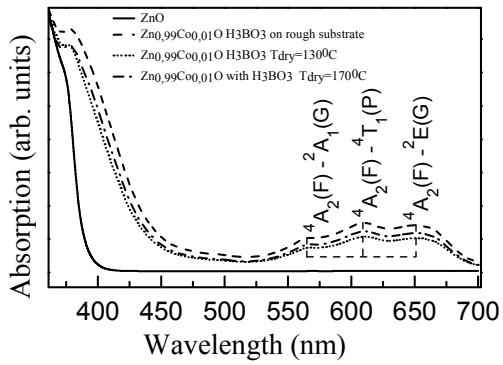


Figure 1. Optical absorption spectra of ZnO and $Zn_{0.99}Co_{0.01}O$ layers prepared under various technological regimes.

The red-shift of the band gap in pure ZnO, as compared with $Zn_{0,99}Co_{0,01}O$ layers, from 387 to 413 nm has been observed in the absorption spectra and is attributed to sp-d exchange interaction between the band electrons and the localized d-electrons of Co ions substituting Zn ions. Observed intra-ion optical absorption at 565, 614 and 654 nm corresponds to the electronic d-d transitions of $Co^{2+}$ ions and confirm the incorporation of Co into the Zn sites of the wurtzite ZnO host lattice.

The observation of the $E_2^{low}$, $E_2^{high}$, $E_2^{high} - E_2^{low}$ and $A_1^{LO}$ modes in the Raman spectra confirms that $Zn_{1-x}Co_xO$ layers have hexagonal wurtzite structure. Addition broad vibrational mode in the range 550 to 580 $cm^{-1}$ has been attributed to disordered Zn-O-Co local vibration modes.

# The Features of Cleavages in Au–Ti–Pd–$n^+$–$n$-Si Ohmic Contacts

Belyaev A.E.[1], Boltovets N.S.[2], Vinogradov A.O.[1], Pilipenko V.A.[3], Petlitskaya T.V.[3], Solodukha V.A.[3], Konakova R.V.[1], Kudryk Ya.Ya.[1], Korostinskaya T.V.[2]

[1] *V. Lashkaryov Institute of Semiconductor Physics, Kyiv, Ukraine*
[2] *State Enterprise Research Institute "Orion", Kyiv, Ukraine*
[3] *Public Corporation "Integral", Minsk, Republic of Belarus*

Here we present the results of investigation of cleavages of both $n^+$–$n$-Si structures and Au–Ti–Pd–$n^+$–$n$-Si contacts before and after thermal treatment at a temperature $T = 450$°C for 20 min. The heavily doped $n^+$-Si layers were obtained using phosphorus ion implantation. The $n^+$-Si layer thickness was ~65 nm, the dopant concentration was $\sim 10^{20}$ cm$^{-3}$. The phosphorus ions were implanted using the "Vesuvius-5" installation. The ion energy was ~60 keV, the implanted dose was $\sim 10^3$ μC·cm$^{-2}$. Thermal annealing of the implanted specimens was made in the oxygen atmosphere at $T = 850$°C for 30 min using a SDOM 3/100 unit. The Au–Ti–Pd–$n^+$–$n$-Si contacts were prepared by successive metal evaporation in a vacuum onto the $n^+$–$n$-Si structure heated to 350°C. Ohmic contacts were formed in the course of metal evaporation. The cleavage surfaces in the $n^+$–$n$-Si and metallized $n^+$–$n$-Si structures were studied before and after annealing using a high resolution scanning electron microscope S-4800. The elemental composition of contact metallization was determined using an energy dispersive spectrometer QUANTEX 200 (Bruker, Germany).

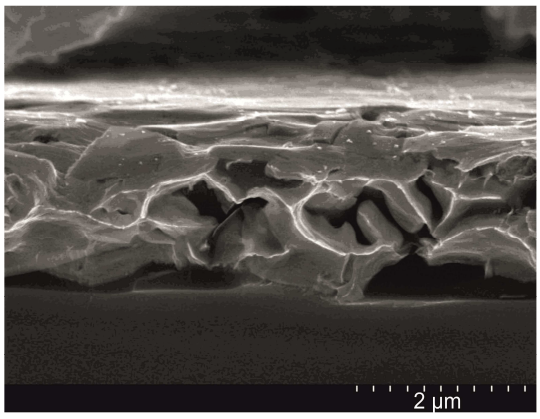


Fig. 1

It was found that, after annealing of ion-implanted $n^+$-Si layer, the cleavages of the $n^+$–$n$-Si structure did not contain any amount of structural defects. After evaporation of contact metallization onto a heated substrate, the degree of imperfection of the near-contact Si layer was bigger than that of the non-metallized $n^+$–$n$-Si structure. However, no considerable smearing of the metal–$n^+$-Si interface was observed.

The morphology of Au–Ti–Pd–$n^+$–$n$-Si cleavage changed drastically after annealing at $T = 450$°C for 20 min. (Fig. 1). Through pores in the contact metallization disturb continuity of the contact-forming layer. Such disturbances of contact metallization may change mechanism of current flow in ohmic contacts. In this case, contact resistivity may increase with temperature which leads to deterioration of parameters of semiconductor devices.

# The Process of Formation and Thermoelectric Properties of Vapor-Phase Condensates PbTe:Bi, PbTe–$Bi_2Te_3$

Bylina I.S.

*Vasyl Stefanyk Precarpathian National University, Ivano-Frankivsk, Ukraine*

The progress of modern science and technology are inextricably linked to the improvement of technology of traditional and new semiconductor materials. In particular, special attention to itself attracts Lead telluride. He is an efficient thermoelectric materials for middle temperatures (500-750 K) of high enough quality factor ZT = 1 [1]. Because of the small prohibited band gap (Eg = 0,32 eV at 300 K) PbTe widely used in devices infrared spectrum [1]. Alloying individual elements, including amphoteric impurity Bi, can greatly modify the basic properties of lead telluride, which is important for practical applications.

Vapor-phase condensates PbTe–$Bi_2Te_3$ and PbTe:Bi obtained by the method of open evaporation in a vacuum on a substrate of pyroceram. The value of $Bi_2Te_3$ varied in the range (1-5) mol.%, and a value of Bi – 1mol.%. For PbTe–$Bi_2Te_3$ the temperature evaporation $T_V$ = 970 K and deposition $T_S$ = 470 K. Variable parameter was deposition time (τ = 15 - 75 s). Condensates PbTe:Bi grown on various technological factors: temperature sample evaporation $T_V$ = (920-1020) K, deposition temperature (substrate) $T_S$ = (420 - 520) K, deposition time τ = (3-120) s. We researched the obtained samples with atomic force microscope (AFM) Nanoscope 3a Dimention 3000 (DigitalInstruments USA) in the periodic contact mode.

Also determined depending on the structural characteristics (medium-sized nanocrystals, their rate of change in the lateral ($D_c$, $D_c$ / τ) and normal ($h_c$, $h_c$/τ) directions to the substrate surface) and thermoelectric parameters (electrical conductivity (σ), Hall concentration (n) and mobility (μ) thermo-EMF (S) and thermoelectric power ($S^2\sigma$)) condensates PbTe–$Bi_2Te_3$ (PbTe:Bi) conditions of their receipt ($T_V$, $T_S$, τ). Is confirmed that the average size of the islands in typical molecular beam epitaxy mode complete condensation bulk of the time grows proportionally $\tau^{1/2}$. It is shown that the dominant process is the Folmer-Weber formation of individual germ on the substrate. The growth of individual nanostructures caused Wagner mechanism (formation of chemical bonds) in the normal direction to the surface deposition and kinetic (diffusion) - in the lateral direction, respectively.

*This research is sponsored by NATO's Public Diplomacy Division in the framework of "Science for Peace" (NATO SPS 984536)).*

1. V.M. Shperun, D.M. Freik, R.I. Zapukhlyak, Thermoelectricity of lead telluride and its analogues, *Ivano-Frankivsk:"Play"*, (2000). – 202 p.

2. G.P. Agrawal, N.K. Dutta, Semiconductor Lasers, *New York: Van Nostrand Reinhold*, (1993). – 547 p.

# Doppler Broadening of Annihilation Line Study of Defect Structure in Advanced Optoelectronic Materials

Kavetskyy T.S.[1,2]

[1] *Drohobych Ivan Franko State Pedagogical University, Drohobych, Ukraine*
[2] *The John Paul II Catholic University of Lublin, Lublin, Poland*

Doppler broadening of annihilation line (DBAL) method in positron annihilation spectroscopy is a powerful experimental tool for structural investigation of materials. The Doppler *S* and *W* lineshape parameters have characteristic values for each material, depending on the electron momentum distribution. Due to their low momentum, the annihilations with valence electrons fall predominantly in the region of the *S*-parameter (shape), while mainly core electrons have momentum values high enough to contribute to the *W*-parameter (wing); thus, *S* and *W* parameters are often called as valence and core annihilation parameter, respectively. When positrons are trapped, the lineshape is characteristic of the trapping defect. The larger concentration of vacancy-type defects, the lower the core annihilation parameter *W* and the higher the valence annihilation parameter *S*. At the same time, the dependence *S* vs. *W* is typically used to study a defect structure of materials. That is, when the samples exhibit the same slope of *S*-*W* plot (or dependence *S* vs. *W* is linear), one may suppose that their defect structure is similar. In the present work the recent results obtained on the DBAL study of defect structure in optoelectronic materials such as chalcogenide glasses [1,2], polymethylmethacrylate [3,4], and organic-inorganic ureasil-based composites [5] are reviewed. The deconvolution procedure with the Gold iterative algorithm used, permitting the measurement of small changes of the annihilation peak with high confidence, is approved.

1. T. Kavetskyy, V. Tsmots, O. Šauša, A.L. Stepanov, *Phys. Status Solidi C,* **9**(12), (2012), 2420.
2. T.S. Kavetskyy, V.M. Tsmots, O. Šauša, A.L. Stepanov, *Semiconductors,* **48**(1), (2014), 9.
3. T. Kavetskyy, V. Tsmots, A. Kinomura, Y. Kobayashi, R. Suzuki, Hamdy F.M. Mohamed, O. Šauša, V. Nuzhdin, V. Valeev, A.L. Stepanov, *J. Phys. Chem. B*, **118**(15), (2014), 4194.
4. T.S. Kavetskyy, V.M. Tsmots, S.Ya. Voloshanska, O. Šauša, A.L. Stepanov, *Abstracts of 6th International Scientific and Technical Conference "Sensor Electronics and Microsystem Technologies" (SEMST-6)* (Odessa, Ukraine, 29 September - 3 October, 2014), 226.
5. T.S. Kavetskyy, O. Šauša, T. Petkova, V. Boev, P. Petkov, A.V. Kukhta, A.L. Stepanov, In book: NATO Science for Peace and Security Series - A: Chemistry and Biology, Chapter 9 "Nanoscience Advances in CBRN Agents Detection, Information and Energy Security" (P. Petkov, D. Tsiulyanu, C. Popov, W. Kulisch, eds.), Berlin: Springer, (2015), 85.

# Long-Term Radiation-Induced Improving of the Mechanical Properties in $As_2S_3$ Glass Probed by Nanoindentation

Kavetskyy T.S.[1,2], Borc J.[3], Nowak J.[2], Stepanov A.L.[4,5,6]

[1] *Drohobych Ivan Franko State Pedagogical University, Drohobych, Ukraine*
[2] *The John Paul II Catholic University of Lublin, Lublin, Poland*
[3] *Lublin University of Technology, Lublin, Poland*
[4] *Kazan Physical-Technical Institute, Russian Academy of Sciences, Kazan, Russia*
[5] *Kazan National Research Technological University, Kazan, Russia*
[6] *Kazan Federal University, Kazan, Russia*

The results of investigation of the mechanical properties (hardness and elastic modulus) in the unirradiated and γ-irradiated g-$As_2S_3$ glass (g- for glassy) using nanoindentation technique with an ultra nano hardness tester (UNHT), developed by CSM Instruments (Switzerland) [1], are reported for the first time. The main improvements of the UNHT compared to the conventional nano indenter (or NHT) design are a new tip and reference fixing system introduced in the ultra indenter head and the use of active top referencing (very low loads applied by the reference, less than 1 g), the possibility of depth and load measurements, one order less noise level, etc.; they allow us to make measurements using the UNHT with high performance.

The hardness and elastic modulus (with a Poisson ratio of the specimen of 0.29 for g-$As_2S_3$ [2]) values were calculated in the load-depth measurements by the method of Oliver and Pharr [3,4] with the software of CSM Instruments for the UNHT [1]. Due to the radiation-induced oxidation effect connected with appearance of $As_2O_3$ (arsenolite) crystals and S phases at the surface of g-$As_2S_3$, forming a white oxidized layer visible to the eye [5], the surface morphology of the investigated γ-irradiated sample is also examined using MIRA (Tescan) field emission scanning electron microscope with EDS detector.

It is established that the γ-irradiated g-$As_2S_3$ with average energy of $^{60}$Co γ-quanta 1.25 MeV and accumulated dose 2.41 MGy, measured 10 years after γ-irradiation, exhibits increasing the hardness and elastic modulus values compared to the unirradiated material in the range of 200-1600 nm indentation depth. The observed long-term radiation-induced improving of the mechanical properties in g-$As_2S_3$ is practically the same for both irradiated samples with and without oxidized layer which was removed by washing and polishing procedures.

1. Introduction on Instrumented Indentation, http://www.csm-instruments.com.
2. T.M. Melnichenko, V.I. Fedelesh, I.M. Jurkin, T.D. Melnichenko, V.M. Rizak, *Phys. Chem. Solid State*, **3**(2), (2002), 292.
3. W.C. Oliver, G.M. Pharr, *J. Mater. Res*., **7**(6), (1992), 1564.
4. W.C. Oliver, G.M. Pharr, *J. Mater. Res.*, **19**(1), (2004), 3.
5. T.S. Kavetskyy, *Semicond. Phys. Quant. Electron. Optoelectron.*, **17**(3), (2014), 308.

# Role of Transition from Atomically Smooth to Atomically Rough Growth Surface at Formation of Condensates Architecture

Kosminska Yu.O., Perekrestov V.I.

*Sumy State University, Sumy, Ukraine*

When depositing substance under near-equilibrium conditions, it is spatially distributed selectivity of fixing of adatoms on a growth surface that determines structure formation of three-dimensional condensates. Extremely low supersaturation corresponds to a certain value of a critical energy of adatoms binding with the growth surface ($E_c$) that divides the whole binding energy spectrum in two parts. Substance condensates onto the area of the growth surface with desorption energies $E_{di}$ higher than $E_c$, and, on the contrary, there is no condensation onto the areas with $E_{di}$ lower than $E_c$. If changing the position of $E_c$ in the binding energy spectrum by varying supersaturation of vapours, the transition from atomically smooth to atomically rough growth surface becomes possible. As a result, one can produce various corresponding architectures of three-dimensional layers. In the present work we study experimentally structure formation of single-component metallic condensates (Ni, Cu, Al, Ti) at varying extremely low supersaturation of deposited vapours. The main focus of the study is transition from tangential to normal growth of structural elements of condensates at reducing the supersaturation.

Substance was deposited in high-pure inert ambient by means of modified magnetron sputtering system with hollow cathode under low discharge power (~2-28 W), high growth surface temperatures (~350-670 $^0$C) and increased working gas pressure (argon) ~3-25 Pa. Structure and surface morphology were investigated by electron microscopy techniques.

General regularities of growth under near-equilibrium conditions are of approximately the same character for all studied metals. When lowering the supersaturation, for example, by increasing the growth surface temperature or reducing the deposited flux in a certain range, faceted structural elements of porous condensates give place to rounded shapes. This is accompanied by change from tangential (layer-by-layer) growth of atomically smooth growth surface to normal growth of atomically rough surface. At the moment of this transition the condition $E_{(hkl)} < E_c < E_{ar}$ is met ($E_{(hkl)}$ is the maximal binding energy of an adatom on atomically smooth surface (*hkl*), $E_{ar}$ is the binding energy of an adatom on atomically rough surface), and the monostep free energy turns into zero. It is found that the porosity character also changes as a result of the above transition, and sizes and concentration of pores usually decrease.

# A Comparison of Methods for Determination of Schottky Barrier Height and Ideality Factor Regarding the Contacts Based on Broad-Band Semiconductors

Kudryk Ya.Ya.[1], Shynkarenko V.V.[1], Slipokurov V.S.[1],
Bigun R.I.[2], Kudryk R.Ya.[2]

[1] *V. Lashkaryov Institute of Semiconductor Physics, NASU, Kyiv, Ukraine*
[2] *Ivan Franko National University of Lviv, Lviv, Ukraine*

Schottky barrier height (ShBH) and ideality factor (n) are the most important parameters of the Schottky contact. A number of methods for their determination, including determination from the current-voltage (I-V) characteristic, is well known. Attempts to generalize and systematize the existing methods were made in a number of papers [1, 2], but estimation of accuracy, carried out in the most of works, does not take into account the peculiarities of contacts to wide-gap semiconductors. Considering the accuracy of determining ShBH, as applied to the contacts based on wide-gap semiconductors, it is necessary to take into account three factors: the accuracy of measurements of initial values (current, voltage), accuracy of the approx method and accuracy of correlation between the proposed mechanism of charge transport and that implemented in reality.

In this work, a batch of Schottky diodes were investigated using different methods, a comparison of these results was made, and the reasons of their differences were discussed. Considering the series resistance and portion of I-V characteristics at V~kT/q can contribute a substantial correction to the value of the determined series resistance, and therefore, the methods of Lien, Werner as well as direct approximation are preferable to determine the height of the potential barrier at the small extent of the exponential portion of the I-V characteristics. The values of ShBH, obtained by the method of activation energy and Sato, are only valid in the absence of the temperature dependence of ShBH. It has ascertained that an inconsistency between the real I-V characteristics and its model – the temperature dependence of the ShBH, n dependence on the voltage – introduces the basic error into the calculated parameters in the diode under study. It can be concluded that for the wide-gap semiconductors, at this stage of their study, the greatest accuracy is inherent to methods allowing to detect and identify a discrepancy between the model and measured data, namely, methods by Lien, Werner and Cheung. The necessity to study the temperature dependence of the ideality factor for correct determination of the mechanism responsible for the charge transfer and Schottky barrier height has been shown

1. V. Aubry, F. Meyer., *J. Appl. Phys.*, **76**(12), (1994), 7973.\
2. K. Sarpatwari. Toward understanding the electrical properties of metal/semiconductor Schottky contacts. PhD Diss. Pennsylv. St. Univ. (2009).

# Structure and Thermoelectric Properties of Doped Telluride Films Condition

Makovyshyn V.I.

*Vasyl Stefanyk Precarpathian National University, Ivano-Frankivsk, Ukraine*

Tin Telluride widely used in semiconductor technology. He also promising thermoelectric material for medium range (500-750) K [1,2]. Getting thin film material greatly expands the boundaries of practical application. Before now remains unresolved by the end of the problem of stability over time of electrical parameters. In addition, the exposure of films in the air due to the acceptor action of oxygen on the surface layer is enriched with native p-type conductivity [3].

Introduction Bi leads donor action in Tin Telluride, manifested in descending order of concentration of holes in the bulk of the film. Results of the study of thermoelectric parameters based on vapor-phase condensation doped Tin Telluride for different compositions given in the table. With increasing dopant content thermoelectric power first increases and then decreases sharply, due to the exit from the region solubility of Bi in SnTe. The maximum thermoelectric power is achieved at the impurity content of about 0.3 mol.%, But condensates obtained on fresh cleavages (0001) muscovite mica, it is much higher than for samples in ceramics.

The thickness dependence of thermoelectric parameters SnTe vapor-phase condensates containing 0.3 mol.% Bismuth, with reduction of condensates d, regardless of the composition, the conductivity increases significantly, and for thickness over d ≈ 0,5 microns virtually unchanged. This is due to increasing concentration of carriers in the small film thickness due acceptor action adsorbed surface oxygen. And the concentration of charge carriers pure Telluride is greater than through the donor doped bismuth action. As the film thickness obtained on mica substrates and Seebeck coefficient increases, leading to a significant increase in the thermoelectric power.

Films obtained on fresh cleavages (0001) muscovite mica-characterized by much higher thermoelectric power thanks to twice the Seebeck coefficient than samples obtained on ceramics, thanks to better structural ordering through the influence of the substrate orientation. Condensate obtained at sytalovyh lining the thickness dependence of the Seebeck thermoelectric power and have a clear maximum in the thickness of ~ 0.6 microns due to the manifestation of size effects at small thicknesses condensate.

There are investigated the thermoelectric properties of vapor-phase condensates based on doped tin telluride SnTe:Bi OF THE different composition obtained in the on ceramics and mica substrate by open vacuum technology. It is shown, that thin films on fresh chips (0001) mica containing ~ 0.3 ml.% Bi characterized by maximum values of the thermoelectric power ~ 42 mkW/K$^2$cm.

**Literature**

1. VM Shperun, DM Freik, RI Zapukhlyak. Thermoelectricity of lead telluride and its analogues. - Ivano-Frankivsk, Play, 2000. - 250 p.

2. DM Freyk, MA Galushchak, LJ Mezhylovskaya. Physics and Technology of thin films. - Lviv: High School, 1988. - 182s.

3. Y. Klanichka, BS Dzundza, LJ Mezhylovska, JS Jaworski // Physics and Chemistry of Solids. - 2011. - T12. - R. 346.

# Carrier Scattering in Thin Films Tin Telluride

Jaworski J.S., Makovyshyn V.I., Yaremkiv R.Ya.

*Vasyl Stefanyk Precarpathian National University, Ivano-Frankivsk, Ukraine*

Tin Telluride is a promising thermoelectric material with stable p-type conductivity for medium range (500-750) K. Thin-film material substantially extends beyond its practical use. The properties of polycrystalline thin films largely depend on electronic processes that occur at interfaces within. Here, in particular, be aware scattering at interfaces and within Intergrain, misfit dislocations and other defects of growth. The localization of current carriers, surface conditions and their capture of dangling bonds at the boundaries of crystallites leading to the formation near the regions of space charge concentration and mobility of charge carriers in can differ from that of the in volume.

From the AFM image of the surface nanostructures can be seen that the vapor-phase condensation of nanosized crystallites formed pyramidal shape. Established that the average size of the nanocrystals condensate thickness increases. Doping Bi condensates SnTe results in reducing the size of nanocrystals.

As for the thickness dependence of the electrical parameters of the vapor-phase condensation, they are as follows. Specific conductivity (σ) of the thickness (d) (1 decrease / d) increases for all of these structures. Thus with increasing Bi content dopant throughout the range of thicknesses condensate σ value decreases.

Current carrier mobility (μ) condensates SnTe: Bi adequately replaced with a thickness (d): slightly increases with d. The latter correlates well as the nature of resizing nanocrystals: increase the size of their saturation characteristic values for condensates with d> 500 nm. It should also be noted the fact that the charge carriers mobility (μ) doped structures in two galleries times higher than for pure Tin Telluride.

Note the two important experimental findings: the impact of dopant (Bi) and the thickness of the condensate (d) their complex structure and electrical properties. With respect to the thickness d-dependency, they can explain the mechanisms of carrier scattering in Intergrain and within interphase [5]. In particular, if the prevalence of carrier scattering on the surface (μP) and grain boundaries (μz) charge carriers mobility in the films is determined Mattisen rule [5].

The influence of the thickness pure and bismuth doped tin telluride films deposited on fresh mica substrates (0001) for their nanostructure and scattering mechanisms of charge carrier are researched. Established that the dominant scattering mechanism is surface scattering and scattering on the intergrain boundaries which determined by the dopant content. Crystal chemistry doping mechanisms which associated with placement of Bi atoms in cationic structures are proposed.

# Study of Contact Structures to *n*-InP at Low Temperatures

Novytskyi S.V.

*Zhytomyr Ivan Franko State University, Zhytomyr, Ukraine*

Stable operation of Gunn diodes under extreme conditions puts special requirements on ohmic contacts connecting the devices into a circuit. Therefore, these contacts must be resistant to different actions and maintain low contact resistivity at Gunn diode operating temperatures.

The problem of contact thermal stability can be solved by applying contact metallization with a diffusion barrier that prevents mass transfer in the contact metallization. We studied the contact structure Au/$TiB_2$/Au/Ge/$n$-$n^+$-$n^{++}$-InP with a $TiB_2$ layer serving as diffusion barrier. An Auger analysis showed diffusion stability of $TiB_2$ at annealing (formation) temperature of 400–490°C. In this case, the contact resistance value did not change.

We studied also how the contact resistivity $\rho_c$ of ohmic contacts Au/$TiB_2$/Au/Ge/$n$-$n^+$-$n^{++}$-InP depended on the ambient temperature $T$. We studied the temperature dependence of contact resistivity $\rho_c$ for InP-based ohmic contacts in the 4.2–300 K temperature range (Fig. 1). The experimental dependence can be described by assuming a diffusion limited current supply of electronic based low-temperature freezing electrons. Ohmicity contact is achieved enriched band bending. Enriched band bending occurs at the ends of the semiconductor in the space charge region, which borders with metal shunts [1, 2].

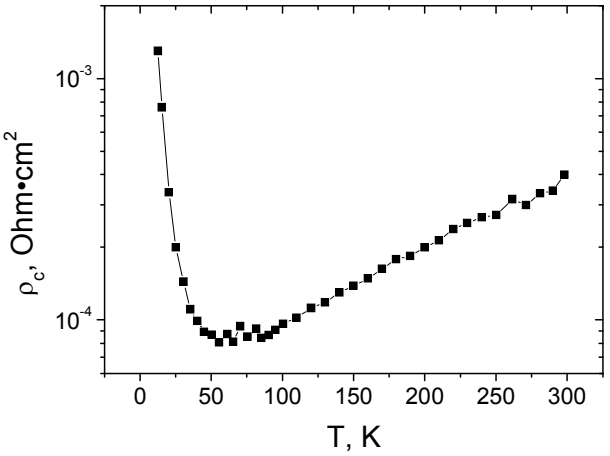


Fig. 1. Temperature dependences of contact resistivity for InP-based ohmic contacts (impurity concentration of $9\times10^{15}$ cm$^{-3}$).

1. A.V. Sachenko, A.E. Belyaev, N.S. Boltovets, R.V. Konakova, Ya.Ya. Kudryk, S.V. Novitskii, V.N. Sheremet, J. Li, S.A. Vitusevich, *J. Appl. Phys*., **111**, (2012), 083701.
2. A. Sachenko A. Belyaev, N. Boltovets, S. Vitusevich, R. Konakova, S. Novitskii, V. Sheremet, *Heidelberg, Germany. - 10th - 17th August 2014,* 13.

# Synthesis of WO3 and NiO Electrochromic Thin Films With Controlled Amount of Hydrogen

Oberemok O.S., Melnik V.P., Nikirin V.A., Khacevych I.M., Sabov T.M.

*V. Lashkarev Institute of Semiconductor Physics NAS of Ukraine, Kyiv, Ukraine*

The transition metal oxide films are commercial attractive material for creation of electrochromic (EC) devices, catalysers, gas sensors, optical switching devices and etc. The conventional EC device consists of glass substrate / transparent conducting electrode (TCO) /cathode EC film / ion-conducting film (IC) / anode EC film / TCO [1]. Such construction provides the enhanced total coloration as a result of successive REDOX reactions in the sandwich structure. It is connected with the charge injection from the anode film NiO (colored in the oxidized state) in the cathode film WO3 (colored in the reduced state) through the IC film.

Depending on the deposition conditions and techniques, films may present considerably different structural, optical and electrical behaviors, and consequently different EC behaviors. Deposited $WO_3$ and NiO films are mainly in the amorphous state. At the same time, the sensitivity and the rate of change in light transmission (colorization and bleaching) oxide films strongly depends on the size of the metal oxide particles. Annealing at temperatures characteristic crystallization allow obtaining the nano-structured films with the high porosity and surface area. It provides greater performance compared to amorphous and polycrystalline films with a great transparency in oxidized ($WO_3$) or reduced (NiO) condition. The most used element for redox reactions in oxide films is hydrogen. Obviously, the amount of hydrogen required for maximum transparency changes oxide films $WO_3$ and NiO in the sandwich structure will depend on many conditions. This is especially important for deposition films at the magnetron reactive sputtering of targets.

One the method of the controlled introduction of hydrogen in the EC film is the ion implantation. In the present work the influence of hydrogen dose, film thickness and structure on the electrochromic film transmittance were investigated by X-ray diffraction, Secondary Neutral Mass Spectrometry, Raman spectroscopy, Transmission electron microscopy, Photoluminescence and Spectrophotometry methods. The quantitative data allowed to determine the optimal parameters of films for the high performance electrochromic cell creation.

1. C.M. Wang, C.Y. Wen, Y.C. Chen, C.C. Wang, …, *International Journal of Chemical, Nuclear, Materials and Metallurgical Engineering*, **8**(7), (2014), 590.

# Properties of Thin Metal Nitride Films Obtained by Laser Deposition

Pavlovskyy Yu.[1], Virt I.S.[1,2], Habinskij V.[1]

[1] *Drogobych State Pedagogical University, Drogobych, Ukraine*
[2] *University of Rzeszow, Rzeszow, Poland*

Aluminium nitride, AlN, in known to be as a semiconductor with a large bandgap (6.2 eV) in its more stable wurtzite crystalline structure and reveals a refractive index of about 2.1-2.2 in the visible range. Exhibits high electrical resistivity, high hardness and it is also a piezoelectric material. AlN is commonly used in fabrication of optical sensors in the ultraviolet-visible region, light emitting diodes (LEDs) with one of the shortest emission wavelength reported (210 nm); and several types of microelectronic-related applications.

The thin films AlN were deposited by pulsed laser deposition, in a laboratory-sized deposition system. Structural details of the films were revealed by transmission electron microscopy TEM. Films for these investigations were deposited onto monocrystal Si substrates. Microhardness measurements were made with a PMT-3 tester equipped with a diamond Knoop pyramid. By applying increasing loads to the indenter it was possible to gather information on layer hardness at increasing penetration depths. Ten impressions were made at each load and the average microhardness values were. Another reason for the lower layer hardness could be the presence of a small oxygen amount in the films.

After annealing, the thickness of the individual layers is changed, and there is an increase in hardness. The best result is to strengthen the surface of the monocrystalline silicon obtained by applying aluminum nitride films: the rise of microhardness by 25% while maintaining the value of fracture toughness.

To study the optical properties of these coatings, some optical measurements (transmittance) were performed. It is thus possible to tune the films optical properties according to the application envisaged, by simply changing reactive gas flow during processing.

1. S. Venkataraj, D. Severin, R. Drese, *Thin Solid Films*, **502**(1-2), (2006), 235.
2. Q. X. Guo, M. Yoshitugu, T. Tanaka, *Thin Solid Films*, **483(**1-2), (2005), 16.

# XPS Study of ZnO Thin Films Annealing in Atomic Oxygen

Rogozin I.V.

*Berdyansk State Pedagogical University, Berdyansk, Ukraine*

Zinc oxide materials have potential applications in optoelectronic devices. In order to create light-emitting devices on the base of ZnO it is necessary to obtain material of both *n*- and *p*- type. However, at present obtaining *p*-type material is a complex technological problem. It is connected with the fact that ZnO films and single crystals have *n*-type conductivity due to the large number of donor intrinsic defects, such as interstitial zinc or oxygen vacancies.

Typical n-type ZnO thin films were prepared using radio frequency magnetron sputtering. Thermally oxidized Si (111) wafers used as substrates. The thickness of the amorphous silicon oxide layer was 500 nm. Sputtering was performed using argon with 99.999% purity. A ZnO disc with 99.999% purity was used as a target. The thickness of the ZnO films about 500 nm. ZnO films were annealing in atomic oxygen at temperatures from 600°C. Atomic oxygen was generated using a 40 W rf discharge at a pressure of 0.1 Pa. The XPS spectra were used to confirm the stoichiometry of ZnO film.

XPS spectra, Zn 2p, Zn LMM and O 1s of the as-deposited and annealed ZnO films were studied. The Zn 2p3/2 peak of zinc in the elemental as well as oxide forms usually consists of a single component at the binding energy of 1021.8 eV. However, an asymmetric Zn 2p3/2 peak with components at binding energies of 1022.5 and 1021.6 eV is sometimes observed. The former is associated with Zn in the oxide form while the latter is attributed to metallic zinc.

Since the Zn 2p3/2 peak shape does not always give an asymmetric feature, the Zn LMM Auger peak analysis is often used to identify the chemical states of the zinc species. The deconvolution of the Zn LMM Auger peak reveals two components at kinetic energies of 991.7 and 988.5 eV, attributed to the presence of elemental Zn in the film and the bonding of Zn with oxygen in ZnO respectively.

We could observe that O1s peak position of the as-deposited ZnO film was at 531.2 eV, which indicated the film was in the oxygen deficient state. However O1s peak position of the annealed ZnO film was at 531.5 eV. We could find that oxygen binding energy shifted towards the large energy direction, which was attributed to increase in the oxygen atoms of the annealed ZnO film. Part of the increased oxygen atoms exist as Zn–O bond, and the rest as free oxygen.

From the results of XPS, we could obtain that the atom ratio of Zn:O equaled, respectively, 1:0.96 before being annealed and 1:1.06 after being annealed which showed that ZnO changed from Zn-rich to O-rich after being annealed in atomic oxygen.

# NATO Project SfP-977982 "X-ray Generator Based on Compton Backscattering"

Shcherbakov A.

*National Science Center «Kharkov Institute of Physics &Technology», Kharkov, Ukraine*

In National Science Center «Kharkov Institute of Physics &Technology» the design and development of a X-ray generator on the base of Compton back scattering **NESTOR** (**N**ew **E**lectron **STO**rage **R**ing) using existed electron storage ring N-100 is one of the promising and priority direction which allows expending of existing accelerator park for experimental investigations in biology and medicine, physics and chemistry, geology and ecology.

The NESTOR X-ray source project is developing within international collaboration using NATO “Science for Piece” program grant SfP-977982. NSC«KIPT» (Ukraine), SSRL (USA), TUE (the Netherlands), LPI (Russia) are the grant participants.

The history and the results of multi-year project of NATO, the basic parameters of x-ray generator NESTOR as well as the possibility of using it in nanotechnology are presented.

# Topology of Nano-Heterostructures Ag2O-HgCdTe

Sizov F.F., Savkina R.K., Smirnov A.B., Udovytska R.S.

[1] *V. Lashkaryov Institute of Semiconductor Physics, NAS of Ukraine, Kyiv, Ukraine*

The samples were irradiated by $Ag^+$ ions on the side of the HgCdTe (MCT) epilayer ($d$ = 17 μm) on "Vezuviy" implanter [1, 2]. The surface morphology of heterostructures, mechanical and electrical properties are studied. It was found that the ion irradiation of the surface of studied specimens gives rise to the formation of a characteristic relief on it. The AFM images of the initial surface of typical heterostructure specimens on the basis of CdHgTe (Figs.1a and 1b) demonstrate a grid of quasipores (3.5 x10) nm in depth and (50 x160) nm in diameter, as well as closely packed grains ranging from 40 to 80 nm in dimensions and located in the surface plane between the pores. The implantation with silver ions gives rise to the emergence of a uniform array of nano-islands 5 to 25 nm in height and with a base diameter of 13 to 35 nm against the background of the insignificant smearing of initial grain boundaries and the constant surface porosity (Fig.1a, 1b) [1].

The observed effects of transformation of the defect-impurity system and structuring of the surface of the heteroepitaxial film of the low-energy-gap semiconductor have been explained using a deformation model. The deformation accumulation is found to lead to the topological instability of the irradiated surface. The calculated mechanical stress is $\sigma_{max} = 2 \times 10^5$Pa [2]. As a result, each of the local volumes (blocks) of the crystal undergoes an action of forces from the neighboring blocks, and their resulting force and its impulse will not be zero because of fluctuations. When the stress will be higher than the ultimate strength of MCT, the action of the forces can brings about the rotation of small crystalline blocks and the structuring of the material.

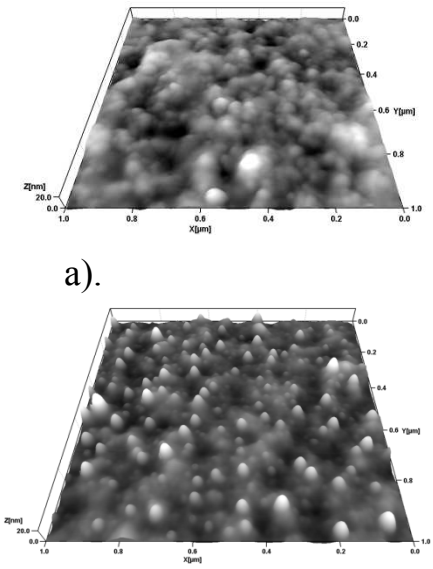

a).

b).

Fig 1 AFM images a) initial $Cd_xHg_{1-x}Te$ b) implanted $Ag^+$

1. A.B. Smirnov, O.S. Litvin, V.O. Morozhenko, R.K. Savkina, M.I. Smoliy, R.S. Udovytska and F.F. Sizov*, Ukr.J.Phys.* **58**, (2013), 872.
2. F.F. Sizov, R.K. Savkina, A.B. Smirnov, R.S. Udovytska, V.P. Kladko at ell. *Physics of the solid state*. **56**, (2014), 2160.

# Investigation of Ohmic Contacts to Silicon IMPATT Diodes

Slipokurov V.S.[1], Kudryk Ya.Ya

*V. Lashkaryov Institute of Semiconductor Physics, NAS of Ukraine, Kyiv, Ukraine*

The maximal output power of impact avalanche and transit time (IMPATT) diodes is related to the properties of *p-n* junction as well as thermal stability of ohmic contact. The investigations of 8 mm-wave IMPATT diodes showed [1] that no degradation of diode active region occurs at temperatures $T$ below 350°C. Thus, to increase the IMPATT diode output power, it is necessary to develop and investigate heat-resistant multilayer ohmic contacts with low contact resistivity $\rho_c$ that could remain stable at temperatures up to 350°C.

We studied ohmic contacts to two multilayer structures with Au-Ti-Pd metallization. The ohmic contacts were formed on $n$-$n^+$-Si with dopant (phosphorus) concentration in $n^+$-Si of about $10^{20}$ cm$^{-3}$. To this end, the layers of palladium (20 μm), titanium (60 μm) and gold were sequentially magnetron-deposited in a single technological cycle onto a silicon substrate (heated to $T$ = 350°C) that was previously exposed to photonic cleaning. The gold layer thicknesses in two specimens studied were 0.1 μm and 1.1 μm, respectively. The Auger concentration depth profiles of contact components (taken before and after rapid thermal annealing at temperatures up to 350°C) indicated contact stability.

When studying a vertical Au-Ti-Pd-$n$-$n^+$-Si structure, contact resistivity $\rho_c = 1.3 \div 5 \times 10^{-5}$ Ω·cm$^2$ at $T$ = 300 K was obtained. We propose a method for error minimization in calculation of contact resistivity in which the value of semiconductor resistivity determined for each template is replaced with the most probable resistivity value for the whole wafer in a case of negative correlation between the contact resistivity and semiconductor resistivity.

1. A.E. Belyaev, et al., *Semiconductors*, **45**(2), (2011), 253.

# Characterization of Grain-Boundary Barriers in CdTe Polycrystalline Films

A. Tkachuk[1], A. Sukach[2], V. Tetyorkin[2], S. Stariy[2], V. Boiko[2]

[1]*V.Vinnichenko Kirovograd State Pedagogical University, Kirovograd, Ukraine*
[2]*V.Ye. Lashkaryov Institute of Semiconductor Physics, NAS of Ukraine, Kyiv, Ukraine*

CdTe polycrystalline thin films are widely used for manufacture different optoelectronic devices such as solar cells and infrared detectors. It is generally believed that their properties are mainly determined by potential barriers at the grain boundaries(GBs). However, their crystalline structure and physical properties still remain unclear.

CdTe polycrystalline films were grown on sapphire substrates by a modified close spaced sublimation technique. The films with the average grain size ranged from ~10 up to ~400 μm were studied by measuring photoluminescence (PL) spectra, in-plain and transverse dark conductivity. For measurement of transverse conductivity films were sandwiched between buffer and cap layers of highly doped polycrystalline p-PbTe. The photoluminescence measurements were performed at 77 K under CW excitation using the 630 nm line of an He-Ne laser.

The correlation between the intensity of the dislocation-related radiation and density of GBs was observed in CdTe polycrystalline films. The most reasonable models of the dislocation-related photoluminescence in CdTe are the radiative emission through the dislocation core states or the states introduced by defect compexes with participation of Cd vacancies. The nonuniform distribution of deep defect inside the grains is proved by means of PL measurements at different excitation geometries.

The transverse conductivity is shown to be ohmic in the temperature range 200-400 K, whereas the in-plane is non-ohmic. The barrier height has been estimated to be ~0.2-0.25 eV. The measured values of intragrain and barrier resistance are comparable. Also, photovoltaic photoresponse measured in Schottky contacts prepared on the investigated films indicates n-type conductivity of GBs.

Based on experimental results possibility of modeling GBs by a dislocation network is discussed. Because the GB dislocations can serve as a getter for point defects, their non-uniform distribution seems to be inherent feature of CdTe polycrystalline films. Conclusions were made about optimal structure and electric parameters of CdTe polycrystalline films for the solar cell applications.

# Properties of Schottky Contacts on Laser-Modified Surface of CdZnTe

Tkachuk A., Tetyorkin V., Sukach A., Matiyuk I.

[1]*V.Vinnichenko Kirovograd State Pedagogical University, Kirovograd, Ukraine*
[2]*V.Ye. Lashkaryov Institute of Semiconductor Physics, NAS of Ukraine, Kyiv, Ukraine*

The surface modification in semiconductors under pulsed laser radiation is increasingly used in opto-and nanoelectronics. By changing the laser processing condition (intensity, duration and repetition rate of laser radiation) the surface structures with characteristic lateral and vertical dimensions ranged from nano- to micrometers can be obtained.

The samples used for the investigations were monocrystalline semi-insulating $Cd_{0.9}Zn_{0.1}Te$ with resistivity (1-2) $10^{10}$ Ω cm at room temperature. The preparation of samples included mechanical grinding and polishing, followed by chemical-mechanical polishing in bromine-methanol etchant. The samples were irradiated by the second harmonic ($\lambda$ = 532 nm) of a Nd:YAG laser with a pulse duration of 10 ns, 5 MW/cm$^2$ intensity and repetition frequency of 10 Hz. To modify the surface approximately $10^3$ pulses were used at each point.

The surface barrier structures have been prepared by electroless deposition of Au at room temperature and thermal evaporation of In on samples heated to 120 °C. The diode-like current-voltage characteristics was observed in Au and In contacts deposited on irradiated and non-irradiated surfaces, respectively. The selective photoresponse peaked at 0.79 μm was observed in In contacts on the non-irradiated surface, whereas additional wide spectral bands peaked at 0.55-0.63 μm were observed in Au contacts. The polarity of the measured signals was analysed to determine the conductivity type of these surfaces.

It has been found that the starting material has p-type conductivity and pulsed laser irradiation results in formation of surface layer with n-type conductivity. The conductivity type inversion occurs on the depth of several microns. The broadening of the photovoltaic response in the Au contacts arises due to appearance of the graded-gap region at the surface.

The observed conversion of the conductivity type is not trivial, since it is generally accepted that the laser irradiation results in formation of cadmium vacancies (stoichiometry violation). Possible reason for the conversion is generation of large amount of dislocations. The presence of the dislocation network at the surface can also explain the observed power dependence of the dark current on temperature. In such a case, the percolation conductivity through the dislocation network can be dominant.

# Physical Interpretation of Anomalous Experimental Temperature Dependences of Contact Resistivity of Ohmic Contacts to Silicon

Vinogradov A.O.

*V. Lashkaryov Institute of Semiconductor Physics of the National Academy of Sciences of Ukraine, Kyiv, Ukraine*

The nanosized layers of contact structures in silicon devices operating at THz frequencies may deteriorate. This results from structure heating to high temperatures. So it is important to know temperature dependence of contact resistivity $\rho_c(T)$ of ohmic contacts over a wide temperature range. The classical mechanisms of current flow cannot explain experimentally observed anomalous $\rho_c(T)$ curves (growing with temperature). However, such behavior can get consistent explanation by the mechanisms of contact formation in crystals with either high density of dislocations with which metal shunts of contact metallization are associated [1] or a $n^+$–$n$-Si doping step [2]. The dislocation density in the silicon near-surface layer (determined from the etch pits after removal of contact metallization) is $\geq 10^7 \cdot \text{cm}^{-2}$.

A model for understanding the above mechanism (with high dislocation density) involves an array of metal shunts with small radius of curvature ($\sim 2 \cdot 10^{-8}$ cm). The features of realization of such mechanism are (i) appearance of strong electric field at the shunt end–semiconductor interface, (ii) presence of potential wells for electrons near the shunt ends because of high potential of mirror reflection force (opposite in sign to the Schottky potential), and (iii) current limitation by diffusion supply of electrons, i.e. $\rho_c(T) \sim 1/\mu(T)$, where $\mu$ is electron mobility.

Application of highly doped $n^+$-layer in the metal–$n^+$–$n$-Si structure leads to realization of the tunneling mechanism of current flow. However, density of structural defects (dislocations) increases as $n^+$ grows. So one should limit the $n^+$ value; as a result, the thermal-field mechanism of current flow is realized. In this case, the thickness of a heavily doped region where electrons are degenerate has to exceed the Schottky layer thickness, and $\rho_c = \rho_{c1} + \rho_{c2}$ (the resistivity $\rho_{c1}$ is related to field-stimulated passage of electrons through the barrier at the heavily doped semiconductor–metal interface, and $\rho_{c2}$ is the resistivity of the weakly doped region). The $\rho_c(T)$ curves in ohmic contacts with a doping step are anomalous because of an accumulation band bending in the weakly doped $n$-Si region near its boundary with the $n^+$-Si layer.

Thus, the mechanisms of formation of ohmic contacts with either high dislocation density or $n^+$–$n$-Si doping step ensure ohmic contacts, if the requirement $\rho_{c2} >> \rho_{c1}$ is satisfied.

1. A.V. Sachenko et al., *JAP*, **112**, (2012), 063703.
2. A.V. Sachenko et al., *SPQEO*, **17**, (2014), 1.

# Morphology of Surfaces of PbTe Films Grown by Pulsed Laser Deposition

Virt I.S.[1,3], Rudyj I.O.[2], Lopatynskyi I.Ye.[2]

[1] *Drogobych State Pedagogical University, Drogobych, Ukraine*
[2] *National University "Lviv Polytechnic", Lviv, Ukraine*
[3] *University of Rzeszow, Rzeszow, Poland*

Laser is a powerful tool in many applications. It is especially useful in material processing. Often the light beam is intense enough to vaporize the hardest and most heat resistant materials. This paper discusses laser methods for fabricating high-quality lead chalcogenides. Lead chalcogenides, such as PbTe, PbS and PbSe, have attracted considerable attention because of their potential applications in thermoelectric and infrared devices. A proposed method is to use a defocused laser to apply energy at a single nucleation site, and then propagate materials growth by scanning the laser along the substrate. The explanation of epitaxy mechanisms in PLD is a most important and difficult problem.

The most popular parameter characterizing the morphology of surfaces is the RMS roughness, which represents the root mean square height of a surface around its mean value. A more complete description is provided by the power spectral density (PSD) of the surface topography.

In this paper, average roughness, $R_a$, is used to describe feature heights and power spectral density is used to describe the contribution of surface features of different lateral sizes to the roughness. $R_a$ is defined as the average absolute deviation of each point in the profile from the mean, and the power spectral density is the magnitude of the Fourier transform (FFT) of the surface profile. In order to quantify the surface quality of three samples, we performed roughness calculation, for a large set of the data for same scan areas as well as different scan areas from different position of the films, involving the RMS roughness – $\sigma$ and $R_a$. The power spectral density by FFT algorithm was applied in analyzing the AFM image data. The taper window function for the FFT algorithm was used to reduce edge effects and to minimize spectral leakage before calculation of the PSD. PSD dependant on the spatial frequency $f$ yields, $PSD(f) = K * f^{-\gamma}$, where K has spatial length to the power of PSD. The $\gamma$ is calculated as the inverse slope in the log-log plot of the high spatial frequency and the PSD. In our study, the length scale ($L$) considered is 3.0 mm. The maximum frequency is limited by the sampling theorem of Nyquist frequency.

The fractal dimension ($D_f$) of the films was evaluated to characterize the surface morphology. The fractal dimension of the surface can be obtained from the parameter $C$ of the k-correlation, $D_f = \frac{(7-C)}{2}$. The dimension value determines the relative amounts of the surface irregularities at different distance scales. $D_f$ = 3 is called the extreme fractal; $D_f$ = 2.5 the Brownian fractal and $f$ = 2 the marginal fractal.

The roughness values for samples with different scan areas are shown in Table 1. As one can see, all PSD curves essentially present the same characteristic shape, consisting in a at response in the lower part of the spatial frequency spectrum and a power law roll-o with frequency in the upper part of the spectrum.

Considering the topographic scattering in applications, it is obvious that this would not be influenced by improving the substrate finish and scatter reduction could be achieved only by changing the $S(f) = \frac{A}{[1+(B\cdot f)^2]^{\frac{C}{2}}}$, deposition conditions.

where *A*, *B* and *C* are model parameters. A is the value of the spectrum in the low-frequency limit, the "shoulder parameter" is a "correlation length" which sets the point of the transition between the low and high-frequency behavior, and *C* is the exponent of the power-law fall-of f at high requencies. At low spatial frequencies ($f_1 = B$) the PSD is constant and equals *A*; at high *f* values, the surface is fractal, its PSD function scaling as $1/f_C$. The ABC model succeeds in describing quite satisfactory the morphologies for both the substrate and all thin filmsamples over the entire spatial frequency range. The *A, B* and *C* parameters of the respective fits are given in Table 1:

Table 1: The roughness values for samples

| films/sustrates | *A* | *B* | *C* |
|---|---|---|---|
| PbTe/Si | 0,6 | 245 | 2,2 |
| PbTe/$Si_3N_4$ | 0,2 | 140 | 2,2 |

Several observations could be drawn from the above results:

- In the mid and high frequency regions, the glass substrate behaves as an ideal fractal surface ($C \geq 2$).

The value of *A* parameter is related to the low frequency component of surface roughness, while the value of *B* parameter (the correlation length), is linked to grain size.

1. Taketsugu, Y. Noriyoshi, *Applied Surface Science*, **253**, (2007), 6196.
2. S. Padilla, O. Drbohlav, P. R. Green, A. Spence, M.J. Chantler, *Perceived roughness of 1/f$^b$ noise surfaces*, **48**, **(**2008), 1791.

## СЕКЦІЯ 1 (стендові доповіді)
## ТЕХНОЛОГІЯ ТОНКИХ ПЛІВОК (МЕТАЛИ, НАПІВПРОВІДНИКИ, ДІЕЛЕКТРИКИ, ПРОВІДНІ ПОЛІМЕРИ) І МЕТОДИ ЇХ ДОСЛІДЖЕННЯ

12-15 травня 2015 р.

## SESSION 1 (poster)
## THIN FILMS TECHNOLOGY (METALS, SEMICONDUCTORS, DIELECTRICS, CONDUCTIVE POLYMERS) AND THEIR RESEARCH METHODS

May, 12-15, 2015

# Methods of Reconstruction and Restoration of Images

Balovsyak S.V., Lutsyk I.V., Fodchuk I.M.

*Yuriy Fedkovych Chernivtsi National University, Chernivtsi, Ukraine*

In the real conditions for a photo and video shooting, as well as obtaining the results of X-ray and electron diffraction techniques, images are often distorted due to defects of sensors and other instrumental factors. This leads to a decrease in visual quality imaging in particular, due to noise and blur.

In this paper analyzes the possibility of using modern methods of reconstruction and restoration of damaged digital images. We describe the advantages and disadvantages of these methods and identified possible areas of use. For the reconstruction and restoration of images used three basic approaches: spatial, frequency and wavelet filtering [1, 2].

The basis of spatial filtering is image processing within local spatial regions, for example, by convolution of the damaged image with the kernel of filter. As the result of this filtration, depending on the type of the used kernel of filter, there is the smoothed image out or, opposite, image with the selected contours. The advantage of spatial filtering is the simplicity and drawback is to decrease performance with increasing the size of the filter kernel.

Frequency filtering is based on the direct and inverse Fourier transform. It is characterized by high performance. For frequency filtering frequencies of noise weakened more than the frequency signal. The frequency filtering is most effective when frequencies the desired signal and noise is not overlap. The main disadvantage is the difficulty of spatially inhomogeneous image processing.

Wavelet processing is one the most perspective methods, which allows to execute multiscale spatial heterogeneous filtration of images. The main disadvantage of wavelet filtering – difficulty of settings adjustment.

Implementation of the program processing a series of images of X-ray topography and magnetic resonance imaging performed by the described above methods in Matlab environment using packages Wavelet Toolbox and Image Processing Toolbox. As a result of the analysis of methods of reconstruction and restoration of images advantages and prospects of their use are defined at the image processing of certain type depending on spatial homogeneity and frequency spectrum of images.

1. Bates R. Restoration and Reconstruction of images / R. Bates, M. McDonnell. – M. : Mir, 1989. – 336 p.
2. Gonzalez R. Digital Image Processing using MATLAB / R. Gonzalez, R. Woods, S. Eddins. – Prentice Hall, 2004. – 609 p.

# Preparation And Dielectrical Studies of "Liquid Crystal – Superionic Nanocrystals" Composites

Demko P.Yu.[1], Bendak A.V.[1], Studenyak I.P.[1], Kovalchuk O.V.[2,3], Lisý V.[4], Kopčanský P.[5], Timko M.[5], Tomašovičová N.[5], Gdovinova V.[5], Miskuf J.[5]

[1]*Uzhgorod National University, Uzhhorod, Ukraine*
[2]*Kyiv National University of Technologies and Design, Kyiv, Ukraine*
[3]*Institute of Physics, National Academy of Sciences of Ukraine ,Kyiv, Ukraine*
[4]*Technical University of Košice, Košice, Slovakia*
[5]*Institute of Experimental Physics, Slovakian Academy of Sciences, Košice, Slovakia*

Last few decades the great interest belongs to the studies of the effect of nanoparticles on the properties of various materials, including liquid crystals, in order to obtain compositions with new functional properties. In present investigation $Cu_6PS_5I$ superionic nanoparticles is used. $Cu_6PS_5I$ compounds belong to the argyrodite family; they are promising materials for creation of solid state batteries, supercapacitors and electrochemical sensors. The ionic conductivity is caused by the presence of $Cu^+$ ions having high mobility as well as to the peculiarities of the crystal structure which provides high concentration of disordered vacancies and, consequently, migration of copper ions.

The synthesis of $Cu_6PS_5I$ compounds was performed as follows: Cu, S, P, and CuI in accordance with the stoichiometry were placed in an evacuated ampoule of quartz glass. The ampoule was heated at a rate 100 K/h to the temperature of 450–500 K and kept at this temperature during 24 h. Then at a rate of 100 K/h the temperature was increased to the maximal value of 1020–1070 K and the ampoule was kept at this temperature during 5-6 days, then they were cooled down to room temperature at a rate 100 K/h. The $Cu_6PS_5I$ powders were milled with a planetary ball-mill. For composites preparation $Cu_6PS_5I$ superionic nanocrystals with different concentrations were added to liquid crystal 6CB. Dielectric properties of the samples were studied within the frequency range $10^{-1}…10^6$ Hz at the temperature 293 K by using the oscilloscopic method. The amplitude of the measuring signal with the triangular shape was 0.25 V.

The frequency dependencies of dielectric permittivity of composites were used for calculation of the frequency dependencies of electrical conductivity. The electrical conductivity values were determined on that part of spectra where the electrical conductivity does not depend on frequency. The high values of electrical conductivity in composites in comparison with liquid crystal 6CB are the evidence of their enhancement due to the introduction of $Cu_6PS_5I$ superionic nanocrystals into the liquid crystal. It should be noted that the increase of concentration of nanocrystals leads to the increase of composite electrical conductivity.

# Substructure properties of MgO thin films obtained by spray-pyrolysis technique

Diachenko O.V., Opanasyuk A.S., Kurbatov D.I.

*Sumy State University, Sumy, Ukraine*

Today more and more areas of electronic equipment used oxide materials as a result - their study is very relevant. Therefore, in this paper the substructure properties of magnesium oxide thin films have been studied.

Magnesium oxide films were obtained on glass substrates 1x1 $cm^2$ by spray pyrolysis technique. Before deposition the substrates surface were cleaned in the tub with ethanol for 300 seconds. We used the 0.2 M magnesium chloride hexahydrate ($MgCl_2 \cdot 6H_2O$) aqueous solution as a precursor solution. Deposition of MgO films was carried out at the substrate temperature range from $T_s$ = 640 K to 690 K with step 10 K.

The diffractometrical method was used for estimation of average values of the coherent scattering domain size (CSD) L and microstrain (ε) by the half-width of the diffraction lines. To separate the diffraction broadening caused by physical and instrumental effects we used approximations of the X-ray line by Cauchy and Gauss functions. Additionally, microstrain and the size of CSD were determined by the method of approximation of the X-ray line as a threefold convolution.

The results of calculations of CSD and microstrain in crystallographic directions are summarized in Table. As it is shown in Table, the values of substructural parameters, obtained with the help of different approximations, correlate well with each other, as it should be on theoretical considerations. This demonstrates the reliability of the results. However, the most accurate values were obtained by threefold convolution of the functions.

*Substructural features of MgO films obtained using different approximations*

| *T, K* | (*hkl*) | *L*, nm | | | $\cdot 10^3$ | | |
|---|---|---|---|---|---|---|---|
| | | Approximations | | From convolution | Approximations | | From convolution |
| | | Gauss | Cauchy | | Gauss | Cauchy | |
| 370 | (111)-(222) | 37.7 | 63.1 | 42,8 | 3.17 | 2.35 | 2.75 |
| 380 | (111)-(222) | 100.1 | 491.5 | 255.9 | 4.37 | 4.04 | 4.29 |
| 390 | (111)-(222) | 16.1 | 17.8 | 16.2 | 2.56 | 0.91 | 1.91 |
| 400 | (111)-(222) | 27.2 | 41.4 | 29.6 | 3.77 | 2.67 | 3.19 |
| 410 | (111)-(222) | 32.5 | 65.2 | 40.7 | 4.82 | 3.99 | 4.35 |
| 420 | (111)-(222) | 32.5 | 65.2 | 40.7 | 4.82 | 3.99 | 4.35 |

# Investigation of the Kinetics of Photoinduced Electronic Transitions in Nanostructures of Bacterial Reaction Centers

Drapikovskyi M.A., Kulish M.P., Zabolotny M.A. Barabash Y.M.

*National Taras Shevchenko University of Kyiv, Kyiv, Ukraine*

The high reactions efficiency of photo-stimulated electron transfer (ET) in biological systems, including the structure of reaction centers attracted attention of many researchers. Analysis of the main factors determining the speed of such reactions is important both in fundamental terms, and in terms of creating artificial systems, storage and energy conversion. Found that ET in biological systems occurs as series of ET in the structure of proteins between the metal centers or organic donor-acceptor groups at a distance of 5-25 Å. In this regard, series of experiments related to ET in the structure of proteins was conducted.

We have researched the kinetics of electron transport in bacterial reaction centers (RC). We have researched the processes of relaxation and photoinduced structural changes in molecular complexes RC Rhodobacter spharoides in the process of intramolecular electron transfer. We have presented results of experimental research of depending transition microspeed between donor and acceptor on the RC illumination intensity and time and on theoretical analysis of relaxation curves by using wavelet transforms.

Following conclusions were done from the research:

1. Kinetics microspeed of the electron transfer from the donor to the acceptor and donor acceptor solutions at RC Rhodobacter sphaeroides, depends on illumination time and intensity. With increasing time or intensity reduction processes are slower, which may indicate the influence of polarization effects on the processes of intramolecular electron transport.

2. The received dependences of optical absorption and quantitative parameters of the kinetics of the oxidation reaction centers at different modes of photo excitation allowed to divide the kinetics of optical absorption to two parts: slow and fast. Fast kinetics characterizes electron transport and slow one - electron transport and slow conformational change RCs.

3. Wavelet analysis examines features of experimental curves of relaxations, depending on the intensity and exposure time. It shows that the restoration and acquisition solutions RC is non-stationary process in time. We make the assumption, that the exponent in the relaxation curves do not act simultaneously and are included in sequence.

4. With the exclusion of light exiting the optical absorption of the solution returned in original condition, which proves that the photo induced changes in the molecular complex RC are reversible. Measurement of the refractive index of the solution by holographic interferometry shows that the change in volume of the molecular complex RC, with its light, is 0.1% -1%. This change in

volume of the RC can be caused by a change in the angle between the bonds M, L, H RC globules that are most labile.

5. Qualitative coincidence of oxidation kinetics of recovery with phytospectrums RC in their light, confirming the relationship between electron transport and conformational changes in RC.

Thus high efficiency reaction photo-stimulated electron transfer in biological systems, including the structure of the reaction centers enables to understand and learn to use photo processes. Analysis of the main factors that determine the rate of such reactions is important as a fundamental and from the point of view of creating artificial systems of conservation and transformation of energy, enabling the improvement and creation of new medical nanoelectronics.


1. Olson J.M., Trornber J.P. Membrane Proteins in Energy Transduction // New York: Marcel Dekker. - 1999. - P. 279-340.
2. Rubin A.B. Biophysics, Moscow: Moscow State Univ., 2000, Vol. 2 (in Russian).
3. Amin M, Vogt L, Vassiliev S, Rivalta I, Sultan MM, Bruce D, Brudvig GW, Batista VS, Gunner MR. Electrostatic effects on proton coupled electron transfer in oxomanganese complexes inspired by the oxygen-evolving complex of photosystem II. J. Phys. Chem. (2013) Vol. 117: 6217-26.
4. Kharkyanen V. N., Barabash Yu. M., Berezetskaya N. M., Lukashev E. P., Knox P. P., Christophorov L. N., Peculiarities of light-induced slow protein dynamics in the photosynthetic reaction center, Chemical Physics Letters, Vol.Том: 512, No 1-3, 2011, 113 - 117
5. Barabash Yu.M., Berezetskaya N.M., Christophorov L.N., Goushcha A.O., Kharkyanen V.N. // J. Chem. Phys, 2002, Vol. 116, No. 10, P. 4339–4352.
6. Kukushkin A.K., Tikhonov A.N. Lectures on Biophysics of Photosynthesis, Moscow: Moscow State Univ., 1988 (in Russian).
7. Barabash Yu.M., Zabolotny M.A., Sokolov N.I., Kharkyanen V.N. // Biofiz., 2002, Vol. 47, No. 6, P. 970-976.

# Charging of Thin Polymer Electret Films in Corona Discharge

Fedosov S.N., Sergeeva A.E.

*Odessa National Academy of Food Technologies, Odessa, Ukraine*

A corona discharge is a self-sustainable electrical discharge occurring when a sufficiently high voltage is applied between asymmetric electrodes such as a point or a fine wire and a plate. The corona discharge is perfectly controllable and thus it can be easily used for charging electrets. The corona charging has the following advantages compared with other poling methods: (a) poling can be performed without deposited electrodes or with only one electrode, (b) higher fields can be achieved in corona poling than in the case of sandwich contact poling, and (c) thin films can be poled in spite of defects, because destructive breakdown phenomena are limited only to small sample areas [1].

By inserting a control grid between the corona electrode and the sample surface, the charging can be supplemented with simultaneous measuring the build-up and decay of the surface potential. The constant current corona triode is mainly applied as an experimental technique for characterizing three types of polymers: nonpolar, ferroelectric and with non-linear optical properties [1].

Non polar polymers of high electrical resistance such as Teflon, capable of storing space charge for a long period of time have been used for electret applications, e.g. microphones. Ferroelectric polymers form a class of electrets with highly ordered and disordered phases coexisting in one material. To induce ferroelectric orientation of dipoles, the polymers such as PVDF, P(VDF-TrFE), P(VDF-TFE) were subjected to a poling procedure usually performed in a corona setup. In the case of a constant current corona triode it has been found that the initial poling and switching processes in ferroelectric polymers consisted of three stages, each one corresponding to a definite part of the sample potential - time curve. Polymers for nonlinear optics attracted interest because of the strong nonlinearity of molecular chromophores as guests, side groups, or main-chain segments. The technique most commonly used for NLO polymers is corona poling performed near the glass transition temperature. We believe that corona poling under well controlled conditions may contribute in optimizing the poling processes of NLO polymers in order to obtain second order nonlinear activity.

Due to its versatility and flexibility, corona charging allows for the optimization of the poling procedure for a given electret. If excess surface or/and volume charge is to eliminated or neutralized, one can easily perform virtual short circuiting in a corona triode by changing the corona polarity with simultaneous grounding of the control grid of the corona triode.

1. J. A. Giacometti, S. Fedosov, M. M. Costa *Brazil. J. of Physics*, vol. 29, 1999, p. 269-279.

# Non-Uniformity of Polarization in Thin Ferroelectric Polymer Films

Fedosov S.N., Sergeeva A.E.

*Odessa National Academy of Food Technologies, Odessa, Ukraine*

Polymer ferroelectrics are increasingly used for creating new types of electroacoustic transducers, as well as pyroelectric and piezoelectric sensors. The performance of such elements strongly depends on the value, stability and uniformity of the residual ferroelectric polarization produced in the process of the high voltage application to virgin samples.

Measurement of polarization and space charge profiles provides valuable information on their relationship in the process of formation of the polarized state and in ensuring of its stability. That is why we have experimentally studied the dynamics of polarization profiles in produced by Plastpolymer polyvinylidene fluoride (PVDF) and of polyvinylidene fluoride with tetrafluoroethylene copolymer P(VDF-TFE) films with a thickness of about 25 μm not only in the process of electrification, but also during and after switching of the voltage polarity in fields close to coercive ones (50-60 MV/m) and in strong fields of the order of 160 MV m, as well as during and after the short circuiting of the samples after electrization carried out either by the contact method or in a controlled corona discharge. Measurements were performed at the University of Stuttgart and at the University of Karlsruhe.

We have found that at the field strength of $E$ = 50 MV/m, a sharply inhomogeneous asymmetric distribution of the residual ferroelectric polarization was formed with the presence of about 5 μm thick zone near the negative electrode, in which the residual polarization was equal to zero.

During the switching of the voltage polarity, the strong non-uniformity of polarization was preserved, and it was not possible to improve it by the application of even very strong fields of the order of 160 MV/m.

It has been found that for obtaining the uniform distribution of polarization, the first electrization of a virgin non-polarized sample should be carried out in strong fields of the order of 150 MV/m. In this case, the uniform polarization was formed along the entire sample thickness. The polarization uniformity was continuing during the short circuiting of the samples after charging, as well as during the switching of the applied voltage polarity.

The obtained results have been confirmed by measurements on the same samples by two independent methods, namely by the piezoelectrically induced pressure step method (PPS) and the light intensity modulation method (LIMM). The sensitivity of the PPS method was 3 μm and the resolution of the LIMM method near the illuminated electrode was claimed to be about 0.1 μm.

# Gold Nanoparticles Arrays in CdS Matrix: Fabrication and Properties

Il'chuk H.A., Kusnezh V.V., Petrus' R.Yu., Rodych V.M.

*Lviv Polytechnic National University, Lviv, Ukraine*

The CdS/CdTe thin-film solar cells (SC) are among top commercial thin-film cells. The world largest photovoltaic 550 MW power station "Topaz Solar Farm" (USA) includes 9 million of the CdTe thin-film photovoltaic modules. Nevertheless CdS/CdTe SC maximal efficiency 19.6% [1] is still far from the theoretical one 28-30%. The efficiency increase can be achieved due to light scattering and absorption on metal nanoparticles (NP), and electromagnetic field amplification by means of surface plasmon (SP) excitation in active layer.

The possibility of gold NP array formation in the chemically deposited CdS thin film matrix was investigated. The gold NP array were fabricated by thermal annealing (400 º C, 120 min.) in vacuum (P~1.3 Pa) of the Au thin films with 6-7 nm nominal thickness obtained by magnetron sputtering (Neo Coater MP-19020 NCTR, Jeol, Japan) on CdS thin (100 nm) films. The surface morphology using an atomic probe microscope was investigated. According to APM data this film consists of NP arrays in the form of oblate spheroids with a mean diameter of 61±3 nm and a mean height of 55 nm. The positions of plasmon resonance peaks at 593 nm wavelength were determined using fiber optic spectrophotometer (AvaSpec-ULS 2048-UA-50, Avantes, Netherlands). The CdS films with 100 nm thickness were chemically deposited on the fabricated Au NP arrays. Therefore the Au NP arrays in CdS thin film matrix were fabricated by subsequent CdS film chemical deposition and Au NP formation between semiconductor layers. The plasmon resonance peak shift from 593 to 604 nm in the absorption spectra has been registered.

1. Green M. A., Emery K., Hishikawa Y., Warta W., Dunlop E. Solar cell efficiency tables (version 44) // Prog. Photovolt: Res. Appl.-2014.-**22.-**P. 701–710.

# Plasmonic Nanoporous Films with Gold Nanoparticles

Kaganovich E.B., Krishchenko I.M., Manoilov E.G.

*V. Lashkaryov Institute of Semiconductor Physics, NAS of Ukraine, Kyiv, Ukraine*

Nanocomposite porous films containing gold nanoparticles (Au NPs) (films of porous gold (por-Au) with porosity 5–60%) were formed using the method of pulsed laser deposition onto substrates which were placed both at a distance from the target (forward clusters transfer from the torch) and into the its plane (backward clusters transfer from the torch). The gold target was irradiated with emission of YAG:$Nd^{3+}$ laser ($\lambda$ = 1.06 μm, $t_p$= 10 ns, $f_p$ =25 Hz) under control of the following technological parameters: gas pressure in the chamber $p_{Ar}=10^{-2}\ldots10^{2}$ Pa, energy density in the pulse j =5…20 J/cm$^2$, number of pulses N= 7500…60000, the distance from the torch axis to definite film area L =5…20 mm. Local surface plasmon resonance with maximum $\lambda_{max}$=540–740 nm was observed in transmission spectra T($\lambda$) of films. The influence of formation conditions of film and its structure on the plasmon features was studied. Set of technological film preparation parameters with controlled plasmon properties LP was determined.

Forward clusters transfer from torch at $p_{Ar}\approx$10 Pa resulted in the formation of clusters with sizes of a few nanometers at high concentrations of ablation particles $n_a$. Films contain a large number of small size Au NPs with small spacing between them. This led to dipol-dipol interaction of Au NP which was responsible for T ($\lambda$) spectra at $\lambda_{max}\approx$740 nm. Argon pressure increase resulted in increasing of clusters size while concentration $n_a$ was decreased. Films contain Au NPs of size up to 10-15 nm with less concentration and much large space size between them. Values $\lambda_{max}$ in the visible spectra were connected with internal size effect in the dipole approximation, taking into account the impact of structural and electronic properties of Au NPs.

In backward clusters transfer from torch the films were obtained with gradient thickness, sizes of Au NPs, nanopores as well as with correspondent maximum in local surface plasmon absorption spectra.

Obtained por-Au films are designed to surface enhanced molecule fluorescence, quantum dots photoluminescence, Raman scattering. On the basis of these films SERS substrates were formed for Rhodamine R6G with concentration $10^{-10}$ M and enhancement factor $3.9\cdot10^{7}$. Great enhancement factor and the best analyte limit detection were achieved due to the nanoporous film structure which was characterized by “hot spots” formation.

# Formation of coating on high-entropy FeCoCrNiVAl alloy during annealing

Karpets M.V.[1], Makarenko E.S.[1], Rockitskaya E.A.[1], Gorban' V.F.[1], Krapivka N.A.[1], Tsebrii R.I[2]., Kantsyr E.V.[3]

[1]*Institute for Problems of Materials Science, NAS of Ukraine, Kiev, Ukraine*
[2]*Ternopil National Economic University, Ternopil, Ukraine*
[3]*National Technical University of Ukraine "Kyiv Polytechnic Institute", Kiev, Ukraine*

The study of phase transitions in cast high-entropy FeCoCrNiVAl alloy using high-temperature (HT) *in situ* X-Ray diffraction in temperature range 293 – 1273 K in a helium atmosphere (fig. 1). In initial state this alloy is a single-phase solid solution on the basis of the BCC structure, ordered according to B2 type. In the temperature range 473 – 873 K changes phase composition is not observed. However, fixed increase in the period of the phase ordered with the B2-type structure, which is associated with the thermal expansion of lattice.

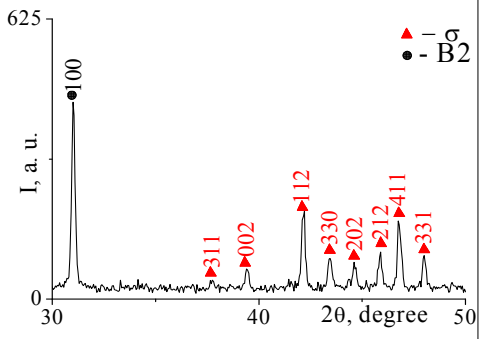


Fig. 1. High-temperature *in situ* XRD patterns of multicomponent FeCoCrNiVAl alloy in a helium atmosphere at 1073 K

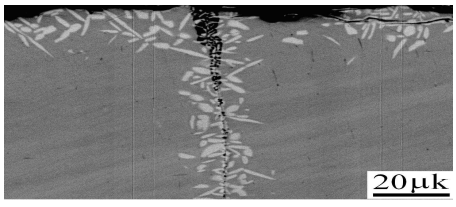


Fig. 2. SEM image of cross-section FeCoCrNiVAl alloy after annealing at 1273 K /2h

At a temperature of 1073 K in addition matrix ordered BCC phase by HT X-ray was recorded reflections of the tetragonal σ-phase type CrFe in an amount of 64 wt. % (Fig. 1). After a slow cooling of the sample in the chamber to room temperature by using X-ray analysis revealed redistribution quantitative ratio in the phases (the number of σ-phase increased to 72 wt. %). To exclude the influence of the helium atmosphere in HT X-Ray camera on the formation of the phase composition of the surface layer additional annealing in a vacuum for 2h at 1073 and 1273 K were performed. Before annealing on surface alloy layer thickness ~40 μk was removed. Annealing does not change phase composition, however, is fixed redistribution in the phase components and increases the period lattice of σ-phase.

Fig. 2 represented SEM image of cross-section FeCoCrNiVAl alloy after annealing at 1273 K /2h. The thickness of the surface layer of σ-phase is about 20 – 22 μk. Precipitation of σ-phase is observed mainly on the sample surface and at least on the grain boundaries, as well as in grains body. σ-phase has an elongated needle-like type.

# Nanoindentation Study of Boron-Ion Implanted Polymethylmethacrylate with Ultra Nano Hardness Tester: Methodological Aspects

Kavetskyy T.S.[1,2], Kukhazh Y.Y.[1], Borc J.[3], Stepanov A.L.[4,5,6]

[1]*Drohobych Ivan Franko State Pedagogical University, Drohobych, Ukraine*
[2]*The John Paul II Catholic University of Lublin, Lublin, Poland*
[3]*Lublin University of Technology, Lublin, Poland*
[4]*Kazan Physical-Technical Institute, Russian Academy of Sciences, Kazan, Russia*
[5]*Kazan National Research Technological University, Kazan, Russia*
[6]*Kazan Federal University, Kazan, Russia*

Depth-sensing indentation, called as nanoindentation, means an instrument which possesses the ability to measure the indenter penetration depth *h* under an applied force *F* throughout the testing cycle [1]. This method gives information about the contact parameters and mechanical properties, which are calculated from the indenter load and the depth measured continuously during loading and unloading. The advantages are very low loads and only minor depths with no special demands on the test specimens. It is capable of measuring both the plastic and elastic deformation of the material under test. The method was originally developed for testing the hardness and elastic modulus from indentation load-displacement data in elastic-plastic materials including fused silica, soda-lime glasses, and single crystals of aluminum, tungsten, quartz, and sapphire [2] and further reviewed with advances in understanding of the mechanics of elastic-plastic indentation [3].

Recently, we have reported [4] a first time the results of investigation of the influence of low dose $B^+$-ion-irradiation on the mechanical properties (hardness and elastic modulus) of polymethylmethacrylate (PMMA) probed by nanoindentation with an ultra nano hardness tester (UNHT) in the range of 300-1100 nm indentation depth. The current work is focused on the nanoindentation study of the B:PMMA samples with the UNHT up to 2000 nm indentation depth, governing three expected layers: (i) “implanted layer” up to 500 nm, (ii) “implanted layer + matrix” up to 1100 nm, and (iii) “implanted layer + matrix” with deeper penetration of indenter into matrix. The methodological aspects of progressive multicycle used for the nanoindentation tests are presented.

1. Introduction on Instrumented Indentation, http://www.csm-instruments.com.
2. W.C. Oliver, G.M. Pharr, J. Mater. Res., Vol. 7, No. 6, 1992, P. 1564-1583.
3. W.C. Oliver, G.M. Pharr, J. Mater. Res., Vol. 19, No. 1, 2004, P. 3-20.
4. T.S. Kavetskyy, J. Borc, Y.Y. Kukhazh, A.L. Stepanov, In book: NATO Science for Peace and Security Series - A: Chemistry and Biology, Chapter 7 “Nanoscience Advances in CBRN Agents Detection, Information and Energy Security” (P. Petkov, D. Tsiulyanu, C. Popov, W. Kulisch, eds.), Berlin: Springer, 2015, P. 65-71.

# Sensory Elements and Devices Operational Diagnostic Blood Glucose

Kogut I.T., Kotyk M.V., Virstyuk V.V.

*Vasyl Stefanyk Precarpathian National University, Ivano-Frankivsk*

Problem research and creation of sensor elements, processing schemes and homeland device for operative diagnostics of blood glucose levels is relevant because of the significant increase the number of diabetic patients. For daily, non-stop and continuous monitoring of blood glucose levels the most promising are issued portable type non-invasive blood glucose meters, because, without mechanical interference with the patient's body to assess the level of glucose. This method, despite the worst accuracy, has several advantages compared to invasive methods.

We considered the physical principles of detection, in particular, the optical spectra absorbtion of blood glucose are shown (Fig. 1), the schematic diagrams opical sensors are shown(Fig. 2).

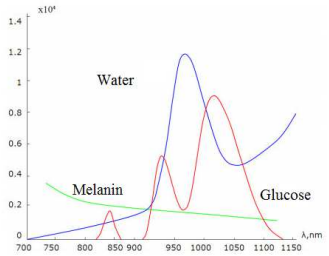


Fig. 1. The optical absorption spectrum of blood glucose.

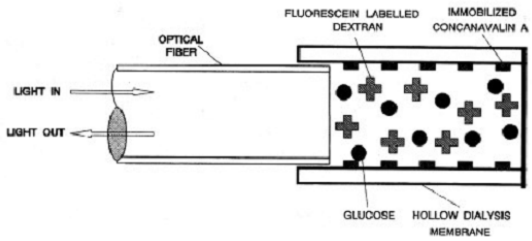


Fig. 2. Schematic diagram of the optical sensor to measure glucose. [1]

This data can be used as a basis for the development of optical sensors and data processing schemes for non-invasive portable blood glucose meters of optical type.

A conceptual block diagram of the blood glucose meter was proposed (Fig. 3). Experimental device pattern is demonstrated (Fig. 4), which confirms the possibility of further work towards building element base non-invasive blood glucose meters.

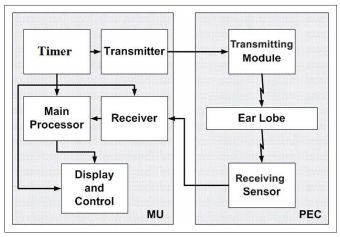


Fig. 3. The conceptual block diagram of non-invasive glucose meter (MU- main unit, PEC - personal ear clip).

Fig 4. The experimental device

1. Mendelson, Y. Optical Sensors, in The Biomedical Engineering Handbook, Bronzino, J.D., Ed. Boca Raton, FL: CRC, p. 764–778, 1995.

# Electron Mobility in Cadmium Sulfide

Malyk O.P.[1], Rodych V.M.[2], Ilchuk H.A.[2]

[1] *Semiconductor Electronics Department, Lviv Polytechnic National University, Lviv, Ukraine*
[2] *Physics Department, Lviv Polytechnic National University, Lviv, Ukraine*

Usually the charge carrier scattering models in cadmium sulfide are considered in the relaxation time approximation. However, these models have essential shortcoming: a) they contradict the special relativity according to which the charge carrier would interact only with the neighboring crystal region; b) they contradict the atomistic hypothesis according to which the charge carrier interacts (and transfers the energy respectively) only with one atom but not simultaneously with many atoms which are situated in different points of space. From the other hand in [1-3] the short- range models of carrier scattering were proposed for $A^{II}B^{VI}$ and $A^{III}B^{V}$ semiconductors (zinc blende and wurtzite structure) in which the above mentioned shortcomings were absent. The purpose of the present paper is to use of short-range models to describe the electron scattering on the various crystal lattice defects taking into account the complex structure of optical vibrations in wurtzite CdS.

The CdS samples with defect concentration $1.68\times10^{16} \div 8.7\times10^{17}$ $cm^{-3}$ were investigated. For the charge carrier scattering on the nonpolar optical and acoustic phonons, neutral defects and static strain potential the interaction radius of the short-range potential is limited by one unit cell. For the charge carrier scattering on the ionized impurity, polar optical and piezoelectric (piezoacoustic and piezooptic) phonons the interaction radius of the short-range potential is founded in a form $R = \gamma\sqrt{3a_0^2 + c_0^2}/2$ ($a_0$, $c_0$ - lattice constants, $\gamma$ – the respective adjustable parameters). To calculate the conductivity tensor components the method of the exact solution of the stationary Boltzmann equation was used [4].

The temperature dependence of the electron mobility in the range 30 ÷ 300 K in wurtzite cadmium sulfide is calculated. The influence of the different scattering mechanisms on the charge carrier mobility is considered. The scattering parameters $\gamma$ for different scattering modes are determined. The temperature dependence of the electron Hall factor is calculated.

1. O.P. Malyk. Physica B:Condensed Matter. 2009. **404**. 5022-5024.
2. O.P. Malyk. Diamond Relat. Mater. 2012. **23**. 23-27.
3. O.P. Malyk. Can. J. Phys. 2014. **92**. 1372-1379.
4. O.P. Malyk. WSEAS Trans. Math. 2004. **3**. 354- 357.

# Optical Properties of Vacuum Condensates Manufactured by Oblique Deposition

Ovcharenko O.P.[1], Gaman D.A.[2], Bilozertseva V.I.[2], Khlyap H.M.[3]

[1]*V.N. Karazin Kharkov National University, Kharkiv. Ukraine*
[2]*National Technical University " Kharkiv Politechnical Institute ", Kharkiv, Ukraine*
[3]*University of Technology, Kaiserslautern, Germany*

Needing fabrication of new materials and wide range variation of their properties stimulates appearing of big number of theoretical and experimental works devoted to studying new thin-film coatings with different structural perfectness. The porous optical layers allowing variation of the refractive index in the range $n = 1.05 \div 1.08$ are of particular interest.

This work reports optical and structural characteristics of porous coverings obtained by thermal evaporation in vacuum ($P < 5 \cdot 10^{-4}$ Pa) under oblique incident beam (angle to the normal of glass substrate is $\approx 70 \div 80^\circ$). Optical transmission of condensates is examined in the range 300 ÷ 1200 nm. Numerical working-out of experimental results allowed determining optical constants of the samples and their dispersion [1]. The microstructure and porosity of the coverings and their connection with optical characteristics are also investigated.

The oblique deposition in vacuum has a disadvantage: the film is deposited inhomogeneously on the substrate surface. It happens due to different distance of the substrate surfaces from the evaporator and various angles of incident substance flows. We also have studied effect of inhomogeneous thickness and optical properties of separate layers on characteristics of bilayer enlightenment covering.

We showed a possibility of manufacturing interference layers with variable properties necessary for optical enlightenment of different optical devices.

1. Ovcharenko A.P., Duong Thi Nhu Tranh, Rakitin I.I., Gaman D.A. Numerical method of determining optical constants and thickness of thin films // Physics and technology of thin films and nanosystems. Proceedings of XII International Conference. – V.1. – May 18 - 23, Ivano-Frankovsk, 2009. p. 219-221.

# Photoluminescent Properties of Composites Based on Polymers with Thiophene Groups and Functionalized Fullerene $C_{60}$

Panarina H.Y.[1],Yefimov Y.L.[2],Olasyuk O.P.[3], Kulish M.P.[4], Dmytrenko O.P.[5]

[1, 2, 3, 4,5]*Taras Shevchenko NationalUniversity of Kyiv, Kyiv, Ukraine*

Solar panels are important because humanity needs the development of alternative energy sources. Therefore, the study of new materials for organic solar cells is widespread [1].

The most interesting are solar photovoltaic cells based on semiconducting conjugated polymers. To implement the bulk heterojunction required donor-acceptor composite polymer (donor) with acceptor material. Fullerene derivatives, polymer and low molecular acceptors are the most commonly used. Functionalized fullerenes same (thanks to the radical) have higher efficiency generation and transport of charge carriers, so and solar energy conversion efficiency of photocurrent. Therefore, the research of composites based on polymers and functionalized fullerenes are important [2-3].

The objects of study in this work are polymer films APFO-3 and functionalized fullerene $C_{60}$ThCBM, which are made by irrigation with dichlorobenzene in crystalline silicon. Samples were prepared from functionalized fullerene mass ratio of fullerene to polymer 1: 2 and 1: 3.

The aim of this work is to analyze the dependence of photocurrent density of the mass fraction of polymer and fullerene. The criterion of effectiveness is the composite value of the photocurrent, so stationary photocurrent was measured in samples with a mass ratio of 1: 3, 1: 2, 1: 1 fullerene to the polymer. To explain the dependencies also were calculated energy and vibrational spectra fullerene and polymer used in the work.

1. Small bandgap polymers for organic solar cells (polymer material development in the last 5 years) / R. Kroon, M. Lenes, J.C. Hummelen, P.W.M. Blom, B. deBoer // PolymerReviews. – 2008. – №48. –P. 531–582.
2. WanzhuCai. Polymer solar cells: Recent development and possible routes for improvement in the performance / WanzhuCai, Xiong Gong, Yong Cao // Solar Energy Materials & Solar Cells. – 2010. – №94. – P. 114–127.
3. S. Gunes. Conjugated Polymer-Based Organic Solar Cells / S. Gunes, H. Neugebauer, N. S. Sariciftci // Chemical Reviews.–2007. – №107. – P. 1324–1338.

# Simulation of Structural Defects and Strains in a Single Crystal $Nd_3Ga_5O_{12}$

Pylypiv V.M. , Garpul O.Z. , Solovko Ya.T.

*Vasyl Stefanyk Precarpathian National University, Ivano-Frankivsk, Ukraine*

Experimental diffraction reflection curves (DRC) single crystal neodymium-gallium garnet (NGG) differ significantly from the theoretical diffraction for a perfect crystal despite correct account of thermal Debye-Waller factor. In this regard, assumed the presence of a crystal dislocation loops in addition, another type microdefects - spherical clusters (particle inclusions of another phase). Considering the presence of crystal clusters and dislocation loops at the same time was much more successful (Fig. 1), however, the simultaneous adjustment of both DRC at default dislocation loops ($R$=100 nm, $n$= $8\cdot10^{11}$ $cm^{-3}$) and only one cluster radius was satisfactory only in certain areas of the measured angular ranges.

But setting two radii of clusters identical for the two reflexes ($R$=10 i 50 nm) by changing the concentration of clusters (respectively $n$= $5\cdot10^{13}$ i $5\cdot10^{11}$ $cm^{-3}$) and a fixed value of the parameter deformation on the edge of the cluster ($\varepsilon$ =0.03) allowed better performance fit with existing statistical dispersion measurements, when the corresponding figures up $r$=12%, $R$=18% i $r$=14%, $R$=17% for the 444 and 888 reflections.

Fig.1.Experimental and theoretical diffraction NGG (markers and thick solid lines) for reflections (444) and (888). The thin solid and dashed lines - coherent components DRC and contributions from diffuse scattering clusters and dislocation loops

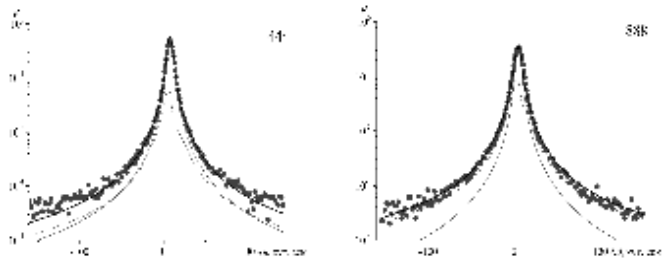

Thus, obtained in our work a good quality fit for each of the measured DRC diffraction in the central parts and in the tails achieved of adequate and self-consistent description coherent intensity and diffuse scattering using generalized statistical dynamical theory of X-ray diffraction in single crystals with uniformly distributed micro-defects [1].

1. X-ray diffractometry dynamic defect structure garnet single crystals/ [V.M. Pylypiv, B.K. Ostafiychyk, T.P.Vladimirova, Ye.M. Kyslovskyy, V.B. Molodkin, S.I. Olikhovskii, O.V. Reshetnyk, O.S. Skakunova, V.V. Lizunov] // Nanosystems, nanomaterials and nanotechnologies. – 2011. – V. 9, № 2. – P. 375-408.

# Temperature Studies of Optical Parameters of $(Ag_3AsS_3)_{0.6}(As_2S_3)_{0.4}$ Thin Films

Ráti Y.Y.[1], Kutsuk M.M.[1], Neimet Yu.Yu.[1], Izai V.Yu.[1], Makauz I.I.[1], Studenyak I.P.[1], Kökényesi S.[2]

[1]*Uzhgorod National University, Uzhhorod, Ukraine*
[2]*University of Debrecen, Debrecen, Hungary*

Ag-doped Ag–As–S chalcogenide glasses and films have found many current and potential applications. The high values of electrical (mostly ionic) conductivity in superionic $Ag_3AsS_3$–$As_2S_3$ glasses and composites in combination with a strong photosensitivity, attracts a great interest towards fabrication and studies of thin films on their base. The present investigation is aimed at the spectroscopic studies of transmission spectra, absorption spectra, refractive indices and their dispersion curves of $(Ag_3AsS_3)_{0.6}(As_2S_3)_{0.4}$ thin films at different temperatures.

Synthesis of $(Ag_3AsS_3)_{0.6}(As_2S_3)_{0.4}$ composite material which consists of crystalline $Ag_3AsS_3$ and glassy $As_2S_3$ was carried out at a temperature of 700°C for 24 h with subsequent melt homogenization for 72 h. $(Ag_3AsS_3)_{0.6}(As_2S_3)_{0.4}$ thin films were prepared by rapid thermal evaporation from the corresponding composite material at near 1350ºC in vacuum ($3\times10^{-3}$ Pa) using a VU-2M setup. The film thickness was measured using an Ambios XP-1 profile meter. The transmission spectra were studied in the interval of temperatures 77–300 K by a MDR-3 grating monochromator; a UTREX cryostat was used for low-temperature studies.

With temperature increase the longwave shift of high-energy parts of transmission spectra and transmittance decrease at interference maxima are observed. Based on the interferential transmission spectra, the spectral dependences of absorption coefficient were obtained. It is shown that the optical absorption edge in the region of its exponential behaviour are described by Urbach rule. Temperature dependences of optical pseudogap $E_g^*$ and Urbach enegry $E_U$ for thin $(Ag_3AsS_3)_{0.6}(As_2S_3)_{0.4}$ films are well described within the framework of Einstein model. The main Urbach absorption edge parameters as well as the temperature dependences of optical pseudogap and Urbach energy $E_U$ are determined.

The dispersion dependences of the refractive index for the thin films were obtained from the interference transmittance spectra. The slight dispersion of the refractive index is observed in the transparency region while it increases when approaching to the optical absorption edge region. It is shown that at temperature increase the refractive index increase.

# The Impact of Technology on the Crystallographic Form Nanostructures PbTe: Sb on Ceramics

Saliy Ya.P., Freik I.M., Bushkov N.I.

*Vasyl Stefanyk Precarpathian National University, Ivano-Frankivsk, Ukraine*

Lead telluride (PbTe) is an advanced semiconductive material in manufacturing optoelectronics devices related to infrared spectrum area, as well as in termoelectronics of medium frequency temperature (500-850) K[1]. PbTe alloing with group 5 impurity heterovalent (Sb, Bi) of Periodical Table are cause modification of electronic and phononic crystal system. Vapor-phase nanostructures on glass ceramics lining have been received from vapor-phase procedure due to open evaporation in vacuum environment ahead of obtaining synthesized compound PbTe:Sb that contains 0.25 at% in different time $\tau$ = (15-240) c and temperatures $T_П$=(420-520) K deposition, according to evaporation temperature $T_В$ = 970 K.

With the help of applied Gwyddion Program the AFM investigation are showed that it is possible to define hardness and size of nanocrystals but not only morphology of condensate surface. We defined polar and azimuth angles of either sides of certain PbTe:Sb glass ceramics nano crystals with clear sides, that helped to find angles between normals towards sides, and finally compare received data with theoretically possible ones. In addition, the results of AFM images of individual nanocrystals and the calculation of the corners first methods of computer simulation using the original Phoenix program written in Visual Basic restored their ideal image. At hasbun shown that the increase of settling time $\tau$ twice applying constant temperature of the substrate, maximum height of nanocrystals would coust the increases twice as well. We defined that certain PbTe:Sb glass ceramics nanocrystals of vapor-phase condensates have been formed by cube system area {100} as well as orthorhombic dodecahetron area {110}, which are electrically neutral and possess the largest reticular atom density.

Having applied computer modeling approaches we have managed to restore in PbTe:Sb glass ceramics condensate the crystal forms that are correspond to different combinations of NaCl area structure. Thus, the establishment features crystalline forms nanocrystals PbTe: Sb explained electrically neutral state crystallographic planes and the nature of the substrate surface ceramics.

1. Dmitriev L.V. Modern trends in the physics of thermoelectric materials. // The success of physical science. –.2010. – V. **180**, №8. – P .821

# Optical studies of $Cu_7GeS_5I$ superionic Thin Films

Studenyak I.P.[1], Bendak A.V.[1], Demko P.Yu.[1], Studenyak V.I.[1],
Izai V.Yu.[1], Vorokhta M.[2], Matolin V.[2], Lisý V.[3]

[1]*Uzhgorod National University, Uzhhorod, Ukraine*
[2] *Charles University, Prague, Czech Republic*
[3]*Technical University of Košice, Košice, Slovakia*

$Cu_7GeS_5I$ crystals belong to the argyrodite family of tetrahedrally close-packed structures and are known as superionic conductors. Due to their high ionic conductivity, they are attractive materials for applications in the different functional elements of the solid state ionics. Thin amorphous films prepared on the base of $Cu_7GeS_5I$ compound are shown to be characterised by a high value of the electrical conductivity which can be used for the creation of miniature solid electrolyte batteries and supercapacitors of new generation.

Thin films of $Cu_7GeS_5I$ superionic compounds were deposited onto silicate glass substrates by non-reactive radio frequency magnetron sputtering. The structure of the deposited films was analyzed by X-ray diffraction; the diffraction patterns show the films to be amorphous. Structural studies were performed using SEM technique and EDX spectra measurements which give the evidence for the formation of a homogeneous two-dimensional structure.

The transmission spectra were studied in the interval of temperatures 77–300 K by a MDR-3 grating monochromator. Based on the interferential transmission spectra, the spectral dependences of absorption coefficient and the dispersion dependences of the refractive index were obtained. The increase of the refractive index dispersion in short-wavelength region as well as increase of the refractive index value with temperature are observed.

It is shown that the optical absorption edge in the region of its exponential behaviour are described by Urbach rule. The main Urbach absorption edge parameters as well as the temperature dependences of optical pseudogap and Urbach energy are determined. The temperature behaviour of the Urbach absorption edge is explained by electron-phonon interaction which increases at the transition from the three-dimensional bulk structure to the two-dimensional planar structure. An essential characteristic of the absorption edge spectra of the thin film under investigation is a lengthy Urbach tail which results in the Urbach energy being more than three time higher than that in the crystal. The transition from the crystalline three-dimensional $Cu_7GeS_5I$ superionic conductors to the two-dimensional amorphous thin films is characterized by a decrease of the electrical conductivity and the optical pseudogap, an increase of the Urbach energy, an enhancement of the electron-phonon interaction as well as an increasing structural disordering.

**СЕКЦІЯ 2 (усні)**
**НАНОТЕХНОЛОГІЇ, НАНОМАТЕРІАЛИ І КВАНТОВО-РОЗМІРНІ СТРУКТУРИ**

12-15 травня 2015 р.

**SESSION 2 (oral)**
**NANOTECHNOLOGIES AND NANOMATERIALS, QUANTUM-SIZE STRUCTURES**

May, 12-15, 2015

# Resonant Stokes Shift in CdS QD

Boichuk V.I., Leshko R.Ya., Sokolnyk O.A., Kropyvnytska K.M

*Ivan Franko Drohobych State Pedagogical University, Drohobych, Ukraine*

In the past two decades, artificial structures with reduced size and dimensions have been fabricated successfully due to advance of material science technologies. Those structures, especially solid solutions $A_2B_6$ are very good and perspective materials for creation of the new elements of nonlinear optics.

The large attentions of reseachers are to paid heed to study of *CdS* quantum dot (QD). The most simplify and informative methods which give possibilities to study the electron structure are light absorption and photoluminescence.

The series of works are dedicated to experimental study of optical properties of *CdS* QDs in colloidal solutions. Besides that there are a lot of theoretical works, which describe optical properties. In particular, the resonant Stokes shift was calculated for different nanocrystals [1-3]. But in those works [2-3] were studied crystals which have a large spin-orbital coupling. Therefore the 4-band model of the valence band was used. But in [1] the density functional was applied to calculation. Since the *CdS* has a small value of spin-orbital interaction the abovementioned methods are not valid. That is why in this work we used the 3x3 model of valence band to describe hole levels and to calculation the exchange interaction which caused the resonant Stokes shift in *CdS* QD. The obtained results show that this approximation is appropriate for this QD. The proof of that are good qualitative and quantitative agreements of obtained results with experimental data.

1. D. O. Demchenko and Lin-Wang Wang. Optical transitions and nature of Stokes shift in spherical CdS quantum dots // arXiv:cond-mat/0603563v1 [cond-mat.mtrl-sci] 21 Mar 2006.
2. Al. L. Efros and M. Rosen. Band-edge exciton in quantum dots of semiconductors with a degenerate valence band: Dark and bright exciton states // PHYSICAL REVIEW B, VOLUME 54, NUMBER 7, P 4843–4856.
3. І.М. Купчак, Д.В. Корбутяк та ін. Зсув Стокса у КТ CdTe // ЖФД. Т 14, №2 , с. 2701 (2010).

# Properties of Low Dimensional Semiconductor Materials Obtained by Electrochemical Methods

Boruk S.D., Dremlyuzhenko X.S., Yuriychuk I.M., Tsaly.V.Z., Klad'ko V.P., Gudymenko O.I.

[1]*Chernivtsy National University, Chernivtsi, Ukraine*
[2]*V.E. Lashkaryov Institute of Semiconductor Physics NASU, Kiev, Ukraine*

Electro-spark method for obtaining of nanostructured and ultrafine powders of metals and semiconductor alloys is one of the most effective. Thus, an important scientific and technical challenge remains to increase the proportion of ultrafine and nanostructured particles in the spark erosion powders.

Cadmium telluride and its solid solutions are of particular interest in terms of both practical and scientific research. This work is aimed in obtaining of low dimensional semiconductor and metallic systems, the study of their characteristics, namely the finding of qualitative and quantitative composition, particle formation mechanism and stability of solutions. We have studied following system: Cd-Cd, Te-Te, K:Cd - Te-A:, K:Te -A: Cd, CdTe in aqueous and thioglycolic acid solution. Semiconductor purity materials are used for making of electrodes. In order to set qualitative composition and size of the highly dispersed systems an X-ray analysis (XRD) have been used. To carry our XRD experiments obtained colloidal solutions were dispersed, and from the resulting sediment there have been made samples in the form of tablets. It is found that at potential difference between the electrodes within 200-240 an electric arc arises. The traces of electrical failure on the anode are visually observed after 30 seconds of current passing. Te (K) - Cd (A); Cd (K) - Te (A); Te(K) - Te(A) solutions show opalescence in the case of using cadmium electrodes. The systems changes color to yellow-brown. Presented studies have confirmed the formation of highly dispersed particles in all studied systems.

According to spectroscopic studies of colloidal solutions the absorption peak gradually shifts toward longer wavelengths over time, and its color intensity decreases. Obtained systems are stable for 12-14 days. The composition of the particles according to XRD data is uniform and correspond to elemental composition of the electrodes.

# Energy Characteristics of Supercapacitors Based on Chemically Modified Carbon

Budzulyak I.M., Vashchynsky V.M., Rachiy B.I., Nykolyuk M.O.

*Vasyl Stefanyk Precarpathian National University, Ivano-Frankivsk, Ukraine*

One of the modern trends of development of rechargeable energy sources is the study of creation Supercapacitors (SC), that operate on the principle of charge/discharge of the electrical double layer (DEL) on polarized electrodes with a large specific surface area. The value of specific capacity IC depends on the type of electrolyte, structure and condition of the developed surface of the electrode material.

The effect of carbonization temperature of raw materials of plant origin on specific capacitance characteristics of the obtained nanoporous carbon (NC), that is used to manufacture SC electrodes, was investigated. Dried apricot pits were used as feedstock. To study the effect of carbonization temperature on the structure and energy characteristics of NC, the feedstock was carbonized in the temperature range of 300 to 900 °C with the interval of 100 °C. Carbonized carbon was activated with potassium hydroxide in different proportions. Samples were numerated according to carbonization temperature and percentage of chemical activator (eg, C63 – material, carbonated at 600 °C and mixed at a ratio of 1: 3 with KOH). Thus, seven series of samples C3 ... C9 were received.

According to galvanostatic research data dependence of capacitance value of NC on discharge current is obtained (Fig. 1). The received results indirectly suggest that these technological methods allow gaining NC, in which a pore system with optimal ratio between the volume fraction transport and operating pores is formed.

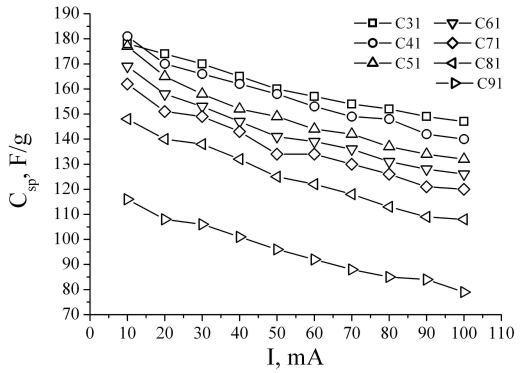


**Fig. 1 –** Dependence of the NC specific capacity on discharge current.

It is established that heat treatment and optimizing of feedstock and KOH enables to provide a carbon material with specific capacity of 150 to 195 F/g at the discharge current of 50 mA, and power surge of generated on its basis SC does not exceed 18 % of the maximum voltage at the discharge current of 100 mA.

# Photoluminescent Properties of the CdTe Nanocrystals Incorporated Into Inorganic Matrices

Budzulyak S.I., Ermakov V.M., Kapush O.A., Korbutyak D.V., Kuryk A.O.

*V.E. Lashkarev Institute of Semiconductor Physics, National Academy of Sciences, Kyiv, Ukraine*

The modern optoelectronics devices made with polymers or inorganic materials and A2B6 semiconductor nanocrystals (NCs) have attracted considerable attention. It is because nanoparticle composites combine key properties required for including low power, low voltage and low weight. The improvements of growth methods, methods of stabilization and other factors result in significant increase of photoluminescence quantum yield of the CdTe NCs grown in colloidal solutions. However, these solutions are ineffective in practical use due to the low reliability and stability.

The synthesis of colloidal solution with CdTe NCs was carried out in a three-neck baffled reactor as earlier described in [1]. In our case, the $Cd^{2+}$ source was the salt $CdI_2$, and the $Te^{2-}$ source was $H_2Te$ gas prepared electrochemically in a galvanostatic cell (reactions at the electrodes: $Te + 2e^- + 2H^+ \rightarrow H_2Te$ at the cathode (+) and $H_2O \rightarrow 2H^+ + 1/2\ O_2$ at the anode (–)). Thioglycolic acid (TGA) was used to stabilize the surface of the CdTe NCs during the synthesis. The preparation of the crystals was performed by mixing 25 mL of a saturated KCl solution (25%) with 5 mL of a CdTe NCs solution ($C_{CdTe} = 1{,}07 \times 10^{-3}$ mol/L based on $C_{Te}^{2-}$).

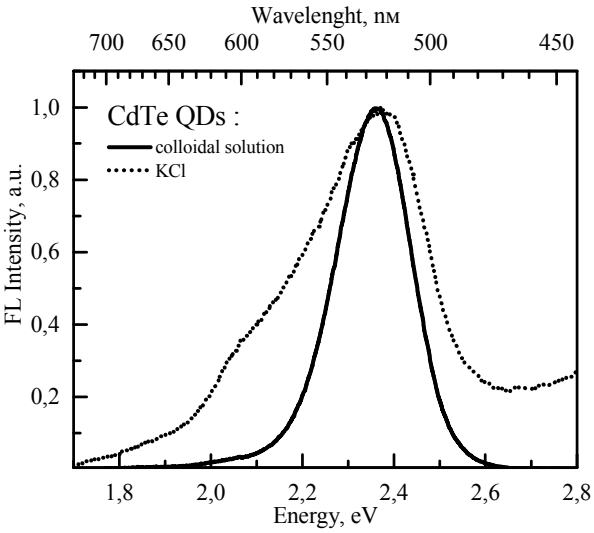


Fig. 1. PL Specta of CdTe QDs in colloidal solution and KCl matrix.

Figure 1 shows the PL spectra of the CdTe NCs in colloidal solution and KCl matrix, taken at room temperature. We have compared PL of starting colloidal solutions of CdTe QDs with the PL of the corresponding CdTe QDs embedded in KCl. Broadening of the main peak was caused evidently by a changing of stabilization conditions. But, obtained KCl powder with embedded CdTe NCs is ready for practical use, especially after mixing with moisture resistant polymers, and can be used as luminescent phosphors.

1. Effect of Thioglycolic Acid on the Stability and Photoluminescence Properties of Colloidal Solutions of CdTe Nanocrystals / O.A. Kapush, L.I. Trishchuk, V.N. Tomashik, Z.F. Tomashik // Inorganic Materials, 2014, Vol. 50, No. 1, pp. 13–18.

# Investigation of Properties Of Nanopowder ZnS:Mn, obtained by the method of selfpropagating hightemperature synthesis

Bulaniy M.F., Kovalenko A.V., Khmelenko O.V.

*Oles Gonchar National University of Dnepropetrovsk, Dnepropetrovsk, Ukraine*

Zinc sulfide doped with various impurities is an important material for optoelectronic devices, that emitting a broad spectral range. In particular, the crystals ZnS:Cu emitting in the blue-green region of the spectrum, ZnS:Mn – in orange region and ZnS:Al – in blue.

The paper deals the results obtain nanosized ZnS powder by selfpropagating hightemperature synthesis (SHS). This method has several advantages compared with other methods of producing ZnS, since it allows to obtain a nanosized powder ZnS and produce doping directly during synthesis.

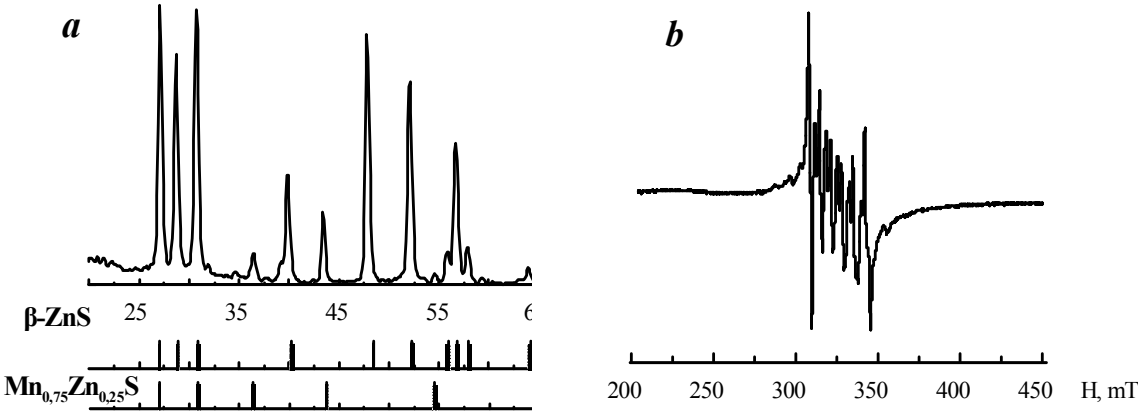


Fig. 1. Data of XR diffraction analysis (***a***) and EPR spectra nanopowder ZnS:Mn (***b***).

Fig. 1 presents the data of XR diffraction analysis and EPR spectra of powder ZnS, obtained by SHS method and doped Mn during synthesis. Preparation of ZnS nanopowder by SHS method was effected in a quartz reactor from mechanical mixture of metallic Zn and S, in the ratio 1:3. For doped ZnS ions $Mn^{2+}$ used of $MnCl_2$ compound, in the ratio $10^{-2}$ gram/gram. Synthesized powder was composed mainly of hexagonal 2H (wurtzite) ZnS compounds and phase $Mn_{0.75}Zn_{0.25}S$. The contribution of the hexagonal phase is (80 ± 5)%. The average crystal size of ZnS:Mn is d ≈ (60 ± 5) nm. EPR spectrum consists of a broad line against which the prescribed six hyperfine structure lines characteristic of paramagnetic centers $Mn^{2+}$ in ZnS. Against the background of these lines can be seen mild structure, which can also be linked to the $Mn^{2+}$ ions in the phase of $Mn_{0.75}Zn_{0.25}S$.

# Doping of ZnO Nanopowders with $Mn^{2+}$ Ions at Ultrasonic Spray Pyrolysis

Bulaniy M.F., Kovalenko A.V., Vorovsky V.Yu., Khmelenko O.V.

*Oles Gonchar National University of Dnepropetrovsk, Dnepropetrovsk, Ukraine*

The processes of ZnO nanopowders doped ions $Mn^{2+}$, obtained by ultrasonic spray pyrolysis. The synthesis of zinc nitrate solution and manganese at T = 670 °C. As carrier gas, air or nitrogen is used. Wherein the manganese concentration was equal to 2,4; 4,8; 9,6 and 38,4 at. %.

XR diffraction analysis method were established crystal structure, chemical composition and average size of nanocrystals ZnO:Mn. Doping was confirmed by ESR spectra by the presence of six lines of the hyperfine structure characteristic of the ions $Mn^{2+}$ (Fig. 1). The possibility of nanopowders doped directly during synthesis, without additional annealing. In the synthesis of a microdroplet spray solution after the rapid heating transformed into spherical particles of a size from 1 to 2 microns. Each particle consists of a large number of nanoparticles as a mixture of the oxides ZnO and $MnO_2$. The average crystal size with increasing manganese concentration to 9.6 at.% decreases from 56 to 24 nm, respectively.

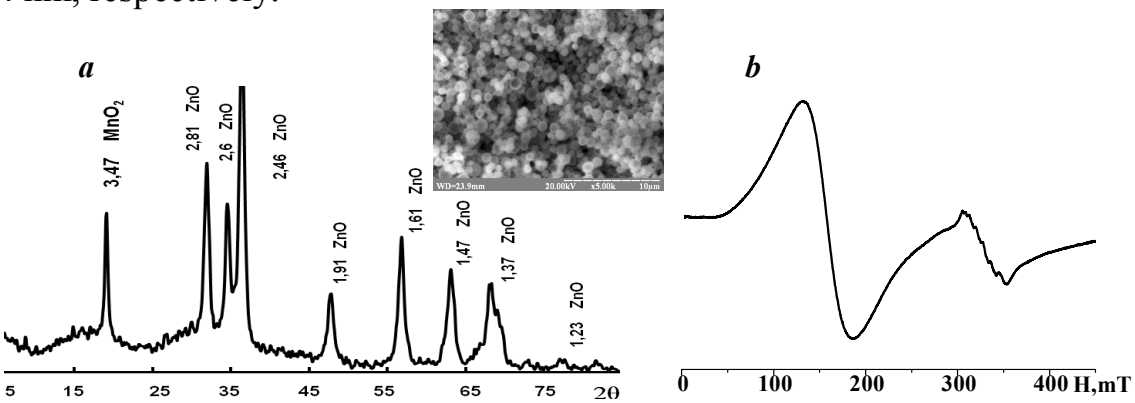


Fig. 1 Data of XR diffraction analysis (***a***) and EPR spectra nanopowder ZnO:Mn (***b***); the inset the form of the surface nanopowder.

The dependence of the final product from the synthesis of the carrier gas type. Nitrogen promotes the formation of a secondary phase $MnO_2$ powder at concentrations of manganese in excess of 2,4 at.%. In samples with manganese concentrations less than 2,0 at.% there is one phase of ZnO c wurtzite type crystal lattice. Studies nanopowder ZnO: Mn by ESR showed that when used as a carrier gas of nitrogen in the EPR spectra in small magnetic fields present broad absorption line with g = 4,2874 (Fig. 1). Perhaps, the presence of this line due to the formation of defects in crystals of ZnO, which occur during the formation of crystals under an inert atmosphere of oxygen deficiency. Such defects are the centers of the acceptor type, so the powder ZnO:Mn may have p-type conductivity.

# Mechanisms of Growth and Topology of Nanostructures in Thin Films of PbTe:Bi, SnTe:Bi

Bylina I.S., Umantsiv R.V., Mykhailyuk V.V., Trynoga Yu.T.

*Vasyl Stefanyk Precarpathian National University, Ivano-Frankivsk, Ukraine*

The efforts of scientists currently focused on the development of new materials using nanotechnology. Atomic force microscopy (AFM), electron microscopy, high-resolution open up new possibilities for observation and analysis of different stages of growth of nanoobjects. Lead and Tin Telluride - promising thermoelectric materials for middle temperatures (500-750) K and devices that operate in the infrared region of the optical spectrum [1]. Alloying PbTe and SnTe Heterovalent impurities fifth group (Bi) Periodic table causes modification of electron and phonon subsystems crystal, which affects whole complex physical and chemical properties[2].

Vapor-phase condensates PbTe:Bi and SnTe:Bi obtained by the method of open evaporation in a vacuum on a substrate of mica and pyroceram. For PbTe:Bi deposition temperature $T_S$ = (420-520) K, the sample temperature evaporation $T_V$ = (920-1020) K and deposition time $\tau$ = (3-120) s.

We researched the obtained samples with atomic force microscope (AFM) Nanoscope 3a Dimention 3000 (DigitalInstruments USA) in the periodic contact mode.

Determined the size of individual crystallites PbTe:Bi, SnTe:Bi and constructed histogram distribution of normal and lateral dimensions. With increasing deposition time is quite adequate increase in the average size of nanocrystals. It is shown that in the process of nucleation Folmer-Weber mechanism dominates, when the three-dimensional nanostructures are formed on the substrate surface. Mechanisms of nanocrystal are growth explained from the standpoint of ostvald maturation. It has been that the surface of ceramics are formed from combinations of individual nanocrystals planes {100} and {110} of NaCl structure.

It is shown that the change in the electrical conductivity $\sigma$ of $T_V$ technology factors, $T_S$ and $\tau$ observed dependence of carrier concentration n, and not their mobility $\mu$, due to the peculiarities of processes like evaporation sample and steam condensation on the substrate.

1. Zimin. S.P., Gorlachev E.S. Nanostructuring lead chalcogenides: monograph. - Yaroslavl: Yaroslavl State University, 2011. - 232 p.
2. Abrikosov N.H., Shelimova L.E. Semiconductor materials based on compounds $A^4B^6$. – M.: "Nauka", 1975. - 195 p.

# The Features of Photolithography Process Based on Reversible Photostructural Changes in Germanium Chalcogenides

Dan'ko V.A., Indutnyi I.Z., Lukaniuk M.V., Myn'ko V.I., Shepeliavyi P.E.

*V. Ye. Lashkaryov Institute of Semiconductor Physics NAS of Ukraine*
*Prospect Nauki, 41, Kiev-03028, Ukraine.*

Photoinduced structural transformations of chalcogenide glasses (ChGs), which lead to changes of their properties (optical characteristics, conductivity, solubility in selective etchants, and even mechanical characteristics), are a basis for wide practical use of GhG films, glasses and fibers. For example, the use of GhG films as a photoresist was based on irreversible change that observed in the thermally deposited films only. In annealed ChG films transient photostimulated structural changes, which exist during illumination, and a small reversible changes after the exposure are observed.

Recently we reported that both the reversible and the transient structural changes are accompanied by a change in the solubility of ChG films, and negative amine-based etchant dissolve illuminated areas of chalcogenide films, i.e. act as positive etchants. But etching selectivity of the annealed films was strongly dependent on the intensity of exposure [1]. Here we present the results of more detail investigations of this phenomenon. The samples for study were prepared by successive thermal evaporation in vacuum at a residual pressure of $2 \times 10^{-3}$ Pa, with a 40-nm thick adhesive layer of Cr and $GeSe^3$ layer with thickness 200 nm, deposited onto substrates. Deposited films were annealed for 1 h near glass transition temperature ($T_g$). Then the samples were irradiated with light pulses of the variable intensity and duration (focused argon ion laser beam, $\lambda = 476.5$ nm, the shutter and neutral density filters were used also) while the exposure was maintained a constant. After exposure the samples were treated in amine-based etchant and studied using microinterferometer MII - 1. It has been found that the dependence between the rate of etching of the irradiated areas of the sample (or the etching selectivity) and the light intensity is nonlinear. Selective etching is observed only at intensities exceeding a certain threshold value. Selectivity wasn't observed in the samples which were annealed repeatedly after exposure at the temperature close to Tg, and appeared again after next exposure (after repeated annealing) at the same conditions. After detail examining of exposure-annealing cycles that were carried out in the same conditions for several times, we have concluded that this selective etching is related to the reversible photostructural changes that occur in annealed ChG films. Selectivity didn't observe in the samples which were annealed repeatedly after exposure at the temperature near $T_g$, and appeared again after repeated exposure (after repeated annealing) at the same conditions. After detail examining of exposure-annealing cycles that were repeated under the same conditions several times, we have concluded that this selective etching is related to the reversible photostructural changes that occur in annealed ChG films.

The results of this experiment allowed us to develop the new photolithography method on annealed ChG films, which is effective for creating of relief micro- and nanostructures of high quality with deep relief [1].

1. Indutnyi I.Z., Kryuchyn A.A., Borodin Yu. et al. Reestraciya, zberigannya i obrobka danyh. – 2013. Vol.15, №4. – P. 3-12.

# Surface enhanced spectroscopy for application in nanotechnology

Dovbeshko G., Gnatyuk.O.

*Institute of Physics, NAS of Ukraine, Kyiv, Ukraine*

Surface enhanced spectroscopy (SES) is a sensitive analytical tool for identification, characterization and obtaining new physical and chemical data about nanostructured systems. This method includes: SEIRA (surface enhanced infrared absorption), SERS (surface enhanced Raman scattering), SEF (surface enhanced fluorescence) spectroscopy. Any spectroscopic technique, in which for increase of output optical signal from molecule, a substrate of metal or non-metal type (e.g. graphene) is used, could be named as SES. In traditional SES spectroscopy the researchers apply rough or periodic metallic substrates as well metallic particles. However, non-metallic substrates, as carbon nanostructures, dielectric and semiconductor structures, could be a good enhancers also. Effect of enhancement of optical transitions of molecules near metallic surface is typically explained by CM (chemical mechanism) and EM (electromagnetic mechanism). CM is due to charge transfer between the probed molecule and the substrate. The nature of EM mechanism is connected with increase of the local electric field caused by plasmon resonance. These two mechanisms always contribute simultaneously to the overall enhancement, while the EM provides the main enhancement. The method could be applied for study metallic clusters, molecules, graphene-type nanostructures, quantum dots, clusters from dielectric materials, etc. Here we present data on study of different cells and biological molecules (DNA, poly-A, DNA bases, proteins, amino acids, lipids) adsorbed on the surface of metallic and non-metallic surfaces as well study of carbon nanotubes and graphene-type structures and their application as support for biological molecules. Discussion of mechanism of enhancement for different graphite- type substrates are presented here.

We thank to Faemcar Project FP7-PEOPLE-2012-IRSES, Marie Curie ILSES project no. 612620, and Ukrainian-Poland project for financial support.

# Changing the Temperature Dependence of Electrical Conductivity on the Opposite in Si Nanocluster Containing Structures

Evtukh A.A., Bratus' O.L.

*V. Lashkaryov Institute of Semiconductor Physics, NAS of Ukraine, Kyiv, Ukraine*

Nowadays, silicon (Si) nanocrystals embedded into $SiO_2$ matrix have perspective of wide applications as the active layer in various electronics and optoelectronics devices. To use this layer in devices the detailed information about the electrical characteristics of Si nanocrystals in $SiO_2$ matrix is needed.

The main purpose of this study was to investigate the mechanisms of conductivity of the MIS structures with nanocomposite $SiO_2$(Si) films obtained by ion-plasma sputtering for subsequent use as a medium for capture and storage of electric charge in the nonvolatile memory structures.

At the beginning $SiO_x$ films have been deposited by ion-plasma sputtering of silicon target in the vacuum on p - type c-Si substrate in argon and oxygen atmosphere. The main parameters of the process were: gas pressure during deposition $P = 8 \times 10^{-4}$ Torr, substrate temperature T=150ºC, deposition rate $v$ = 20-25 nm /min. For transformation of silicon enriched $SiO_x$ film into nanocomposite $SiO_2$(Si) film containing silicon nanocrystals embedded into $SiO_2$ dielectric matrices, high temperature annealing at T = 1100 °C for 30 min in the nitrogen atmosphere has been performed. To measure the electrical characteristics of the films the MIS capacitors have been formed. As aluminum and titanium electrodes were deposited by sputtering of the appropriate target. The MIS capacitors metal electrode square was $7\times10^{-3}$ cm$^2$.

Measurements of current-voltage (I-V) characteristics were carried out using automated complex consisting of a controlled voltage source and ampermeter Keithley-6485. To elucidate the mechanisms of conductivity the measurements of I - V characteristics were carried out in the temperature range 82 K - 350 K.

Fig. 1 shows the temperature dependence of conductivity of n-Si / $SiO_2$ (Si) / Ti MIS structure. The stoichiometry index in initial $SiO_x$ film was $x$ = 1.3. As it can been seen the current through the nanocomposite $SiO_2$(Si) film strongly depends on the temperature. In fields more than $10^5$ V/cm conductivity type changes from the semiconductor to the metal type. The model for explanation this effect has been proposed.

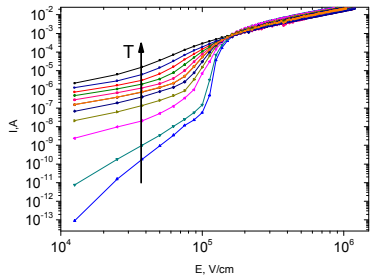


Fig.1. Typical I-V characteristic of n-Si / $SiO_2$(Si) / Ti MIS structure in the temperature range from 83 K to 350 K. The direction of the arrow shows the temperature growth.

# Electroconductivity and Thermopower of Quantum Semiconductor Wire by Thickness Fluctuations

Galuschak M.O.[1], Ruvinskii B.M.[1], Ruvinskii M.A.[2]

[1]*Ivano-Frankivsk National Technical University of Oil and Gas, Ivano-Frankivsk, Ukraine*
[2]*Vasyl Stefanyk Precarpathian National University, Ivano-Frankivsk, Ukraine*

The aim of this work is the theoretical determination of the electroconductivity and thermopower in the model [1] of quantum semiconductor wire by a random field of Gaussian fluctuations of wire thickness.

We present the results for cases degenerate and nondegenerate statistics of carriers. The considered mechanism of relaxation of the charge carriers is essential for sufficiently thin and clean GaAs wire at low temperatures and allows in principle the possibility of increasing the value of thermopower compared to the case of three-dimensional solid model.

1. M.A.Ruvinskii, B.M.Ruvinskii // *FTP* – 2005 – **V39** (2) – P.247-250.

# Photonic Crystal Resonators and Photonic Membranes as Platforms for All-Optical Signal Processing

Glushko E.Ya.[1], Stepanyuk A.M.[2],

[1]*Institute of Semiconductor Physics, NAS of Ukraine, Kyiv, Ukraine*
[2]*Pedagogical Institute, Kryvyi Rih National University, Kryvyi Rih, Ukraine*

The conventional membranes separate particles during the process of its selective transport through the membrane channels. In photonics, the membranes are a kind of thin 2D photonic crystal resonators characterizing as thin and wide systems ordered in both transversal directions and filtering radiation along the normal to surface direction. Photonic bandgap manifestations in the reflectivity of periodically patterned systems were investigated

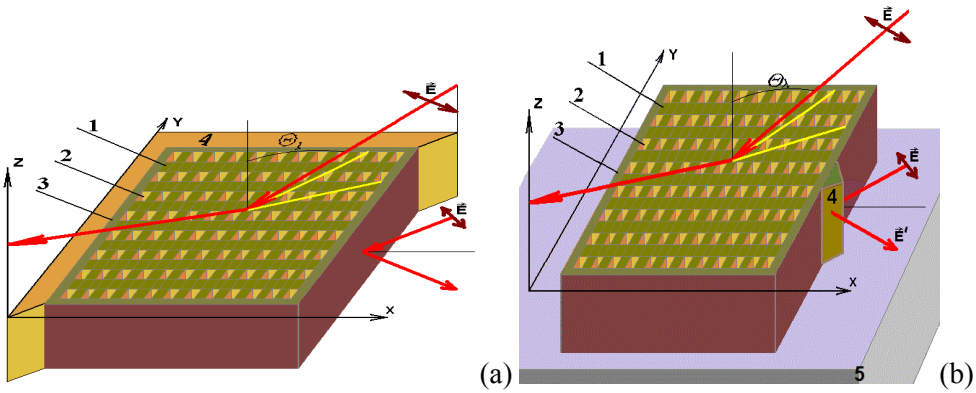


**Fig. 1. Membranes and photonic crystal resonators. (a) A finite porous membrane. Out-of-plane incidence:** s-polarisation, $\Theta_l$, external polar angle of incidence, azimuth angle $\Phi_l=\pi/4$; yellow lines, sector of total internal reflection. **In-plane incidence:** p-polarisation. 1, matrix material; 2, rectangular bar/air wells in matrix; 3, covering layer (nonlinear), 4, external medium. **(b) A finite 8x12 2D photonic crystal resonator**. **Out-of-plane incidence:** s-polarisation, $\Theta_l$, external polar angle of incidence, azimuth angle $\Phi_l=\pi/4$; yellow lines, sector of total internal reflection. **In-plane incidence:** p-polarisation. The is not shown. 1, system matrix; 2, rectangular bar/air wells in matrix; 3, covering layer, 4, input prism, 5, substrate.

experimentally and theoretically in a lot of works by the resonant coupling wave method connecting photonic bands existing for in-plane geometry of incidence with both diffractional signals in reflection and transmission.

The existing terminology distinguishes photonic crystals, photonic membranes or MPC and photonic crystal resonators (PCR). The infinite 2D structures ordered in XY plane which has also infinite size in Z direction are usually called photonic crystals. A photonic crystal resonator is a finite 2D system with perfectly smooth side walls. The latter circumstance leads to a clearly expressed angular area of total internal reflection (Fig. 1a, yellow lines) for a field closed inside the resonator. In the ideal case, the system should have infinite size in Z direction. The only way to excite intrinsic standing waves exists

through the input prisms which allow the external beam to enter the total internal reflection area. Correspondingly, we will tell the difference between above mentioned pure PCR resonators and waveguide/cavity resonators embedded into a PCR. Finally, a photonic membrane may be treated as a thin photonic crystal and in this capacity it exhibits properties of a two-dimensional system. The transfer from a photonic membrane to a photonic membrane resonator makes a 3D system from the initial 2D system.

In this work, we consider some important aspects of electromagnetic field behavior in membranes photonic crystals and PCRs. We develop the approach uniting both external and intrinsic problems, in-plane and out-of-plane geometries of incidence, and resonator properties of MPCs.

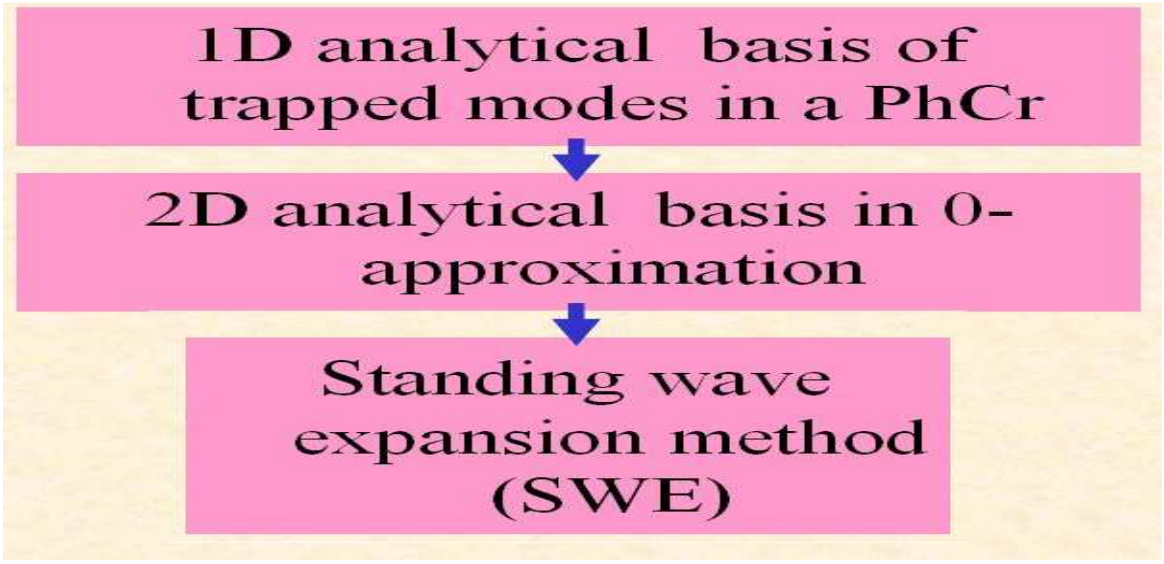


**Fig. 3** A scheme of SWE method use. Two 1D bases generate the 2D analytical basis of standing waves which is a ground of SWE calculation of the eigenproblem for the electromagneric field in a resonator.

To summarise, the approach uniting both external and intrinsic problems, in-plane and out-of-plane geometries was developed to investigate resonator properties of MPC. We have considered light reflection in out-of-plane geometry for rectangular 2D photonic membrane resonators where the incident wave excites trapped standing waves. A novel analytical method SWE is developed to calculate the resonator in-plane standing modes excited by an external source. The proposed SWE method for finite resonators uses open boundary conditions and may be adapted for any symmetry of the lattice as well as for any shape of material 2 bars in matrix material. Finally, a conception of all-optical logic devices based on optical properties of PCR is developed.

1. Glushko, E.,Ya, Glushko, A., E., Evteev, V., N., Stepanyuk, A., N., "All-optical signal processing based on trapped modes of a photonic crystal resonator," Proc. SPIE 7354, 73540L (2009).

# Model Doping Quantum Dots InAs with Bi Impurity by Low-Temperature CVD-Metods

Guba S.K.[1], Peleshchak R.M.[2], Petrovich R.Y.[1], Nayda I.I.[1]

[1]*Lviv Polytechnic National University, Lviv, Ukraine*
[2] *I. Franko Drogobych State Pedagogical University, Drogobych, Ukraine*

Growth of $In_xGa_{1-x}As/GaAs$ heterostructures with embedded arrays of quantum dots (QD) InAs CVD-metods at low temperatures is actual to the needs of nanoelectronics. QD InAs in GaAs matrix is formed by Stranskij-Krastanow mechanism. Growth kinetics and stress distribution in the QD matrix affects the size, shape and location in the matrix [1]. One of the management practices of forming homogeneous coherently deformation InAs QDs is their isovalent impurity doping Bi [2]. Therefore creation of model concepts of formating mechanism of of InAs QDs in GaAs matrix in their isovalent impurity doping Bi at low temperature CVD-metods is scientific novelty.

Epitaxial growth in gas transportation systems is determine by delivery processes of reactive components by gas stream and by the kinetics processes on the substrate. The purpose of this work is to create the mathematical models and numerical algorithms that allow us to investigate the gas-dynamic processes in the chloride system in horizontal gas-transportation reactor.

On the basis of model representations described [3] the growth model of GaAs/InAs(Bi) is constructed for a low temperature CVD-metods. The theoretical model of hetero nanostructures $GaAs/InAs(Bi)/In_xGa_{1-x}As$ growth for low temperature CVD - method is obtained. The model is based on the description of the gas dynamics and kinetics of surface processes of growth $GaAs/InAs(Bi)/ In_xGa_{1-x}As$ hetero nanostructure. The model makes it possible to quantify the change in the rate of growth $GaAs/InAs(Bi)/In_xGa_{1-x}As$ hetero nanostructure. Model also allows to determine the concentration of isovalent doping quantum dots of InAs with Bi admixture along the GaAs substrate in direct-flow horizontal reactor. From the analysis of surface processes kinetics, according to the model representation, the changes in growth rate of heteronanostructures of $GaAs/InAs(Bi)/In_xGa_{1-x}As$ and isovalent doping of InAs QDs by Bi-dope along the GaAs substrate in horizontal straight-through reactor wer quantitatively found out. The effects of input component concentration in the gas phase, the flow rate of gas-carrier $H_2$ and the distribution of the temperature profile along the substrate GaAs on these values were determined.

1. S.K. Guba and V.N. Yuzevich // Semiconductors. – 2014. – Vol.48. – № 7. – P. 905-910
2. R.M. Peleshchak, S.K. Guba, O.V.Kuzyk, I.V. Kurilo, O.O. Dank'iv// Semicnductors. – 2013. – Vol. 47. – № 3. – P. 349-353
3. С.К. Губа, Р.Й. Петрович. // Нові технології – 2008. – № 2. – С.230 –235.

# Investigation of the Structure of Nanoporous Gold Plasmon Films by X-Ray Diffraction and Reflectometry

Gudymenko O.Y., Kryvyi S.B., Kaganovich E.B., Krishchenko I.M., Manoilov E.G., Kladko V.P.

*V.E. Lashkaryov Institute of Semiconductor Physics NAS of Ukraine, Kyiv, Ukraine*

Plasmon nanoporous gold films (npor-Au) are the nanocomposite, nanoporous films containing gold nanoparticles (Au NPs) with the optical properties of localized surface plasmon (LP) resonance. Films prepared by pulsed laser deposition of forward and backward flows particles of erosion torch in argon atmosphere by beam of IAG:$Nd^{3+}$ laser on gold target.

Diffraction measurements were carried on the installation ARL X'tra (Thermo Scientific) using the grazing beam. X-ray reflectometry (XRR) measurements were performed on PANalytical X'Pert PRO MRD using $Cu_{k\alpha 1}$ ($\lambda$=1.5406 Å) characteristic radiation. Simulation and fitting of the reflectometry curves was carried on the X'Pert Reflectivity software.

It was established that the structure of Au NPs belongs to the polycrystalline phase with face-centered cubic lattice (fcc). It was defined that the average size of Au NPs increase from a few nanometers to 10-15 nm with increasing pressure of argon from $P_{Ar}$ = 10 to 100 Pa. Small sizes Au NPs experience compression due to surface tension, the lattice parameter is equal to $a$≈4,0646 Å. The values of lattice parameter Au NPs achieves close to the values in the bulk gold $a$≈4,0852 Å if pressure of argon rise. The smallest value $a$ characterizes lattice of Au NPs in the films obtained by the backward flows clusters on films areas that located far away from the axis torch. The obtained values of the lattice parameters were used to clarify the porosity of the gold films obtained by XRR. Porosity films increase from a few percent to ≈60% with increasing argon pressure. It also increases with decreasing film thickness. In the reverse transfer of torch's clusters it was obtained the films with gradient thickness, size of Au NPs and nanopore. We have studied the influence of film formation conditions (number of pulses in the pulse energy density, etc.) on the structural parameters of the films.

The obtained results are used to control the plasmonic properties of the films. We received films npor-Au with maxima of extinction curves with LP resonance in a wide wavelength range 550-740 nm. Most long-wave region are caused multipole generation, visible spectrum — dipole due to the internal size effect.

# To the Lifshitz-Slezov-Wagner Theory in Metal Alloys

Ivanskii B.V, StasykM.O.

*Yuriy Fedkovych Chernivtsi National University, Chernivtsi, Ukraine*

The Ostwald's ripening (OR) is the final stage of formation of a new phase as a result of phase transformation, such as decay of oversaturated solid solutions. Nanoclusters or nanocrystals (NC) of new phase having different sizes interact through the Gibbs-Thomson effect that results in dissolution of small NC and growth of large ones.

In work [1] the process of coarsening of nanoclusters or nanocrystals (NC) is investigated for the case when cluster growth (dissolution) is governed simultaneously by both diffusion along dislocation pipes and the rate of formation of chemical connections (chemical reaction) at cluster surface, *viz.* the Wagner's growing mechanism. For that, the total flow of atoms to (from) a cluster is represented by two parts, *viz.* diffusion part and Wagner (kinetic) one. The dependence of the rate of growth of NC on the ratio of the parts of the total flow has been determined as well as the NC's size distribution function referred to as the Wagner-Vengrenovich distribution.

Summarizing, it has been shown that the modified Lifshits-Slyozov-Wagner (*LSW*) theory [2] can be applied to nanocluster systems. Theory of the Ostwald's ripening for alloys containing nanocristalline phases must assume taking into account not only diffusion flow, $j_d$, but also kinetic (Wagner's) one, $j_i$, also. It has been shown, for alloys $Al-Sc$ [3] and $Al(Sc,Zr)$ [4] containing, correspondingly, NCs $Al_3Sc$ and $Al_3(Sc_{1-x}Zr_x)$, that the size distribution function is satisfactory fitted by the introduced here Wagner-Vengrenovich (*WV*) distribution.

1. Ivanskii B.V., Moskalyuk A.V., Yarema S.V., Panko I.I., Stasyk M.O. Wagner-Vengrenovich distribution // ISRN Nanomaterials. – 2013. – Vol.2013. – ID651576 (8 pages).
2. Vengrenovich R.D., Ivanskii B.V., Moskalyuk A.V. Generalized Lifshitz-Slyozov-Wagner distribution // JETP. – 2007. – Vol. 131. – P.1040-1047.
3. Novotny G.M., Ardell A.J. Precipitation of $Al_3Sc$ in binary $Al-Sc$ alloys // Material Science and Engineering A. – 2001. Vol.318. – P. 144-154.
4. Fuller Ch.B., Seidman D.N. Temporal evolution of the nanostructure of $Al(Sc,Zr)$ alloys: Part II-coarsening of $Al_3(Sc_{1-x}Zr_x)$ precipitates // Acta Materialia. – 2005. –Vol. 53. – P. 5415-5428.

# Semiconductor N-barrier Structures with Periodically Modulated Localization of 2D-bioionics

Ivashchyshyn F.O., Grygorchak I.I., Shvets R.Ya.

*Lviv Polytechnic National University, Lviv, Ukraine*

The formation of nanointerlayers of histidine ($C_6H_9N_3O_2$) in a three-times expended matrix of *InSe* leads to forty-times increase in the real part of the complex impedance and to almost four-times increase in photosensitivity in the direction perpendicular to the nanointerlayers. At the same time, there is observed the effect of photoinduced "negative capacitance". Co-intercallation of water, with inconsiderable increase in *ReZ* in the most low-frequency range, leads to crucial transformation of frequency dispersion of *ReZ*: highly non-monotoneous variation of *ReZ(ω)* in the frequency interval 0.0015-6.5 Hz (the maximum in the neighbourhood of the point 0.02 Hz being 20 times greater than that for water without intercalation) and further decrease of *ReZ* with the increase in frequency. Co-intercallation of histidine by aquous solution of *KOH* leads to essential decrease in *ReZ(ω)* in the whole frequency range investigated and to multi-valued functional relation: *-ImZ=f(ReZ)*. In both cases, the corresponding branches of Nyquist diagram (Fig. 1) manifest processes of storage and retain of charge in N-barrier structures synthesized. However, their mechanisms are, as it follows from data of cyclic voltampermetry (Fig. 2), generally speaking, different. In the first case, it is, in all probability, caused by electronic processes of capturing and retain of carriers by trap centres, but in the structure *InSe<htd+$H_2O$+KOH>*, we have sufficient reason to assert that pseudocapacitive charge storage at interphase interfaces takes place. The confirmation of the latter is made by curves of galvanostatic charge-discharge (inset of Fig.2), which manifect the fact of formation of a monocrystal nanostructured electric energy storage device. Besides, in this case, the combination of super-high value of dielectric permittivity with super-small value of the tangent of the angle of electric losses in infra-low-frequency range can serve as an evidence of the quantum nature of the energy storage. But for *InSe<htd+$H_2O$>* such combination is observed in the range of 1-120 Hz, which is of prospect for creation of quantum capacitors of super-high capacitance.

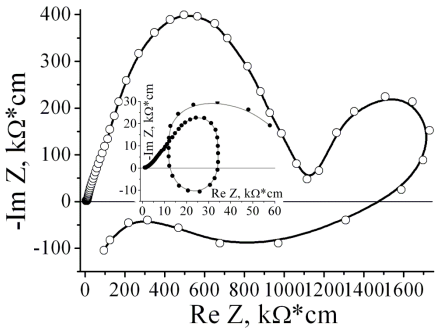


Fig. 1. Nyquist diagram for InSe <htd+$H_2O$> and for InSe <htd+$H_2O$+KOH> (inset) taken in darkness.

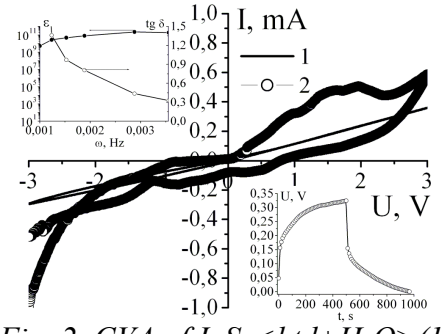


*Fig. 2. CVA of InSe<htd+$H_2O$>(1) and InSe<htd+$H_2O$+KOH> (2). In insets, frequency dependences of tangent of loss angle and of dielectric permittivity (left side); galvanostatic "charge-discharge" with 1 μA current (right side) for InSe<htd+$H_2O$+KOH> are presented.*

# Inequality of 2D Magnetic Conductors Electroconductivity at Contact and Non-Contact Introducing of Electrical Current

Kalinenko A.N.[1], Kopeliovich A.I.[1], Pyshkin P.V.[2], Yanovsky A.V.[1]

[1]*B. Verkin Institute for Low Temperature Physics & Engineering, NAS of Ukraine,*
[2]*Ikerbasque, Basque Foundation for Science, Bilbao, Spain.*

We showed that contact and non-contact methods of inserting to source of current lead to different electron kinetic processes in conductor, and therefore magnitudes of conductivity for these methods are different. The difference is especially large in hydrodynamic situation in electroconductivity [1] in which electron-electron collisions are more frequent than collisions with loss of electron momentum. We showed that at non-contact inserting electron-electron collisions give contribution to electrical resistivity in contrast with contact case. Reason is in space unhomogeneity of polarization charge induced by leads.

We obtain follow expression for electrical field E in 2D conductor by our hydrodynamic approach for "good conductors" [2] for non-contact case:

$$E = m(e\Pi\rho)^{-1}[(\Pi_\uparrow\rho_\downarrow - \Pi_\downarrow\rho_\uparrow)(i\omega + \nu_{ee} + \nu)\Delta u + (i\omega + \nu)\Pi j_p], \quad (1)$$

here m and e are electron mass and charge correspondingly, $\Pi_{\uparrow,\downarrow}$, $\rho_{\uparrow,\downarrow}$ are 2D density of states and density of both of electron spin components, $\Pi$ and $\rho$ are full electron density of states and density, $\omega$ is frequency of applied electrical field, $\nu_{ee}$ and $\nu$ are frequencies of electron-electron and electron-impurity collisions, $\Delta u$ is difference between drift velocities of "spin up" and "spin down" electrons, that was found in the work. Second addend in expression (1) corresponds to contact case. One can see from (1) that effect is large for quantum degenerated electron system, for classical system $\Pi_\uparrow\rho_\downarrow = \Pi_\downarrow\rho_\uparrow$. For electron system on surface of liquid helium quantum parameter $(\Pi_\uparrow\rho_\downarrow - \Pi_\downarrow\rho_\uparrow)/\Pi\rho \approx 10^{-3}$.

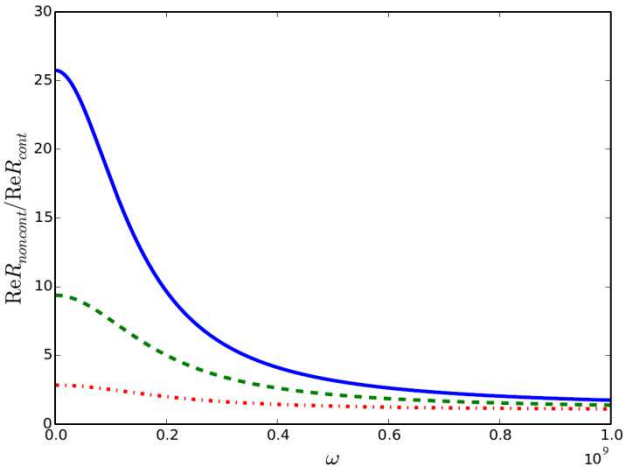


At picture dependence ratio of electroresistance of two inserting cases on frequency is described. Different colors of curves correspond different spin polarizations $\rho_\downarrow/\rho_\uparrow$, difference increase with polarization, $\rho = 6\cdot10^{11}$ m$^{-2}$, $\nu = 10^{10}$, $\nu_{ee} = 10^{11}$.

1. R.N. Gurgi, UFN, **94**, 689, (1968).
2. A.N.Kalinenko, A.I. Kopeliovich, P.V. Pyshkin, A.V. Yanovsky, Low Temp. Phys., **40**, 960 (2014).

# Light-Emitting Structures of CdS Nanocrystals on Oxidized Macroporous Silicon

Karachevtseva L.[1], Kuchmiy S.[2], Stroyuk A.[2], Lytvynenko O.[1], Sapelnikova O.[1], Stronska E.[1]

[1]*V. Lashkaryov Institute of Semiconductor Physics. Kyiv, Ukraine*
[2]*L. Pisarzhevsky Institute of Physical Chemistry. Kyiv, Ukraine*

Nanotechnology of colloidal CdS nanoparticles and its incorporation in the two-dimensional photonic structures of macroporous silicon was provided for the manufacture of compact light emitting elements. We investigated the contribution of electron-phonon interaction to Wannier–Stark effect and photoluminescence in macroporous silicon with nanocoatings.

The macroporous silicon structures to be studied were made using photoelectrochemical etching. $SiO_2$ coatings with thickness of 5÷200 nm were formed on macroporous silicon samples in dry oxygen. The layer of CdS nanocrystals 1.8÷2 nm in size was deposited from colloidal solution with polyethylenimine (PEI) onto oxidized macroporous silicon.

We measured the near-IR light absorption oscillations in 2D macroporous silicon structures with surface CdS nanocrystals and $SiO_2$ nanocoatings. The model of the resonance electron scattering on surface states is realized due to large-time electron scattering in the electric field of the "silicon–nanocoating" boundary, and the Wannier–Stark electro-optical effect is confirmed. We determined the influence of broadening on the oscillation amplitude in IR absorption spectra as interaction of the surface multi-phonon polaritons with scattered electrons.

The photoluminescence quantum yield of CdS nanoparticles on the surface of oxidized macroporous silicon with optimum thickness of $SiO_2$ layer increases of 3-4 times during the first 2 weeks due to evaporation of water molecules from the nanoparticles in the polymer layer and reaches 28%. With further storage of samples range and photoluminescence quantum yield almost no change. High intensity of photoluminescence was obtained due to increasing the flow of electrons from the silicon matrix in the direction of the nanocrystal layers at the maximum of the electric field on the boundary of Si-$SiO_2$. That significantly reduced the rate of nonradiative recombination.

Thus, nanotechnology of synthesis of CdS nanoparticles with the ordered crystal lattices was developed. We prove the possibility of achieving of high efficiency of the nanoparticle photoluminescence on oxidized silicon matrix by the controlled variation of the size of nanoparticles and thickness of the $SiO_2$.layer.

# The Energy of Formation Hexagon-Shaped N-doped Clusters $C_{96-x}N_x$

Karpenko O.S., Kartel N.T., Lobanov V.V.

*Chuiko Institute of Surface Chemistry of the National Academy of Sciences of Ukraine, Kyiv, Ukraine*

Several methods to eliminate some of the imperfection of grapheme – an infinite two-dimensional system of carbon atoms – are insisting. First it is, zero density single-electron states near the Fermi level, and second the lack of band gap. These included too the transition to a carbon nanoclusters (CNC) of finite size, creation of certain sets of mono- and polyatoms vacancies and doping graphene another atoms with an excess or deficiency of electrons in comparison with the carbon atom.

Presented here are the results of quantum-chemical calculations (DFT, B3LYP, 6-31 G**) clusters $C_{96-x}N_x$ (x = 1, 2) graphene-like structure.

Among the clusters $C_{95}N$ considered those, are obtained from the hexagonal $C_{96}$ replacing one of the atoms C on atom N, consistently moving from the central hexagon to one of six zigzag edges. The most stable among them cluster with doubly coordinated nitrogen atom located in one of the zigzag edges with energy of formation, according to the model reaction $C_{96} + N \rightarrow C_{95}N + C$, - 79.8 kJ/mol for the electronic ground-state with multiplicity (M) is equal to four. Despite the rather substantial negative charge (0.38 a.u.) at the nitrogen atom, the spin density in the cluster is allocated in mainly doubly coordinated carbon atoms, as is the case in CNC $C_{96}$ (M=5) [1]. For clusters $C_{95}N$ with various localization of nitrogen atom, the energy of formation is higher and negative charge on N is increasing according to moving the nitrogen atom from zigzag edges to the bulk of cluster, and reaching a maximum value in case when N located in the centre of hexagon. There are several vacant molecular orbitals (α- and β-) in monodoped clusters $C_{95}N$ with negative energy, indicating that transformation the CNC $C_{96}$ (M = 5) into the *n*-type semiconductor with the energy difference between the highest occupied and the lowest unoccupied molecular orbitals ~ 2 eV.

Structural and energetic properties didoped clusters $C_{94}N_2$ (M=3) are largely dependent from the distance between the nitrogen atoms, *d(N-N)*. Thus, in case when one of N placed in the centre of hexagon and the other placed on zigzag edge, and is doublycoordinated, the distance *d(N-N)* is 7,47 Å. The energy of formation cluster $C_{94}N_2$ (M=3), according to a model reaction $C_{95}N$ (M=4) + N → $C_{94}N_2$ (M=3) + C, is already 413.2 kJ/mol. Due to the repulsion between nitrogen atoms (the charges in atom are - 1.08 and - 0.36) the energy of formation $C_{94}N_2$ (M=3) is increase in comparison with the energy of formation cluster $C_{95}N$ (M=4).

1. Karpenko O.S., Lobanov V.V., Kartel N.T. // Chem. Phys. Technol. Syrf. – 2013. – Vol. 4, 2. – P. 123.

# Peculiarities of Electron Transport through Multilayer $SiO_2$-ncSi-$SiO_2$ Structures

Kizjak A.Yu., Evtukh A.A., Steblova O.V., Pedchenko Yu.M.

*V. Lashkaryov Institute of Semiconductor Physics, NAS of Ukraine, Kyiv, Ukraine*

Multilayer structures containing nanocrystalline inclusions (e.g., metalic, or semiconductors particles) in the dielectric matrix are under intensive investigations with aim of their perspective applications in electronics, for example in nonvolatile nanocrystal memory and optoelectronics. One of the significant problems restricting the practical application is to obtain the structures with required electrical parameters.

The purpose of this study was to investigate the electrical properties (conductivity) of layered structures silicon substrate-$SiO_2$-ncSi-$SiO_2$. The amorphous silicon (a-Si) or polycrystalline silicon (poly-Si) films were used as an embedded into dielectric semiconductor layer. The LP CVD (Low Pressure Chemical Vapor Deposition) method was used for obtaining these films. During high-temperature annealing thin a-Si and poly-Si films transform into nanocrystalline clusters.

The first ultrathin $SiO_2$ film was grown on Si wafer by thermal oxidation at T=850°C. Then a-Si or poly-Si films have been deposited by LP CVD at T=500°C and T=680°C correspondingly. The third upper $SiO_2$ layer was grown by thermal oxidation at T=850°C or deposited by LP CVD at T=400°C. After that the structures were annealed at T=1100°C during 1 hour to form nc-Si between $SiO_2$ layers. The total thickness of such three layers structure was variable in the range 17 – 30 nm. The following electrical contacts formation as on front and back sides finished the preparation procedure. The circle capacitors were formed on front side by metal deposition through mask.

I-V and high frequency C-V measurements at various temperatures have been used to characterize the electrical properties of the structures. As was determined the value of the current and transport mechanism significantly depend on the obtaining method of upper $SiO_2$ layer. Based on the analysis of I-V and C-V characteristics the mechanisms of electron transport through multilayered structures have been determined. The important role of traps in dielectric bandgap and tunneling through dielectric layer between Si nanocrystals has been clarified. The thicknesses of dielectric $SiO_2$ layers and size of Si nanoclusters also determine the electron transport mechanism.

# Effect of Geometry on the Fermi Energy Of Metallic Nanowire

Korotun A.V., Pogosov V.V., Koval A.O.

*Zaporozhye National Technical University, Zaporozhye, Ukraine*

The metal wires on semiconductor or dielectric substrates can be considered as one-dimensional electron systems with properties, which are of interest both from the fundamental point of view and from the perspective of their application in nanoscale electronic devices. As a rule, the calculation of the energy spectrum performed for the specific geometry of the metal sample and to obtain the approximate solutions of the Schrödinger equation. The Fermi energy size behavior, in particular, makes a major contribution to the optical conductivity [1, 2]. The solutions for metallic wires with circle cross section are known. However, in experimental conditions the simple geometry delays due to transverse stress or lateral pressure and is close to elliptical one. Therefore, the problem of the Fermi energy calculation for the elliptical nanowires is important.

It is assumed that the conduction electrons of the wire are located in a rectangular potential box with hard walls, so that the box shape reproduces the wire with elliptical cross section. There are exact solutions of the Schrödinger equation [3]. We start from the expression for the energy of an electron $\varepsilon_{mnp} = \hbar^2(k_{mn}^2 - k_{zp}^2)/2m$, where $k_{mn}^2$ and $k_{zp}^2$ are the eigenvalues of transverse and longitudinal components of the electron wave vector, respectively. From equality of the total number of the occupied states to the number of the conduction electrons $\overline{n}$ we obtain the equation for the computation of the Fermi level

$$\overline{n} = \frac{2}{\pi^2 ab}\sum_{m,n}\sqrt{k_{\mathrm{F}}^2 - k_{mn}^2}\ ,$$

where $a$ and $b$ are the half-axes of the ellipse. The summation should be performed over all numbers $m = 0,\pm1,\pm2,...$ and $n = 0,1,2...$ satisfying the condition $k_{mn} \le k_{\mathrm{F}}$. The calculations performed for wide range of sizes $a$ and $b$ and compared with the results for wires with equivalent cross sections.

1. Tomchuk P.M. Oscillations of optical conductivity and luminosity of quantum metal wires // Ukr. Fiz. J. – 2002. – V.47, № 9. – P. 833-841.
2. Kurbatsky V.P., Korotun A.V., Babich A.V., Pogosov V.V. Fermi Energy and optical conductivity of metal quantum wires // Phys. Sol. St. – 2009. – V. 51, № 12. – P. 2371-2378.
3. Van den Broek M., Peeters F.M. Confined states in two-dimensional flat elliptic quantum dots and elliptic quantum wires // Physica E. – 2001. – V.11. – P. 345-355.

# Electric Current and Heat Flux in Landauer – Datta – Lundstrom Transport Model for Nano- and Microelectronics

Kruglyak Yu.

*Odessa State Environmental University, Odessa, Ukraine*

The objectives for this report is to give a condensed summary of Landauer – Datta – Lundstrom (LDL) electron and heat transport model [1] which works at the nano- as well as at macroscale for 1D, 2D, and 3D resistors in ballistic, quasi-ballistic, and diffusive linear response regimes when there are differences in both voltage and temperature across the device.

The generalized LDL transport model for current and heat flux gives:

$$I = \frac{2q}{h}\int T_{el}(E)M_{el}(E)\left(f_1 - f_2\right)dE\,[A],\; Q = \frac{1}{h}\int(\hbar\omega)T_{ph}(\hbar\omega)M_{ph}(\hbar\omega)\left(n_1 - n_2\right)d(\hbar\omega),\; [W]$$

where $M$ is the number of modes of conductivity at energy $E$ or phonon modes at energy $\hbar\omega$, the transmission $T = \lambda/[\lambda + L]$, where $\lambda$ is the mean-free-path for backscattering for electrons or phonons and $L$ is the length of the resistor, Fermi function $f(E)$ and Bose function $n(\hbar\omega)$ are indexed with the resistor contact numbers 1 and 2, Fermi energy as well as temperature may be different at both contacts.

Equation for transmission is valid not only in the ballistic and diffusion limits, but in between as well: Diffusive: $L >> \lambda$, $T = \lambda/L << 1$; Quasi-ballistic: $L \approx \lambda$, $T < 1$; Ballistic: $L << \lambda$, $T \to 1$.

The LDL transport model is developed for linear response regime giving for electric conductance $G = 2q^2h^{-1}\int T_{el}(E)M_{el}(E)W_{el}(E)dE\,[S]$ with the Fermi conductance window $W_{el}(E) = (-)\partial f_0/\partial E$, where the quantum of conductance $G_0 = 2q^2/h$ relates to Klitzing constant and for lattice thermal conductance $K_L = 3\pi^2k^2T\,h^{-1}\int T_{ph}(\hbar\omega)M_{ph}(\hbar\omega)W_{ph}(\hbar\omega)d(\hbar\omega)$ with phonon transport window $W_{ph}(\hbar\omega) = (3/\pi^2)(\hbar\omega/kT)(\partial n_0/\partial(\hbar\omega))$, where the quantum of thermal conductance $g_0 \equiv \pi^2k^2T/3h \approx (9.456\times10^{-13}\,W/K^2)T$ represents the maximum possible value of energy transported per phonon mode and does not depend on particle statistics being universal for fermions, bosons, and anyons.

Expression for conductance above is known as the Landauer equation which is valid in 1D, 2D, and 3D resistors, if we use the appropriate expressions for number of modes $M_{el}(E)$. Conductivity of any material depends on its density of states in the Fermi conductance window with width of $\approx \pm 2kT$ around the equilibrium value of electrochemical potential $E_{F0}$. In the same way the phonon window determines which phonon modes carry the heat current. These two window functions are very similar in shape and play a key role in determining the electrical and thermal conductances.

[1] Yuriy Kruglyak, J. Nanoscience, vol. 2014, Article ID 725420, 15 pages, 2014; DOI: 10.1155/2014/725420.

# High 2D Conductivity of Graphene on Relaxor Film

Kurchak A.I., Strikha M.V.

*V.E. Lashkaryov Institute of Semiconductor Physics, Nat. Acad. of Sci., Kyiv, Ukraine*

A successful attempt [1] was made recently to use graphene as a technological transparent electrode for probable applications to photovoltaics, organic light-emitting diodes, touch screens, displays, and so forth. The main task at the solution of this problem is to obtain the best combination of the transparency (97.3% for a monoatomic graphene layer in the optical and near IR ranges) and the 2D resistivity. In [1] the high 2D graphene channel conductivity was obtained due to graphene doping by the dipoles of the transparent poly[vinylidenefluoride-co-trifluoroethylene] (PVDF-TrFE) relaxor with extremely high spontaneous polarization.

The resistivity, for those systems to be competitive with available indium tin oxide (ITO) coatings, has to be less than 100 Ω, which was in fact observed experimentally. However, the quantitative (and, in some cases, even qualitative) understanding of physical processes that govern the conductivity in such system is still absent, which makes it impossible to talk about directions of the effective improvement of their parameters.

In our work, a quantitative theory is developed for the conductivity in graphene doped with the relaxor PVDF-TrFE dipoles. The theory is based on the model of charge carrier scattering by large-scale static nonuniformities proposed in work [2], with regard for the charge carrier scattering at such nonuniformities arising owing to both the domain structure of the ferroelectric and the nonuniformities in the distribution of chemical dopants over the CVD fabricated graphene surface.

It is shown that the increase of the nonuniformity correlation length gives rise to the decrease of the resistivity. In the case where the distribution of chemical impurities is sufficiently uniform, and the domains in the ferroelectric are large enough, the resistivity can reach a value of 100 Ω and less [3]. Such values make the system “graphene on ferroelectric” competitive against standard conducting transparent ITO coatings for photovoltaics.

1. G.-X. Ni, Y. Zheng, S. Bae, C.Y. Tan, O. Kahya, J. Wu, B.H. Hong, K. Yao, and B. Ozyilmaz, ACS NANO 6, 3935 (2012).
2. F.T. Vasko and V. Ryzhii, Phys. Rev. B 76, 233404 (2007).
3. A. I. Kurchak, M.V. Strikha, Ukr. J. Phys. **59**, 622 (2014).

# Thermoelectric Lead Telluride with ZnO nanoparticles

Matkivsky O.M., Maksymyuk M.

*Vasyl Stefanyk Prekarpathian University, Ivano-Frankivsk, Ukraine*

One of the methods increasing the thermoelectric figure of merit ZT is to reduce the thermal conductivity, the reason is the relationship between the Seebeck coefficient (S) and the electrical conductivity (σ), because with increasing conductivity - thermopower decreases. It is assumed that to achieve this result, requires the use of spatially inhomogeneous materials with inhomogeneities whose size compared with the characteristic wavelengths of electrons or phonons and lying in nanometer plane.

A thermoelectric material properties of lead telluride with ZnO nanoparticles were investigated. In particular, measurement of the electrical conductivity (σ) (fig. 1,a), Seebeck coefficient (S) (fig. 2, b) and thermal conductivity (χ) (fig. 3, c). The calculated value of the specific thermoelectric power (α2σ) (fig. 4, d) and thermoelectric figure of merit (ZT) (fig. 5, e). It was established that the addition of ZnO powder Nanodispersed diameter grains (40-60) nm PbTe reduces the thermal conductivity of the material, while adding 0.5 wt.% ZnO to an increase of lead telluride thermoelectric figure of merit (ZT) to 1.3.

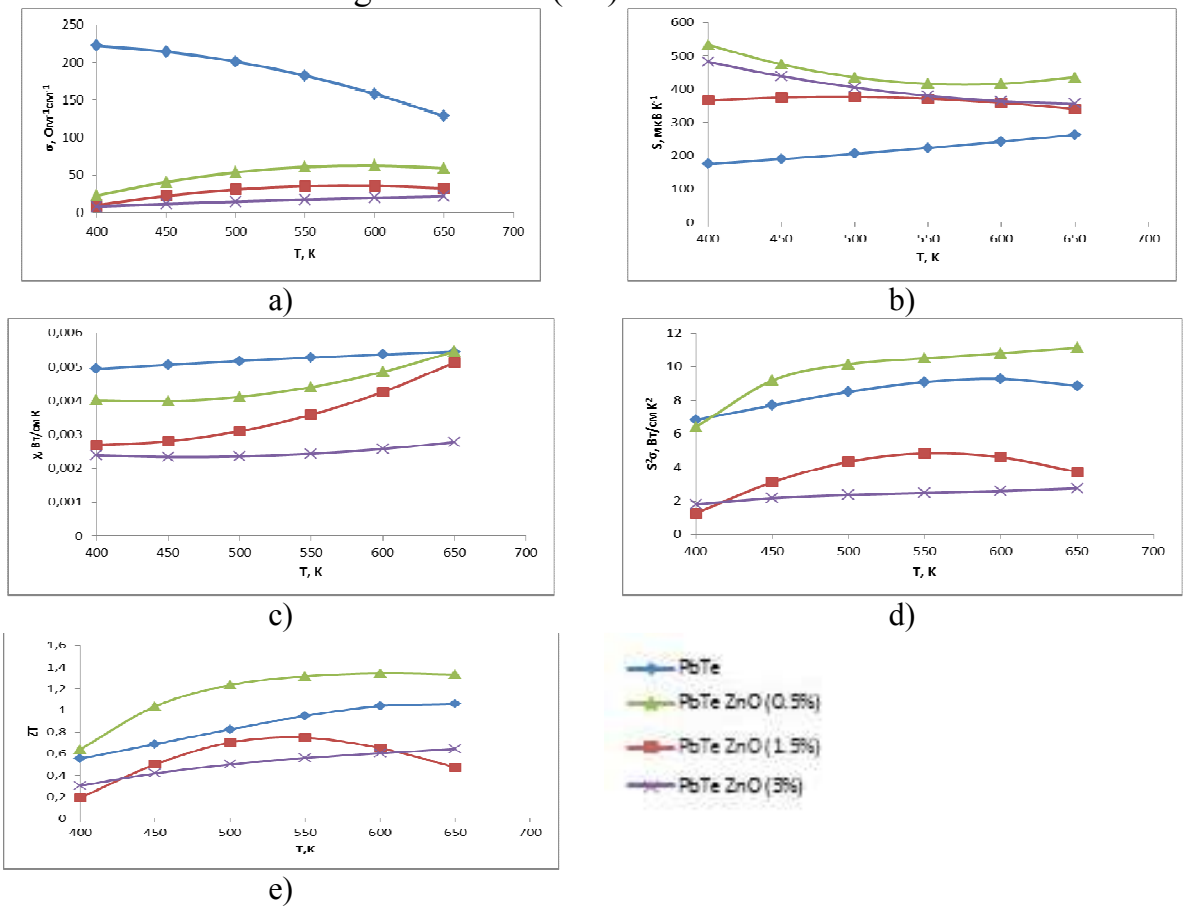


a) b) c) d) e)

Fig 1.Thermoelectric material properties of lead telluride with ZnO nanoparticles.

*This research is sponsored by NATO's Public Diplomacy Division in the framework of "Science for Peace" (NATO SPS 984536)).*

# Optical Properties of Nano-Structures of Eu(II) Compounds in Frozen Saline Melts

Nechyporenko G.V., Zinchenko V.F., Dyshleva L.F., Meshkova S.B.

*O.V. Bogatsky Physico-Chemical Institute of NAS of Ukraine, Odessa, Ukraine*

Nanoscale systems based on Eu(II) compounds are obtained by stabilization intra saline matrices at molten salt systems of crystallization.

In the experimental study of nanostructures of Eu(II) compounds in the salt systems the optical properties not inherent in the individual Eu(II) compounds via the electron spectroscopy of diffuse reflectance, IR spectroscopy, luminescence spectroscopy methods was established. The NaCl – $EuF_2$ mechanical mixture, like $EuF_2$ practically shows no luminescence. Also in frozen melt NaCl – $EuF_2$ the luminescence is weak.

In diffuse reflectance spectra in the near-IR range the distinct absorption bands of low intensity which are caused by 4*f*-4*f* electron transitions in the Eu(III) are available. At the interaction of NaCl and $EuF_2$ the complexation is not present that promotes rapid oxidation of the last one to Eu(III) compound.

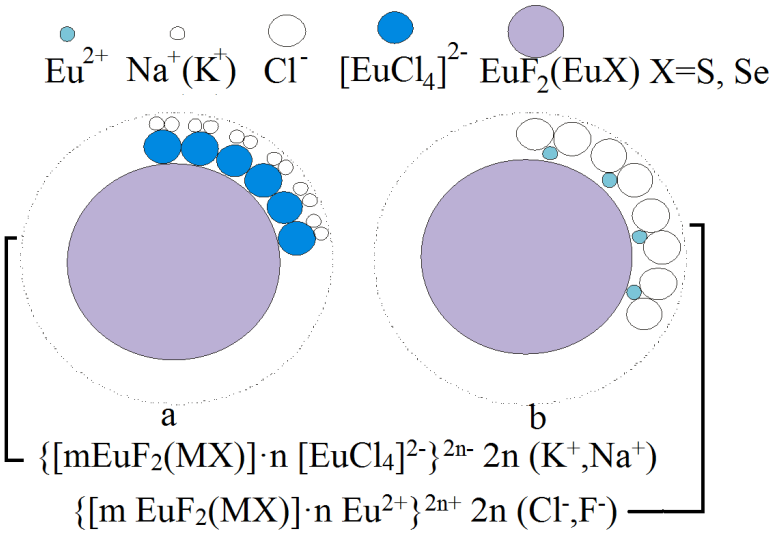


Figure. – Scheme of the electrical structure of $EuF_2$ (EuX) nanoparticles in salt systems:

a) – NaCl–KCl, KCl;

b) – NaCl.

The outer shell of $EuF_2$ nanoparticles in the KCl or NaCl – KCl systems, which includes the $[EuCl_4]^-$ or the $[Eu_2Cl_5]^-$ complex ions, are protected from the oxidation of europium (II) (Fig.). Thanks to this in the systems of KCl – $EuF_2$ and NaCl – KCl – $EuF_2$ an intensive blue luminescence which is caused by 5*d*-4*f* electron transitions in the $Eu^{2+}$ ions is manifested. Thus by comparing the optical properties of the studied systems, it is easy to see that the frozen NaCl – KCl – $EuF_2$ melt is located in an intermediate position between the NaCl – $EuF_2$ and the KCl – $EuF_2$ systems. Influenced by factors such as concentration quenching and coordination environment of Eu(II) the optical properties of nanostructures of Eu(II) compounds appear. There are suggestions that emission is caused not by the nanoparticles of Eu(II) compounds, but by their shells.

# Electron-Beam Recording of Surface Relief's Using $Ge_5As_{37}S_{58}$–Se Nanomultilayers as Registering Media

Paiuk O.[1], Meshalkin A.[2], Achimova E.[2], Stronski A.[1], Abashkin V.[2], Lytvyn O.[1], Sergeev S.[2], Prisacar A.[2], Oleksenko P.[1], Triduh G.[2]

[1]*V. Lashkaryov Institute of Semiconductor Physics NAS of Ukraine, Kyiv, Ukraine*
[2]*Institute of Applied Physics AS of Moldova, Chisinau, Moldova*

Thin films based on chalcogenide glasses have rapidly evolved as light sensitive materials for high density recording media application due to their optical and structural properties. In this work the experimental results showing the surface relief formation in $Ge_5$ $As_{37}S_{58}$-Se nanomultilayer structures under e-beam exposure are presented.

Amorphous $Ge_5As_{37}S_{58}$–Se nanomultilayers were prepared by computer driven cyclic thermal vacuum deposition from two isolated boats with $Ge_5As_{37}S_{58}$ and Se on constantly rotated glass substrate with deposited ITO layer at room temperature in one vacuum deposition cycle. The technology allows depositing thin films with thicknesses from 0.005 up to 3.0μm. The control of the thickness was carried out in-situ during the thermal evaporation by interference thickness sensor at $\lambda$= 0.95μm. Overlapping part of samples contains alternating nanolayers of $Ge_5As_{37}S_{58}$ with thickness of 1020 nm and Se with thickness of 1980 nm. The total number of nanolayers was 200. Control layers of $Ge_5As_{37}S_{58}$ and Se compositions were deposited at the same time onto the same substrate consequently through masks and used to check the composition and calculate the ratio of the sub-layer thicknesses in one modulation period. Diffraction gratings with 1, 2 and 4 μm period (and different exposure) were recorded by e-beam exposure using scanning-electron microscope Tesla BS 300 with programmable exposure control unit. The accelerating voltage was 25 kV and the size of the electron spot at this voltage was about 300 nm. Morphology and surface relief of the obtained gratings were

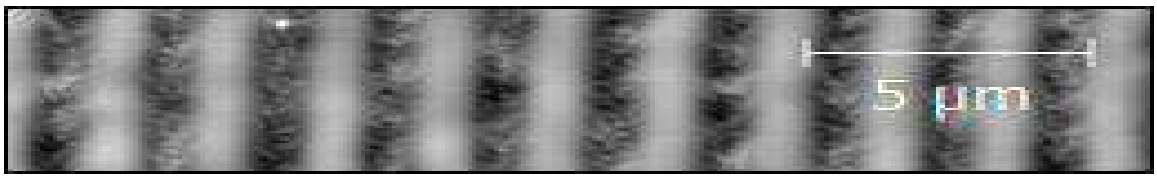


Fig.1 Surface of diffraction grating recorded in $Ge_5As_{37}S_{58}$–Se multilayers

studied by AFM microscopy. In Fig.1 AFM image of surface relief grating with 2 μm period recorded by e-beam exposure is shown. Diffraction efficiencies of the recorded gratings consisted ~ 1-2% on He-Ne laser wavelength (632.8 nm). The obtained results show possibility of $Ge_5As_{37}S_{58}$–Se nanomultilayer structures use as an electron beam assisted recording media.

*The research was supported by the project FP–7 SECURE–R21*

# The Influence of Structure Formation of the Silica Matrix on the Activity of Immobilized Cholinesterase

Payentko V.V.[1], Matkovsky A.K.[1], Kuts V.S.[1] , Matrunchik Yu.V.[2]

[1]*Chuiko Institute of Surface Chemistry, National Academy of Sciences of Ukraine, Kyiv, Ukraine*

[2]*The Institute of General and Inorganic Chemistry, National Academy of Sciences of Belarus, Minsk, Republic of Belarus*

Inclusion of ferments in hybrid organic-inorganic materials permit to obtain active immobilized preparation, since the polymer consisted in system creates the effect near to in vivo and silica matrix preserve biopreparation relative the influence environment. The dependence of the properties of composite material on the way of obtaining of silica constituent part was found by us previously [1] structure of the last may provide for different location of enzyme introduced into polymeric shell.

The goal of present work is to set up influence factors on aggregation of silica particles as the main reason (cause) of high cholinesterase activity of enzyme including composite material.

Microphotographs of materials obtained by drying suspensions of A300/ water (A) and A300/phosphate buffer from scanning electron microscopy(SEM) are shown on Fig.1

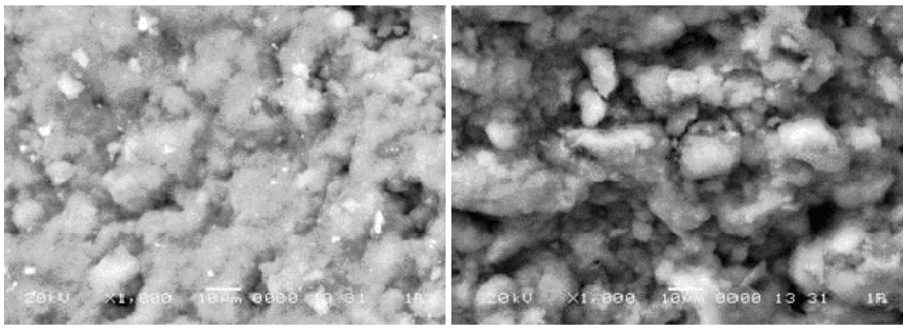

A B

Fig.1.SEM-microphotographs of powder-like materials obtained by drying suspension of A300/ water (A) and A300 /phosphate buffer

Similar results were obtained for systems silica\polyvinyl alcohol and silica\ gelatine. In the case of using polymers with higher molecular mass, the textures of surfaces were less aggregated. Activity of obtained preparations was higher under the less values of molecular mass as result of aggregation silica particles.

These results are in agreement with data of cholinesterase activity of composites obtained of sol-gel method.

Quantum-chemical calculation of charges distribution in the systems under investigation (A300/ water (A) and A300 /phosphate buffer).

1. Payentko V.V., Matkovsky A.K., Matrunchik Y.V. Composites of silica with immobilized cholinesterase incorporated into polymeric shell/Режим доступу/http://www.nanoscalereslett.com/content/10/1/82

# Acoustoelectronic Effects in Nanoheterostructures and Their Practical Significance

Peleshchak R.M.[1], Kuzyk O.V.[1], Dan'kiv O.O.[1], Peleshchak I.R.[2]

[1]*Drohobych Ivan Franko State Pedagogical University, Drohobych, Ukraine,*
[2]*Lviv Polytechnic National University, Lviv, Ukraine*

In works [1, 2] it has been demonstrated that by means of a supersonic wave one can control the transport properties of semiconductors and change their structure due to the processes of impurity atom diffusion, dissolution and formation of complexes, and formation of impurity atom clusters and intrinsic defects in periodic deformation fields. The extrinsic heterogeneous deformation causes the change of point defect chemical potential, thus leading to the directional diffusion flows. In work [3] it has been empirically determined that Si ultrasonic processing can stimulate diffusion at room temperature.

In this work, the deformation-diffusion model of the formation of periodic structures under the influence of acoustic wave in semiconductors with a two-component defect subsystem is constructed. The offered theory considers the deformation, created by an acoustic wave and dot defects. It is shown, that under the influence of an acoustic wave the periodic defect-deformation structures with the period equal to length of a wave are formed in the semiconductor.Within this model the possibility of ultrasonic stimulation of hydrogen passivation of Cl electrically active centers in the CdTe semiconductor and a decrease of dispersion of the sizes of InAs/GaAs strained quantum dots doped by isovalent impurity is analysed.

The obtaining of semiconductor structures with the self-organized nanoclusters by methods of molecular beam epitaxy and ionic implantation, and also possibility control of their physical properties are the subject of intensive researches. Information on nucleation (incipient state of formation) of periodic nanostructures of adsorbed atoms (adatoms) and implanted impurities is important for optimization of technological process and predicted control of physical properties of semiconductor structures with nanoclusters. The theory of spontaneous nucleation of the surface nanometer lattice which is caused by instability in system of the adatoms interacting with the self-consistent surface acoustic wave (SAW) is developed in [4]. Within this theory the conditions of formation of nanoclusters on the surface of solid states are established and the periods of a nanometer lattice as functions of concentration of adatoms and temperature are defined. However, the offered theory adequately describes the processes of formation of nanoclusters only at low temperatures. It is bound to that this model does not consider temperature dependence of concentration of the adatoms, and also interaction of electronic and defect subsystems which significantly depends on the temperature.

In this work, the theory of formation of nanoscale structures of the adsorbed atoms (adatoms), which occurs as a result of the self-consistent interaction of adatoms with surface acoustic wave and electronic subsystem is developed. Temperature regimes of formation of nanoclusters on *n*-GaAs surface under the influence of laser irradiation are investigated. The offered model allows to choose the optimal technological parameters (temperature, doping degree, intensity of laser irradiation) for formation of the surface periodic defect-deformation structures under the influence of laser irradiation. It is shown that at the fixed value of average concentration of adatoms the increase in degree of a doping donor impurities leads to increase in critical temperature below which there are self-organization processes.

The unique electronic and mechanical properties of single-layer graphene, including high carrier mobility at room temperature, the electron-hole symmetry and high values of Young's modulus ($E \sim 10^{12}\ Pa$), make this material very promising for nanoelectronics [5], in particular for creation of generators of mechanical oscillations, infrared light-emitting diodes. Among the main characteristics defining the possibility of practical use of devices on the basis of electromechanical properties of graphene nanotubes there is the frequency characteristic of this device. The higher the frequency of the electric signal to which this device adequately reacts, the greater speed of transformation of information, and eventually, a huge increase in its effectiveness. In this work, the model of the nanoacoustoelectronic converter on the basis of graphene nanotube is constructed. The offered model considers dimensional dependences of elastic constants and the sound velocity in graphene. Within this model, the frequency dependences of amplitude of the deformation, the surface concentration of electrons and the electrostatic potential are established. It is investigated that at increase in an electron concentration, an electron mobility and decrease of radius of nanotube the sensitivity of the converter increases. It is shown that at increase in radius of graphene nanotube there is the monotonic decrease of the amplitude of the electrostatic potential. This results from the fact that graphene nanotubes of the smaller sizes are more sensitive to deformation.

1. O.Ya. Olikh, I.V. Ostrovskii, Physics of the Solid State, vol. 44 (2002), pp. 1249 – 1253.
2. S. Ostapenko, R. Bell, J. Appl. Phys., vol. 77 (1995), pp. 5458 – 5460.
3. I.V. Ostrovskij, A.B. Nadtochij and A.A. Podolyan, Semiconductors, vol. 36 (2002), pp. 367 – 369.
4. V.I. Emel'yanov, Laser Phys., vol. 18 (2008), pp. 1435 – 1438.
5. A.H. Castro Neto, F. Guinea, N.M.R. Peres, K.S. Novoselov, A.K. Gaim, Rev. Mod. Phys., vol. 81 (2009), pp. 109 – 162.

# Regularities of Chromium Condensates Structure Formation under Volmer-Weber Conditions and Critically Low Supersaturations

Perekrestov V.I., Kornyushchenko A.S., Natalich V.V.

*Sumy State University, Sumy, Ukraine*

At present porous materials and three-dimensional structures with developed surface are widely used as sensor, catalysts, sorbents, fuel cells and other active elements. One of the method of low-dimensional porous system formation is based on self-assembling processes at condensation under near thermodynamic equilibrium conditions. The information concerning mechanisms of metal condensates structure formation under Volmer-Weber near equilibrium conditions is limited. At the same time, in our preliminary experiment in this area Cu, Al, C, Ti condensates were obtained in the form of porous three-dimensional system consisting of micro- and nanosized structural elements [1].

In this work the formation regularities of chromium layer under Volmer-Weber conditions at critically low supersaturations have been investigated. The low-dimensional chromium structures with different morphologies (network structures, agglomerations of weakly bounded crystals, columnar structures) have been obtained using unbalanced magnetron stutterer operating under extremely weak vapor fluxes and high growth surface temperatures.

Generalizing the results obtained, it has been established that the near equilibrium Volmer-Weber nucleation processes differ significantly from well-known concepts of substance condensation at the high supersaturations. Under conditions of critically low supersaturations the primary nucleation of subcritical chromium nuclei occurs mainly on active centers of the (001) KCl surface. The following secondary nucleation, as a rule, takes place on the primary clusters-substrate interface or on the structural defects of primary clusters aggregations. The active centers localization near primary clusters aggregation areas leads to formation of network structures and fractal fragments, which serve as a basis for the subsequent low-dimensional porous systems formation. It should be noted that the working gas pressure and the negative bias application to the substrate are very important technological parameters, which influence the structure formation mechanisms significantly.

5. Perekrestov V.I., Kosminska Yu.O., Mokrenko A.A., Kononenko I.N., Kornyushchenko A.S., Structure formation mechanisms of low-dimensional systems under quasi-equilibrium steady-state conditions // Vacuum. – 2011. – V.86**,** №1. – P. 111-118.

# Raman Scattering in Superlattices with SiGe Quantum Dots

Romanyuk Yu.A., Yaremko A.M., Dzhagan V.M., Yukhymchuk V.O.

*V. Lashkaryov Institute of Semiconductor Physics NAS of Ukraine, Kyiv, Ukraine*

In the last two decades under active theoretical and experimental studies of electronic and optical properties of quantum-dimensional crystal structures that create conditions for their practical application as promising materials of modern nano- and opto-electronics [1]. The physical processes occurring in QD and SL, have been studied both experimentally and theoretically in works [1-4].

In our work, a description of the experimental Raman spectra from SL to QD will be held at the microscopic level, which will be considered a real atomic structure of atomic QD and environment. Note that in the theoretical description of Raman spectra and absorption in these structures should be taken into account the convolution dispersion branches phonon modes. Since SL with QD implemented new frequency different from the lattice constant of raw materials, it leads to dispersion branches rolls phonons and manifestation of the spectrum in the range typical of optical phonons.

The theoretical model presented in this study allows analysis of the Raman features for all types of phonons within a microscopic approach using only general parameters of real crystals (phonons of frequency, atomic mass and steel grating). We study superlattices (SL) with layers of SiGe quantum dots (QDs) by Raman (Raman) and proposes a theoretical model that describes the experimental spectra. The model takes into account the real crystal structure of QD and the surrounding matrix, and electron-phonon interaction matrix QD. The intensities of Raman spectra were calculated using the procedure of secondary quantization and Green's function method. The results showed that the crystal structure of the superlattice consisting of Si layers and layers of SiGe quantum dots can be described as a mixed crystal with a certain distribution of "impurities" (SiGe- "atoms"). Qualitative correlation in the position and intensity of bands in the theoretically calculated and experimentally obtained Raman spectra with layers of SiGe quantum dots is observed and the nature of the doublet bands, is explained.

1. K.L. Wang, D. Cha, J. Liu, and C.Chen, Proceedings of the IEEE 95, (2007) 1866.

2. Sung-kit Yip, Yia-Chung Chang, Phys. Rev. B **30** (1984) 7037.

3. M.Cazayous, J. Groenen, A. Zwick, A. Mlayah, R. Carles, J.L. Bischoff, D. Dentel, Phys. Rev. B 66 (2002) 195320.

4. V.O. Yukhymchuk, V.M. Dzhagan, A.M. Yaremko, and M. Ya. Valakh, Eur. Phys. J. B 74, (2010) 10.

# Thermopower of Doped Graphene in Nanoribbons

Ruvinskii M.A.[1], Ruvinskii B.M.[2]

[1]*Vasyl Stefanyk Precarpathian National University, Ivano-Frankivsk, Ukraine*
[2]*Ivano-Frankivsk National Technical University of Oil and Gas, Ivano-Frankivsk, Ukraine*

The theoretical study of the thermoelectric effect in nanoribbons of doped graphene had been fulfilled for the cases [1] of armchair and zigzag with the relevant electronic states (with a gap and no gap in the energy spectrum). The electrical conduction, the thermoelectric coefficient and thermopower were defined by the Boltzman kinetic equation. For the armchair the elastic scattering of charge carriers the screened potential of a charged impurity was considered. For the case of zigzag the effect of electron-phonon interaction was determined. It is shown that the existence of a gap in the energy spectrum and the one-dimensional motion in the nanoribbons lead to increasing of the thermoelectric power in comparison with the case of an unlimited graphene.

1. L.Brey and H.A.Fertig. // Phys.Rev.B – 2006. – **V73 –** P. 235411-1–5.

# Quantum Size Effects in Thermoelectric Parameters of Nanostructures Based on Lead Telluride

Ruvinskyy M.A., Kostyuk O.B., Dzumedzey R.O., Nadraha O.R.

*Vasyl Stefanyk Precarpathian National University, Ivano-Frankivsk, Ukraine*

In the case when thickness of the film is the same order with the wavelength of the De-Broglie's waves for charge carriers the transverse motion of electrons is quantized. Since the spectra have the partially discrete values, the quantum-size effect appears. Terms of appearance of size quantization are performed for the semiconductor films, as they have the De-Broglie's wavelength for the carriers are on several orders higher than the interatomic distance. One of the effects of size quantization of the energy spectrum in two-dimensional systems is the emergence of oscillations in the dependences of thermoelectric parameters from the thickness of condensate. Due to the ability to regulate this data thermoelectric parameters, these structures are interesting for attract attention for detailed study.

Based on the model of quantum flat rectangular and with infinitely high walls pit, the correspondences were calculated and received value of the Fermi energy and kinetic coefficients (conductivity σ, Seebeck coefficient S and thermoelectric power $S^2\sigma$) for n-PbTe, by the Boltzman kinetic equation.

In the cases with strongly degenerate, degenerate and nondegenerate electronic gas in the films of lead telluride with n-type of conductivity are considered separately.

It is theoretically shown oscillating character of dependences of thermoelectric parameters of nanostructures based on n-PbTe for the degenerate and strongly degenerate electron gas (Fig. 1) and it is shown the monotonous character for the case of a nondegenerate electron gas. The conditions for the implementation of quantum-size effects in thin films are investigated. It is shown that quantum-size can be occurring only when the average electron energy is comparable with the characteristic energy quantization.

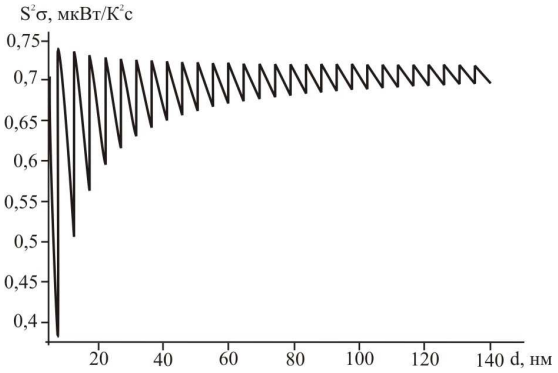


Figure 1. Theoretical dependence of the thermoelectric power $S^2\sigma$ from the thickness d of thin films of n-PbTe at T = 300K

*This research is sponsored by NATO's Public Diplomacy Division in the framework of "Science for Peace" (NATO SPS 984536)).*

# Graphene Membrane Thin Films and Thermomechanical Ripples

Prabhakar S., Melnik R.

*Wilfrid Laurier University, Waterloo, Canada*

It is well known that ripples are a typical feature of graphene sheets and thin films comprised of graphene membranes [1,2]. They are produced by long wavelength corrugations and may greatly affect electronic properties of graphene-based systems and devices.

Several mechanisms of inducing such ripples in graphene have already been discussed in the literature. Among them is electron-induced rippling in graphene [3], as well as elasticity-induced rippling [4], that may, in the general case, include nonlinear effects. The origin of graphene rippling continues to be debated. In the meantime, there is substantial experimental evidence that in order to control such ripples, a pure eleasticity-based picture may not be sufficient [5] and thermal properties of graphene may also be essential.

In this contribution, we illustrate how to develop and apply a fully coupled model that describes thermomechanical processes in graphene sheets. Based on this model, we demonstrate that coupling between mechanical and thermal fields is an important factor in better understanding of the appearance of ripples in graphene. Next, we use a generalization of our multiband model [6] to analyze the effects of such thermomechanically-induced ripples on the electronic properties of graphene. Results of computational experiments are shown for different boundary conditions that allow controlling ripples.

1. Gibertini, M. et al, Electron density distribution and screening in rippled graphene sheets, *Phys. Rev B*, 81, Art. 125437 (2010).

2. Lin, X. et al, Development of an ultra-thin film comprised of a graphene membrane and carbon nanotube vein support, *Nature Communications* 4, 2920 (2013).

3. P. San-Jose, J. Gonzalez, and F. Guinea, Electron-Induced Rippling in Graphene, Phys. Rev. Lett., 106, 045502 (2011).

4. L. L. Bonilla and A. Carpio, Model of ripples in grapheme, *Phys. Rev B,* 86, 195402 (2012).

5. Bao, W. et al, Controlled ripple texturing of suspended grapheme and ultrathin graphite membranes, *Nature Nanotechnology*, 4, 562-566 (2009).

6. S. Prabhakar, R. Melnik, and L. L. Bonilla, Coupled multiphysics, barrier localization, and critical radius effects in embedded nanowire superlattices, *J. Appl. Phys.* 113, 244306 (2013).

# Physical Properties of Three-Barrier Cascade of Terahertz Quantum Cascade Laser

Seti J.O., Tkach M.V., Pan'kiv M.V., Frankiv I.B.

*Chernivtsi National University, Chernivtsi, Ukraine*

The investigation of semiconductor nanostructures used for the fabrication of nanodevices operating in terahertz range, such as quantum cascade lasers, attract the scientific attention due to their actual advances in the operating frequencies enclosing one of the atmosphere transparency window. It is well known [1], that the quantum cascade laser consists of the series of typical nano size superlattice cascades, each of which generates the electromagnetic wave due to the intersubband electronic transitions. The semiconductor materials of cascade and widths of their potential wells and barriers are chosen depending on the demanded frequency of radiation and constant electric field, driving the structure, coordinates the operation of all cascades.

The theoretical investigation of physical properties of quantum cascade lasers is based at the consisted theory for electronic currents flowing through the multi-layer resonant tunneling structure driven by electromagnetic field and taking into account the interaction between electrons and electromagnetic field and with optical phonons as main dissipative subsystem. In the majority of experimental papers the theoretical evaluation of energy spectrum and probability of quantum transitions between the electronic states have been performed without taking into account of electron-electromagnetic field interaction. This interaction is considered in the simplest Frohlich model.

In the proposed paper, using the expanded into Fourier range the analytically obtained exact solution of complete Schrodinger equation, describing the electronic current through the three-barrier resonant tunneling nanostructure in electric and electromagnetic fields, we study the electron quasi-stationary states and dynamic conductivity of the system.

The theory of electron-phonon interaction is developed in the dielectric continuum model using Feynman-Pines diagram technique and temperature Green's functions. At the base of this theory we investigated the dynamics of electronic currents through the cascade of quantum cascade laser in outer fields and took into account the temperature effect of electron-phonon interaction on the renormalization and expanding of operating electron states.

1. C. Gmachl, F. Capasso, D.L. Sivco, A.Y. Cho. Recent progress in quantum cascade lasers and applications // Rep.Prog.Phys. – 2001. – V. 64. – P.1533.

# X-Ray Luminescence Effects in Ag-Dopped Cadmium Bromide Layered Nanostructures

Stetsyk N.V.[1], Antonyuk V.G.,[1] Panasyuk M.R.,[1] Rudka M.M.,[2] Dudyk I.R.[3]

[1]*Ivan Franko National University of Lviv, Lviv, Ukraine*
[2]*Lviv Polytechnic National University, Lviv, Ukraine*
[3]*Lviv National University of Veterinary Medicine and Biotechnology named after SZ Gzhytsky, Lviv, Ukraine*

Optical properties of $CdBr_2$ crystals have been studied in previous works as well as applied research. Cadmium bromide is a layered crystal having fundamental energy gap of 5.4 eV [1,2] and therefore have widely been used as optical material.

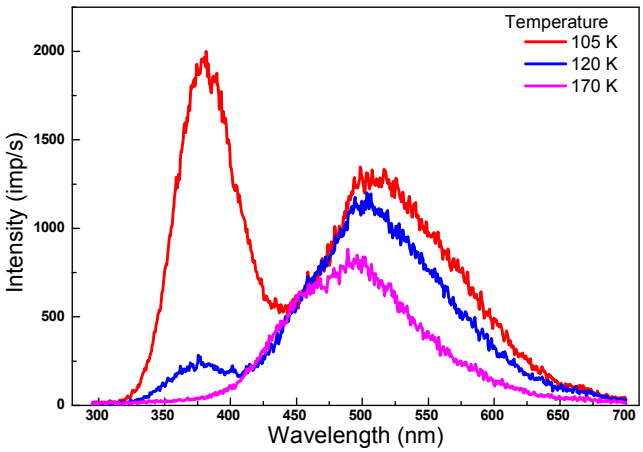


Fig. 1. The rentgen luminescence (RL or X-Ray) spectrum of $CdBr_2$:Ag+ in the short-wavelength region. The main band was a narrow band at 365 nm as well as of some broad bands at about 500, 510, and 525 nm.

The rentgen luminescence in the short-wavelength region is shown by curves in Fig. 1. The emission consisted of a main narrow band at 365 nm as well as of some broad bands at about 500, 510, and 525 nm. As a result the crystals $CdBr_2:Ag^+$ are sensitive to the action of X-rays and ultraviolet light through the flow of photochemical reactions (FHR) in these crystals and FHR cause the increasing of optical density in the samples and decreasing of the luminescence intensity.

1. Stetsyk N.V. , Antonyuk V.G., Rudka M.M.. Luminescence of single crystals cadmium bromide doped with impurities of argentum// Journal of Nano- and Electronic Physics. – 2014. - Vol 6, № 2. - P. 02001-1–02001-3.

2. Stetsyk N. V., Antonyuk V. G., Rudka M. M. , Dudyk I. R.. Luminescence properties of $CdBr_2$:Ag+ nanocrystals// The 17th International Conference on Luminescence and Optical Spectroscopy of Condensed Matter (ICL2014), 13-18 July, 2014, Wroclaw, Poland.Book of Abstracts. – P. 122-123.

# Electron-Phonon Interaction in Four-Well Nanostructure Being an Expanded Active Region of Quantum Cascade Detector

Tkach M.V., Seti Ju.O., Voitsekhivska O.M., Grynyshyn Y.B.

*Chernivtsi National University, Chernivtsi, Ukraine*

The quantum cascade detectors operating in middle and far range have been recently experimentally and theoretically studied on the contrary to the ones operating in near infra red range, researched in details over the last decade. The rising attention to their investigation is caused by the fact that they can operate at room temperatures as it was experimentally shown in [1]. The varying temperature effects at the magnitude of energy gaps of contacting layers of resonant tunneling structure, being an active region of quantum cascade detector and, thus, the heights of potential barriers are varying too, changing the electron energy spectrum in its turn. Therefore, the electromagnetic field absorption bands are shifting for these nano devices. Besides, the increasing temperature of the system increases the occupation phonon numbers and renormalizes the electron spectrum due to the electron-phonon interaction shifting the operating frequency of quantum cascade detector.

In the present investigation, we develop the quantum mechanical theory of electron-phonon interaction in four-well resonant tunneling structure as expanded active region of separate cascade of quantum cascade detector. The electron energy spectrum is calculated within the solution of Schrodinger equation in the model of effective mass and rectangular potential profile for $In_{0.53}Ga_{0.47}As/In_{0.52}Al_{0.48}As$ nanostructure. The spectra of confined and interface phonons are calculated using the transfer matrix method in dielectric continuum model. The electron-phonon Hamiltonian is obtained in the representation of second quantization over all variables of the system.

Using the Hamiltonian, we calculated the mass operator of electron Green's function at any temperature of the system and expanded energy bands at cryogenic and room temperatures. The partial contributions of different mechanisms of electron-phonon interaction (inter-band and intra-band ones within discrete and continuum spectrum) are obtained.

It is shown that the electron-phonon interaction at bigger temperature causes the weak shift of absorption band into the region of higher frequencies. The decreasing heights of potential barriers, due to the varying widths of contacting layers, bring to the essential expanding and shift of electromagnetic waves absorption bands into the region of smaller frequencies according to the experimental data [1].

1. Hofstetter D. 23GHz operation of a room temperature photovoltaic quantum cascade detector at 5.35μm // Appl. Phys. Let. – 2006. – V.89, P. 061119.

# Structure and Formation Energies of Ge Atoms Surface Complexes on the Substrate Si(001)(4×2)

Tkachuk O.I., Terebinska M.I., Lobanov V.V.

*Chuiko Institute of Surface Chemistry of National Academy of Sciences of Ukraine, Kyiv, Ukraine*

Nowadays there is no complete understanding of the physical chemistry of the formation of germanium nanodots Ge/Si, especially with regard to the initial stages of Ge atoms and $Ge_2$ dimers adsorption on the verge of Si(001), due to the lack of reliable data studied and mismatch between there. In experimental studies, the usually structure and properties of Ge islands are determined, and the initial stages of their formation remain unaddressed. In this case, methods of quantum chemistry are useful, which allow us to study nanostructures at atomic level, in particular to clarify the main features of the primary stages of the interaction of germanium atoms with a silicon substrate.

Calculations were performed using density functional theory with the base set 6-31G ** and hybrid exchange-correlation functional B3LYP using a software module GAMESS.

These experimental studies and quantum chemical calculations allowed to offer four different configurations $Ge_2$ dimers on the surface of silicon dimers on the verge of Si(001)(4×2) (Fig. 1.)

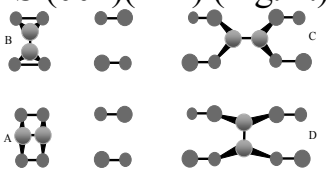


**Fig. 1.** Schematic representation of the structure of possible adsorption complexes of $Ge_2$ on the verge of the reconstructed Si(001)(4×2) surface.

In addition to the formation of clean germanium surface structures, penetration of possible the atoms in to the first substrate layer or more in the deeper layers.

Closest in is energy to the configuration A (A0 in Fig. 2) was A1 configuration that differed from A0 by shift of one *down*-atom in the bulk and by moving in to its place of the silicon atom of the substrate. The energy of this process is 80 meV. The energy difference between the configurations A0 and A1-A4 (see Fig. 2) is quite small, suggesting their possible reciprocal transformation at room temperature, without taking into account the activation barrier of the transitions between them.

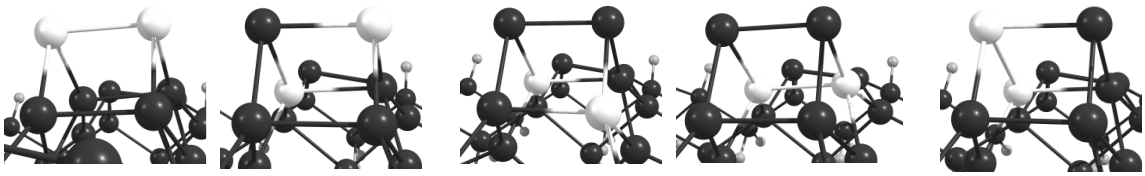

A (0) A1 (80 meV) A2 (120 meV) A3 (220 meV) A4 (220 meV)

**Fig. 2.** The configuration of Ge–Ge dimer (A0) and configurations formed from it by the interchange of Ge atoms and Si atoms on substrate Si(001)(4×2).

# Variation of Surface Characteristics and Sorption Properties of Zirconium Silicate Under Irradiation by Bremsstrahlung Gamma Rays

Vasylyeva H.[1], Yakovlev V.[2], Kylivnyk Yu.[2]

[1] *Uzhgorod National University, Uzhgorod, Ukraine*
[2] *Institute of Sorption and Endoecology problems NAS of Ukraine, Kyiv, Ukraine,*

The effect of Bremsstrahlung gamma rays on the surface parameters of microporous amorphous zirconium silicate and on its ability for sorption is studied. The samples were irradiated using a betatron (electron accelerator) with the maximal energy of the γ-quanta of 10 MeV and 22 MeV. The surface characteristics of the sorbents were studied by low-temperature adsorption/desorption of nitrogen. The experimental data were processed by BET, DR, and BJH methods. The results show that under exposure to Bremsstrahlung gamma rays the micropores of the sorbent under investigation are partly transformed in mesopores.

The ability of zirconium silicate to absorb $Sr^{2+}$ ions from an aqueous solution of strontium chloride is shown to increase noticeably after irradiation by 22-MeV Bremsstrahlung gamma rays. Since some of the zirconium isotopes ($^{40}_{88}Zr$, $^{40}_{89}Zr$, and $^{40}_{90}Zr$) have low gamma ray activation thresholds (5.61 MeV, 11 MeV, and 2.32 MeV, respectively), it is supposed that a certain role in the increased $Sr^{2+}$ ion sorption is played by Zr ion activation which can lead to the formation of vacancies in the sorbent matrix. A similar effect is also observed for another zirconium-containing inorganic sorbent – hydrated zirconium dioxide – and is considerably reduced at the decrease of the gamma radiation energy down to 10 MeV.

# Physicochemical Properties of Metal Oxide Nanopowders and Core-Shell Structures on Their Basis

Zhyrovetsky V.M[1], Popovych D.I.[1,2], Serednytski A.S.[1]

[1] *Pidstryhach Institute for Applied Problems of Mechanics and Mathematics NASU, Lviv, Ukraine*

[2] *National University "Lvivska Polytechnika", Lviv, Ukraine*

In work considered the complex approach to solving the problem that is to develop a laser reactive technology for produce of nanopowder materials and core-shell structures on their base [1] and the use of patented new luminescent methods for detecting gas particles [2]. Established the physical model of the formation of $TiO_2$ and ZnO nanoparticles and core-shell structures on their basis by means of laser reactive evaporation of metallic targets, based on nonequilibrium thermodynamic processes of coalescence and oxidation as a target and the target-cyclone distance and obtained depending dispersion and phase compositions and their structural characteristics of the laser pulse parameters evaporating, geometry and characteristics of chemically active environment. Established physicochemical regularities of formation of adsorption surface electronic states initial and doped nanopowders ($TiO_2$, ZnO) and core-shell structures on their basis during adsorption to gases ($O_2$, $H_2$, $N_2$, CO, $CO_2$). Created the core-shell nanostructure with a given diameter core and the thickness of the outer shell to monitor the type of spatial localization of carriers in the shell and, therefore, the electric field inside the nanoparticles. It was established that the variation of the electric field inside the core-shell structure because of the uncompensated charge regions leading to changes in the spectral position of the electronic transitions at gas adsorption. In obtained Zn-ZnO nanostructures such as "core-shell" observe them as abnormally high (> 1 order) photoluminescence quantum yield (including in gases) and high selectivity response signal on gas. Doped and laser modified nanopowder materials are sensitive indicators of adsorbed gas phase composition on the surface. By-turn, found that surface doping of materials with impurities of noble metals (Ag, Au, Pt) can increase sensitivity to the corresponding gas component and purposefully implement catalytic processes on the surface of nanopowder.

2. Gafiychuk V.V., Ostafiychuk B.K., Popovych D.I., Popovych I.D., Serednytski A.S. ZnO nanoparticles produced by reactive laser ablation // Applied Surface Science. – 2011. – **257**, – P. 8396–8401.
3. Ukrainian Patents №8371, IPC (2004) G01N 30/00. The method of gases registration using luminescence of the oxide nanopowder materials / Kotlyarchuk B.K., Popovych D.I., Serednytski A.S. – №20040604875, publ.15.08.2005, Bul. №8.

## СЕКЦІЯ 2 (стендові доповіді)
## НАНОТЕХНОЛОГІЇ, НАНОМАТЕРІАЛИ І КВАНТОВО-РОЗМІРНІ СТРУКТУРИ

12-15 травня 2015 р.

## SESSION 2 (poster)
## NANOTECHNOLOGIES AND NANOMATERIALS, QUANTUM-SIZE STRUCTURES

May, 12-15, 2015

# The Adsorption Properties of the Diamond Surface (111)-2×1 with the Vacancy Defect: Quantum-Chemical Simulation

Ananina O.Yu.[1], Severina E.V.[1], Lvova N.A.[2]

[1]*Zaporizhzhya National University, Zaporizhzhya, Ukraine*
[2]*Federal State Bugetary Institution "Technological Institute for Superhard and Novel Carbon Materials", Troitsk, Russia*

The goal of this work is simulation of possible states of vacancy defects on the diamond C(111)-2×1 surface and the study of their electronic, geometric and adsorption characteristics. Simulation of graphenes was carried out by a group of methods: semi-empirical MNDO, PM3 and PM6 methods of MOPAC software, and also ab-initio Hartry-Fock methods of PC GAMESS program.

Searching of stable configurations of vacancy defects on a clean surface C(111)-2×1 leads to three states with different geometry, electronic properties, and energy of formation. The total system energy for the cluster in state 2 increases on 0.816 eV (ab initio) and 0.78 eV (semi-empirical) in comparison with that in state 1. In state 3 the total energy for the cluster is 0.272 eV (ab initio) and 0.1 eV (semi-empirical) higher than in the state 1. Formation of the vacancy defect does not lead to significant change in hybridization of carbon atoms orbitals: type of hybridization remains unchanged - $sp^2$+p, change occurs only with the value of s- and p-components of hybrid orbitals. There is no significant change in the charge distribution on the surface with the vacancy defects.

In this paper we have studied the adsorption of the hydrogen $H_2$ and water $H_2O$ molecules on the C(111)-2×1 surface with the vacancy. Potential adsorption sites are the surface atoms in the chains with unsaturated bonds (involved in the formation of delocalized electron clouds) and atoms with the double bonds. During calculation have been estimated the values of energy characteristics of adsorption, such as the activation energy $\boldsymbol{E_{act}}$ of adsorption and binding energy (heat of adsorption, $\boldsymbol{q}$). It was shown that the adsorption of the atomic hydrogen on the region of the vacancy defect have occurs without activation ($\boldsymbol{E_{act}}$=0), unlike the adsorption on the ordered C(111)-2×1 surface wherein $\boldsymbol{E_{act}}$=0.2÷0.45 eV.

The adsorption of $H_2$ and $H_2O$ molecules occurs with the dissociation on the fragments. The chemisorption of hydrogen molecule $H_2 \leftrightarrow H+H$ requires the activation energy $\boldsymbol{E_{act}}$=0,51 eV, which is much smaller than the binding energy in the $H_2$ molecule ($\boldsymbol{E_b}$ = 4.47 eV). For water molecules chemisorption by the mechanism $H_2O \leftrightarrow O+H_2$ need $\boldsymbol{E_{act}}$=1,17 eV, and by the mechanism $H_2O \leftrightarrow OH+H$ the activation energy of adsorption is $\boldsymbol{E_{act}}$=0,76 eV.

Thus, we can conclude that in the region of the vacancy defect on C(111)-2×1 surface having active adsorption centers which will affect the mechanism of adsorption and desorption of molecules and particles.

# The Flow Behavior of Organic Liquids Inside Carbon Nanotube

Balabai R.M., Barilka A.G.

*Kryvyi Rih National University, Kryvyi Rih, Ukraine*

Research efforts over the past 20 years have been focused on the electrical, optical, and mechanical properties of the carbon nanotubes. Although several early experiments had shown the ability to open up carbon nanotubes (CNTs) to serve as nanoscale containers, it is in the past 5-10 years that experimental molecular transport through CNTs, or the interstice between vertically oriented CNTs, has become a subject of intense interest. This interest has been generated by the discovery of the fascinating mass-transport properties of this nanoscale material. For example, the transport rate of water is almost four to five orders of magnitude higher than that of other porous materials of comparable size, and is very close to that of biological membrane channels, such as aquaporin [1].

The aim of this work is to understand the flow behavior of liquids (water and methanol) in nanometrically bounded spaces with a cylindrical geometry, in particular, inside carbon nanotube (SWCNT) with clean walls and covered inside atoms Au (fig.1). Au nanoparticles have been actively studied because of the discovery of quantum size effects and the significant change in physical properties at the nanoscale. In particular, a dewetting event generally starts from the deposition of Au thin films on poorly wetting substrates [2].

We performed calculations of the (diffusion) migration energetic barriers of the water (methanol) molecules inside the zigzag (15,0) nanotube within the framework of the methods of the electron density functional and the ab initio pseudopotential. All calculations have been made with the proprietary source code [3].

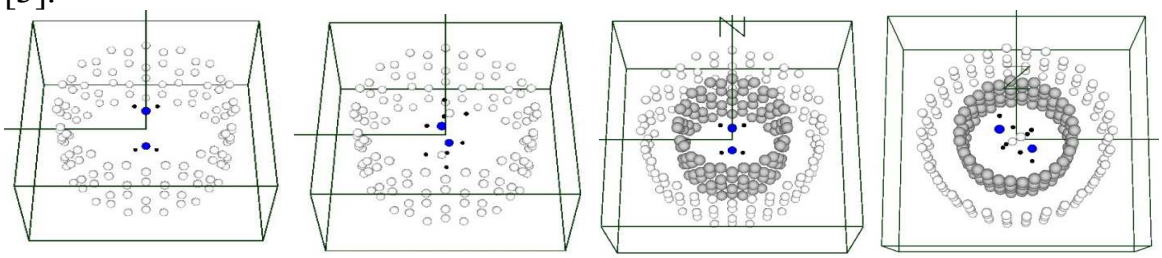

a b c d

Fig. 1. The supercell of the model superstructure for the flow of water or methanol inside nanotube with clean walls (a, b) and inside covered by the gold atoms (c, d).

1. Majumder M. Carbon Nanotube Membranes: A New Frontier in Membrane Science // in: Enrico Drioli and Lidietta Giorno Comprehensive *Membrane Science* and Engineering (*Elsevier* Science). – *2010*. – V. *1*. – P. 291–310.
2. Lee S.-H. et al. Dewetting behavior of electron-beam-deposited Au thin films on various substrates: graphenes, quartz, and $SiO_2$ wafers // Appl. Phys. A . – 2015. – V. 118. – P.389–396.
3. Balabai R.M. Electronic properties of functionalized graphene nanoribbons // *Ukr. J. Phys.* – 2013. – V. **58**, № 4. – P.389-397.

# Surface-Barrier Heterostructures on the Base of Nanoporous InP and GaAs Films with Au Nanoparticles

Barlas T.R., Dmitruk N.L., Kotova N.V., Mamykin S.V

*Institute of Semiconductor Physics, NAS of Ukraine, Kyiv, Ukraine*

Composite nanomaterials based on porous semiconductors attracted great interest in optoelectronics and photovoltaics due to unique optical and electronic properties which are different from the bulk materials [1]. This work is mainly devoted to the study of photoelectric properties of the Au/porous-GaAs and Au/porous-InP structures in combination with electric ones helping to understand the photocurrent behavior. Porous InP and GaAs have been prepared from the n-type (111) and (100) single crystals respectively by anodization in electrolyte containing HCl. Gold nanoparticles were deposited in electrochemical cell from Au salt. Au barrier contacts with 30 nm thickness have been deposited by thermal evaporation in vacuum. Surface morphology and pore structure have been analyzed by SEM. Photoelectric and electric properties of the structures have been studied with help of short-circuit photocurrent spectra in the 0.4-0.9 μm spectral range and forward/backward I(V) and C(V) characteristics. Au/porous-GaAs heterostructures show greater photosensitivity comparing to flat ones. Deposition of the Au nanoparticles into the pores leads to: i) photosensitivity increase of heterostructures due to increase of light absorption (fig. 1); ii) decrease of the saturation current and ideality factor. The physical nature of these effects can be explained by improvement of the barrier characteristics and the decrease of the optical losses [2].

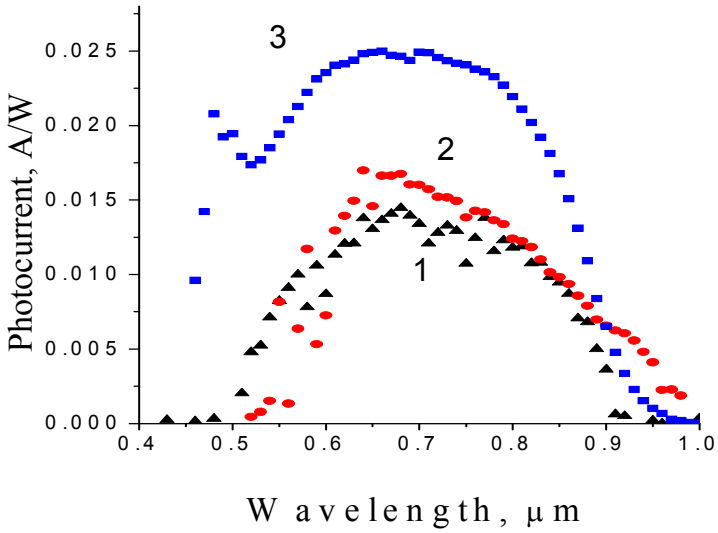


Fig.1. Spectral dependences of the photocurrent for Au/porous-InP structures without Au nanoparticles (1), with small (2) and large (3) amount of Au nanoparticles in the pores.

1. Dmitruk N., Barlas T., Serdyuk V. $A^3B^5$ Porous Semiconductors: Electrochemical Technology, Structure and Optical Properties // Physics and Chemistry of Solid State -2010.-V. 11, № 1 - p. 13-33.
2. Dmitruk N.L., Malinich S.Z. Surface Plasmon Resonances and Their Manifestation in the Optical Properties of Nanostructures of Noble Metals // Ukr. J. Phys.-2014.-V. 9, № 1 - p. 3-37.

# Lithium Power Sources Based on Porous Carbon Material

Barsukov V.Z.[1], Khomenko V.G.[1], Mandzyuk V.I.[2],
Myronyuk I.F.[2], V.M. Sachko[2]

[1]*Kyiv National University of Technologies and Design, Kyiv, Ukraine*
[2]*Vasyl Stefanyk Precarpathian National University, Ivano-Frankivsk, Ukraine*

The paper describes the possibility of using of porous carbon materials (PCM) from plant raw material as anodes of lithium power sources (LPS). The following PCM were chosen for testing: standard 1 – material obtained at carbonization temperature of 1023 K; standard 2 – thermally modified for 2.5 h at a temperature of 773 K standard 1; chemically washed with hydrofluoric (standard 3), salt (standard 4), and nitrogen (standard 5) acids standard 1. To create the laboratory samples of LPS the case details of primary lithium elements of coin design type CR2016 were used. LPS on PCM and lithium counter electrode bases are tested in galvanostatic mode at a current density of *C*/20 (for carbon *C* is 372 mA·h/g). 1 M solution of $LiPF_6$ in a solvent mixture (ethylene carbonate/dimethyl carbonate/diethylene carbonate in the ratio 1:1:1) was used as an electrolyte.

According to the results of the research, the main capacity of material spent in a voltage range of $0 \div 1.2$ V versus $Li^+/Li$. Specific capacity exceeds 450 mA·h/g at the first discharge for all standards. Charge and discharge capacity drastically reduced to 130-250 mA·h/g from the second cycle, but the hysteresis between the charge and discharge curves decreases. This fact points to the gradual stabilization of the electrode structure and its restructuring during cycling. The value of irreversible capacity is $21 \div 63$ % at the first cycle. A main reason is the formation of solid electrolyte interface on PCM surface. Obviously, the higher specific surface PCM has, the more charge (capacity) is spent at its formation. For example, for standard 1 (specific surface area is 343 $m^2/g$) irreversible capacity is 207 mA·h/g (36 %), while for standard 2 (specific surface area is 586 $m^2/g$) – 375 mA·h/g (59 %). The lowest value of irreversible capacity for sample 3 (110 mA·h/g or 21 %) is also associated with the lowest value of its surface (29 $m^2/g$).

From the second cycle, the specific capacitance is reduced almost in half. The difference in the values of the charge and discharge capacity decreases with further cycling, and Coulomb efficiency greater than 95 %. The smallest value of irreversible capacity has LPS on sample 3 base – after 93 charge/discharge cycles its value is 66 %. The highest value has a sample 2 – 86% (after 85 cycles) and sample 5 – 91% (after 90 cycles). Thus, prolonged cycling does not change the charge-discharge characteristics of the electrode, indicating the high stability of electrochemical characteristics of anode materials on PCM bases and the possibility of their use in the LPS.

# Direct Observation of the Empty Liquids Formation by Surface Plasmon Resonance

Boltovets P.M.[1], Manilo M.V.[2], Snopok B.A.[1], Barany S.[3], Lebovka N.I.[2]

[1]*Institute of Semiconductor Physics NAS of Ukraine, Kyiv, Ukraine*
[2]*Institute of Biocolloid Chemistry NAS of Ukraine, Kyiv, Ukraine*
[3]*University of Miskolc, Miskolc, Hungary*

Colloid systems with tunable properties and functionality are very perspective for the bottom-up approach to the self-assembled nanomaterials. From this point of view empty liquids presenting liquid states with vanishing density are of special interest. Here we demonstrate the approach to the investigation of the formation of the empty liquid state by laponite nanoplatelets known by its' possibility to form a solid-like transparent gel. A simple and convenient way for determination of effective optical parameters of complex environments is the surface plasmon resonance (SPR) method. It has been widely used to characterize both various solutions and thin organic films on metal surfaces. In the present work, we demonstrate the aging of aqueous suspension of laponite (2% wt) after the dissolution and homogenization. To our knowledge, it is the first direct on-line observation of the formation spatially organized gel with decreasing refractive index of materials in respect the homogeneous solution of the same components.

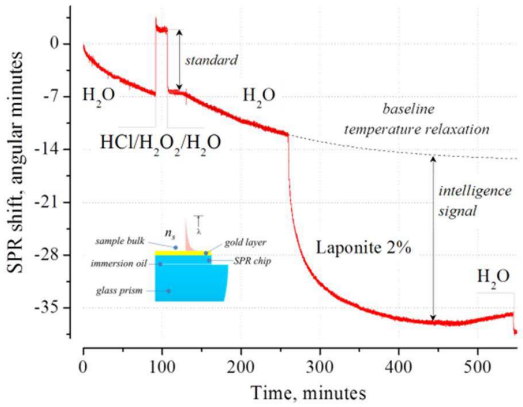


Figure. Typical SPR responses at various stages of surface clearing and formation of gel from initially homogeneous laponite suspension.
Inset: schematic arrangement of the optical components the SPR system at the interface.

Figure demonstrates the dramatic change of the optical properties of the suspensions. The modeling of the variation of the SPR response using Fresnel formalism (Winspall) indicates that observed changes may be explained by the decreasing the bulk refractive index of the formed materials. During the aging the electrokinetic potential of 2% laponite suspension was also studies. It increased from -48 mV (at $t$=0 min) to -62 mV ($t$=20-120 min). After this period of time ($t$ more than 120 min), the zeta-potential became constant. Such changes can be explained by the transfer from glass-like to gel-like structure of the investigated system.

# Ab Initio Study of Structural and Elecronical Properties of ZnO Nanoclusters

Bovgyra R.V.[1], Popovych D.I.[1], Bovgyra O.V.[2], Kovalenko M.V.[2]

[1] *Pidstryhach Institute for Applied Problems of Mechanics and Mathematics NAS Ukraine, Lviv, Ukraine*

[2] *Ivan Franko National University of Lviv, Lviv, Ukraine*

We present results of *ab initio* density functional theory studies of energy spectrum and ground stage parameters of "magic" clusters $(ZnO)_n$ ($n = 34$). Calculations were performed using ultrasoft pseudopotentials in the basis of plane waves, similar to previous studies [1]. The exchange-correlation functional is a generalized gradient approximation (GGA) proposed by Perdew, Burke and Ernzerhof. Optimization of the nanocluster structure was performed using conjugate gradient method. No symmetry restrictions were used during structure optimization.

The ab initio study of ZnO crystals is quite difficult. First, the structure of wurtzite contains twice as many atoms in the unit cell than zincblende structure. Second, oxygen and zinc are so-called "problem" atoms in terms of building their pseudopotentials. In both cases, the valence orbitals of O 2p and Zn 3d don't have core partners with the same orbital angular momentum and as a result are strongly bound, which require a larger basis of plane waves to describe them.

In order to determine the most stable structure for the "magic" clusters $(ZnO)_{34}$ we examined a number of isomers. Among them were fullerene-like hollow structures that satisfy the rule of six isolated quadrangles. Also, frame layered structures $(ZnO)_6@(ZnO)_{28}$ were built.

To analyze the stability of ZnO clusters we calculated binding energy per one molecule of ZnO. Analysis of the energy values shows that in case of $(ZnO)_{34}$ nanocluster the most energetically favorable is fullerene-like hollow structure. All such structures, that satisfy the rule of isolated quadrangles, have approximately the same binding energy. Among the structures in the form embedded clusters more stable are those in which the interatomic distance between the outer and inner shell is greater, i.e. intra cluster interactions are stronger than interaction force between the clusters.

4. О.В. Бовгира. Вивчення структурних та електронних властивостей кластерів ZnO методом теорії функціонала густини. // *Журнал нано- та електронної фізики*. – 2013. – Т.**5,** №1. – С. 01027-1−01027-6.

# Electrochemical Properties of Hybrid Supercapacitors Based on the Nanosized Spinel $LiMn_{1.95}Fe_{0.05}O_4$

Boychuk T.Ya.[1], Budzulyak I.M.[1], Ivanichok N.Ya.[2]

[1]*Vasyl Stefanyk Precarpathian National University, Ivano-Frankivsk, Ukraine*
[2]*G. V. Kurdyumov Institute for Metal Physics of the N.A.S. of Ukraine, Kyiv, Ukraine*

In recent years, hybrid supercapacitors are sharply developing. They are dominating over both the existing power sources and the symmetrical capacitors due to high power density and long cycling life. For today, the search of highly capacitive material for the anode supercapacitor is still continuing. This paper describes the use of spinel $LiMn_{1.95}Fe_{0.05}O_4$ as the anode material for supercapacitor.

This nanosized spinel was synthesized by sol-gel method. At the final stage of the synthesis the samples were annealed at the temperature of 873 and 1073 K. On its basis, anode mixture was formed (75% - spinel, 25% - carbon black). As cathode mixture was used the activated carbon and carbon black. Supercapacitor models in aqueous electrolyte 1M $Li_2SO_4$ discharged at the current of 10 mA in galvanostatic mode.

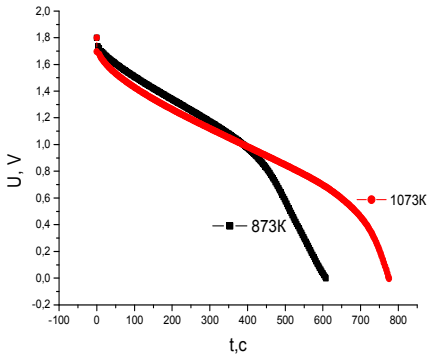


Fig. 1. Discharge curves of supercapacitor based on the spinel anode $LiMn_{1.95}Fe_{0.05}O_4$

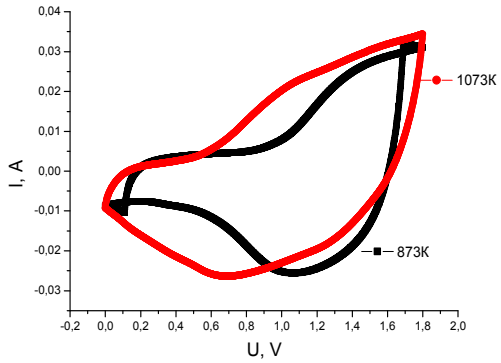


Fig. 2 CVA curves of supercapacitor anode based on the spinel $LiMn_{1.95}Fe_{0.05}O_4$

Discharge curves are characterized by slope in the voltage vicinity of 1.3V. The sample annealed at 1073K shows higher specific capacitance (14.4 mA • h / g) and longer discharge time. Results of galvanostatic experiments were confirmed by CVA method (scan rate of 5mV / s). Potentiodynamic curves have anodic peaks corresponded to lithium intercalation during discharge of supercapacitors (Fig. 2) Experimental data indicate that the investigated materials can be successfully used in the high capacity hybrid electrochemical systems

# Ab Initio Investigations of High-Pressure Behaviour of $Li_6B_4O_9$ Nanoclusters

Chobal I.[1,2], Grebenyuk A.[3], Chobal O.[1], Rizak V.[1]

[1]*Uzhhorod National University,Uzhhorod, Ukraine*
[2]*Institute of Materials Research, Košice, Slovakia*
[3]*Chuiko Institute of Surface Chemistry of National Academy of Sciences of Ukraine, Kyiv, Ukraine*

Numerous works on different physical properties of lithium tetraborate ($Li_2B_4O_7$) crystals point to promising possibilities for applications of these materials in acoustoelectronic devices, ultra-violet solid state lasers, and dosimetry. At the same time, atomic clusters can be building blocks of new nanostructured materials and, consequently, are of interest for intensive investigations with the prospect for applications in future nanotechnologies. At the same time, a study on the nanoparticles under high pressure is considered as a possible path to expand the range of available solid state materials. In this work, we present an *ab initio* theoretical analysis of the compression behaviour of lithium tetraborate nanoclusters.

The equilibrium geometries and energetic characteristics of free $Li_6B_4O_9$ cluster and of model ones where the $Li_6B_4O_9$ clusters are squeezed inside the spherical argon cages $Ar_{30}$ have been calculated from the first principles. All the calculations were performed by means of the GAMESS (US) quantum chemistry package. The calculations on the total energy and equilibrium geometric structure were performed by the spin-restricted Hartree–Fock method (RHF) with the 6-31G valence-split basis set.

Our study is focused on the analysis of changes in the structure and properties of the confined $Li_6B_4O_9$ clusters upon their transition from the free state to the extremely compressed one. The hydrostatic pressure was simulated by reducing the diameter of the spherical argon cages in the range of 15 to 8 Å. *Ab initio* calculations with partial geometry optimization have been performed at each step of compression with a "frozen" cage $Ar_{30}$. According to the results of calculations, all the structures obtained of $Li_6B_4O_9@Ar_{30}$ clusters are stable and correspond to local minima of the potential energy surface. Under hydrostatic pressure which corresponds to the volume reduction (about $0.6V_0$) of $Li_6B_4O_9$ nanocluster, a transformation of cluster structure is observed.

ACKNOWLEDGEMENT
1. Chobal is grateful to the International Visegrad Fund for the support of her research at Institute of Materials Research of SAS.

# Spectral and Morphology Analysis of Ultrathin Gold Films on Glass Substrate

Danylov A.B., Petrus' R.Y., Semkiv I.V.[1], Haiduchok V.G.[2], Zhydachevskii Y.A.[3]

[1] *Lviv Polytechnic National University, Lviv, Ukraine*
[2] *Scientific Research Company "Carat", Lviv, Ukraine*
[3] *Institute of Physics of the Polish Academy of Sciences, Warsaw, Poland*

There are technical applications of gold where its optical properties are of great importance and can assist in solving the various problems. Among the problems is solar cell (SC) manufacturing with maximum light absorption in the cell working range. For thin film SC the gold nanoparticle array can be deposited on the top of photoactive layer to improve SC performance. The nanoparticles interact with solar light that result in light scattering and absorption. The light absorption peak position and sharpness depends on particle shape and size distribution. In the present work we studied technological aspects of gold ultrathin film deposition on optically uniform glass substrate with controlled film thickness up to 0,1 nm and the regimes of thin film annealing to produce nanoparticle array with satisfactory size distribution.

The glass plates of dimension 16x8x0,8 mm were used as substrate. The initial film deposition was carried out by vacuum magnetron sputtering in COM-TH2-SP2-ION device at temperature of substrate 323 K. Rate of deposition was equal to 0,7 Å/s. The thickness and deposition rate control was performed by quartz sensor SQC-330. The film thermal annealing was carried out in air condition for 2 hours at temperature $T = 683$ K.

Optical spectra of absorption and transmission before and after annealing were measured independently by a fiber-optic spectrophotometer AvaSpec-ULS2048-UA-50 and two-beam spectrophotometer Shimadzu UV-3600. Maximum of light transmittance for deposited films is slightly shifted from approximately 485 nm to 510 nm with film thickness increase from 1 nm to 3 nm. The theoretical analysis of optical spectra was performed and optical constants of gold ultrathin films in visible light range in dependence of film thickness were determined. After annealing the absorption peak caused by plasmon resonance effect appears at wavelength about 530 nm. The peak is distinct for samples with initial film thicknesses of 2 and 3 nm, indistinct for 1 nm film, but its position is independent on initial film thickness. The surface morphology and nanoparticle size distribution were analyzed by electron microscopy method. The results of optical spectrometry and electron microscopy studies are discussed and theoretical curves for spectral extinction cross-sections for annealed films with different initial thickness are built.

# The Effect of A Constant Magnetic Field on The Structure and Thermomechanical Properties of Ternary Polyelectrolyte–Metal Complexes and Nanocomposites Based on Them

Demchenko V.L.

*Institute of Macromolecular Chemistry, Natl. Acad. of Sci. of Ukraine, Kiev, Ukraine*

The effect of a constant magnetic field on the structure and properties of ternary polyelectrolyte–metal complexes (TPMC) obtained from a stoichiometric polyelectrolyte complex (PEC) based on pectin and polyethyleneimine with $Cu^{2+}$ ions and nanocomposites formed from these ternary system have been studied by a number of structural techniques and thermomechanical analysis.

It is revealed that as a result of chemical reduction a copper ions in the volume of TPMC under the influence of a constant magnetic field occurs with the formation of nanocomposites based on PEC and nanoparticles which consist of only metallic copper phase. By means of thermomechanical method it is found that under the influence of a constant magnetic field a glass transition temperature $T_g$ increases for PEC–Cu and decreases for PEC and TPMC.

# The Effect of Intense Plastic Deformation on Phase Composition and Structure of Pearlite in Boron-Bearing Alloys

Filonenko N.Yu.[1], Pilyaeva S.B.[2]

[1]*Dnipropetrovsk State Medical Academy, Dnipropetrovsk, Ukraine*
[2]*Oles Honchar Dnipropetrovsk National University, Dnipropetrovsk, Ukraine*

It is known, that intense plastic deformation of iron-based carbon-bearing alloys causes fragmentation of cementite plates. But processes of plastic deformation effect on pearlite morphology for iron-based boron and carbon-doped alloys are not sufficiently studied.

The study was performed for specimens of the size of 30x30 mm with carbon content of 0,25 % (w.) and for alloys with carbon content of 0,25 % (w.) and boron content of 0,005 % (w.). Specimens were preannealed at the temperature of 1123 K for 5 hours and then were deformed to values of relative deformation of 10-40 % or were subjected to high-speed deformation. The microstructure of pearlite of alloys was determined by means of JSM-6490 microscope, optical microscope "Neophot-21" and electron microscope. The X-ray structural analysis was performed by means of diffractometer DRON-3 in monochromated Fe-$K_\alpha$ radiation.

When degree of plastic deformation is 10 %, there are no changes in microstructure of pearlite of iron-based alloy with carbon content of 0,25 % (w.). When deformation degree increases to 25 %, in pearlite grain of alloy partial shattering of cementite plates takes place. Partially in a volume of ferrite grains the formation of cementite inclusions of the size of 1,5-2,5 μm is observed. Under prior plastic deformation with degree of 40 % along with formation of light-side cementite plates there heavy side plates are formed, and occasionally the grained pearlite regions of the size of 2 μm are observed. Besides, volume ratio of pearlite decreases and comes out to 25 %. On the grain boundaries and sometimes inside the ferrite grains the formation of cementite inclusions of the size of 2,0-3,5 μm is observed. In microstructure of steel during high-speed deformation not only pearlite plates, but also ferrite grains are shattering.

Boron doping of iron-based alloy is attended with formation of more finely divided pearlite. When degree of alloy deformation is 20 % the formation of areas of finely divided grained pearlite with volume ratio of 20 % takes place. The enhancement of deformation degree leads to increase of volume ratio for the grained pearlite. Moreover, the formation of single particles of boron cementite $Fe_3(CB)$ inside the ferrite grains is observed in microstructure. It should be noted that phase composition of pearlite consists of ferrite and boron cementite. The high-speed deformation of alloy is characterized by more consertal structure of ferrite, than for carbon alloy. Almost all the pearlite is of grainy morphology. Inside the ferrite grains the finely divided inclusions of $Fe_3(CB)$ phase are observed. The presence of $Fe_{23}(CB)_6$ phase inclusions of the size of 0,05-0,07 μm inside the ferrite grains is revealed by means of electron microscope.

# Structure and Dielectric Properties of Glasses and Nanocomposites in $As_2Se_3$–SbSI System

Gasinets S.M.[1], Gorina O.V.[1], Guranich P.P.[1], Maryan V.M.[1], Mykaylo O.A.[2], Solomon A.M.[3], Rigan M.Yu.[1], Rubish V.M.[1]

[1] *Uzhgorod Scientific-Technological Center of the Institute for Information Recording, NASU, Uzhgorod, Ukraine*
[2] *Uzhgorod National University, Uzhgorod, Ukraine*
[3] *Institute of Electron Physics NASU, Uzhgorod, Ukraine*

Chalcohalogenide glasses on the basis of ferroelectrics SbSI which are the well-known ferroelectric-semiconductors, are of considerable interest.

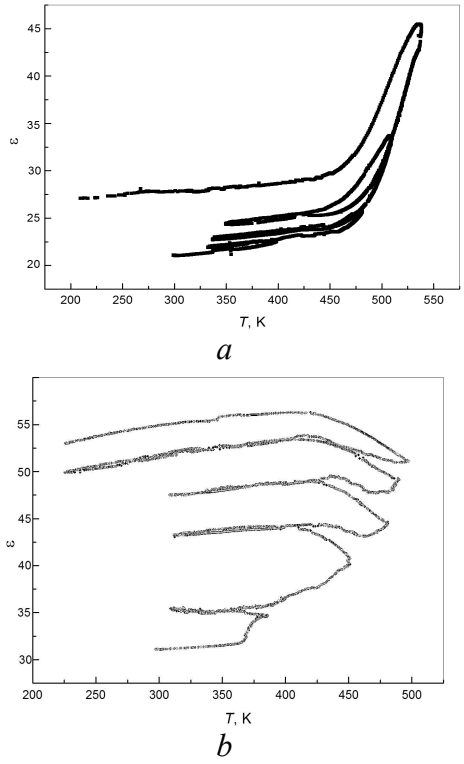


Fig.1 Temperature dependences of ε for $(As_2Se_3)_{30}(SbSI)_{70}$ (*a*) and $(As_2Se_3)_{50}(SbSI)_{50}$ (*b*) glasses measured in continuous regime

In the present report the results of investigation of the structure and dielectric properties of $(As_2Se_3)_{100-x}(SbSI)_x$ glasses (x=10–70) and their change during the heat treatment are given.

Glassy alloys were prepared by vacuum melting method in quartz ampules. The homogenization temperatures and melting times were 780-850 K and 36-48 hours, respectevely. The process of melts cooling was carried out in ice water.

Dielectric permittivity ε and tangent of dielectric loss angle tgδ of glasses were measured at the frequency of 1 MHz in the range of temperature 300-550 K and the heating rate 10 K/min. The parameter of ε was obtained within the accuracy of ±3%, tgδ – of ±10%.

Investigations of X-ray powder diffraction patterns for glassy, crystallized and crystalline materials were carried out on DRON-3 X-ray apparatus (λ=1,5418 Å). It was established that in the studied glasses in conditions of continuous heating prevails the mechanism of crystallization with the separation of SbSI stable phase in the range of $T_g$–$T_c$ ($T_g$ and $T_c$ are the glass-forming and crystallization temperatures). Formations in the glass matrix upon heating the nanocrystals of SbSI and their growth are accompanied by anomalies on the temperature dependences of ε (Fig.1). Glass crystallization is also accompanied by a sharp increase of dielectric parameters.

The influence of annealing times and temperatures on the structure and the dielectric properties of $(As_2Se_3)_{100-x}(SbSI)_x$ glasses are studied.

# The Effect of Carbonate on the Crystallization, Phase Composition and Thermal Behavior of Amorphous Calcium Phosphate with Ca/P=1

Goncharenko A.V.[1], Rokhmistrov D.V.[1], Zyman Z.Z.[1], Epple M.[2]

[1]*V.N. Karazin Kharkiv National University, Kharkiv, Ukraine*
[2]*University of Duisburg-Essen, Essen, Germany*

Amorphous calcium phosphate (ACP) is a precursor in the crystallization of hydroxyapatite. Therefore, ACP is often used as an intermediate phase in the fabrication of calcium phosphate biomaterials. The effect of carbonate on the crystallization, thermal behavior and phase composition of ACP under various conditions has being widely investigated. It was recently shown that ACP has a heterogeneous composition. The reason and mechanism of the inhomogeneity have been poorly studied. The effect of impurities including carbonate ions on the peculiarities in the composition is also unclear. In most cases, the carbonization of calcium phosphates was carried out by their ageing in carbonate saturated solutions. It often resulted in low carbonization, because the penetration of carbonate ions inside the calcium phosphate particles is complicated.

In this work, the preparation of carbonated ACP with Ca/P=1 was carried out in initial solutions which were previously saturated by carbonate dioxide. Analytical grade calcium nitrate tetrahydrate, $Ca(NO_3)_2 \cdot 4H_2O$, and ammonia hydrophosphate, $(NH_4)_2HPO_4$, were used as reactants. The pH values of solutions were within 10–11. The synthesis temperature $5^0$C, the reaction time was about 1 minute. The slurry appeared after mixing was dried by lyophilization.

The powdered samples were examined as-prepared and upon heating to a given temperature in the range 25–1000ºC. XRD, TG-DTA and IR methods were employed.

The as-prepared samples were X-ray amorphous. The effect of carbonate ions on the crystallization, thermal behavior and phase composition of ACP with Ca/P=1 is reported.

# Nanovoid Characterization of $NiMn_2O_4$-$CuMn_2O_4$-$MnCo_2O_4$ Ceramics

Klym H.[1], Ingram A.[2], Hadzaman I.[4] Shpotyuk O.[3]

[1]*Lviv Polytechnic National University, Lviv, Ukraine*
[2]*Opole University of Technology, Opole, Poland*
[3]*Vlokh Institute of Physical Optics, Lviv, Ukraine*
[4]*Scientific Research Company "Carat, Lviv, Ukraine*

Functional temperature-sensitive ceramics based on mixed transition-metal manganites is one of the typical representatives of topologically disordered substances. In bulk ceramics a significant shrinkage of the atomic structure occurs, eventually leading to more or less complex pore topology. These pores (voids) along with specific vacancy-type defects represent free-volume structure of ceramics. The main aim of this work is free-volume or nanovoid characterization of functional oxide materials taking the example of $Cu_{0.4}Co_{0.4}Ni_{0.4}Mn_{1.8}O_4$ ceramics in macro- and micro modifications.

It is shown, that the $Cu_{0.4}Co_{0.4}Ni_{0.4}Mn_{1.8}O_4$ ceramics contained large grains (~10 μm) as well as relatively sharp grain boundaries. So-called "closed" pores have a spherical form and are located mainly near grain boundaries. The $Cu_{0.4}Co_{0.4}Ni_{0.4}Mn_{1.8}O_4$-macro and $Cu_{0.4}Co_{0.4}Ni_{0.4}Mn_{1.8}O_4$-micro ceramics differ only by pores. The neatly shaping grains with comparatively tiny pores (~1 μm) are characteristic for $Cu_{0.4}Co_{0.4}Ni_{0.4}Mn_{1.8}O_4$-micro samples, while $Cu_{0.4}Co_{0.4}Ni_{0.4}Mn_{1.8}O_4$-macro ceramics contain similar crystalline grains with larger pores (reaching in size up to ~10 μm). Open pore size distributions cover significant amount of charge-transferring nanopores depending on sintering conditions and very small number of communication mesopores. The $NiMn_2O_4$-$CuMn_2O_4$-$MnCo_2O_4$ ceramics practically do not possess outside-delivering macropores depending on specific surface area of milled powder. Thus, $Cu_{0.4}Co_{0.4}Ni_{0.4}Mn_{1.8}O_4$ ceramics exhibit so-called one-modal pore size distribution with maximum position near 2 nm and double-maximum near 2.3 and 5.5 nm for $Cu_{0.4}Co_{0.4}Ni_{0.4}Mn_{1.8}O_4$-macro and -micro ceramics, respectively.

Free volume and nanovoids size in studied ceramics are studied also with positron annihilation lifetime measurements. Obtained results are interpreted in terms of unified multi-channel positron annihilation model involving both positron trapping and ortho-positronium decay modes. The shortest component in the lifetime spectra reflects mainly microstructure specificity of the spinel structure with character octahedral and tetrahedral cation vacancies. The extended defects near grain boundaries are supposed to be responsible for middle component at the level of 0.4 ns. The small third component is due to "pick-off" annihilation of o-Ps in the intergranual nanovoids. The observed o-Ps lifetime ~1.8 ns is related to the nanopores with radius of ~2.7 nm based on classic Tao-Eldrup equation.

# Effect of Magnetic Field on Energy Spectrum of Electron in Spherical Multi-Shell Quantum Dots

Holovatsky V.A., Bernik I.B.

*Chernivtsi National University, Chernivtsi, Ukraine*

The semiconductor low-dimensional quantum heterostructures (i.e. quantum wells, wires and dots) are conspicuous in many technological applications such as infrared photo detectors, lasers, light-emitting diodes, single electron transistor, etc. The modern advances in semiconductor technology allow the produce of more complex structures than the simple quantum wells, wires or dots. These structures, such as multiple quantum rings, complex quantum wires and the multi-layered quantum dots (QDs) [1], with various potential profiles of the quasiparticles are extensively studied.

In the paper the theoretical investigation of the energy spectrum and probability densities of the electron in the semiconductor multi-layered quantum dots under the influence of the external magnetic field is hold. We study the different types of the spherical nanosystems with two quantum-bound potential wells: QD with the core-quantum well (three-layered nano-structure) and the QD with the core-quantum barrier (four-layered nano-structure). In the nanosystems of the second type the radii of the curvature of both spherical shells-wells can be increased without any change of the thickness. This property allows to enhance the influence of magnetic field on the spectrum and wave functions of the electron [1].

The calculation of the electron energy spectrum in the QD driven by magnetic field is performed implementing the method of the quasiparticle wave function expansion using a complete set of the electron wave functions in the corresponding nano-structure without the magnetic field:

$$\Psi_{jm}(\vec{r}) = \sum_{n}\sum_{\ell} c^{j}_{n\ell m}\Phi_{n\ell m}(\vec{r})\,. \qquad (1)$$

The dependencies of the energy spectra of electron in double-well spherical nanosystems on magnetic field induction are obtained. It is shown that the influence of the field on the energy spectrum is bigger for the system with the core-quantum barrier due to larger radii of the curvature of the nanolayers. It is established that the quasiparticle localization in the QD can be controlled by the change of magnetic field induction value. That can be used to create new semiconductor devices.

1. Holovatsky V. Effect of magnetic and electric fields on optical properties of semiconductor spherical layer / V. Holovatsky, I. Bernik // *Semiconductor Physics, Quantum Electronics and Optoelectronics.* – 2014. – V. 17, № 1. – P. 7-13.

# Effect of Stressed Heteroborder Quantum Dot - Matrix for Polaron State of a Particle with Degenerate Band Spectrum

Hrushka V.I., Peleshchak R.M., Stara O.V., Radlovska N.S.

*Drohobych Ivan Franko state pedagogical University. Drohobych. Ukraine*

Modern development of nanotechnology [1] requires constructing models that would describe states of charged particles and excitons in mechanically strained-quantum dots (QD). In QD InAs / GaAs (CdTe / ZnTe), obtained in the mode Stranskoho-Krastanov there are significant deformation fields arising at the interface of quantum dot - matrix due to mismatch lattice parameters ($f = \frac{a^{InAs} - a^{GaAs}}{a^{GaAs}} \approx 7\%$). These disagreements lead to increased polaron effects compared to unstrained materials.

In [2] it was shown that polaron effects increases with decreasing size of the QD. Parameter gain polaron effect is the ratio of the radius polaron state $a_0$ to QD radius $R_0$ ( $\frac{a_0}{R_0} \gg 1$). In particular, in [2] was calculated binding energy of the electron and hole polaron in spherical QD-based materials with a high degree of ionicity without deformation of the material lattice QD with a potential hole with infinitely high walls. Availability compression strain material QD (InAs / GaAs, CdTe / ZnTe) will result in additional reinforcement polaron effect as renormalized parameter gain polaron effect will be greater than in the absence of deformation $\frac{a_0}{R_0 - |\vec{U}(\vec{r})|_{r=R_0}} > \frac{a_0}{R_0}$. $\vec{U}(\vec{r})$- displacement of the atoms in the material QD, which is the condition of mechanical equilibrium [3] $\vec{\nabla} \mathrm{div} \vec{U} = 0$. In this problem based on the Shrelsnher equation, which takes into account both deformation potential degenerate conduction band or valence band and the energy of the electron-phonon interaction and phonon own energy found strain energy of electron and hole polaron in mechanically strained QD.

In the experiment polaron states in QDs are shown in interband optical transitions in the event of intense phonon replicas due to the polarization of the medium and large stoksivskoho shift between absorption and emission lines.

1. Ledentsov N.N., Ustinov V.M., Shchukin V.A., Kopev P.S., Alfërov ZH .Y., Bymberh D., FTP, 1998, Volume 32, №4.
2. Ypatova I.P.,. Maslov A, Proshyna A.V., FTT, Vol 33, №4.
3. Teodosyu K. Upruhye models Crystal defects, Moscow, Mir, 1085.

# Formation of Interatomic Bonds on the Fumed Synthesis of Composites $x$-$SiO_2$ +$y$-$Al_2O_3$

Ilkiv V.Ya.[1], Zaulychnyy Ya.V.[1], Yavorskyy Yu.V.[1], Gun'ko V.M.[2], Zarko V.I.[2]

[1]*National Technical University of Ukraine "Kyiv Polytechnical Institute" Kyiv, Ukraine*
[2]*Chuiko Institute of Surface Chemistry, Kyiv, Ukraine*

Consolidation of unique properties of different nanomaterials allows broadening the range of their applications. In contrast to coarse-crystalline materials synthesis of composite nanomaterials can cause appearance of new properties due to significant contribution of interatomic interaction of surface atoms of nanoparticles.

Due to minimal uncontrollable influence of consequences of oxidation of nanoparticles surface in nanooxides and their unique sorption, photo-catalytic and photo-destructive properties they are important objects for investigation of influence of interatomic interaction changes at different treatment methods of nanooxides mixtures on formation of their properties.

The O$K\alpha$- , Si$L\alpha$- and Al$L\alpha$-emission spectra of mechanic mixes in system x – $SiO_2$ + y –$Al_2O_3$ (x=0,8 and y=0,2; x=0,7 and y=0,3; x=0,25 and y=0,75) and fumed synthesis of composites were investigated by the ultra-soft X-ray emission spectroscopy method.

The low-energy widening and shift of the main peak of superposition of the O$K\alpha$-emission bands of mixtures by 1,0 eV in a fumed mixed that indicates significant decrease of the energy of the O$p$-electrons occupying non-binding states. It was found that intensity of the low-energy sub-band reflecting covalent-binding states decreased when increasing $Al_2O_3$ content. Investigation of the Si$L\alpha$- and Al$L\alpha$-emission bands showed in fumed composites electrons occupation of states in low-energy sub-bands increased in Al$L\alpha$ (by 10 %) and in Si$L\alpha$ (by 50 %).

It was shown that such energy redistribution of the electrons is a consequence of formation of O-Si-O-Al-O chemical bonds at fumed synthesis of composites. Increase of occupation of low-energy Si and Al sub-bands and decrease of contribution of the O$p$-states into the covalent-binding sub-band of the O$K\alpha$-spectrum is a consequence of electron charge transfer from oxygen to $s$-states of silicon and aluminum. It leads to shift of the electron density to cations in σ-binding orbitals. Formation of the O$p$-π-bonds caused a decrease of the energy of O$p$-states occupied non-binding states.

# Size distribution of quantum dots on the surface of artificially grown quantum crystals

Ivanskii B.V, Panko I.I, Stasyk M.O, Kryvetskyi V.I.

*Yuriy Fedkovych Chernivtsi National University, Chernivtsi, Ukraine*

Owing to the progress of modern nanotechnologies, new artificial materials are developed that considerably expend functionality of electronic technology in physics and ad-hoc devices in chemistry and biology. In part, the use of pattern self-organization provides achieving precise positioning of QDs for construction of planar and volumetric arrays of QDs [1-2].

To obtain patterns with perfect periodicity, one uses the extreme ultraviolet interference lithography (EUV-IL) technique at wavelength λ=13,5nm [1]. For manufacturing two-dimensional arrays of dots by applying the reactive ion etching technique, gallium arsenide (GaAs) is often used as a subtrate, though silicon (Si) substrates are also in use. Artifical quantum dot crystals ordered in three dimensions grow at such substrates by applying the molecular beam epitaxy technique. X-ray diffractometry and atom-force microscopy (AFM) show high structural perfection of quantum dot crystals growing with the use of the mentioned techniques, as well as narrow size distribution of QDs.

In research [3] The size distribution function for nanodots in artificial three-dimensional quantum dot crystals (Si)Ge/Si and In(Ga)As/GaAs obtained using the patterns with perfect periodicity has been computed. Hut nanodots are modeled by cone-like clusters, for which the Thomson formula has been obtained that in necessary to find out the cluster growth (dissolution) rate under Ostwald's ripening. It follows from the comparison of the theoretical curve with experimentally obtained histograms that the size distribution function is formed under the Ostwald's ripening due to peculiarities of forming quantum dots Ge and InAs at previously patterned substrates Si and GaAs.

1. Grutzmacher D., Fromherz T., Dais Ch., Stangl Ju., Muller E., Ekinci Y., Solak H., Sigg H., Lechner R. T., Wimtersberger E., Birner S., Holy V., and Bauer G. Three-dimensional Si/Ge quantum dot crystals // *Nano Letters*. – 2007. – Vol.**7**. – P. 3150-3156.

2. Kiravittaya S., Rastelli A. and Schmidt O. G. // Rev. Prog. Phys. – 2009. – Vol.72. – P. 046502.

3. Vengrenovich R.D., Ivanskii B.V., Stasyk M.O., Panko I.I. On the size distribution in three-dimensional quantum-dot crystals // Semiconductor structures, low-dimensional systems, and quantum phenomena. – 2014. Vol. 48, №6. – P. 783-791.

# The Photoelectric Characteristics of Thermally Oxidized Macro Porous Silicon Structures on the Intensity of Incident Light.

Karachevtseva L.A., Onyshchenko V.F., Karas' M.I., Lytvynenko O.O., Stronska O.J., Parshin K.A., Konin K.P.

*Lashkaryov Institute of Semiconductor Physics of NAS of Ukraine, Kyiv, Ukraine*

We investigated the samples of thermally oxidized macroporous silicon structures characterized by the [100] orientation, the thickness H=500 μm, the n-type of conductivity, the specific resistance of 4.5 Ω×cm. The macropores had the diameter $D_p$=1-6 μm, the depth $h_p$=40-100 μm, the distance between the pores of *a*-$D_p$=1-4 μm. The silicon oxide layer is equal to 15 nm.

If the concentration of electrons at the surface states increased (see figure, its reciprocal quantity decreases) then decreases the concentration of electrons in the conduction band and the photoconductivity of macroporous silicon structure.

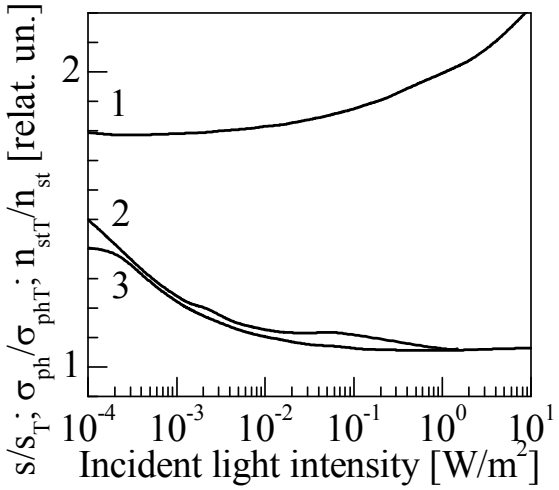


Fig. The calculated dependencies of the thermally oxidized of sample relative of the initial sample: the surface recombination velocity 1, the photoconductivity 2, the reciprocal of the density of filled acceptor surface states 3 on the intensity of incident light (λ = 0.95 micron).

We see from the figure that the photoconductivity of macroporous silicon structures depends inversely proportional on the density of filled acceptor surface states because the curves 2 and curves 3 almost coincide. The increases in surface recombination velocity can also result in decrease in photoconductivity.

It was found that an increase in the photoconductivity of thermally oxidized samples of macroporous silicon structures relative to the initial samples, with an increase in the intensity of the incident light, is connected with the decrease in the number of electrons on the surface levels on the surface of macropores.

1. Onyshchenko V.F., Karachevtseva L.A. Conductivity and photoconductivity of two-dimensional macroporous silicon structures // *Ukr. J. Phys*. – 2013. – Vol.**58**, №9. – P. 846–852.

# Creation of Nano-Track Electronic Devices

Kelesh I.

*South-Ukrainian national pedagogical university, Odessa, Ukraine*

The tracks are formed as a result of the bombardment of thin dielectric films by fast heavy ions. The diameter of tracks is of nanosize. Such structures formed the basis of new electronics, so called “track electronics” (TE). To create novel track devices it’s important to study physical mechanisms of tracks formation, the properties of the internal surfaces of tracks, the processes of penetration of electrolytes through the tracks of different size and shape, peculiarities of ion currents in tracks and so on.

In our theoretical work a model of the track system isworked out. The proposed model is designed on the base of classical moleculardynamics (MD). We developed an appropriate computer program and improved the standard MD approach. In our model quantum effects are accounted.

The model is applied to describe the ion current pulsations in track-containing foils. Typically pulsations ofthe ion current are observed in experiments in which the track-containing polymer foils are embedded in electrolytes, and AC voltage is applied. The interacting currents in tracks are simulated by two-dimensional system of oscillatingmodel particles located in the nodes of a plane lattice. In the model external discontinuous forces areintroduced to simulate an application of AC voltage. Interaction between model particles is varied toclarify its influence on pulsation effect. It is assumed that the average amplitude of oscillations of modelparticles is proportional to the average amplitude of current oscillations in real track structure. Themodel describes adequately the main features of the pulsation effect that were found experimentally.The obtained results are useful for creation and improvement of sensors and other devices of trackelectronics.

Now we continue this work to clarify the influence of geometry parameters and other features of tracks on the characteristics of ion currents through the tracks. We show how to use the results of nanotracks study to create new biosensors.

The work is closely coordinated with investigations of experimental groups in European universities.

# Compositional Investigations of the As-Se Nanolayers Using X-ray Photoelectron Spectroscopy

Kondrat O.[1], Holomb R.[1], Popovich N.[1], Tsud N.[2], Mitsa V.[1]

[1]*Uzhhorod National University, Uzhhorod, Ukraine*
[2]*Charles University, Prague, Czech Republic*

Amorphous films of $As_xSe_{100-x}$ ChG system are currently of interest as materials for optoelectronic devices as well as optical information storage. It was found that $As_{50}Se_{50}$ exhibits high light sensitivity during photostructural transformations due to the presence of homopolar As-As bonds [1]. The excess of As in $As_{50}Se_{50}$ relative to stoichiometric $As_{40}Se_{60}$ leads to an increase of the optical gap $E_g$ (from 1.90 to 1.95 eV for bulk $As_{40}Se_{60}$ and $As_{50}Se_{50}$, respectively) and of other related energy intervals. Evaporated films have been shown to have a large degree of structural disorder which was found to depend on the deposition method and conditions. In addition to structural disorder of the amorphous state connected with the absence of long range order and translation symmetry, the two types of defects: (i) coordination defects (*i.e.* so called charged $D^+$ and $D^-$ centers or valence-alternation pairs (VAPs)) and (ii) homopolar bonds defects (sometimes referred to as "wrong bonds") can be found in non-crystalline structures too.

Amorphous $As_{20}Se_{80}$, $As_{40}Se_{60}$ and $As_{50}Se_{50}$ thin films with thickness of about 0.5 μm were prepared by thermal evaporation from bulk glass on the (100) silicon crystal wafer substrates. The high-resolution photoemission spectra were taken using the Mg K-α (hν=1253.6 eV) X-rays source. The photoelectron As 3d and Se 3d core-level spectra of films were measured and analyzed.

The composition and local structure of the surfaces were determined by curve fitting of the experimental As 3d and Se 3d core levels, and studies show significant Se-enrichment in the top surface layers of the films. The interconnection between the surface composition, local structure formation and the features of the valence band spectra of $As_{20}Se_{80}$, $As_{40}Se_{60}$ and $As_{50}Se_{50}$ films are analyzed and discussed in detail. Obtained results are in a good agreement with results of the compositional analysis of the same samples with using of the synchrotron radiation photoelectron spectroscopy [2].

1. V.M. Lyubin, *J. Non-Cryst. Solids* 97-98 (1987) 47-54.
2. O. Kondrat*, R. Holomb, N. Popovich, V. Mitsa, M. Veres, A. Csik, N. Tsud, V. Matolín, and K.C. Prince, *Journal of Non-Crystalline Solids* 410 (2015) 180–185.

# Temperature Changes of Exciton Absorption Spectra in Semiconductor-Based Flat Nanofilms

Kondryuk D.V., Derevyanchuk O.V., Kramar V.M.

*Yuriy Fed'kovych Chernivtsi National University, Chernivtsi, Ukraine*

In the approximation of a dielectric continuum for phonons, the model of rectangular potential well and approximation of effective masses – for electrons, theoretical studies of the temperature changes of the shape of the exciton absorption band in semiconductor-based nanofilms were carried out by the Green's function method [1]. An evident form of the connection function of the ground excitonic state with confined phonons in the flat nanofilm was obtained.

The mass operator of the exciton-phonon system has been built based on this connection function. Its real ($\Delta$) and imaginary ($\Gamma$) parts defines the spectral and temperature dependence of the exciton absorption band shape function

$$S(\omega,T)=\frac{\Gamma(\omega,T)}{[\hbar\omega-E-\Delta(\omega,T)]^2+\Gamma^2(\omega,T)}.$$

Here $E$ is the energy of transition to the ground exciton state.

Numerical calculations has been made by the examples of a plane double nanoheterostructures $Al_xGa_{1-x}As/GaAs$ with different concentration of aluminum atoms in barrier material ($x = 0.2$ … 0.4), and β-HgS/β-CdS. If the film thickness exceeds 70 nm, the main contribution to the energy of exciton-phonon system in such nanostructures makes the interaction with optical phonons of the confined mode [2].

Spectral dependences of the absorption coefficient by the mechanism of direct transition to the ground exciton state were computed for named types of nanofilms as a convolution

$$\alpha(\omega,T)=2\pi D_0^2\int S(\omega-\omega',T)g(\omega')d\omega'$$

of $S(\omega,T)$ and Gaussian function $g(\omega)$, which takes into account inhomogeneity of the film thickness [3]. The changes in contour of exciton absorption band due to temperature changes in films of both types and composition of the barrier material in $Al_xGa_{1-x}As$ were investigated.

1. M.V. Tkach. Quasiparticles in nanoheterosystems. Quantum dots and wires – Chernivtsy Univ. Press, Chernivtsy, 2003 (in Ukrainian).
2. V.M. Kramar, M.V. Tkach. Exciton-phonon interaction and exciton energy in semiconductor nanofilms // Ukr. J. Phys. – 2009. – Vol. **54**, № 10. – P. 1027-1035.
3. G. Beadie, W.S. Rabinovich, D.S. Katzer, M. Goldenberg. Inhomogeneous broadering of intersubband transitions in $In_{0.45}Ga_{0.55}As/Al_{0.45}Ga_{0.55}As$ multiple quantum wells // Phys. Rev. B. – 1997. – Vol. **55**, № 15. – P. 9731-9739.

# Nanosafety in the Manufacture And Study of Semiconductive Nanomaterials

Koshel V. I., Poplavskyy O. P., Poplavskyy I. O.

*Vasyl Stefanyk Precarpathian National University, Ivano-Frankivsk, Ukraine*

In the XXI$^{th}$ century ecological problems have become especially actual and sharp. Pollution of water and air causes about 5 percent of death nowadays.

Evaluating of research lab conditions is based on impact differential analysis of industrial environment factors. Under the simultaneous influence of several detrimental factors their integral power should be analysed.

Semiconductor devices fabrication includes the use of oxides of aluminum, magnesium, beryllium, barium carbonate, chromium compounds and manganese, mercury, lead and other materials.

Fig. 1. Topogram of film surface

As well as Poisonous fumes, which cause numerous health problems, all manufacturing operations are accompanied by the release of dust and gases. In most cases scientists work with fine polycrystalline materials (see Figure 1). Prolonged exposure to manganese can cause severe changes in the central nervous system. Oxides are toxic and cause ulcers and atrophic processes in the nasal mucosa. The local concentration of harmful substances should not exceed the maximum allowable concentration of a nanopowder.

All manufacturing operations should be carried out in ventilated rooms. Powder dispersing should be carried out wet and completly sealed. Manual processing in a fume hood is allowed with air velocity of 15 m/s. Pressing of nanomaterials should be conducted in the closed equipment.

It is necessary to use personal protective equipment when working with nanomaterials. Overalls should be vacuumed. After the work it is necessary to wash your hands without using soap because soap rubbing facilitates penetration of nanoparticles into the bloodstream.

All these measures will help reduce air pollution and minimize the impact of harmful and hazardous substances.

# Assessment Problems of the Health Risk for Employees, Who Works With Nanomaterials

Koshel V.I., Dzundza B.S.

*Vasyl Stefanyk Precarpathian National University, Ivano-Frankivsk, Ukraine*

Nanomaterials and nanotechnology are widespread around the world. The technologies are developed that gives a nano-objects and nanosystems with desired properties, they are used in microelectronics, energy, chemical and food industries, cosmetology and agriculture [1]. Nanomaterials have opened new possibilities in medicine and pharmacology.

Nowadays the issue of risk assessment in the field of nanotechnology is actively discussed, including occupational hazards in the production and use of nanoparticles. Farther, it is marked on the impossibility of the traditional approaches via physical and chemical properties of nanoparticles, especially via their biological action, insufficiency of full information about indicators of acute and chronic toxicity in vitro and in vivo experiments, the lack of information about the impact on the workplace, which were are use nanotechnology [1 ].

For nano-specific risk assessment studies on the toxicity of nanoparticles of various elements have paramount importance, especially in view of the constant increase of the number of employees who have professional contact with nanomaterials. The nanoparticles can penetrate unchanged across the cell barriers, as well as across the blood-brain barrier into the central nervous system. They can circulate and accumulate in the organs and the tissues, and cause more pronounced pathomorphological changes in the internal organs, and have a long half-life. Risk assessment is difficult because the current approaches do not take into account the physical and chemical properties of nanoparticles and the peculiarities of their biological effect. The size, shape and density of the nanoparticles must be considered when the maximum permissible concentrations are calculated. It should be noted that risk assessment and control it, which requires a much larger base of experimental data than is currently accumulated on this issue.

Work is done according to the scientific topics (the state registration number is 0113U000790).

1. О.В. Демецька. Підходи до оцінки ризику впливу наночастинок та наноматеріалів на робочому місці // Український журнал з проблем медицини праці. – 2011. – Т2, №26 – С. 62–67.

# Nanostructured $Mg(OH)_2$ with the Primary Particle Size Control

Kotsuybynsky V.O, Poplavsky I.O.

*Vasyl Stefanyk Precarpathian National University, Ivano-Frankivsk, Ukraine*

The obtaining of nanostructured inorganic powder materials with particles foreseen morphology (tubes, rods, lamellas) and size is one of the main goals of modern material science. Such structures have anisotropy of physical properties and are suitable for novel composite materials creation. Hydroxide and magnesium oxide are promising materials in this class. Nanostructured $Mg(OH)_2$ for example is used as filler of polymeric materials with fire retardanting properties.

The purpose of our research is the elaboration of magnesium hydroxide nanoparticles synthesis method. The natural $MgCl_2 \cdot 6H_2O$ (bischofite) was used as a feedstock. The nanoparticles of $Mg(OH)_2$ was formed by chemical sedimentation with the control of reaction medium pH by aqueous NaOH solution at a temperature of 20°C. The several samples of nanostructured $Mg(OH)_2$ were obtained at the different pH levels. The final products were washed up to absence of $Na^+$ and $Cl^-$ ions. Synthesized materials were characterized by XRD and scanning electron microscopy. Primary particles sizes was calculated from the Rietveld analysis of XRD data (fig. 1). It was found that the increasing of pH leads to decrease of primary particle size. For example, particles sizes for materials obtained at the pH level 9.0 and 11.0 were about 11 and 6 nm at the same time the agglomerates sizes are close (about 100 μm) (fig.2).

As a result simple one step method of $Mg(OH)_2$ nanoparticles obtaining with the possibility of primary particles size control has been developed.

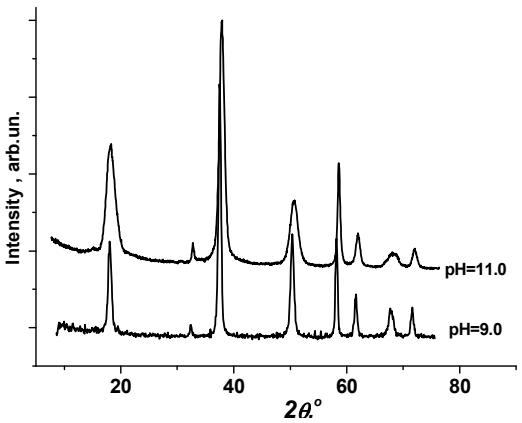


Fig.1. The diffraction pattern of nanostructured $Mg(OH)_2$ obtained at the different pH of reaction medium

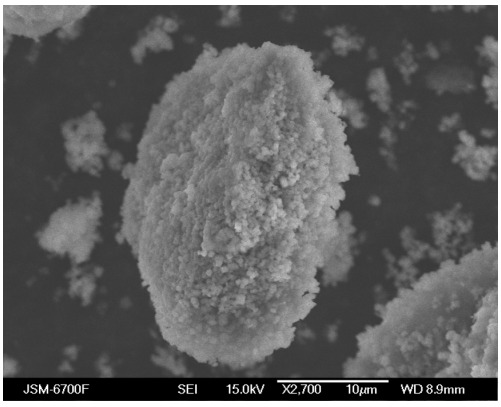


Fig.2. SEM photografy of nanostructured $Mg(OH)_2$ obtained at pH =11

# Electrochemical Properties of Mesoporous γ-$Fe_2O_3$

Kotsyubynsky V.O.[1], Hrubiak A.B.[1], Moklyak V.V.[2]

[1]*Vasyl Stefanyk Precarpathian national university, Ivano-Frankivsk, Ukraine*
[2]*G. V. Kurdyumov Institute for Metal Physics, Kiev, Ukraine*

Mesoporous γ-$Fe_2O_3$ was obtained by thermal decomposition of iron citrate xerogel hydrate synthesized by iron nitrate and citrate acid solutions with 0.3 M molar concentration. Amorphous iron citrate xerogel hydrate calcination in temperature 200ºC within 1.5 hours causes the formation of mesoporous γ-$Fe_2O_3$ with coherent scattering region (CSR) sizes about 7-9 nm. CSR sizes were determined by Debye-Scherer formula. The specific surface area of obtained mesoporous γ-$Fe_2O_3$ is 164 $m^2$/g. Dependences of the pores volume on pores size for both series for all temperatures are characterized by a peak at 5 nm.

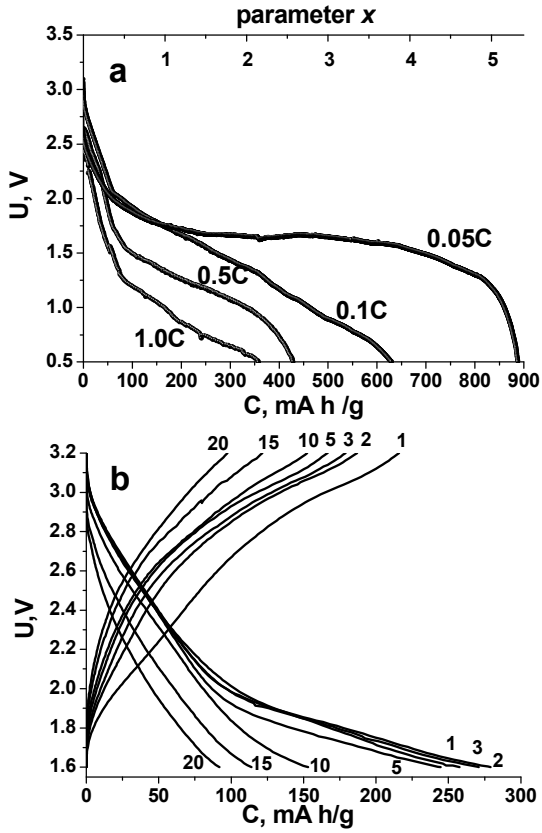


Fig.1

Mesoporous γ-$Fe_2O_3$ was tested as cathode material for lithium power sources (LPS). The cathodes were prepared from a mixture of obtained sample, acetylene black and PVdF with weight ratio of 80:15:5. The anodes were lithium metal and 1M $LiBF_4$ in γ-butyrolactone was used as the electrolyte. The charge and discharge tests were performed at 0.05C, 0.1C, 0.5C, 1.0C rates. Discharge curves of LPS with cathodes based on mesoporous γ-$Fe_2O_3$ at different current rates are shown in Fig. 1, a. Maximum values of specific capacity is 890 mA·h/g at a discharge current 0.05C. The increase of the discharge current leads to the specific capacity reduction: specific capacity is 360 mA·h/g at a discharge current 1.0C.

Mesoporous γ-$Fe_2O_3$ was tested at galvanostatic process charge / discharge. 20 cycles of charge / discharge was carried out at a current density of 0.1 C in the voltage range of 3,2 V - 1.6V (Fig. 1, b). Specific capacitance discharge for several initial cycles varies little within 250 mA·h / g. A sharp decrease in the maximum specific discharge capacity of the material occurs after the fifth cycle, which, after the twentieth cycle is 93 mA·h / g. Coulomb efficiency of the charge / discharge depends nonlinearly on the cycle number and getting the maximum value of approximately 57% for the 3rd cycle.

# Effect of Ph of Synthesis on Cds/L-Cys Colloidal Solutions Optical Properties

Krupko O. V. [1], Khalavka Yu. B. [2], Shcherbak L. P.[2]

[1]*Bukovinian State Medical University, Chernivtsi, Ukraine*
[2]*Yuriy Fedkovych Chernivtsi National University, Chernivtsi, Ukraine*

Nanosized CdS has been extensively studied in the past decades due to its applications as photocatalyst, light-emitting diodes, hybrid solar cells, and others. Capped by bio-conjucting agent L-cystein such nanoparticles (NPs) attract attention as fluorescent probes for biological imaging. In most papers researhers used empirically chosen the precursors concentration range that complicated a total view for the NPs synthesis optimization. In [1] it had been shown advantages of a mathematical method of the experiments planning (simplex-lattice designs suggested by Scheffe) for the data generalization.

The aim of this paper is systematization by the Scheffe method of experimental data on the CdS/L-Cys colloid solutions synthesized at pH=7; 9 and 11 absorption and fluorescence spectra observed at r. t. The $Cd^{2+}$ – $S^{2-}$ – L-cys system composition ranges were first determined from the literature data at various pH (pH= 4 ÷ 11.8). It was obtained that a highest quantum yield QY (up to 35%) demonstrated by the NPs synthesized at pH=7 in the presence of Cd-ions excess or at $[Cd^{2+}]/[S^{2-}] = 1$.

After exclusion the composition of unstable solutions the study was concentrate for the following ones: $[Cd^{2+}]$ ranged 0,1 ÷ 0,35; [L-cys] 0,55 ÷ 0,8; $[S^{2-}]$ 0,1 ÷ 0,35 mM.

The experimental conditions for 1-2 nm spherical NPs production with narrow sizes distribution were determined from TEM-observations. Using the simplex-lattice design gives a possibility to obtain similarity of absorption spectra edge ($\lambda_{edge}$) of NPs synthesized at pH=7 and 9. Increase of pH up to 11 decreases the NPs sizes and consequently the $\lambda_{edge}$ value. This could be attributed to the density of hydroxy-ions on the surface of the nanocrystals that effectively passivate the nanocrystals surface.

It was observed also that an important factor - coordination number (c.n.) = $[L\text{-cys}]/[Cd^{2+}]$ unmonotonically (Gaussian distribution) governs the NPs optical properties. For example, maximum QY at $[Cd^{2+}]/[S^{2-}] = 1$ occurs at c.n.=2,5 at pH=7; 3,5 at pH=9 and 4,5 at pH=11.

1. O.V. Krupko, Y.B. Khalavka, L.P. Shcherbak. Synthesis of CdS/L-cys nanoparticles colloid solutions with predetermined optical properties. Materials Research Bulletin (2014) 60, 264-269.

# A New Approach for Calculating Excitonic Emission Characteristics of Hybrid "Spherical Semiconductor Quantum Dot+Spherical Metal Nanoparticle" Nanosystem

Kryuchenko Yu.V., Korbutyak D.V.

*V.E. Lashkaryov Institute of Semiconductor Physics, NAS of Ukraine, Kyiv, Ukraine*

In all existing theoretical models of the exciton-plasmon interaction in hybrid metal-semiconductor nanostructures with semiconductor quantum dots (QDs) and metal nanoparticles (NPs) the QDs are considered as point dipoles like atomic or molecular *fluorophores*. It is connected with the fact that electric scalar potential formed outside QD by the exciton state (the potential being a superposition of the dipole potential contributions of all crystal unit cells inside QD with corresponding weight coefficients in a form of the exciton envelope wave function) has a typical form of the (point) dipole potential $\varphi_i(\vec{\boldsymbol{r}}) = ed_{exc}\vec{\boldsymbol{r}}\cdot\vec{\boldsymbol{\alpha}}_i/(\varepsilon_{eff}r^3)$, where $d_{exc}$ is the excitonic dipole length which takes values in the range from a few tenths of Å to a few Å depending on a semiconductor, $\vec{\boldsymbol{\alpha}}_i$ are the orts in the directions of corresponding dipole moments, indices $i$=1,2,3 correspond to three possible hole Bloch (site) wave functions of $p$-type. Such "point dipole" representation of QD is quite reasonable when considering direct Förster-type resonant energy transfer (FRET) from excitons in QD to plasmons in NP. However, by considering QD excitonic emission, when transverse electromagnetic field (EMF) is generated, the above representation of a QD becomes invalid.

In this work we have developed a new model of the excitonic emission in QD+NP nanosystem. The total EMF emitted by the exciton in QD has been calculated as a sum of the EMF contributions of all point (unit cell) dipoles emitting inside QD with corresponding weight coefficients. It turns out that the resulting EMF of QD contains only dipole and octupole components of electric type and quadrupole components of magnetic type in contrast to erroneous consideration of QD emission as that of a (point) dipole, when an infinite series of EMF multipole components is generated (these multipole components contribute to a substantial energy absorption in a metal NP and thus are responsible for a strong emission quenching at small interparticle separations).

The nanosystem, which is nonspherical as a whole, has been characterized by three spherical coordinate systems (orientation of the third one is determined by the crystal axes orientation in QD). Multiple scattering between spherical NP and spherical QD of the EM field has been accounted. Characteristic radiative and nonradiative times as well as excitonic radiation efficiency have been calculated as functions of the interparticle separation at different QD and NP sizes and temperatures $T$=4.2 K and $T$=300 K in the particular case of CdTe QD and silver and gold NP.

# Interaction of Electromagnetic Radiation with Multi-Layer Coatings

Kryvoruchko Ya.

*National University of Life and Environmental Science of Ukraine, Kyiv, Ukraine*

The introduction of advanced optical devices and research methods in various fields of science and technology leads to the need not only to create multi-layer metal-dielectric systems with new requirements to their properties, but also to their possible combinations.

The report deals with the problem of the interaction of electromagnetic radiation (EMR) with an arbitrary number of flat nanolayers sharing two dielectric half-spaces. Using impedance method, complex coefficients of reflection and transparency have been found, their modules and phases along with power values of these factors. It allows us to examine both frequency dependence of the coefficients at a fixed wave angle of incidence and angular dependence of the selected range of electromagnetic radiation. Relative magnetic permeabilities of layers are taken equal to unity, and to describe the frequency-dependent dielectric function of metals in model calculations Drude model is applied. Coatings were considered (nanolayers separating two half-spaces) produced from gold or silver, or altering layers of gold and silver, or combined coatings of metal / insulator. Both layers were taken of the same thickness of 20 nm, and the angle of incidence of the electromagnetic wave was $\theta_1 = 20^0$. Comparison with the corresponding dependences for single-layer coatings of gold or silver shows that the dependences of the reflectance versus wavelength have two maxima and two minima instead of one near plasmon frequencies of gold and silver. The order of the layers significantly affects the values of extremes.

Nanocoating were also investigated of eight and ten altering gold and silver nanolayers (thickness of layers is 10 nm). In this case, the angle of incidence was believed to be an option, and calculations were performed for incidence of light at different angles for two types of polarization. As an illustration of the calculations carried out, some results obtained are shown in graphs in Figs. 1 and 2.

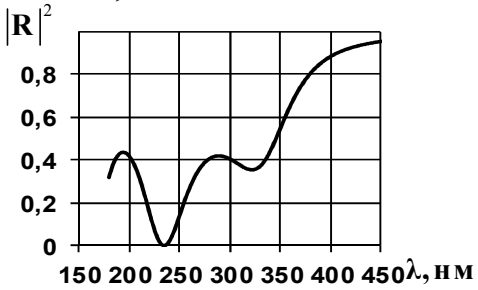


Fig. 1. The spectral dependence of the reflection coefficient at normal incidence waves to 8-layer coverage (polarizations coinside)

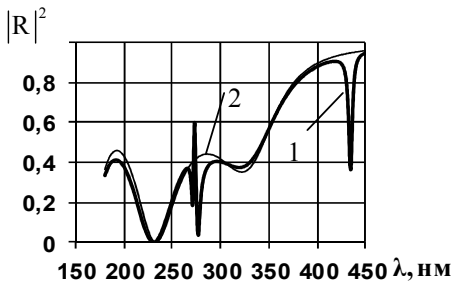


Fig. 2. Spectral dependences of reflection coefficient when wave falls at an angle $20^o$ to 8-layer coverage: 1 – *p*-polarization; 2 – *s*-polarization.

It is seen from the dependences obtained that the frequencies of surface plasmons remain, but the transition between the maxima and minima in the presence of a dielectric is slower.

# Optical Harmonic Generation In Nanostructured And Nanocomposite ZnO Films

Kulyk B. [1,2], Kapustianyk V. [1], Sahraoui B. [2]

[1] *Ivan Franko National University of Lviv, Lviv, Ukraine.*

[2] *Institute of Sciences and Molecular Technologies of Angers MOLTECH, Anjou, France.*

Nanoscale materials are of current interest because of their unique electrical, optical as well as nonlinear optical (NLO) properties which suggest their potential application as frequency converters and logic elements in the optoelectronic circuitry.

We have investigated structural, optical and NLO properties of nanostructured ZnO thin films obtained by RF-magnetron sputtering technique and ZnO/PMMA nanocomposite films which were prepared by embedding of ZnO nanocrystals (NCs) into PMMA polymer matrix. These films manifest a high optical transmittance in near UV-vis region. The temperature study of photoluminescence in ZnO/PMMA nanocomposite films demonstrates the intensive UV emission, which was connected with donor-bound excitons and lower green emission due to the presence of internal intrinsic defects [1].

The second and third harmonic generation studies of ZnO/PMMA nanocomposite films with different concentration of ZnO NCs and nanostructured ZnO films of different thickness were carried out at $\lambda$=1.064 nm with 16 ps pulse duration. It has been found that quadratic NLO susceptibility of nanostructured ZnO film of thickness less than 1 μm is highly dependent on its grain size and exceeds the value for bulk ZnO. The ZnO/PMMA nanocomposite films show quite high second and third order nonlinearity at low ZnO NCs concentration and high resistance to the intensive laser light [2].

1. Kulyk B., Kapustianyk V., Tsybulskyy V., Krupka O., Sahraoui B. Optical properties of ZnO/PMMA nanocomposite films // J Alloy Compd. – 2010. – 502, – P. 24-27.
2. Kulyk B., Sahraoui B., Krupka O., Kapustianyk V., Rudyk V., Tkaczyk S., Berdowska E., Kityk I. Linear and nonlinear optical properties of ZnO/PMMA nanocomposite films // J Appl Phys. – 2009. – 106, – P. 093102(1-6).

# Manipulation of magnetic properties for $Co-Al_2O_3$ nanocomposites

Lashkarev G.V.[1], Radchenko M.V.[1], Bugaiova M.E.[1], Knoff W.[2], Story T.[2]

[1]*I.M. Frantsevych Institute for Problems of Material Science, National Academy of Sciences of Ukraine, Kyiv, Ukraine*

[2]*Institute of Physics, Polish Academy of Sciences, Warsaw, Poland*

Electron beam evaporation of Co and $Al_2O_3$ from two crucibles was used for deposition of granular layers ( $5 \div 7$ mkm) on polycor substrate. The Co amount in ferromagnetic nanocomposite ( FMNC ) determines the dimensions of Co nanoparticles ( NPs ) and the transition temperature ( TT ) from spin-glass state to superparamagnetic state ( SPS ). Thus TT is ~ 200 K at NPs dimensions $d \sim 10 \div 20$ nm, 50 K at $d \sim 3 \div 5$ nm and 12 K at $d < 3$ nm. Consequently a transition from FM to SPS state due to exchange interaction between FMNPs (appearance of hysteresis loop) occurs at lower temperatures for smaller dimensions of Co NPs.

Giant magnetothermoelectric power ( TP ) at low temperatures with a strong dependence on magnetic field was observed. It is due to a hopping spin-dependent transport of electrons between magnetic centers of electron localization containing Co atoms and through a tunnel-transparent alumina interspaces between FM nanoparticles under the influence of a temperature gradient.

The growing of eight sets of FMNC was carried out in magnetic field in parallel and perpendicular orientation to the sample plane (plane of the light magnetization). SEM images of these samples confirm the influence of magnetic field on the process of FMNC formation which is expressed in the preferable orientation of Co NPs long axis in the direction of magnetic field gradient. The latter is the reason for movement of Co atoms at forming Co NPs.

For the samples grown in magnetic field diminishing of electric percolation threshold ( from 43 to 27 at.% Co ) was observed which is due to lowering of a tunnel barrier between Co NPs. The maximum value of negative magnetoresistance ~ 4 % at 2,5 kOe was demonstrated for samples, grown in magnetic field which was perpendicular to the sample plane.

The temperatures of the transition into spin glass state ( Ts ) for samples formed in the magnetic field parallel ( $Ts_{\parallel}$ ) and perpendicular ( $Ts_{\perp}$ ) to the sample plane are different: $Ts_{\parallel} < 5$ K, $Ts_{\perp} \sim 20$ K. It is supposed to be obliged to increasing of magnetic field in a sample plane of light magnetization due to a disposition of long axis of Co NP in this plane.

# Formation of the Primary Nanocrystalline Phases in a Non-equilibrium Crystallization Conditions of Light Lanthanides With Silver Alloys

Lysenko A.B., Zagorulko I.V., Kalinina T.V., Lysenko A.A.

*Dniprodzerzhinsk State Technical University, Dniprodzerzhinsk, Ukraine*

By radiographic investigations of the structure of alloys $E_{100-x}Ag_x$ (E – La, Ce, Pr) depending on the composition ($x$ = 0 – 50 at.%) and the quenching of the liquid state rate ($\upsilon_- = 5\cdot10^4 – 6\cdot10^7$ K/s) identified the concentration ranges of detection and thermal modes of metastable nanocrystalline structures of two types formation. It is shown that in alloys with silver content $x$ = 10 – 35 obtained by rapid quenching at a cooling rate $\upsilon'_к \le \upsilon_- \le \upsilon_к$ crystallizes the metastable bcc-phase of initial chemical composition with the grain size of ~ 30 – 50 nm. In the slow cooling conditions ($\upsilon_- \le \upsilon'_к$) the alloys retains the equilibrium phase composition, elements of which are close-packed modifications of the main component and equiatomic compound E-Ag with the CsCl-type of lattice. When the process accelerating ($\upsilon_- > \upsilon_к$) crystallization is suppressed and the amorphous state is fixed. For all investigated alloys experimentally established the critical cooling rates $\upsilon'_к$ and $\upsilon_к$.

First obtained and identified the diffraction patterns of X-ray amorphous phases formed in the concentration range of $x$ = 5 – 7 at the extreme conditions of the melt quenching ($\upsilon_- \approx 6\cdot10^7$ K/s). It was found that these structures are nanocrystalline (5,5 – 7,0 nm) compounds of a fcc-modifications of the rare-earth elements and metastable bcc-phase containing ~ 10 at.% Ag.

The correctness of the X-ray studies results is confirmed by the theoretical analysis of the structure formation processes of rapidly quenched alloys $E_{100-x}Ag_x$, performed within the concept of kinetic diagrams "temperature-time-transformation".

# Mechanical Nano-Lithography Over Double Layer Chalcogenide Resist

Lytvyn P. M., Induntyi I.Z., Malyuta S., Min'ko V.I., Lytvyn O.S., Dan'ko V.A., Prokopenko I.V.

*Institute of Semiconductor Physics, National Academy of Sciences of Ukraine, Kyiv, Ukraine*

Surface patterning techniques are constantly developing in accordance with the increasing requirements of nano-electronics, plasmonics, nano-medicine and other novel technologies. Nano-lithography with a solid tip driven by scanning probe microscope is a low-cost and versatile technique, which could be applied as a separate operation in some technological cycles or for direct patterning of functional elements for leading-edge devices prototypes. Scanning probe lithography could be applied in materials of different nature (organic, metals, dielectrics) and in variety of ambient (vacuum, liquid, normal atmosphere). Microscope, in this case, used both for surface pattering and controlling of recorded patterns.

We realized mask-production process based on mechanical patterning of double layer chalcogenide resist. The first layer consists from the 5-15nm of a soft material and second layer has a thickness necessary for a lithographic mask formation (50-200nm). Pattern inscribed in a first layer and following selective wet etching process used to translate pattern into a second layer. This approach allows controlled patterning with minimal width of lines near 60nm. Features of smaller sizes (near 5-10nm) could be inscribed after resist quality optimization and improvement of etching process.

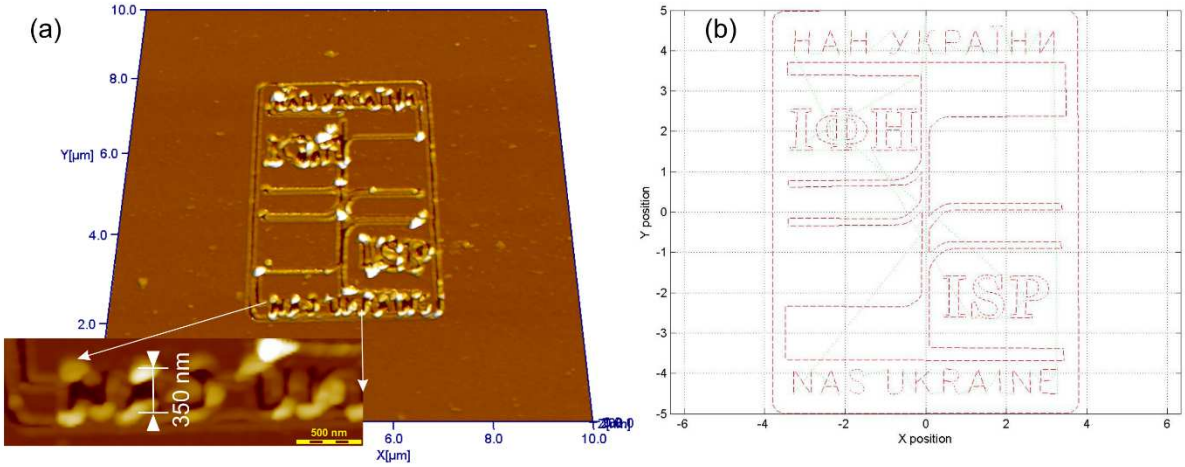


Fig.1. Atomic force microscopy image of the inscribed (a) and programmed (b) pattern of ISP NASU logo.

# Quasi-stationary exciton states in open cylindrical semiconductor nanotube

Makhanets O.M., Kuchak A.I., Voitsekhivska O.M., Iliniuk A.V.

*Yuriy Fedkovych Chernivtsi National University, Chernivtsi, Ukraine*

The multi-shell semiconductor nanotubes have been recently studied both theoretically and experimentally [1,2]. The unique properties of quasi-particles (electrons, excitons and so on) in such nanostructures allow using them as basic elements for the devices of modern nanoelectronics.

The authors of ref. [1] have been grown the arrays of semiconductor nanotubes consisting of the sequence of $GaAs$ and $Al_x Ga_{1-x} As$ nanoshells using the method of molecular beam epitaxy. This nanostructure was covered by rather thick shell of $GaAs$ in order to avoid $Al_x Ga_{1-x} As$ oxidizing.

The multi-shell nanotube under study is an open one because the potential energy of electron in $GaAs$ is smaller than that in $Al_x Ga_{1-x} As$. In open nanotubes, on the contrary to the closed ones, the quasi-particles can tunnel through the potential barrier into the outer medium, creating an additional channel of energy relaxation for the quasi-particles excited in the quantum well. It is clear that the quasi-particles energy spectra in such nanosystems are quasi-stationary and are characterized by the resonance energies and resonance widths.

The theory of exciton and phonon stationary spectra together with the theory of electron- and exciton-phonon interaction well correlating to the experimental data and general physical considerations is already developed for the closed cylindrical and hexagonal nanotubes [2].

The quasi-stationary spectra of electrons, holes and excitons were theoretically studied for the spherically-symmetric quantum dots and single cylindrical quantum wires [3]. In this work, we present the theoretical study of exciton quasi-stationary spectrum in multi-shell open cylindrical semiconductor nanotube. The dependences of exciton resonance energies and resonance widths on nanotube thickness are obtained and analysed.

1. M. Heigoldt, J. Arbiol, D Spirkoska, J. M. Rebled, S. Conesa-Boj, G. Abstreiter, F. Peiro, J. R. Morantece, A. Fontcuberta i Morral, Long range epitaxial growth of prismatic heterostructures on the facets of catalyst-free GaAs nanowires // *J. Mater. Chem.* – 2009. – V.**19**, – P. 840-848.
5. O.M. Makhanets, V.I. Gutsul, N.R. Tsiupak, O.M. Voitsekhivska, Exciton spectrum in multi-shell hexagonal semiconductor nanotube // *Condensed Matter Physics*. – 2012. – V.**15,** №3. – P. 33704: 1–9.
6. N. V. Tkach and V. A. Golovatskii, Quasi-stationary states of electrons and holes in an open composite cylindrical quantum wire // *Physics of the Solid State.* – 2001. – V.**43,** №2. – P. 365-372.

# Optical Properties of Substrates with Surface GaP Quantum-Dimensional Structures

Makhniy V.P., Sklyarchuk V.M., Bodyul G.I., German I.I.

*Yuri Fedkovych Chernivtsi National University, Chernivtsi, Ukraine*

In spite of its indirection, gallium phosphide is still one of the basic materials for producing of sources and detectors of optical radiation, including not well mastered UV region. For example, commercially available metal-GaP photodiodes have detectability ~ 1014 $W^{-1}$ $Hz^{1/2}$ cm in the range of 2.5-6.0 eV, as well as a higher temperature and a radiation resistance for comparison with the receivers based on Si. However, being actual , the search of technologies of producing the photosensitive diode structures that lead to significant reduction of dark currents and the surface recombination velocity. Perspective and promising in this regard may be GaP substrate modification in particular, by creating the surface quantum structures (PKRS) on them. The reason for this are the contacts metal-CdTe, the using of which like technology, helped increase significantly the efficiency of solar cells based on them. The present work is devoted to creating PKRS GaP substrates and studying its impact on their main optical characteristics. The starting substrates were single-crystal n-GaP wafers with a smooth surface which is characterized by the absence of visible photoluminescence (PL). Differential spectrum of the optical transmission $T'_\omega$ such samples submitted with a curve with a maximum at $\hbar\omega_m \approx$ 2,28 eV, which agrees with the bandgap $E_g$ GaP at 300 K. Treatment of substrates in the melt mixture of NaOH + KNO3 leads to a matting surface and a significant change in their optical properties. First of all, we must notice the appearance of the luminescence whose spectrum contains photons with energy much larger $E_g$, curve 2. Such radiation is adequately explained by the quantum-well structure, which occurs on the surface of GaP substrates by treatment and usually consists of two types of nano-grains with lateral dimensions of 10 -30 nm and 100-300 nm . The first group of responsible for the formation of high-energy radiation, and the second - a low-energy "wing" prospectrum of the optical transmittance, curve 3. In addition, researches have shown that Ni- GaP contacts, made on modified substrates have a greater height of the barrier and quantum efficiency than similar structures fabricated on substrates with a smooth surface.

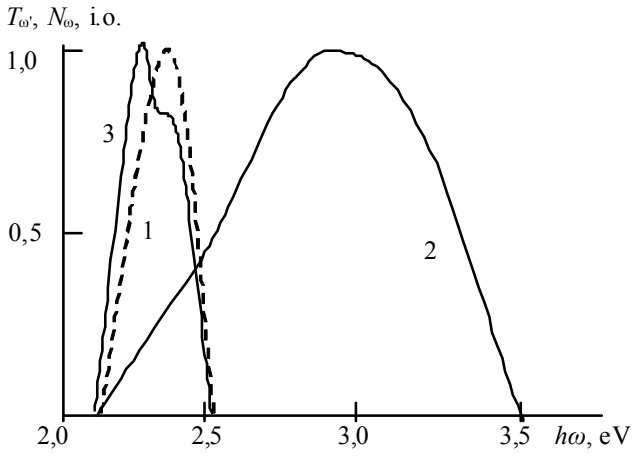

# Polarization Memory of The Luminescence of Si Nanoparticles in Oxide Matrix

Michailovska K.V., Indutnyi I.Z., Shepeliavyi P.E., Sopinskyy M .V.

*V. Lashkaryov Institute of Semiconductor Physics, National Academy of Sciences of Ukraine, Kyiv, Ukraine.*

Measurement of the polarization of the photoluminescence (PL) is a powerful method to study the electronic symmetry of the absorbing as well as luminescent states. The phenomenon, when a certain substance excited by linearly polarized light emits light, which is also linearly polarized, is called polarization memory (PM) effect. Porous silicon and thin-film structures containing Si nanoparticles (nc-Si) embedded in the $SiO_x$ matrix show an intense and wide PL emission peaking in the near-infrared or visible spectrum. However, they differ greatly in the polarization of their PL: PM effect is large in porous Si and non-essential in nc-Si−$SiO_x$ nanocomposites [1].

In this report the PL polarization properties of the dense and porous nc-Si−$SiO_x$ structures were studied for the first time. Investigated samples were fabricated by thermal evaporation of SiO powder in vacuum onto polished c-Si substrates arranged at angles of 0° and 60° to the normal to the substrate surface with the direction to the evaporator (normal and oblique deposition). The films were annealed in vacuum or helium atmosphere during 15 min at temperatures of 975 and 1000°C then were treated in the HF vapor. The PL was excited by linear polarized light of a nitrogen laser at $\lambda = 337$ nm and by a semiconductor laser with $\lambda = 415$ nm.

The obtained dense and column-like porous nanocomposite films containing nc-Si exhibited strong PL emission which can be attributed to recombination of excitons in nc-Si embedded into $SiO_x$ matrix.

It was found that the PM effect is observed only after processing of nanostructures in HF, which is also accompanied by short-wavelength shift of PL maximum and the significant increase in PL intensity. In anisotropic porous nc-Si−$SiO_x$ samples obtained by oblique deposition, there is also well-defined orientation dependence of the PL polarization degree in the sample plane. This dependence is related to the orientation of oxide nanocolumns that form the structure of the porous layer. The above effects are associated with the transformation during etching in HF of symmetric nanoparticles in asymmetric elongated nc-Si. The asymmetric nanoparticles in dense layers are oriented randomly; in the porous structures their preferred orientation is aligned with the orientation of oxide nanocolumns.

1. Kovalev D., Ben Chorin M., Diener J., Koch F., Efros Al. L., Rosen M., Gippius N.A., Tikhodeev S.G. Porous Si anisotropy from photoluminescence polarization // Appl. Phys. Lett. – 2005. – V.**67**, № 11. – P. 1585-1587.

# The Synthesis Conditions Influence on The Phase Stability of Nanodispersed Titanium Dioxide

Mizilevska M.H.[1], Kotsyubynsky V.O.[2], Ostafiychuk B.K.[2], Tadeush O.Kh.[1]

[1]*South Ukrainian National Pedagogical University named after K.D.Ushynsky, Odesa, Ukraine*

[2] *Vasyl Stefanyk Precarpathian National University, Ivano-Frankivsk, Ukraine*

For today, titanium dioxide $TiO_2$ with different polymorphous modifications (anatase, rutile, brookite) is the most promising active material for photocatalytic and photoelectrochemical devices. Its phase composition, morphological characteristics and temperature stability are the parameters determining the efficiency and practical application of such systems.

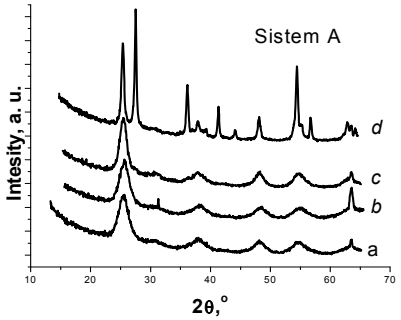


Fig. 1.XRD patterns of system A (a) before and after calcinations at (b) 200°C, (c) 400°C, (d) 600°C

$TiO_2$ nanoparticles were obtained by hydrolysis of titanium tetrabytuloxide in a mixture of anhydrous ethanol, nitric acid, distilled water and PEG300 [1]. Resulted precipitate was received by centrifugation (system B) and then hydrothermally treated at the temperature of 160°C for 5 hours (system A). All samples were additionally annealed on air at the temperatures of 200, 400 and 600°C for 1 hour. X-ray diffraction confirmed that synthesized $TiO_2$ in both cases was the mix of anatase and brookite. System A after annealing at 200°C (Fig. 1) has an anatase relative content increased from 39 to 64 %. The annealing at higher temperature of 400°C caused the appearance of rutile phase (8 %) and the decrease of anatase relative content (55 %). The annealing at 600°C led to the phase transition of anatase/brookite to rutile, the relative content of which exceeds 40 %. In the case of system B (Fig. 2), at the temperature of 200°C the material was a mix of anatase and brookite phases with increased relative content of anatase from 48 to 67 %. At 400°C the phase composition contains 15-17 % of rutile. And after annealing at 600°C rutile became a dominant phase in the sample of the system B, while anatase content does not exceed 2 %. Thus, the method of hydrothermal treatment combined with deposition provides a nanosized titanium dioxide with temperature stable anatase phase while maintaining the average particle size of the material in the vicinity of 4.5 nm.

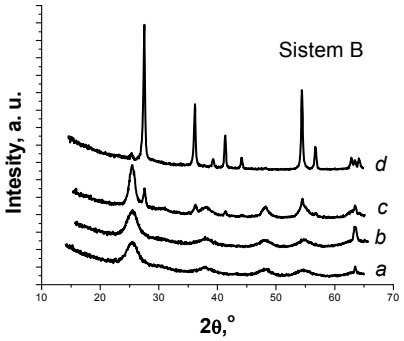


Fig. 2.XRD patterns of system B (a) before and after calcinations at (b) 200°C, (c) 400°C, (d) 600°C

1. K. Yu, J. Zhao, Y. Guo, X. Ding, Y. Liu, Z. Wang, *MATER LETT* **59**, 2515 (2005)

# Synthesis and Structure of Perovskites-Like Materials

Mokhnatskij M. L. Yaremiy I.P.

*Vasyl Stefanyk Precarpathian National University, Ivano-Frankivsk, Ukraine*

Nowadays the basic task of the physical material science is developing and searching of the materials for generational devices energy accumulation. Perovskites-like materials is a break for solar batteries and are used as cathode material for solid fuel elements, and also perovskites-like materials can be used as anodic and cathode material for lithium source current. The main adventure of such structure is its low cost which can decries the common price in 5-8 times in solar batteries comparing with silicon basic analogue.

The samples were synthesized with the aim to research the structure on the basis of perovskite LaXO3, X= Fe, Ni, Co, Cr by sol-gel method with auto burning. The initial materials for the synthesis were nitrates' crystal hydrates of the appropriate metals. Citric acid was used as complex formation. After synthesis, the gained materials as powder were researched by means of the X-rays diffractometer to check their structure and belonging to the perovskites structure.

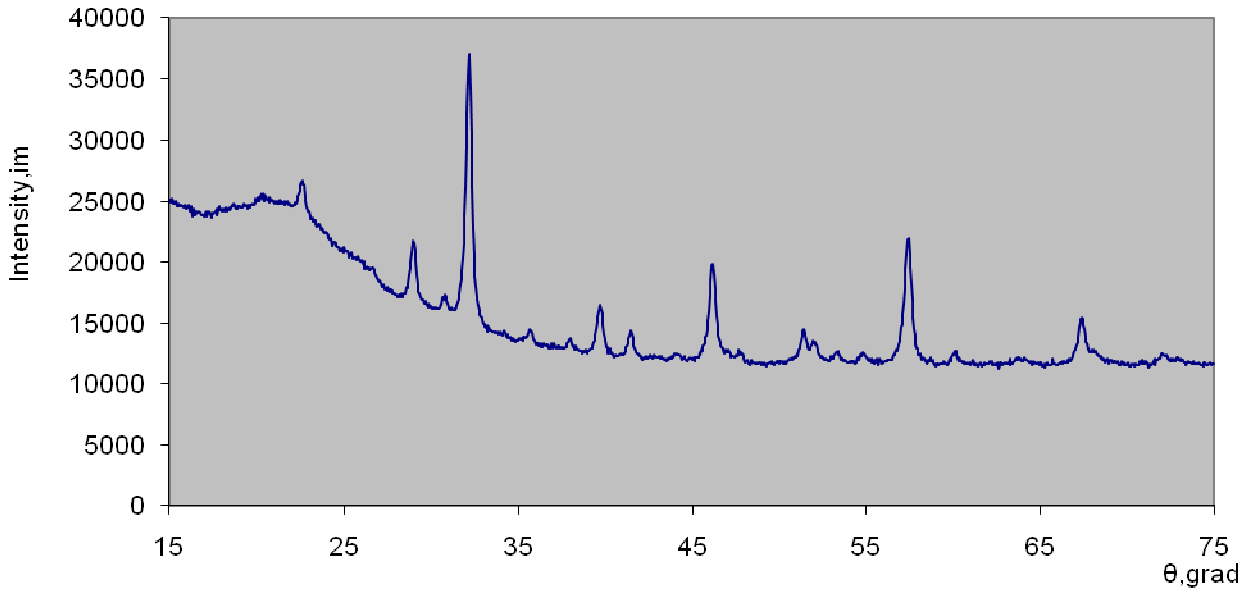


Fig.1. Radiograph $LaFeO_3$ of perovskites structure.

There is radiograph of the perovskites structure LaFeO3 as an example. Decipher figures showed that in all cases nanosized materials were gained from perovskites structure. Afterwards all gained materials will have checking for operational capability as cathode material for the lithium source current, and they will be use for the film production as material for solar batteries.

# Preparation of Nanoporous $FeF_3 \cdot 3H_2O$ as Cathode Materials for Rechargeable Lithium-Ion Batteries

Moklyak V. V.[1], Kolkovskiy P. I.[2], Zbihley L. Z.[1]

[1]*G. V. Kurdyumov Institute for Metal Physics of the N.A.S. of Ukraine, Kyiv, Ukraine*
[2]*Vasyl Stefanyk Precarpathian National University, Ivano-Frankivsk, Ukraine*

Metal fluorides have been widely investigated due to their using as next-generation cathode materials for LIBs in the last years [1].

We have preparated hydrated iron trifluoride using the following reagents: an aqueous solution of $Fe(NO_3)_3$ $9H_2O$, ammonia (25%) and HF (40%). Iron nitrate mixed with ammonia water and washed by distilled water to neutral pH. Next, excessive HF solution was added to the above precipitates and put into a stainless steel autoclave, which was kept at 70 $^0$C for 9 hours. The precipitate was dried at 80 $^0$C for 12 hours at oven in Ar atmosphere.

As a result, according to the X-ray analysis and Mössbauer spectroscopy was obtained β-$FeF_3 \cdot 3H_2O$ phase (PDF: 32-0464) with an average size of coherent scattering regions to 40 nm.

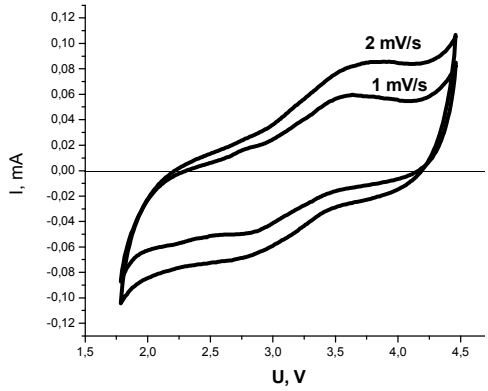


Fig.1. CV curves of β-$FeF_3 \cdot 3H_2O$ at the scan rate 1 and 2 mV/s

Cyclic voltammetry (CV) tests were performed to assess the possibility of using the material in LIBs reversible.

The cathodes for testing cells were fabricated by mixing the cathode material, carbon black, and polyvinylidene fluoride with a weight ratio of 75:15:10, respectively.

CV curves obtained in the range of 1.8-4.5 V at the scan rate 1 and 2 mV/s. Our material shows a pairs oxidation-reduction peaks at ≈ 3.6 V and ≈ 2.8 V, which correspond to intercalation and deintercalation of lithium ions into the material structure. The capacity retention reach up to 90%.

1. Q. Chu, Z. Xing, J. Tian, X. Ren, Abdullah M. Asiri, Abdulrahman O. Al-Youbi, Khalid Ahmad Alamry, X. Sun J. Power Sources 236 (2013) 188 – 191.

# Synthesis, Structural and Colour Characterization of Nanocrystalline Chromic Oxide Green Pigment Doped With Aluminum Oxide

Myslin M.V., Tatarchuk T.R.

*Vasyl Stefanyk Precarpathian National University, Ivano-Frankivsk, Ukraine*

The ceramic pigments with particle size in the nanoscale have a massive potential market, because of their high surface area, which assures higher surface coverage, higher number of reflectance points and hence improved scattering. In this study the chrome alumina green pigment $Cr_{2-x}Al_xO_3$ (where $x$ = 0; 0,2; 0,4; 0,6) was synthesized. The mixture of calculated stoichiometric amounts of metal salts ($NH_4Al(SO_4)_2 \cdot 12H_2O$ and $NH_4Cr(SO_4)_2 \cdot 12H_2O$) was dissolved in distilled water, co-precipitated by using sodium carbonate, thoroughly washed by hot distilled water and dried. Next, the mixtures of the intermediate powder were sintered in air in an electric muffle furnace at 1000$^o$ C for 5 hour and then slowly cooled.

XRD analysis (DRON-3, Cu $K_\alpha$ radiation, $\lambda$ = 1,5408 Å) showed only the single corundum phase. The obtained samples were nanoparticles with an average particle size ranging from 17 nm to 22 nm. Thermal gravimetric analysis (TG-DTA-DTG) were used to investigate intermediate and final products. The thermal degradation pattern of samples was obtained. The weight loss corresponds to the elimination of chemically bounded water, thermal degradation of chromium and aluminium hydroxocomplexes. The Fourier-transformed infrared spectra (FT-IR) of samples was observed. The range of measurement was 400 cm$^{-1}$ to 4000 cm$^{-1}$, and the resolution was set as 6 cm$^{-1}$. The FT-IR spectra of sample shows a broad bands which correspond of hydrogen vibration (stretching vibrations of structural -OH, adsorbed water, and -OH vibrations of hydroxide bonded) and vibration for α-$Cr_2O_3$.

The color of fired pigments was measured in X-Rite Color i7 Benchtop spectrophotometer using standard D65 illumination. The CIE *L*a*b** colorimetric method, recommended by the Commission Internationale de l'Eclairage (CIE) was followed. In this method, *L** is lightness axis: black (0) – white (100), *b** is the blue (−) – yellow (+), *a** is the green (−) – red (+) axis.

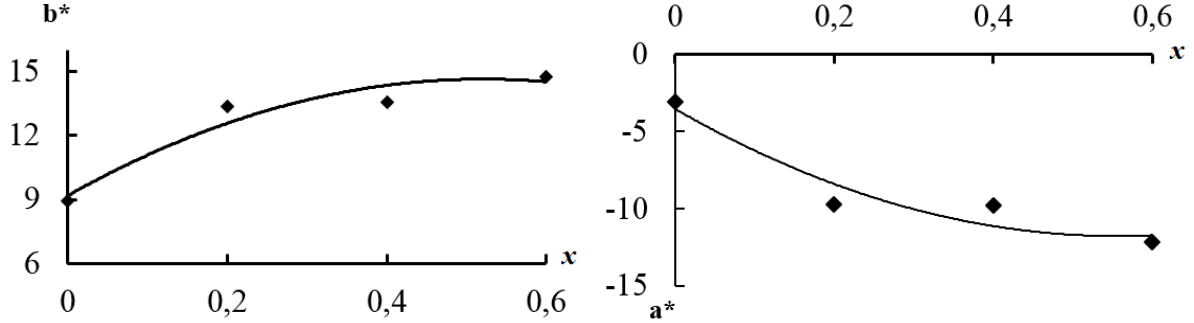


Fig. 1. CIE *L*a*b** colorimetric parameters of $Cr_{2-x}Al_xO_3$ pigments.

# Local Transistor Isolation Using Oxidized Porous Silicon

Novosyadlyy S.P., Bojko S.I.

*Vasyl Stefanyk Precarpathian National University, Ivano-Frankivsk, Ukraine*

Modern microelectronics technology characterized by a number of process parameters called design rules and technological constraints. In particular, for formation of CMOS VLSI with design rules 0.5 microns and below the depth of the dielectric insulation for elements should be the value of <500 nm. For this reason, due to historical trend of reducing temperature in fabrication process, traditional conventional LOCOS technology and its variations (PBZ, SWAMI, SILO, PELOX, NCL) at this stage do not meet the requirements of VLSI structures production with a high yield.

Method includes operations of chemical treatment of n-Si substrate, forming n-$p^+$-p structures, forming $Si_3N_4$ mask using high frequency sputter deposition in N-Ar plasma, lithography, forming wells using anisotropic plasmochemical etching, electrochemical anodizing, oxidization, etching of well bottom and local epitaxy of n doped Si into formed wells.

Special attention should be paid to electrochemical anodizing. It used to form isolation from $p^+$ under p layer. Electrochemical anodizing is conducted in potentiostatic regime in electrolyte that consists of (volume parts):

Sulfuric acid (95%) – 0.549;

Hydrofluoric acid (48%) – 0.376;

Hydrochloric acid (95%) – 0.028;

Acetic peroxyacid ≤ 0.047;

hydrochloric acid added for effective removing of $H_2$ bubbles and increasing of anodizing speed, and acetic peroxyacid causes qualitative wetting of the activated surface. Anodizing process is conducted on device for electrochemical anodizing "Pauk-2K" which has 6 cells for electrochemical anodizing. Porosity of Si is determined by current density (Fig. 1).

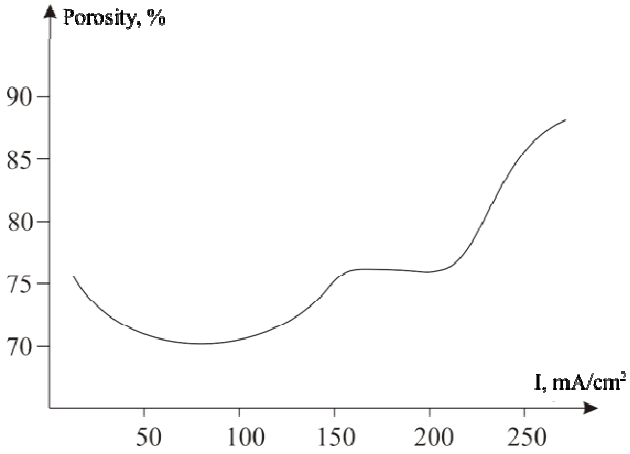


Fig. 1. Porosity of Si vs anodizing current density

Proposed process is easy to automatize for big diameter Si wafers (>150 mm)

Compared to isoplanar technology, proposed method leads to higher device density, higher performance, increased radiation hardness and temperature tolerance and reduced process variability.

# Sensor Properties of The Photovoltaic Structures Poly(3,4-ethylenedioxytiophene) – Porous Silicon

Olenych I.B.[1], Monastyrskii L.S.[1], Aksimentyeva O.I.[1], Yarytska L.I.[2]

[1]*Ivan Franko National University of Lviv, Lviv, Ukraine*
[2]*Lviv State University of Live Safety, Lviv, Ukraine*

The progress in nanoelectronics determines the demand for novel low-dimensional materials, which have specific physical properties due to quantum confinement effect. Recently, hybrid nanosystems on the base of porous silicon (PS) and conductive polymers are in the focus of increased attention. Various electronic and optical systems as well as sensors developed to maximize the use of size effects and large specific surface area of nanoparticles [1-3]. Modification of PS surface by poly(3,4-ethylenedioxytiophene) (PEDOT) may lead to the appearance of new properties or effects that depend on the gas environment and easily recorded. Therefore, the aim of this study was to create hybrid structures of PEDOT–PS–*n*-Si and studying the effect of adsorption of polar gas molecules on their photovoltaic properties.

Thin film PEDOT coatings on PS surfaces were produced by electrochemical polymerization of 0.1 M solution of 3,4-ethylenedioxy-thiophene in water-ethanol solvent (1:1), with 0.5 M $H_2SO_4$ used as an electrolyte. Molecular structure of the PEDOT–PS–*n*-Si composite was explored using FTIR spectroscopy. Modification of the PS surface with conjugated polymer PEDOT led to a change in the nature of the measured CVC. It was observed the rectifier CVC and formation of photosensitive electrical barriers in hybrid structure of PEDOT–PS–*n*-Si. It is established that the photovoltage value of hybrid structure depends on the ambient atmosphere. Increased concentrations of $NH_3$ and $H_2O$ molecules in the air caused decrease in photovoltage. The adsorption of $NO_2$ molecules caused an increase in photovoltaic signal. The analysis of the concentration dependence of adsorption sensitivity showed that the hybrid sensory structure had the greatest sensitivity to adsorption of molecules of $NO_2$. Response time of sensory structure PEDOT–PS–*n*-Si on change in the concentration of $H_2O$ molecules does not exceed 70 s, which is small enough for microelectronic sensors of humidity.

1. Misra S., Bhattacharya R., Angelucci R. Integrated polymer thin film macroporous silicon microsystems // *J. Indian Inst. Sci*. – 2001. – V. 81. – P. 563-567.
2. Olenych I.B., Monastyrskii L.S., Aksimentyeva O.I., Sokolovskii B.S. Humidity sensitive structures on the basis of porous silicon // *Ukr. J. Phys.* – 2011. – V. 56. – P. 1198–1202.
3. Monastyrskii L.S., Aksimentyeva O.I., Olenych I.B., Sokolovskii B.S. Photosensitive structures of conjugated polymer – porous silicon // *Mol. Cryst. & Liq. Cryst*. – 2014. – V. 589. – P. 124–131.

# Synthesis and Structure of Nanosize $Ni_xCo_{1-x}Fe_2O_4$ Particles

Ostafiychuk B.K., Bushkova V.S., Yaremij I.P.

*Vasyl Stefanyk Precarpathian National University, Ivano-Frankivsk, Ukraine*

Spinel ferrites are technologically important ceramic materials because of their excellent electrical and magnetic properties. These classes of materials have been widely used for three decades. Recently, progress in synthesis techniques has initiated a new surge of interest in ferrites in order to improve their physical properties and expand their applications. Ferrospinels, $AFe_2O_4$, where A is Co, Ni, are a very important group of magnetic materials. They cover a wide range of applications from low wave-number to microwave and from low to high permeability including electronic devices, ferrofluids, magnetic drug delivery microwave devices and high density information storage [1]. Among the ferrospinels, the inverse type is particularly interesting due to its high magnetocrystalline anisotropy, high saturation magnetization, and unique magnetic structure.

Nanosize ferrites have been prepared by means sol-gel method with participation of auto-combustion. The chemical reagents used in the preparation were $Ni(NO_3)_2 \cdot 6H_2O$, $Co(NO_3)_2 \cdot 6H_2O$, $Fe(NO_3)_3 \cdot 9H_2O$, citric acid and distilled water. With constant stirring, the pH of the solution was adjusted to about 7 with ammonia solution. The present work deals with the synthesis and structure of nanoparticles of cobalt-doped nickel ferrite ($Ni_xCo_{1-x}Fe_2O_4$ where $x = 0.0$, 0.1, 0.2, 0.3, 0.4 and 0.5).

The phase identification of powders was performed by X-ray diffraction using DRON-3 diffractometer with Cu *Ka* radiation. Surface morphology of the samples was investigated by a JEOL NeoScope JSM-5000 scaning electron microscope. Determination of structural and adsorption characteristics of synthesized samples was conducted by means of nitrogen adsorption/desorption isotherms with the automated sorptometer Quantachrome Autosorb (Nova 2200e).

Studies showed that all the synthesized powders possess single phase of ferrite with spinel structure. According to the obtained results of X-ray analysis and scanning electron microscopy it was determined that the synthesized powder was agglomerated, that was composed of several nanoparticles. It was observed that the lattice parameter decreases with increasing $Ni^{2+}$ content $x$. This behavior of lattice parameter is explained on the basis of difference in ionic radii of $Co^{2+}$ (0.72 Å) and $Ni^{2+}$ (0.69 Å). The experimental result showed that pore size is in the mesoporous range according to IUPAC classification for all samples.

1. M.H. Sousa, F.A. Tourinho. New Electric Double-Layered Magnetic Fluids Based on Copper, Nickel, and Zinc Ferrite Nanostructures // *J. Phys. Chem.* B. – 2001. – V.**105,** №6. – P. 1168-1175.

# Antistructure Modelling of $CoFe_2O_4$ Nanoparticles Prepared by Precipitate Method

Paliychuk N.D., Tatarchuk T.R.

*Vasyl Stefanyk Precarpathian National University, Ivano-Frankivsk, Ukraine*

Spinel ferrite are intensively studied for their good magnetic property and stable chemical property. They shows typical ferromagnetic property at room temperature and it is wildly use as magnetic carrier in adsorbent to realize magnetic separation. Applications of ferrites of nanometer size have prompted the development of several widely used methods, including sol-gel techniques, reverse micelles, co-precipitation, citrate precursor techniques and other, for the fabrication of spinel ferrite nanoparticles.

In this work, the nanocrystalline $CoFe_2O_4$ was prepared using chemical co-precipitation method. The starting materials $Fe(NO_3)_2 \cdot 9H_2O$ and $Co(NO_3)_2 \cdot 6H_2O$ were dissolved in 700 ml of distilled water by intensive stirring, accordingly a homogeneous solution was obtained, and then NaOH was added to the solution until the pH 11,5. After the completion of the reaction, the solid product washed several times with deionized water. The final product was dried oven at 100 $^oC$ for 6 h, then was calcined at 800 ◦C for 2 h. Black powders were obtained and characterized as nanocrystalline $CoFe_2O_4$ ferrites.

The powder X-ray diffraction (XRD) patterns were recorded by use of a DRON-3 diffractometer with $Cu_{K\alpha}$ radiation ($\lambda$ = 1,5406 Å). The diffraction patterns of the sample shows the formation of the spinel phase with cubic structure. In order to calculate the crystallite size, the Scherrer's method was applied. The thermal behavior of powder precursor was characterized by Differential Scanning Calorimetry (DSC) and Thermo-Gravimetric Analysis (TGA) in order to analyze the mass loss and possible energy transitions. The endothermic peak in the DSC curve can be explained by the loss of water (OH-groups), the exothermic peak corresponds to the crystallization of the spinel. The morphologies of obtained sample have been characterized by scanning electron microscopy.

According to crystalloquasichemical model [1], the nature of defects and the mechanism of interaction between CoO and $Fe_2O_3$ oxide phases during the formation of cobalt ferrite spinel structure was described. Processes on the surface CoO and $Fe_2O_3$ are treated separately with the formation of CoO and $Fe_2O_3$ defective phases respectively:

$$(1-\alpha)Co_{Co}^{\times}O_O^{\times} + \alpha\left(Fe_{2/3}^{\bullet}V_{1/3}''\right)_{Co}O_O^{\times} \rightarrow \left(Co_{1-\alpha}^{\times}Fe_{2/3\alpha}^{\bullet}V_{1/3\alpha}''\right)_{Co}O_O^{\times} \quad ,$$

$$(1-\gamma)\left(Fe_2^{\times}\right)_{Fe}\left(O_3^{\times}\right)_O + \gamma\left(Co_2'\right)_{Fe}\left(O_2^{\times}V^{\bullet\bullet}\right)_O \rightarrow \left(Fe_{2-2\gamma}^{\times}Co_{2\gamma}'\right)_{Fe}\left(O_{3-\gamma}^{\times}V_{\gamma}^{\bullet\bullet}\right)_O \quad ,$$

where $\bullet$ is an excess positive charge, $'$ and $''$ is a single and double excess negative charge respectively, $V_{Co}''$ – cation vacancy, $V_O^{\bullet\bullet}$ – anion vacancy, $\times$ is an effective zero charge.

# Spreading of the Lifshitz-Slezov-Wagner Theory on Liquid Media

Panko I.I., Kryvetskyi V.I., Fesiv I.V.

*Yuriy Fedkovych Chernivtsi National University, Chernivtsi, Ukraine*

A generalized Lifshits-Slezov-Wagner distribution [1] for nanoclusters or nanocrystals growth according to two parallel mechanisms (Wagner and diffusion) has been used to explain a series of experimental histograms, which cannot be correctly related to the Wagner or the Lifshits-Slezov distribution separately. A process of the nanoclusters growth at the Ostwald ripening stage of the phase transformation in the solid systems can be correctly described using the generalized distribution of Lifshits-Slezov-Wagner.

The Ostwald ripening stage is also present in a process of formation of a new semiconducting nanoclusters phase (phase transformation of the first type) during chemical synthesis of nanoclusters in the liquid medium. That is why the Lifshits-Slezov-Wagner theory can be used for analysis of the mechanism and kinetics of the *ZnO* and *SnS* nanoclusters [2,3] formation from supersaturated solutions. The theory should be modified taking into account possible joined influences of both (Wagner and diffusion) mechanisms on the process of the growth of the nanoclusters.

As a result, the *SnS* nanoclusters experimental histograms were found in good correlation with the generalized distribution of Lifshits-Slezov-Wagner at various values of $x$. The rate of the nanocluster's growth is controlled mostly by formation of new chemical bonds or a surface chemical reaction, which runs on the nanocluster's surface.

The growth of the *ZnO* nanoclusters can be controlled by any of the Wagner's or diffusion mechanisms.

1. Vengrenovich R.D., Ivanskii B.V., Moskalyuk A.V. Generalized Lifshitz-Slyozov-Wagner distribution // *JETP*. – 2007, – Vol. 131, №6, – P. 1040-1047.
2. Arunasish Layek, Gargi Mishra, Archana Sharma, Marina Spasova, Subhabrata Dhar, Arindam Chowdhury, Rajdip Bandyopadhyaya A Generalized Three-Stage Mechanism of ZnO Nanoparticle Formation in Homogeneous Liquid Medium // *J. Phys. Chem. C*, – 2012, – Vol. 116, – P. 24757-24769.
3. Antoine de Kergommeaux, Jérôme Faure-Vincent, Adam Pron, Rémi de Bettignies, Bernard Malaman, and Peter Reiss Surface Oxidation of Tin Chalcogenide Nanocrystals Revealed by 119Sn–Mössbauer Spectroscopy // *J. Am. Chem. Soc*. –2012, – Vol. 134, №28, – P. 11659-11666.

# Gas Sensing Properties of Metal Oxide Nanopowders

Popovych D.I.[1,2], Savka S.S[1], Serednytski A.S.[1]

[1] *Pidstryhach Institute for Applied Problems of Mechanics and Mathematics NASU, Lviv, Ukraine*

[2] *National University "Lvivska Polytechnika", Lviv, Ukraine*

Environmental monitoring and registration of active gases are important priorities in world politics, especially for highly industrialized regions where great danger toxic and explosive gases. This is the need for improved means of measuring the chemical composition of atmospheric environments and creating new, more efficient and affordable instrumentation. A characteristic feature of the luminescence spectra of the material in the gases is that in addition to the main luminescence bands attached to the phosphor, there are more bands that defined the change of electronic surface states of nanopowders in the gas atmosphere. The ZnO surface has a high adsorption and reactivity ability, due to its intrinsic defect structure. However, a wide range of adsorption centers leads to low selectivity material, causing the need to find ways to improve it. Difficulty of selective detection is the result of a similar mechanism of interaction of reducing gases with ZnO surface. Sensitivity of metal oxides unto the nature and concentration of adsorbed molecules largely depends on the surface microstructure, which can be modified, as by laser annealing or formation of complex heterogeneous systems, in particular, metal-semiconductor type of "core-shell". It is established that the value of the sensory signal increases to saturation with increasing of the nanogranules size, it is determined by growth adsorption ability of nanopowders in conditions of manifestation Debye length. Constructed the principle scheme of semiconductor chemical sensor, which is based on effect of transformation of adsorption level in the luminescent signal, the nature of which corresponds to the number and kind of gas particles adsorbed from the environment. Gas registration carried out by analyzing changes in the spectral characteristics of luminescence of matrix (3x3 or more) of modified nanopowders (ZnO, $TiO_2$ etc.) and core-shell structures on their basis, is located in the gas under the UV excitation and catalytic decomposition of the analyzed gas (fig.1.). Registration luminescence carried out by means of CCD camera with the following digital analysis of the obtained signal, it allows determining the qualitative and quantitative composition of the gas component in the environment.

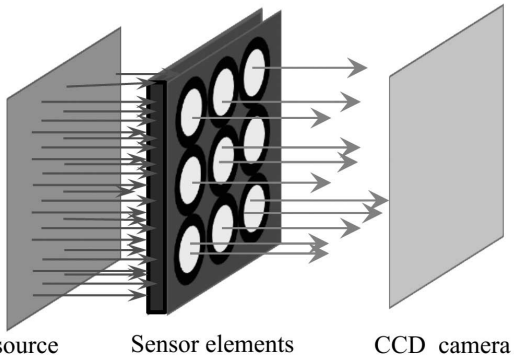


Fig.1. Schematic diagram of luminescence gas sensor

# Structure and Properties of Porous Silicon Films Obtained by Chemical Method

Potashnyk V.Y., Zastavnyi S.P.

*Ivan Franko National University of Lviv, Lviv, Ukraine*

Intensive development of semiconductor electronics is associated with creation and practical application of new materials, in particular by alternative low-cost methods for forming films of those materials. Formation of spatially inhomogeneous nanomaterials of frontal type, such as dispersion-like, island-like, variable-gap, hybrid and porous materials is one of main direction of nanotechnology.

We developed a method of obtaining nanoporous silicon films which is an alternative to electrochemical anodization chemical technology. Porous silicon films with a thickness of 1-10μm were obtained from chemical etching plates of porous silicon with p-type conductivity (KDB-10) and orientations (111) for 10-15 min at room temperature. It was used solution $HF:HNO_3:H_2O$, in which concentration of HF was 48% and concentration of $HNO_3$ - 70%. The obtained porous silicon heterostructures have different morphology depending on the duration of formation. The morphology of the obtained structures differs from that of anodized porous structures. They demonstrate asymmetric CVC which are sensitive to the applied mechanical tension. The influence of conductivity type, silicon carrier concentration and film thickness for por-Si to such structures on mechanical properties was studied.

The relative changes in capacitance of porSi-Si heterojunctions at changes of the applied voltage are investigated for different values of uniaxial pressure. These changes are accompanied with low power consumption and weak self heating of the samples as well as high output linearity and sensitivity to electromagnetic noise. As a characteristic of the effect was decreasing the influence of temperature on the capacity and its dependence on external pressure.

In our opinion, such structures can be used to create the sensors of mechanical tension.

1. Litovchenko V.G., Naseka V.M., Evtukh A.A. Two-Channel Gettering of Recombination-Active Impurity in Polycrystalline Solar Silicon // *Ukr. J. Phys.* – 2012. – V. 57, N 1. – P. 73-79.
2. Kaganovich E.B., Manoilov E.G., Svechnikov S.V. Photosensitive structures on porous silicon // *Phys. Solid State*. – 1999. – V. 33, N 3. – P. 327.

# Cathode Material Based on Ultradispersed Lithium Ferrite Obtained by Ion-Exchange Mechanism

Regush L.

*Vasyl Stefanyk Precarpathian National University, Ivano-Frankivsk, Ukraine*

Lithium pentaferrite $LiFe_5O_8$ is a promising cathode material for lithium power sources due to its structural and thermodynamic properties. Material nanostructured state is an additional factor that contributes to its electrochemical characteristics. Lithium pentaferrite was obtained by ion-exchange reactions in the ethanol. Several series of $LiFe_5O_8$ samples with different duration of the reaction were synthesized. It was found that with increasing duration of synthesis causes a decrease of the specific surface area of the obtained material (Fig.1,a). Changes of the material morphological characteristics affect its electrical properties and determine the effectiveness of its use as part of the electrode composition. As studies have shown (impedance spectroscopy method), the maximum conductivity is recorded for a sample obtained by synthesis duration of 1.5 days (Fig. 2, b). Non-monotonous conductivity $\sigma_{dc}(\omega)$ depending on the synthesis conditions is explained by the influence of two competing factors on the material conductivity. Reducing the particle size leads to an increase in the relative content of interparticle boundaries, but at the same time increasing the number of points of ohmic contact between the particles. Growth of sizes leads to lower reactance component, but deteriorating conditions of the transition between the current carrier particles. Thus superposition of these factors gives to each of the samples certain value of conductivity. These materials were tested as the basis for cathode composition for lithium power sources (LPS). Cathode mixture was consisted of $LiFe_5O_8$ (78 wt.%) with acytelene black (10 wt.%) and PVDF (12 wt.%). Metallic lithium was an anode. 1 M $LiBF_4$ in γ-butyrolactone was an electrolyte. Discharge curves for LPS with cathodes based material $LiFe_5O_8$ obtained by synthesis of various duration are presented in Fig. 3. The maximum capacity is achieved for the material synthesized during 1.5 days and it is 450 mAh/g. This result is consistent with the results of change in conductivity of $LiFe_5O_8$ samples. LPS based on this material was tested by potential-dynamic method. It was proved that the using of ultradispersed lithium pentaferrite is a promising for the design of LPS.

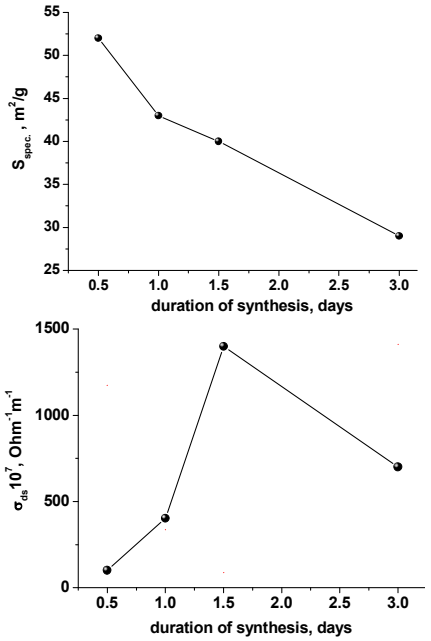


Fig.1.Specific surface area of obtained $LiFe_5O_8$ (a) and their specific electric conductivity (b) as functions of synthesis duration

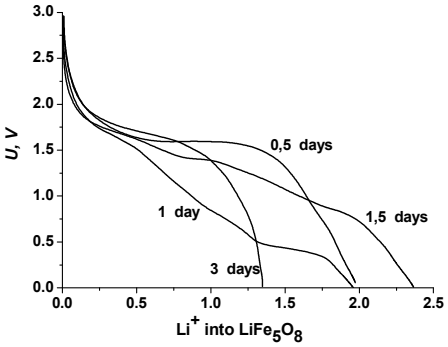


Fig.2. Discharge curves of the LPS with the cathode based on the samples of $LiFe_5O_8$ obtained at the different synthesis duration

# Electrophysical Properties of Polymer-Nanocarbon Composite

Salo A.A., Lyashkov A.Yu., Khmelenko O.V.

*Dniepropetrovsk National University, Dniepropetrovsk, Ukraine*

Composites based on polymer and conductive filler, including polyethylene-nanocarbonic system, have a positive temperature coefficient and high electrical conductivity at room temperature (up to 0.1 $(Om \cdot m)^{-1}$), which makes use of them as one of the promising materials for posistor heaters elements and self-renewing fuses (PolySwitch) [1-2].

In production of composites was used polyethylene with low-density (15803-020) or polypropylene. As a filler was used industrial carbon black marks N330 (according to ASTM D1765) with a particle size of 28-36 nm.

In the resulting nanocomposites with different volume fate of carbon ($\rho_v$) was investigated the temperature dependence of the electrical conductivity $\sigma(T)$, calculated temperature coefficient of resistance ($\alpha$) and conductivity activation energy ($\Delta E$).

*Electrophysical Properties of polyethylene-carbon composite.*

| $\rho_{v,\%}$ | $\sigma_o$, $Om^{-1} \cdot m^{-1}$ | $\alpha$, $K^{-1}$ | $\Delta E$, eV |
|---|---|---|---|
| 5 | 0.00046 | $2.9 \cdot 10^{-3}$ | 0.09 |
| 10 | 0.047 | $4.7 \cdot 10^{-3}$ | 0.11 |
| 15 | 0.21 | $9.7 \cdot 10^{-3}$ | 0.28 |
| 20 | 0.61 | $7.4 \cdot 10^{-3}$ | 0.14 |
| 30 | 0.96 | $1.9 \cdot 10^{-3}$ | 0.05 |

The conductivity increases with increasing volume fractions of nanocarbon. The temperature coefficient of resistance and activation energy first increases, the maximum observed in $\rho_v = 15\%$, and then decreased. This can be explained by the formation of stable continuous conduction channels in the material contains large amounts of carbon.

1. M.F. Wartenberg, J.G. Lahlouh, Toth James. Conductive polymer compositions, and method of making the conductive polymer composition, US Patent, 19960319 (2003).
2. A.V. Degtyar'ov, A.S. Tonkoshkur, A.Yu. Lyashkov. Electrical properties of posistor composite materials based on polyethylene-graphite // Multidiscipline Modeling in Materials and Structures, VSP, 2006, v. 2, №4, p.p. 435-441(7).

# Magneto - Optical Properties of CdMnTe Nanoparticles Dispersed in the Polymer Matrix

Savchuk A. I.[1], Stolyarchuk I. D.[1], Savchuk O. A.[1], Cieniek B.[2]

[1]*Yuriy Fedkovich Chernivtsi National University, Chernivtsi, Ukraine*
[2] *University of Rzeszow, Rzeszow, Poland*

Semiconductor nanoparticles doped with magnetic ions represent an new class of materials - diluted magnetic semiconductors (DMS) [1]. Their unique optical, electronic, and magnetic properties have a potential applications in the field of spintronics and nanomagnetics [2,3]. The defining feature of a DMS is the spin-exchange interaction, which arises between delocalized charge carriers and localized spins on magnetic impurity ions embedded within the semiconductor. These s, p - d exchange interactions are responsible for the giant Zeeman splittings of the bands and excitons states and give rise to the so-called giant Faraday rotation effect [1]. Among these nanomaterials the most experimentally studied are Mn-doped II-VI based DMSs type of CdSe:Mn or ternary solid solutions type of $Cd_{1-x}Mn_xSe$.

In this work, we present results of investigation of magneto-optical properties of Mn-doped semiconductor CdTe nanoparticles prepared by different physical methods. Among physical techniques we have chosen ball milling or mechanical synthesis and pulsed laser ablation in liquids using combined targets. All the samples were characterized by X-ray diffraction (XRD), transmission electron microscopy (TEM), optical absorption, magnetophotoluminescence, and Faraday rotation spectroscopy.

In magnetic field up to 7 T shift of the photoluminescence structure towards long wavelength was observed due to the strong spin-exchange interaction between band carriers and magnetic ions. The linear magnetic field dependence of the Zeeman shifts and Faraday rotation for nanoparticles with low mangan content suggest of increase of the role pairs and antiferromagnetic interaction between $Mn^{2+}$ ions.

1. Furdyna J. K. and Kossut J. Diluted Magnetic Semiconductors // Academic Press, New York – 1988 – **25**.
2. Hedin E.R., Joe Y.S. Spintronics in Nanoscale Devices // Pan Stanford Publishing: Singapore, 2013.
3. Awschalom D.D., Bassett L.C., Dzurak A.S., Hu E.L., Petta J.R. Quantum Spintronics: Engineering and Manipulating Atom-like Spins in Semiconductors // Science. – 2013. – 339. – p. 1174-1179.

# Influence of the Stoichiometry on Raman Spectra of the Amorphous Phase Change Alloys for Future Memory and Display Applications

Shportko K.[1,3], Wuttig M.[1], M. Grueninger[2] and Venger E.[3]

[1]*RWTH University of Technology Aachen, Aachen, Germany.*
[2]*University of Cologne, Cologne, Germany.*
[3]*V.E. Lashkarev Institute for semiconductor physics of NAS of Ukraine, Kyiv, Ukraine.*

Phase change (PC) materials are promising materials for data storage, display and data visualization applications due to the remarkable difference of their electrical and optical properties in the amorphous and crystalline state. Amorphous phase of phase change materials is bonded covalently, while crystalline phase crystalline has resonant bonding. [1].

PC materials have already been employed in optical data storages (CD's, DVD's, Blu-Ray disks). Memories based on PC materials are a candidate to replace flash memory for non-volatile data storage applications [2]. By combining the optical and electronic properties of phase change materials, display and data visualization applications can be created [3].

A fundamental understanding of the properties and stability of the amorphous state of phase change alloys has important implification in optimizing materials for next generation of storage media and smart displays.

Three amorphous Ge-Sb-Te alloys along the co-called pseudo-binary line have been investigated using Raman spectroscopy in this study. In amorphous Ge-Sb-Te alloys the Ge and Te atoms occupy the octahedral and tetrahedral symmetry positions [4]. Several phonon peaks have been observed in Raman spectra of studied $Ge_1Sb_2Te_4$, $Ge_2Sb_2Te_5$, and $Ge_3Sb_2Te_6$ samples at around 70, 127, 155 and 210 $cm^{-1}$. Correlation between stoichiometry, intensity and width of these peaks has been analyzed and discussed.

One of the authors (K. Shportko) gratefully acknowledges the support from the DAAD (German Academic Exchange Service) and the SFB 917 "Resistively Switching Chalcogenides for Future Electronics – Structure, Kinetics and Device Scalability".

1. Shportko K, Kremers S et. al.: Resonant bonding in crystalline phase-change materials. *Nature Materials*: 2008, 7: 653-658.
2. Wuttig M, Yamada N: Phase-change materials for rewriteable data storage. Nature Materials:2007, 6: 824-832.
3. Hosseini P, Wright C D, Bhaskaran H: An optoelectronic framework enabled by low-dimensional phase-change films. *Nature*: 2014, 511:206-212.
4. Kolobov A, Fons P, Tominaga J et al.: Understanding the phase-change mechanism of rewritable optical media. *Nature Materials*: 2004, 3, 703-708.

# The Synthesis of the Nanoparticles With Double-Hierarchical Structure as Promising Materials for Use in Electrochemistry

Shyyko L.O., Kotsyubynsky V.O., Budzulyak I.M.

*Vasyl Stefanyk Precarpathian National University, Ivano-Frankivsk, Ukraine*

In recent years, rechargeable lithium-ion batteries (LIBs) have emerged as the most attractive power source in portable electric devices, and hybrid electric vehicles (HEVs) or electric vehicles (EVs). A lot of different materials were tested as electrode material in such devices [1]. Layered metal dichalcogenides ($MoS_2$, $MoSe_2$, $WS_2$, $WSe_2$, etc) are a a special class of compounds attracted the researchers by its unique structural and electrical properties, due to the weak van der Waals interactions between the individual layers allow to create the space for $Li^+$ ion diffusion path without significant changes in its structure providing relatively high values of specific capacity. However, there is still an issue of low electronic and ionic conductivity and in some cases the problem of nano-particles aggregation and layers restacking during the repetitive cycling and even the drying process of electrodes [2]. One possible way to solve these problems is to use hybrid nanostructures, where the <host> active materials are embedded into the conductive matrix of <subhost> creating the new double-hierachical structure [3]. We present the simple way to obtain such structure consisted of $MoS_2$ and carbon by hydrothermal method using cetyltrimetyl-ammonium cations. According to XRD (Fig.1), TEM (Fig.2) we have received mostly spherical multilayered nanoparticles, in which $MoS_2$ layers alternating with C (atomic ratio is 1:1). Annealing in Ar at 500°C and 1000°C has not significant impact on morphology and composition of the synthesized material.

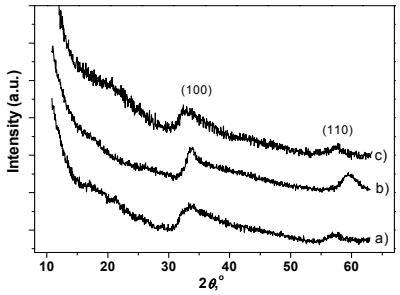


Fig.1. XRD patterns of $MoS_2$/C before (a) and after annealing at 500°C (b) and 1000°C (c)

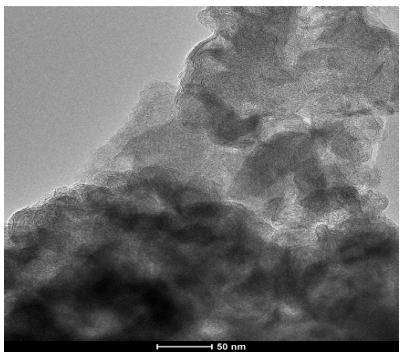


Fig.2. TEM image of $MoS_2$/C

1. Broussely, M., Ph Biensan, and B. Simon. Lithium insertion into host materials: the key to success for Li ion batteries// Electrochimica Acta – 1999. – V. 45, № 1. – C. 3-22.
2. Pumera M., Sofer Z., Ambrosi A. Layered transition metal dichalcogenides for electrochemical energy generation and storage //Journal of Materials Chemistry A. – 2014. – T. 2, №. 24. – C. 8981-8987.
3. Войтович С.А., Григорчак І.І., Матвіїв М.В. Ієрархічна дублетно-матрична структура C<FeS2> для $Li^+$- та $Mg^{++}$-інтеркаляційного струмоутворення//ФІП. – 2010. – Т.8, №1. – С. 43-52.

# Obtaining Regular Porous Gallium Arsenide Surface by Electrochemical Etching.

Simchenko S.V, Dyadenchuk A.F.

*Berdyansk State Pedagogical University, Berdyansk, Ukraine*

The end of the last century has seen a progressive move down in dimensionality of semiconductors. Quantum wires and quantum dots were exotic terms a decade ago, while now they are at the very basis of many devices, e.g. lasers and are the key to the development of the technology of the future, e.g. nanoelectronics [1]. In fact, many possible applications exploit the quantum confinement (e.g. in light emitting diodes) or the high reactivity of its surface (e.g. sensor applications) but to promote real and commercial devices one has to master its quantum sponge nature.

Currently, the most promising is to obtain porous semiconductors such as Si [1], GaAs, GaP [1]. A special place in this series takes GaAs in connection with the prospects of using it as a substrate for growing various heterostructures on which are created efficient sources of radiation (injection lasers, light-emitting diodes) and high-speed photodetectors systems for fiber-optic communication lines. Porous gallium arsenide became the object of many studies [2-3], as a result of which it is possible to receive regular pore structure predetermined dimensions.

Porous GaAs layers were obtained by electrochemical anodic etching of single crystal n-GaAs (111), doped silicon (concentration of majority carriers 1015-1018sm-3) in a cell with a platinum electrode. On the back of the GaAs wafer was done an ohmic contact. In the solutions used as electrolytes HF: C2H5OH = 2: 1, HF: C2H5OH = 1: 1, HF: C2H5OH = 1: 2.

The porous substrate were obtained at different etching conditions that lead to fluctuations in GaAs porosity of 30 to 55 percent and pores from Rather micro to nanometer. The electric current density was varied in the range from 50 to 200 mA / cm2, the etching time was 2-15 min.

Varying the electrolyte composition, time and conditions of etching is possible to obtain high-quality porous structure on the surface of gallium arsenide with deliberately planned parameters. Currently, research is being conducted on the use of these devices as solar cells and gas sensors.

1. Pores in III-V Semicoductors / H. Föll, S. Langa, J. Carstensen et al. // *Advanced Materils*. – 2003. – V. 15, N 3. – P. 183 – 198.
2. Waveguide structures based on porous indium phosphide / S. Langa, S. Frey, J. Carstensen et al. // *Electrochemical and Solid-State Letters*. – 2005. – V. 8, N 2. – P. C30 – C32.
3. Porous III – V compounds as nonlinear optical materials / I.M. Tiginyanu, I.V. Kravetsky.

# Features of Optical Properties of CdSe with Quantum-Size Surface

Slyotov M.M., Slyotov O.M.

*Yu.Fedkovych Chernivtsi National University, Chernivtsi, Ukraine*

Cadmium selenide is one of the most important semiconductors in various functional electronics devices. Their main physical and technical parameters are mainly determined by the state of the surface. Therefore an actual task is both surface modifications with the aim of the state improvement and research of optical processes that provides the possibility of creation of various solid-state electronics devices.

Undertaken studies have shown promising chemical treatment of surface at certain temperatures, etchants compositions and time conditions. Basic cadmium selenide crystals were obtained by Bridgman method. Investigation of their optical, photoluminescent (PL) and photovoltaic (PV) properties using classical methods and λ-modulation revealed a characteristic hexagonal lattice band structure, efficient photoluminescence and photosensitivity. Their spectral characteristics are in a good agreement with well known parameters for CdSe. Chemical treatment allows to significantly changing them. A substantial increase of effective processes is observed in the short-wave region $\lambda < 0{,}7$ μm up to 0,31 μm, Fig. 1. In this case, the mirror surface of substrates is changed.

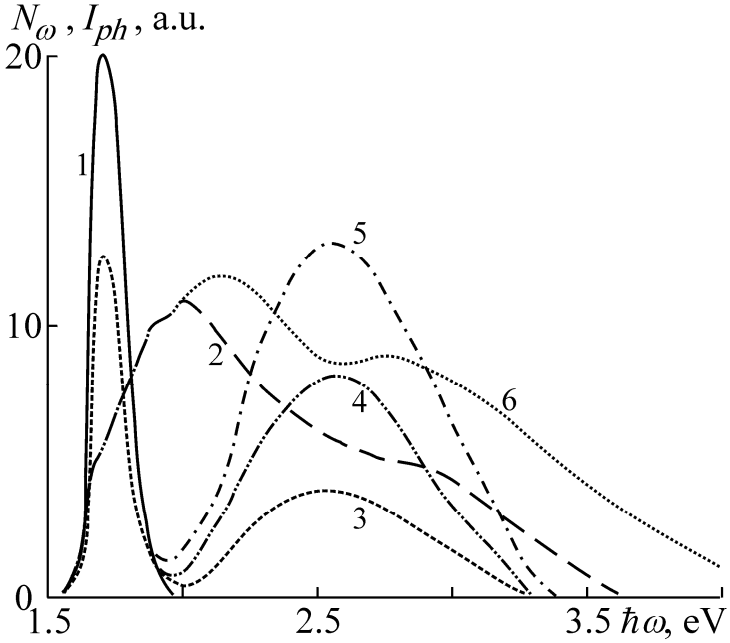


Fig. 1 PL spectra (1, 3, 4, 5) and photo-sensitivity (2, 6) basic (1, 2) and modified (3, 4, 5, 6) layers of CdSe

Investigations of microrelief by atomic force microscopy revealed the formation of rough surface with square roughness of the surface of 45 nm. In the PL spectra wide band in the energy photons $\hbar\omega > E_g$ is observed, which is typical for the quantum-size structures. Its intensity depends from the treatment process that indicates the possibility of controlling the intensity of short-wave radiation. Also varies the photosensitivity of surface-barrier diodes formed on CdSe, which is characterized by a shift of the maximum in a short-wave region with the spectrum expansion, including $\hbar\omega \sim 4{,}25$ eV.

# Topology of Thin Films and Nanostructures II-VI, IV-VI Received vapor Phase Methods

Sokolov O.L.[1], Nagirna N.I.[2] Potyak V.Y.[1]

[1]*Vasyl Stefanyk Precarpathian National University, Ivano-Frankivsk, Ukraine*
[2]*The College of Electronic Devices of Ivano-Frankivsc National Technical University of Oil and Gas, Ivano-Frankivsk, Ukraine*

Today there are a number of methods for the thin films and nanostructures CdTe, including a special place is hot-wall method [1]. This method, due to design features, you can get condensation in a well controlled technological process in many crystalline substrates – as silicon, gallium arsenide, barium fluoride and others. At the same time and even now remains a large number of outstanding physical and technological problems, which become an obstacle to obtaining high-quality structures based on CdTe.

The conditions of forming thin films of CdTe, deposited on the fresh chips (0001) mica-muscovite in quasireserved capacity by hot wall. Evaporation temperature of the batch synthesized compounds CdTe changed within the $T_V$ = (400 - 500) ° C. In this area temperature CdTe evaporates congruent with more than 98% of molecules in a pair CdTe [2]. The temperature of deposition was $T_S$ = (250, 300, 350) ° C. Thickness of obtained films were determined by two methods: optical (interference pattern by optical transmission spectra) and mechanical (using profilometer). The structure of the condensate were studied by microscope MI-4. Rate of condensation on the substrate was V = 0,02-2 mkm/min. Wall temperature maintained at 50° C higher temperature evaporator. Thickness of condensate deposition time asked within (0,1-20) mkm.

In the paper the dependence of grain size b, V condensation rate and film thickness of technological factors in their growth by hot wall. Shown that experimental results can be explained by the peculiarities of evaporation of the batch compounds and adsorption-desorption processes in the zone of condensation.

1. Д.М. Фреик, М.А. Галущак, Л.И. Межиловская. *Физика и технология полупроводниковых пленок*. Вища школа. Львів. 152 с. (1988).
2. Sukarno Olavo Ferreira¤, F´abio Fagundes Leal¤, Tatiana Estorani de Faria, Jos´e Eduardo de Oliveira¤, Paulo Motisuke and Eduardo Abramof. Characterization of CdTe Thin Films Grown on Glass by Hot Wall Epitaxy // Brazilian Journal of Physics. – 2006. – T. 36, №2A. – P. 317.

# Standing Wave Expansion Method: Calculation of a 2D Photonic Crystal Resonator

Stepanyuk A.M.[1], Glushko E.Ya.[2]

[1]*Pedagogical Institute, Kryvyi Rih National University, Kryvyi Rih, Ukraine*
[2]*Institute of Semiconductor Physics, NAS of Ukraine, Kyiv, Ukraine*

The Standing Wave Expansion Method (SWE) [1-2] was developed especially to calculate the electromagnetic spectrum and field distribution inside a kind of ordered finite size objects – photonic crystal resonators (PCR). A PCR looks like a rectangular island deposited on the substrate. Due to the special ways of electromagnetic field exciting inside the total internal reflection (TIR) region of the resonator shown in Fig.1, the system traps irradiation which, in turn, can be processed and redirected out the system. The photonic crystal resonators are of interest for all-optical signal processing as elements of logic devices with extremely high quality factor which may be reached at modern state of technology. The starting basis of 2D eigenfunctions is formed on the ground of standing electromagnetic waves – solutions of the so-called intrinsic problem for field inside the TIR region. A general feature of the solutions corresponding to modes trapped inside the resonator is that all its energy are concentrate inside the resonator whereas outside the resonator we have only falling tails of states. A finite one dimensional problem serves as a generator of analytically determined functions describing X or Y part of the total 2D basis with close periods in both directions. The 2D basis generator works to cover the $N_1 \bullet N_2$ periodic resonator with 1D functions found for $N_1$-period resonator in X direction and $N_2$-period resonator for Y direction. It is easy to understand that the predominant density of field energy is concentrated inside the $N_1 \bullet N_2$ resonator unlike to other approaches based on plane waves. The set of basis' functions $\{|s,g>\}$ found for p-polarised waves may be described with the help of magnetic field.

We calculated several types of PCR differing by intrinsic contrastivity beginning with weak contrastive $SiO_2/SiO_2$ PCR, intermediate $Si/SiO_2$ PCR and strongly contrastive Si/air resonators by the SWE method. In Fig.2, shown is the chosen standing mode $H(x,y,\mathbf{\Omega}_{36})$ coordinate dependence calculated in zero-approximation for the 2D $SiO_2/SiO_2$ PCR situated in air and containing *36* rectangular cells where $\varepsilon_1 = 3.24$, $\varepsilon_2 = 2.25$. The states numbering begins from 0, the lowest state with no node lines and maximal density in middle of the PCR. The lattice and also in the case of nonlinear external covering layers.

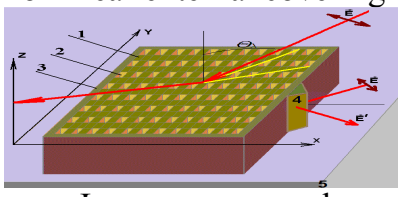


**Fig. 1** The geometry of the problem. Two ways of intrinsic modes (standing waves inside the TIR region) excitation in a 2D 12x8 PCR. 1, 2, period forming layers of width $d_1$ (host material) and (wells); 3, external a-layer (in general case nonlinear) of width $d_a$, 4, input prism, 5 substrate, $\vec{E}$, $\vec{E}'$ are beams incident and reflected.

In summary, we have considered the SWE method to calculate electromagnetic eigenwaves in a finite 2D photonic resonator of rectangular external shape. The 2D basis of standing waves was generated and its properties were studied. The spectrum and field distribution inside the resonator were calculated for several types of PCRs and various shapes of wells. Several types of resonator states were discussed: band, waveguide, surface and pure local states, a classification of 2D modes based on 1D modes and 2D knot theorem was proposed.

1. E. Y. Glushko, A. E. Glushko, V. N. Evteev, and A. N. Stepanyuk, Nanophotonics II, vol. 6988 of Proceedings of SPIE, p. 118, 2008.
2. E. Ya. Glushko, Optics Communications, vol. 247, no. 4–6, pp. 275–280, 2005.

# Sol-gel auto combustion syntesis of nanostructured cobalt aluminate

Tatarchuk T.R., Boyko E.V.

*Vasyl Stefanyk Precarpathian National University, Ivano-Frankivsk, Ukraine*

There are many methods of preparing $CoAl_2O_4$ nanosized powders such as co-precipitation method, hydrothermal method, solid state reactions method and sol-gel method which has some advantage.

In this report cobalt aluminate powder was prepared by sol-gel citrate route. Metal nitrates and citric acid as complexing were dissolved in distilled water with following addition ammonia solution to get pH = 7. After being evaporated obtained sol solution had been transformed to polymeric gel and auto combustion process occurred. Further calcined didn't carry out. In the result dark gray product was obtained. Synthesized sample was characterized by XRD, FT-IR, TG-DSC and colorimetric methods.

The main peaks of XRD pattern are indexed in accordance with spinel structure of $CoAl_2O_4$ and Fd3m space group. The average crystallite size of the cobalt aluminate was estimated by Scherrer's formula. Crystallographic data (X-ray density ($\rho_{XRD}$), specific surface area (S), radius of the ions at octahedral ($r_{oct}$) and tetrahedral ($r_{tetr}$) sites values were calculated using XRD data. Partially inversion of structure also was detected by this analysis.

The IR spectrum was recorded in the 4000-400 $cm^{-1}$ region with an FTIR Brucker Alpha-P spectrometer. Several peaks in 700-450 $cm^{-1}$ range on IR spectrum indicate the formation of $CoAl_2O_4$ spinel. These peaks belonging to vibrations of Me-O groups in tetrahedral and octahedral sublattices.

DSC curve of dried precursor showed two exothermic peaks, first of which corresponding to decomposition of metal complexes and metal oxides formation and the second on spinel phase formation. TG curve of precursor showed weight loss is 87 %.

For colorimetric analysis $CoAl_2O_4$ samples was calcined at 400, 600, 800, 1000$^oC$ and investigated using an X-Rite Color i7 Benchtop spectrophotometer with standard lighting D65. Results showed appreciable color changes depending on calcination temperature. CIE L*a*b* colorimetric parameters of samples were determined.

For prepared spinel antistructure model of formation was described:

$$\left(\mathrm{Co}^{\times}_{1-\beta}\mathrm{Al}^{\bullet}_{\beta}\right)_{\mathrm{Co}}\left(\mathrm{O}^{\times}\right)_{\mathrm{O}}\left(\mathrm{O}''_{0,5\beta}\right)_{\mathrm{i}}+\left(\mathrm{Al}^{\times}_{2-2\delta}\mathrm{Co}'_{2\delta}\right)_{\mathrm{Al}}\left(\mathrm{Co}^{\bullet\bullet}_{\delta}\right)_{\mathrm{i}}\left(\mathrm{O}^{\times}_{3}\right)_{\mathrm{O}}+$$

$$+\left(1+\frac{1}{8}\beta\right)\mathrm{V}''_{\mathrm{A}}\left[\mathrm{V}'''_{2}\right]_{\mathrm{B}}\left(\mathrm{V}_{4}{}^{\bullet\bullet}\right)_{\mathrm{O}}\rightarrow\left(1+\frac{1}{8}\beta\right)\left(\mathrm{Co}^{\times}_{0,2}\mathrm{Al}^{\bullet}_{0,8}\right)_{\mathrm{A}}\left[\mathrm{Co}'_{0,8}\mathrm{Al}^{\times}_{1,2}\right]_{\mathrm{B}}\left(\mathrm{O}^{\times}_{4}\right)_{\mathrm{O}}$$

Sol-gel route is very useful to preparing spinel oxide powders and it gives good results requiring not much time and costs.

# The Effect of Germanium Atom Adsorption on the Si (001) on its Density of Electronic States

Terebinska M.I., Tkachuk O.I., Lobanov V.V.

*Chuiko Institute of Surface Chemistry of National Academy of Sciences of Ukraine, Kyiv, Ukraine*

Different in the electronic properties of nanostructures and in the properties of bulk materials is caused by the presence of spatial quantization effects. The dependence of the band structure of an object from its size can be used for substantially increase the field of application of materials in electronic and optical circuits.

Nanostructures with germanium deposited on Si (001) are the most intensively studied among liked nanostructures and this has a number of objective reasons.

This paper presents the results of quantum-chemical calculations (method of density functional theory, B3LYP, 6-31G**) $Si_{96}H_{84}$•Ge nanostructures, modeling complex of germanium atom adsorption on the face of the Si (001). The energy its binding, of according to the results, was 7.8 eV. Thus there is a significant change in the density of electronic states both clusters representing the substrate and germanium atom. This change depends on the shift of the energy core-levels and valence electrons, so in an isolated atom Ge energy 1s core-level is 10,849.7 while this energy in the $Si_{96}H_{84}$•Ge cluster is 10850.94 eV. This energy shift is due, on the one hand, the displacement of the initial position of the core-level Ge atom at its entry into the modeling of the cluster, and the other - the electron relaxation subsystem original cluster representing of surface of the substrate. These changes can be negative and positive depending on increasing or decreasing the effective charge of the atom.

In addition to these factors to explain the shift direction is considered more Madelung potential - the total capacity, in this case an atom Ge, due to charges on the surrounding atoms. The relative contributions to the chemical shift of these factors are very difficult to individual of assessment.

Whereas Pauling electronegativity of Si and Ge atoms (1,8 and 1,7, respectively) can be explained by the positive shift level 1s Ge atom, assuming the dominant contribution of the first factor.

Core-level the 2s is shifted to 1340.3 (Ge atom) to 1340.9 eV are risen in the cluster, which also indicates the dominant role of the first factor.

Thus, taking into account the small absolute of values of the core-level shifts 1s and 2s atom Ge, it can be argued that the electronic structure of atom Ge undergoing minor changes in spite of the relatively high binding energy.

# Sodium-Substituted and Carbonated Calcium Phosphate Nanoceramics for Bone Substitution

Tkachenko M.[1], Zyman Z.[1], Epple M.[2], Babkina T.[1]

[1]*V. N. Karazin Kharkiv National University, Kharkiv, Ukraine*
[2]*Institute of Inorganic Chemistry, University Duisburg-Essen, Essen, Germany*

Bioactivity of bone implants based on hydroxyapatite (HA) depends on their chemical composition and microstructure. Comparative studies on nanocrystalline and conventional microcrystalline ceramic implants in a biological environment have shown that nanoceramics have greater bioactivity and better integrate with bone tissue. Therefore, effective biomaterials structural and chemical characteristics should be similar to bone mineral. In particular, biomaterial based on HA should be nanocrystalline and incorporate impurity ions that are typical of biological apatite. The ions include $Na^+$, $Mg^{2+}$, $CO_3^{2-}$, etc. The effect of $Na^+$ additions in concentrations ranging from 0.25 to 1.5 wt% on the sintering temperature, crystallinity and characteristics of carbonization of HA powder compacts was studied.

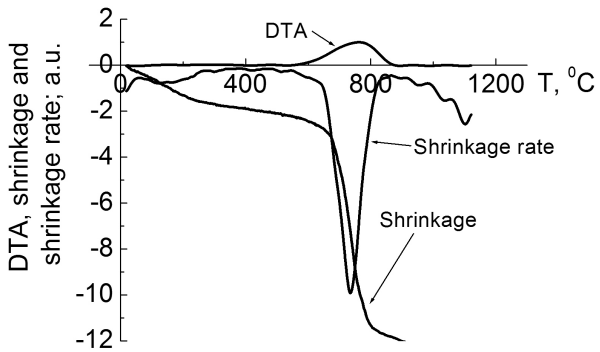


Figure 1

XRD, IR spectroscopy, dilatometric and TG-DTA methods were used.

According to the DTA results a significant exothermic effect associated with solid-state reaction between HA and sodium bicarbonate or nitrate added as a sodium source was found in the temperature range 600-800 °C (Fig. 1). The reaction leads to joint ionic substitutions in cationic ($Na^+$ for $Ca^{2+}$) and anionic ($CO_3^{2-}$ for $PO_4^{3-}$) sublattices of HA. As a result, carbonated sodium-substituted HA (CHA) was formed. The degree of carbonation increased with increasing sodium ion contents. Significant activation in shrinkage of the compacts was also found. The sintered of the finely dispersed sodium-substituted CHA ceramics by microstructure and chemical composition were similar to biological apatite.

# Ostwald ripening of nanocrystals in 2D- and 3D- systems

Vengrenovich R.D., Yarema S.V., Moskaliyk A.V.

*Yuriy Fedkovych Chernivtsi National University, 2 Kotsjubynskyi Str. Chernivtsi, Ukraine*

Currently, the products of nanotechnology (NT) are widely used in electronics, optoelectronics, information technology, medicine, biology, pharmacology, etc. [1]. Especially important is the role of NT for optical industry and, in particular, in the production of light-emitting elements. The perspective branch are the semiconductor light emitting diodes (OLED), as well as new methods of lithography (DUV and EUV).

The comparison of Chakraverti-Wagner distribution [2] and Generalized-Lifshitz-Slezov-Wagner distribution [3] was carried out within modified for the surface (2D- system) and for the volume (3D- system) of LSW theory with the experimental histograms of nanocrystals (quantum dots) obtained with different technologies - electron-beam (molecular beam) epitaxy, liquid phase epitaxy and colloidal chemistry. Matching of experimental histograms with theoretically calculated curves indicates the possibility of nanocrystal growth (dissolution) at the stage of Ostwald ripening simultaneously by two mechanisms - diffusion and chemical reaction which are controlled accordingly by diffusion coefficients $D_s$ ($D_v$) and kinetic coefficient $\beta$. The results of the studies on the mechanisms of nanocrystal growth at the stage of Ostwald ripening might be used in technological processes of their synthesis.

2. *Hartmann U.*, Faszination Nanotechnologie. – München; Heidelberg: Elsevier, Spektrum, Akad. Verl., – 2006. VIII, – 166 p.
3. Vengrenovich R. D., Ivans'kyi B. V., Moskalyuk A. V. Generalized Chakraverty-Wagner Distribution / // Ukranian Journal of Physics. – 2008. – Vol. 11. – P. 1101-1109.
4. Vengrenovich R.D., Ivanskii B.V., Moskalyuk A.V. Generalized Lifshitz-Slyozov-Wagner distribution // JETP. – 2007, – Vol. 131, №6, – P. 1040-1047.

# For Boundary Conditions for Schrödinger Equation on Hetero-Boundary

Voznyak O.M.

*Vasyl Stefanyk Precarpathian National University, Ivano-Frankivsk, Ukraine*

Standard conditions applied to wave function on boundary of two areas reduced to equality of wave functions itself and their derivatives on this boundary [1]. In case of hetero-boundary with different effective masses it goes to complications caused by the fact that if continuity wave function condition is required, than it leads to divergence density of stream, and non-equality of wave functions on hetero-boundary will give kinetic energy variance. Long time as the solution for this problem it was using the method of multiplying wave functions itself or their derivatives on correspondent effective masses. However, this approach often leads to complications.

There is another approach to obtain proper behavior of wave functions and their derivatives on hetero-boundary [2]. It lies in considering of strong-tied model that gives energy zones, which described by effective mass approximation and building strong-relation for merging of two areas with different effective masses for low energy irritations. As an example, we consider the simplest model of linear atomic chain using the method of strong-relation with parameters of effective mass on left and right of boundary are different. We obtained expression for boundary transition coefficient in this model and analyzed it. We came to conclusion that correct boundary conditions obtained by ingesting them on hetero boundary of wave functions divided on root square of correspondent effective masses and their derivatives divided on root square of correspondent effective masses.

1. Vakarchuk I.O. Quantum Mechanics (Ivan Franko LNU, Lviv, 2012).
2. Harrison W. A. Matching Conditions in Effective-Mass Theory. Web: arXiv.org:cond-mat.mtrl.sci/1108.1224/04.August2011.

# Differential Thermal Analysis for Laser Irradiated Composite $TiO_2/C$

Yablon L.S., Khemiy O.M., Budzulyak I.M., Morushko O.V., Rachiy B.I.

*Vasyl Stefanyk Precarpathian National University, Ivano-Frankivsk, Ukraine*

Problem of dehydration of functional nanomaterials for LPS and energy storage devices is quite relevant in view of the fact that water significantly reduces their specific characteristics. We studied the effect of thermal performance and laser irradiation on the change of water content in the composite $(TiO_2)_x/C_{1-x}$, де x = 0,1; 0,2; 0,3 by the method of differential thermal analysis

Fig. 1 presents the results showed that irradiated samples during the heating are losing water much greater than unirradiated, that is crucial for their use in LPS. It was found that the mass loss of composite $TiO_2/C$ (Fig. 1, *a*) most significantly depends on the percentage of $TiO_2$ in the composite and their laser treatment.

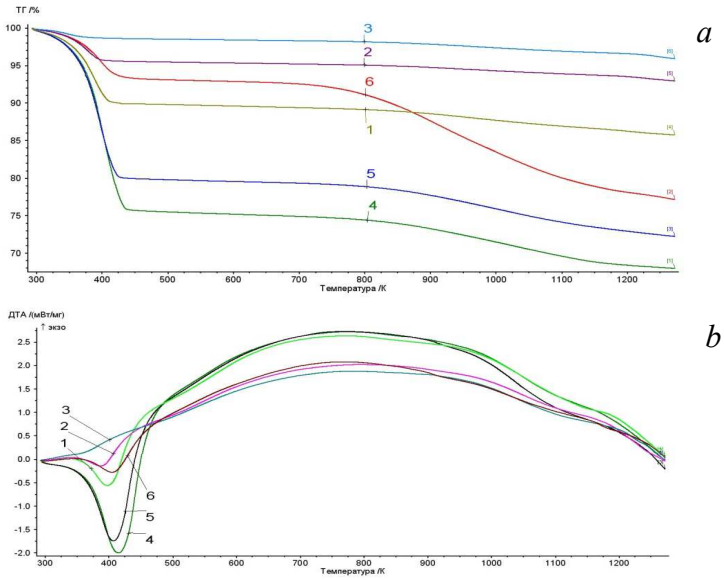


Fig. 1. TG curves (*a*) and DTA (*b*) for composite $TiO_2/C$, where the content of $TiO_2$ is 1 – 10%; 2 – 20 %; 3 – 30 % (unirradiated samples); 4 – 10%, 5 – 20 %; 6 – 30 % (laser irradiated samples)

In the first case, the sample mass loss increases with decreasing of $TiO_2$ amount in the composite, which can be explained by the fact that the content of adsorbed water in nanoporous carbon is much higher than in the nanoscale $TiO_2$, since the carbon surface area in ten times larger than the titanium dioxide surface area.

Also, adsorption ability and morphology of these surfaces should be taken into account since they also contribute to greater water retention of carbon surface than the $TiO_2$ surface. However, laser irradiation reduces the energy of water molecules interaction with the carbon and titanium dioxide surfaces. DTA curves (Fig. 1, *b*) obtained for these samples, where in the temperature range 350-450 K endothermic effects (responsible for water desorption processes) occur, prove the mentioned above.

# Raman Scattering of Composite $TiS_2/C$

Yablon L.S.[1], Strelchuk V.V.[2], Budzulyak S.I.[2], Morushko O.V.[1]

[1] *Vasyl Stefanyk Precarpathian National University, Ivano-Frankivsk, Ukraine*
[2] *Lashkarev Institute of Semiconductor Physics, The National Academy of Sciences of Ukraine, Kyiv, Ukraine*

Raman scattering of light is a quite informative method that allows measurement of the molecules and crystals oscillation frequency. This opens up opportunities for substance identification and research of transformations that occur in it under external influence.

Two intense phonon bands of the first order G and D at ~ 1590 $cm^{-1}$ and 1353 $cm^{-1}$ (Fig. 1) were fixed in the spectra of micro-Raman origin and laser irradiated $TiS_2/C$ samples, whose appearance is caused by one-phonon process of inelastic light scattering on valence fluctuations $sp^2$-bonded carbon atoms and scattering at structure defects, respectively.

The relative integrated intensity of the bands $I_G$ / $I_D$ and their half-width reflect the degree of material structural disordering. In addition, the average size of nanocrystalline carbon regions (nc-C) is proportional to bands $I_G$ / $I_D$ relation and in our case it is 8 nm.

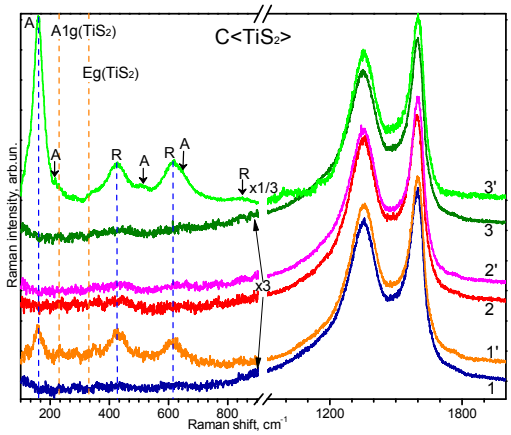


Image 1. Micro-Raman spectra of composite $TiS_2/C$: 1, 2, 3 (1', 2', 3') – pure mechanical mixtures (laser radiated) at a ratio $TiS_2$:C = 10:90, 20:80, 30:70 (%), respectively $\lambda_{зб}$ = 488 nm, T = 300K.

Compared with the original sample for the laser irradiated samples, a decrease of left side of D band at ~ 1208 $cm^{-1}$, whose appearance is caused by mixing $sp^2$-$sp^3$ bonds on the periphery of the crystallites or C-C and C = C valence fluctuations of polyene-like structures.

After laser treatment of $TiS_2/C$ samples new phonon bands are appearing in micro-Raman spectra that are responsible for the inclusion of $TiO_2$ structural phase (Fig. 1 - spectra 1 ', 3'). It is known that the most thermodynamically stable structure is $TiO_2$ with anatase and rutile structure. Anatase structure belongs to the tetragonal symmetry and corresponds to space group symmetry $D_{4h}(I4_1/amd)$. From the group-theoretic analysis it is known that for this structure in Raman spectra there are six active optical modes: $A_{1g}$ (507 $cm^{-1}$) + $2B_{1g}$ (399 $cm^{-1}$ and 519 $cm^{-1}$) + $3E_g$ (144 $cm^{-1}$, 197 $cm^{-1}$ and 639 $cm^{-1}$).

Thus, the local areas with the structure of rutile and anatase in irradiated $TiS_2/C$ composites are formed, and improving the structure of nanocrystalline carbon surface areas.

# The Energy Distribution Changes Of the Valence Electrons of Mixtures x-$SiO_2$ + y- γ -$Fe_2O_3$ Before and After Mechanical Activation

Yavorskyi Y.V.[1], Zaulychnyy Ya.V.[1], Ilkiv V.Ya.[1], Zarko V.I.[2], Karpets M.V.[3], Kotsyubynsky V.O.[4]

[1]*National Technical University of Ukraine "Kyiv Polytechnical Institute", Kyiv, Ukraine*
[2]*Chuiko Institute of Surface Chemistry., Kyiv, Ukraine*
[c] *Frantsevich Institute for Problems of Materials Science, Kyiv, Ukraine*
[d] *Vasyl Stefanyk Precarpathian National University, Ivano-Frankivsk, Ukraine*

Properties of such materials in nano-composites are reciprocally supplemented. Thus, it is important to investigate an electronic structure depending on composition of such nanomaterials and synthesis method. Therefore, it is necessary to study the effect of method mechanical activation on the energy distribution of the valence electrons and charge state of constituent atoms after treatment of iron oxide and silica mixed in different ratios.

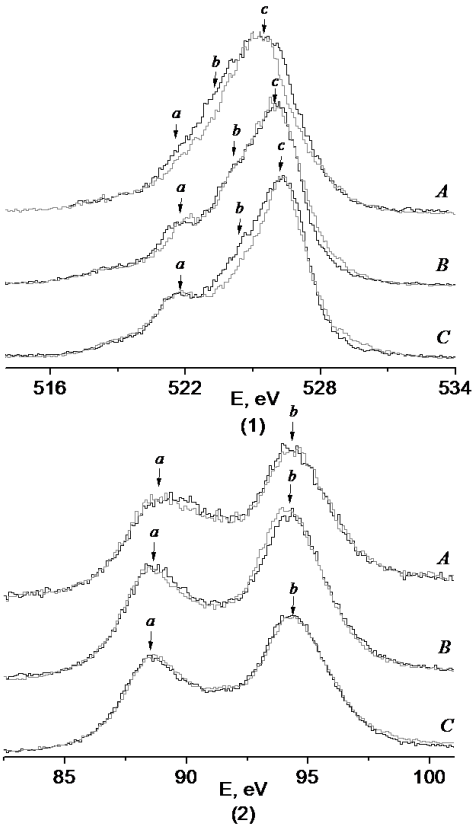


Fig.1. Displacement of contour of the O*K*α -(1) and SiLα-(2) bands after mechanical activation: *a*) 0,2 /0,8, *b*) 0,5/0,5, *c*) 0,8/0,2. Grey lines correspond to the bands of mechanical mixture. Black lines represent the bands of mechanically.

Crystalline and electronic structures of *x*-$SiO_2$+*y*-γ-$Fe_2O_3$ mixtures have been analyzed using X-ray diffraction and ultra-soft X-ray emission spectroscopy. The energy redistribution of Fe*spd*-, Si*sp*- and O*p*-valence electrons due to changes of mass ratio (20/80, 50/50, 80/20) of $SiO_2$ and α-$Fe_2O_3$ initial precursors in mixtures has been studied. The Fe$L_\alpha$-, Si$L_\alpha$-(Fig. 1 (2)) and O$K_\alpha$-(Fig. 1(1)) ultra-soft X-ray emission spectra of $SiO_2$/α-$Fe_2O_3$ mixtures were compared with those of iron oxide and silica powders. During analysis of these bands was detected shape similarity and availability of identical elements of fine structure in OKα and FeLα-emission spectra, whith indicate about high degree of hybridization Op- and Fe3d - valence states of electrons. Expansion OKα and FeLα-emission bands in low energy side is the result of additional splitting energy Op- and Fe3d - levels with increasing degree of hybridization in the mechanical activation processing.

# NGR Investigations of Nanosized Powder of Magnetite

Yuryev S.O., Yushchuk S.I., Dubelt S.P., Loboiko V.I.

*National University "L'vivska Polytechnica", Lviv, Ukraine,*

The fine powder of magnetite $Fe_3O_4$ was obtained by deposition of aqueous solutions of chemically pure More's salt - $Fe(NH_4)_2(SO_4)_2 \cdot 6H_2O$ and $FeCl_3$ to pH = 8.0 using concentrated $NH_4OH$. The fine powders with the particle size from 5 to 25 nm were obtained. Some portions of powders were subjected to heat treatment in air at temperatures of 473, 573 and 673 K.

The NGR spectrum of $Fe_3O_4$ without annealing measured at room temperature in its appearance corresponds to non-stoichiometric magnetite (Fig.1). In the spectrum of this sample for the octahedral and tetrahedral iron ions correspond to sextets with parameter of pure magnetite but these sextets differ of their intensities ratio.

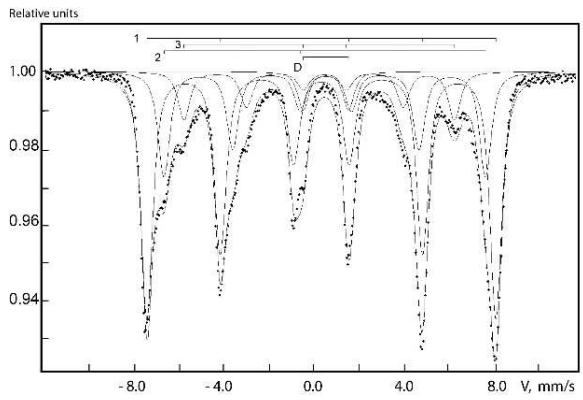


This spectrum was laid out on three sextets and one doublet. The sextet 1 refers to the $Fe^{3+}$ ions which are in tetrahedral positions. The sextet 2 corresponds to ions ($Fe^{2+}$ + $Fe^{3+}$) which are in oxygen octahedral. The intensities of the first and the second sextet differ and are respectively 57.41% and 24.35%.

Fig. 2 shows the NGR spectrum of annealed sample in air at T = 673 K. Compared with the spectrum of not annealing powder the structure of resonance lines is disappeared and their total width is decreased. With the increasing of annealing temperature of nanopowder magnetite in the air, the values of $H_{eff}$ for all sextets increase due to the oxidation of the iron ions and transformation the magnetite ferrite to $\gamma$-$Fe_2O_3$.

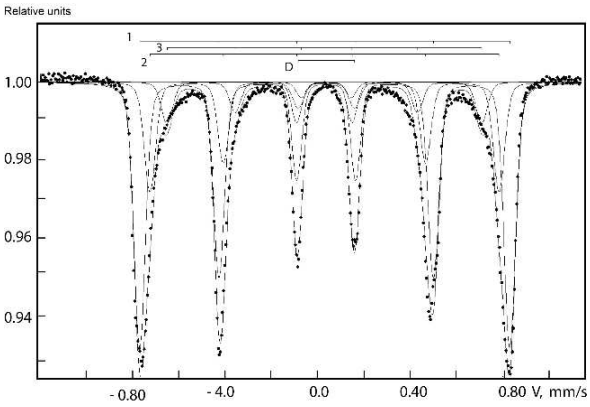


With the increasing of annealing temperature of nanopowder magnetite in the air, the values of $H_{eff}$ for all sextets increase due to the oxidation of the iron ions and transformation the magnetite ferrite to $\gamma$-$Fe_2O_3$.

# Features of Superconductor-Insulator Transition in PbTe/PbS and PbTe/YbS Heterostructures

Yuzephovich O.I.[1,2], Bengus S.V.[1,2], Sipatov A.Yu.[3]

[1]*B.Verkin Institute for low temperature physics & engineering of NAS of Ukraine, Kharkiv, Ukraine*
[2]*International Laboratory of High Magnetic Fields and Low Temperatures, Wroclaw, Poland*
[3]*National Technical University - KhPI, Kharkiv, Ukraine*

Peculiarities of the magnetic field induced superconductor-insulator transition (SIT) in PbTe/PbS i PbTe/YbS heterostructures with different topology of the superconducting interface are investigated. Superconductivity of such $A^{IV}B^{VI}$ heterostructures ($T_c \leq 6.5$K) is determined by the band inversion along the continuous misfit dislocation grid which arises between epitaxial semiconductor layers of a sufficient thickness ($d > 80$nm). While $d$ decreases, the superconducting interface becomes discontinuous, $T_c$ decreases, and conductivity changes from metallic to a semiconductor type [1].

Discontinuity of the superconducting interface is found to be a necessary condition for the magnetic field induced SIT. It has a drastic influence on SIT realization: fan-like set of *R(T)* curves, crossing of *R(B)* curves, maximum on *R(B)* curves and negative magnetoresistance. No sign of SIT found in heterostructures with the perfect interface [2]. So, SIT realization in these heterostructures is determined by the percolation phenomena which are inherent to granular superconductors.

Thus, semiconductor heterostructures of $A^{IV}B^{VI}$-type with the superconducting interface are good model objects for the localized superconductivity effects investigation.

1. O.I. Yuzephovich et al. // *Low Temp. Phys.* – 2008. – v.34. – pp.985-991.
2. S.V. Bengus, A.Yu. Sipatov; S.I. Yuzephovich // *Low Temp. Phys.* – 2013. – v.39. – pp.695-700.

# Classification a New Teoretical Comprehension in Nanotechnology

Zavoiko O.S.

*Chernivtsi Department of NTU "KPI", Chernivtsi, 204A, Ukraine*

Theoretical description and elucidation property condensation surrounings (gas,liguid,firmly body), of departure property compound (atom, molecule) what submit kvantum mechanic [1].

Nanotechnology is complex foundamential and integration science what combination between phisics, chemics, material knowledge, electrotechnical processis in machintool, appara- tus, what direction on through investigation atom-molecule-complex,structure nanomaterial, phisical-chemical processis if sintase, for the obtained nanomanufactured, what worked in micro-opto- electronnomechanics sistems and nanobiorobots.

Nanotechnology include between science [3]:

1. Nanochemy (kvantoom chemi), thet study siutes reaction sistem and inside size efekts.
2. Nanophisical (spintronica, photonica, nanoheterostructure, nanocomposition effect.
3. Nanomaterialization, nanopowder technology, nanoligation, nanobesiege, direct in the complex designer electron-atom nanostructure, chemical nanocomposition for the henceforth task, processing for the process in the condition temperature and radiation influence.
4. Nanoanalise is sistem approach for the definite a basic situation strategic divelopment through nanotechnologyc principls and penetrate element on basic practical science task (work out in nanotechnology nanourans entrich U-238, U-235) [1].

Active plazma electric charge to learn in [2] for the: nanocomposition sistem TiN-AlN, TiN -$TiB_2$, combination SVS and SPS foretell receive nanocompjsition TiN-$TiB_2$ with size grain to 100 nm, firmly Hv = 19 ГПа, crack firm 8 МПа, bend strong – 500 МПа [2].

Especially perspective direction science nanotechnology future is pursuit nanosize effect and appearance in special work out solve design sintese among, create complicated structure, model on conception macro-mezo-pezo-micro-nano-level, and work out on basic new predisposition apparatus, sistem, nanocontact appearance, discavery in new theory(book ) - [3].

1. О.С. Завойко, І.Г. Курек, С.М. Новіков. Теоретичні основи кристалізації та кінетики утворення текстур при термічному розкладі та осадженні з газової фази тугоплавких металів // Науковий вісник ЧНУ, Фізика. Електроніка. вип. 268.
2. А.В. Рагуля Керамические нанокомпозиты на основе тугоплавких нитридов, боридов и карбидов и технологии их изготовления. Тезисы докладов международной конференции MMS-2005. 26-30сент. 2005 г. Киев, с. 643.
3. О.С. Завойко. Теорія міжатомних перетворень покриттів,металів і сплавів фізичного матеріалознавства, Т. 3, Чернівці, « Рута», 2009.

## СЕКЦІЯ 3 (усні доповіді)
## ФІЗИКО-ХІМІЧНІ ВЛАСТИВОСТІ ТОНКИХ ПЛІВОК

12-15 травня 2015 р.

## SESSION 3 (oral)
## PHYSICAL-CHEMICAL PROPERTIES OF THE THIN FILMS

May, 12-15, 2015

# Enhanced Solid-State Solubility of Components in Nanosized Au-Ni Film System

Bogatyrenko S.I., Minenkov A.A., Sukhov R.V., Kryshtal A.P.

*V.N. Karazin Kharkiv National University, Kharkov, Ukraine*

To control structure and properties of binary systems, which are widely used in modern technologies, it's crucial to understand the nature of interaction between components. Such interplay is commonly described by a phase diagram. To this moment, it has been found that main boundaries of a phase diagram shift to lower temperatures with the characteristic size reduction. For instance, eutectic melting temperature lowering and liquidus and solidus lines offset have been predicted for nanosystems. However, there are virtually no reliable experimental data on regularities of formation of solid solutions in binary nanosystems.

In this work we present the results of *in situ* TEM studies of formation of solid solutions in Au-Ni nanoscaled films with entire thicknesses of 140 and 25 nm. This binary is characterized by a cigar-type phase diagram with a minimum and a broad miscibility gap in the solid state at a temperature below 807°C. Besides, the components of the system have the same type of crystal lattice, the parameters of which differ significantly from each other (0.408 nm for Au and 0.3524 nm for Ni). Bilayer film Au (30 ат.%) – Ni was produced in a vacuum of $1 \cdot 10^{-7}$ torr by sequential electron-beam evaporation of the components from independent sources. The components thicknesses ratio corresponded to the composition with the maximum temperature stability of the two-phase region of the phase diagram. *In situ* TEM heating of the film system was performed in the temperature range 20–850°C with a step of 25°C. At each temperature, the film system was maintained for 3–5 min to reach thermodynamic equilibrium. Then, the system state was registered by means of fast electron diffraction and concentrations of solid solutions were calculated according to the Vegard's rule. Electron diffraction studies during *in situ* TEM heating of the layered films also enabled to trace the kinetics of solid solutions formation in a wide temperature and concentration ranges.

In summary, as a result of performed investigation the curve bounding the two-phase region in solid state on the phase diagram was sketched for Au-Ni film with entire thickness of 140 nm. It was shown that obtained data are in good agreement with published data. Moreover, it was found that the formation of solid solutions based on nickel and gold occurs immediately throughout the entire film thickness during heating. For the system with the thickness of 25 nm the two-phase region on the phase diagram narrows and shifts to lower temperatures. This fact clearly indicates an increase in the mutual solubility of the components with in the characteristic size reduction.

# The Studies of Chemical Etching Processes of Highly Radiation Stable $Hg_3In_2Te_6$ Single Crystals for Applying Thin Films Coatings for Schottky Diode

[1]Diychuk V.V., [1]Dremlyuzhenko S.G., [1]Rarenko A.I., [1]Yuriychuk I.M., [1]Tsaly V.Z., [2]Ziółkowska Dorota, [2]Shyichuk Alexander

*[1]Chernivtsy National University, Ukraine*
*[2]UTP University of Science and Technology, Bydgoszcz, Poland*

Semiconductor $A_2^{III}B_3^{VI}$ group crystals and based on them solid solutions have extremely high radiation resistance and electrophotovoltaic parameters to X-, γ-, β- and neutron radiation. The most successful in this area is creation, study and application of semiconductor crystals based on solid solutions of $A_2^{III}B_3^{VI}$ and $A^{II}B^{IV}$ chemical compounds, including composition having a fixed melting point. Among them most attractive is $Hg_3In_2Te_6$ compound (MIT). We have obtained single crystals of MIT solid solution and found that the material consists of $Hg_3In_2Te_6$ phase with lattice parameters $a$=6,2900 Å. It is known that there are unoccupied In sites (stoichiometric vacancies) in $A_2^{III}B_3^{VI}$ group single crystals whose concentration is independent of temperature. These vacancies capture alloying impurities and keep them in an electrically neutral state. This property does not allow to create a simple p-n junction, so we have designed Schottky diodes and photodiodes on MIT substrates. Another feature of MIT crystals with stoichiometric vacancies is low density of surface states that requires special treatment of substrate surface during the formation on it metal thin film coatings or $In_2O_3{\cdot}SnO$ degenerate semiconductor films for Schottky diodes.

The studies of the parting border surface–etchant effectively use the thermodynamic analysis method – the method of Pourbaix diagram. As a result of the construction and analysis of the Pourbaix diagram a prediction of chemical composition of anodic oxide films on $Hg_3In_2Te_6$ surface have been done, and optimum conditions for polishing and selective etching were found. The upper limit of the thermodynamic stability of $Hg_3In_2Te_6$ solid phase line is determined by equilibrium potential in the range from -0.459 V to -1.227 V. The nature of the electrode reactions at each region depends on pH, redox potential and system activity of ions which determine the potential. Optimal conditions for chemical and electrochemical etching, surface oxidation and sulphidation of $Hg_3In_2Te_6$ crystals have been found. Thin film Schottky diode structures, which can be used as near infrared, visible and X-, γ- radiation photodetectors, have been developed on this material.

# Nontrivial damping of ferromagnetic resonance in nanocomposites $Co/Al_2O_3$

[1]Dmitriev A.I., [1]Lashkarev G.V., [1]Radchenko M.V., [1]Bugaiova M.E., [1]Slynko E.I., [1]Timofeeva I.I., [2]Knoff W., [2]Story T.,

*[1]I.M. Frantsevych Institute for Problems of Material Science, National Academy of Sciences of Ukraine, Kyiv, Ukraine*

*[2]Institute of Physics, Polish Academy of Sciences, Warsaw, Poland*

Ferromagnetic nanocomposites (FMNK) $Co/Al_2O_3$ with the Co nanoparticles (NPs) content 41% were grown on the polycor substrates using the laboratory single-chamber electron-beam facility. Ferromagnetic resonance (FMR) studies were performed on a Bruker spectrometer (9,4 GHz) in the temperature range T = (3÷270)K. Amplitude (A) damping for FMR signal lowers with decreasing temperature until it disappears at T ~ 60K, as well as reducing the experimentally determined resonant magnetic field $H_R$.

The resonance condition in inhomogeneous media is the following

$$h\nu=\mu(g + \Delta g)(Hr + \Delta H)$$

where μ - Borr magniton, Δg - correction due to an influence of disturbing factors, ΔH - internal magnetic field.

| T, K | $H_R$, KOe | A, abr.un. |
|---|---|---|
| 261 | 5.63 | 16 |
| 231 | 5.56 | 15 |
| 202 | 5.41 | 14 |
| 161 | 489 | 8 |
| 125 | 3.81 | 6 |

For cobalt g≅ 2 it appears $H_r$ = 3.3 KOe, what is much lower than its experimental values $H_R$ (see. Table.). The temperature variation of g is very small Δg << g. Consequently, there is an internal magnetic field, and temperature-dependent violation for resonant precession of the magnetic moments. The reason for this is the interaction of ferromagnetic NPs with their antiferromagnetic CoO shell. The Neel temperature ($T_N$) for bulk CoO is 291K, but it is strongly dependent on NPs size. For example the low width of CoO shell about 2 nm has $T_N$ = 55K. It is supposed that NPs dispersion determine the smooth damping FMR.

The presence of CoO in FMNK evidenced by our researches: X-ray analysis; bend type temperature dependence of the thermoelectric power. The existence of antiferomagnetic CoO shell also was confirmed by "exchange bias" of the hysteresis loop and the asymmetry of the angular dependence of $H_R$.

Therefore nontrivial FMR damping with decreasing temperature is due to the conflict of ferromagnetic Co NPs and their antiferromagnetic cobalt oxide shells.

# Thermoelectric Properties of Thin Films of Pure and Doped Tin Telluride

Dzundza B.S.

*Vasyl Stefanyk Precarpathian National University, Ivano-Frankivsk, Ukraine*

Tin Telluride widely used in the semiconductor technology. It is a promising thermoelectric material for the region of average temperatures (500-750) K. Getting the thin film material greatly expands the range of the practical applications. Before now, the problem of stability over the time of the electrical parameters remains completely unresolved.

In this paper, the patterns of change thermoelectric parameters of pure and doped Tin Telluride films, which are obtained from the vapor phase thickness on the mica and the sital substrates, are investigated.

Tin Telluride films are characterized by a large concentration of the holes, which for the thick films reach the value of $10^{20}$ $cm^{-3}$, and with decreasing of the thickness increases by more than an order of magnitude. This behavior of the concentration dependences is related with the oxygen adsorption and it diffusion into the interior of film. The conductivity and the Seebeck coefficient increases significantly with the decreasing of the film thickness and reaches values of 5 $10^3$ $Ohm^{-1}$ $cm^{-1}$ and 70 mV/K. It is providing high values of thermoelectric power $S^2\sigma \approx 20$ $mW/K^2cm$. Thick films have a much lower values of the thermoelectric parameters $\sigma$ = 1,5 $10^3$ $Ohm^{-1}$ $cm^{-1}$ and S = 20 mV/K, $S^2\sigma \approx 0{,}5$ $mW/K^2cm$.

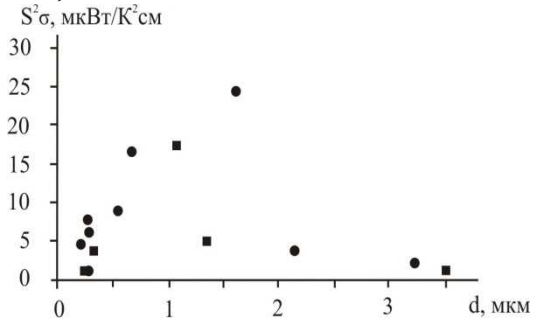


Fig. 1. The dependence of the thermoelectric power $S^2\sigma$ from the thickness d of the films SnTe:Sb. ● – films, which are obtained on the fresh cleavages of mica, ■ - film, which are obtained on the sital substrates.

For the samples, which are doped Stibium, the conductivity of films and the Hall carrier concentration decreases sharply at low thicknesses, and the Seebeck coefficient for the film of the thickness less than 250 nm is 5 times bigger than for the thick. But it is not enough to offset the sharp decline of the conductivity. Therefore, the thermoelectric power ($S^2\sigma$) is observed the maximum in the thickness 1-1.5 μm (Fig. 1) which reaches 25 $mW/K^2cm$.

# The influence of silicon on the boride coatings formation

Fedorenkova L.

*Dnepropetrovsk national University, Dnepropetrovsk, Ukraine*

The peculiarity of the diffusion zone structure, consisting of boride needles, placed in a more plastic matrix of silicide phases, cause high wear resistance borosilicate coatings on steels. With increasing of the silicon-containing component in the saturating **mixture**, the thickness of the diffusion layer decreases. In addition, the increasing of the silicon alloying in the diffusion layer leads to the formation of a significant number of fragile silicide phases distributed under boride, boride and over boride areas and to the stratification of borides borosilicate layer and reduce its strength.

In the work an influence of silicon on the boride coatings formation on steel at chemical-thermal treatment (ChTT) in the powder **mixture** containing boron, molybdenum and silicon are investigated.

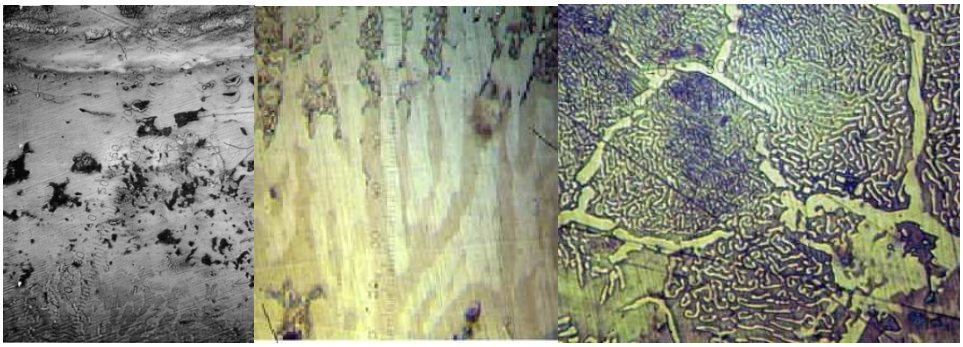

a) x250 b) x1000 c)x1000

Fig. 1 The microstructure of the diffusion layer on steel after ChTT.

The diffusion layer with depth from 400 to 550μm (Fig.1, a), including branched boride layer with formation of eutectoid (Fig. 1, b) and the underlayer, with the typical structure for concentration inhomogeneity peritectic of Fe-C-Si-B with the possible presence of Mo (Fig.1, c) are formed in the saturation. The layer contains inclusions with microhardness of 15-16GPa, and, in addition, the zone with depth of 10-20 μm and hardness of 6,6 GPa formed on the border with matrix. Besides diffusion of the components (Mo, Si) in the diffusion layer is their redistribution in the newly formed boride phase according to the principle of least action. At this stage of saturation microinclusions of iron compounds with diffusate (double and triple phase) located mainly on the boride phase (FeB) boundaries and interphase boundaries are formed.

Thus, the presence of silicon and molybdenum in the saturating mixture produces on the surface of the steel a multiphase composite structure of microcrystalline inclusions of compounds Si and Mo with boron and iron that provides high hardness and heat resistance, resistance to brittle fracture, wear resistance in a wide temperature range.

# Orientation peculiarities vapor-phase condensation PbTe-$Bi_2Te_3$ on substrates of mica and pyroceram

Freik D.M., Saliy Ya.P., Bylina I.S., Lishchynskyy I.M.

*Vasyl Stefanyk Precarpathian National University, Ivano-Frankivsk, Ukraine*

Thanks to its unique properties nanostructured materials occupy a leading position in modern materials science. To create a new semiconductor devices find increasing application multicomponent solid solutions, allowing quite widely varied the parameters of the material. In particular, solid solutions on the basis of lead telluride have proved as useful industrial materials that can be widely used in thermoelectricity. It is important to study the structural characteristics of thin-film condensates solid solutions based on Lead Telluride. It is important to study the structural characteristics of thin-film condensates solid solutions based on Lead Telluride.

By methods of atomic-force microscopy and computer simulations we investigated the effects of orientation and crystallographic form of nanocrystals in vapor-phase condensates of solid solutions PbTe-$Bi_2Te_3$, grown for fresh cleavages (0001) of mica-muscovite and pyroceram by open evaporation in a vacuum at various deposition time ($\tau$ = 15 - 75 s) and the optimal temperature evaporation $T_V$ = 970 K and deposition $T_S$ = 470 K.

We researched the obtained samples with atomic force microscope (AFM) Nanoscope 3a Dimention 3000 (DigitalInstruments USA) in the periodic contact mode. Measuring was conducted in the central portion of samples using serial silicon probes NSG-11 with a nominal tip radius of up to 10 nm.

For the first time based on the analysis of averaged azimuth angles of nanocrystals by discrete transformation methods and the use of the autocorrelation function we determined the dominance of figures, symmetrical to axes of the 6-th and 3-rd order which in most cases are coordinated between themselves and are always coordinated with the figures that have symmetry of the 4-th order.

On the basis of normal distributions for averaged radial angles of nanocrystals for the first time we defined the correlation of steep and gently sloping crystallographic forms of cubic system nanocrystals, their orientation and mutual consistency. We found out the prevalence of planes {110}, {123}, where their relative contribution depends on the time of deposition of the pair on the substrate (thickness of condensates).

Determined that the substrate of pyroceram does not provide a particular orientation of crystallites, and the surface of the samples generated objects formed by planes rhombic dodecahedron and the cube and their combinations.

*This research is sponsored by NATO's Public Diplomacy Division in the framework of "Science for Peace" (NATO SPS 984536)).*

# Electrical diagnostics of h-k dielectrics on InGaAs

[1]Gomeniuk Y.Y., [1]Gomeniuk Y.V., [1]Nazarov A.N., [2]Nazarova T.M.,
[3]Monaghan S., [3]Cherkaoui K., [3]O'Connor É., [3]Povey I., [3]Hurley P.K.

*[1] ISP NAS of Ukraine, pr. Nauky 41, Kyiv, Ukraine,*
*[2] NTUU "KPI", Dep. General and Neorganic Chemistry, Kyiv, Ukraine*
*[3] Tyndall NI, Lee Maltings, Prospect Row, Cork, Ireland*

Using of thin high-κ dielectric film materials in conjunction with III-V substrate is highly required for future progress and improvement of MOSFET performance in high speed logic and RF applications. In this work we present results of a study focused on electrical properties and determination of transport mechanism through dielectric layer in $Pd/Al_2O_3/In_{0.53}Ga_{0.47}As/InP$ MOS system.

In the devices under study high-κ $Al_2O_3$ oxide layer was formed by atomic layer deposition (ALD) of nominal physical thickness $t_{ox}$ of 5, 10, 15 and 20 nm. The top Pd gate metallization was obtained by a shadow mask process. The samples received no post-metallization annealing treatment. Samples with both *n*(S)- and *p*(Zn)- type doped ($4x10^{17}cm^{-3}$) $In_{0.53}Ga_{0.47}As$ epitaxial layers were characterized by capacitance-voltage (*C-V*), current-voltage (*I-V*) measurements over the temperature range of 100 – 300 K using an Agilent E4980A Precision LCR meter and Agilent 4156C Precision Semiconductor Parameter Analyzer.

The similarity of the *J-V* curves for both types of the substrates and the general shape of the characteristics are consistent with a current transport mechanism governed by electron tunneling through the triangular potential barrier at the metal-dielectric or semiconductor-dielectric interface. In both cases, the current can be described by Fowler-Nordheim (FN) tunneling mechanisms. For the case of electron tunneling from the metal electrode, the barrier height, $\varphi_B$, is the same for the 10, 15 and 20 nm thick dielectric and equals to 2.40±0.10 eV. For the electron tunneling from the semiconductor, 10 nm thick dielectric gives the barrier height $\varphi_B$ =2.50±0.06 eV. This value represents the conduction-band energy offset at the $Al_2O_3$/InGaAs interface. The increase of the h-k dielectric thickness results in decrease of the burrier heigth.

Analysis of the *C-V* characteristics has demonstrated that $Al_2O_3$ deposited by ALD on $In_{0.53}Ga_{0.47}As$ surfaces exhibits a fixed positive charge distributed throughout the oxide. This positive charge would modify the barrier at the injecting interface resulting in an apparent reduction in the barrier height with increasing oxide thickness. It was found that no degradation and non-reversible charge trapping in the dielectric occurred. The evidence of the positive charge trapping also could be found from the shift of H-F *C-V* curve toward negative biases. Samples with thicker $Al_2O_3$ oxide demonstrate larger $V_{fb}$ shift thus, the more charge captured in the oxide.

The model of the $Al_2O_3$/InGaAs transition layer transformation during the ALD process is proposed.

# Features of adsorption and electrical properties of nanostructured composites based on porous silicon and metal/oxide nanoclusters

Gorbanyuk T.I., Litovchenko V.G., Solntsev V.S.

*V. Lashkaryov Institute of Semiconductor Physics, National Academy of Science of Ukraine, Kiev, Ukraine*

In this paper we present the results of studies of nanoporous silicon matrix with incorporated copper and copper oxide nanoclasters. It is known that the surface of freshly produced porous silicon covered by layer of hydrides silicon. During storage of the structures or thermal treatments in air is a gradual oxidation of the pore surface and replacement hydride layer on oxide. It was found that this layer greatly influences on the pore filling by copper nanoclusters. The copper doped porous silicon was realized by means of electrolysis deposition method. The morphology of surfaces has been researched by means of scanning electron microscopy. This method allows to estimate that the electrolysis deposition copper on porous silicon surface has appearance of clusters. The copper distributing on depth porous silicon was investigated by second ion mass spectroscopy (Fig. 1). It can be seen during the electrochemical method for pore filling have been observed an accumulation of copper at the interface $Si_{por}$/Si (Fig.1). The morphology of silicon composite was characterised by atomic force microscopy (AFM) and scanning electron microscopy (SEM). The infra red (IR) spectroscopy was used for elemental analysis of gas sensitive composite. It was also found nanoporous silicon doped by Cu and/or $CuO_x$ demonstrates the enhanced adsorboelectric effects in the semiconductor-layered structures. In this case the using of thin catalytic composite metal/Sipor films with d- and sp- metals (Cu, Pd, W) leads to the enhanced adsorption activity and stability to oxidation and ageing process. The physical mechanism has been proposed for explain the observed phenomena. A model based on the combination of hopping and tunneling mechanisms of charge transfer have been proposed.

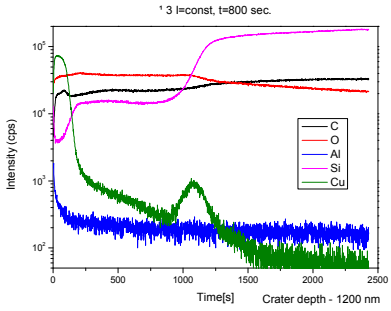


Fig. 1. Second ion mass spectroscopy: distribution of copper in the structure $Si_{por}$/Si at electrochemical method filling the pores by the metal clusters

Our research has been focused on the preparation and characterization of layered semiconductor structures based on nanoporous silicon ($Si_{por}$) with embedded clusters of catalytic (Pd, W) and/or noncatalytic (Cu) metals and its oxides ($CuO_x$, $WO_x$) by means of current-voltage (I-V) characteristics and high-frequency C(V) method under the adsorption of $H_2$ and $H_2S$ gases. To uniformly pore filling by metal clusters the thin metal (Pd, Cu, W) films were deposited on the surface of the porous silicon using the magnetron deposition technique at room temperature followed by annealing at 673-873 K in argon during 30-40 min. The distribution of catalytically active metal on the film thickness of porous silicon was studied by the secondary ion mass spectroscopy (SIMS). It can be seen that copper and copper oxide uniformly distributed in the porous silicon layer. The morphology of silicon composite was characterised by atomic force microscopy (AFM) and scanning electron microscopy (SEM). The infra red (IR) spectroscopy was used for elemental analysis of gas sensitive composite.

It was found that the thin film structures with porous silicon filled by palladium and copper clusters are more sensitive to hydrogen, while the filling of the pores by W and $WO_3$ clusters leads to increased sensitivity to hydrogen sulphide. The physical mechanism has been proposed for explain the observed phenomena. A model based on the combination of hopping and tunneling mechanisms has also been proposed to explain the charge transfer in such structures.

# Electrophysical properties of indium doped $As_2S(Se)_3$ thin films

Grytsyshche I.V., Loya V.Yu.

*Institute of Electron Physics, Ukr. Nat. Acad. Sci., Uzhhorod, Ukraine.*

Amorphous arsenic chalcogenides $As_2S(Se)_3$ are well-known semiconductor materials which, being exposed to light of appropriate energy and intensity, often undergo changes of electronic and atomic structure, composition, phase, physical and chemical properties generally known as photoinduced effects. These changes can be reversible or irreversible and have led to extensive applications of amorphous chalcogenides, the most well known of them being related to optical data storage as well as xerography, photovoltaic and photoconductive elements, laser printers, light-sensitive camera tubes, high-speed optical switches, X-ray radiography, etc. It is known that optical and electrical properties of amorphous $As_2S_3$ and $As_2Se_3$ can be noticeably modified by doping. Moreover, in an amorphous chalcogenide with a high dopant content one can also expect photoinduced phase separation when part of the material crystallizes in a surrounding amorphous matrix [1, 2].

In-doped $As_2S(Se)_3$ films with In content $x$ ranging from 1 to 5 % were obtained by thermal vacuum evaporation from two independent tantalum evaporators on glass substrates at the temperature of 500–550 K for In and 1050–1100 K for $As_2S(Se)_3$. The deposition rates were 3–5 nm/s. Electrophysical studies in the interval 293–373 K were performed by dc measurements on a standard resistance ($R_e$) connected in a series with the sample.

The temperature dependence of the resistance of $As_2S(Se)_3$:In thin films is proved to depend significantly on the modifier concentration. It is shown that the activation energy decreases with In content ($1 \le x \le 5$ %) for $As_2Se_3$:In in the range of 1.5÷1.47 eV and for $As_2S_3$:In the interval of 1.6÷1.53 eV. I-V characteristics of the dark current and the current under the illumination of $As_2S(Se)_3$:In films were investigated. The values of conductivity under illumination and in the darkness are not set instantaneously, but with a certain relaxation time. This relaxation effect can be explained by possible accumulation of charge on the defect levels. Possible mechanisms of photoelectric memory in $As_2S(Se)$:In thin films are discussed.

1. Ke. Tanaka, K. Shinakawa, *Amorphous Chalcogenide Semiconductors and Related Materials* (Springer, Berlin, 2011).
2. T. Ohta and S.R. Ovshinsky, *Phase-Change Optical Storage Media*, in: *Photo-Induced Metastability in Amorphous Semiconductors*, edited by A.V. Kolobov (Wiley-VCH, Weinheim, 2003), 310.

# Structure and thermoelectric properties of the vapor-phase condensation LAST on the ceramics

Jaworski R.S.

*Vasyl Stefanyk Precarpathian National University, Ivano-Frankivsk, Ukraine*

LAST compounds, which are based on PbTe, recently attracte the attention through the considerable sensitivity of their thermoelectric properties to the chemical composition and the ability to obtain n- and p-type conductivity [1,2]. The thin-film material through the impact of the structure, surface, thickness on the transport phenomena, all of these greatly extend useing of the LAST compounds. There are investigated the patterns of changing the thermoelectric parameters and features of the carrier scattering in vapor-phase structures on the ceramics $Pb_{18}Ag_{2-x}Sb_xTe_{20}$ from their thickness in this work.

Based on AFM-images the depending on the size of nanocrystals of conductivity and carrier mobility in the thin film, which are based on the compounds LAST $Pb_{18}Ag_{2-x}Sb_xTe_{20}$ are researched according to their thickness and chemical composition.

Established that electrical conductivity (σ) of the thickness (d) increases for all of these structures. The small values of the conductivity (σ) and the Hall's mobility (μ) with the substantial concentration of n-type carriers (n ≈ 1019 cm -3), were caused by the phase inhomogeneity of the condensate: there were not only PbTe but Sb8Te3 and Sb. The current carrier mobility (μ) of the condensates adequately replaces with a thickness (d): slightly increases with d.

The average length of free path of the current carriers and their mobility are determined at presence scattering on the surface and the intergrain limits of the nanocrystals. It is shown that the dominant carrier is scattering carrier on the surface, not on the intergrain limits, due to its huge size of the nanocrystals in the thin film structures.

The thermoelectric parameters of the surface layer is defined and the significant quantities of their Seebeck's coefficient is found by using Petrits's model.

*This research is sponsored by NATO's Public Diplomacy Division in the framework of "Science for Peace" (NATO SPS 984536)).*

1. K. F. Hsu et al., Science 303, (2004), 818.
2. H. Wang et al., Appl. Phys. Lett. 88, (2006), 092104

# The photoelectric characteristics of thermally oxidized macro porous silicon structures on the intensity of incident light.

Karachevtseva L.A., Onyshchenko V.F., Karas' M.I., Lytvynenko O.O., Stronska O.J., Parshin K.A., Konin K.P.

*Lashkaryov Institute of Semiconductor Physics of NAS of Ukraine, Kyiv, Ukraine*

We investigated the samples of thermally oxidized macroporous silicon structures characterized by the [100] orientation, the thickness H=500 μm, the n-type of conductivity, the specific resistance of 4.5 Ω×cm. The macropores had the diameter $D_p$=1-6 μm, the depth $h_p$=40-100 μm, the distance between the pores of *a*-$D_p$=1-4 μm. The silicon oxide layer is equal to 15 nm.

If the concentration of electrons at the surface states increased (see figure, its reciprocal quantity decreases) then decreases the concentration of electrons in the conduction band and the photoconductivity of macroporous silicon structure.

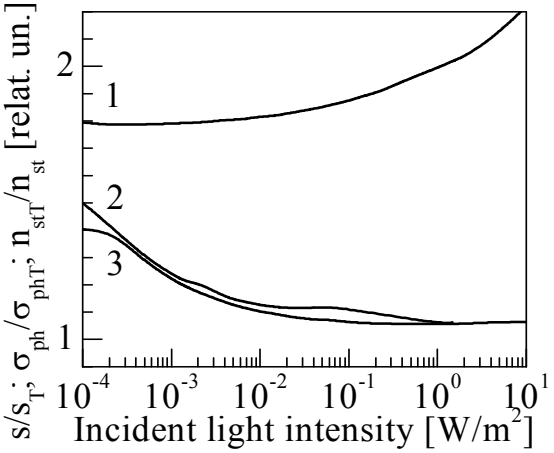


Fig. The calculated dependencies of the thermally oxidized of sample relative of the initial sample: the surface recombination velocity 1, the photoconductivity 2, the reciprocal of the density of filled acceptor surface states 3 on the intensity of incident light (λ = 0.95 micron).

We see from the figure that the photoconductivity of macroporous silicon structures depends inversely proportional on the density of filled acceptor surface states because the curves 2 and curves 3 almost coincide. The increases in surface recombination velocity can also result in decrease in photoconductivity.

It was found that an increase in the photoconductivity of thermally oxidized samples of macroporous silicon structures relative to the initial samples, with an increase in the intensity of the incident light, is connected with the decrease in the number of electrons on the surface levels on the surface of macropores.

1. Onyshchenko V.F., Karachevtseva L.A. Conductivity and photoconductivity of two-dimensional macroporous silicon structures // Ukr. J. Phys. – 2013. – Vol.**58**, №9. – P. 846–852.

# Structure and Morphology of Metal Films on Silicon Monocrystalline Surface

Koman B.P., Kulik B.Ya., Rovetskii I.M.

*Ivan Franko Lviv National University, Lviv, Ukraine*

Thin metal films were thermally deposited on the surface of monocrystalline silicon. It's structural features were investigated by ACM technique with Solver P47PRO. Structural features such as surface morphology, surface profile, geometrical sizes of nanocrystals and other parameters were conducted for metal films with thicknesses *d*: 2,5 nm, 10 nm, 50 nm, 100 nm, deposition rate 0,8 nm/c. Surface profile of all metal films is characterized by random topography and granularity hierarchy. Most probable growing mechanism for all metal films is Folmer-Weber mechanism. In particular, at start condensation during nucleation of metal film new phase is formatting as columnar pyramids with diameters 20-40 nm and height 10-15 nm. After Cu and Al metal films formation process is finished the distinctions between it's surface morphology become unnoticeable. The surface profile heights of all metal films demonstrate stochastic irregularity without any laws during thickness growth. Thin chromium films have significantly different surface morphology. At a minimum thickness randomly placed nanoobjects with pyramidal geometry the average distance between them 2-3 nm is observed. But most exotic phenomena is existents of clear and almost cylindrical nanovoids for thickness $d_2$ with average depth 1 to 4 micrometers. They reach the surface of substrate it's diameter around 2 nm and they are located at a distance 2 nm. With increasing of film thickness such peculiarities disappears after that the series of pyramid like columnar nanostructures with specific sizes is occurred. With surface morphology and profile investigation of thin metal films the statistical analysis of cluster images wich obtained by the standard method of cut on certain height. For numerical description of the clusters the Hoshena-Kopelmana algorithm were used. The statistical investigation of average distances between clusters showed that for Cu films that average distances is around 40-60 nm. With father increasing of film thickness the average distances do not change dramatically 51-56 nm. In the case of Al metal films we observe greater statistical dispersion and greater value of distances up to 170 nm but average distances approximately 52-90 nm. The Cr films demonstrate greater statistical dispersion in comparison with Cu and Al film but distances can reach up to 1300 nm. The average distances between closest clusters significantly increases up to 495-747 nm. Abnormally low value of surface inhomogeneitys observer for Cr films - 5,5 nm in comparison with Cu films that value is 0,3–0,4 micrometer. The surface morphology parameters of investigated metal films on silicon substrate first of all depend on thermalization of film created particles. It's depend on distinctions of the energy dissipation kinetics of molecular beam of specific metal for it's transition from strongly nonequilibrium state on substrate in metastable film state and peculiarities of interfacial interaction in the system of condensate-substrate. Those phenomena are characterized by energy and adhesive parameter such as: interfacial energy – $\gamma_m$, interfacial tension – $\sigma_m$, adhesion work – $A_{ad}$ and adhesion energy – $\gamma_{ad}$ in "metal-silicon" system.

# The Optic Absorption Spectra of Polytoluidine Thin Films Doped With Inorganic Nanoclusters

Konopelnyk O.I., Aksimentyeva O.I., Horbenko Yu.Yu., Savytsky N.S.

*Ivan Franko National University of Lviv, Lviv, Ukraine*

The development of nanotechnology attaches great importance to research materials that combine several functions, including "own" conductivity, optical absorption, touch sensitivity with flexibility, ease plasticity of polymers. Among these materials actively investigated conjugated polymers – polyaniline and their derivations: polytoluidine, polymethoxianiline and others. Manage of the optical and the electrical properties of these polymers is possible by doping with nanoparticles of different nature. In work, the features of the absorption spectra of polyorthotoluidine (PoTI) films doped by nanosilver (Ag), ferric chloride ($FeCl_3$) and complex $K_3$ [Fe $(CN)_6$] were studied.

The optical absorption spectra of PoTI are characterized by three bands. The first peak at a wavelength of 320 – 340 nm corresponds to π-π* transition in polyaminoarene band gap. Absorption in the 620 - 650 nm can be attributed to the n-π* transition in the amino-quinoid fragments in the polymer system. Absorption at $\lambda >$ 800 nm due to the presence of charge carriers of the polaron type which form own polaron zone [1].

It is shown the significant changes of optical absorption of PoTI-Ag films in comparison with the spectrum of undoped PoTI. The decreases of intensity and half-width of π-π* transition band, the appearance of the absorption band with a maximum at 612 nm and leveling bipolaron broad band in the 800-950 nm were observed. These changes can be explained by the interaction of silver nanoparticles with a polymer chain, and at high levels of doping - plasmon resonance [2].

The doping of PoTI films with ferric chloride can be explained by the mechanism of recovery acceptor doping of Fe (3+) to Fe (2+). In this case can form a complex with charge transfer by $[PoTI]^+$ $[FeCl_4]^-$ type, which leads to an increase in intensity of the first absorption band. Introduction to the PoTI film of $K_3[Fe(CN)_6]$ complex causes the increase an intensity of the band at 620 nm and the disappearance of absorption induced by delocalized charge carriers.

The received results show a possibility to predict and control the optical properties of polyaminoarenes thin films using doping level and nature of dopant.

1. Konopelnyk O.I. Aksimentyeva O.I. Thermochromic effect in conducting polyaminoarenes // Photoelectronics. - 2011. - V.**20**, - P. 18-22.
2. Choudhgury A. Polyaniline/silver nanocomposites: dielectric properties and ethanol vapour sensitivity // Sensors and Actuators B. - 2009. - V.**138**, - P. 318-325.

# Radiation Spectrum of Electrons Moving Along a Spiral in Medium

[1]Konstantinovich A.V., [1,2]Konstantinovich I.A.

*[1]Chernivtsi National University, Chernivtsi, Ukraine*
*[2]Institute of Thermoelectricity, National Academy of Sciences and Ministry of Education and Science of Ukraine, Chernivtsi, Ukraine*

The time-averaged radiation power $\overline{P}^{rad}$ of sequence of electrons moving one by one along a spiral in transparent medium can be calculated by the instrumentality of spectral distribution $W(\omega)$ [1]

$$\overline{P}^{rad} = \int_0^\infty W(\omega)d\omega,$$

$$W(\omega) = \frac{2e^2}{\pi c^2}\int_0^\infty dx\mu(\omega)S_N(\omega)\omega\frac{\sin\left\{\frac{n(\omega)}{c}\omega\eta(x)\right\}}{\eta(x)}\cos\omega x\left[V_\perp^2\cos(\omega_0 x)+V_\parallel^2-\frac{c^2}{n^2(\omega)}\right],$$

where $\eta(x)=\sqrt{V_\parallel^2x^2+4\frac{V_\perp^2}{\omega_0^2}\sin^2\left(\frac{\omega_0}{2}x\right)}$, $\omega$ is the cyclic frequency, $r_0 = V_\perp\omega_0^{-1}$, $\omega_0 = ec^2B^{ext}\widetilde{E}^{-1}$, $\widetilde{E} = c\sqrt{p^2+m_0^2c^2}$, the magnetic induction vector $\vec{B}^{ext}\|0Z$, $V_\perp$ and $V_\parallel$ are the components of the velocity, $\vec{p}$ and $\widetilde{E}$ are the momentum and energy of the electron, $e$ and $m_0$ are its charge and rest mass, respectively, $\Delta t_l$ is the time shift of the $l^{th}$ electron, $c$ is the velocity of light in vacuum.

In the case of sequence of electrons moving one by one along a spiral the coherence factor $S_N(\omega)$ takes the form:

$$S_N(\omega) = \sum_{l,j=1}^{N}\cos\left\{\omega\left(\Delta t_l - \Delta t_j\right)\right\}.$$

The oscillations [1] in the spectral distribution of radiation power of the one, two, three, and four electrons are founded and studied for the case when the transversal component of velocity (perpendicular to the magnetic induction vector) is bigger than the light phase velocity ($V_\perp > c/n(\omega)$) in the medium.

For the small time shifts between electrons, in radiation spectra of two, three, and four electrons moving along the spiral in vacuum and in transparent medium we have found the existence of the coherent radiation of harmonics with $S_N(\omega)=N^2$ ($S_N(\omega)$ is the coherence factor of $N$ electrons). The conditions at which the radiation power for these systems tends to zero are analyzed [1].

1. Konstantinovich A.V., Konstantinovich I.A. Fine Structure of Radiation Spectrum of System of Electrons Moving in Spiral in Medium // Romanian Reports in Physics. – 2014. – V. 66, No 2. – P. 307–318.

# Passivation Properties of Nanostructured SiC Films on Silicon

Kostylyov V.P., Chernenko V.V., Slusar T.V., Vlasyuk V.M., Korkishko R.M., [1]Semenov O.V.

*V.E. Lashkarev Institute of Semiconductor Physics, Kyiv, Ukraine*
*[1]Institute for Single Crystals, National Academy of Sciences of Ukraine, Kharkov, Ukraine*

In order to reduce the recombination and optical losses in silicon solar cells special passivation layers are applied on their front surface. These layers reduce the effective surface recombination velocity $S_{ef}$. In the work the passivation properties of nanostructured SiC/Si heterojunctions were experimentally investigated. The SiC films were formed on the front surface of silicon substrate using direct ion deposition method [1].

The thickness of the SiC film on Si substrates varied in the range from 0.1 to 4 μm. The structure and composition of nanostructured SiC films varied in a controlled manner. We investigated the spectral dependence of short circuit photocurrent and open circuit voltage of samples nc-3C-SiC, (-3C-SiC) 80% + nc-Si (~10%), (nc-3C-SiC, nc-21R-SiC) 80%+nc-Si (~10%), (nc-3C-SiC, nc-21R-SiC) 80%+nc-Si (~10%) and (nc-3C-SiC) 70%+nc-Si (~20%) with inclusions of amorphous phase.

The photocurrent and small signal open circuit voltage spectral dependencies at constant monochromatic power mode in the wavelength range 400...1200 nm were measured on the experimental SiC/Si samples.

It was experimentally shown that the effective surface recombination velocity $S_{ef}$ on silicon surface coated with nanostructured SiC film have minimum value in the case using film (-3C-SiC) 80% + nc-Si (~ 10%) annealed in air.

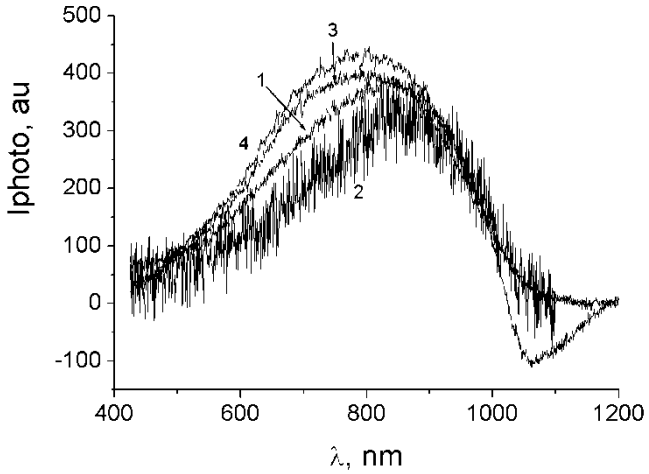


Fig. 1 Experimental spectral dependencies of short circuit photocurrent (1-3) i and open circuit voltage (4) heterojunction SiC/Si samples 7354.10 (1), 7356.10 (2), 7368.10 (3,4).

1. Semenov A.V., Puzikov V.M. at all. Low-temperature fabrication of silicon carbide films of different polytypes. *Semiconductors*, **43**, 5, (2009), 685.

# The Surface Influence to the Thermoelectric Properties of Vapor-Phase Condensates LAST Pb-Ag-Sb-Te

Kostyuk O.B.

*Vasyl Stefanyk Precarpathian National University, Ivano-Frankivsk, Ukraine*

The thermoelectric properties and features of carrier scattering in the thin films $Pb_{18}Ag_{2-x}Sb_xTe_{20}$ are researched, which were obtained by the condensation of vapor in the high vacuum on the ceramics and mica substrates. Based on a two-layer Petrits model the electrical parameters of surface layers are found. It is shown that the condensates of thickness near $d < 1$ micron are characterized by the improved thermoelectric properties. The obtained results are interpreted by the adsorption of oxygen on the surface and its diffusion into the interior of condensate. It is established that the dominant role plays carrier scattering on the surface, but not on intergrain boundaries of the nanocrystals, whose sizes increase with the thickness of the vapor-phase structures.

Films for the investigation are received by the deposition of the vapor on pre-synthesized material in vacuum for the fresh chips (0001) of muscovite mica, and sital. The measurement of the thermoelectric parameters of condensates was realized at the room temperature in the constant magnetic and electric fields on the developed automated installation. This installation provides as a process for measuring the electrical parameters, as initial registration and as initial data processing.

The experimental results are explained within the framework of a two-layer Petrits model. Thin film in this model is composed of two layers: a surface layer and a bulk layer, which are connected in to parallel. The designated thermoelectric parameters of the surface layer are significantly different from the bulk layer by the electrical conductivity, the Hall concentration and the Seebeck coefficient.

The thickness d-dependences of mobility are obtained experimentally. They are explained by the mechanisms of carrier scattering on the surface and on the intergrain boundaries of condensates.

On the basis of the research results could be argued that the main contribution into the mobility of the charge carriers are made by the diffuse scattering on the surface ($\mu p$). The impact of the intergrain boundaries is significantly lower due to increase the grain size.

*This research is sponsored by NATO's Public Diplomacy Division in the framework of "Science for Peace" (NATO SPS 984536)).*

1. R.L. Petritz. Theory of an Experiment for Measuring the Mobility and Density of Carriers in the Space-Charge Region of a Semiconductor Surface // Phis. Rev. (110), P. 1254 (1958)..

# Carbazole-Based Azo Polymer: Characterization and Surface Relief Grating Formation

[1]Meshalkin A., [1,2]Robu S., [1]Prisacar A., [3]Shepel D., [1]Boiarinov Yu., [1]Achimova E.

[1] *Institute of Applied Physics AS of Moldova, Chisinau, Moldova*
[2] *State University of Moldova, Chisinau, Moldova*
[3] *Institute of Chemistry AS of Moldova, Chisinau, Moldova*

Recently polymer materials with azo dyes become attractive materials for holographic recording due to possibility of surface relief grating fabrication with high diffraction efficiency and resolution. It has been reported that large surface modulations can be obtained on azo polymer films upon exposure to an interference pattern of laser beams.

In this study, novel type of carbazole-based azo polymer have been synthesized through a polymerization azo-coupling scheme. As carbazole-based polymer the epoxypropilcarbazole (EPC) 90% and as azo dye the Disperse Orange 3 (DO) 10% were selected respectively. DO was purchased as a commercial product with dye content 90% from Sigma-Aldrich Company. FTIR characterization of synthesized copolymer EPK:DO has proved the introduction of azo group in polymer matrix confirmed by the peak at 1580 $cm^{-1}$ in the IR spectrum corresponding to the N = N stretching frequency. Copolymer film was prepared as thin film spin-coated at glass substrate. The film thickness was measured with microinterferometer MII-4 and was 140 nm. The transmittance spectra for obtained films coated on glass substrates were measured over the range 200 – 900 nm. The broad absorption band in the range 420-580 nm with $\lambda_{max}$=460 nm is assigned to strongly absorbing azobenzene groups. The surface-relief-grating (SRG) formation process was studied for obtained thin films. An interferometric holographic recording was used to expose linear grating. The interference pattern of DPSS laser beams was produced by two spatially symmetrical s-polarized beams ($\lambda$=532 nm and power density 120 $mW/cm^2$). It was shown that s/s-polarization condition is not efficient for SRG formation process. While using two circularly polarized interfering beams (left-circularly polarized: right-circularly polarized LCP:RCP) good quality SRG were direct produced without any chemical treatment and with diffraction efficiency more than 20%. Fig. shows atomic force microscopy image of the recorded sinusoidal surface relief structures with spatial period 1 μm. The depth of the grating was in the range from 80 nm to 130 nm.

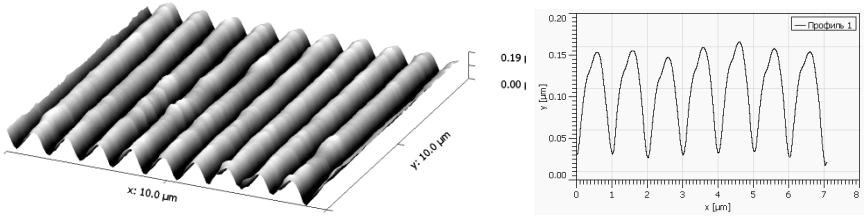


*The research was supported by the project 080-208 (ININC JINR) and 14.819.02.20A (ASM)*

# Eutectic Temperature Lowering in Nanoscaled Ag/Ge Films

Minenkov A.A., Kryshtal A.P.

*V.N. Karazin Kharkiv National University, Kharkov, Ukraine*

Multi-layer and multi-component films are essential to a number of modern technologies. However, for successful application of such systems it's vital to understand the nature of components interaction. This becomes crucial with reduction the components size since it leads to a significant change of multicomponent system properties and to an emergence of new ones. Unfortunately, fundamental understanding of the phase diagrams at nanoscale is currently insufficient. Available experimental data are scant and don't allow to trace phase diagram evolution in an entire size range. Moreover, further investigation becomes actual since our recent studies have shown that below a threshold size of Sn-Bi and Au-Ge binary systems the melting at the eutectic temperature doesn't occur [1, 2].

In this work we present the results of systematic experimental studies of the effect of scale on the eutectic melting in Ag-Ge binary system.

Layered Ag/Ge film is a convenient model object for the phase transitions in binary nanosystems studying. Thus, it was chosen as the object under study. Ag and Ge form the phase diagram of a simple eutectic type with a rather restricted solubility in solid state. The eutectic composition is formed at 24.5 at.% Ge and the temperature of 651°C. Terminal solubility of germanium in silver achieves 9.6 at.% at the eutectic temperature, while at room temperature it doesn’t exceed 0.1 at.%. Solubility of silver in a solid germanium is negligible.

We have used two experimental approaches on studying the eutectic temperature in Ag-Ge layered films. The first method involves the study of crystalline structure of the film during *in situ* TEM heating. The second one is based on the detection of abrupt change in the morphology of the film system under melting. The samples were produced at room temperature by sequential thermal evaporation of components from independent sources at a vacuum of $5 \cdot 10^{-8}$ Torr.

In summary, the Ag/Ge eutectic temperature $T_E$ as a function of Ag film mass thickness (1-50 nm) has been systematically measured. Few hundreds degrees lowering of $T_E$ with the thickness reduction was registered. It has been revealed that the liquid-phase formation in the system at the eutectic temperature takes place only if the silver film mass thickness value are greater than the critical one (1.2 nm). While the onset temperature for liquid phase formation at the metal-semiconductor interface was found as 200°C.

1. A.P. Kryshtal, R.V. Sukhov, A.A. Minenkov, *Journal of Alloys and Compounds,* **512**, (2012), 311.
2. N.T. Gladkikh, A.P. Kryshtal, R.V. Sukhov, *Physics of the Solid State,* **52.** **(**2010), 633.

# Modern Problems of CAD Topology Speed VLSI Structures

Novosiadliy S. P, Melnyk L.V, Varvaruk V. M, Novosiadliy S.V, Marchuk S.M.

*V.Stefanyk Precarpathian National University, Ivano-Frankivsk, Ukraine*

**Introduction**

When designing the topology of high-speed VLSI structures used different methods. The main of them are:

- A manual calculation scheme for the previously prepared analytical calculation formulas of its elements;
- Physical modeling, ie the study of objects of a physical nature by means of objects having a second physical nature, but identical to the first mathematical description of the structure elements, based on the principles of physical modeling of electro analogies;
- Full-scale layout with elements and devices previously diluted PCB aided mathematical modeling using computers (PCs) using special software).

The disadvantage of a manual calculation circuit LSI and its topology - a low accuracy, limited functionality, inability to take account of parasitic effects (elements) and design rule design and technological constraints.

Physical modeling as a way of designing structures and CEA LSI is used very rarely, most often it is used for a detailed study of individual processes, such as heat, mathematical modeling which is rather complicated and time-consuming and is usually electrophysical diagnostics elements (processes).

Full-scale layout - is one of the oldest and common ways of designing REA, which under certain conditions can be transferred to WSI structure for ensuring maximum reliability of the results arising from work with real signals, devices, rather than their closest model. In addition, the full scale layout determines the appearance of the results in the form of options and features. Its main drawback - high cost of preparing a layout that provides development duration, limited prototyping in taking into account the actions of parasitic elements and processes, including transient.

For automated mathematical design on the PC usually refers to the full range of issues associated with all phases of design, functional, logical, schematic, technological, physical and topological, which created mathematical models that provide the full range of procedures for calculation, analysis, synthesis and optimization of topological solution with high density layout. Compared with other methods of automated mathematical modeling using modern software tools (Cadence, TCAD, PCAD, MATHCAD, MATLAB, Stalker, OTTO, OrCAD, MicroCap) has the following advantages.

In problems of calculating circuits using the model can always find the original settings circuits (including dynamic) and their characteristics that can not be measured directly in the layout because of the unavailability of

measurement points that are especially characteristic of high-speed VLSI structures.

In problems of modeling analysis allows to analyze the output parameters and characteristics of schemes boundary and over boundary modes that are physically impossible to implement, such as transients taking into account the actions of parasitic elements. In addition, the simulation allows you to calculate mass production and analysis of various statistical characteristics of the circuit without its launch in series production, analysis of the scheme of action of external conditions without real climatic tests using test electrophysical diagnostics, calculate hurt security schemes, and simulate analog-digital circuitry together.

In optimization problems possibility of technological model is limited by a small number of regulatory elements, while the new model can be varied parameters, achieving maximum improvement parameters and characteristics, especially speed. Optimization and minimization of elements in the scheme reduces power consumption and chip area, which increases the yield of VLSI structures.

The role of modeling in problems of synthesis allowed to clearly verify proper operations of synthesized circuits and topology taking into account the parasitic elements by minimizing their topological layout and routing.

Obviously, it is impossible to AC / VLSI and CEA varying degrees of difficulty to analyze and design with the same power of the detail, including at the processes that occur in each active element (transistor). Therefore, CAD design presents multi-hierarchical process. The content and the number of stages of the design depends on many factors, especially where there are features of an object and its ultimate goal of designing used electronic components and technologies of topology structures Mathematics (software) tools. As technology of VLSI structures CAD software tools should be improved in the shortest possible time to eliminate the above problems today.

**References**

1. Novosyadlyy, S. P. (2010). Sub–nanomykron technology structures LSI. Ivano–Frankivsk: City NV, 456.

2. Novosyadlyy, S. P. (2003). Physical and technological bases submicron VLSI. Ivano–Frankivsk: *Si*myk, 52–54.

*Si*mon, V. V. Kornilov, L. (1988). Equipment of ion implantation. *Radio and Communications,* 354.

# Graphene Enhanced Raman Scattering From Deoxyribonucleic Acid Constituents

[1]Pidhirnyi D., [1]Dovbeshko G., [2]Kaplas T., [2]Svirko Yu., [3]Lange S., [3]Kiisk V., [3]Jaaniso R., [3]Dolgov L., [3]Sildos I.

[1]*Institute of Physics, NAS of Ukraine, Kyiv, Ukraine*
[2]*Institute of Photonics, University of Eastern Finland, Joensuu, Finland*
[3]*Institute of Physics, University of Tartu, Tartu, Estonia*

Graphene enhanced Raman scattering is comparatively new spectroscopic branch of science, which is connected on the one hand with graphene applications in optical biosensing and on another hand with fundamental understanding of Surface Enhanced Raman Scattering mechanisms [1]. These mechanisms traditionally include electromagnetic and chemical enhancements. First one is connected with strongly localized near the surface light induced electric fields. They can appear as a result of resonant interaction of incident light with electron plasma oscillating near the surface of thin metal or semiconductor films and nanoparticles. Such interaction in case of graphene occurs in the THz spectral range. So we do not consider this effect, because our samples were excited by visible laser light 488 nm and 514 nm. Nevertheless for such constituents of deoxyribonucleic acid as adenine and constituents of protein as glycine, we obtained 2-10 times enhancement of Raman signal. We associate this enhancement with charge transfer effects appearing in case of close contact between the tested molecules and graphene surface. As a result of this charge transfer change of molecule polarizability can occur and result in enhanced Raman response. The features of this so-called chemical mechanism of Raman enhancement are discussed in our work relatively to the constituents of deoxyribonucleic acid.

This investigation was supported by DORA T5 grant of SA Archimedes (agreement No 30.1-6/886), institutional grant IUT34-27 TLOFY15027I, Marie Curie ILSES project no. 612620, NATO SPS project NUKR.SFPP984702 and partially by European Regional Development Fund project TK114.

1. Xu W., Mao N., Zhang J. Graphene: A Platform for Surface-Enhanced Raman Spectroscopy // *Small*, 9, 8, (2013), 1206.

# Effect of Surface Doping on The Gas Sensitivity of Si and GaAs P-N Junctions

[1]Ptashchenko O. O., [2]Ptashchenko F. O., [1]Gilmutdinova V. R., [3]Bogdan O. V., [1]Masleyeva N.V., [1]Pecheryans'kyi O.V. , [1]Sevastyan A. P.

*[1]Odessa National I. I. Mechnikov University, Odessa, Ukraine*
*[2]Odessa National Maritime Academy, Odessa,Ukraine*
*[3] Odessa State Academy of Building and Architecture, Odessa,Ukraine*

Si and GaAs *p-n* junctions are perspective as chemical sensors, having a lower threshold $NH_3$ concentration for detecting, than porous Si membranes and Si nanowires. The sensitivity of a *p-n* junction as gas sensor was defined as

$$S_I = \Delta I / \Delta P, \quad (1)$$

where $\Delta I$ is the change in the current (at a fixed voltage) due to a change $\Delta P$ in the corresponding gas partial pressure. The presence of $NH_3$, $H_2O$ and $C_2H_5OH$ vapors in the ambient atmosphere strongly increased the direct and reverse currents in studied *p-n* junctions due to forming of *n*-conducting channel, which shorts the depletion region. The gas sensitivity was strongly affected by presence of surface centers. In the homogeneous channel section, the surface free electrons density is defined by

$$N_{ns} = N_i - N_{sf}^- - N_{ss}^- - N_{sA}^- + N_{sD}^+, \quad (2)$$

where $N_i$ is the surface density of adsorbed donor like ions; $N_{sf}^-$ and $N_{ss}^-$ denote the surface densities of the ionized fast and slow acceptor centers, respectively; $N_{sA}^-$ is the surface density of ionized acceptors in the surface depletion layer; $N_{sD}^+$ is the surface density of ionized donors. It is seen from (2), that the electrons number $N_{ns}$ in the channel can be increased by $N_{sD}^+$ growth, i. e. by surface doping with donor like atoms (molecules).

The surface doping of *p-n* junctions was carried out by two methods: a) by a prolonged exposure of the *p-n* junctions in moist ammonia vapors with a partial pressure of 12 kPa; b) by exposure in a $Na_2S$ aqueous solution.

The ammonia-sensitivity of Si and GaAs *p-n* junctions at a reverse bias voltage of -1 V before treatments was of ⊔ 50 nA/kPa and ⊔ 50 μA/kPa, respectively. After the ammonia doping the sensitivity rised by factors of ⊔ 30 and 5, accordingly. The effect of S-doping was analogous.

A durable storage of the treated samples in a neutral atmosphere lowered their gas sensitivity. The characteristic time of this process in GaAs *p-n* junctions was of $5 \cdot 10^5$ s and was of the same order of value in Si *p-n* junctions. The isochronal annealing of the treated Si *p-n* junctions showed that the degradation was due to destruction of centers with a thermal activation energy of ⊔ 0,2 eV. In GaAs *p-n* junctions the degradation rate was constant in the temperature range 290–370 K.

# Localized Surface Plasmon Resonance in Gold Porous Films

Stetsenko M.A., Maksimenko L.S., Rudenko S.P.,
Krischenko I.M., Manoilov E.G., Kaganovich E.B., Serdega B.K.

*V. Lashkaryov Institute of Semiconductor Phisics, NAS of Ukraine, Kyiv, Ukraine*

Gold porous (por-Au) films are the nanocomposite porous films with Au nanoparticles (NPs) produced by the method of pulsed laser deposition with a YAG:$Nd^{3+}$ laser ($\lambda$=1.06 mkm, j=15 j/$sm^2$, $t_i$=10 ns, $f_i$=25 Hz) in an argon atmosphere with a pressure of 70 Pa and laser shot number 1500 [1]. The aim of this study is the adoption of wide information abilities of the modulation polarimetry technique developed in [2] for diagnostic of localized surface plasmons resonances (LSPR) in por-Au films. The angular and spectral characteristics of polarization difference $\rho(\theta, \lambda)=R_s^2-R_p^2$ of reflection coefficients for *s*- and *p*-polarized radiation are measured in the ranges of wavelengths $\lambda$=400÷1000 nm and incidence angles $\theta$=20÷60 degree. Two types of LSPR are detected: the first is on isolated Au NPs in the short-wavelength range and the second is between Au NPs caused by dipole-dipole interaction, when the dipole fields of plasmons on one Au NPs induces the surface plasmons oscillations in neighboring. The LSPR of the second type is observed in the long-wavelength range at the incidence angles above the critical angle of total internal reflection ($\theta > \theta_{cr} \sim 43^0$) under the phase synchronous condition fulfillment. A separation of the contributions of different resonant mechanisms is performed by means of analysis of characteristics $\rho(\lambda)$. The corresponding frequency dependencies of $\rho(\omega)$ are decomposed into elementary components from Gaussian functions with fundamental frequencies $\omega_1$ and $\omega_2$, $\omega_2'$ and the oscillation relaxation times $\gamma_1$ and $\gamma_2$, $\gamma_2'$, respectively, for the first and second type of LSPR, which are observed at the certain incidence angles of *s*-, *p*-polarisations. The extremum of $\rho(\lambda)$ at $\theta < \theta_{cr}$ is shifted in the long-wavelength range, if the incidence angle is increased. This indicates on the existence of radiative modes of LSPR with the first type. The dispersion characteristics $\omega(k)$ of surface plasmons are shown for nonradiative modes: one branch for the first resonance type and two branches for the second resonance type, respectively. The obtained experimental results contain the information about the morphological peculiarities of por-Au films and the inhomogeneous space distribution of Au NPs. The interaction of electromagnetic radiation with por-Au films has a LSPR character which is determined by the topologic size effect.

1. E. B. Kaganovich, S. A. Kravchenko, L. S. Maksimenko, E. G. Manoilov, I. E. Matyash, O. N. Mishchuk, S. P. Rudenko, B. K. Serdega, Polarization properties of porous gold and silver films. Opt. Spectrosc. 110(4) (2011) 513-521.
2. B.K. Serdega, S.P. Rudenko, L.S. Maksimenko, I.E. Matyash, Plasmonicoptical properties and the polarization modulation technique, in: M.I. Mishchenko, Ya.S. Yatskiv, V.K. Rosenbush, G. Videen (Eds.), Polarimetric Detection, Characterization and Remote Sensing, Springer. (2011) 473-500.

# The Diagnostics of Nanosized Tin Disulfide Films by Modulation Polarimetry Technique of Surface Plasmon Resonance

Stetsenko M.A., Maksimenko L.S., Rudenko S.P.,
[1]Vozny A.A., Opanasyuk A.S., Serdega B.K.

*V. Lashkaryov Institute of Semiconductor Phisics, NAS of Ukraine, Kyiv, Ukraine*
*[1]Sumy State University, Sumy, Ukraine*

The tin-sulfur system can form a variety of crystalline phases such as SnS, $Sn_2S_3$, $SnS_2$ with a different band gaps. A number of these compounds can be obtained by both p- and n-type conductivity. This allows to create a solar cells (SC) with a heterojunction based on different phases of the same compound (eg, n-SnS2/p-SnS), which significantly simplifies their production and reduces cost [1]. The increasing of SE efficiency needs the optimization of the structural characteristics of the surface layers $SnS_2$ as a syllabic element. The application of modulation polarimetry technique of surface plasmon resonance allows to characterize the structure of nanosized films by studying of their polarization features [2]. The samples of $SnS_2$ films were obtained by thermal evaporation method of compound in a quasi-closed volume in the installation VUP-5M (P = $5\cdot10^{-3}$ Pa) at a different substrate temperature $T_s$=175-275°C. The mass thickness of samples was d=50nm. It is shown, that there are two mechanism of resonance interaction of radiation with the electron subsystem of samples which expressed in the angular and spectral characteristics of the polarization difference $\rho(\lambda,\theta)=R_s^2-R_p^2$ ($R_s^2$ and $R_p^2$ are the internal reflection coefficients of s- and p-polarized radiation, respectively) in the $\lambda$=400-1000nm wavelength range. The resonance excitation of the localized surface plasmons (LSP) and the surface plasmon polaritons (SPP) were found by light. As a results of spectrums analysis $\rho(\lambda)$ the dispersion characteristics $\omega(k)$ consisted of three frequency branches were obtained. One of them is low-frequency branch corresponds to the excitation of SPP (non-radiative region), two others are high-frequency branch corresponds to the excitation of LSP on nanoparticles (radiative region) and on roughness (non-radiative region). The ratio between the amplitudes of LPP and SPP resonances is determined by the structural features of $SnS_2$ films due to various $T_s$. The practical application of experimental data conclude in the fact that the increasing of the substrate temperature leads to formation of a more homogeneous lower layer of film with increasing of surface roughness with a further formation of aggregates on the surface of $SnS_2$ films. Our studies show the perspective of modulation polarimetry technique for diagnostics of structural homogeneity of nanocomposite films.

1. A. Sanchez-Juareza, A. Tiburcio-Silverb, A. Ortiz, *Thin Solid Films* 480, (2005), 452.
2. B. K. Serdega, S. P. Rudenko, L. S. Maksimenko, I. E. Matyash. Polarimetric Detection, Characterization and Remote Sensing / NATO Science for Peace and Security Series C. Springer Science + Business Media. B.V, (2011), 473.

# The Influence of an External Magnetic Field on the Stripe Domains in Epitaxial YIG Films Studied by Force Gradient Microscopy

[1]Synhaivska O.I., [1]Lytvyn P.M., [2]Yaremiy I.P., [1]Prokopenko I.V.

*[1]Institute of Semiconductor Physics, National Academy of Sciences of Ukraine, Kyiv, Ukraine*

*[2]V. Stefanyk Precarpathian National University, Ivano-Frankivsk, Ukraine*

Epitaxial yttrium-iron-garnet films (YIG) have a set of structural and magnetic properties, which enables their application as an active medium of electronic devices. Epitaxial YIG structures are used in microwave technology devices, planar waveguide structures and lasers, magneto-optical devices and sensors of visual magnetometry.

The aim of our research was to study the distribution of magnetic domains on the surface of the YIG films with different thicknesses in the external magnetic field. The study was carried out using a scanning probe microscope "NanoScope IIIa Dimension 3000" using the methods of the magnetic field gradient measurements.

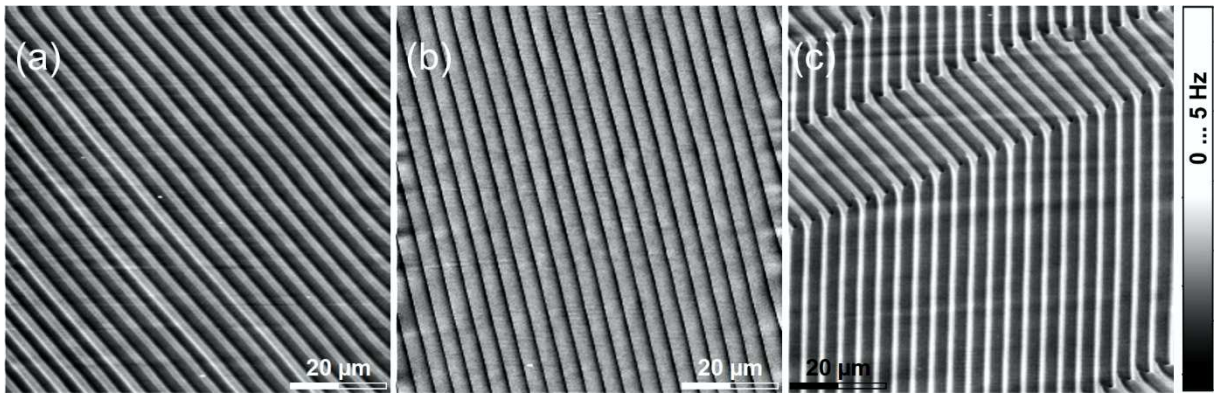


Fig.1. MFM images of the same area on the 2.9 μm YIG film scanned before (a) under (b) and after (c) application of external magnetic field of 4 mT. Field applied along horizontal direction.

We observed the stripe domain structure in YIG films with thickness 2.9 μm and 5.11 μm in external magnetic field of 2-10 mT. It was found that in the external magnetic field stripe domains in YIG film thickness of 2.9 μm expanding, which is not observed in the film thickness of 5.11 μm. Also there are bends or alignment of domain structure.

These results are important for understanding the physics of the processes occurring in thin films of YIG.

# Electroluminescence Spectra of Light-Emitting $In_xGa_{1-x}N/GaN$ Heterostructures at Reverse Bias at $T$ = 300 K and 77 K

Vlasenko O.I., Veleschuk V.P., Kisselyuk M.P., Vlasenko Z.K.

*V.E. Lashkaryov Institute of Semiconductor Physics of the NAS of Ukraine, Kyiv, Ukraine*

Separated bands and peaks of the luminescence spectra, also displayed at lower temperatures, contain valuable information on the energy levels of recombination centres and various defects. For effective non-destructive control of quality and characterization of GaN (InGaN, AlGaN) structures often used the local photo-, electro-, cathode-luminescence (PL, EL, CL). At the same time, application of a reverse voltage to GaN structure produces controlled microplasma (MP) breakdown that takes place mainly in the regions of extended defects, and is accompanied by luminescence. In general, the EL spectra at reverse bias investigated in typical InGaN/GaN AlGaN/GaN heterostructures, GaNP, ZnO / GaN, Si and GaAs structures (for example, see [1]).

But depending on the indium (In) content in the $In_xGa_{1-x}N$ quantum well EL spectra at reverse bias is not investigated, also at $T$ = 77 K. For the first time we measured EL spectra of the LED $In_xGa_{1-x}N/GaN$ heterostructures at reverse bias for $x$ = 0.05, 0.15, 0.2, 0.3, and also at liquid nitrogen temperature.

In the MP spectrum, one can observe the main peak of quantum wells (QW) $In_xGa_{1-x}N$ with the maximum corresponding to the energy of the band gap $E_g$ $In_xGa_{1-x}N$ and the shoulder (or peak) near 400 nm related to GaN layers. The shoulder corresponds to recombination on donors and (or) acceptors in the *p*- and *n*- GaN layers. Also “yellow” (defect) luminescence is observed.

It is revealed appearance of EL bands from defects, as well as bands, the form of which is identical to typical EL spectra at forward bias. The observed both temperature narrowing of the width of EL spectra and shift of the peak of EL spectra of microplasmas.

It was found that at $T$ = 77 K electroluminescence spectra of microplasmas for $In_{0.2}Ga_{0.8}N/GaN$ structures are divided into two peaks, which correspond to recombination in two areas - the quantum well and *p*-GaN layer. EL spectrum microplasmas $In_{0.3}Ga_{0.7}N/GaN$ structures at $T$ = 77 K contains main 1 peak due to the higher conductivity $In_{0.3}Ga_{0.7}N$ layer.

1. M. Lahbabi, A. Ahaitouf, M. Fliyou, E. Abarkan, J.-P. Charles, A. Bath, A. Hoffmann, S.E. Kerns and D.V. Kerns. Analysis of electroluminescence spectra of silicon and gallium arsenide p-n junctions in avalanche breakdown // J. Appl. Phys. **95** (2004) 1822.

## СЕКЦІЯ 3 (стендові доповіді)
## ФІЗИКО-ХІМІЧНІ ВЛАСТИВОСТІ ТОНКИХ ПЛІВОК

12-15 травня 2015 р.

## SESSION 3 (poster)
## PHYSICAL-CHEMICAL PROPERTIES OF THE THIN FILMS

May, 12-15, 2015

# Oxygen Adsorption on the Be-covered Mo(112) Surface: DFT Study

Afanasieva T.V.[1], Petrova N.V.[2], Yakovkin I.N.[2]

[1] *National Taras Shevchenko University of Kyiv, Kyiv, Ukraine*
[2] *Institute of Physics of National Academy of Sciences of Ukraine, Kyiv, Ukraine*

It has been shown that both on a clean and (1×1)Be-covered Mo(112) surface, oxygen will readily dissociate, without any noticeable barrier, and the presence of Be in the furrows rather facilitates than hinders the dissociation. The $O_2$ molecules can be adsorbed also on Be rows in several metastable configurations, which can be considered precursor states for the dissociation. The O atoms will occupy bridge-on-row sites, which remain available for oxygen in presence of the (1×1)Be monolayer, because Be atoms occupy adsorption sites in furrows. However, the co-adsorbed Be – O monolayer is found to be unstable (or metastable). In particular, O atoms, being slightly shifted from the symmetrical position in the bridge-on-row sites, tend to move towards Be atoms and spontaneously form $Be_2O$ or, at higher oxygen exposures, BeO, which is consistent with recent AES studies for this system. The estimated gain in energy due to reaction of the BeO formation on the Mo(112) surface is of 1.17 eV. At lower oxygen coverages, the formation of $Be_2O$ is more favorable (by 0.15 eV) than the configuration of BeO with some non-oxidized Be adatoms on the surface.

# Doping Semiconductors on the Base of IV-VI for Thermoelectric

Ahiska R.[1],Freik D.[2], Chavjak I.[2], NykyruyL.[2]

[1]*Gazy University, Ankara, Turkey*
[2]*Vasyl Stefanyk Precarpathian National University, Ivano-Frankivsk, Ukraine*

The analysis of the topology vapor-phase thin films and nanostructures deposited on monocrystalline, polycrystalline, and amorphous substrates executed by surface condensates modeling methods on the mode of atomic force microscopy and cellular automata [1]. The proposed geometric model of the terrain allows to describe all stages of nanostructures formation in axiomatic form depending on the both the conditions growth and physical parameters of the system.

It was define the spatial forms of nanocrystallines, their mutual orientation, and orientation relative to the substrates in heterostructures. It is shown, the investigated values of technological factors is implemented in all cases the Folmer-Weber mechanism taking into account the orientation and energy influencing. Was proposed and implemented distribution histograms represent of height of nanoformations on their superposition of three Gaussian functions. It is shown, that the size of individual nanoislands defined processes of Ostwald maturation provided simultaneous action the diffusion and Wagner mass transfer mechanisms, whose contribution depends on technological factors and evaporation temperature deposition [2].

The relation for thermoelectric parameters, such as Seebeck efficient (S), specific conductivity (σ) received in semi-classic approximation on the base of Boltzmann transport equation by model of quantum well with high walls [3]. This model considers the change of Fermi energy due their wide. There were developed software package, and calculated the theoretical dependence of energy and thermoelectric parameters of the width of the quantum well. It was reasonable to use the model of the quantum well with high walls to describe the behavior of thermoelectric parameters of vapor-phase nano-condensates.

There is shown that doping of lead (tin) telluride by antimony and bismuth leads to a drastic change in the kinetic properties of nanostructures PbTe(SnTe):Sb(Bi), leading to an improvement of thermoelectric power.

The stable n-type of conductivity and high carrier concentration define the substitution of lead ions $Pb^{2+}$ by ions of $Sb^{3+}(Bi^{3+})$ in cationic sub-lattice of main matrix $Sb_{Pb}^{3+}(Bi_{Pb}^{3+})$ for solid solution of $PbTe\text{-}Sb_2Te_3$ $PbTe\text{-}Bi_2Te_3$ vapor-phase condensates deposited on sital and fresh chips of (0001) mica. And, the dominant scattering mechanisms explained of the diffuse scattering on surface and inter-grain boundaries.

*This research is sponsored by NATO's Public Diplomacy Division in the framework of "Science for Peace" (NATO SPS 984536)).*

[1]. D. Freik et al. J. Eng. Phys. and Thermophys. 85 (2012) 1011.
[2]. D. Freik et al. Phys. Chem. Solid St. (Ukr.) 10 (2009) 789.
[3]. D. Freik et al. J. Mat. Res. 27 (2012) 1157.

# The Influence of Obtained Conditions for Fundamental Absorption Edge in $Y_2O_3$ Thin Films

Antonyuk V.G., Bordun I.O., Kukharskyy I.Yo., Polovynko I.I.

*Ivan Franko National University of L'viv, Lviv, Ukraine*

Thin films $Y_2O_3$ with thickness 0.3–1.5 μm obtained by the method of discrete evaporation and RF-sputtering in this work have been investigated. X-ray diffraction data shoved the polycrystalline structure with predominant orientation in plain (222) and (440).

As a result of our studies, we established that regardless of the sputtering atmosphere and the heat treatment atmosphere, the absorption coefficient $\alpha(h\nu)$ for the thin films in the fundamental absorption edge region is described by a power-law dependence

$$\alpha\left(h\nu\right)=\frac{A\left(h\nu-E_g\right)^{1/2}}{h\nu}, \qquad (1)$$

from which we can determine the bandgap width $E_g$. Such behavior of the absorption edge is typical for allowed direct photon-assisted transitions.

Table 1

Energetic prameters in equation (1) and consolidated effective mass of free charge carriers in $Y_2O_3$

| Films | $E_g$, eV | $A$, $sm^{-1}eV^{-1/2}$ | $\mu$ |
|---|---|---|---|
| I | 5.90 | $2.96\times10^5$ | 0.335m |
| II | 5.84 | $2.83\times10^5$ | 0.322m |
| III | 5.77 | $2.65\times10^5$ | 0.308m |
| IV | 5.65 | $2.23\times10^5$ | 0.388m |

It was ascertained that the optical band gap Eg increases from 5.65 eV for $Y_2O_3$ films, obtained by methods of discrete evaporation (IV), to 5.77 eV for films, obtained by ion-plasmous sputtering in atmosphere of argon (III), to 5.84 eV for films, obtained by ion-plasmous sputtering in atmosphere of 50% argon and 50% oxygen (III) and to to 5.90 eV for films, obtained by ion-plasmous sputtering in oxygen atmosphere(I). Consolidated effective mass of free charge carriers in $Y_2O_3$ films was estimated. It was found that the concentration of charge carriers in $Y_2O_3$ films obtained by ion-plasmous sputtering at addition in argon atmosphere 50 % of oxygen is $N\approx1.34\times10^{17}$ $cm^{-3}$ and after sputtering in 100 % of oxygen $N\approx1.38\times10^{18}$ $cm^{-3}$, which is typical for degenerated semiconductors. It was shown that the shift of fundamental absorption edge in $Y_2O_3$ thin films after addition in sputtering atmosphere of oxygen is caused by Burstein-Moss effect.

# Kinetics Peculiarities Describing *in-situ* Photodarkening in Thin As-Se Films

Balitska V.O., Shpotyuk O.I.

[1] *Lviv State University of Vital Activity Safety, Lviv, Ukraine*
[2] *Scientific Research Company "Carat", Lviv, Ukraine*

Amorphous chalcogenides like binary arsenoselenides are known to be unique disordered materials possessing extremely high sensitivity to external factors. As an example, the photo-induced optical effects typically revealed themselves in photodarkening (e.g. long-wave shift of fundamental optical absorption edge), have been put in a ground for chalcogenide-based sensors, optical memory and switching devices, information storage systems, etc. These photoinduced effects clearly demonstrate two principally different components in chalcogenide films, the transient changes occurring under *in-situ* photoexposure and metastable or permanent ones leaving for a long time in the illuminated films after photoexposure stopping (*ex-situ* photodarkening)

In this work the realistic governed kinetics *in-situ* photodarkening in amorphous arsenoselenide films of different thicknesses (from 0.54 to 4.07 μm), pre-history (virgin and annealed) and chemical composition ($As_{40}Se_{60}$, $As_{50}Se_{50}$ and $As_{60}Se_{40}$) pumping with the same light beam having different penetration depth in each sample were studied.

$As_{100-x}Se_x$ films of different thicknesses ($d$=0.54÷4.07 μm) were prepared by flash thermal evaporation in a vacuum onto glass substrates held at 100 $^oC$. One part of films was additionally annealed at T=120 $^oC$ during 1 hour to produce small darkening in respect to un-annealed films.

To initiate photostructural transformation in the studied films, a He-Ne laser (λ=633 nm, W=10 mW) operated in CW irradiation mode was used. Experimental set-up allowed simultaneous photodarkening activation and *in-situ* optical transmission measurements at the same wavelength of $\lambda$=633 nm.

It was shown the *in-situ* photodarkening in amorphous arsenoselenide As-Se films is non-dispersive in nature, its kinetics description on thickness, thermal pre-history and chemical composition being governed by penetration depth parameter (the inverse value of the absorption coefficient) of pumping light beam in respect to film thickness: the greater penetration depth of pumping light, the smaller non-dispersivity in the resulting photodarkening kinetics. In contrast, if film thickness is less than penetration depth, the stretched exponential relaxation kinetics tents towards simple exponential one.

# Quantum Charge Transport in Ultrathin Noble Metal Films

Bihun R.I., Buchkovska M.D., Stasyuk Z.V.

*Ivan Franko Lviv National University, Lviv, Ukraine*

Rapid development of modern micro- and nanoelectronics requires the electrical circuits dimension geometry reducing and increase their reliability and efficiency. The reducing of conductor linear sizes will increase working elements density on working surface of integrated circuits. It will enhance the performance of these systems. Under such dimensional sizes the influents of size effects on electron transport will be predominant, because the impact of surface electron scattering will be commensurable with bulk. The influents of surface asperities on electron states and electron scattering peculiarity in metal film are highly important for quantitative description of the electron transport phenomena in such system. The exact solution of Schrödinger equation for metal film with corrugated boundaries is sufficiently difficult problem that is why we can only estimate the asymptotic solution of the problem [1-2]. This problem is the understanding key of electron-surface phenomenon in metal films electron transport. Quantum mechanical approaches based on investigation of electron subsystem Hamiltonian $H$. Electrons located in sample restricted between two inhomogeneity surfaces. The influents of surface inhomogeneities on electron transport dissipation were calculated with additive item $\delta H$ to Hamiltonian $H_0$. The Hamiltonian $H_0$ describes electron subsystem located in sample restricted between two homogeneity surfaces. Calculations were conducted under perturbation theory with small inhomogeneity approximation $h << d$, where $h$ – characteristics of surface asperities, which were used in TJT, TA, FC, SHW and mSHW quantum approaches [3]. That is why we developed one dimension model of metal films conductivity in Boltzmann approach for quantum electron transport. The fluctuation of film boundary has dramatic influents on electron spectra. It changes electron scattering under quantum size effect. In the frame work of developed model size dependences of metal films conductivity were calculated. The developed model was used for quantitative description of the experimental data of monocrystalline $CoSi_2$ films and fine-grained gold metal films. In the film thickness ranges of the quantum electron transport and transition to the semiclassical electron transport the comparison of calculations results of metal film size dependences conductivity were conducted for our model with others theoretical approaches. The developed quantum model of charge transport in films with metallic conductivity can more successfully describe the transition from purely quantum to semiclassical charge transport in comparison to mentioned theories [3]. This was possible because the proposed model considers the perturbation energy states in the whole volume of the film due to the existence of macroscopic inhomogeneities on the metal film surface. In consequence of this approach became possible to include a consideration of partial additive contributions of bulk and surface carrier scattering. When the film thickness is changed the relative value of the electron states only changes. Perturbation calculated in the linear approximation with assumption that $\Delta h$ is $d$ independent.

1. Y. Amirat, G. Chechkin, R. Gadyl'shin, Applicable Analysis, (2007), **86**(7), 873.
2. G.A. Chechkin, A. Friedman, A.L. Piatnitski, J. Math. Anal, **231**, (1999), 213.
3. R.I. Bihun, Z.V. Stasyuk, Metallofizika i noveishie tekhnologii, **36(**6), (2014), 723.

# The Electronic Structure in the Transition d-Metal Films of Nanometer Thickness

Bihun R.I., Gavrilyukh V.M., Kravchenko O.E., Stasyuk Z.V.

*Ivan Franko Lviv National University, Lviv, Ukraine*

The electron kinetic size phenomena in thin metal films give us useful information about the evolution of electronic structure of limited size samples such as transition *d*-metal films. It is interesting to determine the minimum film thicknesses after which electronic structure of sample are identical of bulk metal electronic structure. Setting the limits of theoretical models suitability which describe size kinetic phenomena in metal film thermoelectric power allow to estimate the critical films thicknesses at which electronic structure of the samples are changed. The investigation of transition *d*-metal such as Ni, Pd and Cr electrical conductivity, thermoelectric power size dependence and structure had allowed to get valuable information about critical film thickness after which the energy band structure became similar to electronic structure of bulk material.

The preparation and electron kinetic parameters investigation of metal films were conducted under ultrahigh vacuum conditions (residual dynamic gas pressure ~ $10^{-7}$ Pa) in metal experimental devices. Similar to [1] technique was used. The investigated metal film were deposited on glass substrate at 78 K (clear or coated germanium underlayers with mass thickness of 1-2 nm) with speed deposition 0,1-0,2 nm/s by condensation of thermally evaporated metal. The control of germanium underlayers and metal film thicknesses were performed by shift of quartz vibrator resonance frequency placed in the metal vapor flux. After deposition metal films were thermostabilized to room temperature to improve it's structure and electrical properties.

The experimental dependence of the resistivity $\rho = \rho(d)$ and temperature coefficient of resistance $\beta = \beta(d)$ can be quantitatively described by polycrystalline inhomogeneous layer thickness model [2]. It was shown that germanium underlayers reduce crystallites linear sizes of metal films and have effect on the electron transport properties of them. Deep analysis of resistivity and thermoelectric power size dependences of deposited on germanium sublayers metal films show that the dimensional dependence was well described by a model of two independent groups of current carriers with different effective masses. It was shown that in the case of palladium film with average linear sizes of crystallites D = 10 nm, the ratio between the conductivity of different groups of charge carriers is $\sigma^+/\sigma^- = 0{,}8$ and for palladium films deposited on germanium sublayers with mass thickness of 0,5 nm; $\sigma^+/\sigma^- = 0{,}75$. It was found that critical mass thickness after which electron structure become identical to bulk metal electron structure is compiled in electrically continuous palladium films close to 5 nm. This result had good agreement to [3].

1. Bihun R. I., Kravchenko O.E., Stasyuk Z.V., Leonov D.S. Metallofizika i noveishie tekhnologii.– 2012.– V.34, № 4.– P. 469 –476.
2. Stasyuk Z. V. Journ. Phys. Studies.– 1999.– V. 3.– P. 102.
3. Katrich G.A. , Naumovets A.G. In: Physics of Solid Surfaces, ed. by J. Koukal, Elsevier, Amsterdam – 1988. – P. 123-130.

# Dynamic Conductivity of Ultrathin Copper and Gold Films

Bihun R.I., Stroganov O.V.

*Ivan Franko Lviv National University, Lviv, Ukraine*

Optical properties of thin metal films provide important information about electron transport phenomenon in metal films. Optical properties of thin silver and gold films have been studied already but fundamental analysis of thickness dependencies of effective optical parameters is lacking. We have developed methodology for assessing transport kinetic parameters on the basis of the thickness dependent optical constants of the films. Ultrathin silver films in the vicinity of percolation threshold have been studied. The critical thickness of the films, mean linear grain size and grain boundary scattering parameters of charge curriers have been determined from the size dependencies of the effective optical constants. The experimental data are in good agreement with those obtained by structural and electron transport investigations of the samples.

Ultrathin metal films have been fabricated by the thermal evaporation on the glass substrate under high vacuum condition ($P \sim 10^{-7}$ torr) at the room temperature. Mass thicknesses of the films have been assessed by the shift of the resonance frequency of the piezoquartz vibrator. Measuring the resistance of the films was carried out electronically by the Ohmmeter Ц301-1. Transmittance and reflectance spectra were measured by broadband spectrophotometer Shimadzu UV-3600.

Dynamic conductivity size dependencies of silver films with thicknesses from 8 to 25 nm in the wavelength range 200-2500 nm were investigated. Optical coefficients $n$ and $k$ have been calculated from the spectral data using Murmann's equations [1]. Optical conductivity, effective charge carrier mass, effective relaxation time, skin depth values were calculated. The critical thickness at which metallic phase is formed was found to be 15 nm. It was determined within the framework of the percolation theory [2] (in the vicinity of the percolation threshold transmittance and reflection spectra do not depend on the frequency). This is confirmed by the dynamic conductivity data which are frequency independent for this thickness value of the film. Another proof is the dramatic change of the sign of the first derivative of the dielectric permittivity on frequency ($d\varepsilon_1/d\nu$) around the thicknesses of silver layer 15-16 nm. The effective mass of the charge carrier was around $1{,}2 \pm 0{,}2\ m_0$, which allowed us to use the free electron model [3] in finding of dielectric constants. Mean grain sizes were estimated. They proved to be commensurable with film thicknesses. For example, for film thickness $d = 15$ nm linear grain size is $D = 22$ nm and for thickness $d = 20$ nm, $D = 25$ nm. The skin depth thickness was evaluated [4]. It was shown, that its thickness dependence has descending character up to the percolation region. For thin films with thicknesses above 15 nm this parameter remains constant and approximately 25 nm. Structural investigations of the films showed that grain sizes of the samples similar to those obtained by the optical studies. The intergrain tunneling coefficient for thin silver films with metallic type conduction were calculated. It is value about $t \sim 0{,}6\text{-}0{,}7$. The data is in good agreement with those investigations by the direct electro transmission microscopy of the films in the framework of grain boundary scattering theories.

On the basis of the curried out optical and structural studies was found kinetic charge transport parameters for the silver films with the thicknesses 8-25 nm. It is shown, that the average linear grain sizes obtained in different ways are the same and are commensurable with the thickness of the films. Grain-boundary scattering parameters obtained from spectral characteristics are in full agreement with those previously obtained values from electrical resistivity studies of the films. Effective critical thickness of silver film with metal phase conductivity was estimated and, it was found to be 15 nm.

1. Barybin A., Shap V. International Journal of Optics, **2010**, (2010), Article ID 137572, 18 p
2. Smilauer P. Contemporary Physics.– 1991.– Vol. 32, № 2.– P. 89-102.
3. Dressel M., Grüner G. Cambridge University Pres.– 2002.– 474 p.
4. Gilberdt P.W., J. Phys. F: Met. Phys.– 1982.– Vol. 12.– P. 1845-1860.

# Comparison of Background Donor Concentration in HgCdTe Grown with Different Technologies

Bonchyk O.Yu.[1], Mohylyak I.A.[1], Savytskyy H.V.[1], Fitsych O.I.[2], Voitsekhovsky A.V.[3], Izhnin I.I.[4]

[1] *Pidstrygach Institute for Applied Problem of Mechanics and Mathematics, Lviv, Ukraine*
[2] *Army Academy named after Hetman Petro Sahaydachnyi, Lviv, Ukraine*
[3] *National Research Tomsk State University, Tomsk, Russia*
[4] *Scientific Research Company "Carat", Lviv, Ukraine*

Background donor concentration (BDC) is the important parameter for HgCdTe (MCT) because all types of MCT–based photodetectors use some kind of *n*–type material, including photoconductors, photodiodes, and most recently, nBn detectors. As a background donor concentration, we understand a total concentration of residual donor dopants ($N_{RD}$) and intrinsic donor defects ($N_{ID}$). The problem with establishing BDC in MCT, relates to the fact that detection limits of many popular physical and chemical methods are much higher than doping levels of practical interest. To determine BDC in *p*–type material one needs to convert it into *n*–type and to bring to the minimum the level of electrical compensation. For *n*–type material, maximum reduction of the level of compensation is needed.

The unique method of BDC determination in HgCdTe is the using of ion milling (IM). At IM, the crystal is supersaturated with mercury interstitial, which during the diffusion completely annihilates mercury vacancies (intrinsic acceptors), and forms a donor complexes and centers with all the most known acceptor impurities in MCT (As, Sb, Cu, Ag, Au, etc.). After the finishing of IM, these complexes decompose even at room temperature, and after relaxation, the electron concentration adequately reflects the background donor concentration.

The proposed methodology was used to study the BDC in HgCdTe epitaxial films grown by different methods: molecular beam epitaxy (MBE), liquid phase epitaxy (LPE), Metal-Organic Chemical Vapour Deposition (MOCVD) in various research centers. It is shown that the lowest BDC (level $(2\text{-}4)\cdot10^{14}$ $cm^{-3}$) was observed for MBE films grown on Si substrates (Rzhanov Institute of Semiconductor Physics, Siberian Branch of RAS) and LPE films (JSC Research and Design Institute of Rare Materials Industry «GIREDMET»). Films grown with MOCVD (VIGO System SA) and with MBE (from various manufacturers) on GaAs substrates showed significantly higher BDC of the order of $\sim(2\text{-}4)\cdot10^{15}$ $cm^{-3}$. The possible reasons for the observed features are discussed.

In general, the studies showed the effectiveness of ion milling as a method of reducing electrical compensation in *n*–type MCT and an excellent tool for studying BDC, especially for samples extrinsically doped with acceptor dopants.

# Dispersion of Refractive Index of Thin Films Based on β-$Ga_2O_3$

Bordun O.M., Medvid I.I., Bordun B.O., Matviishyn M.V.

*Ivan Franko National University of L'viv, Lviv, Ukraine*

$Ga_2O_3$ thin films (0.2–0.8 μm) were prepared by radiofrequency (RF) ion-plasma sputtering on *v*-$SiO_2$ fused quartz substrates. Deposited films were heat treated in oxygen or Ar at 1000–1100°C and in $H_2$ at 600–650°C. X-ray powder patterns showed that the films were polycrystalline and differed depending on the heat treatment method. The results indicated that the films were oriented in the (400), (002), (111), and (512) planes after annealing in oxygen. Films oriented in the (400), (002), (111), and (512) planes also dominated after annealing in Ar. Films annealed in $H_2$ showed a weakly developed structure in which reflections from the (400), (002), and (512) planes also dominated.

We used a single-oscillator three-parametric model to describe the refractive index dispersion of films that were annealed in an atmosphere of oxygen (I), Ar (II) in the studied spectral range. It was to a certain extent a modification of the Zelmeer approximation:

$$n^2 - A = \frac{E_0 E_d}{E_0^2 - E^2}. \qquad (1)$$

Here $A$ is the approximation coefficient; $E_0$, the energy at the absorption band maximum that determined the spectral course of the refractive index; and $E_d$, the dispersion energy (oscillator strength)

Regression analysis made it possible to determine the approximation parameters in equation (1) for the studied films.

Table 1.

Crystal-chemical and energy parameters of dispersion curve for β-$Ga_2O_3$ thin films from equation (1)

| Films β–$Ga_2O_3$ | $A$ | $E_0$, eV | $E_d$, eV | $f_i$ | $N_c$ |
|---|---|---|---|---|---|
| I | 1.04 | 7.70 | 14.53 | 0.73 | 4.17 |
| II | 1.48 | 6.98 | 10.01 | 0.83 | 3.21 |

For films, which annealed in hydrogen was observed the anomalous dispersion and for films annealed in oxygen or argon observed the normal dispersion was demonstrated. At normal dispersion spectral dependence of refractive index in visible region is mainly determined by the transition from the top of the valence band formed by the 2p-states of oxygen to the bottom of the conduction band formed by the hybridization 2p-states of oxygen and 4s-states of gallium. For investigated films with normal dispersion the parameters of the one-oscillator approximation are determined, the dispersion energy, ionicity degree and coordination number are calculated.

# Electronic and Vibrational Structure of Complexes Formed by $C_{60}$ Fullerenes and Squaraine Dyes

Brusentsov V.A.[1], Pavlenko O.L [1], Kulish M.P.[1], Dmytrenko O.P.[1], Stubrov Yu.[2], Kachkovsky O.D.[3]

[1] *Taras Shevchenko National University of Kyiv, Kyiv, Ukraine*
[2] *V. Lashkaryov Institute of Semiconductor Physics, National Academy of Sciences of Ukraine, Kyiv, Ukraine*
[3] *Institute of Organic Chemistry, National Academy of Sciences of Ukraine, Kyiv, Ukraine*

$C_{60}$ fullerenes are an allotropic form of carbon known to act as efficient charge donors are acceptors, which makes them a lucrative choice in the design of organic solar power cells. A natural and straightforward way to functionalize the fullerenes would be to link them to molecular structures that convert solar radiation energy into charge in a specific region of photon energies. These conditions are satisfied by dyes, specifically squaraine dyes [1], derived from squaric acid, which form a bond with the fullerene via their central cycle.

The point of interest in this research is to study the electronic and vibrational properties of complexes formed by $C_{60}$ fullerenes and several squaraine dyes (such as one shown on Fig. 1) in order to determine the specifics of the mechanisms, by which they interact.

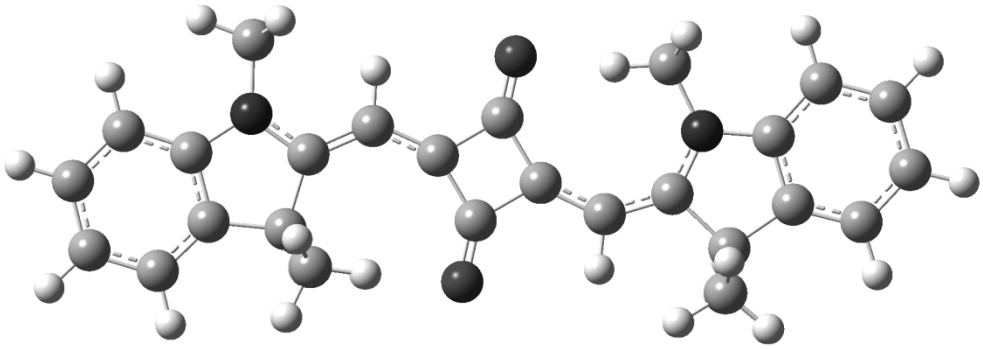

Fig. 1. A Ball and Bond Type model of a sample squaraine dye.

We use UV-VIS absorption, Raman scattering and photoluminescence measurements along with quantum-chemical calculations to explore the properties of the complexes and discuss the charge transfer, excited states, shapes of molecular orbitals and nonlinear features on experimental spectra.

Extra attention is given to the bridge that connects the squaraine dye to a fullerene, as it plays a sufficient role in the vibrational picture of the complex and the reallocation of charge.

1. G. Chen, D Yokoyama, H. Sasabe et.al., *App. Phys. Lett*, **101**, (2012), 08390.

# Photon Crystal Defect Mode in 1D Photonic Crystal Terminated by a Metal Film for Using in Sensorics

Dmitruk N.L., Korovin A.V., Mamykin S.V., Sosnova M.V.

*Institute of Semiconductor Physics, NAS of Ukraine, Kyiv, Ukraine*

Nowadays, plasmon-polariton photodetectors and optochemical sensors are widespread in different fields of science, medicine and industry. This is a stimulus for an active research to enhance the working characteristics of these systems (sensitivity, selectivity, geometric specification etc.).

The excitation of photon crystal defect mode can be realized in the case of the photonic crystal (PhC) terminated by a metal film. The position of this defect mode highly depends on geometrical and optical properties of the PhC and its boundaries [1]. In this work we study the active plasmon-polariton devices based on Schottky barrier that is united with the 1D PhC deposited on the top of a periodically profiled thin metal film located on semiconductor substrate (1D PhC/Au/GaAs).

The modeling of light transmittance through multi-layered structure with periodically profiled metal film in the framework of the differential formalism is presented in the figure 1 for varied thickness of the front layer of 1D PhC that can be base of selectively sensitive layer. The 1D photonic crystal is based on Bragg mirror consisting of repetition of sequence of two dielectric films with refractive indices, $n_1$, $n_2$ ($n_1$=1.47, $n_2$=2) and thicknesses, $d_1$, $d_2$, that equal to quart-length of photonic band gap (we chose 700 nm) in corresponding media. The geometrical parameters of texturized metal (gold) film with correlated sine profiles are a period of 700 nm, a thickness of 50 nm and a profile depth of 50 nm. The defect mode of 1D PhC is located inside PhC band gap (600-900 nm) and rapidly blue-shifted at decreasing of the thickness of first layer of 1D PhC.

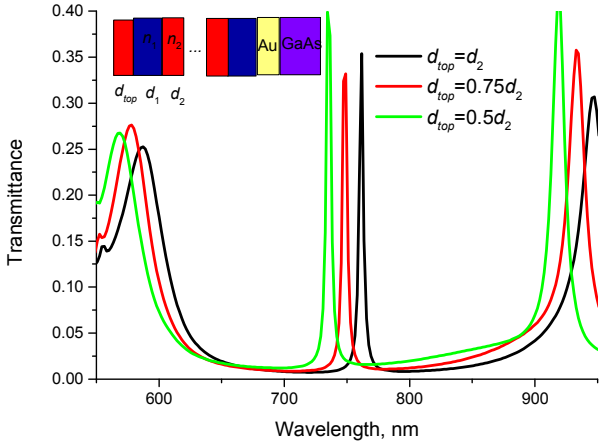


Fig.1. Calculated transmittance of *p*-polarized light through multilayered plasmonic-photonic structure based on Schottky barrier (1D PhC/Au/GaAs) for varied thicknesses of front 1D PhC layer.

# High Temperature Oxidation of Nickel Silicides Films Formed from Thin Ni Films

Dranenko A.S., Koshelev M.V.

*Frantsevich Institute for Problems of Materials Science of NASU, Kyiv, Ukraine*

Transition metal silicides (NiSi, TiSi2, CoSi2, etc) are widely used in the semiconductor industry, e.g. complementary metal-oxidesemiconductor (CMOS) devices, as ohmic contact, gate electrodes, diffusion barriers and local interconnects. Nickel silicides are one of the most widely studied silicide systems due to their high temperature performance and micro/nanoelectronics application.

In this work the phase formation and thermal oxidation stability of NiSi and NiSi2 thin films on n-type Si (111) substrates have been investigated. The objects to study were thin-film layers of Ni (200nm) on crystalline Si substrate of orientation (111) doped with phosphorus. Thin-film system Ni/Si obtained by electron-beam deposition in vacuum $2 \cdot 10^{-4}$ Pa. After deposition the samples were annealed in a furnace with oil-free vacuum pumping $1.33 \cdot 10^{-3}$ Pa in the temperature range 470 – 1270 K.

As-deposited and annealed films were examined with an EMR-100 electron diffraction unit. The calculated values of interplanar spacing were compared with the corresponding tabulated values. The thermogravimetric analysis was carried out with a ″Derivatograph Q-1500D″ unit in the following conditions: temperatures range 300–1270 K, sample weight ~ 20mg, open air, heating rate 10 K/min.

In the initial state, the Ni (200 nm)/Si thin-film system with a layer of ″natural″ oxide $SiO_2$ (~ 6–10 nm) was present nickel phase. At annealing temperature 770 K a number of nickel phase remains after annealing the system. Further increase in annealing temperature to 970 K leads to formation of $Ni_2Si$ and NiSi. Remaining phase of nickel is not observed. Nickel disilicide formed at temperature of 1270 K.

According to data TGA, high-temperature oxidation of the NiSi films and the associated increase in weight begins at about 250 degree higher than the oxidation of a silicon substrate. The oxidation of NiSi film starts at 930 K, which is approximately 100 K below the temperature at which $NISi_2$ films start oxidising. For both NiSi and $NISi_2$ oxidation types the $SiO_2$ thin protective layers have been formed. When temperature increases, the mass increment NiSi films becomes greater than that of $NiSi_2$ films. This difference is three times as great at 1270 K, which is due to the difference in their structure and stoichiometry. Due to high silicon content, nickel dicsilicide forms dense layers of silica on the surface during oxidation, which has substantial impact on the oxidation rate.

# Amorphization of Helium Implanted YIG Films

Fedoriv V.D., Kurovets V.V., Garpul O.Z.

*Vasyl Stefanyk Precarpathion National University, Ivano-Frankivsk, Ukraine*

The mechanism of amorphization in helium implanted single crystalline YIG films was investigated. The possibility of the radiation disordered region formation in the film at helium implantation with energy of 100 keV is shown. It received distribution of the displaced matrix ions at high-energy helium ions collisions with target atoms. The formation of radiation disordered region with the greatest number of atoms observed in the near-surface area of the material, but the maximum number of them is at a depth of 370 nm.

It was calculated degree of amorphization Ω YIG film in dependence of the helium implantation dose according to [1]. With the value of Ω = 0,85 is the association of some amorphous zones in a continuous layer and amorphization dose for our experimental conditions will be $8 \cdot 10^{16}$ см$^{-2}$. In the range of doses $1 \cdot 10^{15}$-$1 \cdot 10^{16}$ $He^{+}$/см$^2$ the degree of amorphization of YIG film increases linearly from 0.02 to 0.21.

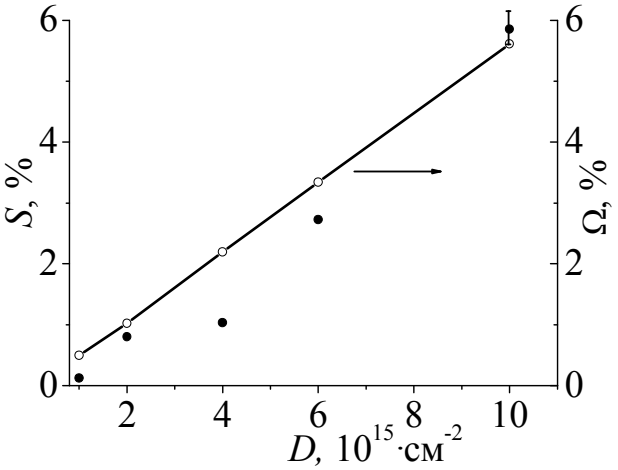


Fig. 1. The relative integral intensity of the paramagnetic doublet *S* in the CEM spectra and theoretically calculated degree of amorphization Ω as function of dose for helium implanted single crystalline YIG films

Radiation disordered regions at room temperature are represented as paramagnetic inclusions in ferrimagnetic matrix. Comparative analysis of the relative integral intensity of the paramagnetic doublet *S* in CEM spectra of implanted single crystalline YIG films and theoretically calculated degree of amorphization Ω at the dependence of helium ions dose (fig. 1) shows the consistency of theoretical calculations with experimental data.

1. A. Markelis, L. Pranevičius. On mechanism of suppression of hard bubbles in garnet films // *Lietuvos fizikos rinkinys*, **18** (5) pp. 647-652 (1978).

# Magnetic Microstructure of Dispersed Yttrium Iron Garnet Obtained by Sol-Gel Method

Fedoriv V.D., Stashko N.V., Moklyak V.V.

*Vasyl Stefanyk PreCarpathian National University, Ivano-Frankivsk, Ukraine*

Ferrimagnetic garnets are very well suited for magnetism studies, as these materials have a uniquely defined cation distribution. However, to improve their present applications a full understanding of their magnetic properties is required. Magnetic properties depend critically on the structure and microstructure of the materials [1]. We have synthesized $Y_3Fe_5O_{12}$ with a single garnet phase sample by a sol–gel method. This method enables to get finely dispersed polycrystalline porous material with a homogeneous size particles.

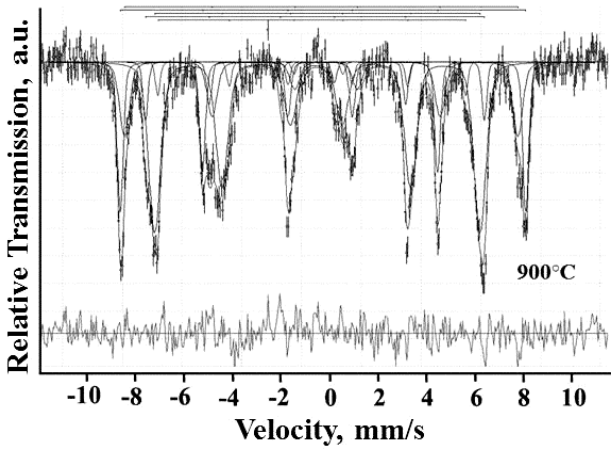


**Fig. 1.** $^{57}$Fe Mössbauer spectrum recorded from the YIG particles prepared at 900 °C.

Annealing at 900 ºC in air leads to the formation of the garnet single-phase system in which iron ions are in two non-equivalent a-positions and in three non-equivalent d-positions. The presence of a significant number of non-equivalent positions of $Fe^{3+}$ ions can be associated with the distortion of oxygen octahedrons and tetrahedrons, respectively. Annealing of system at 1000 ºC and 1100 ºC has not made any significant changes of the magnetic microstructure. Slight decrease of line width of some sextets of the Mössbauer spectrum is apparently caused by decrease of the number of oxygen vacancies as a result of increasing the annealing temperature, which is confirmed by the growth of the magnetic field at the iron nuclei in a-position from 474 kOe to 480 kOe.

1. Sanchez R.D., Rivas J., Vaqueiro P., Lopez-Quintela M.A., Caeiro D. Particle size effects on magnetic properties of yttrium iron garnets prepared by a sol–gel method // Journal of Magnetism and Magnetic Materials. – 2002. – №247. – P.92 – g 98.

# Dependence of Yttrium Iron Garnets Magnetic Domain Structure on Structural Parameters

Fodchuk I.M.[1], Dovganiuk V.V.[1], Gutsuliak I.I.[1], Lytvyn P.M.[2], Safryuk N.V.[2], Kladko V.P.[2], Syvorotka I.M.[3], Bonchyk O.Yu.[4], Kotsyubynsky A.O.[5],

[1] *Yuriy Fedkovych Chernivtsi National University, Chernivtsi, Ukraine*
[2] *V.E. Lashkaryov Institute of Semiconductor Physics NASU, Kyiv, Ukraine*
[3] *Scientific Research Company "Carat", Lviv, Ukraine*
[4] *Institute of Applied Problems of Mechanics and Mathematics of NASU, Lviv, Ukraine*
[5] *V. Stefanyk Prykarpatskyy University, Ivano-Frankivsk, Ukraine*

Comprehensive research of influence of the transition layer thickness, spatial distribution of macrodeformations and microdefect structure on the formation of crystalline and magnetic domain structure of epitaxial yttrium iron garnet films (YIG) of different thicknesses (Fig. 1) was carried out. Scanning atomic-force (Fig. 1), magnetic-force microscopy (Fig.1b) and high-resolution X-wave diffractometry (Fig.1c) was used. $Y_3Fe_5O_{12}$ epitaxial films with thicknesses of 2.3 (sample №1), 6.41 (№2) and 94.4 microns (№3), grown in SRC "Carat" on $Gd_3Ga_5O_{12}$ (111) substrates, were used as objects of research.

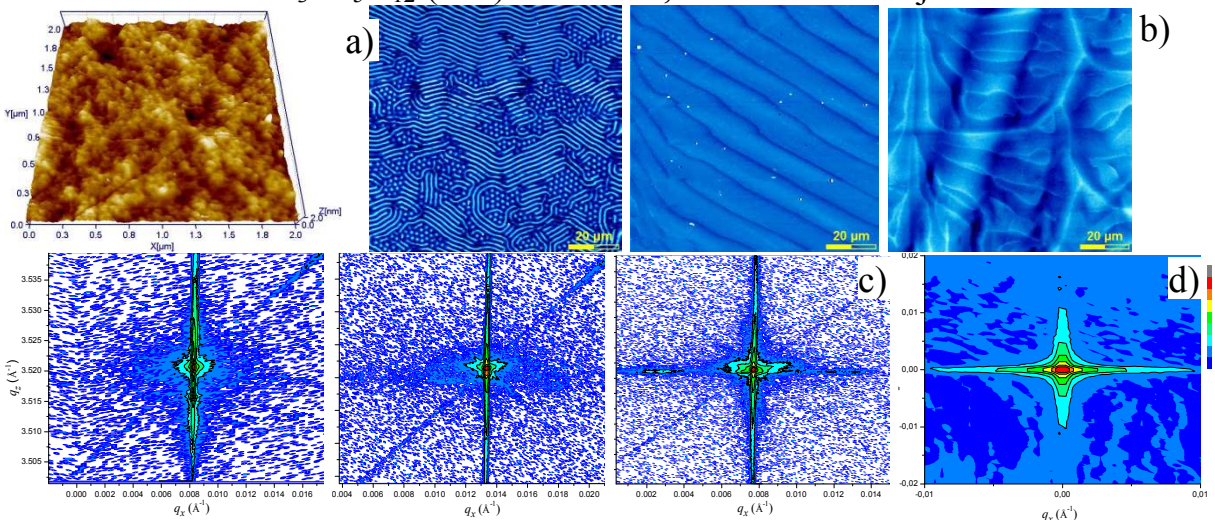


Fig. 1. YIG: a) AFM, sample №1; b) MFM, №1-№2; c)RSM, №1-№3; d) simulation.

Simulation of reciprocal space maps (RSM) (Fig. 1d) was carried out using equations of Krivoglaz kinematic theory [1]. The transition layer model is presented in the form of two sets of mismatch dislocations of different density that differ by directions of the Burgers vector. It was established that the thickness of film-substrate transition layer, dislocation density, lateral nonstoichiometry, character of macrodeformations distribution along the thickness and the presence of various types of microdefects has significant influence on the magnetic stripe domain structure (Fig.1b).

1. M. A. Krivoglaz, X-Ray and Neutron Diffraction in Nonideal Crystals. Springer, Berlin, 1996, 460 p.

# Critical Properties of Ferroelectric and Ferromagnet Models

Galdina A.N.

*Oles Honchar Dnipropetrovsk National University, Dnipropetrovsk, Ukraine*

Solving the problem of description of the behaviour of thermodynamic parameters near the critical points one considers either the simplest models, for which the partition function can be evaluated exactly, or an approximate solution of the problem. At the first approach the exactly solvable 2-dimensional models [1] are of great importance. The second approach is connected mainly with examination of the asymptotic behaviour of thermodynamic parameters near the critical points, as well as with the development of the scaling law hypothesis, the universality hypothesis and the renormalization group approximation and has appreciably succeeded. Indeed, the large class of real systems and models satisfies the scaling law and the universality hypotheses. The existence of real systems and exactly solvable 2-dimensional models, for which these hypotheses are violated, is also remarkable. The 6-vertex ferroelectric Lieb model and the 8-vertex Baxter model [1] are such examples. These models give a reasonable fit to real ferroelectrics (antiferroelectrics) and ferromagnets (antiferromagnets), because there are a lot of crystals with strong horizontal and weak vertical bonds in the nature, for which 2-dimensional models are suitable.

The properties of 2-dimensional exactly solvable Lieb and Baxter models in the critical region are considered on the base of thermodynamical method developed for investigation of critical state of one-component system. From the point of view of the thermodynamic stability the behaviour of the whole set of thermodynamic characteristics of stability for these models is analyzed. The reasons for the violation of the scaling law hypothesis and the universality hypothesis for the models are clarified. For ferroelectric Lieb model it is ascertained that in subcritical and supercritical areas two types of critical behavior, different in fluctuation growth of energy and electric polarization are realized. This results in symmetry breaking of subcritical and supercritical indices, in essentially different behaviour of the same thermodynamic parameters on each side of a critical point. Baxter model is characterized by the same two types of critical behaviour, one of which is also presented in three cases, depending on a slope of phase equilibrium curve at the critical point. The type of the behaviour is varying dependently on the interaction parameter of the model. It is interesting to emphasize that in each model while one hypothesis is violated, another nevertheless holds. In addition, the special case of the 8-vertex Baxter model, where the universality hypothesis is violated, is the Lieb model, in which the universality hypothesis is satisfied, but the scaling law hypothesis is violated, and the Ising model, where both hypotheses are fulfilled.

1. R.J. Baxter Exactly Solvable Models in Statistical Mechanics. – London: Academic Press, (1982). – 488 p.

# Morphology and Vibrational Structure of Multi-Wall Carbon Nanotubes

Gaponov A.M.[1], Salyi M.Ya.[1], Busko T.O.[1], Kulish M.P.[1], Dmytrenko O.P.[1], Strelchuk V.V.[2], Stubrov Yu.Yu.[2]

[1] *Taras Shevchenko National University of Kyiv, Kyiv,Ukraine*
[2] *V. Lashkaryov Institute of Semiconductor Physics, National Academy of Sciences of Ukraine, Kyiv, Ukraine*

In recent time multi-wall carbon nanotubes (MWCNs) were used for organic bulk heterojunction structure [1]. The preparation of controlled morphology in which uniform distribution of MWCNs in the whole bulk of films is necessary. The MWCNs prefer to form agglomerates to homogenic distribution. As the diameter of MWCNs is less than the film thickness of organic photovoltaic cells, the MWCNs planar location can leads to surface conductivity. Fig. 1, 2 show SEM images of as-prepared MWCNs and made by Langmuir–Blodgett (LB) after ultrasonic treatment in chloroform solution (2 hours) 0,1 mg/ml, respectively. The parameters of ultrasonic treatment: frequency 40 kHz, power 50 watt and volume 0.5 L. The transfer of film on glass substrate was due to horizontal lifting in LB method.

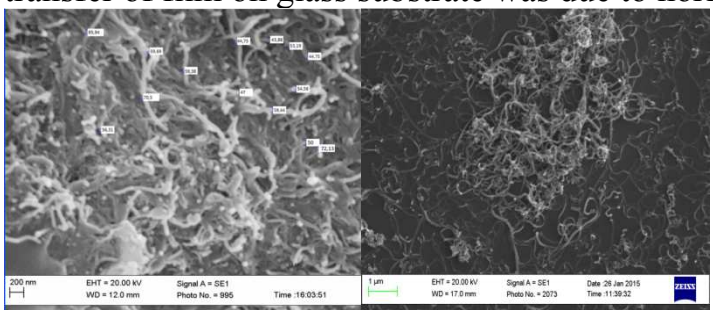

Fig. 1. SEM images of as-prepared MWCNs.



Fig.2. SEM images of MWCNs made by LB method.

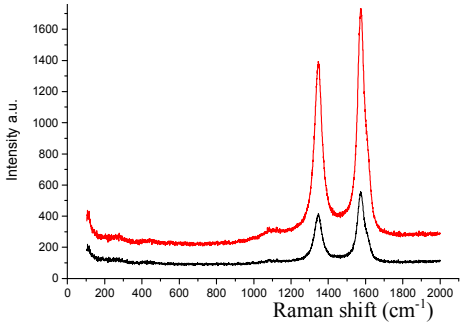


Fig.3. Raman scattering of as-prepared MWCNs (black curve) and MWCNs made by LB method (red curve).

The mean diameters of MWCNs after 2 hours of ultrasonic treatment is 54.28 nm, which is not very different from as-prepared (55,82 nm). Also, there is no difference of their length that average is about 3.5 μm before and after ultrasonic treatment. There are G, D modes in Raman spectrum of MWCNs at frequencies 1346 and 1574 $cm^{-1}$, respectively. As shown in Fig. 3 shows the Raman spectrum of MWCNs. The position of G, D modes of both before and after treatment identical to within $cm^{-1}$. The *G*/*D* ratio remains almost unchanged. Based on experimental results we can say that MWCNs before and after ultrasonic treatment stay almost the same structure. LB method allows to obtain a monolayer MWCNs films.

1. J. Arranz-Andre´s, W. J. Blau. Enhanced device performance using different carbon nanotube types in polymer photovoltaic devices // Carbon.– 2008. – 46, 2067.

# Films Based on Colloidal Silver Nanoparticles for Surface-Enhanced Raman Scattering of Rhodamine 6G

Golichenko B.O.[1], Strelchuk V.V.[2], Kravchenko S.O.[2], Kolomys O.F.[2]

[1] *Taras Shevchenko National University of Kyiv, Kyiv, Ukraine*
[2] *V.E. Lashkaryov Institute of Semiconductor Physics NAS of Ukraine, Kyiv, Ukraine*

Films with colloidal metallic particles for Raman scattering are often used for studying vibrational structure of organic and bio-molecules. These films give a possibility to obtain significant amplification of the signal and to detect a small amount of the substance. In addition, they are cheap and very simple in preparation. Varying the parameters of synthesis of the colloidal particles results in formation of films with optimal thickness and size of the silver particles. These factors influence on plasmonic enhancement of SERS-substrates.

Colloidal Ag-nanoparticles with the density 20 $\mu m^{-2}$, 9 $\mu m^{-2}$ та 4 $\mu m^{-2}$ were prepared on the thin silicon substrate by a method of the "silver mirror reaction". Obtained SERS-substrates were immersed in solution of Rhodamine 6G with concentration $10^{-8}$ Mol/L.

In micro-Raman experiment laser with excitation wavelength $\lambda = 488$ nm was used. Figure 1 shows the Raman spectra of Rhodamine 6G adsorbed on colloidal Ag-nanoparticles. For Ag-nanoparticles with different densities the factors of SERS-enhancement $5.2\times10^6$, $1.3\times10^6$ and $7\times10^5$ were obtained.

Mechanisms of SERS-enhancement discussed.

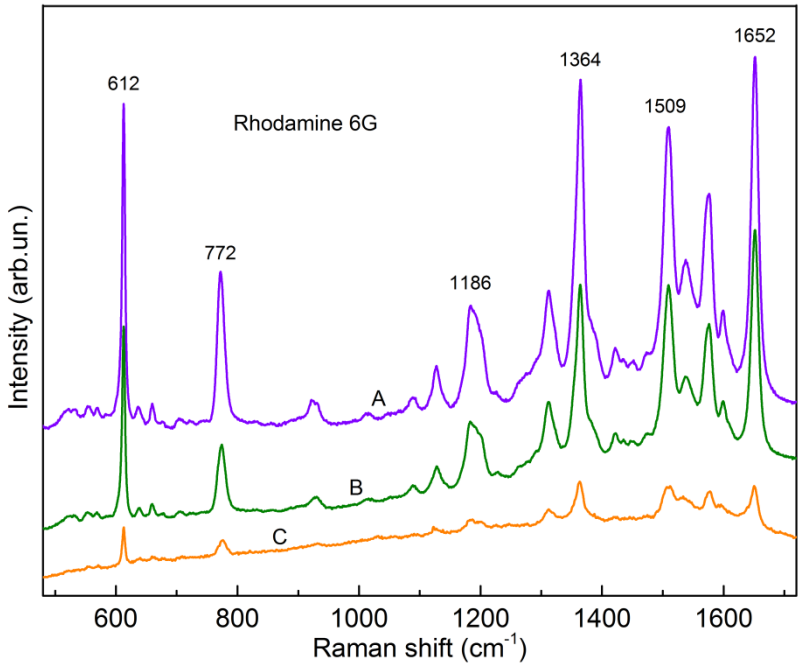


Figure 1. Micro-Raman spectra of R6G $10^{-8}$ Mol/L on SERS-substrates with density of colloidal nanoparticles 20 $\mu m^{-2}$ (A), 9 $\mu m^{-2}$ (B) and 4 $\mu m^{-2}$ (C).

# Compositional Dependence of the Optical Properties of Amorphous $In_x(Ge_{40}S_{60})_{100-x}$ Thin Films

Horvat H.T.[1], Vlcek M [2], Rizak V.M.[1]

[1] *Uzhhorodskyy National University, Uzhhorod, Ukraine*
[2] *University of Pardubice, Pardubice, Czech Republic*

Chalcogenide glasses are one of the most widely known families of amorphous materials and have been studied for several decades, because of their interesting fundamental properties and wide range of applications. These glasses have attracted considerable attention due to their infrared transparency, low phonon energy and high refractive indices. They have been explored as promising candidates for optical memories, gratings, switching devices. They are used for optoelectronics as infrared elements and devices for acousto-optic devices, holography, xerography and information storage media

Ge–S amorphous system are very good glass-former. The addition of dopants such as Indium (In) controls its electrical and optical properties. Moreover, the Ge–S–In system is of special interest, and it forms glasses over a wide composition range. It occurs up to 15 at.% In and 60–90 at.% Se and the rest is Ge. Various studies have reported on the structural, electrical and optical properties of Ge–S–In glasses. They are characterized by high refractive index, low optical losses and good infrared transparency.

Amorphous $In_x(Ge_{40}S_{60})_{100-x}$ thin films with different compositions ($x$ = 3, 5 and 7 at.%) were deposited onto glass substrates by thermal evaporation. Bulk chalcogenide glasses of the appropriate composition were synthesized by the usual melt quenching technique.

The effect of Indium content on the optical properties of $In_x(Ge_{40}S_{60})_{100-x}$ films was analyzed in the wavelength range 400–2500 nm. The refractive index was found to decrease with the increase of the In content. The behavior of the refractive index with the wavelength was explained using the model of single oscillator proposed by Wemple and Di Domenico. Band gap energy and cohesive energy increase with increasing In concentration.

# Electrochemical Properties of Composites $C/Ni(OH)_2$ and $C/Ni(OH)_2/MoO_3$

Khemiy O.M., Yablon L.S., Budzulyak I.M., Ostafiychuk B.K.

*Vasyl Stefanyk Precarpathian National University, Ivano-Frankivsk, Ukraine*

Nickel hydroxide and molybdenum trioxide are cheap alternative materials exhibiting capacitive behavior similar to ruthenium oxide, which is too expensive for commercial use. To increase the conductivity of these materials we used nanoporous carbon, which is a good conductive additive and can solve the problem of nanoparticles coagulation when the electrode material is nanodispersed.

Fig. 1 shows the cyclic voltammogramms of nanocomposite electrodes $C/Ni(OH)_2$ and $C/Ni(OH)_2/MoO_3$ at the scanning speed of 1 mV/s. There are two redox peaks responsible for pseudocapacity: one peak - anode (positive current density) during the oxidation of $Ni^{2+}$ to $Ni^{3+}$, and the second - cathode (negative current density) in the reverse process. These peaks are fast reversible redox processes occurring at the interface of $Ni(OH)_2$ and $Ni(OH)_2/MoO_3$ from one side and the electrolyte from the other. This shows that the capacitance characteristics are mainly regulated by faradic reactions, not only the capacity of the electrical double layer.

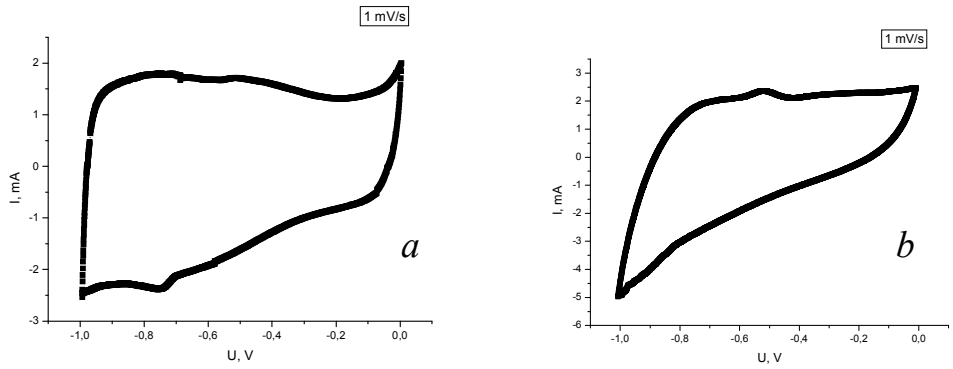


Fig. 1. Cyclic voltammogramms of electrochemical cell formed based on the composites: *a*) $C/Ni(OH)_2$, *b*) $C/Ni(OH)_2/MoO_3$ at the scanning speed of 1 mV/s

Voltage dependence of the cell current is not linear during the charge/discharge, due to the redox processes that occur at the cathode during charge and discharge.

Analysis of the charge/discharge curves of electrochemical cells formed on the basis of the composites shows that the cell, which electrode formed from the composite $C/Ni(OH)_2/MoO_3$, specific capacity reaches a maximum value at the current of 1 mA; this value is reduced more than twice with the current increasing up to 5 mA. For composite $C/Ni(OH)_2$ specific capacity is practically unchanged with the current increasing.

# Strain Distribution in Synthesized Diamonds

Khomenko V.[1], Borcha M.[1], Fodchuk I.[1], Balovsyak S.[1], TkachV.[2]

[1] *Yuriy Fedkovych Chernivtsi National University, Chernivtsi, Ukraine*
[2] *V.Bakyl Institute for Superhard Materials of NAS of Ukraine, Kyiv, Ukraine*

The complex of experimental methods (electron backscattering diffraction, X-ray microanalysis, X-ray topography) was used for determination of local strain distributions in diamond crystals synthesized in different growth systems: by a temperature-gradient method in a Fe–Al–C system (first sample), and diamond film Mg–C + B grown on diamond single crystal of Ni–Mn–C system (second sample). EBSD patterns (Kikuchi patterns) were obtained by using of scanning electron microscope "Zeiss" Evo-50 with CCD detector.

A new ways for determination of planar distribution of local strains in crystal from Kikuchi patterns were proposed including histogram method and method of direct two-dimensional Fourier transformation. Relationships between changes of fine structure of two-beam Kikuchi lines and multi-beam areas and crystal imperfections were established [1]. It gave possibility to determine strains in local areas of samples.

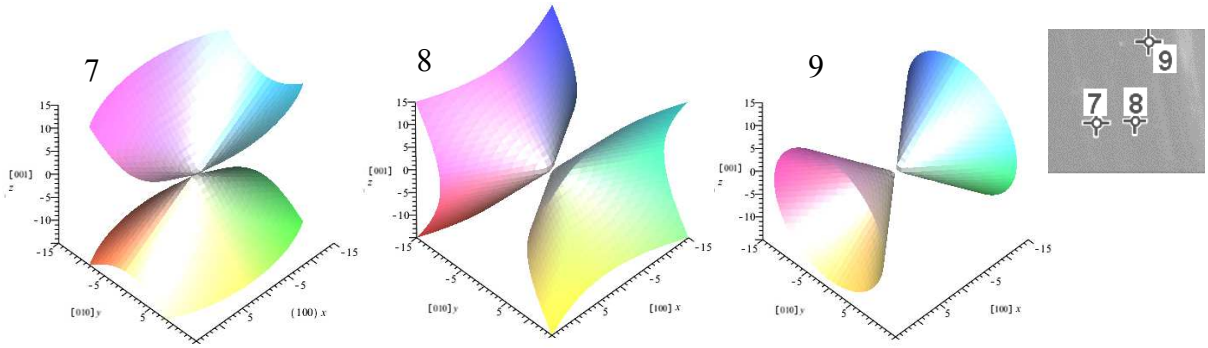


Fig. 1. Characteristic surfaces of strain tensor (a), which correspond to different local areas 7, 8, 9 of diamond crystal (b)

The researches of displacements of Kikuchi-band intersections and changes of integral intensity along crosssection of Kikuchi band allowed to determine the strains in $[\bar{4}00]$, $[\bar{1}11]$ and [022] directions for a local areas of synthesized diamond crystals. It is shown that $(\bar{1}11)$ planes are the most strained and $(\bar{4}00)$ planes are the less strained for the first sample. The second sample revealed the increase of strains in all directions, especially in [022] direction.

1. Borcha M.D. Local strains in diamond crystals determined by Fourier-transformation of Kikuchi patterns / M.D. Borcha, S.V. Balovsyak, I.M.Fodchuk, V.Yu.Khomenko, O.P.Kroitor, V.N. Tkach // Journal of Superhard Materials. – 2013. – Vol.35, Issue 5. – P. 220-226.

# The Features of the Formation a Thin Silicon Oxide Layer on the Surface of Silicon Carbide in the Oxidation in Ozone Pairs

Konakova R.V.[1], Okhrimenko O.B.[1], Lytvyn O.S.[1], Svetlichnyi A.M.[2],

[1] *Lashkarev Institute of Semiconductor Physics, ,Kiev, Ukraine*
[2] *Southern Federal University, Taganrog, Russia*

One of the most important factors which determining the reliability of functional devices based on MOS - structure, is the quality of the insulating oxide, which is located between the locking electrode and the semiconductor. In this regard, the using of $SiO_2$ is very attractive, not only due to its dielectric properties, but also because of its capability of growing SiC on the surface of standard methods of oxidation.

In the present study the morphological properties of $SiO_2$, which obtained by SiC oxidation into ozone and oxygen was compared.

On the Figure 1 the AFM images of the $SiO_2$/SiC structures surface, obtained by oxidation under temperature 1000°C in ozone pairs (Figure 1a) and in the oxygen vapor (Figure 1b) was shows.

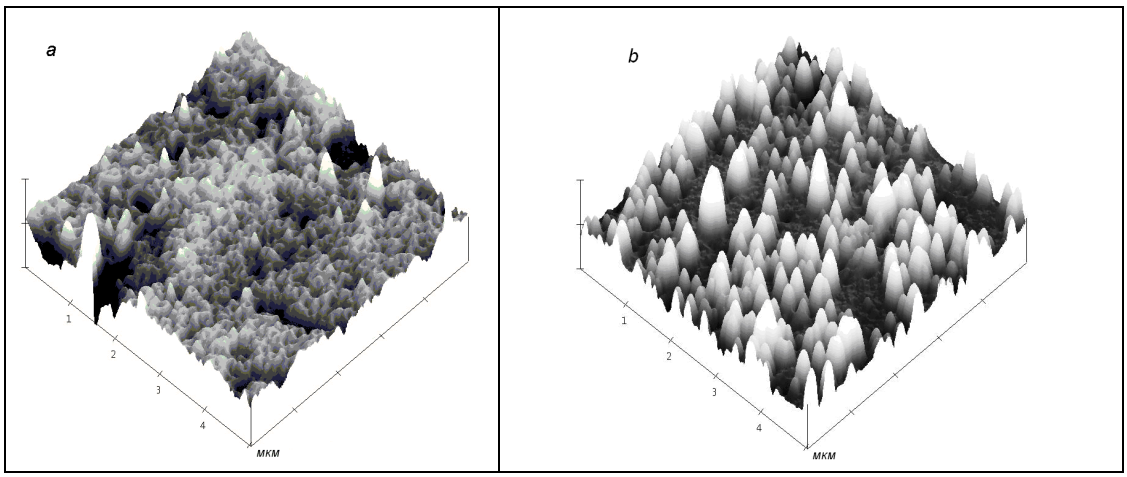


Figure 1. AFM images of the of $SiO_2$/SiC structures surface. *a* - oxidation in ozone pairs, *b*- in oxygen vapor.

As seen from Figure 1, the oxidation of silicon carbide an the ozone pairs allows to form the $SiO_2$ layer with a smoother surface than in the case of silicon carbide oxidation an oxygen vapor. An increase in temperature oxidation to 1100°C in both cases leads to a smoothing of the microrelief of the oxide layer. AFM data correlate with the data obtained from the transmission spectra of $SiO_2$/SiC structures.

Thus, from the above morphological studies of the $SiO_2$/SiC surface structures, it can be concluded that the oxide layer which is formed in the ozone vapor is better than in the oxygen pairs.

# Increase of $TiO_2$ Photoanodes Efficiency as a Consequence of Surface Modification with Catalyst for Dark Oxidation Reaction of Water

Korablov S.F., Danko D.B., Sylenko P.M., Khyzhun O.Y., Solonin Y.M.

*Institute for Problems in Materials Science, Kyiv, Ukraine*

Dark water oxidation reaction have been studied by recording the anode current density dependences from potential in the 3-electrode cell with Ni cathode and silver chloride comparison electrode in a solution of 1 M KOH. The electrode potential was changed using a stabilized voltage source B5-44. The current was measured with microammeter. Photoanodes for research were produced through $TiO_2$ deposition on a Ti substrate in the CVD process. Catalyst films of Mn that accelerate the dark reaction of the water oxidation were formed by thermal deposition in vacuum over $10^{-4}$ Torr. In the case of thin layers of manganese (deposition time < 20s), there was only unstable effect of accelerating of water oxidation compared to the unmodified electrode (Fig. 1). The same effect caused a mechanical wiping of thick (the deposition time 450s) layer of manganese catalyst. However, in the case of electrochemically passivated Ti-anode (Fig. 2), which is a model of $TiO_2$ photoanode, a significant and sustained effect in reducing the potential of $O_2$ release was registered. Study of modified anode surface by X-ray photoelectron spectroscopy (Fig. 3) revealed the presence of a Mn oxides (IV/III) mixture. At optimal thickness of $MnO_2$ layer (the deposition time 20s) an uniform oxygen evolution was observed over the entire surface of the modified electrode. When a thick layer of Mn oxide was obtained (deposition time > 300s), the energetic oxygen evolution was observed only at the ends of the modified electrode. This means that the active places for the passage of the water oxidation reaction are situated exactly on the border of $MnO_2/TiO_2$. Thus, thin layers of Mn oxides on the surface of $TiO_2$ photoanodes accelerate the dark water oxidation reaction.

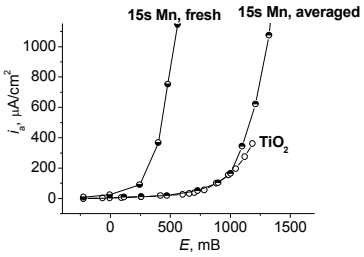


*Fig. 1 Current density dependencies of $O_2$ release on potential of $TiO_2$ photoanodes modified by Mn*

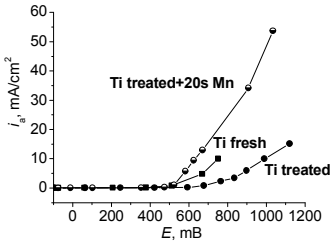


*Fig. 2 Current density dependencies of $O_2$ release on Ti-anode potential in the initial state (fresh), passivated (treated) and modified (Mn)*

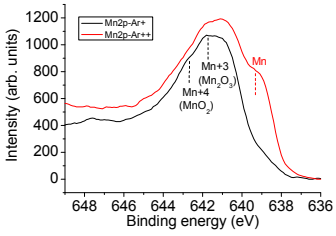


*Fig. 3 XPS spectra of Ti anode modified by Mn*

# Structure and Mechanical Properties of Splat-Quenched Al-Co-Cr-Fe-Ni-V Alloys Films

Kushnerov O.I., Bashev V.F.

*Oles Honchar Dnipropetrovsk National University, Dnipropetrovsk, Ukraine*

Most conventional alloys traditionally have been based on one solvent element to which various solute atoms are added for improving specific properties. In recent years, one kind of new alloys, high-entropy alloys (HEA) with multiple principal elements, has received more and more attentions due to its unique structure and excellent properties in hardness and wear resistance, exceptional high-temperature strength, good structural stability, radiation and corrosion resistance [1]. Each principal element in HEA should have a concentration between 5 and 35 at.%. Because of high mixing entropy of HEAs (12-19 J/(K·mol)), they usually consists of some simple solid solutions, instead of complex phases or inter-metallic compounds. Structure and mechanical properties (microhardness) of splat-quenched films (cooling rate~$10^6$ K·$s^{-1}$) of HEAs of Al-Co-Cr-Fe-Ni-V system are investigated in this paper.

The XRD patterns were used to determine the phase composition, lattice parameters, and the parameters of the fine structure (size of coherent scattering areas) and microstresses. The density of dislocations ρ was estimated based on the profile of the first diffraction maximum. The results obtained are given in Table. XRD analysis allowed us to establish what splat-quenched films of $Al_xCoCrFe_yNiV$ HEAs have single-phase body-centered cubic (BCC) structure. The lattice parameters shows that the solid solution are based on chromium as the element with the highest melting point (the lattice parameter of Cr $a$= 0.2884nm). High microhardness values of alloys can be explained by the presence of the dissimilar atoms of elements with different size, electronic structure and thermodynamic properties in the crystal lattice. This leads to significant distortion ($\Delta a/a$) of crystal lattice. Consequently the hardness of $Al_xCoCrFe_yNiV$ alloys films has been increased.

Table.

Phase composition, coherent scattering areas (L), degree of crystall lattice distortions (Δa/a), microhardness ($H_\mu$) and dislocation density (ρ) in films

| Alloy | Phase composition | $L$, nm | $\Delta a/a$ | $H_\mu$, MPa | ρ, $cm^{-2}$ |
|---|---|---|---|---|---|
| AlCoCrFeNiV | BCC ($a$=0.2883 nm) | 33±2 | $2.0\cdot10^{-3}$ | 6600±300 | $1.55\cdot10^{12}$ |
| $AlCoCrFe_2NiV$ | BCC ($a$=0.2880 nm) | 24±2 | $2.8\cdot10^{-3}$ | 6200±200 | $6.30\cdot10^{11}$ |
| $Al_2CoCrFeNiV$ | BCC ($a$=0.2889 nm) | 34±2 | $1.3\cdot10^{-3}$ | 7500±300 | $4.60\cdot10^{11}$ |
| $Al_2CoCrFe_2NiV$ | BCC ($a$=0.2882 nm) | 33±2 | $1.7\cdot10^{-3}$ | 5600±200 | $4.52\cdot10^{12}$ |

1. Murty B.S., Yeh J.W., Ranganathan S. High-Entropy Alloys.– London:Butterworth-Heinemann, 2014.–218p.

# Change of Microhardness of Amorphous Thin-Films of the System Ge-As-Se Under the Influence of Laser Irradiation

Kuzma V.V.[1], Bilanych B.V.[1], Flachbart K.[3], Lofaj F.[2], Csach K.[3], Bilanych V.S.[1], Rizak V.M.[1],

[1] *Faculty of Physics, Uzhgorod National University, Uzhgorod, Ukraine*
[2] *Institute of Materials Research of SAS, Kosice, Slovak Republic*
[3] *Institutes of Experimental Physics of SAS, Kosice, Slovak Republic*

This paper presents the results of studies of photoinduced changes in microhardness of amorphous films $Ge_xAs_ySe_{100-x-y}$ under influence of laser irradiated (laser power of 50 mW, wavelength of 655 nm). For realization of researchers chalcogenides glasses for such syllables were prepared: $Ge_4As_4Se_{92}$, $Ge_9As_9Se_{82}$, $Ge_8As_{32}Se_{60}$, $Ge_{16}As_{24}Se_{60}$, $Ge_{24}As_{16}Se_{60}$, $Ge_{32}As_8Se_{60}$ and $Ge_{40}Se_{60}$. The thin films were got thermal evaporation method of glasses by analogical syllables in a vacuum ($10^{-3}$ Pa) on surface from quartz glass. Measuring of microhardness of *H* was conducted by means of PMT-3 instrument with the used of indenter of Vickers on-loading 0.05 Pa. At including of laser microhardness exponentially diminishes during the first 25-30 min in dependence on chemical composition lowering of microhardness of films makes a 10 - 27 %. Increase of time of irradiation over 30 min results in stabilizing of microhardness.

It is educed that at increase of mane coordinating number of Z in an interval a 2.12 - 2.48 size $\Delta H$ changes poorly enough. At Z=2.67 ($Ge_{24}As_{16}Se_{60}$) there are the minimum relative photoinduced changes of microhardness. At the increase of Z from 2.67 to 2.80 sizes $\Delta H$ swiftly grows approximately in 7 times ($Ge_{40}Se_{60}$). The indicated intervals of the photoinduced changes of microhardness of films of $Ge_xAs_ySe_{100-x-y}$ correlate with position of areas of glasses with different structural flexibility on the diagram of glass formation in the system Ge - As - Se. As a point at Z=2.67 is a 2d-3d topological structural transit point is possible to assert that the maximal photoinduced changes of mechanical parameters of chalcogenide glasses of the system Ge - As-Se, take place in glasses with a three-dimensional structure. This feature can be explained within the structure of intermolecular structural model of the photoinduced plasticity of chalcogenides glasses. The structure of films of the system Ge - As - Se at $Z > 2.67$ under the action of laser irradiation passes the broken of the homopolar bonds in (As - As, Ge - Ge) and transformation of formed by them has volume (3-measurable) structural units of the plenary trivial oriented complexes. As a result of such processes structure of dimension and it structural has inflexibility fall down.

Reduction of the relative photoinduced changes of hardness is at $Z < 2.67$ it can be contingently the subzero dimension of structure in the initial films of system $Ge_xAs_ySe_{100-x-y}$ by irradiation.

# Role of Metal Impurities in Generation of Defects in Anodic Layers $Nb_2O_5$

Skatkov L.[1], Gomozov V.[2], Liashok L., Tulskiy G., Deribo S., Tulskaya A.

[1] *PCB "Argo", Beer Sheva, Israel*
[2] *NTU "KhPI", Kharkov, Ukraine*

Key role in formation of the properties of the anode layers of niobium pentoxide is related to defects of their own or additive nature, while the main defects are oxygen vacancies . The aim of this work – analysis of additive influence in niobium on formation of defects in Nb2O5.

The object of the study were layers of Nb2O5, formed by anodic oxidation of the sintered niobium pellets of two types (denoted as A and B), differ by the presence on the surface of A type samples of Mg additive, controlled by X-ray photoelectron spectroscopy (XFES). It shall be noted that XFES - initial analysis of the niobium powder applied at generation of samples of both types, has shown no differences in the composition of additives; presence of Mg has only been detected on the surface of the pellets formed by high-temperature vacuum powder sintering. This fact affirms that additives located in the niobium powder as a result of sintering are concentrated on the pellet's surface probably according to the bulk diffusion mechanism. Anodic oxidation of niobium was similarly carried out in two stages: in a galvanostatic mode, and subsequent aging at a constant voltage. Concentration of charged defects is determined from the current-voltage characteristics (C - V) according to Mott -Schottky equation. The results can be interpreted as follows: at the first (galvanostatic) stage of anodic oxidation of samples part of A atoms displaced from the metal oxide pellets are represented by additive metal atoms (Mg), which behavior in electric field is determined by mechanisms specific for anionic defects. As a result, after galvanostatic stage less quantity of defects as compared to B sample case will be carried out to the oxide / electrolyte border. Further, at the transition to the potentiostatic oxidation mode, $Mg^{2+}$ cations along with the basic (anionic) defects are moved to the outer boundary of the oxide layer, which leads to an increase in concentration of the charged defects in the surface layer $Nb_2O_5$.

# Surface Potential Variation under e-Beam and/or Light Induced Mass-Transport in As-Se Films

Lytvyn P.M.[1], Trunov M.L.[2,3], Durkot M.O.[3], Lytvyn O.S.[1], Rubish V.M.[3], Prokopenko I.V. [1],

[1] *Institute of Semiconductor Physics, National Academy of Sciences of Ukraine, Kyiv, Ukraine*
[2] *Uzhgorod National University, Uzhgorod, Ukraine*
[2] *Uzhgorod Scientific-Technological Center of IIR NAS Ukraine, Uzhgorod, Ukraine*

Chalcogenide glasses (ChG) exhibit a number of remarkable structural and optical changes when exposed to light or electron beam. One of them is mass-transport induced by band-gap laser light [1] or electron beam irradiation with moderate energy (10-30 kV, 3-10 nA) [2], which opens capabilities for one-step, direct microfabrication of ChG.

The transformation of the mass-transport in ChG into commercially viable applications could be realized with the improvement of our knowledge on the basic mechanisms underlying the effect. This mechanism, however, is still not well studied, despite some attempts to develop appropriate model with a complete description of the basic microscopic mechanism [3].The scanning Kelvin probe force microscopy is a unique technique for direct measurements of surface topography and corresponding surface potential (SP) mapping. We present unusual behavior of surface relief gratings (SRGs) preliminarily written in a-Se and $As_{20}Se_{80}$ films by photoinduced mass-transport and further treated by electron beam. Gratings of small periods smoothed whereas gratings of larger periods increased their amplitudes. Peculiarities of light-induced lateral mass transport in Se and $As_{20}Se_{80}$ ChG films under e-beam and band-gap light excitation will be discussed in the frame of *in-situ* and *ex-situ* measurements of SP transformations.

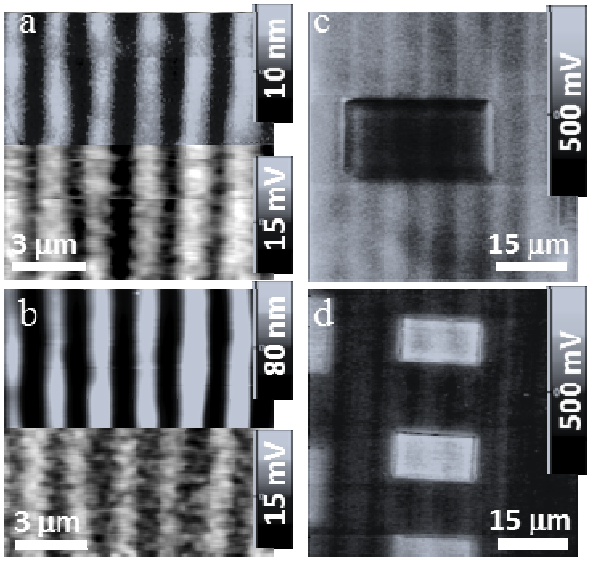


Fig.1. SP transformations in Se (a,c) and $As_{20}Se_{80}$ (b,d) SRGs inscribed optically (a,b) and e-beam treated (c,d). Topography and SP maps of the same areas presented in top and bottom of (a,b), correspondingly.

1. Trunov M.L. Polarization-dependent laser-induced giant mass transport in glassy semiconductors // JETP Letters.-2007.- 86.-P. 313-316.
2. Trunov M.L, Cserhati C., Lytvyn P.M., Kaganovskii Y., Kokenyesi S. Electron beam-induced mass transport in As–Se thin films //J. Phys. D: Appl. Phys.- 2013.- 46. –P. 245303 (9pp).

# Effect of Filler Nature on Chemical Resistance and Microhardness of Epoxy Composite Films

Martinyuk G.[1], Zakordonskyi V.[2], Aksimentyeva O.[2], Skoreiko N.[1],

[1] *Rivne State Humanitarian University, Rivne, Ukraine*
[2] *Ivan Franko National University of Lviv, Lviv, Ukraine*

Introduction of fillers to the polymer composites including epoxy ones, not only considerably improves technological properties of polymers, but also substantially influences on water and chemical resistance, and also on microhardness and other characteristics of composite films on their basis.

We investigated water absorption processes, chemical stability and microhardness of investigated samples, which contained as a polymeric matrix epoxy resin (UP-655) and mineral fillers: graphite, mica, aluminum oxide, and polymer filler - polyaniline (PANI) at their content (0-30% mass).

Film samples of composites in size 30×15 mm were hardened with 100°C for 2 hours and maintained within 30 days in the water vapor atmosphere of hydrochloric and acetic acid.

Introduction of mineral fillers, specifically polymer ones significantly affects on all complex of operating films. The most water and acid absorption processes took place for 24 hours exposure of films in acid solution. The higher effect on water absorption processes and chemical resistance to the acid action is caused by mica, which is connected with high concentration of hydroxyl groups -OH on the filler surface. Increasing of filler content reduces the amount of water absorption and deceleration of this process.

Researching physical and mechanical properties of filled epoxy composites it was found that introduction of mineral filler substantially influences on their microhardness. Thus the character of this influence largely depends on the type of filler and its content. At presence of fillers in matrix of epoxy resin the change of maximum value of conical point of fluidity ($F\infty$) or microhardness takes place with large content of filler (>20% mass) in an epoxy matrix is the decrease of microhardness and at 25-30% mass in the filler's content the integrity of the sample is violated. Thus the most influence on the microhardness changing is caused by aluminum oxide $Al_2O_3$. Introduction of mica leads to a decrease of microhardness in comparison with $Al_2O_3$, probably, by the reduction of the concentration of the reacting substances in the unit's volume. A slight increase of microhardness in case of filling with graphite is determined, probably, by a low concentration of hydroxyl groups -OH that absorbed graphite's surface prevailing over carboxyl COOH- groups, which are sedentary at the catalysis of reactions.

# Optical Properties of $(As_2S_3)_{100-x}$ $(Sb_2S_3)_x$ Amorphous Films with Small Content of Antimony

Maryan V.M.[1], Pop M.M.[2], Gera E.V.[1], Mykaylo O.A.[2], Gatsenko A.A.[2], Horvat Yu.A.[1], Kostyukevych S.O.[3], Mykulanynets-Meshko O.S.[1], Yurkin I.M.[2]

[1] *Uzhgorod Scientific-Technological Center of the Institute for Information Recording, NASU, Uzhgorod Ukraine*
[2] *Uzhgorod National University, Uzhgorod, Ukraine*
[3] *V.E. Lashkaryov Institute of Semiconductor Physics, Kyiv, Ukraine*

Present report is devoted to investigation of influence of laser illumination on transmission spectra and optical parameters of $(As_2S_3)_{100-x}(Sb_2S_3)_x$ (x=2, 4, 10 and 15 mol.%) amorphous films.

Thin films were obtained by vacuum evaporation of the glasses of corresponding compositions from quasiclosed effusion cells onto cold (293 K) silica substrates. The films thickness was ~ 1 μm. Uniform thickness of layers was provided by planetary rotation of substrates. Unfocused illumination of semiconductor laser (λ=530 nm, P=100 mW) was used for exposure of films. Investigation of transmission spectra of films was carried out by means of "МДР-23" spectrometer in the wavelength region of 450 - 800 nm at T=300 K.

The investigations have shown that with growing of Sb content (from 0.8 to 6 at.%) in the composition of films, transmission spectra are shifted into longwave region testifying to decrease of pseudoforbidden gap width ($E_g$) of films. Refractive index (n) in this case is growing (Table).

| x, mol.% | Parameter | Exposure, min | | | |
|---|---|---|---|---|---|
| | | 0 | 1 | 3 | 5 |
| 2 | $E_g$, eV | 2.354 | 2.298 | 2.292 | 2.287 |
| | n | 2.275 | 2.323 | 2.332 | 2.340 |
| 4 | $E_g$, eV | 2.349 | 2.309 | 2.305 | 2.297 |
| | n | 2.284 | 2.316 | 2.320 | 2.326 |
| 10 | $E_g$, eV | 2.342 | 2.264 | 2.262 | 2.260 |
| | n | 2.366 | 2.430 | 2.442 | 2.448 |
| 15 | $E_g$, eV | 2.334 | 2.276 | 2.270 | 2.267 |
| | n | 2.442 | 2.496 | 2.508 | 2.514 |

With the illumination time growing absorption edge of films is shifting into longwave region. $E_g$ of films under illumination is decreasing and n is growing. Here, maximum edge shift under equal expositions conditions is observed for films with antimony content 4 at.%.

The obtained results are discussed from the point of view of films structure and photostructural transformations in them.

# Dispergation Cinetics Under Annealing in Vacuum Copper Nanofilms Deposited onto Nonmetallic Materials

Naidich Yu.V., Gab I.I., Stetsyuk T.V., Kostyuk B.D.

*Frantsevich Institute for Materials Science Problems of NAS of Ukraine, Kyiv, Ukraine*

Copper coverings onto metal surfaces are widely used in technics for the various purposes, for example, for the products brazing. At the same time it is possible to deposit of copper coverings onto nonmetals, in particular, onto oxides for the same purposes.

Dispergation processes of copper nanofilms by 100 nm thickness which were deposited onto sapphire, nonoxide ceramics ($Si_3N_4$) and carbon materials (monocrystal SiC, graphite, carbon glass) and annealed in vacuum were investigated at temperatures up to 1100 °C under various time of endurance at these temperatures.

Nonmetallic substrates were small thin plates having sizes 4x3x1 mm. One of flat surfaces of each sample has been well polished up to roughness $R_z$ = 0,03 ÷ 0,05 mcm except for samples from monocrystals SiC in which used the initial raw smooth side. After polishing all samples have been carefully degreased and annealed in vacuum at temperature 1100 °C during 1 h.

On annealed surfaces of samples copper films by 100 nm thickness were deposited by electronic beam, which after had been annealed in vacuum under temperature 800 – 1100 °C.

Annealed samples were investigated with the help of scanning electronic and atomic-power microscopes. As result were received microphotos. With using of these microphotos the islands areas metal onto nonmetallic substrates surface by planimetric method of weighing, i.e. definition of weight of metallized elements surfaces of substrates have been made.

It is established, that copper nanofilms in result of annealing at 800 °C remain practically without changes on all investigated nonmetallic materials even at long annealing. Some changes of morphology copper films are observed at annealing not less than 10 min at 900 °C, and already after 20 min annealing copper films onto all samples essentially dispergate. During increasing of temperature annealing the copper films from 900 °C up to 1100 °C her dispergation it is considerably intensified on all materials.

On the basis of given researches results it is possible to draw a conclusion, that for joining of the investigated nonmetallic materials were metallized by copper at temperatures 800 – 950 °C duration of brazing process should not exceed 15 min, and at 1000 °C it must be no more then 5 min.

# Structure of Oxide Film Formed on ZnSe Surface at the Contact with Air

Odarych V.A.

*Taras Shevchenko Kyiv National University, Kyiv, Ukraine*

The surface condition of the semiconductor crystals has a significant influense on the foto- and microelectronic devices performance. It is determined by the characteristics of the surface interaction with the environment. Here we report an ellipsometric measurements realized on freshly made single-crystal zinc selenide cleaves for a long time from the moment of their production to one year exposing in atmospheric conditions. It has been shown that the process of surface interaction with air is formed two-layer system. The inner layer is formed mainly within the first few tens of days, and external layer show itself at the final oxidation period in last of months. Ellipsometric parameters changing with time of oxidation in the first stage can be described in the model of the absorbing layer, on the contrary, in the last months of the oxidation process can be described by using the transparent outer layer model. Optical constants – refractive index n, absorption index κ and the thickness d of the layers were obtained. Ellipsometric parameters changing over time well describe by the obtained parameters values. The figure shows the measured ellipsometric parameters tgψ and Φ (symbols) in comparison with the theoretical curves, calculated on the basis of the parameters founded (table). The inner layer corresponds to the curve AB, the outer – curve BD.

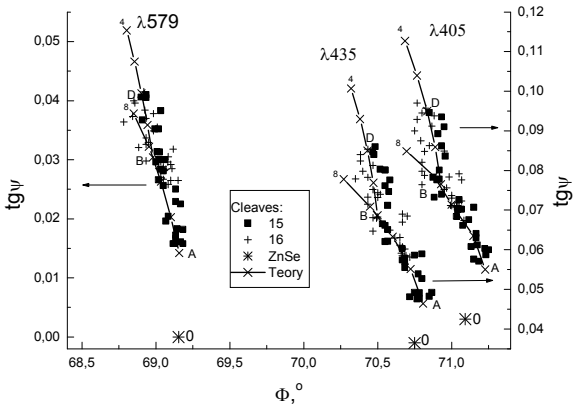


| Λ, NM | INNER LAYER | | | OUTER LAYER | |
|---|---|---|---|---|---|
| | $n_2$ | $\kappa_2$ | $d_2$, nm | $n_1$ | $d_1$, nm |
| 579 | 2,33 | 0 | 8 | 1,2–1,4 | 2,5 |
| 435 | 2,53 | 0,13 | 7 | 1,21–1,3 | 3 |
| 405 | 2,6 | 0,2 | 7 | 1,305–1,4 | 2,5 |

Because optical constants inner layer is less than the optical constants zinc selenide, he probably formed by the mixture of base material and a stable oxide (ZnO). The outer layer may be formed by a mixture of air and an unstable oxide of the type $SeO_2$.

# Luminescence and Structural Features of ALD $TiO_2$ Coated Porous Silicon Surface

Pavlenko M.M.[1], Iatsunskyi I.R.[1,2], Smyntyna V.A.[1],

[1] *Odessa I.I. Mechnikov National University, Odessa, Ukraine*
[2] *Adam Mickiewicz University, Poland, Poznan*

In the present work, we investigated luminescence and structural features of Atomic layer deposition (ALD) $TiO_2$ coated porous silicon (Si) surface fabricated by metal-assisted chemical etching. We assume that combination of these two materials promises the great benefits in advanced technologies and it requires further investigations.

$TiO_2$ thin (3-20 nm) films were grown on p type Si (100) nanostructures by ALD using $TiCl_4$ and water as precursors. The crystalline structure, chemical composition, and morphology of the deposited films and initial PSi were investigated by scanning electron microscopy (SEM), energy dispersive spectroscopy (EDS), micro-Raman spectroscopy, X-ray diffraction, and atomic force microscopy. It was found that layer of $TiO_2$ on the nanostructured silicon surface has granular structure and the approximate size of titanium dioxide nanocrystallites are laying in the range 7-15 nm (Fig.1). The photoluminescence (PL) spectra were measured at room temperature. Some interesting features were found on the PL spectra. We observed the evolution of PL due to annealing of obtained structure that caused by the transition of the amorphous phase to the crystalline one (Fig.2).

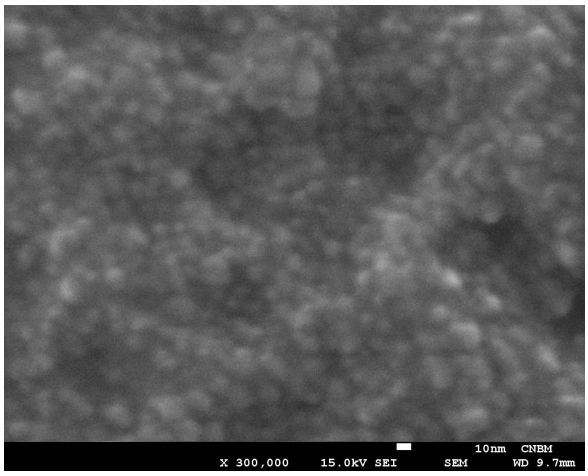


Fig.1. Plane view SEM image of $TiO_2$-PSi surface.

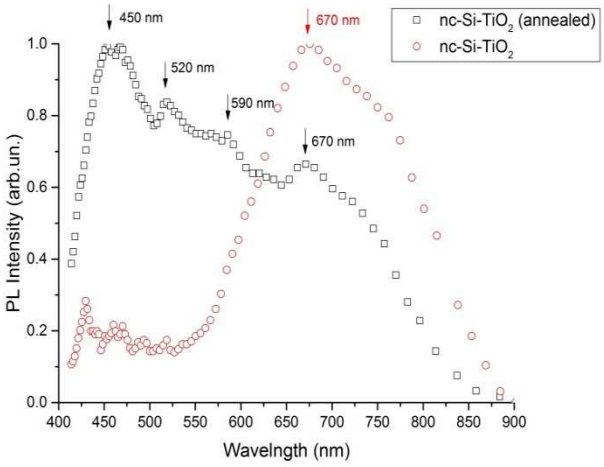


Fig.2. PL spectrum of $TiO_2$-PSi before and after annealin for an hour at 400°C in the air.

# The Influence of the Average Grain Size on the Internal Size Effect in Polycrystalline Films of Lead

Petrushenko S.I., Dukarov S.V., Sukhov V.N., Parfylo T.O.

*V.N. Karazin Kharkiv National University, Kharkiv, Ukraine*

The presence of a large number of grain-boundaries in thin polycrystalline films, with which excess energy is connected, leads to the internal size effect appearance. It can be explained by the fact that grain-boundaries, separating a grain from neighboring ones, disappear while melting. Energy gain in this process is determined by the grain size and its orientation with respect to the surrounding grains. As a result, each of the crystallites in the film starts to melt at its own temperature. The internal size effect was experimentally observed previously in polycrystalline films of metals. It has been found, that while melting of such films on the substrates with a temperature gradient, the crystal-melt boundary has a finite width, in which a partial melting of the film is observed. Due to the large value of the grain-boundary energy contribution, even for polycrystals, consisting of micron-size grains, the melting range can reach 3–4 K.

It is naturally to suppose, that the temperature width of the partial melting will increase together with the rise of the grain-boundary energy contribution into the total energy of the polycrystalline film. This contribution is determined by the mean grain size, which in its turn depends on the conditions of films production.

In this paper, we present the results of the internal size effect investigation in Pb films with different mean grain size. The samples were formed on the prolonged glass or $Al_2O_3$ substrates with pre-deposited amorphous carbon layer. To produce samples with different grain size the substrate temperature was varied in the range 150–400 K during the condensation of Pb. It enabled us to obtain Pb film samples with a grain size of 2–12 microns. It can be seen on Fig. that the width of the melting area increases with the mean grain size reduction. Such evolution is well described by a hyperbolic dependence, which follows from the triple junction model. Using obtained data, we determined the mean grain-boundary energy value, which was estimated to be 230 mJ/m$^2$. This value is constant at all sizes studied.

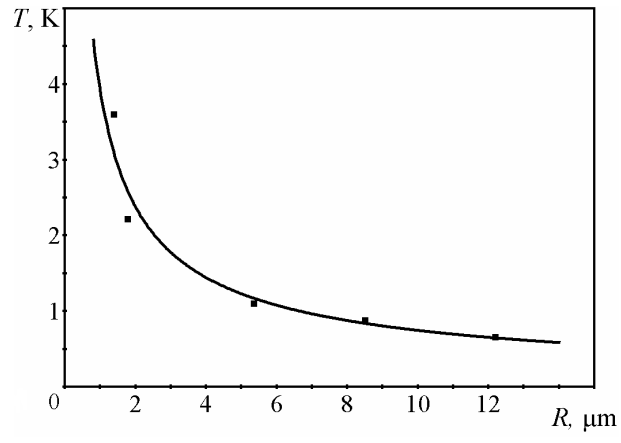

# Quasi-Chemical Analysis of Point Defects in Cadmium Telluride Crystals Doped by Bromine

Prokopiv V.V.[1], Pysklynets U.M.[2], Starko I.Yu.[1], Maliarska I.[1]

[1]*Vasyl Stefanyk Precarpathian National University, Ivano-Frankivsk, Ukraine;*
[2]*Ivano-Frankivsk National Medical University, Ivano-Frankivsk, Ukraine*

Cadmium telluride is a promising material for creating highly efficient optoelectronics devices and detectors of ionizing radiation. To improve and stabilize the characteristics of the material can be achieved by doping with various impurities, in particular bromine. For the development of science-based technologies CdTe: Br needed reliable information about its defective condition.

In this paper, using quasichemistry reaction modeled the formation of point defects in crystals of cadmium telluride doped with bromine and based on this calculated concentration dependence of the point defects and free carriers from technological factors of the two-temperature annealing.

It is shown that alloying effect of bromine impurity in CdTe crystals deal with replacing defects $Br_{Te}^{+}$ and with them complexes of own point defects $\left(2Br_{Te}^{+}V_{Cd}^{2-}\right)^{0}$, which is dominant throughout the all studied range of annealing process parameters and determine the concentration of free charge carriers in the material.

Calculated Isothermal and Isobaric concentration dependence of the free charge carriers (electrons *n* and holes *p*) and its dominant own and impurity point defects: doubly ionized cadmium vacancies $\left[V_{Te}^{2+}\right]$ and tellurium $\left[V_{Cd}^{2-}\right]$; interstitial atoms of cadmium $\left[Cd_{i}^{2+}\right]$ and tellurium $\left[Te_{i}^{2-}\right]$; singly ionized atoms of bromine in the node tellurium $\left[Br_{Te}^{+}\right]$ and complexes $\left(2Br_{Te}^{+}V_{Cd}^{2-}\right)^{0}$ in bromine doped cadmium telluride crystals under conditions of two-temperature annealing in a couple of cadmium.

Determined equilibrium constant of complex formation of impurity replacement defects with own point defects $\left(2Br_{Te}^{+}V_{Cd}^{2-}\right)^{0}$.

The calculation showed that the concentration of electrons *n* does not depend from the annealing temperature T and at the same time linearly depends from the vapor pressure of cadmium $P_{Cd}$, which well agrees with experiment. This confirms the adequacy of the chosen model of creating defects in the crystals of cadmium telluride doped by bromine in which dominant defects are singly ionized impurity atoms in the node tellurium $Br_{Te}^{+}$ and complexes $\left(2Br_{Te}^{+}V_{Cd}^{2-}\right)^{0}$.

# Magnetism of Gd-Fe System

Prysyazhnyuk V.I., Mykolaychuk O.G.

*Ivan Franko National University of Lviv, Lviv, Ukraine*

Investigation of magnetic properties of films of $GdFe_2$, $GdFe_5$ and $Gd_2Fe_{17}$ compounds are complete. Films have been gained by a method of thermal evaporation on teflon substrates at room temperatures.

Values of Curie temperature, curves of specific magnetisation, and hysteresis curves for massive and thin-film samples are determined. It is spotted that the Curie temperature of massive samples corresponds to references. At examination of thin-film samples Curie temperature reduction was observed. Such depression of Curie temperature speaks expansion of a crystalline lattice owing to formation of microdefect (films were is amorphous-crystal).

Temperature dependences of magnetic saturation for compounds and films of Gd-Fe system are determined. The given dependences characteristic for materials of such class. Magnetic saturation of films $Gd_2Fe_{17}$ and $GdFe_2$ at room temperature are measured.

1. Zinkevich M. Reassessment of the Fe-Gd (Iron-Gadolinium) System. / M. Zinkevich, N. Mattern, and H.J. Seifert // Journal of Phase Equilibria. – 2000. –V.21, No.4. –P.385–394.
2. Андреенко А. С. Магнитные свойства аморфных сплавов редкоземельных металлов с переходными 3d-металлами / А. С. Андреенко, С. А. Никитин // УФН. –1997. –Т.167, №.6. –С.605–622.

# A Structure and Physical Properties of Pure Mn, Bi and MnBi Films Obtained by Method of Triod Ion-Plasmous Sputtering

Ryabtsev S., Bashev V., Gusevik, P., Kurdukova C.

*Oles Honchar Dnipropetrovsk National University, Dnipropetrovsk, Ukraine*

The regularities of formation of Bi, Mn and MnBi metastable film structures obtained by modified three-electrode ion-plasmous sputtering method (IPS) were researched in this work.

X-ray analysis showed that in the as-deposited Mn films there is formed a mixture nanocrystalline β-Mn (the size of coherent scattering region L = 7.5 nm), and oxide MnO. The Mn film heat treatment in a vacuum at a temperature above 700 K leads to its complete oxidation. Initial Bi film are a mixture of rhombohedral Bi phase (L = 6.5 nm), and traces of cubic Bi. Heat treatment leads to the enlargement of the grains and the complete disappearance of Bi with a cubic lattice. MnBi films are a mixture of rhombohedral Bi phase and β-Mn in the initial state. After heat treatment, except those phases appear traces of $Bi_2Mn$ and MnO.

The temperature dependence of the resistivity analysis revealed that the pure Mn and Bi activation energy of the phase transitions are $E_A \sim 5000$ K and $E_A \sim 8500$ K respectively. The activation energy of MnBi films are in the range of $E_A \sim 3500$ - 5000 K. After heating the Bi and MnBi films to the temperatures above 670 K and subsequently cooled to a temperature of 490 K is an abrupt change in resistance.

Analysis of the demagnetization curves showed that the hysteresis of the magnetization is observed only in the containing Bi films, because the assumed occurrences of the ferrimagnetic properties of Bi oxide in the nonequilibrium state.

# Simulation of Electronic Structure and Properties for Amorphous $GeSe_2$ - $X_2Se_3$ (X= As, Sb) Films

Savchenko N.D., Shchurova T.N., Opachko I.I.

*Uzhgorod National University, Uzhgorod, Ukraine*

One of the top problems in the development of novel electronic devices is the prediction of the electronic properties of functional materials. Wide spectrum of chalcogenide compounds find application in nano- and opto-electronics, infrared optics, information recording et al. The main purpose of the present work was to explain the peculiarities of concentration dependences of the optical band gap, conduction activation energy and trapping centres in ternary chalcogenide thin films based on the studies of electronic structure - properties relationship.

Amorphous thin films thermally deposited in vacuum from ternary glassy chalcogenides of $(GeSe_2)_x(As_2Se_3)_{1-x}$ (x=0-0.8) and $(GeSe_2)_x(Sb_2Se_3)_{1-x}$ (x=0.4-0.9) families have been the subject of the investigation. For the materials under investigation the results of the calculation of the top of the valence band, the bottom of the conduction band, the optical band gap, the Fermi level, the position of the levels formed gap by the homopolar bonds and clusters have been presented. The calculation procedure has been based on the linear combination of the atomic orbitals and pseudo-potential methods [1]. The energy values have been determined in the Γ-point - the centre of the Brillouin zone. The atomic terms taken from the generalized periodic table [2] have been used in the calculations, as well as the available experimental data on the photoemission [3] and average interatomic distances [4]. For the films the experimental data on the absorption edge, temperature dependence of d. c. conduction, photoconduction and thermally activated depolarization currents have been given.

The quantitative agreement between calculated energy band diagram and experimental data for the studied materials has been shown. The peculiarities of the composition dependences for the properties of the films under investigation have been discussed.

1. Harrison W.A. Elementary Electronic Structure. – London: World Scientific Publishing Co., 2004. – 838 p.
2. Harrison W.A. Theoretical Alchemy. Modelling Matter. – New Jersey, London, Singapore: World Scientific Publishing Co., 2010. – 196 p.
3. Spectral Distribution of Photoemission Quantum Efficiency for $(As_2Se_3)_{1-x}$ $Ge_x$ Glasses / T. Shchurova, N. Savchenko, A. Spesivykh, N. Baran // Jap. J. Appl. Phys. – 2000. – Vol. 39, Suppl. 39-1. – P. 334–335.
4. Short-range order in amorphous $(Ge_{1-x}M_x)Se_2$ (M = As, Sb and Bi)/ O. Uemura, Y. Nagata, T. Usuki, Y. Kameda // J. Non-Cryst. Solids. – 1995. – 192&193. – P. 74-78.

# Comparison of Polarization Switching in PVDF and P (VDF-TFE) Thin Ferroelectric Films

Sergeeva A.E.[1], Fedosov S.N.[1], H. von Seggern[2]

[1] *Odessa National Academy of Food Technologies, Odessa, Ukraine*
[2] *Darmstadt Technological University, Berlin, Germany*

Copolymers have some advantages over pure PVDF in a group of polymers based on vinylidene fluoride. The most studied is a trifluoroethylene copolymer P(VDF-TrFE), while only a few studies were devoted to tetrafluoroethylene copolymer P(VDF-TFE). That is why our goal was to study formation and relaxation of the polarized state in the P(VDF-TFE) in terms of its applicability for the manufacturing of sensors with high and stable polarization.

The method developed for PVDF [1] was applied to polarization switching in P(VDF-TFE). The films were electrified in a strong field for 200 s to obtain a fully polarized state. Then, the switching voltage pulses from 10 μs to 100 s duration from were applied. After each switching, the formatting was performed. The difference between the electric displacement in the first and in the second case gave the kinetics of the ferroelectric polarization switching [1].

The following conclusions were made from comparison of the PVDF and P(VDF-TFE) data: (a) the value of switchable polarization in the copolymer was significantly higher than in PVDF; (b) the total switching occurred in $t \sim 10^{-4}$ s, whereas saturation in PVDF was not reached even after 100 s; (c) displacement graphs had almost rectangular shape indicating the absence of the unstable polarization; (d) abrupt changes in displacement during the switching in the case of P(VDF-TFE) was significantly smaller than in PVDF indicating the smaller value of the effective permittivity in P(VDF-TFE) compared to PVDF.

These features were, probably, due to the lack of the amorphous phase and the lower conductivity. The characteristic shape of the charging current with the presence of a flat section was marked in the first microseconds. By subtracting the capacitive current from the total current, we obtained the polarization switching current, which has a maximum at 3 μs. Namely this value can be considered as the switching polarization time for P(VDF-TFE).

The dependence of polarization switching from the applied field and exposure time were studied. A comparison with the corresponding graphs for PVDF shows that the coercive field has the same order as in PVDF (~ 50 MV m). Therefore, the application of lower fields is impractical, because polarization is very small. At the same time, if the field of 120 MV/m is used, there is no significant difference in applying pulses of 5 ms, 50 ms, or even 5 seconds, because of very fast switching of the ferroelectric polarization.

1. H. von Seggern, S. N. Fedosov *IEEE Trans. Diel. Elect. Insul.* 2004. – v. 11, – p. 232– 241.

# Experimental Measurement of the Effective Electrical Conductivity of Thin Ferroelectric Polymer Films

Sergeeva A.E.[1], H. von Seggern [2], Fedosov S.N.[1]

[1] *Odessa National Academy of Food Technologies, Odessa, Ukraine*
[2] *Darmstadt Technological University, Berlin, Germany*

We have developed two methods of determining the effective conductivity of a ferroelectric polymer films. Experiments were performed on 11.5 μm-thick Kureha films of polyvinylidene fluoride (PVDF). The total current density $j$ during repeated poling of an already completely polarized sample has three components, namely, the capacitive one $j_c$, the component related to the unstable reversible displacement $j_{unst}$ and the conductivity component $j_{cond}$.

$$j=dD/dt=j_c+j_{unst}+j_{cond} \quad (1)$$

where $D$ is the total ‘‘apparent’’ displacement containing in addition to the usual displacement the current density resulting from conduction. The capacitive component $j_c$ is decreasing almost exponentially and approaches zero at times larger than about 5 $R_sC_s$=0.4 μs for a current limiting resistor of $R_s$=500 Ω_ and a sample capacitance of $C_s$=160 μF. The unstable part of polarization completely aligns or switches back in about 10 ms, so one can assume that $j_{unst}$=0 at $t$>10 ms. Therefore, the total current density $j$ after a few seconds of voltage application to a completely poled sample contains only the conductivity component $j_{cond}$. Since $j_{cond}$ depends on the conductivity $g_o$, its value can be determined experimentally either from the slope of the $D(t)$ curve for t> 10 ms, or from the residual charge on the measuring capacitor after short-circuiting of the sample, because this charge is accumulated due to conduction of the sample.

$D(t)$ is linearly increasing with time and $g_o$ can be determined from $g_o=D(t)/E$. The conductivity obtained from the residual charge on the measuring capacitor amounts to $g_o = C_mV_{cond}/EAt_{ch}$ where $V_{cond}$ is the voltage at the measuring capacitor $C_m$=0.2 μF, $t_{ch}$=150 s the charging time and $A$=0.2 cm$^2$ the sample area. There is a reasonable agreement between the two methods, and the average values are of the same order of magnitude ($10^{-12}$ S/m).

Ohm’s law is not valid, since the current-voltage dependence is non-linear. From our data $I=\gamma V^{1.6}$. The exponent of 1.6 indicates that the conductivity has a mixed origin with a quadratic dependence typical for the space charge limited injection currents superimposed with a linear Ohmic dependence caused by intrinsic conductivity of the sample. From the linear component the intrinsic conductivity of $g_{in}=0.63\cdot10^{-12}$ S/m has been derived and the quadratic component delivers a mobility of injected excess charge carriers of $\mu=9.3\cdot10^{-12}$ cm$^2$/V·s utilizing Child’s law.

# Optical, Structural and Photocatalytic Characteristics of Iron-Doped Titania Films Synthesized by Sol-Gel Method

Shestopal N., Linnik O., Smirnova N.

*Chuiko Institute of Surface Chemistry, National Academy of Sciences of Ukraine, Kyiv, Ukraine*

Sol-gel technology is a well-regulated technique to obtain the nanostructured systems and allows the homogeneous distribution of the components on the atomic level. The synthesis of sol-gel doped $TiO_2$ films requires the special approaches depending on the stated goal such as i) an incorporation of dopant ions into $TiO_2$ crystal lattice; ii) solid solution formation ($Ti_{1-x}Zr_xO_2$) or iii) spinel phase formation ($Ti_xX_yO_z$) [1]. It known that $TiO_2$ absorbs only 4% of ultraviolet light and it is inert in the whole visible range of the solar spectrum. The challenge is therefore to extend the sensitivity of $TiO_2$ towards the visible range of the spectrum. Our work presents the correlation of the synthesis conditions with optical and structural peculiarities as well as the photocatalytic properties of iron doped titania films.

The non-porous films are prepared by sol-gel method using titanium tetraisopropoxide and unhydrous iron(III) chloride. The films were deposited by a dip-coating technique with the withdrawal rate of 1.5 mm/s. The films are thermal treated at 450 and 600 ºC. The significant shift in the optical absorption edge to the visible part of absorption spectra is observed for $Fe^{3+}/TiO_2$ films comparing with bare titania. A change in the band-gap calculated by extrapolating the linear parts of the $(\alpha h\nu)^{1/2} \sim f(h\nu)$ curves (the indirect electronic transition) corresponds to 2.2 eV for films at 450 ºC and two values: 1.9 and 2.2 eV for the films at 600 ºC. XRD results show that the treatment temperatures influence on the phase composition of the films. No anatase, but only pseudobrookite ($Fe_2TiO_5$) structure is registered for the doped films treated at lower temperature while the film structure (600 ºC) contains the numerous phases (rutile, $Fe_2TiO_5$, $Fe_2Ti_2O_7$ and $Fe_2O_3$). Photocatalytic activity was studied in the processes of toxic dichromate ions reduction and tetracycline hydrochloride (TC) degradation. Activity of the films (450 ºC) is increased 3-4 times during TC degradation and more than three times during dichromate ions reduction under both UV and visible light in comparison with the $Fe^{3+}/TiO_2$ films (600 ºC) and bare $TiO_2$ films. Thus, the certain phase composition of the doped semiconductive films is responsible for a more efficient separation of photogenerated electron-hole pair that led to improvement of the photoactivity.

1. Nataliia Smirnova, Yuriy Gnatyuk, Nadiia Vityuk, Oksana Linnik, Anna Eremenko, Vera Vorobets, Gennadiy Kolbasov // Nanosized $TiO_2$ - Based Mixed Oxide Films: Sol-gel Synthesis, Structure, Electrochemical Characteristics and Photocatalytic Activity // International Journal of Materials Engineering 2013, 3(6): 124-135.

# Nature of Edge Luminescence of α-ZnSe Heterolayers

Slyotov M.M., Gavaleshko O.S.

*Yu.Fedkovych Chernivtsi National University, Chernivtsi, Ukraine*

Zinc selenide is one of the most promising semiconductors for creation of radiation sources in the blue optical wavelengths. They are formed on the base of materials with cubic lattice modification (band gap $E_g \approx 2{,}7$ eV at 300 K). However, it remains small studied obtaining and investigation of hexagonal zinc selenide properties, and especially its layers as active region of functional electronics devices.

α-ZnSe heterolayers formed by isovalent substitution method due to α-CdSe crystals annealing in saturated pair of Zn. On the surface of the substrate with black color the compound formed with yellow-green color appropriate to ZnSe. By means of λ-modulation method the optical reflection (OR) and photoluminescence (PL) were studied. Differential OR curves consists of three peaks corresponding for the optical processes in materials with a hexagonal lattice. This spectrum allowed to determine the band gap of α-ZnSe $E_g = 2{,}89$ eV, and the value of the valence band splitting due to spin-orbit interaction $\Delta_{so} = 0{,}37$ eV and crystal field $\Delta_{cr} = 0{,}07$ eV. Intense photoluminescence in the edge region inherent for the obtained α-ZnSe heterolayers with a maximum at photon energies $\hbar\omega = 2{,}7$ eV. The studies of differential spectra revealed two main components of radiation. The dominant band has the following properties: maximum displacement in the region of lower energies with increasing of excitation level $L$; the intensity $I$ of $L$ is in accordance with the law $I \sim L^{1,5}$. These basic properties with contour asymmetry and exponential dependence of the band edge intensity from the photons energy $\hbar\omega$ indicate the nature of the dominant exciton emission. Importantly, this emission is observed at 300 K. The second component of the radiation in the range $\hbar\omega > E_g$ is determined by the interband radiative recombination of free carriers. Note that transitions with participation of subzone split by crystal field $\Delta_{cr}$ are also observed in the luminescence spectra of α-ZnSe heterolayers. In general, an edge emission at 300 K indicates the possibility of using heterolayers in different types of functional electronics devices. What is important is stability in time of their properties. This caused by the peculiarities of heterolayers formation by means of isovalence replacement. They grow in "depth" of the matrix, and therefore determine the substrate lattice and stabilize the crystal structure of formed heterolayer. Possible inconsistency of crystalline and thermal parameters of contacting materials is compensated by corresponding graded-gap solid solution.

# Electronic and Vibrational Structure of Complexes Formed by $C_{60}$ Fullerenes and Squaraine Dyes

Brusentsov V.A. [1], Stubrov Yu.Yu., Pavlenko O.L.[1], Kulish M.P.[1], Dmytrenko O.P.[1], Strelchuk V.V.[2], Kachkovsky O.D.[3]

[1] *Taras Shevchenko National University of Kyiv, Kyiv, Ukraine*
[2] *V. Lashkaryov Institute of Semiconductor Physics, National Academy of Sciences of Ukraine, Kyiv, Ukraine*
[3] *Institute of Organic Chemistry, National Academy of Sciences of Ukraine, Kyiv, Ukraine*

$C_{60}$ fullerenes are an allotropic form of carbon known to act as efficient charge donors are acceptors, which makes them a lucrative choice in the design of organic solar power cells. A natural and straightforward way to functionalize the fullerenes would be to link them to molecular structures that convert solar radiation energy into charge in a specific region of photon energies. These conditions are satisfied by dyes, specifically squaraine dyes [1], derived from squaric acid, which form a bond with the fullerene via their central cycle.

The point of interest in this research is to study the electronic and vibrational properties of complexes formed by $C_{60}$ fullerenes and several squaraine dyes (such as one shown on Fig. 1) in order to determine the specifics of the mechanisms, by which they interact.

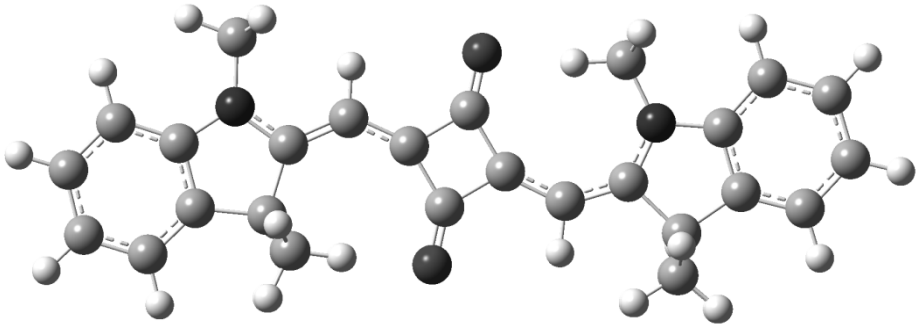

Fig. 1. A Ball and Bond Type model of a sample squaraine dye.

We use UV-VIS absorption, Raman scattering and photoluminescence measurements along with quantum-chemical calculations to explore the properties of the complexes and discuss the charge transfer, excited states, shapes of molecular orbitals and nonlinear features on experimental spectra.

Extra attention is given to the bridge that connects the squaraine dye to a fullerene, as it plays a sufficient role in the vibrational picture of the complex and the reallocation of charge.

1. G. Chen, D Yokoyama, H. Sasabe et.al. Optical and electrical properties of a squaraine dye in photovoltaic cells // App. Phys. Lett. – 2012. – 101, 08390.

# Structural Features of $Sn_xS_y$ Thin Films

Voznyi A.A., Kosyak V.V., Opanasyuk A.S.

*Sumy State University, Sumy, Ukraine*

Today $Sn_xS_y$ could be considered as a perspective material for thin film solar cells (SC). This is presupposed by the fact that it fully meets demands to highly effective SC, possess bang gap $E_g$ = 1.16 – 2.4 eV, has *p*- and *n*-type conductivity and includes no toxic or rare elements. Besides of that, the SnS, $Sn_2S_3$ and $SnS_2$ compounds with different band gaps and conductivity type could be formed within sulfur-tin system. This gives an opportunity to create heterojunctions SC based on the *n* - $SnS_2$/*p* – SnS.

The present work deals with the study of the structural properties of the $Sn_xS_y$ thin films deposited by the closed-space vacuum co-evaporation (CSVCE) method. The effect of growth conditions on surface morphology and structural properties of $Sn_xS_y$ films were studied. Surface morphology of obtained films was determined by the scanning electron microscope (SEM-102E). Structural investigations of the films were performed with the X-ray diffraction (XRD) method. The analysis of chemical composition of the layers was carried out by by energy dispersive X-ray (EDAX) spectroscopy. Influence of the substrate temperature on chemical composition of thin films and their structural properties was also investigated.

It was showed that obtained layers consist of platelet-shaped grains about 300 μm thickness. There was observed increasing in size of crystals from 0.7 μm to 4.2 μm with the increasing in the substrate temperature. Chemical composition of the layers depended on the substrate temperature and changed in the range from $\varphi = C_S/C_{Sn}$ = 1.03 to 1.41. Hereby their stoichiometry was becoming better when condensation conditions were close thermodynamic equilibrium. The most stoichiometric samples ($\varphi = C_{Sn}/C_S$ = 0.96) were deposited at 573 K.

At XRD patterns a range of peaks, which were identified as reflections from (103), (011), (111), (112) crystallographic planes and other orthorhombic phase were observed. Positions of this peaks coincides with the JCPDS data for $Sn_2S_3$. Parameters of the crystal lattice of the material were calculated *a* = 0.88741 – 0.89129 μm, *b* = 0.37525-0.37568 μm, *c* = 1.40209-1.40948 μm.

# Structure-Phase Composition and Thermoresistive Properties of Film Systems Based on Fe and Cu

Kondrakhova D.M., Protsenko Z.M., Shamardin A.V., Protsenko I.Yu.

*Sumy State Pedagogical University by name A.S. Makarenko, Sumy, Ukraine*

According to the phase diagram Cu-Fe for bulk samples of the system components do not mix. The structural state of this samples can be interpreted as pseudoalloys. In addition, the study magnetoresistance (MR) of two-component films based on Cu and Fe, obtained simultaneously [1 - 3] or layers [4, 5] condensation, indicating the formation of their granular state and, as a result, implementation of the spin-dependent scattering of electrons (SDSE) and the effect of giant magnetic resistance (GMR). Since the solubility of Fe atoms in the Cu matrix is very limited, it is somewhat unclear is the question of the mechanism of formation of granular state.

The purpose of this work is study the crystal structure, diffusion processes and the possibility of stabilizing the situation in granular multilayers $[Cu/Fe]_n/S$ obtained at relatively low speeds and high thermal and electro-chemical deposition. It was found that the samples in both cases with two-phase structure of fcc-Cu + bcc-Fe (sign of pseudoalloys), although studies using secondary-ion mass spectrometry indicate weak mutual diffusion of atoms with the diffusion coefficient order $10^{-19}$ $m^2/s$. Analysis indicates that this is not effective diffusion due mainly ion-stimulated diffusion limits on crystalline Cu or Fe with little contribution condensation-induced diffusion. Measurement of defense indicate that the samples obtained from the low deposition rate ($10^{-2}$ nm/s), implemented with effect amplitude GMR from 0,2% ($[Cu\ (2nm)/Fe\ (2nm)]_4/S$) to 0,4% ($[Cu\ (2)/Fe\ (2)]_{10}/S$). When the deposition of relatively high rate (1 - 2 nm/s) MR has all the features of AMR with amplitude 0,15 – 0,30%. The results are discussed in terms of a possible mechanism SDSE.

1. K. Wakoh, T. Hihara, T.J. Konno et all. // Mater. Sci. Engin.A. – 1996. – V. 217/218. – P. 326-330.
2. V. Kuncser, I. Mustata, C.P. Lungu et all. // Surf. Coatings Technol. – 2005. – V. 200. – P. 980–983.
3. A. Tiwari, M.S. Kumar // Physica B. – 2007. – V. 387. – P. 63–69.
4. T. Sakai, G. Oomi, K. Okada et all/ // Physica B. –1997. –V. 237–238.- P. 275–277.
5. K. Nowakowska-Langier, K. Zdunek, T. Lucinski // Surf. Coatings Technol. – 2007. –V. 201. – P. 5333–5335.

## СЕКЦІЯ 4 (усні доповіді)
## ТОНКОПЛІВКОВІ ЕЛЕМЕНТИ ЕЛЕКТРОННИХ ПРИСТРОЇВ, НАНОЕЛЕКТРОНІКА

12-15 травня 2015 р.

## SESSION 4 (oral)
## THIN FILM ELEMENTAL COMPOUNDS FOR ELECTRONIC DEVICES

May, 12-15, 2015

# Space and Polarization Dependences of Light Transmission by Multilayer Interference Systems

Fekeshgazi I.V.[1], Sidenko T.S.[1], Mitsa A.V.[2], Petsko V.I.[2]

[1]*V. Lashkaryov Institute of Semiconductor Physics, National Academy of Sciences of Ukraine, Kyiv, Ukraine*
[2]*Uzhgorod State University, Uzhgorod, Ukraine*

The dependences of transmission by multilayer interference systems on incidence angle values for s- and p-polarization of parallel light beams were investigated by developed program on Delphi 7 language. The considered structures of multilayer interference systems were: S-HL...HLHHLH..LH→ S-$(HL)^4 2H(LH)^4$ and S-$(B/2\times H\times B/2)^8$ or S-$(H/2\times B\times H/2)^8$ . They contained 17 layers with altering of H and L layers with high ($n_H$) and low ($n_L$) refractive indices and optical thickness equal to quarter of functional wavelength $\lambda_0$ for the normal beam incidence deposited on transparent substrate S with refractive index ($n_S$).

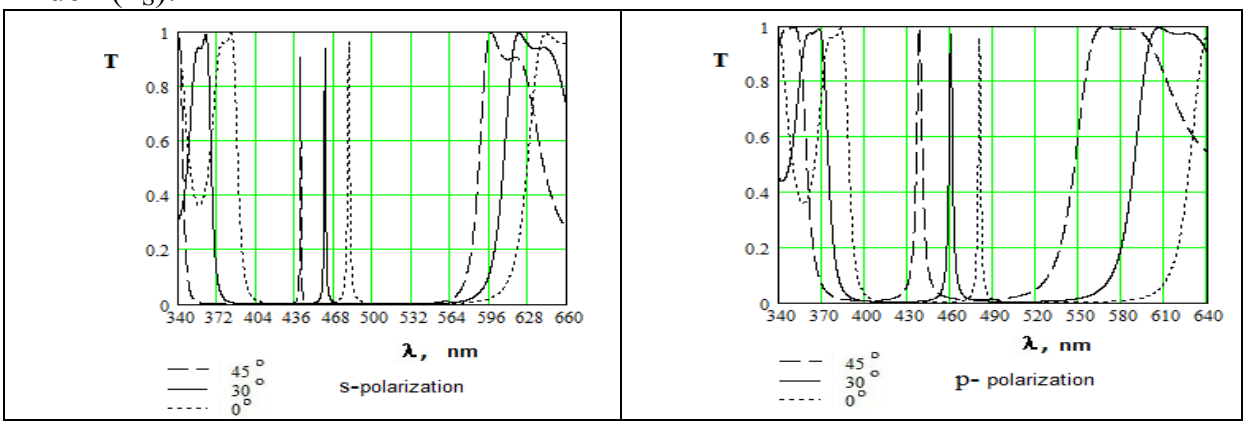


The obtained transmission spectra are shown on figures. It was established that with the increasing of incidence angle of light beams on multilayer interference system the:

- maximum $T_{max}$ values of transmittance for s-polarized light beam decrease, while for the p-polarized one increase, remaining always higher;
- position of the maxima transmission $\lambda_{max}$ always shifted in the short-wave region, being higher for s- polarized light;
- half-width $\delta\lambda_{0,5}$ and $\delta\lambda_{0,1}$ of bands transmission for s- polarized light decreases, while for the p- polarized one are growing, remaining always higher;

The limit values of spatial divergence angles for filtered beam's always determined only by the total internal light reflection due to high refractive index of incoming layer and substrate.

# Some Peculiarities of Hybrid Organic-Inorganic Silicon-Based Solar Cells Formation

Gorbach T.[1], Smertenko P.[1], Melakh V.[1], Roshchina N.[1], Kostylyov V.[1], Wisz G.[2]

[1] *V.Lashkarev Institute of Semiconductors Physics, NAS of Ukraine, Kyiv, Ukraine*
[2] *Institute of Physics, Rzeszow University, Rzeszow, Poland.*

The new solar cell hybrid architecture by a chemical deposition of the organic layer from aqueous solution of heterocyclic amines onto the patterned *Si* substrate has been developed. The hybrids were fabricated at room temperature during from 0.3 hour up to 170 hours. Aqueous solutions of the thiamine diphosphide (cocarboxylaze hydrochloride) (TD) and the metamizole sodium (analgin) (MS) were used.

The chemical deposition it is found to form morphology evolution from pyramid like to the spherulite formation and separate organic crystals. The morphology, current-voltage and spectral characteristics were studied. Organic layers of thiamine diphosphide and metamizole sodium modified the morphology, chemical composition and physical properties of porous patterned substrates. This modification does not depend on solution chemistry and is determined by deposition time, i.e. layer thickness. For thin organic layers ($\leq$ 100 $\mu$m) the layer contour is the same as substrate and terrace-step-kink (TSK) growth mechanism is realized. For more thick layers (up to some micrometers) self organized assemblies are formed but with preference of pre-pattern substrate. On the interface of TD layer – porous patterned substrate the barrier is formed and PV characteristic is observed.

Chemical solution deposition at room temperature is newly simple technological process useful for realization of hybrid organic-inorganic structures. The further progress in this field strongly depends on control of ligand incorporation.

1. T.Ya. Gorbach, V.P.Kostylyov, P.S. Smertenko. New organic materials for organic-inorganic silicon-based solar cells // Mol. Cryst. Liq.Cryst. – 2011. – V.**535.** – P. 174-178.
2. T.Ya. Gorbach, V.P.Kostylyov, V.G. Melakh, N.M.Roshchina, P. S. Smertenko, G.Wisz. Formation of self-organized organic-inorganic hybrids // Proceedings of Ukrainian Material Research Society. – 2015 (in press)

# Scientific School B.T. Boyko in the Field of Thin Film Solar Cells

Khrypunov G., Kopach G., Khrypunova A.

*National Technical University "Kharkiv Polytechnical Institute", Kharkiv, Ukraine*

One of the most perspective forms of renewable energy in Ukraine is solar energy.

This year would have been 85 years since the day of birth Doctor of Sciences, Professor Boyko Boris Timofeevich, alumnus of L.S. Palatnik scientific school in the area of thin films physics. In 1973 prof. Boyko B.T. during 6 years worked in Paris in the UNESCO department of science. During the energy crisis in Europe (1974-1975), he led the program of using solar energy in the world. After returning Ukraine in 1979, he continues to work as professor of "The Physics of Metals" department in National Technical University (NTU "KhPI"). All scientific potential accumulated over the years at UNESCO, international relations and numerous contacts he acquired it using to develop new subjects - the conversion of solar energy into electrical in Ukraine. According to the decision of the Ukrainian government for prof. Boyko B.T. laboratory in Kharkiv allocated the building on the Gamarnika street, 2, where in 1988 he organized the "Materials for electronics and solar cells" (MESC) department. It was the first in the USSR department that prepares specialists in the field of solar energy. In the 90 years Boyko B.T. puts a lot of effort to work with foreign partners, signed new contracts, projects, through which members of the MESC department could go for an internship in Germany and Switzerland. The MESC department becomes the sole representative of Ukraine - European party programs on the use of solar energy (INTAS), as well as an associate member of Solar Energy Center in Germany (Stuttgart). In the list of Boyko B.T. publications - 214 publications, including 52 published in foreign journals, 18 copyright certificates, 4 textbooks and teaching aids. In 1997 prof. Boyko B.T. was awarded the title "Honored Worker of Science and Technology". In NTU "KhPI", he created a scientific school for the development of physical principles and technology of efficient film solar cells for terrestrial applications.

After 2009 year MESC department participated in 10 international projects. Staff of department published more than 100 scientific articles, including 30 in journals included in SCOPUS database, 5 manuals, defended 8 PhD and 2 doctoral dissertations and received 10 patents, including one international. This year, three young researchers of the MESC department were awarded by the State Prize of Ukraine for young scientists.

# Thermophysical and Structural Investigations of Ge-S-Ag Chalcogenide Glasses

Lishchynskyy I.M.[1], Kaban I.[2], Klanichka V.M.[1], Zapukhliak R.I.[1], Varvaruk V.M.[1], Vasylyshyn I.D.[1]

[1]*Vasyl Stefanyk Precarpathian National University, Ivano-Frankivsk, Ukraine,*
[2]*Leibniz Institute for Solid State and Materials Research, Dresden, Germany*

This work presents the results of thermodynamic and structural investigations of rapidly $GeS_3$, $(GeS_3)_{100-x}Ag_x$ alloys and $Ge_{42}S_{58}$, $(Ge_{42}S_{58})_{100-x}Ag_x$ alloys (x= 5, 10, 15, 20, and 25 at.%).

The thermal properties of the amorphous alloys were investigated using a differential scanning calorimeter NETZSCH DSC 404. All compositions $(Ge_{42}S_{58})_{100-x}Ag_x$ show a single glass transition. The glass transition temperatures decrease with the increase of silver.

X-ray diffraction data measurements were taken at the BW5 high energy x-ray diffractometer (Hasylab). The energy of incident radiation was *100.0 keV (λ=0.124 A)*. Raw data were corrected for background scattering, detector deadtime, and Compton scattering.

Images of glass surfaces at various magnifications were recorded using the ZEISS Digital Scanning Electron Microscope DSM 982 Gemini. SEM micrographs of $(GeS_3)_{100-x}Ag_x$ samples are shown in Fig. 1.

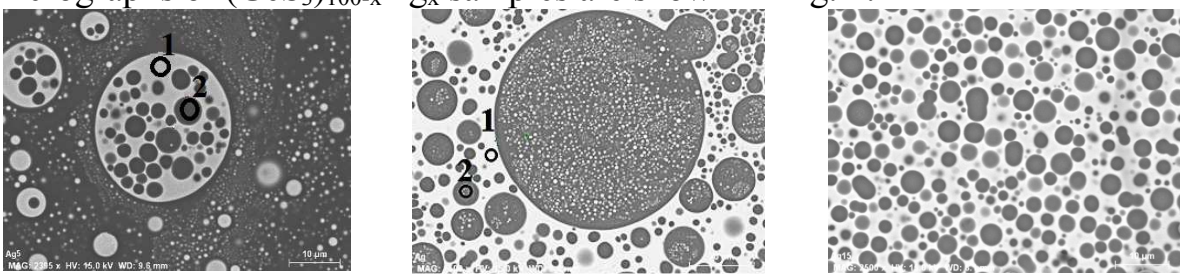


x =5 at.% x =10 at.% x =15 at.%

Fig. 1. SEM micrographs of the $(GeS_3)_{100-x}Ag_x$, glasses.

Energy dispersive X-ray analysis (EDX) techniques were used to investigate the phase separation of the $(GeS_3)_{100-x}Ag_x$. As expected, the images of the matrix $(GeS_3)$ and the $(GeS_3)_{75}Ag_{25}$ glass reveal homogenous glasses. Light and dark regions of the other images correspond to Ag-rich and Ag-poor phases, respectively. Interestingly, the larger Ag-rich domains contain inclusions of Ag-poor phase of various sizes. For higher Ag concentrations, i.e. for x = 15 at.%, the situation changes drastically and the Ag-rich phase becomes the dominant one.

Similar SEM images and EDX spectrum were obtained for $(Ge_{42}S_{58})_{100-x}Ag$, bat the samples exhibits no phase separation, while at x = 25 at.% the Ge cristalls in the glassy matrix is observed.

# Mutual Solubility in Thin Cu-Pb Film

Petrushenko S.I., Dukarov S.V., Sukhov V.N.,. Churilov I.G.

*V. N. Karazin Kharkiv National University, Kharkiv, Ukraine*

Understanding of changes in the solubility with transition from bulk samples to nanoscale ones is of great practical importance. In particular, the stability of microelectronic devices depends on the mutual solubility of the components from which they are made.

It has been found that small addition of lead (about 0.3 at.%) significantly reduces the disintegration temperature of continuous polycrystalline copper films to the island ones. The observed collapse of continuous copper films is probably caused by the acceleration of the mass transfer of copper, with the appearance of liquid lead on its surface. However, in accordance with literature data the solubility in the bulk is negligible in this system; it is less than 0.09 at.% at 900 K. This work is devoted to studying the mutual solubility in Cu-Pb binary system, in which one of the phases is in a highly dispersed state. Multilayer Cu-Pb films, produced in a vacuum of $10^{-6}$ torr, have been chosen as an object under study. The films were studied by electron diffraction during heating and cooling directly in an electron microscope. The value of the solubility was determined in accordance with Vegard's law. Such calculation was based on a change of the lead lattice parameter, with respect to the copper lattice parameter. To take into account the influence of the lattice parameter thermal expansion, we used Cu-C-Pb standard, which was produced in the same experiment. The thick carbon layer separated the metal layers and, as a result, served to prevent the interaction between components.

In summary, it was shown that up to temperatures of 400-420 K the lattice parameters of the component in Cu-Pb films and Cu-C-Pb standard are equal. However, with increasing temperature, we observed the solubility rise, which is linear in a first-order approximation. The mutual solubility reached 0.8 at.% near the melting point of lead. This value is at least one order of magnitude greater than one of Cu-Pb bulk.

# Devices Based on Silicon Carbide with a Quantum Structure

Sklyarchuk V.M., Melnik V.V., Sklyarchuk O.F.

*Yuriy Fedkovych Chernivtsi National University, Chernivtsi, Ukraine*

The unique properties of silicon carbide, such as high hardness, chemical and radiation resistance, make it possible to use carbide devices in such operating conditions, where similar devices on silicon can not be used. High sensitivity to spectral plot 0.2-0.4 microns and its absence in the visible spectrum offers a unique opportunity to use Au-SiC photodiode structures in metrology of ultraviolet (UV) radiation.

In this paper, the effect of surface treatment on photoluminescence and photoelectric properties of single crystals 6H-SiC were investigated. As a result of chemical etching of silicon carbide crystals in the melt-mix $1KOH:(50\div100)NaNO_3$ microrelief in the form of a sphere-like grain diameter 0.5÷1.0 microns or less formed on the surface $(000\bar{1})C$. To create a photosensitive Schottky diodes semitransparent gold contacts were deposited in vacuum $10^{-6}$ Torr on heated substrate by thermal evaporation. The thickness of the gold film was about 10 nm, which ensured its relatively high optical transparency with sufficient electrical conductivity. Ohmic contacts were formed by vacuum deposition of the same metal with following burning in with laser pulse ($\lambda$ = 1,06 μm). The resulting devices had high stability and well-marked diode properties. Photosensitivity of Au-SiC diodes covers the spectral area 200-350 nm, with sensitivity considerably higher than the value of the sensitivity diodes that were created on the mirror surface for comparison. In the photoluminescence spectra of samples radiation with photon energies $\hbar\omega$, larger band gap 6H-SiC present. This can be explained by the dimensional quantization of energy carriers, which occurs as a result of the creation of microrelief on the surface of the semiconductor. In this case, the photon energy is determined by the formula

$$\hbar\omega = E_g + \Delta E = E_g + \frac{\pi^2\hbar^2}{2d^2}\left(\frac{1}{m_n^*} + \frac{1}{m_p^*}\right) \qquad (1)$$

where $m_n^*$ and $m_p^*$ - the effective masses of electrons and holes respectively, and $d$ - the size of nano-objects on the surface of the crystal. Substituting known values of constants and effective mass and the experimental data $\hbar\omega$ into (1) allows to obtain value $d$ = 4 nm.

# The Use of Semi-Insulating Crystals Cd (Zn) Te: in Detectors for Ionizing Radiation

Sklyarchuk V.M.[1], Zakharuk Z.I.[1], Fochuk P.M.[1], Rarenko A.I. [1], Danilchenko B.A.[2], Klad'ko V.P.[3]

[1]*Yuriy Fedkovych Chernivtsi National University, Chernivtsi, Ukraine*
[2]*Institute of Physics of NASU, Kiev, Ukraine*
[3]*V.E. Lashkaryov Institute of Semiconductor Physics NASU, Kiev, Ukraine*

Semi-insulating crystals of Cd(Zn) Te with weak n-type conductivity, doped with indium during growth, which can be used for the manufacture of detectors of ionizing radiation were investigated in Shottky photodiodes design.

Crystals were grown through a solution-melt tellurium at 800°C by the zone melting method. Polycrystalline blank placed in quartz ampoule that moved through the heater zone at a speed of 2 mm per day. Synthesis of polycrystalline piece performed at 1150°C. Crystal plates 5×5 $mm^2$ and a thickness of 0,8-2,0 mm cut from different parts of the ingot. To investigate the electrical properties of crystals the ohmic contacts were made by thermal spraying of indium in a vacuum. Thus the structure created In / Cd (Zn) Te / In.

The current- voltage characteristics (CVC) demonstrated two specific areas: linear $I \sim V$ and quadratic $I \sim V^2$. The voltage $V_o$ was determined at the point of intersection of the continuation of ohmic and quadratic dependences of current on voltage. It was found differences in the magnitude of the resistivity determined from linear plots of CVC for crystals cut from different parts of the ingot: ~ (3-6) $\times 10^{10}$ Om×cm for the middle and (1-2)$\times 10^{10}$ Om×cm for the end of the ingot at 293 K and different temperature dependence of voltage $V_o$. This behavior of the CVC we explain within the model of space charge limited currents (SCLC). Based on the joint study of the temperature dependence of ohmic current areas of CVC and SCLC for crystals Cd (Zn) Te doped indium during growth, we defined that impurity energy level, responsible for the dark conductivity, has the donor nature. The observed features of the electrical properties of the crystals from the analysis of the statistics of electrons and holes from the electroneutrality equation explains the specifics of compensatory processes of semiconductor material. The method of determining the ionization energy, the degree and nature of compensation deeper level, responsible for the dark conductivity of the material proposed. Relationship between the degree of compensation deeper level of semiconductor crystals with detecting properties of structures fabricated on them were investigate. Established that for close values of material resistivity detective properties are better for structures made from crystals in which dark conductivity caused by poorly compensated deep level.

## СЕКЦІЯ 4 (стендові доповіді)
## ТОНКОПЛІВКОВІ ЕЛЕМЕНТИ ЕЛЕКТРОННИХ ПРИСТРОЇВ, НАНОЕЛЕКТРОНІКА

12-15 травня 2015 р.

## SESSION 4 (poster)
## THIN FILM ELEMENTAL COMPOUNDS FOR ELECTRONIC DEVICES

May, 12-15, 2015

# *n*-CdTe-Based Thin-Film Solar Converters

Bobrenko Yu.N., Pavelets S.Yu., Semikina T.V., Stadnyk O.A.,
Sheremetova G.I., Yaroshenko M.V.

*V. Lashkaryov Institute of Semiconductor Physics, NAS of Ukraine, Kyiv, Ukraine*

The *n*-CdS/*p*-CdTe solar converters (SC) belong to the most efficient thin-film SC. The advances obtained using *n*-CdTe in this area are less substantial because there is no optimal broad-band "window" of *p*-type. Here we propose application of strongly degenerate digenite $Cu_{1.8}S$ as a *p*-type component of *n*-CdTe-based SC. Based on *p*-$Cu_{1.8}S$/*n*-II–VI surface-barrier structures, efficient photoconverters of UV and visible radiation are obtained. The investigations presented in this work show that the above surface-barrier structure is also promising for application in solar power engineering.

Cadmium telluride was grown on Mo/CdSe substrates through a graded-gap $CdSe_xTe_{1-x}$ interlayer using the quasi-closed volume technique. A multilayer *p*-$Cu_{1.8}S$/*n*-CdTe/*n*-CdSe/Mo structure was prepared that made it possible to increase the degree of structural perfection of thin photosensitive *n*-CdTe layers without application of additional high-temperature treatments, as well as to obtain an ohmic back contact without additional doping of CdTe. A thin layer of insulating $TeO_2$ oxide was grown on the *n*-CdTe surface to raise SC quantum efficiency. When growing $TeO_2$, accumulation of cadmium on the CdTe surface is possible, with formation of a low-resistance near-surface region. The low-resistance layer leads to redistribution of drag electric field whose maximal values are localized at the $Cu_{1.8}S$/CdTe interface. This results in 15-20% increase of SC efficiency over the whole spectral sensitivity area. Presence of a low-resistance near-surface layer was supported by the results of studies of *I–V* and *C–V* curves.

The main operating parameters of SC were measured at natural solar lighting. The emittance of incident radiation was 0.74 mW/cm$^2$. The best parameters were demonstrated by the $Cu_{1.8}S$-CdTe SC in which CdTe was doped with indium. For such SC, the peak open-circuit emf $U_{oc}$ = 0.71 V, fill factor of load characteristic FF = 0.7, short-circuit current density $I_{sc}$ = 15.8 mA/cm$^2$, efficiency $\eta$ = 10.7%. The SC area (with allowance made for ~10% shadowing with the upper current-collecting electrode) was $S$ = 0.25 cm$^2$.

# Investigation of Physico-Chemical Properties of Organic Materials for Creation of Thin Film Piroelectric Elements of Infrared Radiation Detectors

Boichuk V.I., Peleshchak R.M., Kravtsiv M.M.

*Drohobych State Pedagogical University, Drohobych, Ukraine*

The results of investigations of organic materials based on the films of poly-crystalline organic poly-cycle compounds, which are characterized by the non-symmetric crystalline structure and belong to the naftaline and dyphenile class, have been presented in the work. There are many dielectric materials to be known which possess electrical polarization at the absence of external electrical field. The organic semiconductors based on the thin film of poly-crystalline organic poly-cycle compounds have been chosen as objects for the research. The best piroelectric characteristics have been obtained for the films based on the dephynile class.

The samples have been prepared by vacuum thermal evaporation of organic matter on the dielectric substrates with further crystallization of the formed phase. The thickness and the parameters of film have been determined by the time and regime of the organic matter evaporation. The correct orientation has been obtained for 1 μm films.

The films of poly-crystalline organic poly-cycle compounds present themselves as ordering conglomerate of micro-crystals which possess microscopic spontaneous polarization toward normal of substrate, giving therefore piroelectric properties of the films [1]. The films morphology can be obtained under microscope in the view of many-centered spheroid structure, characterizing a statistical meaning of any crystallographic axes in the plane of substrate.

The films are characterized by the piroeffect which is explained by the strong temperature dependence of interrelated situation of polar groups in the organic molecules [2]. In respect to own parameters, the poly-crystalline films of organic compounds are similar with known piroelectrics.

The using of such films testifies on their perspective application as materials for creation of new type piroelectric detectors of infrared radiation.

1. Dorozhkin L.M., Lazarev V.V., Pleshkov G.M. Thin film piroelectric detector based on the organic compounds for measuring parameters of impulse laser radiation // Quantum electronics. – 1983. -V.10. – P.1107-1112.
2. Mykola Kravtsiv. On the mechanism of formation of the photoelectret state in 4-nitro-4′-aminodiphenyl thin films. // Materials Science.- 2014- Vol.20 - № 4. – P.69 – 75.

# Influence of Localized Charge Distribution on Thin Film CdS-$Cu_2S$ Nonideal Heterojunction Photovoltaic Properties

Borschak V.A., Brytavskyi Ie.V., Smyntyna V.A.

*I. I. Mechnikov Odessa National university, Odessa, Ukraine*

The work is devoted to theoretical generalization, modeling and control of accumulation and re-read signal effect in optical sensors based on nonideal heterostructures.

The work is dedicated to the analysis of the characteristics of sensor properties and component composition of thin-film heterojunction CdS-$Cu_2S$. In this regard, a complex research aimed at processes modeling in the tunnel barrier layer, the study of samples chemically modified phase composition, investigation of sensor properties degradation was carried out [1].

The main results present a model that describes the kinetics of concentration of positive charge, accumulated in deep traps after photoexcitation and takes into account both thermal and tunnel holes release mechanisms. Numerical calculations of localized charge distribution changes over time, found out that this distribution in terms of dynamic equilibrium has an exponential character. Close compliance between calculated and experimentally obtained dependences was demonstrated.

The mechanisms of signal relaxation, associated with the removal processes of nonequilibrium charge from the space charge region of the image sensor on the basis of non-ideal heterojunction were investigated. The mechanism of the observed two-stage process was determined. Novel results concerning CdS-$Cu_2S$ heterojunction surface morphology and impurities depth distribution were obtained. In particular, the question of observed variation of surface photosensitivity and components interdiffusion on heteroborder was clarified [1]. Also the comparison of samples formed by two different methodics (electrodynamical spraying and vacuum evaporation techniques) was made. X-Ray diffraction (XRD) was performed in order to detect $Cu_xS$ compounds at CdS-$Cu_2S$ heterojunctions.

[1]. V. A. Borschak, V. A. Smyntyna, Ie. V. Brytavskyi, S. V. Zubritskiy, M. I. Kutalova, Ya. I. Lepikh. Microstructural features and componential analysis of thin film CdS-$Cu_2S$ photosensing structures as element of image sensor // Photoelectronics. – 2013. – № 22. – P. 98-102.

# Schematic and Topological Elements Optimization of Transfer Signals Circuits for Analytical Microsystems-on-Chip

Kogut I.T., Dovhij V.V., Holota V.I.

*Vasyl Stefanyk Precarpathian National University, Ivano-Frankivsk, Ukraine*

When designing the elements of integrated circuits (ICs) and specialized in integrated realizations analytical microsystems-on-chip based on silicon-on-insulator (SOI) MOS transistors is necessary to consider such parameters as speed, signals delay in information channels, power consumption and area on chip [1]. These parameters are particularly important in analytical microsystems-on-chip, which are, for example, systems for investigated non-silicon's elements monolithically integrated directly into the crystal of specialized chips.

The optimal base for such systems for constructively-technological realizations, possibilities of creating in the short term, and improved characteristics are specialized CMOS gate array with SOI-structures.

In this paper the results of schematic, layouts design and computers simulation of signals generators with using trigger elements in the information transferring channels for integrated circuits to select the optimal power and time characteristics circuit solutions are presented. Also, level shifters with two levels of signal voltage was designed and investigated. Such level shifter can be effective signals generator with good delay parameters and power consumption at the same voltage.

Trigger element with dual controls, which has much steeper amplitude-transmitting characteristics comparatively with series-connected inverters, is taken as a basis for such converters. For example, is represented electrical circuit (a) and designed CMOS SOI gate array layout (b) for this generator of signals is shown on Fig.1.

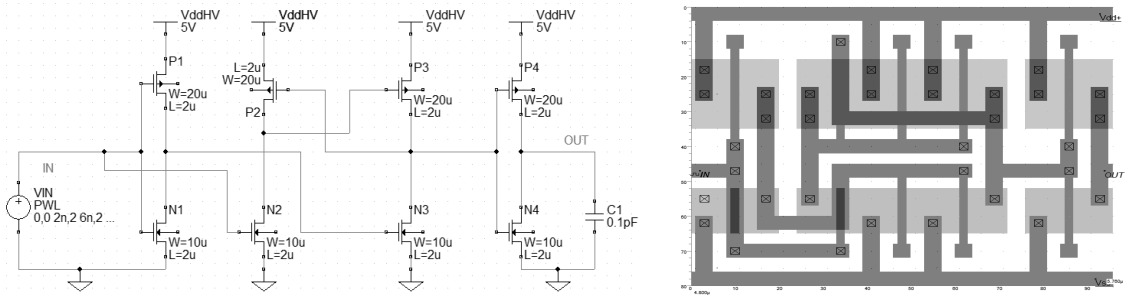


a) b)

Fig.1 Signals generator on trigger element: a) electrical circuit; b) layout.

The obtained results can be used in the design of integrated circuits and microsystems-on-chip.

1. Kogut I.T., Dovhij V.V. Research outputs cascades of CMOS gate array with silicon on insulator structure // Modern problems of Radio Engineering, telecommunications and Computer Science Proc. of the 10th Inter. Conf., TCSET"2010.

# The Influence of Own Point Defects on Luminescence Of α-ZnSe Heterolayers

Slyotov O.M., Gavaleshko O.S., Ulyanitskiy K.S.

*Yu.Fedkovych Chernivtsi National University, Chernivtsi, Ukraine*

Wide-gap II-VI-semiconductors are widely used in functional electronics. Among them the most interest is attracted by zinc selenide. As well know, the undoped β-ZnSe specially own point defects reveals themselves. They form different energy states that affect on material properties and behavior of impurity atoms in it, especially isovalent. Such information may be significantly supplemented by investigation of properties of hexagonal modification α-ZnSe layers, that's the main aim of this work.

Heterolayers of α-ZnSe were obtained by isovalent substitution method. The hexagonal structure of the grown layers is confirmed, in particular, undertaken studies of optical reflection of $R_\omega$. On the differential curves $R'_\omega$, obtained by using λ-modulation, characteristic of this type of crystal structure features were observed. They are caused by the band structure of the relevant parameters: $E_g = 2{,}89$ eV, $\Delta_{SO} = 0{,}37$ eV, $\Delta_{CR} = 0{,}07$ eV. Specially undoped heterolayers inherent luminescence in the photons energy $\hbar\omega < E_g$. It is characterized by the presence of three main components bands, which is marked by means of symbols *A*, *B*, *C*. They correspond to the energy centers with the ionization energy $E_i$ at 0,06 eV, 0,135 eV and 0,583 eV, respectively. They are defined from the studies of temperature dependence of conductivity and luminescence. For the bands *A* and *B* are inherent peculiarities of small centers – maxima correspond $\hbar\omega_m = E_g - E_i$, and bands form adequately approximated by Gaussian distribution. The obtained values of $E_i$ in a good agreement with the depth of singly charged vacancies of selenium $V^{\bullet}_{Se}$ and zinc $V'_{Zn}$ in β-ZnSe (0,03 eV and 0,18 eV). We can assume that such own point defects (OPD) is also involved in the formation of α-ZnSe emission. The nature of *C* band with $E_i = 0{,}583$ eV is explained by recombination via deep levels in according to the model of Kopylova-Pihtina. This is evidenced by the following main features: asymmetric band shape, its large half-width (which increases with the excitation level *L*), and the independence of the $\hbar\omega_m$ with changes of *L* values. Under certain conditions on the differential curves of luminescence can be observed the equidistantly excesses with the interval of 21 meV, corresponding to the LO-phonon energy in α-ZnSe. Position of the C-band maximum at $\hbar\omega_m = 2{,}43$ eV corresponds to the following equation $E_i = E_g - \hbar\omega_m - \Delta$, where $\Delta$ – Frank-Condon shift. Calculations by the known expressions give $\Delta = 0{,}123$ eV, which is close to $\Delta = 0{,}2$ eV for β-ZnSe. The most likely explanation of the deep centers nature is that interstitial atoms of cations sublattice $Zn_i$, as in the case of β-ZnSe. Possible assumptions about the nature of these indicated OPD analyses by the method of quasichemical reactions.

# Flexible Elements of Gas Sensors Based on Conducting Polymers

Tsizh B.[1,2], Aksimentyeva O.[3], Chokhan M.[2], Konopelnyk O.[3], Horbenko Yu.[3]

[1]*Kazimierz Wielki University in Bydgoszcz, Bydgoszcz, Poland*
[2]*S.Gzytsky Lviv Natoina lUniversity of Veterinary Medicine and Biotechnologies, Lviv, Ukraine*
[3]*Ivan Franko National University of Lviv, Lviv, Ukraine*

One of the most promising among sensor elements is gas sensing polymer films due to their high process ability, easy of synthesis and low cost and in some cases by better technological performances [1]. It is proposed a method of formation of the sensitive to polar gas free standing elastic films of the conjugated polyaminoarenes embedded in the polyvinyl alcohol (PVA), polyacrylic (PAA) and polymethacrylic acid (PMAA) matrices. The structure, optical and thermo mechanical properties of the obtained composite films were studied. It's shown that action of ammonia causes spectral and corresponded visible changes in the films colour. On this basis the method of obtaining the flexible colour indicators for express control ammonia content in gas environment has been developed [2]. Flexible sensor films sensitive to action of ammonia were formed on the base of conducting polymers and dielectric polymer matrices by template synthesis. It has found that content of composite and nature of polymer matrix causes a complex character of specific conductivity of composites. For composites of polyorthotoluidine, PoTI-PAA a specific conductivity achieves maximal value at 5,7-6,5% content of PoTI. With follow increasing concentration of polyaminoarene it decreasing, this may be caused by poor mechanical properties of composites. Specific conductivity of PoTI-PVA composites achieves a maximal value on the level $10^{-4}…10^{-6}$ S/cm. A shape of dependence of specific conductivity from volume content of conducting polymer is evidence to percolation character of conductivity in obtained composites. With help of structure investigations is confirmed the formation of linear chains of conducting polymer in dielectric matrix due to an appearance of structure matrix effect. Existence the structure of this type provides a safety of the properties characteristics for flexible polymer matrices PVA and PAA, and also a semiconductor character of conductivity of conjugated polymers

1. B. R. Tsizh, O.I. Aksimentyeva, Ya. I. Vertsimakha, P. M. Lutsyk, M. I. Chokhan. Molec. Cryst.&Liq. Cryst. – 2014. – Vol. 589. – P. 116 – 123.
2. O.I. Aksimentyeva, B. R. Tsizh, M. I. Chokhan, O.M. Yevchuk . Patent № 65401, Ukraine. Sensor visual control ammonia content. – Publ. 12.12.2011, Bul. № 23.

# Microplasma Characteristics of the Light-Emitting InGaN/GaN Thin-Film Structures on Various Substrates at Reverse Bias

Veleschuk V.P., Vlasenko O.I., Kisselyuk M.P., Vlasenko Z.K.

*V. Lashkaryov Institute of Semiconductor Physics, NASU, Kyiv; Ukraine*

At increasing the area for the epitaxial thin-film InGaN/GaN heterostructures arises the urgent problem of express detection and non-destructive control of electrically active extended defects (imperfect regions) in such heterostructures of power light-emitting diodes (LEDs).

Except for various methods of diagnostics and reliability prognostication based on diversity of elemental and structural analysis techniques, different electro-physics methods effective in non-destructive characterization and control of quality of GaN (InGaN, AlGaN) structures are local photo-, electro-, cathode-luminescence (PL, EL, CL). But it is not always possible to detect critical electrically active extended defects (defects regions) influence of which is dominant on electric and luminescent functional parameters of InGaN/GaN structures.

At the same time, application of a reverse voltage to GaN structure produces controlled microplasma (MP) breakdown that takes place mainly in the regions of extended defects, and is accompanied by luminescence [1].

Studied in this work is the microplasma controlled breakdown of InGaN/GaN heterostructures in power LEDs ($P_{el}$ = 1 W, $I_{nom}$ = 350 mA, $\lambda_{peak}$ = 460…470 nm), prepared on various substrates - SiC, AuSn/Si, $Al_2O_3$. It has been ascertained that the luminescent and electric parameters of the microplasmas for InGaN/GaN power LEDs are related with the InGaN/GaN functional parameters. It is ascertained that among these three investigated heterostructures on the different substrates (SiC, AuSn/Si, $Al_2O_3$) the heterostructure on the SiC substrate has the best quality and, respectively, the best functional parameters, in contrast to the heterostructure on the sapphire substrate that has the highest amount of critical defects.

It is established that the sources of microplasmas in the InGaN/GaN heterostructures of power LEDs in the most cases are corresponding to them extended defects at the grain boundaries of GaN crystallites.

1. V.P. Veleschuk, O.I. Vlasenko, M.P. Kisselyuk, and O.V. Lyashenko. Microplasma breakdown of InGaN/GaN heterostructures in high-power light-emitting diodes // *Journal of Applied Spectroscopy*. – 2013. - Vol. 80, N 1. – P 121 - 127.

# The Photosensitivity Nanostructures Based on II-VI Semiconductors

Vuichyk M., Tsybrii Z., Svezhentsova K., Smirnov O., Bilevych O., Sizov F.

*V. Lashkaryev Institute of Semiconductor Physics NAS of Ukraine, Kyiv, Ukraine*

Perspective materials to create a solar converters are composite structures based on $A_2B_6$ (CdTe, ZnO) semiconductor films, which activated by CdS, CdSe quantum dots. Their basic electrical properties depend on the structure of the atomic lattice and its defects. Carrier transport efficiency is defined microstructure sensitive layer. The study of the physical properties of such structures is necessary in view of the fact that such heterostructures are promising when used as active elements photosensitive converters for solar cells.

In work are studied the photoelectric properties of nanostructured $A_2B_6$ thin films and heterostructures based on them, and surface morphology of thin layers at each stage of production prototype solar cell (SC). SC prototype consisted thin nanostructured layers of CdTe, CdS on glass substrate with gold contacts.

To study the surface morphology was used atomic force microscope “FemtoScan”. Depending on the choice of growing conditions observed two characteristic surface relief with a large (d ~ 100-200 nm) and a small (d ~ 10-30 nm) nanorods CdTe. Fig. 1 shows the surface morphology of the heterostructure CdTe/CdS at an intermediate stage of manufacture SC.

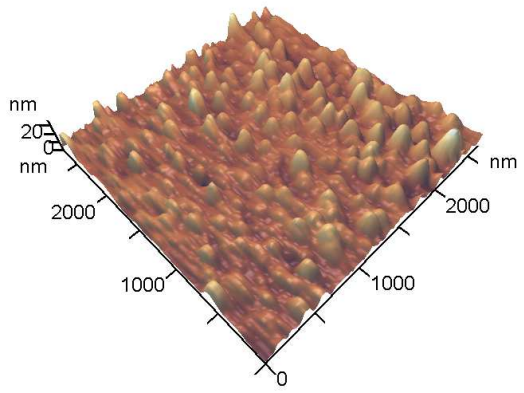


Fig. 1. Morphology of surface CdTe/CdS heterostructure.

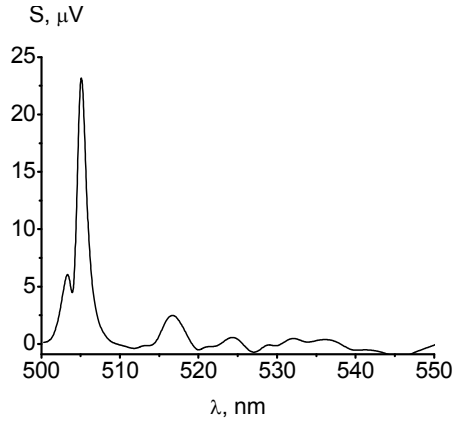


Fig. 2. Photoresponse's spectral dependence for the prototype solar cell at T = 300K.

Spectral dependencies of photosensitivity (Fig. 2) were measured at using SPM-2 spectrometer with a prism G-60 and nanovoltmeter UNYPAN-232V without prior amplification mode. As the result, the structures of this type characterized spectrally narrow strip of photoresponse in the visible spectrum with a peak sensitivity at 505 nm, which confirms the promising use this structures for photovoltaic systems.

# Advanced Capacitive Converters Based on Al/ITO/Polyimide/$Al_2O_3$ Heterostructures

Zaitseva L.V.[1,2], Khrypunov G.S.[1], Zaitsev R.V.[1], Momotenko O.V. [1]

[1]*National Technical University "Kharkiv Polytechnical Institute", Kharkiv, Ukraine*
[2] *OJSC «Turboatom», Kharkiv, Ukraine*

The necessity of simplification the control technology of metal products in industrial production led to further development of widely implemented acoustic methods. Significant experience of practical utilization of piezoelectric method has identified areas where it is not effective: for control of products with contaminated surface, affected by corrosion or coated. Thus, devices that will perform liquidless acoustic control need to be created for practical defectoscopy purposes. The promising ones can be based on the capacitive method for generating and receiving of acoustic signals, which has fundamentally different physical mechanism for generating of an acoustic signal in control object, its surface is one of the capacitive plates and generates a signal without liquid for acoustic contact. However, existing capacitive compositions do not allow obtaining of the required sensitivity.

It appears to be quite actual to use a polyamide film with thickness of 15 to 125 microns as a dielectric layer and a basis for capacitive converters, that is 10 times less than the thickness of the classic dielectric layers, on which can be fabricated the capacitive converters by coating of the surface with thin film layers of ITO layer (0,2-0,3 μm) as a converter conductive plate and $Al_2O_3$ dielectric layer (1 μm) for increase the dielectric constant value. In general, the capacitive converter can be based on ITO/polyimide/$Al_2O_3$ heterostructures.

Past studies of the film layers crystal structure, their electrical properties and surface morphology allowed to determine the optimum technological conditions of manufacturing such capacitive converters. They also allowed creating a prototype of a thin film capacitive converter based on Al/ITO/ polyimide/$Al_2O_3$ heterostructure for acoustic control of metallic products with ten times higher sensitivity comparatively with classic capacitive converters.

1. Zaitseva L.V. Flexible film capacitive converters based on the ITO/ polyimide/$Al_2O_3$ structure / L.V. Zaitseva, G.S. Khrypunov, R.V. Zaitsev, A.L. Khrypunova // Physical surface engineering – 2014. –№4. – P. 505–509.

## СЕКЦІЯ 5 (усні)
## ФУНКЦІОНАЛЬНІ КРИСТАЛІЧНІ МАТЕРІАЛИ: РІСТ, ФІЗИЧНІ ВЛАСТИВОСТІ, ВИКОРИСТАННЯ

12-15 травня 2015 р.

## SESSION 5 (oral)
## CRYSTAL'S GROWTH AND THEIR PHYSICAL PROPERTIES

May, 12-15, 2015

# Quasi-Chemical Model of Point Defect Equilibrium in ZnO Single Crystal

Berestok T.O., Kosyak V.V., Kshnjakina S.I., Opanasyuk A.S.

*Sumy State University, Sumy, Ukraine*

Practical application of device structures based on single crystals and films of zinc oxide is determined by electro-physical and optical characteristics of the material, which is largely conditioned by the ensemble of point defects of the material. Point defects can be traps, luminescence and photoconductivity centers, act as donors and acceptors. Therefore, the ability to obtain semiconductors with controlled ensemble of point defects by varying the deposition condition determines the possibility of using the material.

In the work we report the results of improvement of modeling of the point defects equilibrium in zinc oxide single crystals, which is based on the consideration of the formation of point defects under thermodynamic equilibrium between gas phase and solid state [1].

The developed approach allowed us to obtain the balance of chemical potentials between perfect crystal and defect-containing crystals. On the basis of this approach we developed the equations that allowed more adequately calculations of the concentration of various types of point defects of zinc oxide during changing the external temperature of deposition or annealing.

Using obtained equations, translation, vibrational and rotational motions of the total defect energy were determined and estimation of the chemical potentials of the atoms of zinc ($\mu_{Zn}$) and oxygen ($\mu_O$) were made. As a result the dependence of the dominant point defect concentration and free charge carriers concentration on the growth conditions ZnO were studied. The values of the defects formation energy and transition energy levels calculated from the first-principles were taken from [2]. The concentration of free charge carriers and charged point defects were calculated using Fermi-Dirac statistics. On the basis of these values the concentration of point defects were expressed as a function of zinc and oxygen in the material by the values of the chemical potentials.

Moreover comparing analysis of results obtained by propounded model and traditional model of point defect ensemble modeling

1. Kosyak V., Mortazani Amiri N.B., Postnikov A.V., Scarpulla M.A. Model of native point defect equilibrium in $Cu_2ZnSnS_4$ and application to one-zone annealing // *Journal of Applied Physics*, **114**, (2013), 124501.
2. Zhang S.B., Wei S.-B., Zunger A. Intrinsic n-type versus p-type doping asymmetry and the defect physics of ZnO // *Physical Review B,* **63**, (2001), 07205.

# Characterization of Zn(Mn)Se/GaAs(001) Layers by Multi-Beam X-Ray Diffraction

[1]Borcha M., [1]Fodchuk I., [2]Baidakova M, [2]Klimko G,
[2]Sedova I., [2]Sokolov R., [2]Sorokin S., [2]Yagovkina M.

[1]*Yuriy Fedkovych Chernivtsi National University, Chernivtsi, Ukraine*
[2]*Ioffe Physical-Technical Institute of the Russian Academy of Sciences, St.-Petersburg, Russia*

X-ray multi-beam diffraction (MBD) is not often used for characterization of complicated multilayered semiconductor systems due to complexity of diffraction pattern governed by both multi-beam effects and complex real structure influence. However X-ray MBD is a high-precision tool for determination of lattice parameters, chemical composition and strain distribution in crystalline materials [1-2].

The technique of high-resolution X-ray MBD with the using of coincidental coplanar / non-coplanar diffraction [2] was developed for multilayered systems comprising $ZnMn_xSe$ (x=0.05÷0.15) layers on GaAs (001) substrate. Experimental approbation of this technique was carried out on the 1-μm-thick ZnMnSe layers grown by molecular beam epitaxy (MBE) pseudomorphically on GaAs (001) substrate via a GaAs buffer epilayer at a temperature of $T_S$= 280°C by using a double-chamber MBE setup (Semiteq, Russia). X-ray MBD measurements were performed using the high resolution x-ray diffractometer (Bruker D8 Discover) equipped with an Eulerian quarter circle, a graded parabolic mirror and a double-crystal symmetric Ge (220) monochromator. CuKa1 radiation from a 6 kW rotating anode x-ray source was used.

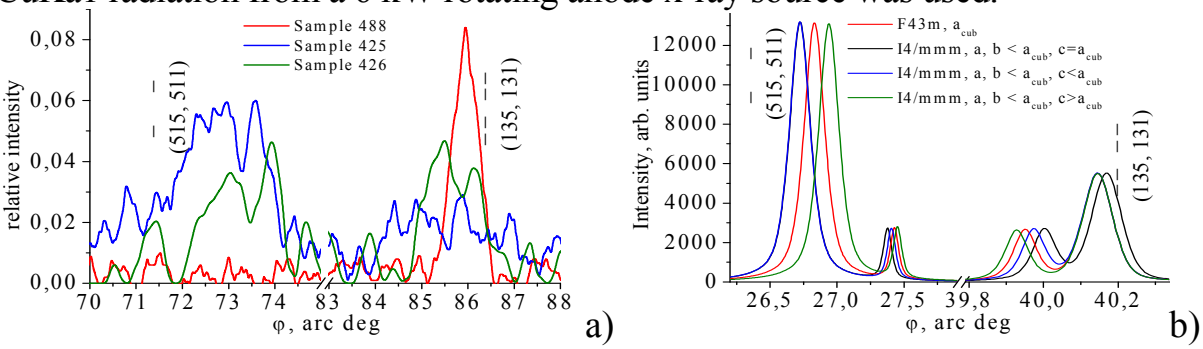


Fig. 1. Fragment of multi-beam X-ray diffraction scan for $Zn_{1-x}$ $Mn_xSe$ layer.
a) experiment; b) calculations, the cubic-to-tetragonal transition in layer is taken in account. φ is a scanning angle, primary reflection is (006), CuKα-radiation.

Application of the developed X-ray MBD technique enables one to study the structural disordering near the II-VI/III-V heterovalent interface, the degree of interdiffusion of chemical elements between ZnMnSe and GaAs layers and to determine the depth of heterovalent interface mixing for the multilayered structures based on Zn(Mn)Se (Fig. 1).

1. Chang S-L, *Journal of Physics and Chemistry of Solids,* **62**, (2001), 1765.
2. Borcha M *et al.* (2009). Physica status solidi A **206**, N 8, 1699.

# Studying of Fine Structure of Coatings and Deformed High Entropy Alloys With the Using of Analytical Electron Microscopy

Danylenko M., Gorban V., Firstov S.

*Institute for problems of Materials Science NAS of Ukraine, Kyiv,Ukraine*

The recently developed high-entropy alloys (HEAs) are the new class of alloys which typically consist of at least five principal elements with atomic concentration between 5% and 35%. The HEAs demonstrate high properties [1-3] and show great potential for aircraft and engineering applications due to their promising properties in hardness, wear resistance, corrosion resistance, and high-temperature stability.

The method of analytical transmission electron microscopy was used for studying of fine structure of coatings and high deformed HEAs [4]. High locality of quantitative x-ray microanalyses is achieved by studying of thin foils (thickness about 100 nm) and fine electron beam (0,5-1,5 nm).

Chemical composition of HEAs in the initial state varies in the range of 10 percent at a distance of a few nanometers. After ECAP alloy becomes more homogeneous (the deviation is 1-2 at.%). Hardness increased to 5,1 GPa, with a slight increasing the elasticity modulus up to 78 GPa.

The phase and chemical compositions do not undergo significant changes during magnetron sputtering. But the application of a negative bias voltage to the substrate allows to form the homogeneous structure instead of a columnar one, which leads to increasing the hardness from 14 to 17.5 GPa of the AlCrFeCoNiCuV coatings.

1. Yeh J.W., Chen Y.L., Lin S.J. and Chen S.K. High-entropy alloys – a new era of exploitation // Materials Science Forum, 560, (2007), 1.
2. Zhang Y. and Zhou Y. J. Solid Solution Formation Criteria for High Entropy Alloys // Materials Science Forum, 561, (2007), 1337.
3. O.N. Senkov**,** J.M. Scott**,** S.V. Senkova**,** D.B. Miracle Microstructure and room temperature properties of a high-entropy TaNbHfZrTi alloy//Journal of Alloys and Compounds, **509**(20), (2011), 6043.
4. V.F.Gorban', V.A.Nazarenko, M.I.Danylenko, M.V.Karpets, N.A.Krapivka, S.A.Firstov, and E.S.Makarenko Influence of deformation on the structure and the mechanical properties of a high_entropy $Fe_{25}Cr_{20}Ni_{20}Co_{10}Mn_{15}Al_{10}$ alloy// Russian Metallurgy (Metally), 10, (2014), 773.

# Calculation of Thermoelectric Parameters PbTe:Ag

Dzumedzey R.O., Boryk V.V., Pavliuk M.F., Kal'ka O.Yu, Zapuhliak J.R.

*Vasyl Stefanyk Precarpathian National University, Ivano-Frankivsk, Ukraine*

Now one of the most promising alternative energy is thermoelectricity. It is known for this application of lead telluride and compounds based on it are the most promising in the medium temperature range. Efficient thermoelectric converter is realized through the establishment of needed characteristics at the material that ensure, in "permanent" electronic subsystem, a significant deterioration phonon component of the crystal. Promising ways for that is doping material. For create effective thermoelectric converters necessary materials as n- and p-type conductivity.

Among the most famous acceptor impurity can be identified thallium and alkali metals. However, they have several disadvantages in particular, thallium is highly toxic, and with alkali metals there are many technological problems, due to their high chemical activity which significantly complicates the process of synthesis material. Silver impurity also has acceptor action in Lead Telluride and does not have aforementioned drawbacks.

This work is devoted to the study of thermoelectric parameters PbTe: Ag with different silver content: 0.05; 0.1; 0.15; 0.2 and 0.3 at. %.

Determined that the maximum figure of merit at 300 K observed when the silver content of 0.15 at. %.

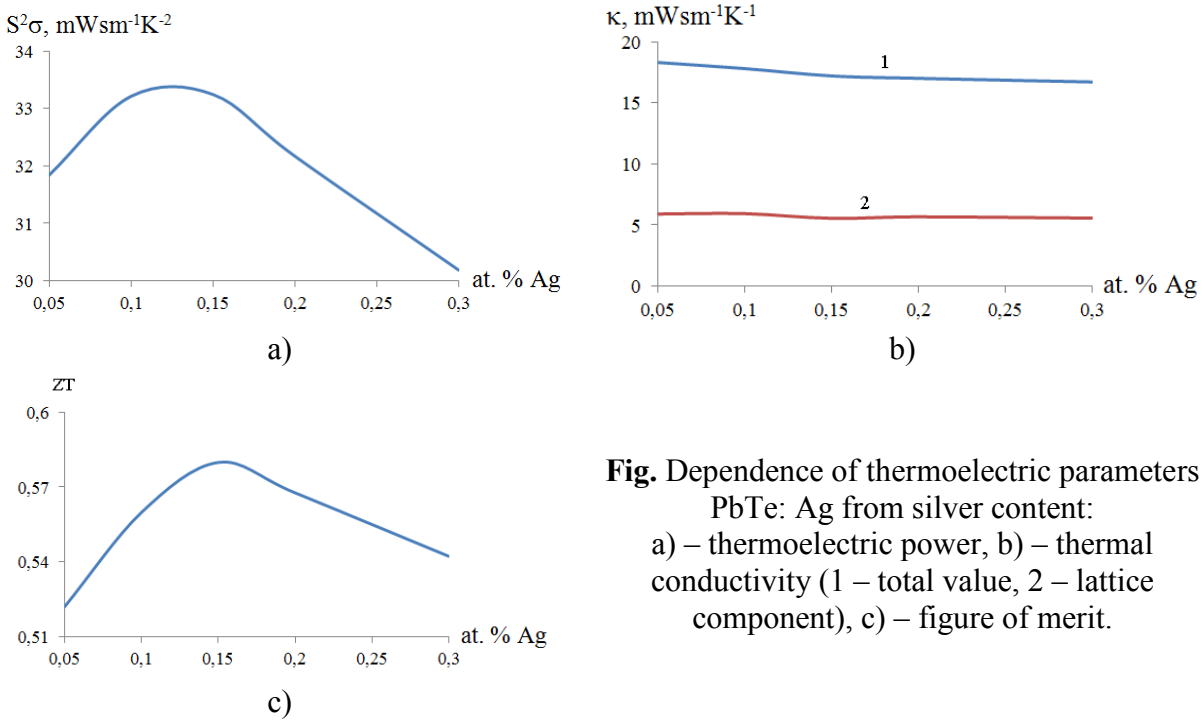


**Fig.** Dependence of thermoelectric parameters PbTe: Ag from silver content: a) – thermoelectric power, b) – thermal conductivity (1 – total value, 2 – lattice component), c) – figure of merit.

*This research is sponsored by NATO's Public Diplomacy Division in the framework of "Science for Peace" (NATO SPS 984536)).*

# The Inclusions' Behavior in Cd(Mn,Zn)Te Crystals

Fochuk P.[1], Kopach O.[1], Verzhak Ye.[1], Shcherbak L.[1], Panchuk O.[1], Bolotnikov A.[2], James R. B.[2]

[1]*Chernivtsi National University, Chernivtsi, Ukraine*
[2]*Brookhaven National Laboratory, Upton, USA*

The quality of gamma- and X-ray detectors prepared from Cd(Mn,Zn)Te crystals at the current time can be sufficiently improved by inclusion size/content reductions. This is possible by long-term thermal annealing under Cd overpressure. Another possible method is to move inclusions in a temperature field gradient. Therefore our task was to study the inclusions' behavior in Cd(Mn,Zn)Te crystals under thermal treatment in or without a temperature gradient field.

Cd(Mn,Zn)Te single crystals were grown by the Bridgman method. A series of annealing experiments under different conditions (temperature, Cd overpressure, annealing time, and cooling rate) was performed. The obtained results allowed us to determine the optimal temperature and time for sample treatment at ~1100 K and times up to 1 hour (Fig. 1). No visible inclusions can be detected by IR microscopy after annealing under these conditions. Annealing in a temperature field gradient under a Cd overpressure was performed at different temperature gradients in range of 900-1000 K. The experiments demonstrated inclusion movement in Cd(Mn,Zn)Te crystals if the inclusion dimensions exceeded ~30 microns. The optimal temperature for inclusion migration is 950 K.

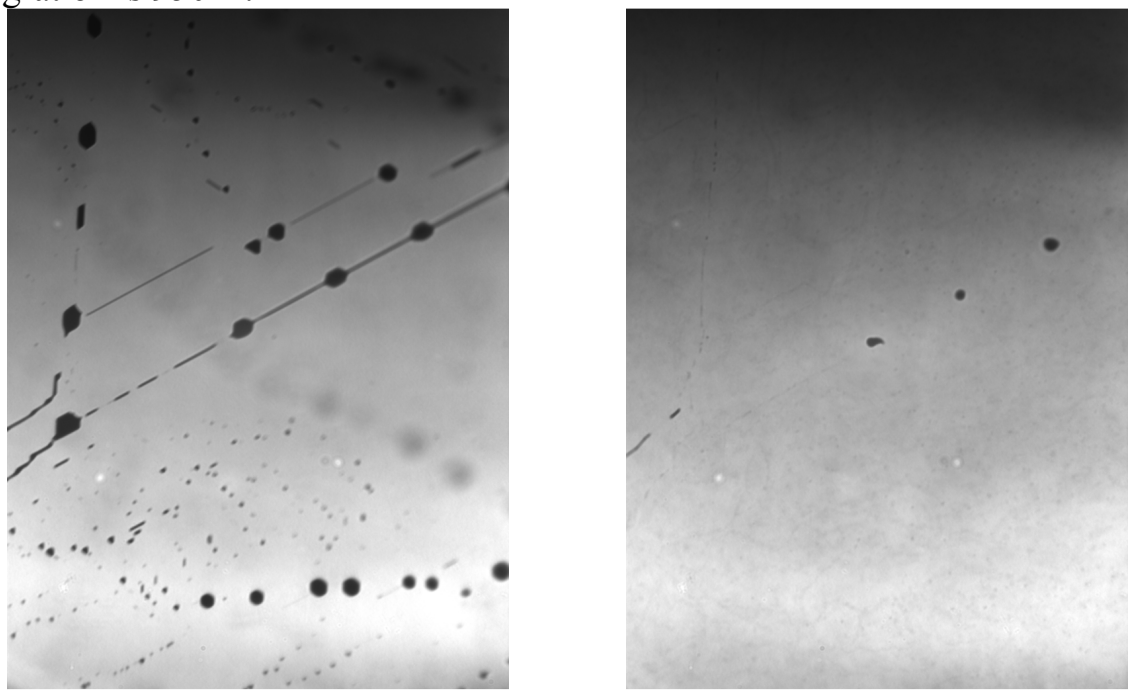

Fig. 1. The IR images of Cd(Zn)Te before (left) and after (right) annealing at 1100 K during 60 min. under Cd overpressure.

# Technology and Thermoelectric Properties of Semiconductor Materials Based Systems Pb-Sb-Te

Galushchak M.O., Krynytsky O.S.

*Ivano-Frankivsk National Technical University of Oil and Gas; Ivano-Frankivsk, Ukraine.*

Compound $A^{IV}B^{VI}$ semiconductor materials promising for creating thermoelectric devices operating in the temperature range from room to 900K. Among which compares favorably with properties PbTe - many valley nature of the energy spectrum (N = 4); lattice thermal conductivity of low value ($\chi_g$ = 2,09·10 $^{-2}$ W·K$^{-1}$·cm$^{-1}$) relatively high carrier mobility ($\mu \approx 10^3$ cm$^2$·V$^{-1}$·s$^{-1}$); the most important values $\mu\chi^{-1,}$ leading to a significant increase maximum thermoelectric figure of merit ($Z_{max}$).

The efficiency of thermoelectric materials is determined by a dimensionless figure of merit, figure of merit (ZT): $ZT = (\alpha^2\sigma/\chi)T$, where $\alpha$, $\sigma$, $\chi$, T respectively Seebek coefficient, electrical conductivity, thermal conductivity and absolute temperature. Low values of ZT commercially available thermoelectric materials limits the use of thermoelectric devices. To thermoelectric generators were competitive in the large and powerful business devices need to look for materials with significantly higher values of ZT [1].

The electrical resistance of pure Lead Telluride depends on the temperature and changes in metals, increases with increasing temperature. Absolute Seebeck coefficient for PbTe show a tendency to increase with increasing temperature. PbTe samples with maximum values of power factor $\alpha^2\sigma$ at room temperature (16 mW·cm$^{-1}$·K$^{-2}$), which decreases with temperature. The value of thermoelectric figure of merit (ZT) for PbTe has a maximum at 723 K, ZT = 0,48.

Established that doping Sb lead telluride leads to increase basic thermoelectric material characteristics. In particular, when the content of impurities 0,3 at.%. electrical conductivity is ≈ 700 (Ohm cm)$^{-1,}$ and thermoelectric coefficient ≈ 300 μV/K of solid solutions PbTe-$Sb_2Te_3$ containing 0,3 mol.% defined $\sigma \approx$ 350 (Ohm cm)$^{-1,}$ $\alpha \approx$ 350 μV / K [2].

1. Freik D.M., Galushchak M.O., Krynytsky O.S., Matkivsky O.M. New thermoelectric nanocomposite materials (review) // Physics and Chemistry of Solids 14 (2) (2013).
2. Freik D.M., Mudry S.I., Gorichok I.V., Dzumedzey R.O., Krynytsky O.S., Lyuba T.S. Charge carrier scattering mechanisms in thermoelectric PbTe: Sb // Ukrainian Journal of Physics 2014. - Vol. 59, № 7. - P.706-711.

# Pressure Influence on Transitions in Spin-Crossover Nanostructures

Gudyma Iu.V., Ivashko V.V.

*Chernivtsi National University, Chernivtsi, Ukraine*

A compressible model of spin-crossover nanostructure in framework of the Ising-like model with two order parameters and effect of elastic strain on interaction potential is presented [1]. By using this model can be effectively studied the influence of pressure on the spin transition. Magnetic ions occupy a simple regular cubic lattice with homogeneous and isotropic deformations. The Hamiltonian of the model is given by

$$H = -h\sum_i s_i - \sum_{\substack{i,j \\ i\neq j}} J_{ij} s_i s_j + \frac{1}{2}K\xi^2 - P\xi . \qquad (1)$$

Here $h = -(\Delta - k_B T \ln g)$ is generally the energy distance between the HS (High-Spin) and the LS (Low-Spin) states, where $\Delta$ is directly related to the strength of crystal field per site, $k_B T$ is the thermal energy, $g = g_H/g_L$ is the electro-vibrational degeneracy ratio between the HS and LS states. Variable $s_i$ is a fictitious classical spin which has two eigenvalues ±1, corresponding to the LS and HS states respectively, $J$ is the inter-ion interaction potential upon homogeneous elastic strain, $K$ is the bulk modulus of the lattice (the elastic constant). Variable $\xi = (a - a_0)/a_0$ indicates the change of the relative inter-ion distance, where $a_0$ is the average distance between neighboring spins at an equilibrium temperature $T_{eq}$ and an atmospheric pressure, $a$ is the average distance between neighboring spins at a temperature $T$, $P$ is the external uniform pressure.

On the basis of this model, the thermodynamic function (entropy) of the system was obtained:

$$S = k_B \ln[z(x)] + k_B(\ln g - x) < s > -(\partial K/\partial T)\xi^2 , \qquad (2)$$

where $z(x)=2\cosh(x)$, $x=(2zJ<s> + h)/k_B T$, $<s>=2n_H - 1$, $p=P/N$, $K=K/N$, $n_H$ and $\xi$ are two order parameters of the system, and $N$ - number of molecules.

The entropy had shown us the existence of two basic types of transitions that occurs in a framework of our model: continuous high–spin ↔ low–spin transitions over a broad temperature range; discontinuous high–spin ↔ low–spin transitions associated with a first-order phase transition at a definite temperature.

Also we have obtained a phase diagram witch gives more complete description of diffusionless processes occurring in the spincrossover nanostructure [1]. The results obtained show that the increase of the strain component leads to the forthcoming first-order phase transition. The kind of phase transition, in general, depends on the magnitude of inter-ion interaction.

1. Gudyma Iu., Ivashko V., Linares J. Diffusionless phase transition with two order parameters in spin-crossover solids // *Journ. of Appl. Phys*, **116(**17), (2014), 173509.

# Defective Subsystem and Modification of Crystals' Properties of Compounds $A^2B^6$

Hurhula H.Ya, Vintoniak T.P., Yaremiychuk O.

*Vasyl Stefanyk Precarpathian National University, Ivano-Frankivs, Ukraine*

Metal chalcogenides of the second subgroup of the periodic table are perspective materials in electronic engineering for making detectors for $\gamma$ - and x-rays, photo receiving and radiating structures of visible and infrared light spectrum. These materials are characterized by high quantum yield of photo-luminescence and cathode excitement. However, the largest quantum yield can be obtained only in homo-n-p-transition, which requires the ability to grow material of hole and electron conductivity type.

It is known that the basic electrical and photovoltaic properties of semiconductors are determined by their own defects and impurities, which are almost always present in the crystal. The concentrations of different types of defects depend on each other, and therefore, the development of the model of point defects that would enable, on one hand, to identify the relationships that exist between the concentrations of defects and on the other - to establish qualitative and quantitative dependency of the physical crystals' properties of compounds $A^2B^6$ on the concentration of defects.

In this work, the crystalquasichemical formulas of non-stoichiometric metal chalcogenides of the second subgroup of n- and p-type conductivity have been proposed provided the existence of the complex defect subsystem after the scheme of Schottky-Frenkel. On their basis, the concentration dependencies of the prevailing defects have been calculated, as well as major current carriers and Hall concentration which would depend on the degree of deviation from the stoichiometric disproportion of the charge state of point defects.

By using the obtained crystalquasichemical formulas one can determine not only the prevailing types of point defects, but also their concentration depending on chemical composition, in particular, the magnitude of deviation from stoichiometry ($\alpha$, $\beta$) and content of alloying elements (M, X) respectively. Based on quasi-chemical equations of the formation of point defects, the annealing processes of double temperature treatment of MX crystals have been described and the dominant defects have been determined. Crystalquasichemical formulas of the non-stoichiometric n- and p-MX (M – Zn, Cd; X – Te, Se, S) have been proposed provided the realization of the complex spectrum of point defects. Besides, the analysis of the principal models of point defects in ZnX crystals with the concomitant process of self alloying by p-MX and chacolgenide – n-MX has been performed when interacting with oxygen, and also the mechanisms of defect formation in solid solution on the basis of metal chalcogenides.

*This research is sponsored by NATO's Public Diplomacy Division in the framework of "Science for Peace" (NATO SPS 984536)).*

# The Structure of Resistant Surface Layer in High-Entropy Alloys of System $VCrMnFeCoNi_x$

Karpets M.V[1], Myslyvchenko O.M[2], Rokitska O.A[1],
Krapivka M.O[1], Marchenko S.V.[3]

[1]*Institute for Problems of Materials Science, NAS of Ukraine*
[2]*National Technical University os Ukraine "KPI", Kyiv,* Ukraine
[3]*Sumy State University (SumSU), Sumy, Ukraine*

In 2007 J.W.Yeh worked out the scientific fundamentals and proposed the formal criteria of material adequacy to new class of alloys, which were names as high-entropy alloys (HEA) [1]. According to these criteria such alloys which contain not less than 5 elements are referred to HEA, though the amount of every element mustn't exceed 35 at. % mustn't be less than 5 at. %. This class of alloys is new; because the processes of phase formation and the mechanism of mechanical characteristics are considerably differ from the similar processes in traditional alloys. The latter alloys are those where the main elements are Fe, Al, Cu and others, which defined the crystal lattice of the material. The goal of this work is to research the surface layers of friction zone of HEA of system $VCrMnFeCoNi_x$ (where x= 1; 1,5; 2 in molar correlation (in the text they will be named as $Ni_1$, $Ni_{1,5}$, $Ni_2$).

Table1. The results of X-ray diffraction analysis and mechanical characteristics of alloys of system $VCrMnFeCoNi_x$.

| Alloy | Phase compos. | | Lattice period, nm | Inside the friction zone | | Outside the friction zone | |
|---|---|---|---|---|---|---|---|
| | Struct. | Mass., | | H*, GPa | E**, GPa | H*, GPa | E**, GPa |
| Ni | σ | 68 | a = 0,8787<br>c = 0,4664 | 15±0,7 | 175±9 | 9,1±0,5 | 140±4,2 |
| | FCC | 32 | a = 0,3599 | | | | |
| $Ni_{1,5}$ | σ | 16 | a = 0,8841<br>c = 0,4603 | 6,5±0,3 | 160±8 | 5,4±0,3 | 134±4,1 |
| | FCC | 84 | a = 0,3625 | | | | |
| $Ni_2$ | FCC | 100 | a = 0,3603 | 5,4±0,3 | 148±7 | 3,6±0,2 | 131±3,9 |

* microhardness, ** Young modulus

These alloys gained by the method of argon-arc melting, some plates were cut from them to do the test on resistance for abrasive wear. The determination of wear resistance was done according to State Standard 23.208-79 (Material test method for wear resistance at friction on flexible fastened abrasive particles). An arithmetical mean loss of weight of the pieces was: $g_{Ni1}$=0,0204 g; $g_{Ni1,5}$=0,037 g; $g_{Ni2}$=0,0412 g, relative resistance was: $K_{Ni1}$= 3,03; $K_{Ni1,5}$= 1,69;

$K_{Ni2}$= 1,54 properly. This test showed, that alloy $Ni_1$ had the highest level of abrasive resistance.

The phase composition of researched alloys in initial condition is marked in table 1. In all investigated concentration interval of content changes of Ni the number of phases are changed from two (solid solution with structure FCC+ σ-phase of type CrFe) to one (solid solution with structure FCC). That is for the increasing of amount of Ni in system the amount of solid solution with structure FCC is also increased. The ratio of lattice spacing c/a, for σ-phases in formed HEA is in the interval 0,517-0,518, that is practically coincided with the correlation c/a (~0,517) for the double and triple σ-phases.

The morphology of surface layers of friction space was investigated with a help of Scanning Electron Microscopy and is shown on the picture 1.

The intensive nicks are formed in alloy $Ni_1$, oriented to the way of friction. it should be noted, that abrasive particles in pointed zones-lines are not matched. In alloy $Ni_2$ the considerable changes are caused on the friction surface. It has the flat surface with fine and chaotically distributed scratches.

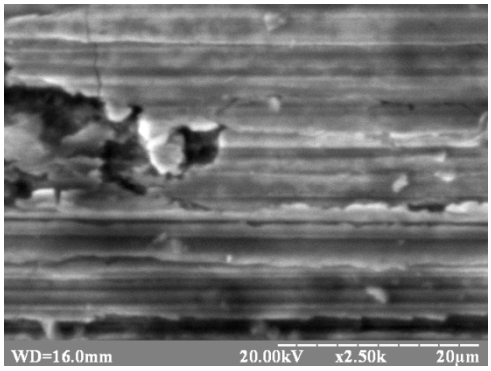


а

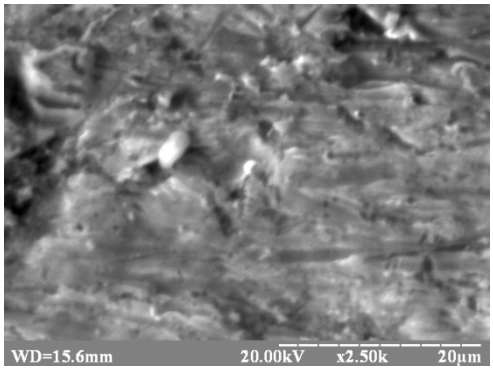


б

Picture1. – The Friction Surface in Secondary electrons (SEI) of alloys: a) $VCrMnFeCoNi_1$, × 2500; b) $VCrMnFeCoNi_2$, × 2500

The mechanical characteristics of materials in and out of friction zones are changed (table 1.). As the results of X-ray diffraction analysis showed, qualitative and quantitative changes of phase compound in the friction zone were not occurred. The increasing of micro hardness in the process of friction on the surface of the material is explained of formation of nanosrtuctural components. During hardness measuring by Rokvel method (HRC) the difference in and out of friction zone was not occurred, that indicated the small thickness of nanostructures layer.

1. Yeh J.W., Chen Y.L., Lin S.J. High-entropy alloys – a new era of exploitation // *Materials Science Forum*. 560, (2007), 1.

# The Radiation Stimulated Rise of Mobility of Current Carriers in the Cadmium Antimonid Monocrystals, Alloyed by Indium

Koval Yu.V.[1], Zakharchuk D.A.[1], Yashchynskyy L.V.[1], Fedosov S.A.[2]

[1]*The State Technical University of Lutsk, Lutsk, Ukraine*
[2]*Lesya Ukrainka East European National University, Lutsk, Ukraine*

An irradiation by parts of high energies is mighty and good by the control block method of management by the efficiency degree in solids. Research of defects of crystalline grate and establishment of tie between them and physical properties of crystals is of large scientific and practical interest and behaves toward the major problems of physics of solid and semiconductors.

Kinetic effects were explored in the given work in cadmium antimony monocrystals, alloyed by indium, before and after $\gamma$-irradiation. The conductivity and the Hall effect were measured, that settled to get both concentration of current carriers and their mobility. A sharp growth of mobility of majority carriers in the exposed to rays crystals is noticed. This fact we explain by presence of effect so called of "small doses". It is known, that probability of appearance of radiation defects in the mechanically tense regions crystal substantially higher, than for the untense regions. That is why at the small doses of irradiation of introduction of defects the place takes mainly in the locally tense fields of grate, that is close to atoms of alloying admixture (*In*). Entered in the irradiation crystals the acceptor centers partly neutralize a charge of ionic remains, placed in the grate knots.

That is, the growth of mobility of current transmitters look after in the given work arises up not on account of rise of perfection of crystals in case of their radiation treatment, and on account of decline of efficiency of dispersion of current transmitters on the admixture ionic remains during the partial neutralization of charge by the opposite on sign charge of defects. The got results and their interpretation conform to the known experimental data for the exposed to rays by the small doses crystals of silicon and to the germanium.

# Vibrational Spectra of Co-Doped Hexagonal ZnO

Kupchak I.M., Serpak N.F., Korbutyak D.V.

*V. Lashkarev Institute of Semiconductor Physics of National Academy of Sciences of Ukraine, Kiev, Ukraine*

Zinc oxide (ZnO), due to the large direct band gap (Eg ~ 3.3 eV) at RT, large exciton binding energy (Ex ~ 60 meV) and strong excitonic emission, is widely used as a material for filters and detectors of UV radiation [1]. Doping with transition metal atoms opens another field of ZnO QDs applications. Diluted magnetic semiconductor QDs are the interesting materials for spintronics. Particularly, they can serve as memory cells and even as the logic elements for data processing due to their ability to store both electric charge and spin.

Despite ZnO is already well-studied and widely used in technology, the nature of its magnetic properties, which appear due to transition metal doping, is still far from clear understanding.

One of the most informative methods for studying such structural disorders is the Raman light scattering. In particular, micro-Raman studies are applicable even in the case of nanocrystals, while the X-ray analysis does not always allow to identify their structure distinctly. In contrast to undoped ZnO samples**,** Raman spectra of ZnO:Co samples demonstrate additional bands between LO and TO phonon modes, the intensity of which increases with the Co atoms' concentration.

In this work, vibrational density of states of 12.5% cobalt doped bulk hexagonal ZnO has been studied by the density functional theory method using generalized gradient approximation (GGA). We have considered various mutual positions of cobalt atoms in the structure including cases of single atoms and their complexes, as well as the possibility of cluster formation. It has been shown, that cobalt introducing into ZnO leads to appearing of additional vibrational modes with their frequencies dependent on the relative positions of the cobalt atoms. The magnetic and vibrational properties have been studied also of highly Co-doped ZnO samples, which are characterized by a high possibility of the metal clusters formation.

It has been found that two cobalt atoms forming Co-O-Co chain lead to a redistribution of vibrational density of states, and its maximum shifts to the region between TO and LO modes of ZnO. In addition, the cobalt clustering also may lead to appearing of additional modes with frequencies between TO and LO modes frequencies of ZnO, which are associated with the vibrations of Co-O-Co chains.

1. Ü. Özgür, Y. I. Alivov, C. Liu, A. Teke, M. A. Reshchikov, S. Doğan, V. Avrutin, S. J. Cho, H. Morkǫ, A comprehensive review of ZnO materials and devices // *J. Appl. Phys,* **98**, (2005), 1.

# Fractal Approach to Non-Crystalline States

Mar'yan M.I., Yurkovych N.V.

*Uzhhorod National University, Uzhhorod, Ukraine*

Based on the analysis of literary sources for the study of non-crystalline materials and the transition to non-crystalline state of the possibility fractal approach to describe them. Shows a description of the fractal structure using the system dynamic equations, which takes into account the flow of negative entropy of the surrounding environment.

Found that the formation of fractal dissipative structures in non-crystalline solids associated with the creation of self-consistent fields of soft atomic configurations and thermal behavior of such structure-sensitive characteristics that meet the minimum energy dissipation for a given external parameters - velosity cooling and process modes receipt. It is shown that this fact makes it possible to determine the non-crystalline structure through the processes of self-organization.

The calculation of the temperature dependence and computer simulation of particle atoms in soft configurations, mean-square displacements depending on the cooling rate in case of non-crystalline materials of the system As-S(Se). The temperature change in the fraction of atoms in soft configurations, their relationship with fractal structure and fractal dimension. It is shown that the fractal dimension can be described by the relation fractal Cantor, reduced to three-dimensional case.

# First Empirical Investigations of The Thermodynamic Properties in II-VI Chalcogenide Crystals

Parashchuk T.O., Ivanyshyn I.

*Vasyl Stefanyk Precarpathion National University, Ivano-Frankivsk, Ukraine*

In this paper the cluster approaches for calculations of thermodynamic parameters of zinc chalcogenides have been proposed. Specifically there were determined formation enthalpy $\Delta H$, formation energy $\Delta E$, entropy $\Delta S$, Gibbs free energy $\Delta G$, heat capacity at constant volume $C_V$ and constant pressure $C_P$ of crystals. On the base of temperature dependences of Gibbs free energy for sphalerite and for wurtcite phases there were determined the transition temperatures between these phases. And on the base of temperature dependences of heat capacity at constant volume were determined the temperature dependences of Debye temperature $\theta_D$. The calculation was carried out within the cluster approximation with using of DFT-method with the valence basic set B3LYP. All calculations have been spending in quantum-chemical computer packet PCGamess (FireFly).

For the calculation of sphalerite we used two cluster models of zinc chalcogenides: clusters A and B. The model A includes a zinc atom which is surrounded by two ligands, and has the general formula $ZnC_2H_2X_4$. The general formula of the cluster B is $Zn_4C_6H_6X_{13}$, contains a Zinc atom which is surrounded by four chalcogen atoms, it can be corresponded to a real crystal, all these atoms are four-coordinated. We used six $HCX_2$-ligands, which had saturated the dangling bonds.

Wurtzite structure was studied by using three models: C, D and E. Cluster C (general formula $Zn_{15}X_{15}$) was the base for the calculation of the spatial and electronic structure and the thermochemical quantities. This model consists of 30 atoms and contains two pairs of four-coordinated, eight pairs of three-coordinated and five pairs of two-coordinated couples of atoms. Cluster D (the general formula $Zn_{11}X_{11}$) consists of 22 atoms. It contains one four-coordinated, six three-coordinated and four two-coordinated pairs of atoms. Cluster E of wurtzite modification (with the general formula $Zn_{10}X_{10}$) consists of 20 atoms. It contains one four-coordinated, four three-coordinated and five two-coordinated pairs of atoms.

*This research is sponsored by NATO's Public Diplomacy Division in the framework of "Science for Peace" (NATO.NUKR.SFPP 984536).*

# Anomalous Lattice Expansion of $Sm_{0.5}Pr_{0.5}FeO_3$ Derived From X-Ray Synchrotron Powder Diffraction Data

Pavlovska O.B., Vasylechko L.O., Ubizskii S.B.

*Lviv Polytechnic National University, Lviv, Ukraine*

Complex oxides with perovskite structure $R$FeO$_3$, where $R$ are rare earth metals, represent an important class of functional materials. The $R$FeO$_3$ compounds are used in thermoelectric devices and solid oxide fuel cells, as membranes for partial oxidation of methane and oxygen cleaning, as catalysts for CO oxidation and decomposition of $NO_x$, and as sensory materials. Complementary, the interest in the rare earth ferrites is stimulated by their interesting fundamental physical properties, such as spin-reorientation transitions at 80–200 K and the para- to antiferomagnetic transitions at 620–750 K. Just recently, $SmFeO_3$ has attracted considerable attention due to its reported multiferroic properties above room temperature.

Mixed samarium-praseodymium ferrite $Sm_{0.5}Pr_{0.5}FeO_3$ was synthesized by conventional solid state reaction technique in air at 1473 K for 20 h. Lattice parameters at room temperature are in good agreement with the end members of the $SmFeO_3$–$PrFeO_3$ system, thus proving a formation of the continuous solid solution $Sm_{1-x}Pr_xFeO_3$. Thermal behaviour of the structure has been studied *in situ* in the temperature range of 298–1173 K by means of high-resolution X-ray synchrotron powder diffraction technique. Corresponding experiments were performed at synchrotron laboratory *HASYLAB/DESY* (Hamburg, Germany).

As it was established, $Sm_{0.5}Pr_{0.5}FeO_3$ remains orthorhombic in the whole temperature range investigated. No structural phase transitions were detected. However, strongly anisotropic anomalous lattice expansion is observed. The lattice parameters exhibit an anomalous kink around 670 K that is obviously indicative for magnetoelastic coupling at the magnetic ordering temperature $T_N$, similar to recently reported for $SmFeO_3$ [1].

**Acknowledgments**: The work was supported in parts by the Ukrainian Ministry of Education and Sciences (project ”KMON”) and *ICDD* Grant-in-aid program.

[1] C.-Y. Kuo, Y. Drees, M.T. Fernández-Díaz, L. Zhao, L. Vasylechko *et al*. $k$=0 magnetic structure and absence of ferroelectricity in $SmFeO_3$. *Phys. Rev. Letters* 113 (2014) 217203.

# Abnormal Deformation Properties of some Single Crystals of Tetragonal System

Raransky M.D., Balazyuk V.N., Gun'ko M.M., Gorda O.M.

*Yu.Fedkovych Chernivtsi National University, Chernivtsi, Ukraine*

One of the most informative parameters in classical theory of elasticity is Poisson's ratio which by definition is equal to relation of transverse relative compression to longitudinal relative elongation with uniaxial crystal tension. For isotropic materials Poisson's ratio is a scalar quantity and lies in the range of $0 \le \mu \le 0{,}5$ [1]. The negative values of Poisson's ratios are mostly observed in certain crystallographic directions. Absolute auxeticity, i.e., $\mu < 0$ in all crystallographic directions is extremely rare, and, as a rule, occurs close to phase transition points [2].

To analyze the regularities of origination of the abnormal deformations, we have created a program that permits to calculate the negative values of Posson's ratios in all possible directions, to choose the negative values of μ and their respective directions and to build the indicating auxeticity surfaces of single crystals. By way of example, Fig. 1 shows the indicating surfaces of $(NH_4)H_2PO_4$, $KH_2PO_4$, $RbD_2AsO_4$ and $RbH_2AsO_4$ single crystals.

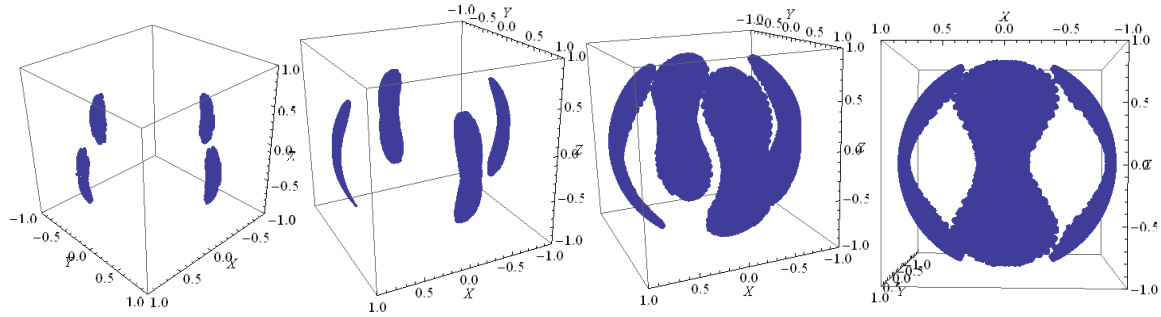

$(NH_4)H_2PO_4$ $KH_2PO_4$ $RbD_2AsO_4$ $RbH_2AsO_4$

Fig. 1. Indicating auxeticity surfaces.

These crystals are characterized by a spontaneous electric polarization (ferroelectrics), a spontaneous deformation (ferroelastics) and an extremely low ultrasonic wave propagation velocity (~330 m/s). It is established that for all crystals the negative values of Poisson's ratios are concentrated in crystallographic directions [100], [010], $[\bar{1}00]$ and $[0\bar{1}0]$ - axial auxeticity.

1. L.D.Landau, E.M.Lifshits, *Theory of Elasticity* (Moscow: Nauka, 1965), 203p.
2. D.A.Konyok, K.V.Wojciechowski, Yu.M.Pleskachevsky, and S.V.Shilko, Materials with Negative Poisson ratios (Review), *Mechanics of Compositional Materials and Structures* **10** (1), (2004), 35.

# Synthesis and Properties of High-Efficiency Thermoelectric Materials basis on the Systems Pb-Ag-Sb-Te

Gorichok I.V, Semko T.O., Mateik G.

*Vasyl Stefanyk Precarpathian National University, Ivano-Frankivsk, Ukraine*

In recent years, the issue of improving the efficiency of conversion of thermal energy into electrical energy gained special importance in connection with the realization exhaustion of fossil fuels and significant emissions into the atmosphere during combustion of harmful gases that pollute the environment, damage the ozone layer and cause global climate change .

The efficiency of thermoelectric materials is determined by the figure of merit (ZT):

$$ZT = \left( \frac{S^2 \sigma}{k} \right) T,$$

where S, σ, k, T Seebeck coefficient, electrical conductivity, thermal conductivity and absolute temperature, respectively. Modern TEG are based on materials with ZT≈1. Increase of this parameters complicated interconnectivity with values S, σ, k.

The abstract presents the results of research and X-ray measurements of thermoelectric parameters (Seebeck coefficient S, electrical conductivity σ and thermal conductivity k) materials based on Lead Telluride: PbTe, PbTe:Sb, PbTe-$Sb_2Te_3$, $Pb_{18}Ag_1Sb_1Te_{20}$, $Pb_{18}Ag_2Te_{20}$ and PbTe-$Ag_2Te$. Established that the highest values of thermoelectric figure of merit have PbTe: Sb (0.3 at.%) and system $Pb_{18}Ag_1Sb_1Te_{20}$, $Pb_{18}Ag_2Te_{20}$, in the first case due to a significant increase in the electrical conductivity of the material, and the other two - as an increase in the Seebeck coefficient and significant reduction in thermal conductivity compared to pure PbTe.

*This research is sponsored by NATO's Public Diplomacy Division in the framework of "Science for Peace" (NATO SPS 984536)).*

# Appearance of Electret Effect in The Cathodoluminescence of Intercalated GaSe

[1]Tovstyuk N.K., [2]SavchynV.P., [1]Krushelnytska T.D.,
[2]Demkiv L.S., [3]Mykytyuk O.Yu.

*[1]National University "Lvivska Politechnika", L'viv, Ukraine,*
*[2]Ivan Franko National University of L'viv, L'viv, Ukraine,*
*[3]Bukovinian State Medical University, Chernivtsi, Ukraine*

Intercalation by foreign atoms (guests) of different nature allows to modify significantly the physical properties of the semiconducting compounds and to use them as sensitive materials of microelectronics. Layered GaSe crystals intercalated by $NaNO_3$ or oligomer possessing the different dipole moments, can be successfully used in optoelectronics, particularly in the structures with high dielectric screening.

In this contribution we show the experimental results for cathodoluminescence (CL) spectra of GaSe crystals intercalated by $NaNO_3$ and oligomer, received at low temperatures. The CL spectra were measured at 80K with a set-up based on a DMR-4A monochromator and a PMT FEU-106 under pulsed e-beam excitations (duration of pulse of 2μs at frequency of 30-3 Hz) with an energy of electrons of 9keV and a beam current of 100 μA. The CL spectrum of GaSe intercalated by $NaNO_3$ (oligomer ) presents the luminescence shifted with respect to the pure GaSe on 0.1eV (0.08eV ) and with half-width 0.08eV(0.1eV).

Appearance of additional maxima shifted by 0.1eV for GaSe<$NaNO_3$> and 0.08eV for GaSe<oligomer> we explained within the framework of the model of virtual guest-crystal with additional band of guest states [1]. Density of electron states of pure layer crystal and guest virtual crystal is described by Fivaz dispersion law. We considered: i) the anisotropy of electron host-guest overlapping; ii) nonmonotonic change of lattice constant along the main crystallographic axis *C* depending on guest concentration. In the case when electret effect appears we consider positioning of the intercalant (guest) in two different potential wells $T_1$ and $T_2$ of different depth in he unit cell; the concentrations $p_1$ and $p_2$ are different. Our calculations showe that if $p_1=0.98$ and $p_2$ changes from 0.2 to 0.7 the width of additional gap that appears due to the itercalation changes in a monotonic way. The shift of the additional gap depends strongly on the value of the intercalant ground state energy ($\varepsilon_1=\varepsilon_2$) and on its position (below or above the bottom of the conduction band). It is shown that in the case of ordered electret like distribution of intercalant in the van der Waals gaps the shift of peaks of electron density of states can be explained by Keldysh-Frantz effect.

1. Tovstyuk N.K. Band structure of GaSe with guest components of different nature. Visnyk of Ivan Franko LNU. Physics Series - 2013.- v.48 . - P.109-119.

# Cluster Models and *ab initio* Calculations of Thermodynamic Parameters of Lead Chalcogenides

Volochanska B.P.

*Vasyl Stefanyk Precarpathian National University, Ivano-Frankivsk, Ukraine*

Lead telluride can be used in semiconductor optoelectronics for deep infrared thermal photovoltaics as materials that works in 300-950 K temperature range. PbX (X = Te, Se, S) can be used as the components of infrared detectors and emitters of infrared lasers, photodetectors, solar cells, thermoelectric devices, field effect transistors and as telecommunication appliances. The effective using of this materials both in model studies and practical applications caused by set of unique properties of lead telluride, in particular, bocouse the small band gap, high carrier mobility and high dielectric constant.

The first step for the quantum-chemical calculation of the cluster properties was the determination of the lowest energy configuration. All calculations started with SCF (Self-Consistent Field) convergence and geometry optimization; after obtaining a stable minimum, the frequencies were calculated. The calculations of the lowest energy structure were carried out using Hartry-Fock method on the basis of the Stevens-Basch-Krauss-Jasien-Cundari (SBKJC) parameterization. In this basic set only the valence electrons which are directly involved in chemical bonding are considered.

The calculation of thermodynamic parameters have been spent using the software package Firefly (PCGamess) within the density functional theory method (DFT), using hybrid valence electrons basic set B3LYP [1]. Visualization of spatial structures was carried out using Chemcraft.

Analytical expressions for temperature dependence of the energy ΔE, enthalpy ΔH, Gibbs free energy ΔG and entropy ΔS of PbTe crystals for the temperature range from 80 to 1000 K are represented by the following expressions respectively:

$$\Delta \mathrm{E(T)} = 0,0271 \cdot \mathrm{T} + 64,494, \quad (1)$$

$$\Delta \mathrm{H}(T) = 0,0243 \cdot T + 64,494, \quad (2)$$

$$\Delta \mathrm{G(T)} = 0,0241 \cdot \mathrm{T} + 64,54, \quad (3)$$

$$\Delta \mathrm{S(T)} = 0,0271 \cdot \ln \mathrm{T} - 54,11, \quad (4)$$

Obtained by us analytical expressions of temperature dependencies of heat capacity at constant volume $C_v$ and heat capacity at constant pressure $C_P$ are shown by the following equations:

$$C_V = 50,7 + 6,6 \cdot 10^{-3} T - 0,044 \cdot 10^5 T^{-2}, \quad (5)$$

$$C_P = 45,1 + 6,6 \cdot 10^{-3} T - 0,044 \cdot 10^5 T^{-2}. \quad (6)$$

*This research is sponsored by NATO's Public Diplomacy Division in the framework of "Science for Peace" (NATO SPS 984536)).*

1. S. Pashinkin, M. S. Michailova, A. S. Malkova, V. A. Fedorov, Inorganic Materials, 45 (11), (2009), 1226.

# New Areas of Optimization of Thermoelectric Parameters of Lead Telluride and Germanium Telluride Based Solid Solutions

Yurchyshyn L.D.

*Vasyl Stefanyk Precarpathian National University, Ivano-Frankivsk, Ukraine*

IV-VI semiconductor compounds and their solid solutions are basic materials for thermoelectric energy converters that operate in the medium temperature area [1-2]. Point defects and their complexes largely responsible for the physical and chemical properties of the material. At present there is no consensus about the nature of these defects and their charge states. Lead telluride hasn-type conductivity in metal excess presence relative to stehiometry and p-type conductivity in chalcogen excess presence and germanium telluride has only hole conductivity [1].

The basis of the method of crystalquasichemical analysis is superposition of doping cluster formed on the basis of lead telluride antistructure, and the crystal formula of stoichiometric compound. Crystalquasichemical model of nonstoichiometric PbTe with a complex range of Frenkel defects ($V_{Pb}^{2-}$, $V_{Pb}^{-}$, $V_{Te}^{2+}$, $Pb_i^{2+}$, $Te_i^{0}$), and *p*-GeTe ($V_{Ge}^{2-}$,$V_{Ge}^{4-}$), and based on them ternary systems have been offered. Dependences of concentration of point defects, electrons and holes, and the Hall concentration of current carriers on the size and nature of deviation from stoichiometry of *n*- and *p*-PbTe and solid solution composition have been calculated on the basis of the first developed crystalquasichemical formulas and equations of full electroneutrality. Thus hole conduction of lead telluride relates to a vacancy in cation sublattices $V_{Pb}^{2-}$, $V_{Pb}^{-}$, and electronic – in anion sublattices $V_{Te}^{2+}$, of lead telluride crystal structure.

The influence of chemical composition and the deviation from stoichiometry on the side of tellurium on the ratio between two- ($V_M^{2-}$) and fourfold charged ($V_M^{4-}$) cationic vacancies (dominant defects in this case) and thermoelectric properties of PbTe-SnTe solid solution have been specified.

A similar analysis has been done for germanium telluride and germanium telluride based solid solutions. Thus that the main areas of optimization of thermoelectric parameters of PbTe, GeTe based materials are decrease of the thermal conductivity (PbTe-SnTe, PbTe-$Sb_2Te_3$), and increase of electric conduction and activity of point defects (PbTe-SnTe, PbTe-GeTe), and the incorporation of noncentral dopant ions in solid solutions (Pb-Te-Se-S).

1. Abrykosov N.Kh., Shelimova L.E.: Semiconductors Materials on the basis of combinations of AIVBVI, M. Science, 1975, 196 p.
2. Ioffe A.F.: Semiconductor thermoelements. M.-H. Publishing House of USSR Academy of Sciences, 1960, 346 p.

# Superconductivity of Surface Layers of PbTe Crystals Grown From Melt by a Bridgman Technique

[1]Zayachuk D.M., [2]Mikityuk V.I., [2]Shlemkevych V.V., [3]Kaczorowski D.

[1]*Lviv Polytechnic National University, Lviv, Ukraine*
[2]*Yuri Fedkovich Chernivtsy National University, Chernivtsy, Ukraine*
[3]*Institute of Low Temperature and Structure Research, Polish Academy of Sciences, Wroclaw, Poland*

Superconductivity of surface layers of *PbTe* crystals was firstly detected in the study of ingots grown from the melt with low initial concentration of the doping impurity of *Eu*, which is entirely pushed out onto the lateral surface of the ingot during the process of growth of the doped crystal [1]. Recently the same effect was detected in the study of surface layers of undoped *PbTe* crystals too [2]. It was suggested that the observed superconductivity is caused by a mixture of the superconducting inclusions of *Pb* as type-I superconductor and the normal phase. Here we present the results of in-depth study of this phenomenon by method of magnetic measurements in undoped *PbTe* crystals, grown from melt by a Bridgman technique. High purity (99.9999 %) *Pb* and *Te* were used for the growth of crystals, which were afterwards additionally purified. The crystals had hole conductivity with typical for *PbTe* hole concentration of the order of $3 \cdot 10^{18}$ $cm^{-3}$.

The magnetization and magnetic susceptibility of the surface layers were investigated. Since only powder samples could have been manufactured out of surface layers of crystalline ingots, powder samples were used for the study. Particular reference was done on extra-low temperature range up to 1.7 K and low magnetic fields. Meissner effect was used as an indicator of the appearance of superconductivity. As grown and annealed in the atmosphere of oxygen samples were studied.

It is shown that the probability of occurrence of surface superconductivity of *PbTe* crystals correlates with their total magnetic susceptibility. The sample is weak diamagnetic or paramagnetic at high temperature the probability of its superconducting state at low temperature is higher. Superconductivity of *PbTe* surface layers has characteristic features of non-uniform type-II superconductor, such as temperature hysteresis of magnetic susceptibility upon transition to superconducting state, field hysteresis of magnetization and preservation of features of intermediate state in magnetic fields exceeding critical field of type-I superconductor *Pb* at $T \rightarrow 0$ K. Annealing in the atmosphere of oxygen destroys the superconducting state of the samples.

1. Zayachuk D.M., Mikityuk V.I., Shlemkevych V.V., Kaczorowski D., and Ilyina O.S. *Physica C* **483,** (2012), 1.
2. Zayachuk D.M., Ilyina O.S., Mikityuk V.I., Shlemkevych V.V., and Kaczorowski D. *Solid State Sciences*, **38,** (2014), 30.

# Dosimetry Application of the $YAlO_3$:Mn Based Materials

[1,2]Zhydachevskii Ya., [3]Luchechko A., [1]Martynyuk N., [4]Morgun A., [1]Ubizskii S., [4]Chumak V., [2]Berkowski M., [2,5] Suchocki A.

[1] *Lviv Polytechnic National University, Lviv, Ukraine*
[2] *Institute of Physics, Polish Academy of Sciences, Warsaw, Poland*
[3] *Ivan Franko National University of Lviv, Lviv, Ukraine*
[4] *National Research Centre for Radiation Medicine, Kyiv, Ukraine*
[5] *Institute of Physics, University of Bydgoszcz, Bydgoszcz, Poland*

Application potential of $Mn^{2+}$-doped $YAlO_3$ (YAP) for thermoluminescent (TL) dosimetry of ionizing radiation has been shown previously [1-2]. For this purpose, one of two types of detectors can be used. The first type detectors have green emission near 530 nm in the main TL peak at 200°C [1], whereas the second type detectors have orange emission around 640 nm in the TL peak near 350°C [2]. The first type detectors have strong daylight effect on fading and optical stimulation by blue light can be used for their readout. On the other hand, the second type detectors with TL peak near 350°C have no daylight effect on fading.

High chemical and time stability, radiation damage resistance and high sensitivity to ionizing radiation (up to 40 relative to TLD-100), extremely wide range of linearity (from few μGy up to few kGy) and the optical emission in visible are the most attractive properties of the material. The material is a good candidate for low, middle- and partially high-dose dosimetry of ionizing radiation, when tissue equivalence is not required. The material possesses relatively high efficient atomic number ($Z_{eff}$ = 31.2), therefore the radiation energy response should be taken into account especially for the radiation energies below 0.5 MeV.

The present work demonstrates main features and dosimetric properties of the $YAlO_3$:Mn based detectors in the form of single crystalline and ceramic materials, including the calculated and experimental energy response of the material in the range from 0.005 to 10 MeV.

**Acknowledgements:** The work was partially supported by the EU within the European Regional Development Fund through the Innovative Economy grant (POIG.01.01.02-00-108/09) and by NATO within the Science for Peace and Security Programme (Project NUKR.SFPP 984649).

1. Ya. Zhydachevskii, A. Suchocki, M. Berkowski, P. Bilski, S. Warchol, *Radiat. Meas.* 45 (2010) 516–518.
2. Ya. Zhydachevskii, M. Berkowski, S. Warchol, A. Suchocki, *Radiat. Meas.* 46 (2011) 494–497.

## СЕКЦІЯ 5 (стендові доповіді)
## ФУНКЦІОНАЛЬНІ КРИСТАЛІЧНІ МАТЕРІАЛИ: РІСТ, ФІЗИЧНІ ВЛАСТИВОСТІ, ВИКОРИСТАННЯ

12-15 травня 2015 р.

## SESSION 5 (poster)
## CRYSTAL'S GROWTH AND THEIR PHYSICAL PROPERTIES

May, 12-15, 2015

# Crystallization and Phase Transition of Solid Solutions in the $Cu_8GeX_6$-$Ag_8GeX_6$ (X-S, Se) Systems

Alverdiyev I.J. [1], Abbasova V.A. [1], Gahramanova A.S. [2], Yusibov Y.A. [1], Babanly M.B. [2]

[1] *Ganja State University, Ganja, Azerbaijan*
[2] *Institute of Catalysis and Inorganic Chemistry ANAS, Baku*

Copper and silver chalcogenides with germanium are particular interest because possess ionic conductivity and are perspective materials for photoelectrodes, electrochemical converters of solar energy, ionselective sensors, photoelectro-chemical imaging etc.

Ternary compounds $Ag^I_8GeX_6$ ($A^I$-Cu, Ag, Sn; XS, Se) have phase transition. Their high-temperature modifications are isostructural and crystallize in cubic (*F*-43*m*) system, however low-temperature ones crystallize in orthorombic or hexagonal system. This allows us to expect the formation of wide series of solid solutions in $Cu_8GeS_6$-$Ag_8GeS_6$ (A) и $Cu_8GeSe_6$-$Ag_8GeSe_6$ (B) systems.

This work is devoted to investigation of phase relations in the systems (A) and (B) and some properties of solid solutions.

Starting compounds were synthesized from high-purity elements (at least 99.999 wt.% purity) in sealed silica ampoules under vacuum ($10^{-2}$Pa). Synthesis was carried out in a two-zone furnace. Samples of the systems (A) and (B) were prepared by melting of the pre-synthesized compounds in sealed silica ampoules under vacuum followed by homogenizing annealing at 900 K for about 500 h.

DTA, XRD and EMF measurements were employed to analyze the samples. The XRD data were collected using a Bruker D8 ADVANCE diffractometer (Cu-$K_\alpha$ radiation). DTA of the equilibrated alloys was carried out using a NETZSCH 404 F1 Pegasus system. For the EMF measurements, the reversible cells of following type were assembled:

(-) Cu (solid) | $Cu_4RbCl_3I_2$ (solid) | (Cu in alloys) (solid) (+) (1)

EMF was measured by the compensation method in the temperature range of 295–380 K with the accuracy of ±0.1 mV, using the high-resistance universal B7-34A digital voltmeter.

Based on experimental data the T-x diagrams, concentration dependences of crystal lattice parameters, microhardness and EMF measurements are constructed.

It was shown that both systems are characterized by continuous series of solid solutions between high temperature modifications and limited solid solutions based on their low-temperature ones. Formation of solid solutions decreases the temperature of polymorphic transitions of compounds down to room and low.

# Electroluminescence of Powder ZnS:Cu Obtained by the Self-Propagation High-Temperature Synthesis

Bacherikov Yu.Yu.[1], Zhuk A.G.[1], Okhrimenko O.B. [1], Kozytskyi S.V.[2], Kardashev D.L.[2]

[1]*V. Lashkaryov Institute of Semiconduktor Physics, National Academy of Sciens of Ukraine, Kyiv,Ukraine*

[2]*Odessa National Maritime Academy, Odessa, Ukraine*

The self-propagation high-temperature synthesis method (SHS) is low expenses technology, therefore, perspective for obtained phosphors on the basis ZnS. As it has been defined in [1], for recombination of the radiation in semiconductors, except the centres of recombination, are necessary free electrons and holes and heterojunction between different phases. In zinc sulfide electroluminescence (EL) samples doped copper such phase is copper sulphide, therefore excitation process of EL it is set of processes of injection and multiplication of carriers of a charge in heterojunction ZnS–$Cu_{2-x}S$.

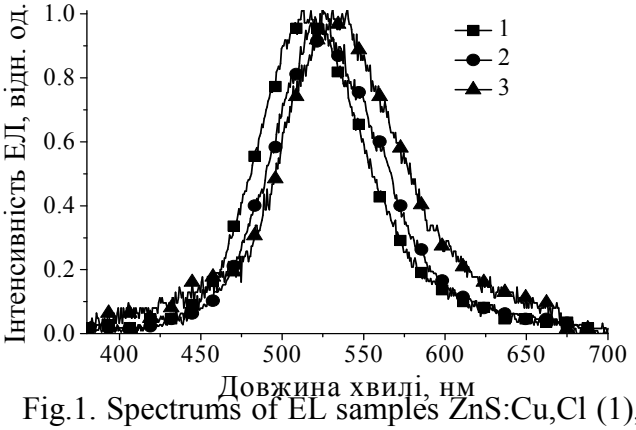


Fig.1. Spectrums of EL samples ZnS:Cu,Cl (1), ZnS:Cu,Ga (2) and ZnS:Cu,Ga (3) annealing at $400^0$C.

The EL spectra of powders synthesized by method SHS are presented in Fig.1.The EL spectra look like wide band in the blue-green spectral range with maxima at $\lambda_{max}$~515 nm, $\lambda_{max}$~525 nm, $\lambda_{max}$~535 nm according to curves 1, 2 and 3. Thus, gallium introduction leads to increase intensity of radiation of dark blue photoluminescence (PL) strip and shift in the long-wave part of spectrum. Additional annealing ZnS:Cu, Ga has led to the further increase intensity of a dark - blue strip and shift of a green strip to the long-wave part of EL spectra. Impurity distribution, ratio of phases, etc., is a consequence of nonequilibrium conditions of obtains of a material in some minutes at change of temperature from $300^0$ K to 2500-$3000^0$ K for this time. Annealing after synthesis leads to more uniform distribution of an impurity of copper in the volume of material and promotes more active embedding of Cu in lattice knots. It is promoted by presence co-activator Ga. Influence of Ga on PL as co-activator [2] is connected with necessity of indemnification of a charge of internal defects of a material that promotes copper embedding in knots sublattice zinc or to filling of vacancies of Zn. It leads to increase in the contribution of a green strip in luminescence. Occurrence of a dark-blue strip in a spectrum PL at introduction Ga (Fig.1, curve 2-3) it is connected, obviously, with formation of the centres of close DA-pair $Cu_i$-$Cu_{Zn}$.

1. Samelson H. Fluorescence of cubic ZnS:Cl crystals. / H. Samelson, A. Lempicki // Phys. Rev. – 1962. - V.125. №.3. - P. 901-909.

2. Морозова Н.К. Сульфид цинка. Получение и оптические свойства/ Н.К. Морозова, В.А. Кузнецов. – М.: Наука, 1987. – 200 с.

# Graphene-based Photonic Crystal: Ab-initio Calculation

Balabai R.M., Gritsulia D.Yu., Zdeshchyts A.V.

*Kryvyi Rih National University, Kryvyi Rih, Ukraine*

Photonic crystals are one of the modern, rapidly developing areas in solid state physics. Photonic crystals have a strictly ordered arrangement forming structural elements in one, two or three dimensions. Forming elements are generally considered monodisperse in geometric and identical in the dielectric parameters [1]. Photonic crystals with dielectric, metal or semiconductor constituent elements have different photonic band and transmittance spectrum. Attenuation of electromagnetic waves is also different in all these photonic crystals.

In these computing experiments, we consider periodically arranged stacks that form a two-dimensional photonic crystal. Stacks consist from the graphene planes, which separated by an insulator ($SiO_2$) (fig.1). We attempt to study the influence of the geometric parameters of stacks on the band gap, density of states, dielectric function. Electron response of solids to the impact of the electromagnetic field closely related to the structure of the energy bands. We calculated the electronic spectrum of the model atomic systems, the spatial distributions of the valence electrons density (fig.1), the distributions of the Coulomb potential and the static dielectric function using its own software complex [2].

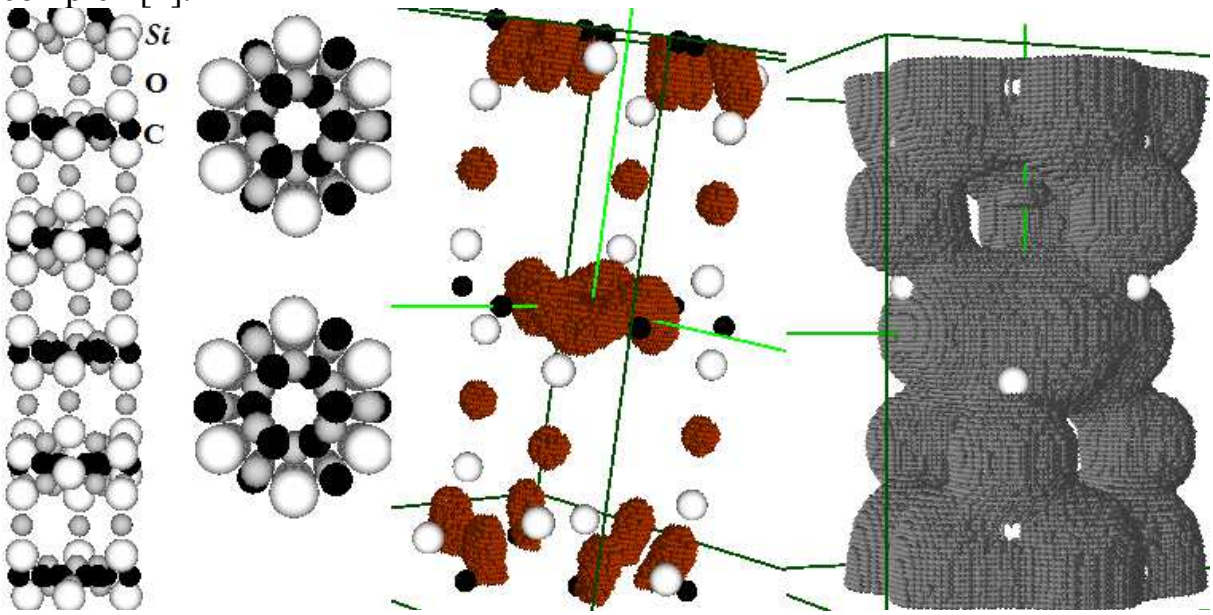


Fig.1. The model of photonic crystal that includes the periodically arranged stacks consisting the graphene planes and the $SiO_2$ slab with the electron density.

1. Yablonovitch E. Inhibited Spontaneous Emission in Solid-State Physics and Electronics // Phys. Rev. Lett . – 1987. – V.58. – P.2059-2062.

2. Balabai R.M. Electronic properties of functionalized graphene nanoribbons // Ukr. J. Phys. – 2013. – V. 58, № 4. – P.389-397.

# Photonic Crystal with Electrical Properties: Ab-initio Calculation

Balabai R.M., Gritsulia D.Yu., Zdeshchyts A.V.

*Kryvyi Rih National University, Kryvyi Rih, Ukraine*

Photonic crystals are materials that are able to control the light, their unique properties inherent in orderly arranged structural elements of the crystal. Due to ordering of elements-lenses photonic crystals are called crystals.

University of Illinois researchers discovered a way to change the three-dimensional structure of a well-established semiconductor material to enable new optical properties while maintaining its very attractive electrical properties [1]. They epitaxy grew the GaAs crystal through the complex template.

In these computing experiments, we investigated the static dielectric function of two-dimensional (2-D) GaAs-based photonic crystal using its own software complex [2]. Our model photonic crystal includes the porous GaAs wire array (fig.1). In this structure, the dielectric constant is periodic in one plane (usually defined as the *xy* plane) and extends infinitely in the third direction (*z* direction). Electron response of solids to the impact of the electromagnetic field closely related to the structure of the energy bands. That is why we calculated the electronic spectrum of the model atomic systems, the spatial distributions of the valence electrons density and crossings of these spatial distributions, the distributions of the Coulomb potential and the static dielectric function.

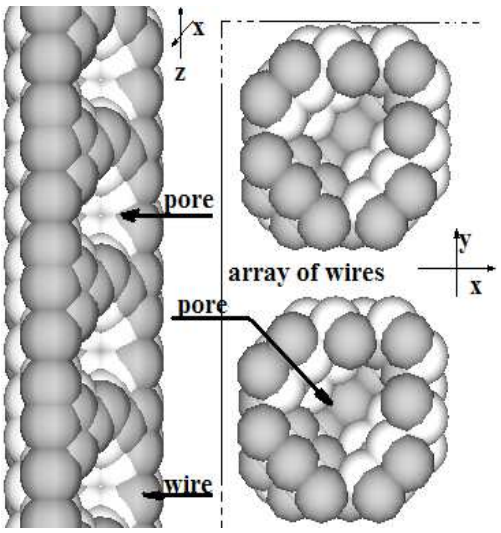


Fig.1. The model of photonic crystal, one includes the porous GaAs wire array.

1. Nelson E.C. at all. Epitaxial growth of three-dimensionally architectured optoelectronic devices // Nature Materials. – 2011. – V.**10**. – P.676-681.

2. Balabai R.M. Electronic properties of functionalized graphene nanoribbons // Ukr. J. Phys. – 2013. – V. 58, № 4. – P.389-397.

# Formation of Electro- and Photoelectret States in $CdI_2$ Crystals with $PbI_2$ Nanoinclusions

Bolesta I.M.[1], Galchynsky O.V.[2], Gloskovska N.V.[3], Yarytska L.I.[4]

[1] *Ivan Franko Lviv National University, Lviv, Ukraine*
[2] *Lviv Medical Institute, Lviv, Ukraine*
[3] *Bogolyubov Institute for Theoretical Physics, Kyiv, Ukraine*
[4] *Lviv State University of Vital Activity Safety, Lviv, Ukraine*

Layered structure of lead and cadmium iodide crystals is specified by the coexistence of different types of chemical bonding in them: ionic-covalent within the structural layeres and interlayer van der Waals. At low temperatures these crystals can be used as ionizing-radiation detectors in the nanosecond range and at temperatures higher than 150 K they can form a medium for information recording. Study of the electret properties is of scientific interest as the method to investigate structural defects of the photoelectrets.

To obtain electroelectret state, an electric field was applied to the sample at room temperature (without irradiation). After 10-minute interval the temperature in the cryostat was reduced to 80 K. Short-circuited sample was heated at a constant rate of 0.06 deg/sec. Thermally stimulated depolarization current was registered as a function of temperature.

Photoelectret state in the crystals was produced after their exposure to light at the intrinsic absorption edge of $CdI_2$ (3.5 eB) at 80 K. Energy distribution functions of populated localized states were calculated on the base of thermally stimulated depolarization curves of electro- and photoelectret states.

Electroelectret state is generated mainly by the trapping levels with the depth 0.3-0.56 eV (distribution function peak is located at 0.44 eV). This is due to the dipole polarization of $PbI_2$ molecules that compose monolayers of nanoinclusions [1].

Photoelectret state of the crystals, in addition to the dipole polarization, typical for electroelectert state, contains the trapping centers stipulated by the point defects (at 0.05, 0.17 and 0.36 eV) and the deepest trapping centers near 0.56 eV. The latter are thermally ionized at the temperatures 300-320 K and possess specific spectral sensitivity area near 3.1 eV [2]. This allows us to attribute them to the linear defects of $CdI_2$ structure with $PbI_2$ nanocrystals localized in the vicinity.

1. Galchynsky O.V., Gloskovskaya N.V. and Yarytska L.I. Deep acceptor trapping centers in $CdI_2$-$PbI_2$ crystal system // Functional materials. – 2014.- V.**21**, №3. - P.243-246.

2. Gal'chinskii A.V., Gloskovskaya N.V. and Yaritskaya L.I. Carrier trapping and delocalization in $PbI_2$-containing $CdI_2$ crystals // Inorganic Materials.- 2012. - V.**48**, №4. - P.423-427.

# Structure and Channels of Cationic Conduction of Ag8SnSe6 Argyrodite

Chekaylo M.V. [1], Ukrainets V.O. [1], Il'chuk G.A. [1], Akselrud L.G.[2], Ukrainets N.A. [1], Semkiv I.V. [1]

[1]*Department of Physics, Lviv Polytechnic National University, Lviv, Ukraine*
[2]*Ivan Franko National University of Lviv, Lviv, Ukraine*

The solid state materials with high ionic (superionic) and mixed electronic-ionic conductivity (solid electrolytes) belong to prospective materials of the near future [1]. Crystalls of $Ag_8SnSe_6$ argyrodite, which we had grown by means of pseudosublimation method, served as the object of X-ray diffraction (XRD). The structure of the low-temperature β′-phase (t = 20÷83ºC, space group $Pmn2_1$) and the high-temperature γ-phase (t = 83÷140ºC, space group $F\bar{4}3m$) of $Ag_8SnSe_6$ were investigated by means of method of temperature XRD, and with the use of Frank-Kasper (FK) polyhedra modeling of their space structures has been carried out. Since it is ionic conduction that is characteristic of argyrodite type structures, the concept of partial occupation of crystallographic positions of Ag was used to describe the positions of Ag atoms in the structural model.

The refinement of the structure was carried out with the use WinCSD (Version 4.14) packet of software [2]. In the elementary cell of β′-$Ag_8SnSe_6$ argyrodite, there are 7 positions of Ag atoms, 4 of them are completely filled, and 3 are partially filled. The completely filled positions of Ag1 and Ag3 atoms in $Ag_8SnSe_6$ structure have thetraedric surrounding of Se atoms, and the completely filled positions of Ag2 and Ag4 atoms have trigonal coordination of Se atoms. The partially occupyed (Occ) positions of Ag in the structure β′-$Ag_8SnSe_6$ are situated in tetrahedric voids, which are formed by Se atoms. The Ag atoms with partially occupied positions (Ag5 (Occ = 0.921), Ag6 (Occ = 0.047), Ag7 (Occ = 0.102)), which form potential channels of conduction.

It is shown that the structure of the high-temperature γ-phase of $Ag_8SnSe_6$ can be represented with help of FK polyhedra. In the tetrahedral voids of pyramids and bi-pyramids of these FK polyhedra, there are three partially filled positions of Ag atoms: Ag1 (Occ = 0.3243), Ag2 (Occ = 0.301), Ag3 (Occ = 0.068). The structural elements (tetrahedra and triangular bi-pyramides) of γ-phase of $Ag_8SnSe_6$, being joint by common faces, form continuous channels of conduction. The connection of such channels between each other by common tetrahedra lead to the existence of 3D network of ionic conduction.

1. International Technology Roadmap for Semiconductors (ITRS). http://www.itrs.net/home.html. 2012.
2. L. Akselrud, Yu. Grin. WinCSD: software package for crystallographic calculations (Version 4.14) // J. Appl. Crystallogr.– 2014.– P. 47.

# Nanoindentation Studies of $LiKB_4O_7$ Single Crystals

Chobal I. [1, 2], Kováč F. [2], Petryshynets I. [2], Adamiv V. [3], Burak Ya. [3], Chobal O. [1], Rizak V. [1]

[1] *Uzhhorod National University,Uzhhorod, Ukraine*
[2] *Institute of Materials Research, Košice, Slovakia*
[3] *Institute of Physical Optics named after O.G. Vlokh, Lviv, Ukraine*

The $LiKB_4O_7$ single crystal is new promising material for application in non-linear optical and acousto-optic devices. Mechanical properties of $LiKB_4O_7$, however, are little investigated, although they are obviously important for all kinds of device application. The present work is devoted to experimental studies of mechanical properties of the $LiKB_4O_7$ single crystals in [100], [010] and [001] crystallographic directions by means of nanoindentation.

The indentation tests were performed on „Nanoindenter G 200“, using a pyramidal diamond Berkovich indenter tip. The procedure is to apply load to indenter and record the depth of penetration. This is done on loading and unloading. The samples were measured with a maximum force of 100, 300 and 500 mN. The calculation was done according to the standard ISO 14577.

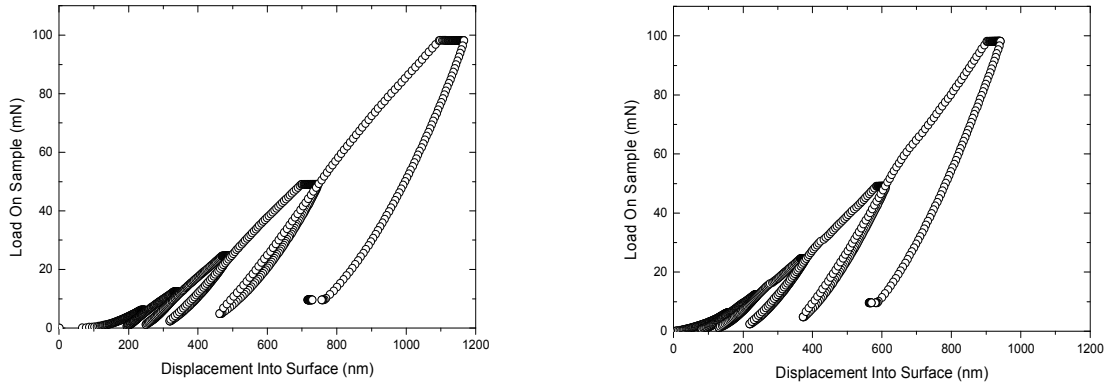


(*a*) (*b*)

Fig. 1. Experimental load-displacement curves for (100) plane indentation (*a*) and (010) plane (*b*) of $LiKB_4O_7$ single crystal

From the resulting load-displacement curves (Fig. 1), the Young's modulus and hardness of the $LiKB_4O_7$ single crystals in all three directions have been determined. The orientation dependences of the Young's modulus are correlated with the available results of acoustic measurements of $LiKB_4O_7$ crystals.

**ACKNOWLEDGEMENT**

I. Chobal is grateful to the International Visegrad Fund for the support of her research at Institute of Materials Research of SAS.

# Spectroscopic Characteristics of $Er^{3+}$ Ions in Glassy $Li_2B_4O_7$

Danyliuk P.S.[1], Rizak V.M.[1], Krasylynec V.M.[2], Birov M.M.[2], Chychura I.I.[2], Turok I.I.[2], Puga P.P.[2]

[1] *Uzhhorod National University, Uzhhorod, Ukraine*
[2] *Institute of Electron Physics, National Academy of Sciences of Ukraine, Uzhhorod, Ukraine*

The X-ray luminescence (XRL) spectra for different concentrations of $Er_2O_3$ in the glassy lithium tetraborate have been studied in the range of 200–800 nm. The spectra were excited using a BSV-21 X-ray tube with cobalt anticathode at 30 kV voltage and 15 mA current, and studied at room temperature using an automated complex based on an MDR-23 monochromator. As a detector, we used an FEU-106 photomultiplier. The experimental data at the FEU exit were recorded using a computer program controlling the necessary number of photon counts in each point of the studied spectral range and the spectral scan step with subsequent result processing.

The analysis of obtained dependencies $I_{XRL} = f(\lambda)$ shows that increasing $Er_2O_3$ concentration within the range of 0.0005–0.015 has no significant effect on XRL spectrum structure or the intensity of emission bands in the whole studied range. At dopant concentration of 0.01 mol. % the effect of concentration quenching is observed, caused by change of charge compensation, occurrence of vacancies of interstitial ions, and local symmetry change of $Er^{3+}$ ion. These changes cause intensity redistribution and inhomogeneous line broadening without considerably shifting the centers of gravity of individual multiplets. At the maximum $Er_2O_3$ concentration (0.05 mol. %) the structure of the spectrum changes significantly.

The XRL spectra were interpreted in accordance with the data on energy position of levels in free $Er^{3+}$ ion that forms an active optical center in $Li_2B_4O_7$ matrix. In general there were 36 maxima detected in the dependency $I_{XRL} = f(\lambda)$, of which we could identify 18. All identified maxima are determined by parity-forbidden intraconfigurational radiative transitions within 4f configuration of $Er^{3+}$ ion from the excited levels of higher-lying multiplets $^2K_{\mathbf{J}}$ ($\mathbf{J}$ = 13/2, 15/2), $^4F_{\mathbf{J}}$ ($\mathbf{J}$ = 3/2, 5/2, 7/2, 9/2), and $^4S_{\mathbf{J}}$ ($\mathbf{J}$ = 3/2), onto the ground level $^4I_{15/2}$. It is shown that for most of the transitions there is violation of strict selection rules for total angular momentum ($\Delta\mathbf{J} > 1$), and also for spin ($\Delta\mathbf{S} > 0$) and orbital momentum ($\Delta\mathbf{L} > 1$) in LS coupling approximation, caused by the internal field of the matrix having effect on triple-charged erbium ions via non-centrosymmetric interaction, which leads to different parity states being mixed, resulting in removing the prohibition of parity and total orbital momentum selection rules, which are strictly obeyed in the spectra of free $Er^{3+}$ ions. The unidentified maxima might be determined either by transitions from excited states onto the ground level $^4I_{15/2}$, or by transitions between excited states.

# Electronic Structure of $Tl_3PbI_5$, a Prospective Nonlinear Optical Material

Denysyuk N.M. [1], Khyzhun O.Y. [1], Bekenev V.L. [1], Parasyuk O.V.[2]

[1]*Institute for Problems of Materials Science, National Academy of Sciences of Ukraine, Kyiv, Ukraine*

[2]*Department of Physics, Volyn National University, 13 Voli Ave., Lutsk 43025, Ukraine*

The first appearance of the $Tl_3PbI_5$ compound was detected when studying the pseudo-binary TlI–$PbI_2$ system [1]. It was found that $Tl_3PbI_5$ melts congruently at 639 K. Olekseyuk et al. [2] have discovered that $Tl_3PbI_5$ crystallizes in the orthorhombic (space group $P2_12_12_1$) $Tl_3PbBr_5$-type structure, with the lattice parameters: a = 16.205 Å, b = 9.676 Å, and c = 8.952 Å.

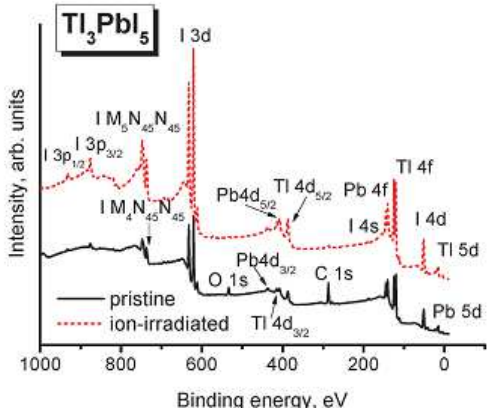


Fig. 1 Survey XPS spectra recorded for a pristine (solid line) and $Ar^+$-ionbombarded (dashed line) surface of the $Tl_3PbI_5$single crystal

Fig. 1 presents the survey XPS spectra of the pristine and $Ar^+$-ion irradiated surfaces of the $Tl_3PbI_5$ single crystal. It is apparent that all the spectral features, except for the carbon and oxygen 1s levels for a pristine surface, are assigned to be the constituent element core-levels or Auger lines. Fig. 1 shows that the relative intensity of the C 1s core-level line for the pristine $Tl_3PbI_5$ single crystal surface was found to be rather weak, and the line almost completely vanishes after the $Ar^+$ ionbombardment of the surface. As can be seen from Fig. 1, the present survey XPS data show that there is no active chemical interaction with oxygen when the $Tl_3PbI_5$ single crystal surface is exposed to air for comparatively long time (about 1 month): the O 1s line is rather weak on the studied pristine surface and no trace of the O 1s line is detected after the $Ar^+$ ion-bombardment of the surface. Therefore, our XPS results reveal the low hygroscopicity of $Tl_3PbI_5$, the property that is very important for handling this compound as an efficient laser source operating in ambient conditions.

1. E. Yu. Peresh, V. B. Lazarev, V. V. Tsigika, Y. V. Voroshilov and V. S. D'ordyai, Zh. Neorg. Khim., 1980, 25, 1368.
2. I. D. Olekseyuk, G. E. Davidyuk, A. A. Fedonyuk, L. V. Sysa and A. M. Padalko, Inorg. Mater., 1998, 34, 445.

# Anisotropic Light Scattering by Magnetite Nanoparticles in a Presence of External Magnetic Field

Dmitruk N.L.[1], Malynych S.Z.[1,2], Moroz I.E.[3], Kurlyak V.Yu.[4]

[1] *V.E Lashkaryov Institute of Semiconductors Physics, NAS of Ukraine, Kyiv, Ukraine*
[2]*Hetman Petro Sahaydachnyi Army Academy, Lviv, Ukraine*
[3]*National University "Lviv Polytechnic", Lviv, Ukraine*
[4]*Ivan Franko National University of Lviv, Lviv, Ukraine*

Nanoparticles possessing magnetic moment exhibit a number of interesting optical properties. These are magnetic dichroism, magnetically induced birefringence, Faraday rotation and ellipticity, to name a few. Zero backscattering and weak localization of light in a suspension of magnetic nanoparticles subjected to the external magnetic field was also observed. Those unusual optical effects are attributed to the delay of light propagation that result from the formation of standing waves within the scatterer due to the resonances in backscattered efficiency and forward-backward anisotropy factor. Based on Mie theory calculations it was found that the intensity of light scattered by magnetic nanoparticles depends on incident wave configuration with respect to the direction of the external magnetic field [1]. Photonic Hall effect was predicted and experimentally confirmed for a scattering medium subjected to the transverse magnetic field. Despite a great deal of works on the optical effects in the magnetic nanoparticle assemblies some aspects of those phenomena remain unexplored. In particular, few studies consider variations in scattered light intensity of a magnetic nanoparticle suspension when the latter is subjected to the transient magnetic field.

In present work we report experimental results on fast variations in the optical transmission of superparamagnetic magnetite $Fe_3O_4$ nanoparticle aqueous suspension depending on mutual orientation of the incident electromagnetic wave and the magnetic field direction. The nanoparticles were 10–15 nm in diameter with a volume fraction of 0.0012. He-Ne laser with a 632.8 nm wavelength was used as a light source. It was found that optical transmittance of the suspension varies in the range of 10–15% when the DC operated magnet was switched on. The characteristic time of those variations is less than 1 ms which makes magnetite nanoparticle assembly an appealing platform for high-speed magneto-controlled optical devices. Our studies reveal that fast optical response is due to orientation of the magnetic moments associated with each nanoparticle along the applied magnetic field. Our findings are important for understanding of the interaction of light with magnetic nanoparticles as well as for practical applications.

# Reconstruction of Residual Deformation Field from Moiré Patterns in the X-ray Interferometry

Fodchuk I.M., Novikov S.M., Yaremchuk I.V., Struk Ya.M.

*Yuriy Fedkovych Chernivtsi National University, Chernivtsi, Ukraine*

The aim of this work is a search of approaches for the solution of inverse problem – reconstruction of the spatial distribution of the residual strain field from the features of change of moiré fringe periods, shape and intensity. Based on the method of numerical calculation of moiré patterns, developed in [1], for different model representations as series of local concentrated sources of residual strains, arising after scribing, the influence of size and distribution features of strains on change of shape and periods of moiré fringes was studied (Fig.1c-g).

The comparison of calculated and experimental moiré patterns (Fig.1a,b) [1,2] allows us to assert about the presence of maximum deformations at the edges of scratches, which corresponds to more intensive indenter indentation at the beginning of scribing (Fig.1c,d). Introduction of structural moiré allows to characterize the contribution of each source deformation to the total field is not only near but far from scratch.

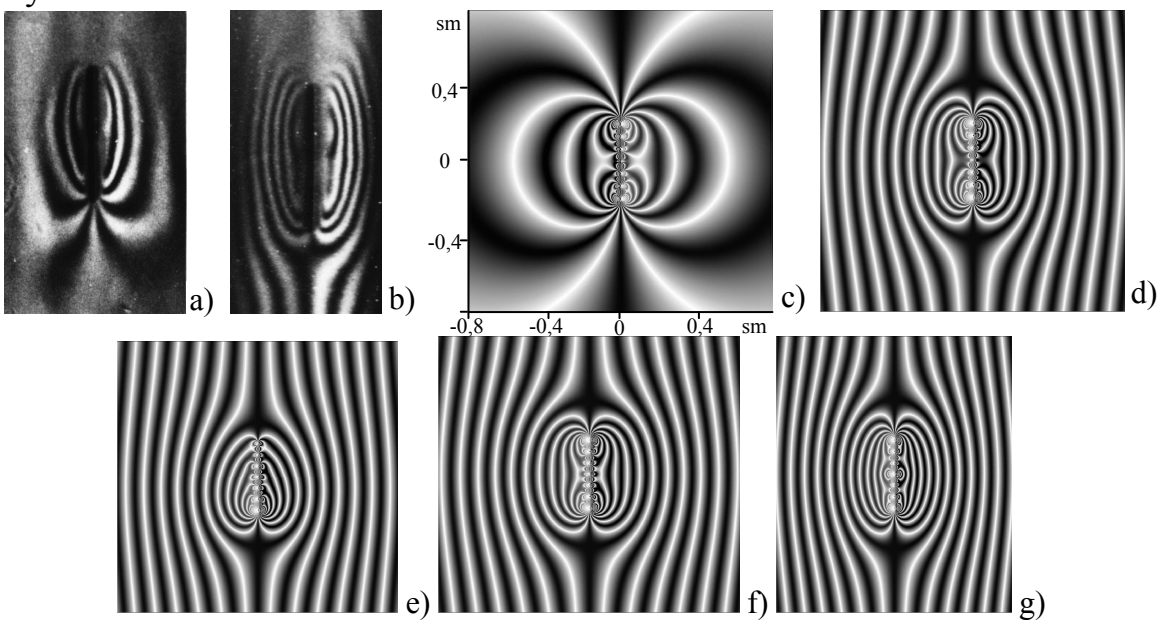


Fig. 1. Experimental moiré images [1] of scratch placed perpendicular to the diffraction vector (220), Cu$K_{\alpha 1}$ radiation (a,b). Calculated moiré images in dependence on the character of force displacement in a rows: without structured moiré $\Lambda$=0 (c), and with structured moiré $\Lambda$=1200 μm. Force distribution: parabolic (c,d), exponential (e), uniform in central part and rapidly increasing at the ends (f), chaotic (g).

7. Raransky M.D., Shafraniuk V.P., Fodchuk I.M. // Sov. Metallofizika. – 1985. – Vol. **7**, No.5. – P.63.
8. Fodchuk I.M., Raransky M.D. // J. Phys. D: Applied Physics. – 2003. – Vol.**36**. – P.A55.

# Crystal-Chemical Analysis of Defect Subsystem at the Doped and Annealed in a Pair of Selenium Crystals ZnSe:Mn

Freik D.M., Boichuk V.M., Levkun M.P.

*Vasyl Stefanyk Precarpathian National University, Ivano-Frankivsk, Ukraine*

Zinc selenide used to create laser screens, LED injection, scintillation sensors, photoconductive, sources of spontaneous and coherent radiation in the blue region of the spectrum. Crystal-quasi-chemical formula for Magnesium doped crystals of n-ZnSe:Mn and p-ZnSe:Mn allows to calculate the concentration dependence of the dominant point defects, free carrier and Hall's concentration from dopant content.

Doping crystals of n-ZnSe by Magnesium increases the electrons concentration and due to doping crystals of p-ZnSe by Magnesium is conversion of conductivity from p- to n- type and further increases of the electrons concentration, confirming the donor effect of Mn (Fig. 1).


a) b)

**Fig. 1.** Dependence of concentration of dominant point defects N: 1 - $[V_{Se}^{2+}]$, 2 -$[V_{Se}^{+}]$, 3 - $[Zn_i^{+}]$, 4 - $[Zn_i^{2+}]$, 5 - $[V_{Zn}^{2-}]$, 6 - $[Mn_{Zn}^{x}]$, 10 - $[V_{Zn}^{-}]$, main carriers 7 - n, 8 - p and Hall's concentration 9 - $n_H$ from dopant content of Mn for n-ZnSe:Mn (a) and p-ZnSe:Mn (b) ($\alpha = 0{,}1 \cdot 10^{-4}$ at. %, $\gamma = 0{,}99999$, $\delta = 0{,}1$; $\beta = 0{,}1 \cdot 10^{-4}$ at. %, $\mu = 0{,}1$, $\varepsilon = 0{,}1 \cdot 10^{-4}$).

Annealing of n-ZnSe:Mn in a pair Se leads to decrease in the concentration of electrons, conductivity conversion from n- to p-type and further increase in the concentration of holes. During this also increases current carriers in crystals of ZnSe:Mn<Se (Fig. 2).


a) b)

**Fig. 2.** The spatial dependence of the Hall's concentration $n_H$ from stoichiometric deviation α (Zn) – a, β (Se) – b and content [Se] for crystals n-ZnSe:Mn<Se> (a) and p-ZnSe:Mn<Se> (b), annealing in a pair Se.

# Crystal-Chemical Interpretation of Amphoteric Influence of Bismuth Impurity in Tin Telluride

Freik D.M.[1], Turovska L.V.[2], Boichuk V.M.[1]

[1]*Vasyl Stefanyk PreCarpathian National University, Ivano-Frankivsk, Ukraine*
[2]*Ivano-Frankivsk National Medical University, Ivano-Frankivsk, Ukraine*

Tin telluride is the special material of IV-VI compounds over a wide enough range of homogeneity, which lies completely on the side of chalcogen; it is characterized by only *p*-type of conductivity and high concentration of holes, which increases with the content of tellurium [1]. Optimization of parameters of SnTe is associated with the need to reduce the concentration of current carriers by influence on the defect subsystem. This can be achieved by doping with various impurities, among which elements of V group of the Periodic Table (in particular, bismuth) are important [2].

In this paper within the crystal-quasichemical formalism defect subsystem of tin telluride crystals doped by bismuth has been analyzed. In SnTe:Bi the dopant is distributed between the cationic and anionic sublattices. Thus, dopant, replacing tin in its sublattice, is ionized from the state $Bi^0(s^2p^3)$ into the state $Bi^{3+}(s^2p^0)+3e^-$ (where it is a donor) and relatively to $Sn^{2+}$ sublattice it is $Bi_{Sn}^{1+}$. In tellurium sublattice dopant is ionized $Bi^0(s^2p^3)\rightarrow Bi^{3-}(s^2p^6)+3h^+$ (where it is an acceptor) and relatively to $Te^{2-}$ sublattice it is $Bi_{Te}^{1-}$. This leads to the experimentally observed amphoteric effect of dopant.

The character of change of disproportionation of dopant charge state ($Bi^{3+}$, $Bi^{3-}$) and its effect on the electrical properties of the material have been determined. In particular, it has been found that in the initial stages of doping (up to 1.5 at.% of Bi) there is a predominance of impurity ions in the cation sublattice $Bi_{Sn}^{1+}$. With increasing impurity concentration (> 1.5 at.%) processes of self-compensation are amplified, indicating the increasing the share of bismuth ions in tellurium positions $Bi_{Te}^{1-}$, which leads to the increase of the concentration of holes, and consequently increase of the electrical conductivity.

On the basis of the proposed crystal-quasichemical formulae the analytical expressions for the concentration of point defects and Hall concentration of current carriers in SnTe:Bi crystals have been derived, and their dependences on the dopant content have been calculated. It has been shown that the dominant point defects are bismuth ions in lattice sites of tin telluride $Bi_{Sn}^{1+}$, $Bi_{Te}^{1-}$, doubly charged tellurium $V_{Te}^{2+}$ and tin $V_{Sn}^{2-}$ vacancies; the ratio between them is determined by the concentration of dopant Bi.

1. Brebrick R.F. Deviations from stoichiometry and electrical properties in SnTe // J. Phys. Chem. Solids. – 1963. – V. 24, No. 1. – P. 27-36
2. Shperun V.M., Freik D.M., Prokopiv V.V. Teluryd olova. Fizyko-khimichni vlastyvosti. – Ivano-Frankivsk: Plai, 2002. – 250 p.

# Structural Phase Transitions on the Free Cleavage Surfaces of GaTe Layered Crystals

Galiy P.V.[1], Nenchuk T.M. [1], Mazur P. [2], Poplavskyy O.P. [3], Yarovets I.R. [1]

[1] *Ivan Franko Lviv National University, Lviv, Ukraine*
[2] *University of Wroclaw, Wroclaw, Poland*
[3] *Vasyl Stefanyk Precarpatian National University, Ivano-Frankivs'k, Ukraine*

Gallium telluride semiconductor crystal belongs to the layered III-VI group chalcogenides and is attracting great interest for applications in "nanoscale-generation" of optoelectronics devices, radiation detectors and solar cells. The structural studies of bulk GaTe crystal indicate the presence of hexagonal and monoclinic structural modifications. However, the phase state of the surface that is obviously more important for novel GaTe application has been studied less, in particular, by "direct" scanning probe methods.

1. GaTe single crystals were grown by the Bridgman method. Previous bulk-structure investigations indicated the hexagonal structure of the studied GaTe crystals with unit cell parameters $\boldsymbol{a} = \boldsymbol{b} = 4.06$ Å, $\boldsymbol{c} = 16.96$ Å. The surface was studied by scanning tunneling microscopy/spectroscopy (STM/STS) and low electron energy diffraction (LEED). The STM/STS data were acquired using the Omicron NanoTechnology STM/AFM System, at room temperature under ultrahigh vacuum (UHV) conditions ($4 \cdot 10^{-9}$ Pa). The STM images were taken in the constant-current mode. The STM/STS data processing was carried out using the WSxM v.4.0 of Nanotec Electronica. LEED data were analyzed using the SPECS SAFIRE Diffraction Image Acquisition and Processing System for LEED and RHEED. LEED analysis was carried out using incident beam energies 10-150 eV, and spot size less than 1 mm.

The results of the combined scanning probe and electron diffraction study of the GaTe cleavage surface indicate the presence of different structures: hexagonal on macroscale and local monoclinic, randomly distributed at the nanoscale. The hexagonal unit cell parameters $\boldsymbol{a} = \boldsymbol{b} = 4.08$ Å, $\boldsymbol{c}$ □ 16 Å STM-determined are in good agreement with the bulk ones and, besides, planar parameters ***a, b*** obtained using LEED. The monoclinic unit cell parameters $\boldsymbol{a}$ □ 24 Å, $\boldsymbol{b}$ □ 4 Å, $\boldsymbol{c}$ □ 10 Å are consistent with one of the known monoclinic modifications. LEED and STS data indicate that the GaTe surface is not flat, but is characterized by a well-developed staircase structure formed by cleavage. The possibility of partial on-nanoscale reconstruction of the basic hexagonal structure towards a monoclinic one is directly related to the number of surface defects, such as the loosely distributed steps which are as high as a single Te-Ga-Ga-Te packet.

# Technology and Thermoelectric Properties of Semiconductor Materials Based System Pb-Bi-Te

Galushchak M.O., Krynytsky O.S., Mateik G.D.

*Ivano-Frankivsk National Technical University of Oil and Gas, Ivano-Frankivsk, Ukraine*

Lead telluride – efficient thermoelectric materials for medium field (500-850) K. The high interest in his research that does not diminish over the years, due to a unique physical and chemical properties and relatively simple technology to obtain high-quality crystals.

The efficiency of thermoelectric materials is determined by a dimensionless figure of merit, figure of merit (ZT): $ZT = (\alpha^2\sigma / \chi)T$, where $\alpha$, $\sigma$, $\chi$, T respectively Seebeck coefficient, electrical conductivity, thermal conductivity and absolute temperature. Low values of ZT commercially available thermoelectric materials limits the use of thermoelectric devices. To thermoelectric generators were competitive in the large and powerful business devices need to look for materials with significantly higher values of ZT [1]. One of the main methods for improving thermoelectric material parameters are doping and formation of solid solutions.

For the synthesis of semiconductor thermoelectric compounds used method of direct fusion of mixing of the components. The resulting ingots ground in an agate mortar and by selecting the size fraction (0,05 – 0,5) mm and pressed. Thermoelectric coefficient $\alpha$ and specific conductivity $\sigma$ was determined by the standard method. The specimen is clamped two copper rods placed in a furnace $U_1$, which heats the sample to the desired temperature measurement. For one copper rods wound furnace $U_2$ to create a temperature gradient (≈10 K) in the sample. Temperature measurements were carried out by two chromel-alumel thermocouples placed in holes drilling in the sample. Electrical conductivity was determined by measuring the voltage drop on the sample generated by voltage source $U_3$. Thus, one of the legs of each thermocouple was used as conductor of current.

A study was conducted of lead telluride doped Bi and the main characteristics of the thermoelectric material. In particular, when the content of impurities 0,1 at.% Electrical conductivity is ≈ 630 $(\text{Ohm cm})^{-1}$, and thermoelectric coefficient ≈ 350 μV/K concerning solid solution is for $PbTe\text{-}Bi_2Te_3$ containing 1 mol.% defined $\sigma \approx 1000$ $(\text{Ohm cm})^{-1}$, $\alpha \approx 350$ μV/K.

1. Freik D.M., Galushchak M.O., Krynytsky O.S., Matkivsky O.M. New thermoelectric nanocomposite materials (review) // Physics and Chemistry of Solids 14 (2) (2013).

# Effect of CaO and BaO Additions on the Electrical Parameters of $SnO_2$ Based Varistor Ceramics with Nano-Sized Intergranular Phase

Gaponov O.V., Vorobiov O.V., Vasyliev A.M.

*Oles' Gonchar Dnipropetrovs'k National University, Dnipropetrovs'k, Ukraine*

The high nonlinear $SnO_2$ based ceramics which can be used as a varistor material has intensively been investigated for the last two decades. Along with the widespread ZnO based ceramics $SnO_2$ based ceramics can be used for producing the overvoltage-protective devices. In this article $SnO_2$-$Co_3O_4$-$Nb_2O_5$-$Cr_2O_3$-CuO ceramics baked at 1520 and 1620 K with CaO or BaO additions is studied. The structure of the investigated material consists of $SnO_2$ grains divided by the layers of Cu-rich intergranular phase. The width of this phase is the same as for the ZnO based ceramics and equals to several nanometers.

In ceramics obtained at both burning temperatures the electrical conductivity in the low electric field decreases with CaO addition and even more decreases with BaO. It correlates with the increase of potential barrier height at the grain boundaries from 0.6 to 0.8 eV. The nonlinear coefficient $\beta = 36$ is the highest in the ceramics with 0.5 mol. % BaO addition baked at 1620 K. The electric field $E_1$ of samples obtained at 1520 and 1620 K is increasing with CaO and BaO additions. This process is caused by decreasing of the average grain size. It explains the obtained parameters of the dielectric permittivity which decreases in the samples with alkaline-earth metal oxide additions. The normalized nonlinear coefficient $\beta_E = \beta / E_1$ decreases with adding CaO and BaO. The $SnO_2$-$Co_3O_4$-$Nb_2O_5$-$Cr_2O_3$-CuO ceramics baked at 1620 K has the highest $\beta_E = 0.016$.

The specific resistance of $SnO_2$ grains estimated from high-current pulse measurements [1] differs greatly for different $SnO_2$ based ceramics and amounts to from 5 to several tens Ohm·cm. The estimated average size of $SnO_2$ grains is 2-7 $\mu m$ which correlates with the data of scanning electron microscopy.

In the studied $SnO_2$-$Co_3O_4$-$Nb_2O_5$-$Cr_2O_3$-CuO system with CaO and BaO additions the rise of burning temperature leads to the increase of linear shrinkage, grain size, electrical conductivity in the low field, normalized nonlinear coefficient and dielectric permittivity and the decrease of the electric field $E_1$. The coordinated changes of these parameters uphold the barrier mechanism of conductivity in the $SnO_2$ based ceramics. The nonlinear coefficients and normalized nonlinear coefficients are higher for the samples baked at higher temperatures. The addition of alkaline-earth metal oxides allows to increase the potential barrier height at the grain boundaries and produce the varistors with the lower values of leakage current.

1. Glot A.B. Electrical properties of $SnO_2$ ceramic varistors withstanding high current pulses / A.B. Glot, Z.Y. Lu, Z.Y. Zhou, A.I. Ivon // Superficies y Vacio. – 2011. – 24(2). – P. 61-67.

# Optical Spectroscopy of High Resistance CdTe(III) Single Crystals at the Fundamental Optical Transitions $E_0$

Gentsar P.O., Vlasenko O.I.

*V. Lashkaryev Institute of Semiconductor Physics NAS of Ukraine, Kyiv, Ukraine*

Recently, more attention is paid to the technology of growth high resistance CdTe crystals and solid solutions based on them. The development of technology based on the control of the synthesis, determining the defect structure and its impact on the physical properties of the material. Conditions for obtaining material determine the composition and distribution of point defects that materially influence on electronic processes in the material. It is known that CdTe is used to make not cooled detector of gamma radiation. One of the main problems when using $A_2B_6$ semiconductor compounds as the base material optoelectronics is to obtain a homogeneous volume of material.

In order to characterize highresistance CdTe (III) single crystals with a resistivity $10^9$-$10^{10}$ ohm·cm were conducted optical study of the material at the fundamental optical transition $E_0$.

Reflection and transmission spectra at the fundamental optical transition E0 of CdTe(III) single crystals (range 800-1100 nm) were measured using diffraction lattice monochromator MDR-23.

Working brink of samples subjected to different treatment including mechanical polishing, removing layers of damaged layer using chemical-dynamic etching and free etching, and chemical treatment to remove the products of etching.

In the spectral dependence of reflectance observed a clearly expressed band from 829 to 910 nm. From the transmission spectra determined the values energy that corresponds to the fundamental optical transition $E_0$ for CdTe single crystals (E = 1.44 eV).

It is known that the peak refractive index corresponds to the fundamental absorption edge. The band-gap of samples associated with complex energy band structure of the valence band and the conduction band gap, technological conditions crystal growth. Features of the energy band structure of functional materials for electronic equipment are observed in the experimental spectra classical spectroscopy (reflection and transmission).

Thus, studies of optical properties (reflectance and transmittance spectra in the range 800 - 1100 nm) are shown that the investigated crystals have high (detector) quality, which is crucial for the production of highly sensitive and high resolution sensors of ionizing radiation.

# Laser-Stimulated Processes in Silicon

Gentsar P.O., Vlasenko O.I., Levytskyi S.M.

*V. Lashkaryev Institute of Semiconductor Physics NAS of Ukraine, Kyiv, Ukraine*

Due to intensive development of nanophysics and nanoelectronics the research of electronic phenomena that occur in the optical spectra of surface layers and bulk of functional materials for electronic equipment is important. In recent years laser irradiation very successfully used for surface treatment (surface layers). By use the laser treatment of functional materials for electronic equipment can be change their optical and electrical properties. Study of the laser irradiation is important for the further progress of laser technology.

In this work are shown the results of optical investigations of the reflection spectra in the range 0.2 - 1.7 μm before and after laser irradiation in the energy interval 66 - 108 mJ/cm$^2$. As semiconductor wafers are used n-Si (100) and n-Si (111) single crystals with a resistivity of 4.5 - 5.5 Om□cm at room temperature. Samples were subjected to laser treatment, namely the crystal surface was uniformly irradiated at room temperature (T = 300 K) pulses of neodymium laser (λ = 532 nm) nanosecond duration (τ = 7-8 ns) of the energy density E from 66 to 108 mJ/cm$^2$.

So in n-Si single crystals a structural gettering, i.e. the absorption due to the presence of sites with defective structure and have the ability to actively absorb point defects and impurities bind. In silicon the role of getter perform $SiO_x$, $SiO_2$, $Si_3N_4$, $SiO_{2-x}P$, SiC layers and others.

Increasing of the reflectivity of n-Si (100) and n-Si (111) single crystals can be explained as follows: the processing of crystals is modification of thin surface layers and resulting in the total reflection effect contributes thin surface layer and bulk material. Another way this is a result of interference of reflected light (electromagnetic) waves from the boundaries of the air - a thin surface layer and a thin surface layer - the crystal volume. Reflecting the ability of crystals is determined by refractive index $n$ and extinction coefficient $\chi$. Differences of optical characteristics of the surface layer and bulk (complex refractive index of the surface layer $\tilde{n}_s = n_s + i\chi_s$ is different from the complex refractive index of the volume of material $\tilde{n}_v = n_v + i\chi_v$) and leads to the integral effect.

Experimentally shown that high-intensity peak in single crystal n-Si $E_1 = \Lambda_1^c - \Lambda_3^v$, which is located at energy 3.38 eV after laser irradiation increases.

Thus, the laser processing of thin surface layers allows changing the physical properties (optical, electrical and other) functional materials for electronic equipment, which is crucial in the study of fundamental problems of nanostructured systems, nanomaterials and nanotechnology.

# Non-Stationary Temperature Distribution of Anisotropic Optical Thermoelement Based On Bi

Gutsul I.V., Gutsul V.I.

*Chernivtsi National University, Chernivtsi, Ukraine*

In the paper we provide the investigation of non-stationary temperature distribution of anisotropic optical thermoelement (AOT) which has the shape of rectangular parallelepiped, fabricated from the thermoelectric anisotropic Bi crystal with the length $a$, height $b$ and width $c$. The uniform ray current with density $q_0$ falls at the upper side of thermostat which has thickness $b_1$, fabricated of optically transparent material in the observed spectral range of wave lengths. The upper side of AOT is in thermo optical contact with the lower side of thermostat which has the temperature $T_0$. The lateral sides of AOT are isolated adiabatically. The homogeneous monochromatic ray current with density $q_0$ passes through the thermoelement volume and flow out of its lower side. The part of this current of energy $\Delta q$ is absorbed by thermoelement volume creating the temperature gradient. This, in its turn, causes the appearance of themoelectromotive force which definitely determines the magnitude of falling ray current density $q_0$. The kinetic coefficients of AOT material are assumed as temperature independent.

The non-stationary temperature distribution in AOT is obtained from the equation of thermal conductivity

$$\frac{\partial T}{\partial t} = A^2 \frac{\partial^2 T}{\partial y^2} + B\, e^{-\gamma(b-y)}, \qquad (1)$$

where $A^2 = \frac{\chi_{22}}{C_0 d}$, $B = \frac{q_0 \gamma}{C_0 d} \exp[-\gamma_1 b_1]$, $C_0$ – specific thermal capacity, $d$ – density of AOT material, $\chi_{22}$ – component of thermal conductivity tensor, $\gamma$ – absorption coefficient of the thermoelement material, $\gamma_1$ – absorption coefficient of the thermostat material. The boundary and primary conditions for the equation of thermal conductivity (1) are the following

$$\left.\frac{\partial T}{\partial y}\right|_{y=0} = 0; \quad T|_{y=b} = T_0; \quad T|_{t=0} = T_0. \qquad (2)$$

The solution of equation of thermal conductivity (1) is obtained as a sum of general solution of homogeneous equation and partial solution of non-homogeneous one. The obtained solution proves that the temperature distribution inside of AOT shows the complicated non linear dependence both on coordinate $y$ and time $t$. Besides $T(y,t)$ depends on anisotropic coefficient of thermal conductivity $\chi$ and on the absorption coefficient $\gamma$ of the AOT material and one of the thermostat material $\gamma_1$.

# Influence of the Composition of Solutions $HNO_3$-HI-glycerol on the Process of Chemical Etching of CdTe and Solid Solution $Zn_xCd_{1-x}Te$ and $Cd_xHg_{1-x}Te$

Gvozdiyevskij Ye.Ye.[1], Denysyuk R.O.[1], Tomashyk V. M.[2], Tomashyk Z. F.[2]

[1]*Ivan Franko Zhytomyr State University, Zhytomyr, Ukraine*
[2] *V. Ye. Lashkaryov of National Academy of Science of Ukraine, Kiev, Ukraine*

CdTe and solid solutions on its base have sufficiently wide practical use. There is need at first prepare accordingly there surface for made work items with used under named semiconductor materials for itch use chemical mechanic and chemical dynamic polishing (CDP).

There is used the methodic of rotating disk in order to develop and optimize new etching compositions with low rate of non-alloyed CdTe and solid solutions $Zn_{0,04}Cd_{0,96}Te$, $Zn_{0,1}Cd_{0,9}Te$ and $Cd_{0,2}Hg_{0,8}Te$ dissolution. The $HNO_3$ – 70%, HI – 57%, $C_3H_8O_3$ – 20 % aqueous solution have been used for the preparation of solutions (all the reagents are chemically clean). At first, the surface of the chemically treated semiconductors was washed in 0,2 M $Na_2S_2O_3$ solution for complete dissolution of iodine, and then it was washed in distilled water and dried out in the air.

On the basis of the obtained results, the structure of the polished etching compositions, as well as the techniques and modes of CDP for making the kind of semiconductor devices (table 1) have been developed and optimized.

Table 1

**The structures of the polished iodine-educing compositions on the basis of $HNO_3$ – HI – Glycerin system for CDP (T = 298K, $\gamma$ = 80 min.$^{-1}$)**

| **Semiconductor** | **CdTe** | **$Zn_{0,04}Cd_{0,96}Te$** | **$Zn_{0,1}Cd_{0,9}Te$** | **$Cd_{0,2}Hg_{0,8}Te$** |
|---|---|---|---|---|
| **$HNO_3$ – HI – $C_3H_8O_3$, V. %** | (5-25) : (55-95): (0-40) | (5-50) : (75-95): (0-40) | (15-25):(75-95): (0-40) | (5-25) : (60-95): (0-40) |
| **Speed CDR, mkm/min** | 1-11 | 1-10 | 1-13 | 3-11 |

The given study of kinetic regularities of chemical digestion processes of $Zn_XCd_{1-X}Te$ and $Cd_XHg_{1-X}Te$ solid solution in etching solutions of $HNO_3$ - HI - Glycerin allowed to establish that the process of dissolution in the polishing compositions has a mixed nature, as the apparent activation energy is equal to 20-50 kJ/mol. It is confirmed by the speed of dissolution and dependence on the speed of rotation of the disk.

The developed iodine-educing etching compositions can be used for the CDP of under investigated semiconductor single crystals, whereupon the surface should be washed in the 0,2 M $Na_2S_2O_3$ solution and distilled water. In addition to that the surface is qualitatively polished ($R_z \leq 0,05$mkm).

# Thermodynamics of Point Defects and Their Electrical Activity in ZnTe Crystals

Horichok I.V., Pylyponiuk M.A., Freik N.D.

*Vasyl Stefanyk Prekarpathian University, Ivano-Frankivsk, Ukraine*

Zinc telluride (ZnTe) is a relatively little studied direct band gap semiconductor and is of interest in terms of the expansion of element basis of modern electronics [1]. Also, as a direct band gap semiconductor, ZnTe has high photosensitivity and can be successfully used for efficient solar energy conversion [1]. Its effective practical use depends on the defective subsystem.

In this paper, the predominant type of point defects in the two-temperature crystal annealing process is calculated using the method of thermodynamic potentials. It has been established that under annealing in zinc vapor ($P_{Zn}$ = 13300 Pa) at temperatures T = (1000-1200) K the dominant defects are doubly ionized zinc vacancies, and under annealing in tellurium vapor ($P_{Te}$ = 13300 Pa) in the same temperature range the dominant defects are once ionized zinc vacancies. A close agreement between the formation energy of neutral zinc vacancy that has been calculated in our work and theoretically known values, and a satisfactory correlation of our values of concentration of free charge carriers with experimental data indicate the adequacy of the presented defect subsystem model and of conclusions that have been made on its basis.

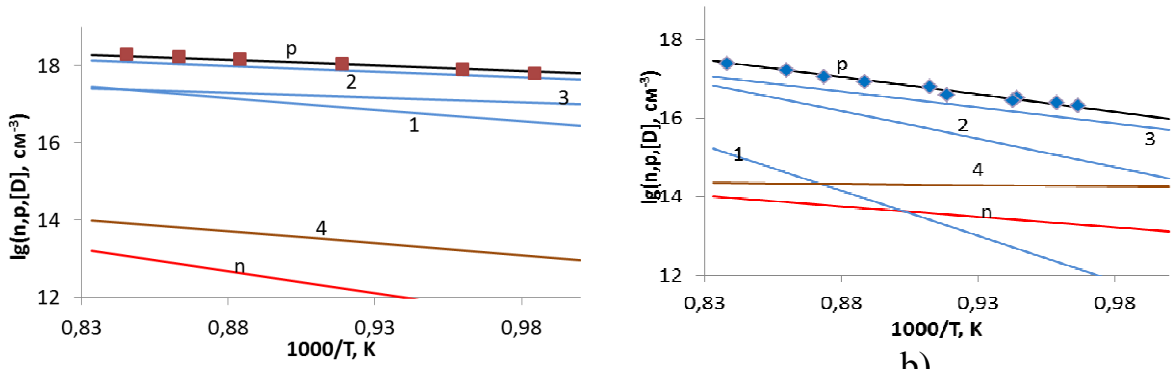


**Fig.** The dependence of concentrations of electrons (n), holes (p), point defects ([D]) on temperature T under two-temperature annealing at tellurium vapour ($P_{Te}$ = 13300 Pa) (a) and zinc vapour ($P_{Zn}$ = 13300 Pa) (b). (1 – , 2 – , 3 – , 4 –). Solid curves are calculation; points are experiment [2].

*This research is sponsored by NATO's Public Diplomacy Division in the framework of "Science for Peace" (NATO SPS 984536)).*

1. A. Sakalas, Z. Yanushkevichyus, “Point defects in semiconductor compounds”. Nauka, Moscow, p.153, 1988.
2. F. T.J. Smith, “High temperature study of native defects in ZnTe” J. Phys. Chem. Solids, Vol. 32, pp. 2201 - 2209, 1971.

# Fabrication and Some Properties of Solid Solutions in the $Tl_5Te_3$-$Tl_9GdTe_6$ System

Imamalieva S.Z.[1], Gasanly T.M.[2], Mehdiyeva I.F.[1], Sadygov F.M.[2]

[1]*Institute of Catalysis and Inorganic Chemistry of ANAS, Baku, Azerbaijan*
[2]*Department of General and Inorganic Chemistry, BSU, Baku, Azerbaijan*

Narrow-band gap heavy metal chalcogenides have attracted an increasing level of attention because of their promising thermoelectric properties.

Thallium subtelluride, $Tl_5Te_3$ owing to features of the crystal structure has a lot of ternary analogs which are thermoelectric with anomaly low thermal conductivity.

In our previous study we reported some new ternary compounds $Tl_9LnTe_6$ which crystallize in $Tl_5Te_3$ structure type [1,2]. These compounds might exhibit good thermoelectric properties. Lanthanide elements are lighter than thallium or bismuth elements resulting in significant mass fluctuation between the Tl and Ln atoms, which may further lower the thermal conductivity. On the other hand, the magnetic properties are popular among the f-block metal compounds as all the $Ln^{3+}$ ions contain unpaired electrons.

In present report phase equilibria in $Tl_5Te_3$-$Tl_9GdTe_6$ system for obtaining of solid solutions with $Tl_5Te_3$ structure are discussed.

The samples were prepared by heating the high purity elements into graphitized silica ampoules. The ampoules were heated to maximal temperature 1000 K and were kept at this temperature during 4 h. After that they were cooled slowly to 700K and annealed at this temperature during 1000h.

Investigations were carried out by using DTA, XRD and EMF measurement of concentration cell concerning gadolinium electrode with liquid electrolyte (300-450K). Based on experimental data the T-x phase diagram of $Tl_5Te_3$-$Tl_9GdTe_6$ system and concentration dependences of crystal lattice parameters are constructed.

It was shown, that system is characterized by formation of continuous fields of solid solutions with $Tl_5Te_3$-type structure. The partial molar thermodynamic functions of gadolinium and integral thermodynamic functions of formation and entropy for the $Tl_9GdTe_6$ and solid solutions $Tl_{10-x}Gd_xTe_6$ are calculated based on the results of the EMF measurements

Moreover, thermoelectric and magnetic properties of $Tl_9GdTe_6$ compound and solid solutions $Tl_{10-x}Gd_xTe_6$ are discussed.

## Reference

1. Babanly M.B., Imamaliyeva S.Z., Babanly D.M. // Azerb. Chem. J., 2009, №2, p.122-125
2. Imamalieva S.Z., Sadygov F.M., Babanly M.B. (2008). // Inorganic Materials, v.44, No.9, pp.935–938

# Polishing Properties of the $KIO_3$–KI–Organic Acid Etchants to the CdTe and $Zn_{1-x}Cd_xTe$ Surfaces

Ivanits'ka V.G., Shcherbak L.P., Tomashik V.M., Fochuk P.M., Tomashik Z.F.

[1]*Yuriy Fed'kovych Chernivtsi National University, Chernivtsi, Ukraine*
[2]*V.E. Lashkaryov Institute of Semiconductor Physics, Kyiv, Ukraine*

Our previous research has revealed that solution, containing potassium iodate ($KIO_3$) and potassium iodide (KI) in acidic medium find out polishing properties concerning CdTe and $Zn_xCd_{1-x}Te$ surfaces. As an acid agent, aqua solutions of citric and lactic acids were used. In this study to $KIO_3$–KI etching system an aqueous solution of 2, 3-dihydroxybutanedioic (tartaric) acid ($C_4H_6O_6$) was added. Tartaric acid has higher acidity value ($pK_{a1}$ = 2.89) in comparison with citric and lactic acids. Besides, there are two carboxyl groups in $C_4H_6O_6$ molecule and the tartrate-anion is bidentate complexing ligand. The use of tartaric acid in etching solution can result in a binding of poorly soluble interaction products in stable complexes. The complexation will intensify removal of interaction products from semiconductor crystals and this enable us to obtain high-quality clean surface without sediment and films.

Samples under investigation were cut from CdTe and $Zn_{0.04}Cd_{0.96}Te$ single-crystals. The 5 % $KIO_3$, 55 % KI and 25 % $C_4H_6O_6$ aqueous solutions were used as mother solutions for the etchant preparation. The etched surfaces microstructure was observed on the Leitz/Laborlux 12HL optical microscope. The surface roughness measuring was carried out on noncontact 3D surface profiler "New view 5022 S". Mathematical simulation of experimental data using the simplex-method was applied and etchant compositions optimization for polishing treatment of CdTe and $Zn_xCd_{1-x}Te$ surface was carried out.

The semiconductor dissolution rate in $KIO_3$–KI–$C_4H_6O_6$ etching solutions was found to vary from 0.3 μm/min to 6.5 μm/min for CdTe and from 0.3 μm/min to 8 μm/min for $Cd_{0,96}Zn_{0,04}Te$. Thus the studied etching composition can be attributed to the category of slow etchants the same as citric and lactic acids containing $KIO_3$–KI etching composition. The maximum of dissolution rate of all samples in studied concentration regions was observed in solutions enriched by potassium iodate and potassium iodide simultaneously.

Microscopic and profilographic studies show high-quality polishing properties of the developed etching compositions. It was revealed that etched semiconductor surfaces are smooth, clean and whatever visible films free.

The dependence of the etching rate versus time of solution storage was studied. It was found that $KIO_3$–KI–$C_4H_6O_6$ etching system can be characterized as age high-resistance. The polishing properties of etchants did not disappear over a period of solution storage. On the ground of obtained results it is possible to draw conclusion that the studied etchant compositions can be used for the controlled removal of the semiconductor materials and polishing treatment of CdTe and $Zn_xCd_{1-x}Te$ surface.

# Peculiarities of Thermoelectric half-Heusler Phase Formation in {Gd,Lu}-Ni-Sb Ternary Systems

Kaczorowski D.[1], Romaka V.V.[2], Romaka L.P.[3], Horyn A.M.[3], Kovbasyuk T.[2], Stadnyk Yu.V.[3]

[1]*W. Trzebiatowski Institute of Low Temperature and Structure Research, Polish*
[2]*National University "Lvivska Politechnika", Lviv, Ukraine*
[3]*Ivan Franko National University of Lviv, Lviv, Ukraine*

Semiconductor compounds which crystallize in MgAgAs structure type (so called half-Heusler phases) belong to the objects, which are very intensively investigated as the perspective materials for the direct conversion of the heat energy into electric current. The semiconducting properties of the half-Heusler intermetallic phases are in many cases very sensitive to the heat treatment, suggesting some structural disorder and the existence of the homogeneity domains. For the proper understanding of these influences, a detailed knowledge of the phase relations is necessary. The phase equilibria in the Gd-Ni-Sb and Lu-Ni-Sb ternary systems have been studied in the whole concentration range by means of X-ray and EPM analyses at 873 K. The interaction between the elements in Gd-Ni-Sb system results in formation of five ternary compounds at investigated temperature: GdNiSb (MgAgAs-type), $Gd_5Ni_2Sb$ ($Mo_5SiB_2$-type), $GdNi_2Sb_2$ ($CaBe_2Ge_2$-type), $GdNiSb_2$ ($HfCuSi_2$-type) and $Gd_5Ni_{0.965}Sb_2$ ($Yb_5Sb_3$-type). The Lu-Ni-Sb ternary system is characterized by formation of three ternary intermetallics at 873 K: LuNiSb (MgAgAs-type), $Lu_5Ni_2Sb$ ($Mo_5SiB_2$-type) and $Lu_5Ni_{0.56}Sb_{2.44}$ ($Yb_5Sb_3$-type). Under used conditions according to EPM analysis the composition of the half-Heusler RNiSb compounds deviates from stoichiometry toward to lower Ni content indicating the disordering in their crystal structure. The electrical properties measurement performed in the temperature range 80-380 K showed that GdNiSb and LuNiSb compounds with MgAgAs structure type are heavily-doped semiconductors.

# Calculation of Refractive Indices of Triple Chalcogenide Crystals

Kamenshchikov V.N. , Suslikov L.M.

*Uzhgorod National University, Uzhgorod, Ukraine*

$AgGaS_2$, $CdGa_2S_4$, $CdGa_2Se_4$ crystals belong to the large class of triple chalcogenide compounds. These crystals are widely used in various nonlinear optical devices. Therefore calculation of optical properties of these compounds is important.

In this work high frequency refractive indices are calculated by using Harrison's bond-orbital method.

For investigation of crystal properties, the calculated energies of the $V_2$ covalent bond and $V_3$ ionic bond are used. Using the above mentioned theory, it is possible to find out that the interaction of *s* and *p* orbitals of the cation and the anion is represented by the energy

$$\varepsilon_k = \frac{\varepsilon_s + \varepsilon_p}{2} \pm \sqrt{\left(\frac{\varepsilon_s - \varepsilon_p}{2}\right)^2 + f(k)^2 V_{sp\sigma}^2} \qquad (1)$$

where $f(k)^2$ depends on phases and orientations of neighboring orbitals and coincides with the number of neighbors around the given atom (coordination number $N_c$). The first and the second terms under the square root represent $V_3$ and $V_2$ energies, respectively. Because of the interaction of *p* orbitals of both the cation and the anion, energy $\varepsilon_s$ of the cation in (1) is replaced by $\varepsilon_p$, and the energy $V_2$ will represent the interaction of these orbitals. Table 1 contains the values of Hartree–Fock terms for atoms of $AgGaS_2$ and $CdGa_2S(Se)_4$ crystals [1]. The method of calculation is presented in [2].

Table 1. Hartree–Fock values for the valence levels

| Energy level | Ag | Cd | Ga | S | Se |
|---|---|---|---|---|---|
| $\varepsilon_s$, eV | -5.99 | -7.21 | -11.55 | -24.02 | -22.86 |
| $\varepsilon_p$, eV | -3.29 | -3.89 | -5.67 | -11.60 | -10.68 |

For comparison with experimental data, we calculated the dielectric susceptibility $\chi$. Experimental data are taken from [3, 4, 5], where the dielectric susceptibility was defined as the squared high frequency refractive index at $\omega \rightarrow 0$ [6]. The results of calculations are presented in Table 2.

Table 2. Calculated parameters of $AgGaS_2$ and $CdGa_2S(Se)_4$ crystals

| Bond type | $N_c$ | $d$, Å | $V_2$, eV | $V_3$, eV | $\alpha$, Å$^3$ | $X$ | $\gamma$ | $N_{theor}$ | $N_{exp}$ |
|---|---|---|---|---|---|---|---|---|---|
| $AgGaS_2$ | | | | | | | | | |
| Ag-S (s-p) | 4 | 2.556 | 3.31 | 2.80 | 5.847 | 0.044 | 0.5 | 1.97 | 2.37 |
| Ga-S (p-p) | 4 | 2.276 | 4.06 | 2.97 | 17.717 | 0.188 | 1.5 | | |

| | | | | | | | | | |
|---|---|---|---|---|---|---|---|---|---|
| $CdGa_2S_4$ | | | | | | | | | |
| Cd-S (s-p) | 4 | 2.52 | 3.41 | 2.19 | 12.552 | 0.098 | 0.5 | 2.25 | 2.34 |
| Cd-S (p-p) | 4 | 2.52 | 3.31 | 3.85 | 6.575 | 0.051 | 1.5 | | |
| Ga-S (p-p) | 4 | 2.31 | 3.94 | 2.96 | 17.199 | 0.174 | 1.5 | | |
| $CdGa_2Se_4$ | | | | | | | | | |
| Cd-Se (s-p) | 4 | 2.59 | 3.23 | 1.73 | 24.061 | 0.173 | 0.5 | 2.46 | 2.53 |
| Cd-Se (p-p) | 4 | 2.59 | 3.14 | 3.39 | 9.113 | 0.066 | 1.5 | | |
| Ga-Se (p-p) | 4 | 2.59 | 3.14 | 2.50 | 22.687 | 0.163 | 1.5 | | |

By determining the polarizability of $AgGaS_2$ and $CdGa_2S(Se)_4$ crystals and susceptibility $\chi$, it is possible to write the refraction index as $n^2 = 1 + 4\pi\chi$. In such a way, we obtain the values presented in Table 2. The performed calculation shows a satisfactory agreement with experiment: 96 and 97% for $CdGa_2S_4$ and $CdGa_2Se_4$, respectively, and 83% for $AgGaS_2$.

Thus, the results obtained in the present work confirm the possibility of application of this approximation for analysis of optical properties of complex crystalline compounds with a large number of atoms in a unit cell.


1. Walter A. Harrison. Elementary electronic structure. 1999.
2. Harrison W.A., Phys. Rev. B. 2006. V. 74. P. 205101.
3. Hobden M.V, Optical activity in an non-enantiomorphous crystal: $AgGaS_2$. Acta Cryst. – 1968. – V. A24, N3. – P. 676-680.
4. Дисперсия показателей преломления и двулучепреломления тиогаллата кадмия. Л.М. Сусликов, З.П. Гадьмаши, Д.Ш. Ковач и др. Оптика и спектроскопия. – 1982. – Т.53, № 3. – С. 480-488.
5. Дисперсия показателей преломления и двулучепреломления монокристаллов $CdGa_2Se_4$, Л.М. Сусликов, З.П. Гадьмаши, Т.А. Зацаринная, В.Ю. Сливка. Укр-физ. журнал. – 1987. – Т.32, N10. – С. 1481-1485.
6. Мосс Т., Баррел Г., Эллис Б. Полупроводниковая оптоэлектроника. М. Мир, 1976. 431 с.

# EBSD Based Studies of Strain Distribution in Weld Joint of NiCrFe Alloy

Khomenko V.[1], Borcha M.[1], Fodchuk I.[1], Balovsyak S.[1], TkachV.[2], Yuschenko K.[3], Zvyagintseva A.[3]

[1]*Yuriy Fedkovych Chernivtsi National University, Chernivtsi, Ukraine*
[2]*V.Bakyl Institute for Superhard Materials of NAS of Ukraine, Kyiv, Ukraine*
[3]*E. O. Paton Electric Welding Institute, Kyiv, Ukraine*

Electron backscattering diffraction technique (EBSD) in the scanning electron microscope has been applied for determination of local strain distributions near the cracks of NiCrFe weld joint, which appears in the areas of thermal influence. Since NiCrFe weld joints are well used in nuclear industry it was necessary to establish the reasons of formation of microcracks during the heat processing. In this study, the series of Kikuchi patterns from the local areas of specimen (40 $nm^2$) near the crack which have been obtained using the scanning electron microscope "Zeiss" Evo-50 with CCD detector and were analyzed [fig. 1]

To minimize the subjective factors during the image processing of EBSD and X-ray patterns, the methods of direct 2-D Fourier transform was used since Fourier spectra parameters and integral intensity along cross section of Kikuchi band are related to the interplanar distances. It gave possibility to determine strain distribution in local areas of samples.

It was established that for some cracks the dependence of strain on distance from the crack has exponential character. Maximal strain values in an area around crack are distributed along the low angle boundaries of subgrains. X-ray microanalysis investigations indicate the presence of impurities (predominantly C, O atoms), which can cause the formation of characteristic microstructure (precipitates).

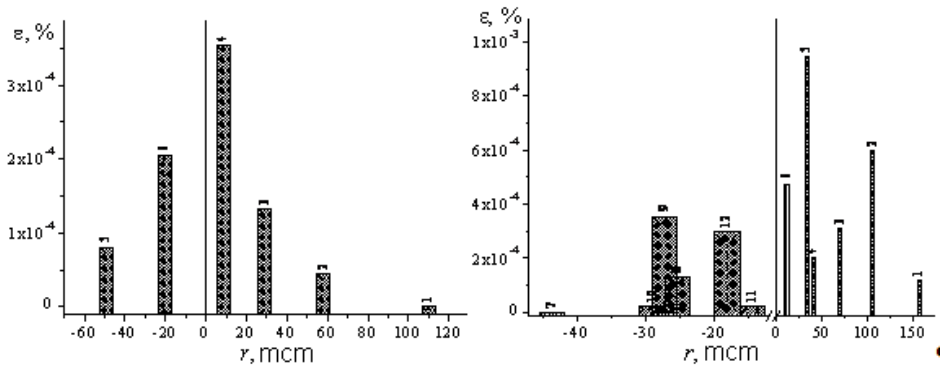


Fig 1. Strain-distance to crack dependence for two specimens from different groups.

1. Borcha M., Fodchuk I., Balovsyak S., Garabazhiv Ya., Tkach V. Phys. Status Solidi A. – 2011. – **208, № 11**. – P. 2591-2596.

# Influence of Impurities Gd and Yb on the IR Transmission of the Crystal ZnSe<Te>

Kinzerska O.V. [1], Makhniy V.P. [1], Maistruk E.V. [1], Pavluk M.D. [2]

[1] *Yuri Fedkovych Chernivtsi National University, Chernivtsi, Ukraine*
[2] *Vasyl Stefanyk Precarpathian NationalUniversity, Ivano-Frankivsk, Ukraine*

Due to the rapid development of infrared laser technology in recent years is a very urgent problem of the choice of highly transparent material for the manufacture of optical elements – windows, lenses, prisms, mirrors, beam splitters, etc. Successful promptness of optical, mechanical and thermal properties of zinc selenide led to its widespread use in the power of IR-optics. However, note that the good (50-60%) transmission in the spectral range of 5-20 microns has only a high-purity material. That fact is illustrated by curve 1 for monocrystal ZnSe, grown from the melt of stoichiometric composition under pressure of an inert gas. The main drawback of such designs is the poor resistance to high-power laser radiation, which can be increased nearly 5 orders of magnitude by doping during the growth of crystals in an isovalent impurity Te [1]. However, studies have shown that samples of ZnSe<Te> are almost opaque to radiation with a wavelength of $\lambda \geq 7$ microns, curve 2. This makes it impossible to use this material as an element of the optical systems, which contain the $CO_2$-laser ($\lambda_m \approx 10{,}6$ microns). We have found a significant decrease in absorption crystal ZnSe<Te> at $\lambda \geq 3$ microns with a result of doping with rare earth elements from the vapor phase. Transmittance at 10,6 microns reaches 30% and 50% for samples doped with Gd and Yb, as can be seen from the figure curves 3 and 4, respectively. Possible mechanisms responsible for the formation of IR transmittance are discussed.

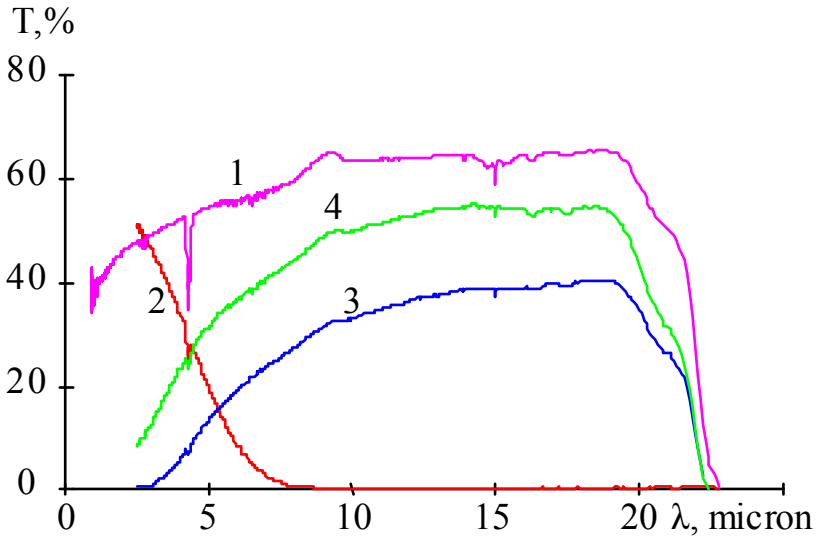


1. Ryzhikov V.D. Scintillation crystals of semiconductor compounds $A^{II}B^{VI}$. Preparation, properties and application. M.: NIITEKHIM, 1989, 123 p.

# Sensitive Elements of Magnetic Field Sensors Formation as Spin-Valve Type Multilayer Structures Based On Co and Cu

Kostenko M.V., Nahornyi S.S., Cheshko I.V.

*Sumy State University, Sumy, Ukraine*

Multilayer spin-valve structures with spin-dependent electron scattering based on Co and Cu are widely used in modern micro-instrument engineering and sensor techniques as sensing elements for high density recording systems. In this work we study the magnetoresistive properties of model film systems based on Co and Cu in the form of sandwich structures, received under the scheme magnetic/nonmagnetic/magnetic layer, which is the basis of simple spin valves and modified spin valves, in which as upper or lower magnetic layer used multilayer Co/Cu with different number of fragments.

The experiments have been performed under high vacuum condition (the base pressure was $10^{-4}$Pa) and samples have been prepared by method of thermal evaporation. The layer thickness during the deposition process was controlled by the quartz resonator method. Results of the study magnetic properties of film samples in the form of spin-valves Co/Cu/Co/S(substrate) fixed magnetic layer thickness of 20 nm Co (bottom) and Co 5 nm (upper) shows, that for such systems value magnetoresistance (MR) at room temperature in the range of 0,1-0,2 %. The annealing to temperatures 700 K and 900 K simple and modified spin-valve based on Co and Cu leads to a slight increase in the values of MR and significant changes in the forms of dependency MR. These changes can be explained by the processes of mixing layers as a result of thermal diffusion, which may in turn lead to the formation of granular state of magnetic Co solid solution in the matrix.

Analyzing the experimental data we can conclude that multilayer film system in the form of spin-valve Co(5)/Cu(8)/Co(20)/S advisable to modify using as the upper magnetic layer multilayer based on Co and Cu. This modification will increase the value of MR, increases performance and somewhat improves temperature stability of the system. These characteristics can be useful in the manufacture of electronic components spintronics working in digital mode and the manufacture of magnetic memory elements, switches and so on.

This work was done in the framework of the project № 52.20.01-01.15/17.3Ф

1. Fert A. The origin, development and future of spintronics // Successes of physical sciences – 2008. – V. 42. – P. 1336-1348.
2. Yang G.H. Thin Film Magnetoresistive Sensors // Thin Solid Films – 2012. – V. 42. – P. 12946-12962.

# Investigation of $Zr_{1-x}Ce_xNiSn$ Thermoelectric Material

Romaka V.A.[1,2], Krayovskyy V.Ya.[2], Rogl P.[3], Romaka L.P.[4], Stadnyk Yu.V.[4], Kaczorowski D.[5], Korzh R.O.[2], Horyn A.M.[4]

[1]*Ya. Pidstryhach Institute for Applied Problems of Mechanics and Mathematics National Academy of Sciences of Ukraine, Lviv, Ukraine;*
[2]*National University "Lvivska Politechnika", Lviv, Ukraine;*
[3]*Universität Wien, Wien, Österreich;*
[4]*Ivan Franko National University of Lviv, Lviv, Ukraine;*
[5]*W. Trzebiatowski Institute of Low Temperature and Structure Research, Polish Academy of Sciences, Wroclaw, Poland*

The increasing of the thermoelectric power factor $Z^*(x)$ values while doping *n*-ZrNiSn intermetallic semiconductor with Ce atoms was obtained for the first time. It was found that Ce atoms are in $Ce^{4+}$ valence state that generated structural defects of donor nature in the crystal.

Attempts to get thermoelectric materials with high efficiency conversion of thermal energy into electrical by doping *n*-ZrNiSn with rare-earth metals (R) have failed [1] because the default valence state in rare earth metals is $R^{3+}$. As a result, in the crystal substitution of Zr atoms by R ones generates the acceptor structural defects. It caused a drift of the Fermi level from the conduction to the valence band and decreasing of resistivity and thermopower coefficient values.

Taking into account the feature of Ce to change the valence state from $Ce^{3+}$ to $Ce^{4+}$, the crystal and electronic structures, temperature and concentration dependences of magnetic susceptibility, electrical resistivity and thermopower coefficient of $Zr_{1-x}Ce_xNiSn$ thermoelectric material were investigated in the ranges: K, $x = 0.01–0.10$, $H \leq 10$ kOe.

A complex mechanism of the compensation degree change in $Zr_{1-x}Ce_xNiSn$ was revealed as a result of the simultaneous reduction in the number of defects with donor nature (Ni atoms in 4*a* positions of Zr) and generation of defects with donor nature in the same positions due to substitution of Zr atoms by Ce in $Ce^{4+}$ valence state. Investigated solid solution $Zr_{1-x}Ce_xNiSn$ is a promising thermoelectric material.

1. V.A. Romaka, V.V. Romaka, Yu.V. Stadnyk. *Intermetallic semiconductors: properties and applications* // Lvivska politekhnika, Lviv, 2011, 488 p.

# Influence of Pressing Conditions on Thermoelectric Properties of $PbTe-Sb_2Te_3$

Kryskov Ts.A., Lyuba T.S., Optasyuk S.V., Tsykaniuk B.I., Rachkovsky O.M.

*Ivan Ohienko Kamyanets-Podilsky National University, Kamyanets-Podilsky, Ukraine*

Thermoelement legs are made by the method of cold pressing. Samples are maintained at pressing some time for improving of uniformity and partial relaxation of mechanical stress. The influence of maintaining time in the state of stress in samples on their thermoelectric properties was investigated.

The compounds $PbTe-Sb_2Te_3$ with concentration of 0,3 mol.% $Sb_2Te_3$ were synthesized by direct fusion method with mixing of the components at the melting point. Pre-cleared Pb, Te and Sb were used as initial components for synthesis. $Sb_2Te_3$ compound was synthesized in advance. All materials of B4 purity class were taken in stoichiometric ratio. From the samples were formed compacts by grinding and pressing at pressure 0,2 GPa with maintaining time 5, 10 and 15 minutes.

Temperature dependences of the Seebeck coefficient were determined by standard method [1].

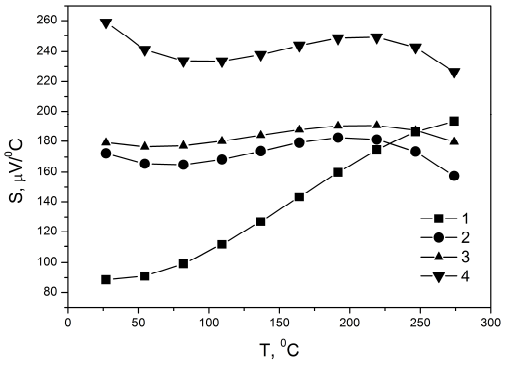


Fig. 1. Temperature dependence of the Seebeck coefficient: 1 – PbTe (5 min), 2 – PbTe + 0,3 mol. % $Sb_2Te_3$ (5 min), 3 – PbTe + 0,3 mol. % $Sb_2Te_3$ (10 min), 4 – PbTe + 0,3 mol. % $Sb_2Te_3$ (15 min)

The temperature dependences of the Seebeck coefficient for the samples show that the value of the S for PbTe increases throughout the temperature range. Seebeck coefficient for PbTe + 0,3 mol. % $Sb_2Te_3$ solid solutions increases with the pressing time. For samples 2-4 curves of the temperature dependence S (T) are identical. The sharp increase in S compared with other observed for sample 4. The difference in curves 1 and 2-4 can be explained by the influence of impurities on the plasticity of the material.

1. I.A. Drabkin, O.E. Kvyatovsky, B.Ya. Moyjes, L.M. Sysoyeva. FTS, 21, 188 (1987).

# Kinetic Phosphorescence of Ceramics ZnS-Cu from a Doze of a Proton Irradiation

Kuchakova T., Makara V., Kuchakova I.

*National University Taras Shevchenko, Kyiv, Ukraine*

Was studied kinetic of the light sum accumulation at an isothermal mode after an irradiation by protons of ceramics ZnS-Cu by dozes 1014, 1015p/sm2 with energy 50 Mev. The excitation luminescence and the light sum accumulation were carried out by integrated study x-ray tube (Mo, 35κV, 10 mA) at temperature 85K. In work the method accumulation of the light sum is used at increase of time of excitation. The method allows qualitatively estimating changes in system of local levels of samples.

The researches stationary luminescence have shown, that at an irradiation of initial samples the doze 1014p/sm2 observes increase of intensity roentgen luminescence (RL) and the size reserved the light sum under a curve phosphorescence (Ph) grows. The fall of intensity RL and strong reduction reserved the light sum under a curve Ph is characteristic for samples irradiated by a doze 1015p/sm2. For all three sets of samples experimental dependence's of recession of intensity Ph after the first minute of attenuation is satisfactory approximation by hyperbolic dependence. After an irradiation of ceramics by protons has changed kinetic radiation relaxation Ph. The increase of a parameter of a degree hyperbola $\alpha = Ln(J) / Ln(t)$ is established, for the irradiated samples, where **J** - intensity Ph, **t** - the time of registration Ph, from time of excitation, in an initial sample α decreases with increase of a degree of excitation. The received dependence's of rate of accumulation the light sum (**t**) during an interval of registration Ph testify to participation in attenuation of two grades of traps differing on the mechanism radiation of transitions. And, the presence of radiating defects differently changes processes of the light sum accumulation on these grades of traps. For initial sites Ph τ depends on time of achievement of saturation Ph and size of intensity RL, it is supposed that this grade of a trap is a part of a uniform complex responsible for "green" a luminescence in ZnS-Cu. The character of change τ for the second grade of traps explains by increase of channel recombination after a proton irradiation. The reduction increase of values τ for samples irradiated by a doze 1014p/sm2 contacts to increase of concentration interstitial of zinc (Zni) responsible for long low- temperature Ph. For samples irradiated by a doze 1015p/sm2 the received values t are explained by possible displacement Zni in regular places, that is reduction of concentration Zni and vacancies S. The fall radiation of ability of samples irradiated by a doze 1015p/sm2 is explained by occurrence of the center's nonradiative recombination.

# Hand-Held Gamma Detector Based on High-Pressure Xenon Gas

Kutny V.E., Rybka A.V., Pudov A.O.

*National Science Center "Kharkov Institute Physics and Technology", Kharkiv, Ukraine*

Gamma-radiation detectors based on high-purity Xenon (HPXe) gas at high pressure have very promising potential applications, including security applications (detecting radioactive materials at ports of entry), as well as fuel cell lifecycle monitoring. HPXe detectors have wide operation temperature range, do not require cryogenic cooling, can have large sensitive volume, and yet have excellent detecting qualities. The goal of this presentation is to report on the progress of the project work aimed at developing a hand-held HPXe detector with optimized parameters.

# Structure and Morphology of Alumina Materials Prepared by Aluminum Nitrate Nonahydrate Decomposition

Myronyuk I.F., Mandzyuk V.I., Sachko V.M.

*Vasyl Stefanyk Precarpathian National University, Ivano-Frankivsk, Ukraine*

The paper studied the mechanism of $Al(NO)_3 \cdot 9H_2O$ decomposition in argon atmosphere and alumina phase formation in the range of 100-1200°C.

Thermogravimetry dependences of $Al(NO)_3 \cdot 9H_2O$ decomposition, as well as XRD and IR spectroscopy data of products of its thermodestruction allowed to find out that chemical state of precursor at growth temperature to 1200°C changes according to scheme:

$Al(NO_3)_3 \cdot 9H_2O$ (100-140°C) → $[Al(OH_2)_6]^{3+} \cdot 3NO_3^-$ (140-152°C) → $[AlOH(OH_2)_5]^{2+} \cdot 2NO_3^-$ (152-210°C) → $AlONO_3 \cdot H_2O$ (210-525°C) → AlOOH (525-1000°C) → γ-$Al_2O_3$ (1100°C)→ α-$Al_2O_3$.

The peculiarity of this process is that amorphous and crystalline motifs of boehmite AlOOH consist of globules of 6-10 nm in diameter at temperatures above 210°C (fig. 1). The globules of amorphous phase consist of randomly combined alumina monomer chains –AlO(H)–O–AlO(H)– of 1-5 nm in length. Mesoporous aluminum hydroxide with a pore size of 2.4-4.9 nm, pore volume of 0.138 $cm^3 \cdot g^{-1}$, and specific surface area of 175 $m^2 \cdot g^{-1}$ is formed at 350-525°C.

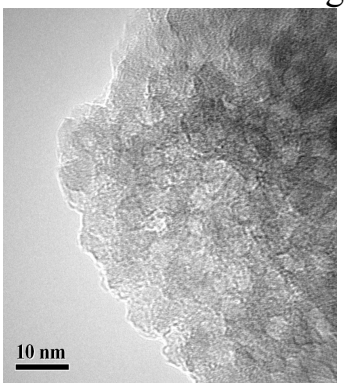


Fig. 1. Globular structure of phase AlOOH, formed at 480°C.

The calcination of precursor at 850°C forms a mesoporous γ-$Al_2O_3$ with pore size of 5.0 nm, pore volume of 0,084 $cm^3 \cdot g^{-1}$, and specific surface area of 72 $m^2 \cdot g^{-1}$. The increase of γ-$Al_2O_3$ lattice parameter on 2 % is due to the Laplace pressure that occurs in particles of nanometer scale. The countering to approachment of aluminum atoms in the structure of the oxide material reduces interatomic interaction in Al – O-chains and leads to their extension.

α-$Al_2O_3$ prepared at 1100°C has a heterogeneous porous structure and contains mesopores of 8-40 nm in size. Their volume is 0.070 $cm^3 \cdot g^{-1}$ and specific surface area 13 $m^2 \cdot g^{-1}$.

# The Synthesis of $Ti(OH)_3Cl{\cdot}2H_2O$ Crystal Hydrate Precursor

Myronyuk L.S.[1], Sachko V.M.[1], Karpets M.V.[2],
Mandzyuk V.I.[1], Myronyuk I.F.[1]

[1]*Vasyl Stefanyk Precarpathian National University, Ivano-Frankivsk, Ukraine*
[2]*Frantsevich Institute for Problems of Materials Science of NAS Ukraine, Kyiv, Ukraine*

The investigations related to the receipt of $Ti(OH)_3Cl{\cdot}2H_2O$ crystal hydrate compound, used as a precursor to produce of $TiO_2$ nanocrystalline modifications (rutile or anatase), are conducted.

This crystal hydrate compound is crystallized from $[Ti(OH_2)_6]^{3+}{\cdot}3Cl^-$ solution. A solution of titanium aqua-cations is obtained by mixing $TiCl_4$ with concentrated hydrochloric acid:

$TiCl_4 + 6H_2O = [Ti(OH_2)_6]^{3+}{\cdot}3Cl^- + 1/2Cl_2$.

Coordinating bond of water molecules with titanium atoms in precursor cations reduces the activation energy of the reaction of their dissociation because chemical equilibrium in a solution is disturbed at the temperature more that 30°C:

$Ti^{3+} + H_2O + Cl^- \rightarrow Ti(IV)OH + H^+ + 1/2Cl_2$.

$[Ti(OH)(OH_2)_5]^{3+}$ cations formed, then also change their chemical state under the temperature influence, increasing the hydroxility degree of titanium atoms:

$[Ti(OH)(OH_2)_5]^{3+} \rightarrow [Ti(OH)_2(OH_2)_4]^{2+} + H_2O$.

The crystal hydrate form of titanium precursor is obtained as result of "cold" dehydration of solution. For this purpose, the partial pressure of $H_2O$ and HCl molecules was low over the solution, using CaO adsorbent. $[Ti(OH)_3(OH_2)_3]^+{\cdot}Cl^-$ complex compound is transformed into $Ti(OH)_3Cl{\cdot}2H_2O$ crystal hydrate at the end of the dehydration process.

Needle-shaped rutile nanoparticles of 3-5 nm in diameter and 12-18 nm in length are formed from the precursor solution in an aqueous medium at a temperature of 40°C.

Spherical anatase nanoparticles of 4-6 nm in diameter are formed at the presence in solution of small amount $SO_4^{2-}$or $PO_4^{3-}$ anions-promoter.

# Taking into Account the Orientation of Disc-Shaped Clusters in the Static Debye-Waller Factor Calculation

Ostafiychuk B. K., Umantsiv M. M., Yaremiy I. P., Tomyn U. O., Yaremiy S. I.

*Vasyl Stefanyk Precarpathian National University, Ivano-Frankivsk, Ukraine*

Presence of defects in crystals affects their physical properties. It is important to know not only the type, size and concentration of existing defects, but in the case of spherically asymmetric defects (dislocation loops, disk-shaped clusters) also their spatial orientation. X-ray diffractometry enables to define these characteristics. A powerful theoretical tool is statistical dynamical theory of X-rays scattering [1]. The presence of defects oriented perpendicular to the diffraction vector, leads to higher intensity of X-rays diffuse scattering than presence of defects oriented at some angle to the diffraction vector [2]. The lowest diffuse scattering values are observed when defects are located in parallel to the diffraction vector planes. In X-ray diffractometry it leads to a change in values of the crystallographic parameters such as static Debye-Waller factor $E = \exp(-L)$ and the absorption coefficient due to diffuse scattering on defects $\mu_{DS}$. In the presence of a disc-shaped clusters in a crystal static Debye-Waller factor can be given by the formula:

$$L_{d.cl} = \frac{3\Gamma\varepsilon R_0}{4\pi}\frac{c(Hh_p)^{3/2}}{V_c}\eta(\vec{H}_o,\vec{n}_{cl})$$

where $c$ is a clusters concentration, $V_c$ – crystal unit cell volume, $h_p$ – cluster thickness, $R_0$ – an average cluster radius, $\varepsilon$ – cluster boundary deformation, $\Gamma = (1+\nu)(1-\nu)^{-1}/3$, ν – Poisson's ratio, $H$ – module of diffraction vector, $\vec{H}^0 = \vec{H}/H$ – unit vector in the diffraction vector direction, $\vec{n}_{cl}$ – unit normal to the cluster surface. The assumption that the disk-shaped clusters are formed in all equivalent crystallographic planes with equal probability and averaging over all their probable orientations lead to values of $\eta(\vec{H}_o,\vec{n}_{cl})$ close to 0.5. Since the value of $\eta(\vec{H}_o,\vec{n}_{cl})$ depends only on the relative orientation of the vectors $\vec{H}^0$ and $\vec{n}_{cl}$, then for calculating the static Debye-Waller factor in the case of a presence in a crystal of disc-shaped clusters only certain orientations one can use the values obtained by the authors of [2].

1. Даценко Л. И. Динамическое рассеяние рентгеновских лучей реальными кристаллами / Л. И. Даценко, В. Б. Молодкин, М. Е. Осиновский. – К. : Наукова думка, 1988. – 200 с.
2. Вплив анізотропії в орієнтації радіаційних дефектів на значення поглинання Х-променів / Б.К. Остафійчук, І.П. Яремій, У.О. Томин, С.І. Яремій // Фізика і хімія твердого тіла. – 2013. – Т. 14, № 1. – С. 202-209.

# Physico-Chemical Interaction in Systems Based on Quaternary Compounds Cu(Ag)In(Cr)$P_2S_6$($Se_6$)

Potorij M.V., Milyan P.M., Motrya S.F., Tovt V.V.

*Uzhgorod National University, Uzhgorod, Ukraine*

The investigation of phase equilibria in systems based on Cu(Ag)In(Cr)$P_2S_6$($Se_6$) compounds was held with the purpose of studying the possibility of formation of solid solutions. Electronic structure of atoms, ionic and covalent radii, electronegativity of the components, crystal structure data of quaternary compounds, similarity of chemical bonding and structure of initial substances indicate the possibility of formation of solid solutions between them.

In all investigated systems there are substitutional solid solutions where the substitution of singly charged ($Cu^+ \leftrightarrow Ag^+$) and triple charged ($In^{3+} \leftrightarrow Cr^{3+}$) cations and double charged anions ($S^{2-} \leftrightarrow Se^{2-}$) is realizing.

Phase diagrams of these quazibinary systems can be divided into three types according to the type of physico-chemical interaction:

The formation of continuous solid solutions between the initial quaternary compounds ($AgInP_2Se_6$-$CuInP_2Se_6$, $AgInP_2S_6$-$AgInP_2Se_6$).

Peritectic interaction with limited solubility of components ($CuInP_2S_6$-$AgInP_2S_6$, $CuCrP_2S_6$-$AgCrP_2S_6$, $CuInP_2S_6$-$CuInP_2Se_6$).

Eutectic interaction with limited solubility of components ($CuCrP_2S_6$-$CuInP_2S_6$).

We explain that physico-chemical interaction in the studied systems depends on the size of ions, electronegativity, crystal structure data, the type of formation and the difference of melting points of quaternary compounds, as well as the values of average first quantum number, ionic component of chemical bonding and polarization properties of ions.

# Quasichemical Models of Point Defects in CdTe:Br

Pysklynets U.M.

*Ivano-Frankivsk National Medical University, Ivano-Frankivsk, Ukraine*

The influence of dopant and annealing conditions on electrical properties of cadmium telluride monocrystals doped with bromine, grown by Bridgman technique and annealed in an atmosphere of cadmium at temperatures $T$ = (800-1100) K and pressure of cadmium vapour $P_{Cd}$ = ($10^3$-$10^5$) Pa have been studied and analyzed. To explain the electrical properties of CdTe:Br two models of quasichemical reactions of defect formation have been considered. In these models, addition to own point defects $V_{Cd}^{-}$, $V_{Cd}^{2-}$, $Te_i^{-}$, $V_{Te}^{2+}$, $Cd_i^{2+}$, it has been taken into account that all introduced impurity in the studied range of technological parameters is completely dissolved as singly ionized defects $Br_{Te}^{+}$, and its donor effect can be compensated by: 1) own acceptor point defects, in particular $Te_i^{-}$, $V_{Cd}^{2-}$, $V_{Cd}^{-}$; 2) complexes of impurity defects of substitution with own point defects $(Br_{Te}^{+}V_{Cd}^{2-})^{-}$.

Based on the model of defect subsystem of the material without associative centres experimental isothermal and isobaric dependences of the concentration of current carriers couldn't be explained satisfactorily by compensation of donor action of bromine dopant by only own point defects. In the case of the model of compensation of bromine dopant by complexes of impurity defects of substitution with own point defects $(Br_{Te}^{+}V_{Cd}^{2-})^{-}$, calculated dependences of concentration of current carriers on the annealing process conditions consistent with experimental data both quantitatively and qualitatively.

The nature of the curves of the concentration of current carriers is explained by dependences of concentration of point defects in the material. Dominant defects in CdTe:Br are singly ionized impurity bromine atoms in the tellurium sublattice $Br_{Te}^{+}$ and acceptor complexes $(Br_{Te}^{+}V_{Cd}^{2-})^{-}$.

With the increase of the partial pressure of cadmium vapour concentration of associative centres $(Br_{Te}^{+}V_{Cd}^{2-})^{-}$ decreases. This leads to the almost linear increase of the concentration of current carriers that satisfactory agreement with experiment. Changing the annealing temperature in the range of (800-1100) K at constant pressure of cadmium vapour practically does not change the ratio between the concentrations of $Br_{Te}^{+}$ and $(Br_{Te}^{+}V_{Cd}^{2-})^{-}$, which leads to keeping of the electron concentrations at the same level.

In quasichemical model of defect subsystem of CdTe:Br crystals equilibrium constant and enthalpy of quasichemical reaction that describes the formation of acceptor complexes of impurity defects of substitution with own point defects $(Br_{Te}^{+}V_{Cd}^{2-})^{-}$ have been taken equal to: $K = 1 \cdot 10^{-22} \exp(1.15 / kT)$.

# Elastic and Non-Elastic Properties of Auxetic Crystals

Raransky M.D., Oliynych-Lysyuk A.V., Taschuk O.Yu., Kurek E.I.

*Yu.Fedkovych Chernivtsi National University, Chernivtsi, Ukraine*

Auxetic structures characterized by an abnormally negative value of the Poisson coefficient belong to materials with essentially nonlinear deformation properties and make it possible to vary and improve considerably the properties of the existing structural materials. The first reports on the existence of auxetic structures capable of expanding in the direction normal to their tension appeared long ago [1]. However, the problem of experimental, as well as theoretical study of their properties is still far from being solved. This applies especially to partially auxetic crystalline materials whose properties change considerably as a function of the direction in crystal and of the state and dynamic properties of their defective subsystems.

Beryllium belongs to partially auxetic hexagonal crystals and has negative values of tensor components of the Poisson coefficients $\nu_{ij}$ only in certain crystallographic directions [2]. Moreover, both positive and negative values of $\nu_{ij}$, due to specific elastic properties of this structural material, lie in the range from 0.02 to 0.05, which has essential impact on the behaviour of its defective subsystems, specifically the "dislocation-impurity" one.

In this paper, we have studied the elastic (effective shear modulus $G_{ef}$) and non-elastic (low-frequency internal friction $Q^{-1}$) properties of beryllium of various purity level: from 98% to 99.95 % Be on the as-prepared samples, as well as after natural aging. Characteristics in question were studied with a change in temperature in the range from -50 to 450 □C, amplitude of torsional strain in the range from 1 to 70□$10^{-6}$ and time with different temporal aging bases. It is shown that the anomalies of $G_{ef}$ and $Q^{-1}$ in Be in the investigated temperature range "correlate" with the appearance of auxetic properties.

[1] D.A.Koniok, K.V.Woiciechovski, Yu.M.Pleskachevsky, and S.V.Shilko, Mechanics of Compositional Materials and Structures, 1(35) (2004).
[2] R.V. Goldstein, V.A. Gorodtsov, and D.S. Lisovenko, Letters on Materials, 3 (7), (2013).

# Phase Relations in the YbTe-SnTe-$Bi_2Te_3$ System

Rasulova K.D. [1], Aliyev Z.S.[2], Yusibova I.M. [2], Babanly M.B.[2]

[1]*Department of General and Inorganic Chemistry, BSU, Baku, Azerbaijan*
[2]*Institute of Catalysis and Inorganic Chemistry of ANAS, Baku, Azerbaijan*

Tellurides of bismuth and tin and complex phase on their based are perspective materials for creation of novel high-performance materials for thermoelectric and topological insulators.

This work presents the results of investigation of phase relations in the YbTe-SnTe-$Bi_2Te_3$ system.

The samples were prepared by melting of the high purity elements in evacuated ($10^{-2}$Pa) graphitized ampoules. The synthesis was realized in a tube furnace. The ampoules were heated to maximal temperature 1200 K. Then in order to achieve a state close to equilibrium, the reaction mixture was pressed into pellets and annealed at 800-1000K for 1000h.

DTA (NETZSCH 404 F1 Pegasus system), XRD (Bruker D8 ADVANCE diffractometer) and SEM–EDS (FEI Quanta™ 250 scanning electron microscope with Oxford Instruments energy dispersive X-ray spectrometer) techniques were employed to check the purity of the synthesized starting compounds and analyze the samples.

Based on experimental data the T-x phase diagrams of YbTe-SnTe, YbTe-$Bi_2Te_3$ systems, some isopleth sections, isothermal sections at 300 and 800 K of the phase diagram, as well as the projection of the liquidus surface (T<1400K) have been constructed.

It was found that the quasi-binary system YbTe-SnTe characterized by formation of continuous high-temperature solid solutions field with a cubic structure (α-phase). At temperatures below 950K the solid solutions are decompose. Solubility of the YbTe and SnTe are determined to be about 35 and 3 mol% at room temperature.

The system YbTe-$Bi_2Te_3$ is quasi-binary too and has a eutectic phase diagram. According to the SEM and XRD samples quenched from 800 K, the solubility YbTe in $Bi_2Te_3$ is about 12 mol%. Isothermal section of the phase diagram of the system YbTe-SnTe-$Bi_2Te_3$ at 300 and 800 K shows that the dominant role in the formation of phase areas in the subsolidus the solid solutions based YbTe are playing. This solid solutions form tie lines with all other phase.

*The work was supported by the Science Foundation of the State Oil Company of Azerbaijan Republic (Grant for the project "Preparation and investigation of new functional materials based on complex metal chalcogenides for alternative energy sources and electronic engineering", 2014).*

# Vapor Phase Crystal Growth and Properties of Ag- and Cu-doped $PbI_2$ Crystals

Rybak O.V.

*Lviv Polytechnic National University, Lviv, Ukraine*

Thin-film light-sensitive $PbI_2$-Ag and $PbI_2$-Cu structures are promising detecting media [1]. Doping of lead iodide (Ag, Cu) improves its photosensitivity and enhances non-linear optical effects in it.

The purpose of this work is to examine the effect of silver and copper acceptor impurities on the vapor phase growth of lead iodide crystals in a closed system in the presence of excess iodine and on the properties of the crystals.

Under optimal conditions for the preparation of undoped lead iodide single crystals, we studied the effect of dopant concentration in the source material (0,001 to 30 at %) on the rate of $PbI_2$ transport and the dopant concentration in the single crystals. The present results demonstrate that, at dopant concentrations in the source material from 0,001 to 0,1 at.%, the mass transport rate is on the same order as in undoped crystals. The dopant concentration in the grown single crystals is proportional to that in the source material. The rate of mass transport decreases with increasing (0,5 to 30 at.%) dopant concentration in the source material. At dopant concentrations within 1 at. %, the mass transport rate is on the same order as in undoped $PbI_2$. Further increasing the dopant content in the range 1-5 at.% leads to a sharp drop in mass transport rate: from $3\times10^{-5}$ to $2\times10^{-5}$ mol/($m^2$s). At high doping levels (10-30 at.%), the mass transport rate decreases more gradually: from $1,93\times10^{-5}$ to $1,72\times10^{-5}$ mol/($m^2$s) in the case of copper and from $1,31\times10^{-5}$ to $0,88\times10^{-5}$ mol/($m^2$s) in the case of silver. X-ray microanalysis results demonstrate that, at dopant concentrations in the source material from 0,1 to 0,5 at.%, the doping level of the single crystals is on the same order. At dopant concentrations in the source material from 1 to 30 at.%, the doping level of the single crystals is an order of magnitude lower. Increasing the dopant concentration in the system from 5 to 30 at.% reduces the number and dimensions og single crystals and leads to deposition of polycrystalline material.

Copper doping of $PbI_2$ in the range 0,001-0,01 at.% shifts the excitonic band in its low-temperature (5 K) photoluminescence spectrum to longer wavelengths, reduces its intensity, and increases its full width at half maximum. In addition, a band emerges around 600 nm, and its intensity increases with copper content. This band was assigned by Derenzo et al. [2] to a copper-related deep acceptor level.

1. Indutnyi I.Z., Kostyshin M.T., Kasyarum O.P. Fotostimulirov. vzaimodeistv. v struct. metal-poluprov. Kiev: Nauk. Dumka, 1992, 240 c.

2. Derenzo S.T., Bourret E., Yan Z. et al. Experimental and theoretical studies of donor-acceptor scintillation from $PbI_2$// J.Lumin.- 2013, V.134, p.28-34.

# Particularities of the Thermodynamic Functions of Fermi Gas of Electrons in Strongly Anisotropic Materials

Tovstyuk C.C.

*Lviv Polytechnic National University, Lviv, Ukraine*

Thermodynamic functions of the electron gas in strongly anisotropic materials have a number of particular propertieseven in a quasi-classical case. The presence of closed and openedequipotential surfaces leads to no monotonic dependences of the internal energy*(U)* and heat capacity*(C)*as functions of the anisotropy parameter *(γ)*in one particle spectrum withFivazdispersion (FD). These peculiarities are explained by transition from closed to opened equipotential surfaces, which are typical for such crystals. It is shown that changingofγ affects the open equipotential surfacessignificantly then the closed. We obtain the maxima shiftsof *U* and *C* into low temperatures while theanisotropy parameter increases. It means that the transition from closed to open equipotential surfacesoccurs at lower values of energy and indicates the limits of application of the parabolic dispersion(PD) while anisotropy increases.

For Fermi – gas we compared the thermodynamic functions for FD and PD in one particle spectrum.For strong anisotropic case we got the analytical expressions for the internal energy,Gibbs potential*(Ω)*,specific heat and entropy*(S)* as functions of temperature*(T),* chemical potential*(μ)* and anisotropy parameter and compared them with the investigations completed using theknown expression for thermodynamic functions in PD both for closed and opened equipotential surfaces. In all the cases the values of thermodynamic functions are smaller for strong anisotropic crystals and their temperature dependences are much weaker than in materials with the parabolic dispersions. These dependences are still smaller for opened equipotential surfaces in strong anisotropic crystals. We obtained the region of positive values of thermodynamic potential for strong anisotropic Fermi gas by small values of chemical potential. The similar result for phonon gas may leadto negative value of the thermal expansion coefficient, known in GaSe. This feature is due to the one particle energy spectrum (FD), and does not associate with the presence of bending vibrations, which were not found experimentally in GaSe. The dependences of the internal energy of the chemical potentialis controversial for FD and PD. So there is a region of small energies (small μ) for which the internal energy of strong anisotropic Fermi gas dominates. Whileμ increases the energy of the electron gas with PD increases strongly and begins to dominate. Further increasing of μ leads to the prevalence of PD internal energy more and more explicitly.Moving from closed to opened equipotential surfaces we obtained the particular points in specific heat and entropy.

# The Phenomenon of Double Diffraction at TEM-identification of Mn-like phases in Fe-based Spinning Ribbons

Velikanova T.A.[1], Karpets M.V.[1], Kuprin V.V.[1],
Graivoronskii N.A.[2], Zaslavskii A.M.[3]

[1]*Institute for Problems of Materials Science, NAS of Ukraine, Kiev, Ukraine*
[2]*National Technical University of Ukraine "Kyiv Polytechnic Institute", Kiev, Ukraine*
[3]*National University of Life and Environmental Scienses of Ukraine*

The presence of nanostructural stable and/or metastable α- and β-Mn-like phases in high-speed crystallizated Fe-based materials improves useful properties significantly. There are specific peculiarities at identification of Mn-like phases, main causes of which are almost identity of sets of interplanar distances its crystal structures and the phenomenon of double diffraction.

For example, *by the XRD-method* (Fig. 1) the phase composition of $Fe_{75,5}Mo_{10}C_{14,5}$ % at. spinning ribbons (flat molding spinning method, cooling rate ~$10^6$ K/c, ribbon thickness 30 mkm) is almost *π-phase*: 96π + 4γ.

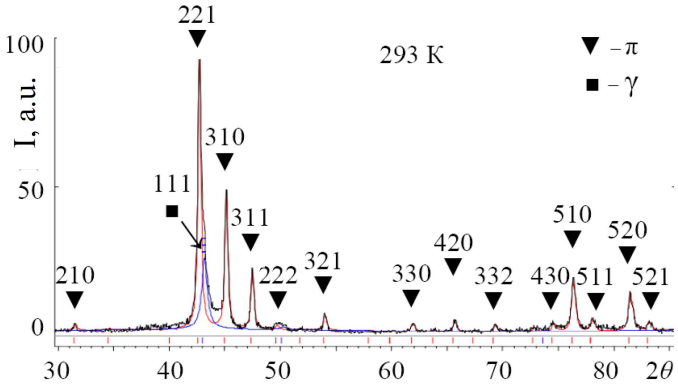


Fig. 1. Rietveld-analysis (Powder Cell 2.4-program) of the XRD-pattern (DRON-UM1, Cu*K*α-radiation, monochromator on diffracted beam) from a powder of $Fe_{75,5}Mo_{10}C_{14,5}$ spinning ribbons: π – β-Mn-like phase, $P4_132$, $a$=0,6370 nm; γ – fcc-phase, $Fm\bar{3}m$, $a$=0,3646 nm.

In contradiction to XRD-patterns *by the TEM-method* the phase composition of $Fe_{75,5}Mo_{10}C_{14,5}$ spinning ribbons is almost *χ-phase* (α-Mn-like phase, $I\bar{4}3m$, $a_{TEM}$ ≈ 0,891 nm): χ + γ. This is evidenced by the fact that the most selected areas TEM-diffraction studies found the reflex corresponding to interplanar distance 0,63 nm for α-Mn-like structure only but not for β-Mn-like structure within „fine" grids. However, the angle between the corresponding planes was incorrect. Other a few selected areas TEM-diffraction studies found the reflexes of γ-phase as „large" grid.

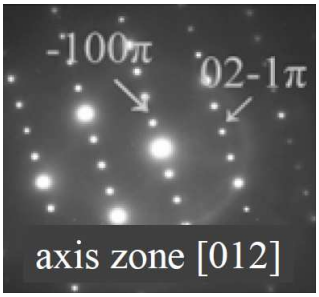


Fig. 2. TEM-pattern of $Fe_{75,5}Mo_{10}C_{14,5}$ spinning ribbon (JEM-100, ion etching, 2,25 nm × мм)

Discovered contradictions may well be explained by phenomenon of double diffraction. Thus, the (100)-type reflexes, prohibited by extinction laws in the β-Mn-type structure appear by the double diffraction from a family of planes {110}π and {111}π, wherein d(100)π ≈ d(110)χ (Fig.2).

# Structural changes in La, Ga: YIG under laser irradiation

Yaremiy I.P., Kozub V.V., Yaremiy S.I., Kravets V.I.

*Vasyl Stefanyk Precarpathian National University, Ivano-Frankivsk, Ukraine*

Laser irradiation of high power acting on monocrystalline ferrite-garnet films (FGF) significantly affects their structural reorganization. With the help of laser irradiation can effectively recover the crystal structure of monocrystalline films and deliberately generate defects of different nature, which cause certain characteristics of irradiated samples. The nature of the structural transformations in the irradiated sample essentially depends on the ratio between the energy of the quantum laser radiation hv and a band gap of monocrystalline FGF $E_g$.

Irradiation La, Ga-substituted FGF, implanted with ions of fluoride in the dose range of $1 \cdot 10^{13}$ - $1 \cdot 10^{14}$ $cm^{-2}$ with the energy of 90 keV, was performed by pulses YAG: *: $Nd^{3+}$*- of laser, which worked in the modulated merit mode, with radiation energy – $E$ = 0,04 J ($\tau$ = 15 ns, f = 56 Hz) for t = 30 s. The structure of the subsurface layers FGF was investigated by the method of X-ray structural analysis.

With the implantation of fluorine ions at doses of $6 \cdot 10^{13}$ $cm^{-2}$ and $1 \cdot 10^{14}$ $cm^{-2}$ deformation profile is nonmonotonic with decreasing, almost the equal speed in both directions from the position where the deformation is maximal. It is established that under the laser irradiation there is a decrease in deformation maximum value and its gradient from the side of the surface. This is, first of all, due to the motion of defects to the film surface, ie, under laser irradiation the determining factor of movement and relaxation of defects is a temperature gradient, which stimulates the diffusion of defects. Using statistical-dynamical theory of X-rays, parameters of complex radiation defects were calculated.

# Features of Structure and Phase Composition of Calcium Phosphates Synthesized From Eggshell

Zyman Z.Z., Rokhmistrov D.V., Lytkova M.Yu., Goncharenko A.V.

*V.N. Karazin Kharkiv National University, Kharkiv, Ukraine*

Hydroxyapatite (HA) is a main mineral component in hard tissues of human and animals. It is widely used in medical practice as implant. There are several methods of HA production. Nowadays the synthesis of HA from biological waste product is becoming more and more popular due to environmental protection. In this connection use of eggshell as a calcium source is promising because of simplicity and efficiency. However, due to the HA synthesis depends on the several factors, the obtained product has often variable phase composition and the structure. The aim of this work was to synthesize HA from eggshell and study its structure and phase composition.

Eggshell was collected from 10 eggs. It was treated during 2 hour in boiled water in order to remove the organic substances. Then the shell was dried at 60$^{o}$C for 3 days. The dry shell was milled in mixer to obtain the fine powder, which was used as a source of calcium in the synthesis. The XRD of the powder have shown, that it contain one phase – $CaCO_3$. HA was synthesized by reaction between $CaCO_3$ and $H_3PO_4$ [1]. The ratio of reagent was chosen in order to get the stoichiometric HA (Ca/P=1.67) [2]. The synthesis was performed at 25$^{o}$C for 24 h. The synthesized product was filtered at Buchner funnel and dried at 60$^{o}$C for 3 days. The powder was pressed into cylindrical pelts, which then fired from room temperature to 1250$^{o}$C for 1 h. The samples were examined by XRD and X-ray qualitative phase analysis.

The XRD of the samples have shown that the samples fired at low temperatures have the structure of calcium-deficient hydroxyapatite (CdHA), which then transform to tricalcium phosphate (TCP) at higher temperatures. Heating of the samples at 950$^{o}$C led to the formation of CaO and β-$Ca_3(PO_4)_2$. The quantity of CaO in the samples is tend to decreasing when the temperature rise up to 1250$^{o}$C. This route of the synthesis opens ways for production of new calcium phosphate biomaterials based on HA.

1. M. Jarcho, C.H. Bolen, J. Mater Sci., 11, 2027 (1976).
2. Narasaraju T. S. B., Phebe D. E., J. Mater. Sci., 31 (1996), 1-21.

# Solid-Phase Interaction in the Bilayer Eutectic Nanofilms

Doroshenko T.

*V. Lashkaryov Institute of Semiconductor Physics NAS of Ukraine, Kyiv, Ukraine*

Low-temperature solid-phase interaction in the simple eutectic pairs of metal- semiconductor thin films is one of the ways to create new materials for engineering of nanoplasmonic and nanophotonic structures. Such eutectic pairs of films can be used for recording media, in the optical sensors and photonic crystals. In present report bilayer systems of semiconductor and metals that are forming simple eutectic pairs Ge-Au, Ag, Al were investigated. The aim was to study the changes of structural and optical properties of bilayer eutectic nanofilms during the laser and thermal annealing. Bilayer eutectic nanofilms systems were prepared by thermal evaporation in vacuum with computer control technique.

The nanostructure with total thickness 45 - 50 nm and width of pits 0,5mkm was obtained via laser beam treatment of two-layer eutectic system Ge-Au, Ag, Al. The annealing was performed by laser radiation with a wavelength of 530 mkm. The laser annealing power of this structures on glass substrates is represented in Table 1.

*Table 1. The annealing power of two-layers structures on glass substrates*

| Systems | Layers thickness, nm | Pulse length, ns | Recording power for local interaction, mW | Recording power for perforation, mW |
|---|---|---|---|---|
| Ge-Al | 45 | 150 | 4,2 | 11 |
| Ge-Ag | 50 | 150 | 11 | 19 |
| Ge-Au | 45 | 150 | 5,7 | 11 |

The results of bilayer eutectic nanofilms thermal annealing demonstrate the changing of transmission and reflection index. At the same time AFM images of samples before and after the thermal annealing show the same structure. The temperatures of solid-phase interaction of investigating samples was 1,5-3 times less then eutectic temperatures. Spectra of binary mixtures Ge-metals were measured in situ during the thermal annealing. They show the changes of transmission as a function of the annealing temperature. Also be noted that reflection index spectra of the systems Ge-Au,Ag,Al before and after annealing are different. All features of the investigated systems described above were used by us for creation photonic crystals.

One of the most sensitive modern optical sensors are devices based on SPR. System Ge-Au make it possible to extend the range of the studied biological objects. Annealing this bilayer systems shows the shifts of curves of surface plasmon resonance and give the possibility to obtain the required curves.

Such advantages of these materials as low-energy interactions, long lifetime and environmental make them promising for neoteric technology.

## СЕКЦІЯ 7 (стендові доповіді)
## ІННОВАЦІЙНІ МЕТОДИКИ ІЗ ВИКЛАДАННЯ НАВЧАЛЬНИХ ДИСЦИПЛІН

12-15 травня 2015 р.

## SESSION 7 (poster)
## INNOVATIVE METHODS FOR TEACHING

May, 12-15, 2015

# Monitoring at the Ukraine-Romania Cross-Border Region in Teaching Methods of Environmental Sciences

Kurta S.A., Voronych O.L., Matkivskyi M.P., Dzhura U.Ya.

*Vasyl Stefanyk Precarpathian National University, Ivano-Frankivsk, Ukraine*

Abstract published for program ENPI CBC Hungary-Slovakia-RomaniaUkraine 2007-2013 funds Project Clean Air Management in the Romania-Ukraine Transboundary Area (CLAMROUA).

Between July and November 2014 project expert group from State High Educational Institution «Precarpathian National University named after Vasyl Stefanyk» was held clean air mobile monitoring campaign in Ivano-Frankivsk region. During the monitoring campaign following parameters were measured: the contents of carbon oxide, carbon dioxide, sulfur dioxide, nitrogen dioxide, hydrogen sulfide, formaldehyde, alpha-, beta-particles and gamma radiation contamination in the area. For this purpose were used 5 automatic analyzers «DOZOR C-P" for each of the above gases individually, certified and produced by NPP "Orion" m. Kharkiv Ukraine and the appropriate dosimeter-radiometer. The principle of automatic analyzers «DOZOR C-P" is based on electrochemical or infra-red method of detection and each of these six gases individually in the natural atmosphere of the analyzed air [2].

As shown by measurements in more than 200 cities and villages of IvanoFrankivsk region the expert group from the university has overcome more than 1500 km and visited all parts of the Ivano-Frankivsk region. Mainly air at the region is clean and complies with the regulatory parameters according the laws of Ukraine. The exception was the village Broshniv (Rozhnyativ District), where revealed numerous exceeding of maximum permissible concentration for formaldehyde (daily average maximum permissible concentration in the air of localities - 0,003 ppm, or mg/m$^3$). Formaldehyde included in the group of chemical carcinogens and has general toxic effect at a concentration 0,012 mg/m$^3$and discovers allergenic effect at a concentration 0,011 mg/m$^3$. MPC of formaldehyde in water - 0.05 mg/L, in the breathing zone for workplaces - 0,035 mg/m$^3$. Lethal dose 35% solution of formaldehyde is 10 ... 50 grams. [3].

Obtained data were used in teaching environmental sciences at the Institute of Natural Sciences State High Educational Institution «Precarpathian National University named after Vasyl Stefanyk»

1. Clean Air Management in the Romania-Ukraine Transboundary Area (CLAMROUA), registration number: HUSKROUA 1101/127 approved by the Joint Monitoring Committee of the Joint Operational Programme Hungary-Slovakia-Romania-Ukraine European Neighbourhood and Partnership Instrument Cross-border Cooperation Programme. — 8 p. 2013.
2. Instruction of gas analyzer «DOZOR C-P". Developed by "SPE ORION" / S.Yu.Sokolov. - M. Kharkov Ukraine - 13 p..
3. Formaldehyde - Living Planet. http://www.ecolabel.org.ua/slovnuk/276-s.html.

# Special Course "Physics and Technology of Thin Films" for Students of Specialty "Applied Physics

Prokopiv V.V.

*Vasyl Stefanyk Precarpathian National University, Ivano-Frankivsk, Ukraine*

Obtaining high quality and reproducible electrical parameters for the thin film layers is one of the most important technological processes of forming structures as discrete diodes and transistors, and active and passive elements IC. Reliability and quality of microelectronic products, technical level and economic indicators of their production, the effectiveness of modern equipment for applying thin films largely depends on the level of personal training. So important and topical is reading course "Physics and Technology of Thin Films" for students specialty "Applied Physics".

The course is read in two semesters. The first dealt with technological aspects of thin film materials, during the second - the main focus is on the physics of thin films.

During the study of thin film technology, students acquire various methods of their creation, particular, methods of thermal evaporation and ion sputtering, liquid and gas phase epitaxy, molecular-beam epitaxy. At the same time study various vacuum systems and equipment for creation thin films, especially the technological modes and control parameters of their creation. The program of special course involves acquaintance of students with the basics of electronic vacuum hygiene and safety at growing thin films.

In the second semester are studied processes of nucleation and films growth, their physical properties. In particular, consider the following question: electric current in thin films, internal tension in films and coatings, thermoelectric properties.

Are considered experimental and theoretical study of the effect of technological factors of growing on properties of thin films based on lead chalcogenides and tin telluride. The use of thin films in semiconductor devices and microcircuits.

The program of special course provided for fulfillment of four laboratory works:

1. Preparation and measurement of high vacuum.
2. Obtaining thin films by thermal evaporation in open vacuum.
3. Obtaining thin films by hot wall method.
4. Measurement of electric parameters of thin films.

*This research is sponsored by NATO's Public Diplomacy Division in the framework of "Science for Peace" (NATO SPS 984536)).*

# Specific Features of Teaching a Newly Introduced Subject "Fundamentals of Radiochemistry" in Uzhhorod National University

Vasylyeva H.V.

*Uzhgorod National University, Uzhgorod, Ukraine*

A new subject, Fundamentals of Radichemistry, was introduced for teaching in Uzhgorod National University for the students specializing in Ecology at the Faculty of Chemistry. The importance of this subject being introduced is related with the following reasons:

(1) Radiochemistry is an important field of chemical sciences. It is closely related to the contemporary environmental problems, including utilizing nuclear power plant waste. Another reality now is a danger of radioactive pollution due to terrorist attacks or use of nuclear weapons.

(2) Previously, radiochemistry had not been included into the curricula of Uzhgorod National University; meanwhile, the facilities available at the university provide sufficient equipment for carrying out laboratory studies.

The authors analyze the experience of teaching radiochemistry in Ukrainian universities and propose a series of innovations. They include, in particular, the teachers' emphasis on the basic differences of radiochemical processes from purely chemical, correct formulation of the vision of relationship of nuclear physics, radiochemistry, chemistry, and environmental science and safety of work and natural resource management.

The innovations also include a series of new laboratory works devoted to the processes of isotope exchange, water radiolysis under ionizing radiation as well as co-precipitation processes which will enable the students to become specialists in this field and face the possible challenges of today and the future.

## AUTHORS INDEX

## Для нотаток/For notes

## Для нотаток/For notes

Наукове видання

**ФІЗИКА І ТЕХНОЛОГІЯ ТОНКИХ ПЛІВОК ТА НАНОСИСТЕМ**
Матеріали XV міжнародної конференції
МКФТТПН-XV

**PHYSICS AND TECHNOLOGY OF THIN FILMS AND NANOSYSTEMS**
Materials of XV International Conference
ICPTTFN-XV

Редактор *Роман Дзумедзей*
Технічний редактор *Олександр Соколов*
Верстка *Оксана Костюк, Богданна Волочанська, Іван Биліна, Остап Матківський*
Відповідальний за випуск *Володимир Прокопів*

***Усі матеріали подано у авторській редакції***

Підписано до друку 22.04.2015.
Формат 60x84/16. Ум. др. 16,83 арк. Гарнітура «Times New Roman».
Папір офсетний, друк цифровий. Тираж 350 примірників.

Видавництво
Підприємець Голіней О.М.,
вул. Галицька, 128, м. Івано-Франківськ, 76018
Тел. +38(0342)580432, +38(050)5403064

**Фізика і технологія тонких плівок та наносистем.** ***Матеріали XV Міжнародної конференції*** / За заг. ред. заслуженого діяча науки і техніки України, д.х.н., проф. **Фреїка Д.М**. – Івано-Франківськ: П-ць Голіней О.М., 2015. – 400 с.